Evaluation of Sentinel-1 & 2 time series for the identification and characterization of ecological continuities, from wooded to crop-dominated landscapes

Audrey Mercier

DOCTORAT SOCIETES BRETAGNE TEMPS LOIRE TERRITOIRES

UNIVERSITÉ RENNES 2

THESE DE DOCTORAT DE

L'UNIVERSITE RENNES 2

ECOLE DOCTORALE N° 604
Sociétés, Temps, Territoires
Spécialité : *Géomatique*

Par

Audrey Mercier

Evaluation of Sentinel-1 & 2 time series for the identification and characterization of ecological continuities, from wooded to crop-dominated landscapes

Thèse présentée et soutenue à Rennes, le 21 janvier 2021
Unité de recherche : LETG – UMR CNRS 6554

Rapporteurs avant soutenance:

Agnès Bégué	Directrice de recherches, CIRAD – UMR TETIS
Hervé Nicolas	Professeur des universités, Agro Campus Ouest – UMR SAS

Composition du Jury:

Présidente :	Sandrine Petit-Michaut	Directrice de recherches, INRAE – UMR Agroécologie
Examinateurs :	Paola Mairota	Directrice de recherches, Université de Bari Aldo Moro
	Samuel Corgne	Professeur des universités, Université Rennes 2 - LETG
Dir. de thèse :	Laurence Hubert-Moy	Professeure des universités, Université Rennes 2 - LETG
Co-dir. de thèse :	Jacques Baudry	Directeur de recherches, INRAE Rennes - UMR BAGAP

ACKNOWLEDGMENTS

Tout d'abord, je tiens à remercier mes directeurs de thèses, Laurence Hurbert-Moy et Jacques Baudry. Des stages de master au doctorat, je vous remercie de m'avoir fait confiance et de m'avoir donné ces opportunités. Je remercie Laurence pour ses conseils, sa rigueur scientifique, ses soigneuses relectures et ses bons choix de direction lorsque je m'égarais. Je remercie Jacques tout d'abord pour m'avoir fait découvrir l'écologie du paysage et enseigner ses bases, ensuite, pour les discussions passionnantes à l'INRA, au knock puis par visioconférence (confinement oblige), pour sa disponibilité et sa réactivité et enfin merci de m'avoir permis de rencontrer des gens tout autant passionnés que lui à de nombreux événements scientifiques (terrains, réunions, conférences, colloques) à travers l'Europe et au Costa Rica.

Je tiens à adresser des remerciements particuliers à Julie Betbeder qui a été exceptionnelle durant cette thèse de par son soutien, ses enseignements méthodologiques et ses idées brillantes. Je me rappelle également de ses aides spontanées lors de ses passages à l'INRA durant mon stage de Master 1 puis de son encadrement très enrichissant lors de mon stage de Master 2. Ta détermination et ton énergie sont pour moi une grande source d'admiration. Merci pour tous tes conseils autant pour la thèse que pour mon avenir professionnel. Aussi, je te remercie sincèrement de m'avoir donné l'opportunité de te rejoindre au CATIE, ces quatre mois ont permis de donner un bel élan à cette thèse, et enfin, merci de me donner l'opportunité de continuer dans la recherche avec un post-doctorat qu'il me tarde de commencer prochainement au CIRAD.

Je remercie Agnès Bégué, Paola Mairota, Sandrine Petit-Michaut, Samuel Corgne et Hervé Nicolas d'avoir accepté de participer à mon jury et d'évaluer mon travail.

Je remercie Eric Pottier pour sa bienveillance et ses explications incroyablement claires dans le domaine du radar lors des comités de suivi annuel.

Cette thèse a débuté et s'achève avec le projet WOODNET qui a réunit une équipe de chercheurs/ ingénieurs/doctorants/stagiaires de Belgique, d'Espagne et de France. Je tiens à remercier toute l'équipe du projet pour ce partage de connaissances très enrichissant et la bonne ambiance lors des réunions entre la Sierra Morena et Louvain-la-Neuve. Ce projet a été pour moi l'occasion de découvrir le superbe territoire des ours bruns dans les Monts Cantabriques et celui des Lynx dans la Sierra Morena. Merci à l'équipe espagnole pour l'organisation de ces terrains. J'adresse mes sincères remerciements à Carlos et sa famille qui m'ont accueillie et avec qui j'ai partagé de très bons moments. Mes remerciements s'adressent également à Miguel pour sa bienveillance et sa bonne humeur lors de nos échanges et notre visite à Madrid.

Je remercie l'équipe de l'INRA BAGAP pour son accueil lors de mes stages de master puis de mes passages tout au long de ces trois années de thèse.

Je remercie l'équipe de l'unité Forêt et Sociétés du CIRAD de Montpellier pour son accueil lors des sessions de travail avec Julie. Un grand merci à Guillaume pour les optimisations précieuses de mes codes R, et à Valéry et Lilian pour leurs apports

enrichissants sur les forêts tropicales. Je remercie chaleureusement Anthony, Clément, Florence, Jasper, Laura et Sarah pour leur aide et les bons moments passés à leurs côtés à Montpellier.

La suite de mes remerciements s'adresse à l'ensemble du personnel du CATIE qui m'a permis de venir travailler au Costa Rica durant quatre mois et de découvrir un pays magnifique. Merci à Lenin, Christian, Sergio, Emily et Alan de m'avoir accueillie dans leur unité. Merci aux colocs d'Andino d'avoir fait de ce séjour une suite de joyeuses échappées et de moments conviviaux. Je remercie particulièrement Sacha pour ses tips et astuces de vie en milieu tropicale et Ophélie, organisatrice de voyage hors pair et véritable soutien dans les moments délicats.

Je remercie l'ensemble des personnes qui m'ont aidée lors du terrain sur la ZAA ; en amont avec l'établissement du protocole en collaboration avec Hervé Nicolas, le prêt gracieux des capteurs par Christophe Langrume et l'aide au bricolage de Jean et Julien; pendant la fameuse journée avec Elodie, Hortense, Julien, Maxime et Yonnie ; et enfin en aval lors des traitements avec Paul lors de son stage.

Je tiens à remercier toute l'équipe du LETG Rennes, le personnel administratif, les permanents, doctorants, post-doctorants, ingénieurs et stagiaires avec qui j'ai passé de très bons moments professionnels et personnels. A mon arrivée, il y avait Marianne, Perrine et Adeline qui nous ont dorlotés, nous les nouveaux doctorants plein d'entrain et d'espoirs, merci à vous! Mille mercis à Julien, mon éclaireur sur les missions de reconnaissances radar et Sentinel. Merci à Clémence, Elodie, Guglielmo, Gwenaël, Narges, Pierre-Gilles, Roberta et Wei pour leur écoute et leurs encouragements. Des remerciements tout particulier à Olivier pour son grain de folie et ses idées de jeux farfelues et un immense merci pour son soutien infaillible et son aide durant la dernière ligne droite. Enfin, j'adresse de tendres remerciements aux doctorants et amis avec qui j'ai fait mes premiers pas en doctorat et avec qui j'ai créé beaucoup de précieux souvenirs : Damien, Fanny et Florent.

Je remercie mes amis rencontrés à Rennes pour les bons moments passés à leur côté lors du marché des Lices, des soirées en ville ou des randonnées sur les côtes Bretonnes: Anne Sophie, Chloé, Eléonore, Elvira, Pierre, Jeremy, Léa, Mathilde, Maeva et Pascal.

Enfin, je remercie mes amis de Charente-Maritime qu'il fait toujours bon de retrouver : Alexis, Angélique, Benjamin, Benoit, Camille, Florine, Helena, Laura, Leslie, Lila, Manon, Mickael, Paul, Quentin, Samantha et Valentin.

Enfin, je remercie mes parents, ma sœur, mon beau-frère et mes grands-parents pour tout le bonheur et la motivation qu'ils m'apportent. Merci à mes merveilleux parents qui m'ont toujours soutenu dans mes choix, cru en moi et sur qui je peux compter en toutes circonstances. Merci du profond intérêt que vous avez porté à mes différentes réalisations et l'amour que vous me témoignez chaque jour. Je me sens extrêmement chanceuse d'être votre fille.

Enfin, merci à mon meilleur collègue pour ses leçons de programmation et nos discussions interminables sur les méthodes scientifiques. Au-delà du cadre professionnel, je tiens à te remercier pour ton écoute, ton soutien et tes encouragements tout au long de ces trois ans de thèse et pour ta patience durant les derniers mois.

LIST OF ACRONYMS

ALOS *Advanced Land Observing Satellite*

AVHRR *Advanced Very High Resolution Radiometer*

CFA *Correspondence Factor Analysis*

CNRS *National Center for Scientific Research*

DB *Dry Biomass*

ERS *European Remote Sensing*

EVI *Enhanced Vegetation Index*

FAPAR *Fraction of Absorbed Photosynthetically Active Radiation*

fCover *Fraction of green vegetation cover*

GNDVI *Green Normalized Difference Vegetation Index*

GPR *Gaussian process regression*

GRD *Ground Range Detected*

INRAE *National Research Institute for Agriculture, Food and Environment*

Inverted Red-Edge Chlorophyll Index IRECI

JERS *Japan Earth Resources Satellite*

LAI *Leaf Area Index*

LETG *Littoral - Environnement - Télédétection - Géomatique*

LiDAR *Light Detection And Ranging*

LTER *Long Term Ecological Research Network*

MCARI *Modified Chlorophyll Absorption in Reflectance Index*

MODIS *Moderate Resolution Imaging Spectroradiometer*

MSAVI *Modified Soil Adjusted Vegetation Index*

MTCI *MERIS Terrestrial Chlorophyll Index*

NDI *Normalized Difference Index*

NDVI *Normalized Difference Vegetation Index*

NDWI *Normalized Difference Water Index*

NIR *Near-InfraRed*

OA *Overall Accuracy*

PA *Producer's Accuracy*

PALSAR *Phased Array L-band Synthetic Aperture Radar*

PSSRa *Pigment Specific Simple Ratio*

RaDAR *Radio Detection And Ranging*

REIP *Red-Edge Inflation Point index*

RF *Random Forest*

S-1 *Sentinel-1*

S-2 *Sentinel-2*

S2REP *S-2 Red-Edge Position index*

SAVI *Soil Adjusted Vegetation Index*

SE *Shannon Entropy*

SLC *Single Look Complex*

SNAP *Sentinel Application Platform*

SPOT *Satellite Pour l'Observation de la Terre*

SRTM *Shuttle Radar Topography Mission*

SVM *Support Vector Machine*

SWIR *ShortWave InfraRed*

UA *User's Accuracy*

UMR *Unité Mixte de Recherche*

WB *Wet Biomass*

WC *Water Content*

WDVI *Weighted Difference Vegetation Index*

ZAA *Zone Atelier Armorique*

Table of contents

GENERAL INTRODUCTION

The survival of humanity is closely linked to the maintenance of biodiversity. Biodiversity is " *the sum total of all plants, animals, fungi, and microorganisms on Earth, their genetic and phenotypic variation, and the communities and ecosystems of which they are a part*" (Dirzo and Raven 2003). Climate regulation, support to agriculture (soil fertilization, pest regulation), production of food and material resources, and transformation of waste and pollutants are among the multitude of ecosystems services provided to humans (Bolund and Hunhammar 1999; Baudry et al. 2000; Krieger 2001). Anthropogenic pressures have led (and still lead) to habitat loss and degradation causing massive extinction of biodiversity (Pimm et al. 1995). Habitat loss can decrease connectivity by isolating habitat patches from other patches at the landscape scale. However, movement is essential for the sustainability of species because they need to move throughout their life cycle, particularly to feed, find refuge and reproduce. Furthermore, the movement supports genetic mixing, a key element for the maintenance of fauna and flora species.

Ecological corridors are one of the main tools used to increase the landscape connectivity by facilitating the movement of species. Ecological corridors connect the patches of habitats to form a whole called "ecological continuities" (Bennett 2004). The ecological functions of continuities are complex due to the diversity of structure and composition of landscape elements and their different contexts from local to landscape scale. In addition, there is a diversity of species that react differently to the landscape elements (Dennis et al. 2013). Therefore, maintaining and creating ecological continuities require a good understanding of the interactions between landscape elements and species to achieve relevant conservation strategies. In wooded landscapes, the main threat on biodiversity is deforestation and forest degradation. In these landscapes, primary forests and large patches of habitats are considered to be the most effective landscape elements for biodiversity conservation. However, secondary forests and small habitat patches play an important role for species persistence by potentially increasing landscape connectivity (Lindenmayer et al. 2006; Vidal et al. 2016). In crop-dominated landscapes, many studies have focused on semi-natural elements such as permanent grasslands and wooded elements (woodlands and hedgerows), that are key elements of ecological continuities (Burel et al. 2013). Originally, crop-dominated landscapes were described as a set of semi-natural elements within a neutral agricultural matrix by landscape ecologists (Burel et al. 2013). However, heterogeneous crop-dominated landscapes with semi-natural elements have a high potential for biodiversity (Tscharntke et al. 2005; Billeter et al. 2008; Fahrig et al. 2011). Crops induce spatial heterogeneity due to their diversity and the complexity of their configuration beneficial for biodiversity. In addition, temporal heterogeneity induced by crop rotation, management and phenology affects the movement of species across the landscape. Therefore, corridors may temporarily appear within crop-dominated landscapes (Burel et al. 2013).

Now, the notion of ecological continuity is a key concept in public policies dealing with environmental protection laws, protected areas, land use planning tools, etc from the international level to local level. The identification and characterization of ecological continuities are at the basis of biodiversity conservation strategies and represent a major scientific challenge due to the structural and functional complexity of ecological systems. However, in wooded landscapes, small habitat patches and secondary forests are being neglected in favour of primary forests and large habitat patches. In landscapes dominated by crops, the mosaic of crops is rarely integrated into maps of ecological continuities that

include only semi-natural elements such as permanent grasslands and wooded elements. Moreover, the temporal dynamics of these landscapes are not taken into account while it impacts the functionality of ecological continuities.

In this context, time series of satellite images are a relevant tool for mapping and monitoring the elements constituting ecological continuities in crop-dominated and wooded landscapes over large areas. Images acquired by optical satellites have already shown high potential for identifying and characterizing landscape elements. The optical sensors Moderate Resolution Imaging Spectroradiometer (MODIS), Advanced Very High Resolution Radiometer (AVHRR) and Landsat have been widely used to map land use and land cover (Congalton et al. 2014; Gómez et al. 2016) and to detect deforestation and forest degradation (Bourgoin 2019) at large scales due to their high temporal resolution and large swathes. However, the low spatial resolution of these data (30m to 1.1km) does not allow the fine identification of landscape features or their characterization. Very high spatial resolution images such as SPOT (Satellite Pour l'Observation de la Terre), Formosat-2 optical, Quickbird, WorldView and IKONOS (<5m) have shown high potential to identify fine hedgerows (Vannier and Hubert-Moy 2014), estimate yield, leaf area index (LAI), biomass and crop phenological stages (Quarmby et al. 1993; Doraiswamy et al. 2004; Mulla 2013; Bontemps et al. 2015; Pan et al. 2015; Betbeder et al. 2016b) or mapping the above-ground biomass of tropical forests (Singh et al. 2014; Pargal et al. 2017). The temporal resolution is also an essential element in characterizing the temporal dynamics of landscape features. Since the 2000s, studies have demonstrated the value of high spatial resolution SAR (Synthetic Aperture RaDAR) satellite data for crop mapping and characterization (Steele-Dunne et al. 2017). Polarimetric indicators derived from RADARSAT-2 or TerraSAR-X are relevant for estimating the phenological stages, height and biomass of various crops (Jiao et al. 2009; Wiseman et al. 2014; Mascolo et al. 2015; Jin et al. 2015; Betbeder et al. 2016b; Pacheco et al. 2016; Canisius et al. 2018; McNairn et al. 2018; Homayouni et al. 2019). In wooded landscapes, the ALOS-SAR sensor has shown high performance in producing a global forest/non-forest map (Shimada et al. 2014; Zhou et al. 2018). However, the low temporal resolution of these sensors, their necessary programming and the cost of the images constitute strong constraints for the monitoring of crop-dominated and wooded landscapes.

The free high spatial and temporal resolution data acquired by the Sentinel-1 (S-1) SAR satellite since 2014 and the Sentinel-2 (S-2) optical satellite since 2016 offer new possibilities for mapping and monitoring ecological continuities. Recent studies have demonstrated the potential of S-2 time series for mapping land use in wooded (Jönsson et al. 2018) and crop-dominated landscapes (Csillik and Belgiu 2017a; Denize et al. 2019a). For crop-dominated landscapes, spectral bands, vegetation indices and biophysical variables derived from S-2 data accurately estimate LAI (Delegido et al. 2011b; Frampton et al. 2013; Clevers et al. 2017; Pan et al. 2018; Wang et al. 2019), biomass (Veloso et al. 2017; Ghosh et al. 2018; Ganeva et al. 2019) and phenological stages (Veloso et al. 2017; Ghosh et al. 2018; Stendardi et al. 2019) of various crops. However, the exploitation of optical data is limited by cloud cover presence. In addition, they provide information only on the top layer of vegetation and the signal saturates with high biomass and LAI levels (Wang et al. 2016a). Despite the fact that S-1 data are sensitive to soil conditions (roughness, moisture), they are an alternative to S-2 data as they are insensitive to atmospheric conditions and the SAR signal penetrates the canopy (Lee and Pottier 2009). Recent studies have shown the interest of backscatter coefficients and

VH:VV ratio derived from S-1 data for mapping five global land cover types (water, forest, urban, bare soil and agricultural area) in Turkey (Abdikan et al. 2016) and detecting coniferous forests, deciduous forests and non-irrigated arable land in Germany (Balzter et al. 2015). In crop-dominated landscapes, the potential of these same S-1 variables has been demonstrated for detecting changes in the structure of rapeseed, maize and winter cereals (Vreugdenhil et al. 2018), identifying the phenological stages of wheat (Song and Wang 2019) and estimating biomass, water content (WC) and LAI of wheat (Kumar et al. 2018). However, to our knowledge, no studies have been conducted with polarimetric indicators derived from S-1 to characterize crops (Jin et al. 2015; Stendardi et al. 2019).

Consequently, the combined use of optical and SAR data should improve the mapping of ecological continuities. Indeed, the fusion of optical and SAR data improves the identification of land use/land cover (Kussul et al. 2017; Zhou et al. 2017; Laurin et al. 2018; Reiche et al. 2018) and crop types (Orynbaikyzy et al. 2019). The optical domain is sensitive to the vegetation physiology, while microwaves are influenced by geometry (roughness, texture, geometrical structure) and surface moisture. This complementarity between the optical and SAR domains is little exploited to characterize ecological continuities. A few studies have used both optical and SAR data to characterize crops (Betbeder et al. 2016a; Veloso et al. 2017; El Hajj et al. 2019). However, these studies use the Normalized Difference Vegetation Index (NDVI), derived from optical data as a reference for evaluating SAR data. Although the actual combination of optical and SAR data improves the results of land use and crop type classification, it remains little used to predict crop parameters (Jin et al. 2015; Stendardi et al. 2019).

The objective of the thesis is twofold : 1) comparatively evaluate the S-2 optical and S-1 SAR time series to identify and characterize the constituent elements of ecological continuities using land cover and land use classifications and crop characterization in wooded and crop-dominated landscapes, 2) assess the influence of the spatio-temporal structuring these landscape mosaics on biodiversity using metrics derived from S-1 and S-2 time series.

The first part of the thesis explains the basis of ecological continuities and remote sensing with a focus in wooded landscapes and crop-dominated landscapes, and highlights the associated challenges. Then, study areas and field, species and remote sensing data used in this thesis are detailed.

The second part of the thesis aims at answering the following question : What are the most efficient Sentinel sensor and variables to identify the potential constitutive elements of ecological continuities in wooded landscapes?

For that purpose, we evaluated the potential of S-1 data alone, S-2 data alone and the combined S-1 and S-2 data to identify and characterize land cover in forest-agricultural mosaic landscapes. The study focused on two wooded landscapes with contrasting vegetation gradients: a temperate mountainous landscape in the Cantabrian Range (Spain) and a tropical humid forest landscape in Paragominas (Brazil). The satellite images were classified using an incremental procedure based on the ranks of importance of the input variables derived from S-1 and S-2 time series. The developed algorithm automatically

selects the relevant variables and time periods to be used to best classify land cover and land use in each landscape.

The third part of the thesis focused on the following the question: What are the most efficient Sentinel sensor and variables to identify and characterize the potential constitutive elements of ecological continuities in agricultural landscapes?

To answer this question, we focused on wheat and rapeseed, which are two of the most important crops in the world in terms of area harvested (FAO, 2017). We evaluated the potential of S-1 data alone, S-2 data alone and the combined of S-1 and S-2 data to identify the principal and secondary phenological stages of wheat and rapeseed in Picardy (France). More specifically, the aim of this study was to evaluate the interest of polarimetric indicators derived from S-1 data and to determine the number and type of S-1 and S-2 variables necessary to discriminate the phenological stages of wheat and rapeseed. We estimated the performance of spectral bands and vegetation indices derived from S-2 and backscatter coefficients and polarimetric indicators derived from S-1. Satellite images were classified using the incremental method developed in the previous study (Mercier et al. 2019b).

We continued our research on crop characterization by evaluating the potential of S-1 and S-2 data to estimate the LAI, wet biomass (WB), Dry Biomass (DB) and WC of wheat and rapeseed in Brittany (France). We compared the predictive power of spectral bands and vegetation indices derived from S-2 and backscatter coefficients and polarimetric indicators derived from S-1 using Gaussian process regressions (GPR).

The fourth part of the thesis focused on the following question: What is the impact of landscape structure on crop phenology and biodiversity in crop-dominated landscapes?

Based on the results obtained in the previous part of the thesis, we assessed the impact of the spatio-temporal structuring of the crop mosaic on biodiversity. For that purpose, we analyzed the influence of biophysical heterogeneity on wheat phenology and associated biodiversity in Brittany, Picardy and Wallonia study areas. The vegetation index named Weighted Difference Vegetation Index (WDVI) calculated from S-2 data was used as a metric of biophysical heterogeneity and as an indicator of wheat phenology. First, we analyzed the relationships between crop mosaic, landscape grain and biophysical heterogeneity. Then, we studied the effect of biophysical heterogeneity on wheat phenology. Finally, the distribution of two carabid beetle species was estimated using the biophysical heterogeneity metric.

This thesis contributes to the WOODNET project (Connectivity patterns and processes along a gradient of European landscapes with woody vegetation and spatial heterogeneity), which is part of the European BIODIVERSA program. This is an interdisciplinary project that combines ecology, geography, hydrology, agronomy and law and involves researchers from Belgium, France and Spain. The researches that are presented in this thesis focus on one of the main activities of the WOODNET project, that is the evaluation of new satellite images for landscape mapping (https://woodnetweb.wordpress.com/project/).

I ECOLOGICAL CONTINUITIES AND REMOTE SENSING

Contents

Introduction

The first part of this manuscript presents the thematic basics necessary for a clear understanding of the thesis and details the study areas and data used.

The objective of this part is to present the challenges posed by landscape ecology and remote sensing applied to ecological continuities based on the scientific literature.

In the first chapter, the basic terms and concepts related to ecological continuities are defined. We explain the global issues related to ecological continuities and those specific to wooded and crop-dominated landscapes. Finally, the integration of ecological continuities in public policies is described from the international to the national and regional scales, focusing on policies in the sites studied in this thesis.

In the second chapter, we first define the basics terms and concepts related to optical and SAR remote sensing data. Then, we provide an overview of research using these data for the identification and characterization of constitutive elements of ecological continuities from wooded to crop-dominated landscapes, with particular emphasis on Sentinel-1 and 2 images. Finally, we explain how ecological continuities functions are evaluated using remote sensing data.

Finally, in the third chapter, we present the eight sites studied in this thesis: first, the wooded landscapes located in Spain and Brazil and second, the crop-dominated landscapes located in France and Belgium. Then, the remote sensing data used and associated preprocessing are described. Finally, field data, species data and the field protocols developed for their collection are presented.

CHAPTER 1

Ecological continuities from wooded to crop-dominated landscapes

Contents

1.1. Introduction

This chapter first defines the basic terms related to ecological continuities and their functions. Then, the second and third sections focus on ecological continuities in wooded and crop-dominated landscapes, respectively. The implications of ecological continuities in public policies are described and reviewed in a final section.

1.2. Habitat fragmentation and ecological continuities

Habitat loss is the main driver of the current mass extinction of biodiversity (Pimm et al. 1995). Biodiversity is "the sum total of all plants, animals, fungi, and microorganisms on Earth, their genetic and phenotypic variation, and the communities and ecosystems of which they are a part" (Dirzo and Raven 2003). An operational habitat is defined as an unit that is lived in, occupied by, or consumed by one or more species (Vandermeer 1972). A habitat is therefore directly linked to the notion of species and is not relevant without it. More recently, Hall et al. (1997) defined habitat as "the resources and conditions present in an area that produce occupancy-including survival and reproduction-by a given organism". Then, Mitchell et al. (2012) introduced a fitness-based definition of habitat by considering that individuals have an ideal knowledge about the distribution of resources and move between patches to maximize fitness. The main causes of habitat loss are human pressures, i.e. intensification of agriculture, natural resource extraction (mining, fishing and logging) and urbanization (cities, roads, dams and power lines) (Dirzo and Raven 2003).

Over the last 3 years, the effects of habitat fragmentation have been debated in the ecology community (Fahrig 2017; Fletcher et al. 2018; Fahrig et al. 2019). "Fragmentation occurs when a large expanse of habitat is transformed into a number of smaller patches of smaller total area, isolated from each other by a matrix of habitats unlike the original" (Wilcove et al. 1986). Habitat fragmentation is frequently associated with habitat loss and perceived as negative for biodiversity. While the effects of habitat loss have been widely demonstrated to be detrimental to biodiversity, habitat fragmentation independent of habitat loss has mostly rare and positive effects (Fahrig 2017). Indeed, for the same total area, small separated habitats have an ecological value equivalent or higher than a single large habitat (Figure 1-1). Fahrig (2017) reviewed 161 author's explanations for positive responses (water quality, plants, inverterbrates, mammals etc.) to habitat fragmentation and identified 7 possible causes: an increase of functional connectivity (higher patch encounter rate and higher edge density), a higher diversity of habitat, positive edge effects, a stabilization or increase of persistence of predator-prey and host-parasitoid systems, a reduction of intraspecific and interspecific competition, a spread of the extinction risk and an increase of landscape complementation.

Either way, connectivity plays a crucial role for biodiversity. The connectivity is defined as the degree of isolation of a patch from the other patches at landscape scale (Hanski 1999) or the degree of permeability of the landscape to the movement of species (Taylor et al. 1993). Connectivity is considered at a species-specific scale; the defined study landscape should be a function of the dispersal capacity and preferred habitats of the studied species. Movement is essential for the sustainability of species as it allows them to feed, reproduce, avoid predators and colonize new habitats (Wiens et al. 1993). Thus, patch isolation has negative

effects on biodiversity (Virgós 2001; Heller and Zavaleta 2009; Bailey et al. 2010) impeding mechanisms such as genetic rescue, inbreeding avoidance, colonization of unoccupied habitat and adaptation to climate change (Clobert et al. 2012). The corridor is a widely used tool to reduce patch isolation by connecting habitats together to increase and maintain landscape connectivity (Beier and Noss 1998).

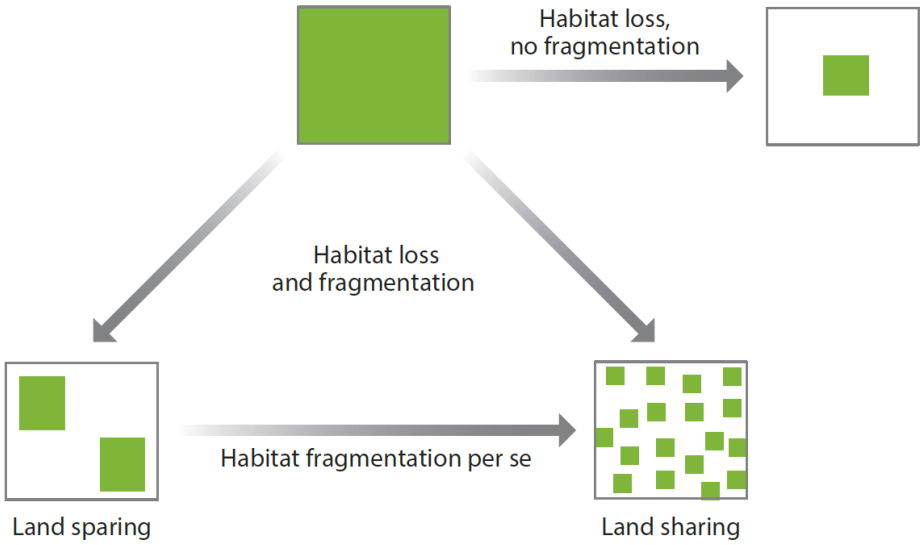

Figure 1-1. Illustration of habitat loss and habitat fragmentation concepts in Fahrig (2017). Higher fragmentation results in higher number of smaller patches with less distance between them. Land-sharing will usually result in a higher ecological value than land-sparing. Habitat fragmentation per se = habitat fragmentation independent of habitat amount.

Originally, corridors were designated as linear elements that facilitate the movement of species (Spellerberg and Gaywood 1993). On the contrary, barriers impede movement. More recently, Dennis et al. (2013) define a corridor "as any structure, distinct from neighboring ones, that facilitates relatively more transfers per unit area and unit time between contributing habitat units than predicted from the surrounding matrix". The landscape consists of features that promote or discourage species movements within it. For example, hedgerows are considered corridors for diverse forest herb communities (Roy and de Blois 2008) and forest carabid beetles (Petit 1994) while transports infrastructure and urban areas are barriers for brown bears (Gastón et al. 2017). However, corridors and barriers vary considerably in terms of structure (vegetation, management, topography), composition, energy flow (moisture, heat, light, wind), resources and landscape context, resulting in very heterogeneous functions for one population, species or individual (Dennis et al. 2013). Indeed, a corridor more or less facilitates movement depending on the resistance of surrounding landscape matrix. A landscape feature may be a corridor or a barrier, depending on the direction of dispersal flow of a species. For example, roads are barriers if considered perpendicular flows, whereas roads verges can be corridors considered longitudinally (Villemey et al. 2018). Also, the orientation of a landscape feature and its landscape context modify energy flows affecting certain species. For example, flying insect species benefit from the microclimate provided by the hedgerows by accumulating near hedgerows in windy weather (Lewis 1969). Finally, the functions of corridors vary over time with mowing of grassland for butterfly (Aviron et al. 2007) or tree canopy closure in hedgerows for European badger (Dondina et al. 2016). The diversity of organisms also

contributes to the complexity of corridor functions (Dennis et al. 2013). A landscape feature can be a corridor for one species and a barrier for another. For example, hedgerows are barriers for the butterflies *Lysandra bellargus* (Thomas 1983) and corridors for forest carabid beetles (Petit 1994). Corridors can be at the kilometer scale for mammals (Kautz et al. 2006) or at the meter scale for butterflies (Delattre et al. 2010). Also, individuals within the same species may react differently to the same landscape feature because they are all different (i.e. speed of movement, physical capacity and life span) (Dennis et al. 2013). All these reasons make it irrelevant to establish a standard list of barriers and corridors.

Ecological continuities are composed of habitats (core area), corridors varying in structure and function (landscape corridor, linear corridor, stepping zone corridor), and a buffer zone that protect the continuities and are mainly transition zones between the continuities and the surrounding matrix (Bennett 2004).

.

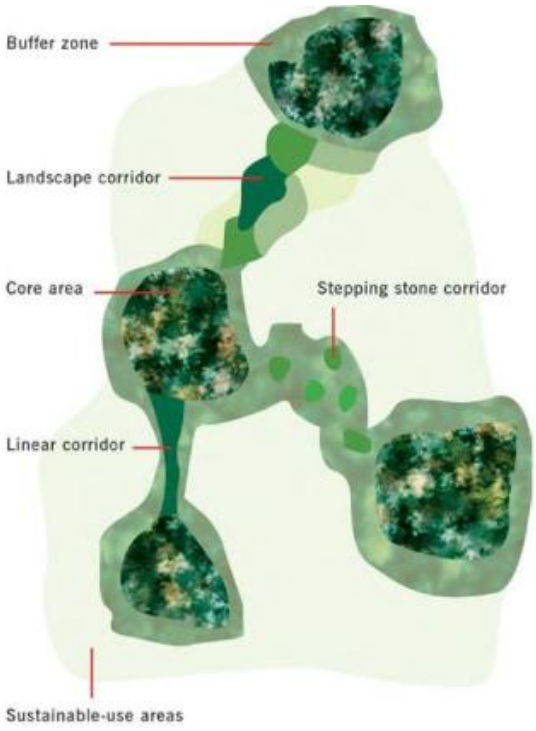

Figure 1-2. Elements composing an ecological continuity. Source: Bennett 2004.

Although most studies demonstrate the effectiveness of corridors for the movement of species and the conservation of biodiversity (Resasco 2019), some studies highlight their potential adverse effects (Simberloff et al. 1992; Haddad et al. 2014). Simberldorff and Cox (1987) and Sinberloff et al. (1992) first noted that corridors could have five negative effects: (1) increase dispersal of species antagonistic to conservation targets, (2) create edge, (3) increase dispersal of exotic species, (4) facilitate spread of disturbances and (5) synchronize population dynamics (Figure 1-3). However, Hadad et al. (2014), who reviewed 46 studies on these five corridor effects, found no evidence that corridors are systematically detrimental in a way that overcomes their established benefits and advised further research to clarify their potential negative effects. No evidence was found implicating corridors in the spread of invasive species or the facilitation of disasters such as fire spread (Haddad et al. 2014). However, corridors may introduce predatory species that threaten the species to be

conserved, such as seed predators, plant parasites and protozoa in microcosms. Therefore, consideration of food webs in corridor design is necessary (Haddad et al. 2014). Edges can increase predation by migratory birds (nestlings) and fish and be traps for species that prefer edges. This problem could be addressed by creating wider corridors or less contrast between corridors and the surrounding matrix. The synchronization of population dynamics can lead to an increase in likelihood of simultaneous extinction, but this effect is unlikely for slow-growing, poorly dispersed species that are often conservation targets.

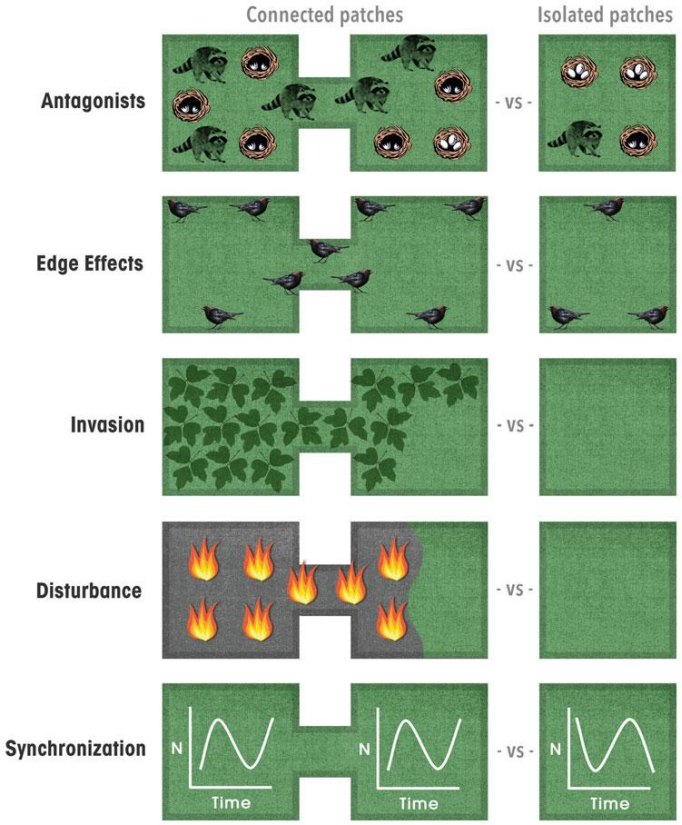

Figure 1-3. The five potential negative effects of corridors reported by Simberloff et al. (1992) illustrated by Neil McCoy in Haddad et al., 2014.

Ecological continuities, as ecosystems, provide benefits to human populations, i.e. ecosystem services. In all environments, they provide habitats for many species and have recreational and cultural values (Bolund and Hunhammar 1999; Baudry et al. 2000; Krieger 2001; Duru et al. 2015). In crop-dominated landscapes, services can be delivered through landscape structure and the biodiversity resulting from ecological continuities (Baudry et al. 2000; Duru et al. 2015). Semi-natural habitats such as hedgerows and grasslands are habitats for arthropods that provide pollination and natural pest control services. Hedgerows provide a large set of services: protection against soil erosion, water drainage, windbreak, carbon storage, wood production (Baudry et al. 2000). In wooded landscapes, natural forests contribute significantly to human well-being and health. These ecosystems regulate the climate, improve air quality by trapping carbon and airborne particular matter, product food and raw materials (timber, fodder, medicines products etc.) and purify water with soil filtration (Krieger 2001). In cities, vegetation zones (parks, urban forests, street trees, wetlands) and water surfaces (lakes and rivers) contribute to improve air quality, regulate the microclimate, reduce noise, improve water flows and purify waste water (Bolund and Hunhammar 1999).

1.3. Ecological continuities in wooded landscapes

Forests are essential for biodiversity conservation as they support 65% of terrestrial taxa (World Commission on Forests and Sustainable Development, 1999) and have the highest diversity for many species such as birds and invertebrates (Lindenmayer et al. 2006). In wooded landscapes, the main threats to biodiversity are deforestation and forest degradation. Deforestation is mainly caused by logging and the expansion of crops and pastures (Angelsen and Kaimowitz 1999; Kaplan et al. 2009) leading to habitat loss. Forest degradation is a vaguer process than deforestation, which is simply the removal of a forested area. Degradation is a loss or reduction of functions or services (e.g. carbon storage, water quality, wood resources, biodiversity conservation) that can take multiple paths in time and space (Putz and Redford 2010; Ghazoul et al. 2015). Ghazoul et al. (2015) emphasized the fact that forests are resilient, therefore, a forest is not degraded if the dynamics allowing it to return to its former state are conserved. The main causes of tropical forest degradation are unsustainable logging, intensive hunting and low-intensity slow-moving undergrowth fires (Putz and Redford 2010). Primary forests are defined as mature forests that have been little or not exploited (Margono et al. 2014), while secondary forests are forests that were developed as a result of deforestation, e.g. through abandonment of crops or pastures (Vidal et al. 2016). Primary forests are reservoirs of biodiversity, e.g. in the Brazilian Amazon, which have many more native species (25%) compared to secondary forests (8%) or plantations (11%) (Barlow et al. 2007). However, secondary forests and plantations have an important role to play in biodiversity conservation as they provide habitat for forest species, ensure the persistence of some primary forest species (Barlow et al. 2007) and can increase landscape connectivity (Lindenmayer et al. 2006).

While large forest patches are considered one of the most effective elements for biodiversity conservation in wooded landscapes (Lindenmayer et al. 2006; Vidal et al. 2016), studies showed that species respond differently to the size patches. Hoover et al. (1995) showed that wood thrushes in Pennsylvania are more abundant in large habitat patches (72%) than small ones (43%) due to a lower predation rate. In Finland, Suorsa et al. (2004) found that fat and protein storage by treecreeper chicks was higher in larger habitats. In contrast, Jokimäki et al. (1998) found lower numbers of flying arthropods, small arthropods, and seven different arthropod taxa in large patches compared to small ones in a pine forest in Finland due to the presence of saplings, deciduous shrubs, and spruces, and a well-developed and diverse understory in small forest patches. Forest structure maters, sometime more that size. Foaublomme et al. (2008) found that forest carabid beetles were more abundant in large forest patches along an urbanization gradient in Belgium. Finally, Norris et al. (2010) found that armadillos were in large patches at night and small patches when searching for food during the day. Regarding large ecological reserves, Lindenmayer et al. (2006) noted that they are relatively free from human disturbance and provide a reference for comparing human impacts in managed forests. Furthermore, they mentioned that many species require large habitats to live, and interactions with humans that are undesirable for some species are limited in large habitats. However, small isolated forest fragments have also an important role to play in biodiversity conservation (Lindenmayer et al. 2006; Vidal et al. 2016). They provide habitats for some species with little or no presence in large forest patches (Lindenmayer et al. 2006) and may contain high levels of biodiversity (Vidal et al. 2016). They also act as "stepping stones" and thus increase the connectivity of wooded

landscapes. Small isolated forest fragments may have a role in supporting biodiversity in highly modified wooded landscapes such as intensive agricultural matrices (Vidal et al. 2016). Given that small fragments constitute a significant part of forest habitats, e.g. 80% of the forest cover in the Brazilian Atlantic Forest (Ribeiro et al. 2009), their consideration is essential for biodiversity conservation. Tree planting, seed collection for nurseries and the creation of corridors between forest fragments are examples of tools to improve the habitat quality of small fragments and landscape connectivity in wooded landscapes (Lindenmayer et al. 2006; Vidal et al. 2016).

1.4. Ecological continuities in crop-dominated landscapes

In crop-dominated landscapes, semi-natural elements such as grasslands and woodlands (hedgerows and forests) are key elements of ecological continuities. Burel et al. (2013) showed that the abundance of diptera decrease with the decrease of semi-natural elements. Avignon et al. (2005) showed that large forest carabid beetles are found in landscapes with a high proportion of semi-natural elements whereas small winged species prefer a high proportion of cultivated land. Originally, crop-dominated landscapes were described as a set of semi-natural elements within a neutral agricultural matrix by landscape ecologists (Burel et al. 2013). However, many species perceive the landscape in a more complex way than a set of habitats containing all the necessary resources within a hostile matrix (Fahrig et al. 2011). While farming practices (e.g. pesticides, fertilizers, herbicides, intensive grazing, etc) resulting from intensive systems have shown negative effects on biodiversity (de Snoo and van der Poll 1999; Desneux et al. 2007), heterogeneous crop-dominated landscapes with semi-natural elements have a high potential for biodiversity (Tscharntke et al. 2005; Billeter et al. 2008; Fahrig et al. 2011). Some arthropod (Vasseur et al. 2013) , bird (Freemark and Kirk 2001), mammal (Delattre et al. 1999) and weed (Petit et al. 2011) species use crops (including grasslands) during their life cycle. At the same time, biodiversity provides benefits to farmers, for example, pollination by insects or crop pest control by birds.

The value of crop-dominated landscapes lies in particular in their high potential heterogeneity, a key element for biodiversity (Burel and Baudry 2003). While functional landscape connectivity is important for species movement, heterogeneity is equally important for the dynamics of resource patches (Schooley and Branch 2011). In crop-dominated landscapes, the diversity of crop types induces spatial heterogeneity. Spatial heterogeneity increases with the increase of different cover types and the complexity of their configuration (Figure 1-4). It is beneficial for species because it brings different types of resources and is essential for species that use different types of habitats during their life.

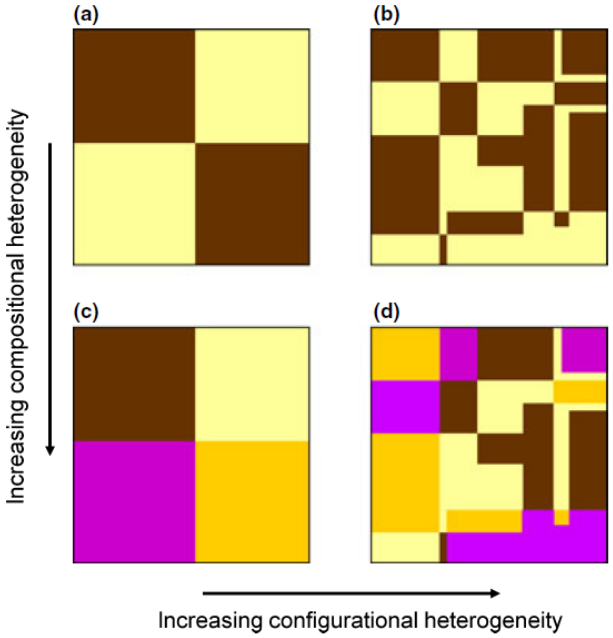

Figure 1-4.Illustration of spatial heterogeneity and its two components: compositional heterogeneity and configurational heterogeneity. Source: (Fahrig et al. 2011)

Farming practices, crop rotation and crop phenology induce additional temporal heterogeneity to which species respond (Vasseur et al. 2013). Several studies have demonstrated the influence of past landscape structure on current ecological processes and a lag in the response of organisms to landscape change (Burel et al. 1998; Ernoult et al. 2006; Krauss et al. 2010). Fahrig (1992) has shown that in dynamic landscapes, habitat turnover and associated landscape structure change can be more important than the spatial organization of resource patches for species survival. For example, intensive mowing of grasslands decreases butterfly movement between habitats because it reduces the quality of resources (vegetation height, available nectar), and early mowing (before the butterflies activate their wings) prevents their full development (Aviron et al. 2007). Conversely, late mowing is beneficial for butterflies as it ensures continuous nectar resources and grasslands provide shelter and food for larvae to develop (Feber and Smith 1995). The phenology of maize and peas affects the movements of the agricultural carabid beetle *Pterostichus melanarius* due to its preference for crops with dense canopy cover (Vasseur 2012). Indeed, in early summer in Brittany, maize crops have bare soil and pea crops have dense vegetation, thus *Pterostichus melanarius* move from maize to peas. At the end of July, the opposite movement occurs because the maize has grown and the peas have been harvested. Also, Fitzgibbon et al. (1997) and Ouin et al. (2000) found that landscape connectivity increases for small forest mammals when crops are grown high and dense. Corridors may therefore temporarily appear within crop-dominated landscapes.

In a context of increasing demand for food coupled with the extinction of biodiversity, understanding the role of crops as ecological continuities and their consideration for biodiversity conservation is essential.

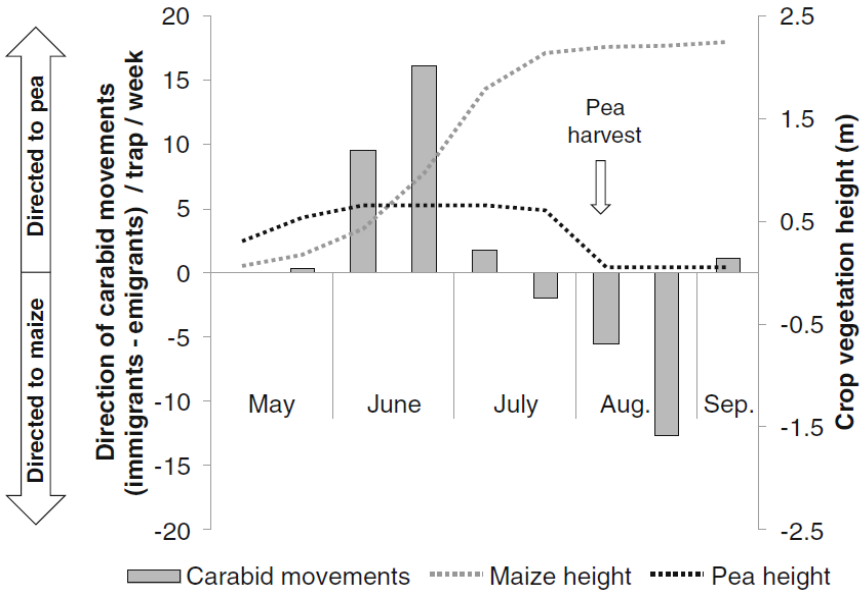

Figure 1-5. Carabid movements between maize and pea fields, and crop vegetation height from May to September. Source: Burel et al. 2013

1.5. Ecological continuities and public policies

Since 1972, the United Nations (UN) has been organizing Earth Summits inviting member states (132 members in 1972, 193 in 2020) in order to establish the main thrusts of an international environmental policy. The integration of biodiversity conservation into public policies first appeared at the first Earth Summit (1972) with the creation of the United Nations Environment Program (UNEP). This organization aims to coordinate the environmental actions of member states and to assist countries in implementing environmental policies. It introduced the notion of sustainable development with the Brundltand Report in 1987 and created, in association with the World Meteorological Organization (a United Nations institution), the Intergovernmental Panel on Climate Change (IPCC) in 1988. This expert group is an organization including the member states and aims to analyze and synthesize international research on human impacts on climate. In 1992, the 3rd Earth Summit in Rio de Janeiro led to the creation of the Convention on Biological Diversity, which aims at the conservation of biodiversity, the sustainable use of biological diversity and the fair and equitable sharing of the benefits arising from the use of genetic resources. Finally, the importance of ecological networks was recognized in 2002 at the 4th Summit in Johannesburg. The UN therefore encourages initiatives in favour of areas of biological richness and other areas essential for biodiversity and the realization of ecological networks at national and regional level.

Heavy pressure has been exerted on Brazil since the Earth Summit in Rio to conserve forests. The State has implemented numerous environmental measures such as the Satellite Project to Monitor Deforestation in Legal Amazonia (PRODES) in 1988, the creation of the Brazilian Institute of Environment and Renewable Natural Resources (IBAMA) in 1989, the Action Plan for the Prevention and Control of Deforestation in the Legal Amazon (PPCDAm) in 2004, the "Black list" published by the Brazilian Ministry of Environment in 2007 (subject municipalities with the highest deforestation to restrictions such as access to agricultural credits) and the National Policy for the Restoration for Native Vegetation Recovery

(PROVEG) in 2017. For example, the municipality of Paragominas (Pará) was included in the black list in 2007. From 1980, wood production, beef exploitation, then charcoal production and finally the expansion of crops (rice, corn, soybeans) in the early 2000s led to massive deforestation. In order to comply with the legislation, the "município verde" (green municipality) was created in 2008. The aim of this action plan was to fight against deforestation by stopping deforestation, monthly monitoring of forest cover, training of personnel for environmental control and management, environmental education, establishment of a land registry of farms, encouraging the reforestation of degraded soils and the adoption of good agricultural, livestock and forestry practices. The municipal authorities of Paragominas and large private producers signed a territorial pact that includes these objectives and are supported by environmental NGOs and funds from companies operating in the region. Deforestation has thus been reduced by 80% between 2007 and 2010 and the municipality was taken off the blacklist in 2010. At present, the priorities are the fight against fires, the fostering of family farming, carbon storage, education in rural areas and the reconstruction of forest continuity and efficient landscapes (Piketty et al. 2015, 2017; Laurent et al. 2017).

In Europe, environmental issues have initially been linked to the simple economic framework since the creation of the European Economic Community in 1957. Then in the 1970s, several environmental disasters (pollution of the Rhine in 1969, accidental release of dioxins at Seveso in 1976, oil spill following the sinking of the Amoco Cadiz in 1978) and the gradual rise of environmental issues on the international scene (first Earth Summit in 1972) led the member countries to launch a European environmental policy in Paris in 1972 (Bertrand and Fournier 2009). From 1973 onwards, Environment Action Programmes have been regularly adopted. More specifically about ecological continuities, these programmes led to the creation of the Natura 2000 network. In 1995, the Pan-European Biological and Landscape Diversity Strategy launched by the European Environment Ministers aims to establish ecological continuities at the regional and national scales and a pan-European ecological network. In 2011, the European Union aimed to halt the loss of biodiversity by 2020 by adopting a biodiversity strategy. This aim has not been reached, and the dead line was postponed to 2030. One of the objectives is the preservation of ecosystems and their services with the establishment of a green infrastructure and the restoration of at least 15% of degraded ecosystems. The European commission defined green infrastructure as “a strategically planned network of natural and semi-natural areas with other environmental features designed and managed to deliver a wide range of ecosystem services such as water purification, air quality, space for recreation and climate mitigation and adaptation” (https://ec.europa.eu/environment/). More specifically, the green infrastructure strategy is based on four elements: (1) promoting green infrastructure in key European policy areas, (2) supporting green infrastructure projects at the European level, (3) improving access to finance for green infrastructure projects, and (4) improving information and promoting innovation (https://ec.europa.eu). The Review of progress on implementation of the EU green infrastructure strategy published in May 2019 indicates that 179.6 million euros have been invested to support green infrastructure projects; it also highlights the difficulty of deploying infrastructures at transnational scale (https://eur-lex.europa.eu/homepage.html, COM(2019) 236 final).

In France, ecological continuities were integrated into public policies under the impetus of the Ministry of Ecology with the Grenelle I and II laws adopted in 2009 and 2010, respectively. The policy called "Trame Verte et Bleue" (green and blue network) came from these laws. French administrative regions have to identify ecological continuities in order to improve and maintain them. Ecological continuities are implemented at the local level by integrating them into urban planning documents (local urban planning plans and territorial coherence schemes) and at the regional level with the Regional Ecological Coherence Schemes (SRCE). The SRCEs are elaborated by each region and include documents aimed at identifying and preserving ecological continuities, such as a diagnosis of the territory related to biodiversity, an action plan, maps of ecological continuities and a summary for public actors. At the national level, the State has elaborated a framework document named "National Guidelines for the Preservation and Restoration of Ecological Continuities". In 2017, a national map was produced for illustrative purpose by merging the SRCEs maps (Figure 1-6).

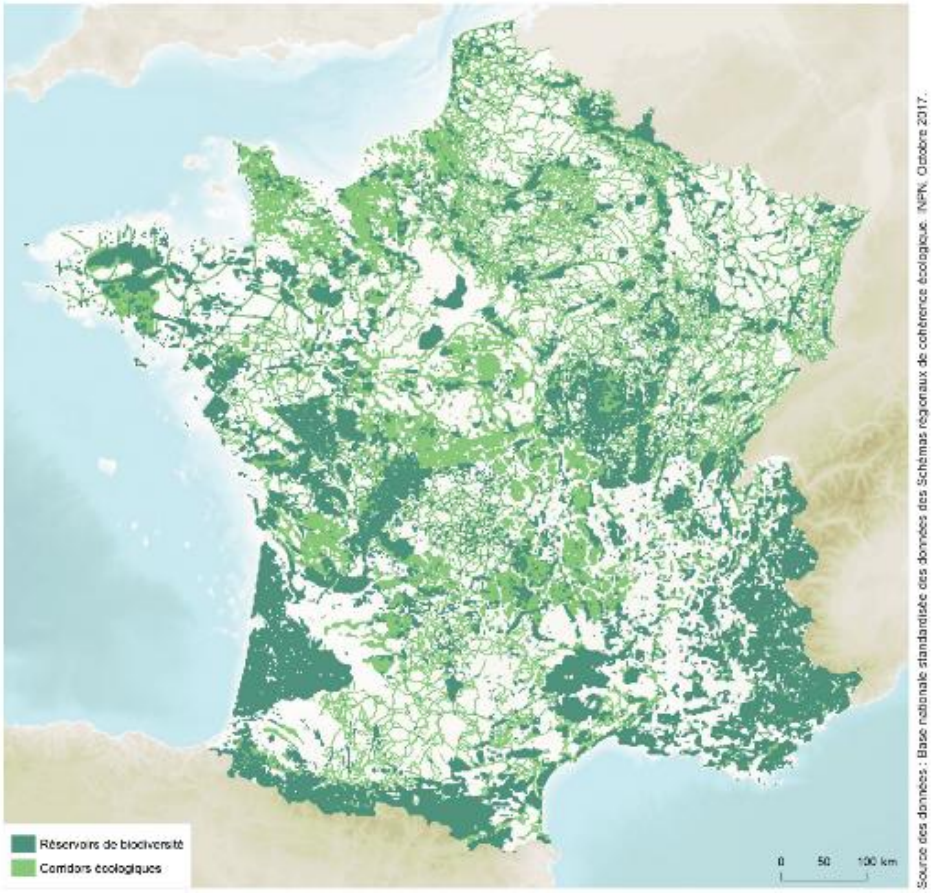

Figure 1-6. National synthesis of regional “trames vertes”. This map shows the ecological continuities identified within the framework of regional ecological coherence schemes (SRCE) in metropolitan France.. “Réservoirs de biodiversité” = Biodiversity reservoirs. “Corridors écologiques” = Ecological corridors. Source: https://inpn.mnhn.fr/

In Belgium, protection of biodiversity began in 1973 with the law on nature conservation. This law provides several tools to protect natural areas such as protected areas, species and biotope protection. In 1993, the Wallon region launched a program of Inventory of Sites of Great Biological Interest (SGIB) to identify remarkable natural terrestrial or aquatic areas. Six years later, the regional development plan (SDER) was defined in the Walloon code of territorial development, urban planning and heritage. This document consists of an

analysis of the territory and a strategy for future planning. Among the objectives of this document is the protection and development of the natural heritage with the implementation of an ecological network. It indicates the reinforcement of protection of Natura 2000 sites. In addition, it is planned that Sites of Great Biological Interest (SGIB) will be identified on public land with the help of scientific inventories coordinated by the Department of Natural and Agricultural Environment Studies in order to be integrated into the Natura 2000 network. The areas classified as "green spaces" and "parks" are intended to be integrated into the ecological network. Finally, the use of linear infrastructures (bicycle and pedestrian paths and roads) is encouraged for the constitution of ecological continuities. The set of ecological continuities is called Main Ecological Structure (SEP) and is composed of central areas where nature protection is a priority and development areas where protection is less and human activities are in accordance with biodiversity conservation. These areas can be habitats, corridors or buffer zones protecting the continuities. In 2014, Wallonia abandoned the protection of the SGIBs not yet protected with the project of a new regional development plan (SDER) called Territorial Development Code (CoDT). In the same year, several researchers called on the Walloon government to reiterate this objective. The Territorial Development Code (CoDT), that became effective in 2017, stipulates that only sites recognized by the law on nature conservation (1973) must be taken into account in land use planning. The text provides for the identification of a "trame verte et bleue" (green and blue network) at the communal level with an indicative value (Born et al. 2014). A map of ecological continuities (Figure 1-7) was adopted by the Walloon government in 2019 and included in the territorial development plan (SDT) (tool defined by the CoDT). This map lists five types of continuities: deciduous forest massifs, limestone grasslands and associated environments, Ardennes ridges, high Ardennes valleys and alluvial plains (http://lampspw.wallonie.be/dgo4/site_amenagement).

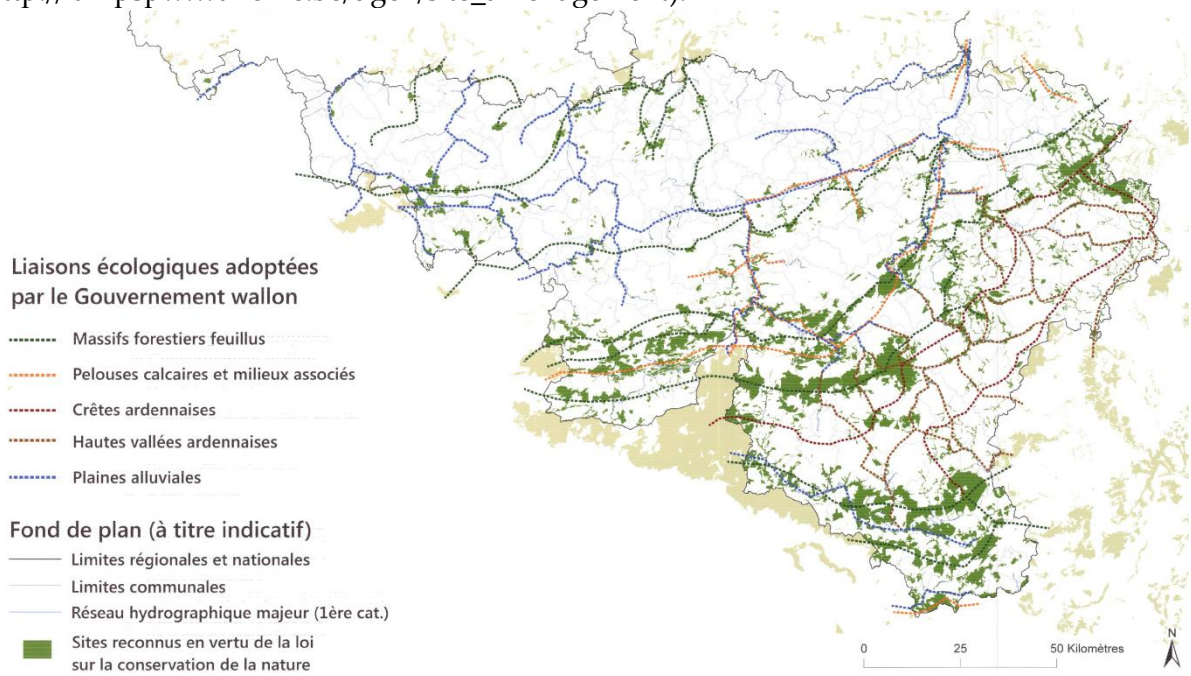

Figure 1-7. Ecological continuities adopted by the Walloon government. Massifs forestiers feuillus = deciduous forest massifs. Pelouses calcaires et milieux associés = limestone grasslands and associated environments. Crêtes ardennaises = Ardennes ridges. Hautes vallées ardennaises = high Ardennes valleys. Plaines alluviales = alluvial plains. Source: http://environnement.wallonie.be/legis/consnat/cons070.htm

In Spain, the Natural Heritage and Biodiversity Act of 2007 defines three types of protected areas: (1) protected natural areas, (2) protected areas Red Natura 2000 and (3) areas protected by international instruments. The Ministry of Agriculture, Food and Environment is responsible for protected areas in marine areas under national sovereignty or jurisdiction. The Autonomous Communities are responsible for protected areas in the terrestrial and marine space within their territories. The first type of protected areas named "natural protected areas" includes land or sea areas that meet one of the two following constraints: (1) contain natural systems or elements that are representative, unique, fragile, threatened or of special ecological, scientific, landscape, geological or educational interest or (2) be specially dedicated to the protection and maintenance of biological diversity, geodiversity and associated natural and cultural resources. At the state level, these areas are classified into five categories (Parks, Nature Reserves, Protected Marine Areas, Natural Monuments and Protected Landscapes), while autonomous communities use more than forty different designations. Examples of areas protected by international instruments in Spain are Wetlands of International Importance under the Ramsar Convention, Protected Areas under the Convention for the Protection of the Marine Environment of the North-East Atlantic (OSPAR), Biosphere Reserves declared by UNESCO, and Biogenetic Reserves of the Council of Europe. A national register listing the various protected areas is being prepared as a result of the 2007 law (https://www.miteco.gob.es/). Ecological corridors between Natura 2000 areas were identified by a team of researchers from the ETSI of Forestry and Environment of the Polytechnic University of Madrid (UPM) in collaboration with the WWF (De la Fuente et al. 2018). Figure 1-8 shows the map of the ecological continuities to be conserved and restored (De la Fuente et al. 2018).

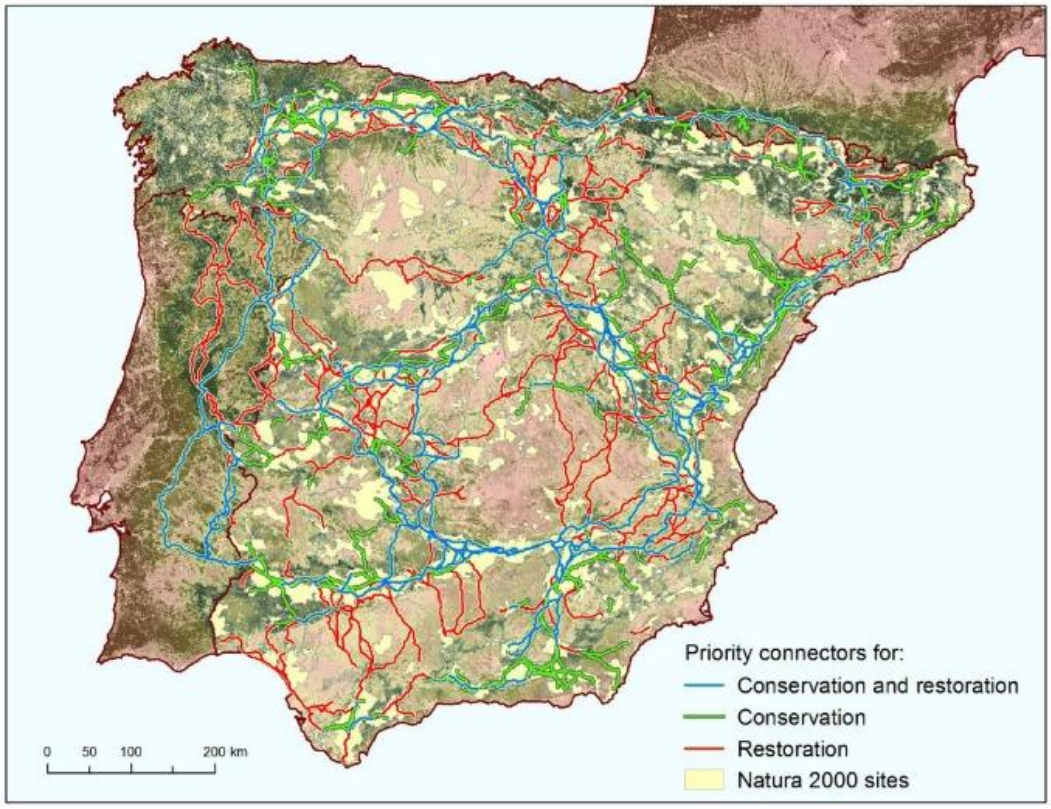

Figure 1-8. Priority connectors for conservation and restoration for the network of Natura 2000 woodland sites in mainland Spain. Source: De la fuente et al. (2018)

CHAPTER 2

The use of remote sensing imagery for the identification and characterization of ecological continuities

Contents

2.1. Introduction

This chapter aims to present the use of remote sensing data to identify and characterize ecological continuities. First, the basics of optical and SAR remote sensing are explained for a good understanding of this these. The following section provides an overview of research using optical and SAR remote sensing data for the identification and characterization of ecological characteristics from wooded to crop-dominated landscapes, with particular emphasis on Sentinel-1 and 2 images. Finally, examples of applications are described to illustrate how ecological continuities functions are evaluated using remote sensing data.

2.2. Basics of remote sensing

Remote sensing refers to the set of techniques allowing the acquisition of information on the Earth's surface without physical contact with it. The information measured by the sensors is derived from the electromagnetic radiation reflected by the objects. The visible domain, from 380 to 780 nm, is only a small part of the spectrum exploited in remote sensing; radiations in the infrared (near-infrared (NIR), short-wavelength infrared (SWIR), thermal infrared) and microwaves are also commonly used (

Figure 2-). Passive sensors record radiations emitted by an external source, either solar or thermal radiations emitted from the Earth. On the contrary, active sensors emit radiations and record their returns. These types of sensors emit microwaves in the case of SAR sensor and optical laser pulses in the case of Light Detection And Ranging (LiDAR) sensor. Radiations are absorbed, transmitted and reflected differently depending on the materials encountered and the part reflected to the atmosphere is registered by airborne, UAV or spaceborne sensors.

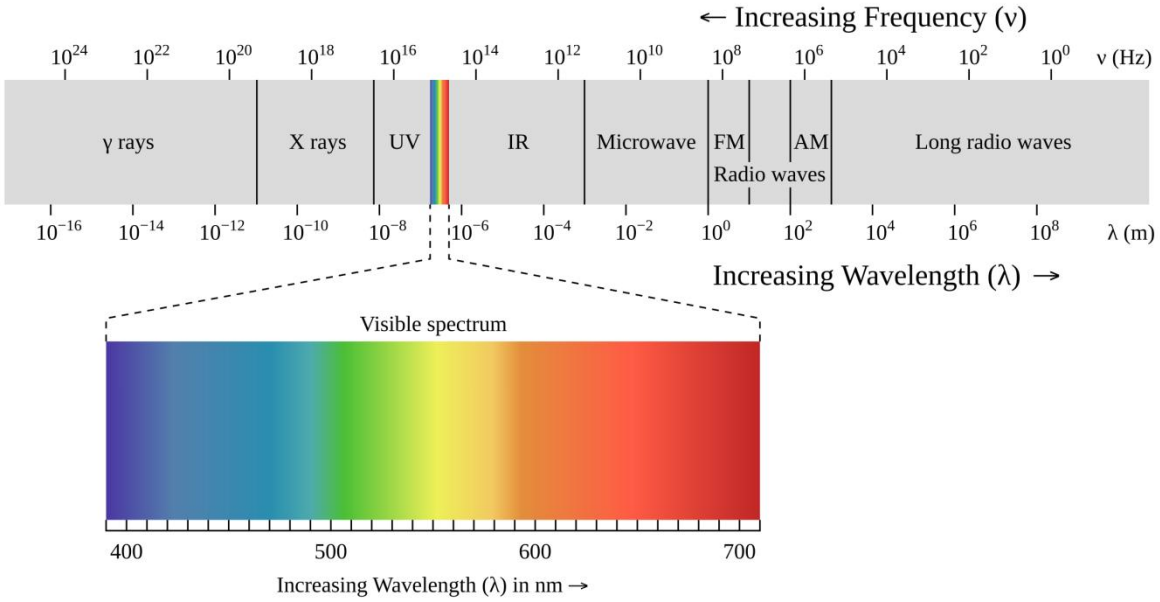

Figure 2-1. Electromagnetic spectrum and related fields, By Philip Ronan, file licensed under the Creative Commons Attribution-Share Alike 3.0 Unported license.

In the case of optical or SAR imagery, the signals received by the sensors are synthetized into raster images where each pixel corresponds to a digital count of reflectance. The swath corresponds to the area scanned by the antenna beam. Spatial resolution is defined by the size of the smallest element that can be detected (Figure 2-2). Spectral resolution is the ability

of a sensor to distinguish different electromagnetic wavelengths in the spectrum. The higher the spectral resolution, the more parts of the spectrum the sensor records and the more detailed the spectral signature of an object is. Parts of the electromagnetic spectrum are called spectral bands and their widths vary from sensor to sensor. Temporal resolution corresponds to the revisit time of the sensor to monitor the same area. The selection of the sensor depends on the objectives of the study, the size of the study area, the available funding, the available land data etc. Note that generally the higher the spatial resolution (fine pixel), the lower the temporal resolution (long revisit time) and vice versa (Wegmann et al. 2016).

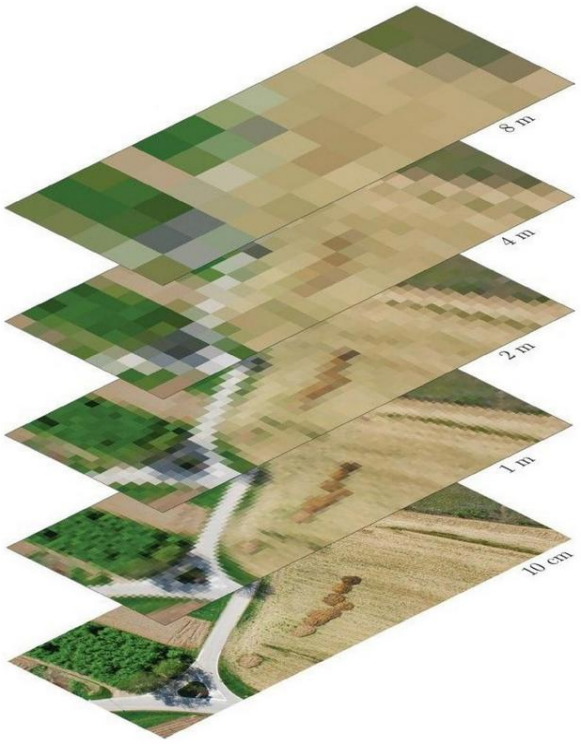

Figure 2-2. Different spatial resolutions (10cm - 8m) for the same landscape. Source: Wegmann et al. 2016.

2.2.1. Passive optical remote sensing

2.2.1.1. Basics

Optical images are widely used to map land cover types and monitor vegetation. Optical sensors cover the visible and infrared spectrum, including NIR, SWIR and thermal infrared, with varying spectral resolutions. Panchromatic sensors have the lowest spectral resolution, consisting of a single wide band ranging from blue to red wavelengths. Multispectral sensors (eg. SPOT, QuickBird, ASTER and S-2) have from three to twenty large bands while hyperspectral sensors (eg. CASI, AVIRIS and HySpex) can record several tens to hundreds of fine bands. Concerning the interactions of visible spectrum wavelengths with vegetation, chlorophyll absorbs blue and red wavelengths and reflects a higher proportion of green. Green vegetation strongly reflects NIR wavelengths due to its cellular structure and water in the leaves absorbs SWIR wavelengths near 1450 and 1900 nm (Figure 2-3). The interactions between vegetation and optical wavelengths are determined by vegetation chlorophyll content, cellular structure and WC. Hence, optical remote sensing images allow identifying

plant species, phenological stages or estimate water stress. However, optical wavelengths are reflected from the first layer of the canopy and signal saturation is observed when the leaf surface is high. Moreover, the acquisition of optical images is dependent on cloud cover and their exploitation requires atmospheric corrections due to the sensibility of short wavelengths to water vapor and clouds. These corrections are necessary when different dates or images are compared.

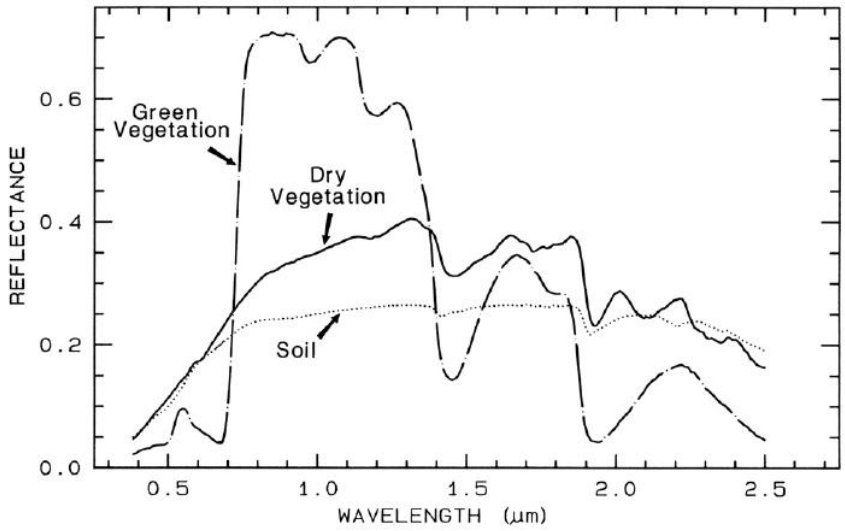

Figure 2-3. Spectral signatures of dry and green vegetation. Source: Clark 1999.

2.2.1.2. Vegetation indices and biophysical variables

Many indices have been developed by combining the spectral bands of optical sensors. The best known is the NDVI (Rouse et al. 1973). This index exploits the red and NIR bands to determine the chlorophyll content of the vegetation. The Normalized Difference Water Index (NDWI) including NIR bands and SWIR (Gao 1996) or green (McFeeters 1996) bands is commonly used to detect hydric stress. Other vegetation indices take into account effect of soil such as the Soil-adjusted Vegetation Index (SAVI) (Huete 1988) and the Modified SAVI (MSAVI) (Qi et al. 1994, p. 199) or the combined effects of soil and atmosphere such as the Enhanced Vegetation Index (EVI) (Huete et al. 1999). Some of them indices were specifically developed from a sensor such as the EVI from MODIS or the S-2 Red-Edge Position (S2REP) index from S-2.

Biophysical variables are commonly used to study the structure and functioning of vegetation and estimate the water and carbon balances of surfaces. The LAI, the Fraction of Absorbed Photosynthetically Active Radiation (FAPAR) by green vegetation and the fraction of green vegetation cover (fCover) are the most commonly used to study vegetation. The LAI is defined as the total area developed by green leaves per m² on the ground. The FAPAR is the fraction of solar radiation absorbed by plants for photosynthetic activity. Finally, the fCover is the fraction of the soil surface covered by vegetation observed at nadir. These biophysical variables can be measured in the field, directly with samples or indirectly using digital hemispherical photography, LAI sensors such as the LAI-2000 PCA or TRAC (Claverie 2012), terrestrial scanning LIDARs. Optical satellite images are widely used to estimate biophysical variables, using radiative transfer models that simulate the processes of radiative transfer in the soil-vegetation system. The PROSPECT-PROSAIL model is one of the best known and is notably integrated in the S-2 data processing chains in order to map

biophysical variables (Jacquemoud et al. 2009). Relationships between biophysical variables and spectral bands or indices such as NDVI can then also be explored in time over large areas.

2.2.2. Active SAR remote sensing

2.2.2.1. Basics

SAR sensors operate in the microwave region of the electromagnetic spectrum, from 0.75 to 100 cm, between Ka-band and P-band (Table 2-1). The signal penetration capacity increases with the wavelength, the signal being sensitive to objects of at least the same size (Figure 2-4). Concerning the satellite sensors, the bands used are X-band (e.g., TerraSAR-X), C-band (e.g., S-1 and RADARSAT) and L-band (e.g., ALOS-PALSAR (Phased Array L-band Synthetic Aperture RaDAR and JERS (Japan Earth Resources Satellite)). The other parts of the spectrum are exploited with airborne sensors such as RAMSES and SETHI for the Ka, K, Ku and S bands, and AIRSAR and OrbiSAR for the P band.

Table 2-1. SAR bands and their associated frequencies and wavelengths.

Band	Frequency (GHz)	Wavelength (cm)
P	0.03-3	100-30
L	0.3-1	30-15
S	2-4	15-7.5
C	4-8	7.5-3.75
X	8-12.5	3.75-2.4
Ku	12.5-18	2.4-1.67
K	18-26.5	1.67-1.13
Ka	26.5-40	1.13-0.75

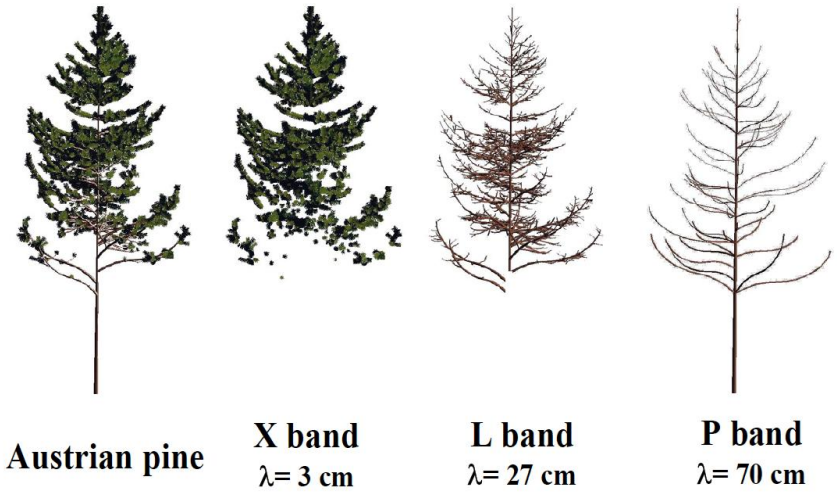

Figure 2-4. Main diffusers of vegetation according to SAR bands. Souce: Le Toan 2007

In contrast to optical sensors, SAR sensors are active, and therefore independent of solar illumination, allowing the acquisition of images day and night. Moreover, SAR signal pass through clouds, fog and rain, which is particularly interesting in areas with heavy cloud cover such as tropical areas (Lee and Pottier 2009).

The SAR imaging system is a side-looking Radio Detection and Ranging (RaDAR) sensor with an antenna that illuminates the scene perpendicular to the flight line direction. The SAR imaging geometry can be briefly described with the following technical terms (Figure 2-5):

- The height and velocity of the SAR imaging system.
- The angle of incidence between the antenna beam direction and the nadir.
- The "slant-range" defined as the RaDAR-line-of-sight, i.e., the antenna beam direction.
- The "ground range" that is perpendicular to the flight line direction.
- The "azimuth range" that is parallel to the flight line direction.

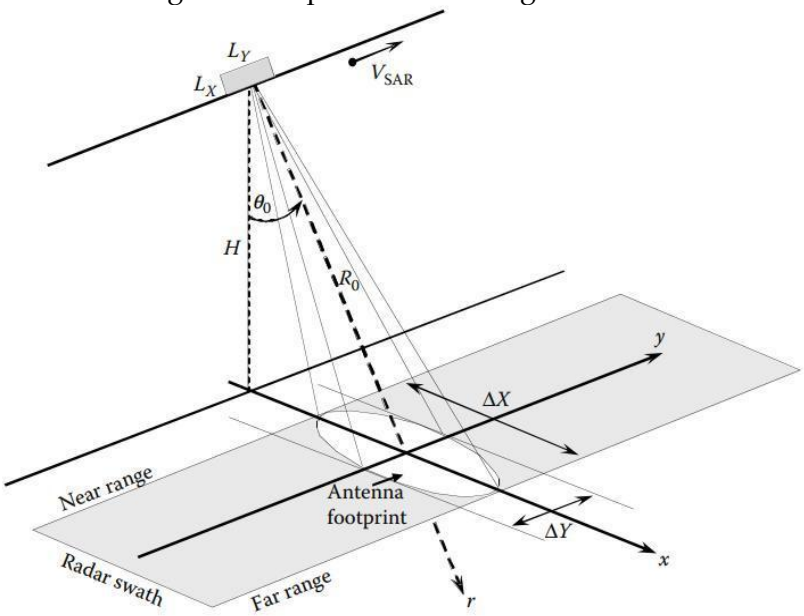

Figure 2-5. SAR imaging geometry in strip-map mode. L_X and L_Y=physical dimensions of the antenna, V_{SAR}=Velocity, H=Height, θ_0=incidence angle, r="slant-range", x="ground range", y="azimuth range", R_0=distance between the sensor and the antenna footprint center, ΔX=range swath, ΔY=azimuth swath. Source: Lee and Pottier 2009

SAR images are subject to geometrical distortions due to their cross-track dimension. The main distortion sources are the "foreshortening" and "layover". In mountainous areas, foreshortening is dominant especially with high angles of incidence. It occurs when the beam reaches the top of a relief before its base, so the relief appears folded on the image and the length of the slope is smaller than in reality. The layover is the opposite phenomenon, when the beam reaches the base of the top before the base of the slope. On the images, the slope appears inverted; the top is in front of the base of the slope. Finally, if the angle of the slope on the reverse of the relief is steeper than the angle of incidence, a RaDAR shadow appears on the image because no signal is returned (Figure 2-6Figure 2-7).

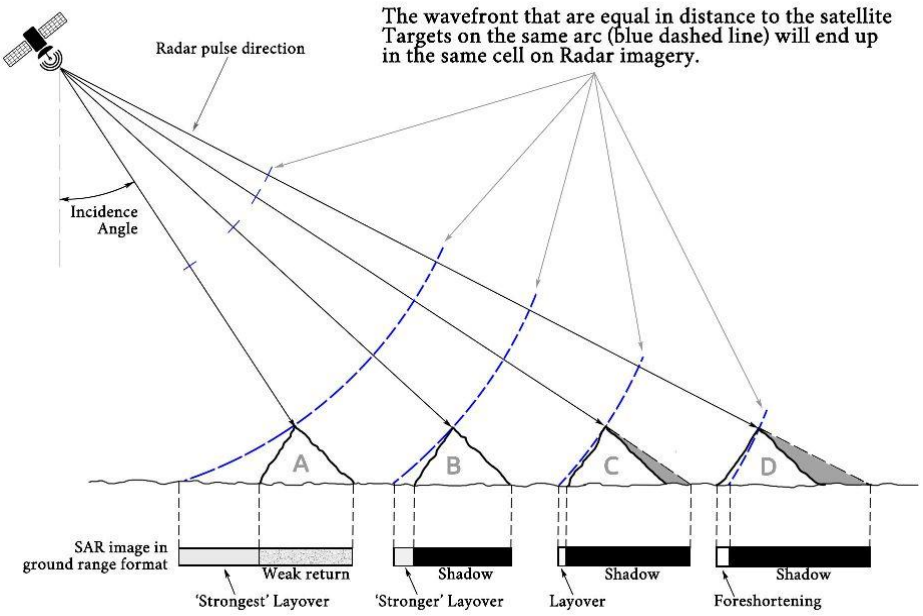

Figure 2-6. Illustration of distortion effects. Source: Lillesand et al. 2015.

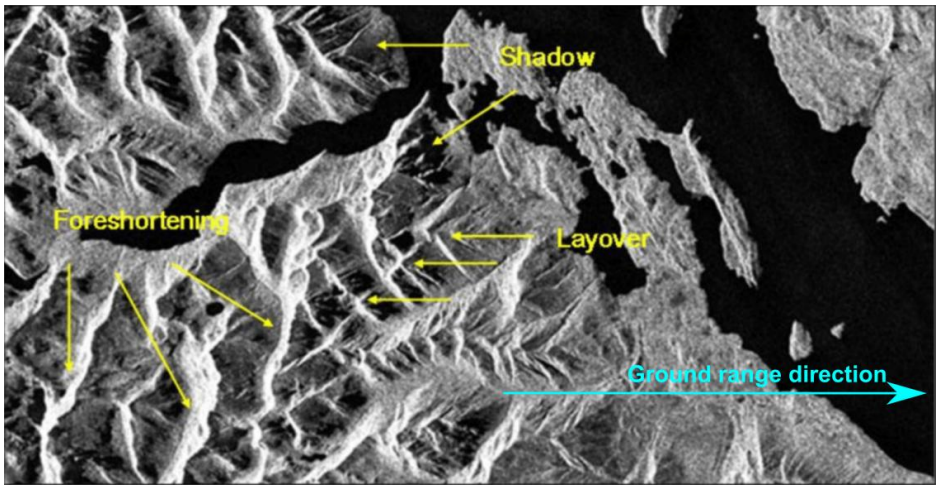

Figure 2-7. Geometric distortions observed in SAR images. Adapted from Toth et al. 2014.

"Each pixel of SAR images provides a complex number, including amplitude and phase information, associated to the reflectivity of all scatterers contained in the SAR resolution cell" (Lee and Pottier 2009). The amplitude is a measure of the signal strength (i.e., the height of the wavelength), the higher the quantity of radiation returning to the sensor, the higher the amplitude. The amplitude depends of surface properties that induces different scattering mechanisms. The phase indicates the instantaneous situation in the cycle of a microwave. Its measurement refers to its starting point or its progression from an arbitrary origin and is expressed in radian or degree. The phase depends on the surface properties and the distance between the sensor and the earth's surface. The resulting images look like noise and cannot be used directly. The surface reflectivity is sensitive to the SAR sensor parameters such as frequency, incidence angle and polarization, and of the surface properties such as topography, roughness, moisture, dielectric properties and incidence angle (Lee and Pottier 2009).

Random variations in gray levels called speckle appear on SAR images. These variations are caused by waves reflected from many scatterers within the same resolution cell. Since these scatterers are at random distances from the sensor, the waves received are not coherent in phase. The received signal is strong if the waves of each disperser add relatively constructively (constructive interference); the signal is weak if the waves are out of phase (destructive interference). This effect complicates the interpretation of SAR images, as well as their segmentation and classification. The SAR image multi-look processing and filtering methods are commonly used to reduce speckle noise. The multi-look processing consists in treating separately "looks", i.e. sub-apertures, then averaging the values of the same target to smooth the speckle. The filtering methods consist in applying sliding windows that compute an algorithm, for example, median, boxcar, lee refined or lee sigma. The spatial resolution of the processed image decreases as the window size increases. Larger windows provide more speckle smoothing, while smaller windows provide better texture preservation (Lee and Pottier 2009).

RaDAR remote sensing yield different types of information such as the SAR signal intensity, the SAR polarimetry or the SAR interferometry (phase difference analysis to measure extremely fine altitudes and small displacements). In this thesis, the intensity and polarimetry were used because of their suitable applications to identify and characterize ecological variables.

2.2.2.1. Intensity

The backscatter coefficient, also called “sigma nought” or σ^0, is a measure of the SAR signal intensity that is proportional to the ratio between the received power and the emitted power. The values of the backscatter coefficients vary according to a set of parameters related to the sensor characteristics (frequency, polarization, incidence angle, etc.) and the target characteristics (geometric structure, surface roughness, dielectric constant, physical properties, etc.). The intensity is measured in natural values (m^2/m^2) with the following equation (Eq. 2.1):

$$\sigma^0 = \frac{4\pi r^2}{A_0} \frac{\langle |\vec{E}_S|^2 \rangle}{|\vec{E}_I|^2} \quad (2.1)$$

Where A_0 is the illuminate area, $\vec{E}_S$ is the power that the target intercepts from the incident wave electric field called scattered field and $\vec{E}_I$ is the power reradiated by the same target in the form of the scattered wave called scattered field.

The backscatter coefficients are converted into decibels (dB m^2/m^2) on a logarithmic basis using the following equation (Eq. 2.2):

$$\sigma^0_{dB} = 10.log10(\sigma^0) \quad (2.2)$$

2.2.2.2. Polarimetry

SAR polarimetry is the study of the polarization state of an electromagnetic wave. Microwaves are polarized, i.e. there is an orientation of the electric field in a plane perpendicular to the wave direction of propagation. SAR systems emit microwaves with horizontal (H) or vertical (V) polarization, and receive the backscattered waves with horizontal or vertical polarization. Thus, four combinations are possible: HH, VV, HV and VH, with the first letter corresponding to transmission and the second to reception. The HH and VV polarizations are so-called parallel or co-polarized, while HV and VH are crossed polarizations. Multi-polarization SAR systems enable the transmission of H or V polarizations and can receive parallel or cross polarizations. Polarimetric SAR systems can transmit and receive in both V and H polarizations and, therefore, provide the four possible combinations. The single, dual and quad polarizations correspond to SAR systems including one, two and four combinations, respectively. More specifically, polarimetry is the study of the modification of the wave polarization during its interaction with a target. The modification of the wave polarization is related to the target properties such as its structure, shape, orientation and physical properties. The depolarization of the backscattered wave (superposition of many waves) can be revealed by several decompositions of the sccattering matrix (Cloude and Pottier, 1996, Freeman and Durden, 1998).

In the case of quad-polarized data, the complex 2 x 2 matrix called coherent scattering matrix, $[S]$, also called Sinclair matrix, transcribes the change in polarization. The $[S]$ matrix consists of four complex numbers calculated from the amplitude and phase of the polarized channels. The diagonal corresponds to the co-polarized channels and the other elements to the cross-polarized channels.

$$\begin{bmatrix} S_{hh} & S_{hv} \\ S_{vh} & S_{vv} \end{bmatrix} \tag{2.3}$$

The span of the matrix $[S]$ is the total power scattered by a target and is calculated with the following equation (Eq. 2.4):

$$span = |S_{hh}|^2 + |S_{hv}|^2 + |S_{vh}|^2 + |S_{vv}|^2 \tag{2.4}$$

When the transmitter and receiver are located at the same location, which is the case for most SAR systems, S_{hv} and S_{vh} are equal, based on the reciprocity assumption. Thus, it is possible to represent the information scattered with the 3-D lexicographic feature vector from the $[S]$ matrix as (Eq. 2.5):

$$k_L = \begin{bmatrix} S_{hh} \\ \sqrt{2}S_{hv} \\ S_{vv} \end{bmatrix} \tag{2.5}$$

Pauli decomposition is used to derive the 3-D Pauli feature vector from the $[S]$ matrix (Eq 2.6).

$$k_p = \frac{1}{\sqrt{2}} \begin{bmatrix} S_{hh} + S_{vv} \\ S_{hh} - S_{vv} \\ 2S_{hv} \end{bmatrix} \tag{2.6}$$

These two target vectors are consistent representations of the $[S]$ matrix and their norm is equal to the span (Eq. 2.4). The 3-D lexicographic feature vector is directly related to the measurable elements of the system. The 3-D Pauli feature vector is closely related to the physical properties of the scatterers and can be interpreted in terms of elementary scattering mechanisms with the single bounce (or surface scattering) corresponding to $S_{hh} + S_{vv}$, the double bounce to $S_{hh} - S_{vv}$ and the volume scattering to $2S_{hv}$ (Figure 2-8).

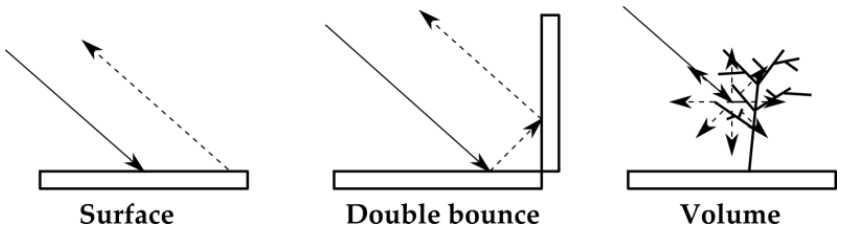

Figure 2-8. The main scattering mechanisms.

From the target vectors k_L and k_p, complex polarimetric coherence matrices, $[T_3]$, and covariance, $[C_3]$, can be constructed. This is an incoherent representation of the signal derived from the variance of the signals in the different polarization channels and their mutual correlation. The covariance matrix $[C_3]$ is the product between the target vector k_L and its conjugate transpose k_L^T (Eq. 2.7):

$$C_3 = \langle k_L k_L^{T*} \rangle = \begin{bmatrix} \langle |S_{hh}|^2 \rangle & \sqrt{2}\langle S_{hh} S_{hv}^* \rangle & \langle S_{hh} S_{vv}^* \rangle \\ \sqrt{2}\langle S_{hv} S_{hh}^* \rangle & 2\langle |S_{hv}|^2 \rangle & \sqrt{2}\langle S_{hv} S_{vv}^* \rangle \\ \langle S_{vv} S_{hh}^* \rangle & \sqrt{2}\langle S_{vv} S_{hh}^* \rangle & \langle |S_{vv}|^2 \rangle \end{bmatrix} \quad (2.7)$$

The coherence matrix $[T_3]$ is the product between the target vector k_p and its conjugate transpose k_p^T (Eq. 2.8):

$$\begin{aligned} T_3 &= \langle k_p k_p^{T*} \rangle \\ &= \frac{1}{2} \begin{bmatrix} \langle |S_{hh} + S_{vv}|^2 \rangle & \langle (S_{hh} + S_{vv})(S_{hh} + S_{vv})^* \rangle & 2\langle (S_{hh} + S_{vv}) S_{hv}^* \rangle \\ \langle (S_{hh} - S_{vv})(S_{hh} - S_{vv})^* \rangle & \langle |S_{hh} - S_{vv}|^2 \rangle & 2\langle (S_{hh} - S_{vv}) S_{hv}^* \rangle \\ 2\langle S_{hv}(S_{hh} + S_{vv})^* \rangle & 2\langle S_{hv}(S_{hh} - S_{vv})^* \rangle & 4\langle |S_{hv}|^2 \rangle \end{bmatrix} \end{aligned} \quad (2.8)$$

These matrices aim to characterize "non-coherent" targets, also known as non-pure targets. In reality, a target has a complex scattering response due to its complex geometry and reflectivity properties. Interpretation of a target response is difficult because the target response is the sum of several mechanisms within the resolution cell. Therefore, canonical targets are used because their polarimetric signature and $[S]$ matrices associated are known (Table 2.2). Geometric representation of canonical targets and associated Sinclair matrix adapted from Lee and Pottier (2009) (Table 2.2). For example, the $[S]$ matrix of the trihedron corresponds to single bounce, that of a dihedral oriented at 0° to double bounce and that of a dihedral oriented at 45° to volume scattering.

Table 2-2. Geometric representation of canonical targets and associated Sinclair matrix adapted from (Lee and Pottier 2009).

Geometric representation	Canonical target	Sinclair $[S]$ matrix
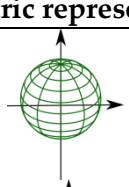	Sphere	$S = \frac{1}{\sqrt{2}}\begin{bmatrix}1 & 0\\ 0 & 1\end{bmatrix}$
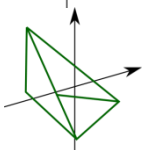	Trihedron	$S = \frac{1}{\sqrt{2}}\begin{bmatrix}1 & 0\\ 0 & 1\end{bmatrix}$
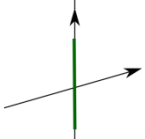	Vertical dipole	$S = \begin{bmatrix}0 & 0\\ 0 & 1\end{bmatrix}$
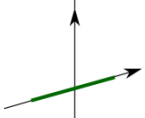	Horizontal dipole	$S = \begin{bmatrix}1 & 0\\ 0 & 0\end{bmatrix}$
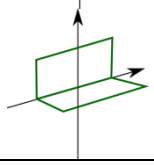	Dihedral oriented at a θ angle	$S = \frac{1}{\sqrt{2}}\begin{bmatrix}\cos 2\theta & \sin 2\theta\\ \sin 2\theta & -\cos 2\theta\end{bmatrix}$

Polarimetric decomposition models are used to extract the different scattering mechanisms of targets to better discriminate objects. Canonical targets are used to partially analyze the results of polarimetric decompositions. The aim is to analyze an incoherent matrix, such as $[C_3]$ or $[T_3]$, and to translate it into a sum of matrices associated with canonical targets. The best known decompositions are the Freeman-Durden (Freeman and Durden 1998) based on the $[C_3]$matrix and the Cloude and Pottier (Cloude and Pottier 1996) based on the $[T_3]$ matrix. The first decomposition aims to separate the scattering mechanisms. As the penetration capacity increases with the wavelength, the induced mechanisms differ according to the SAR sensors (Figure 2-9). Figure 2-10 gives an example of a classification processed by Cloude and Pottier based on the Freeman-Durden decomposition (Lee and Pottier 2009). Specular returns occur on smooth surfaces such as still water. Surface scattering occurs on more or less rough surfaces such as water or bare soil. Double bounce is produced by two locally orthogonal surfaces. Finally, the volume scattering is observed on objects with complex structures such as trees. Figure 2-10 shows that surface scattering corresponds to the ocean and the specular returns are due to the small incidence angles on the ocean surfaces and are scattered in city blocks. Volume scattering correspond to trees and vegetation. Finally, double bounce show street patterns associated with the city blocks and are scattered in park areas (Lee and Pottier 2009).

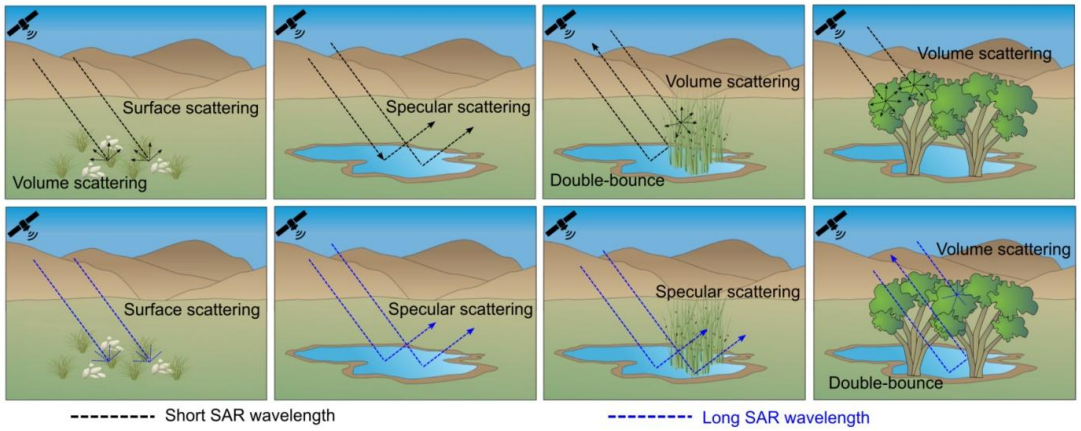

Figure 2-9. Example of scattering mechanisms on a wetland landscape with different wavelengths. Short wavelength = X-band and C-band, Long wavelenght = L-band. Source: Wohlfart et al. 2018.

(a) Classification map

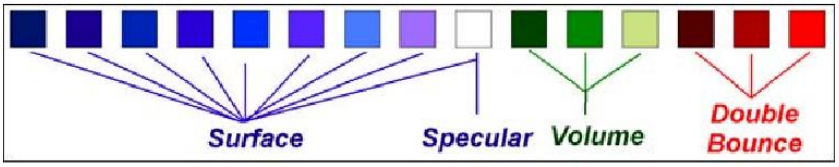

Figure 2-10. Classification map using the Freeman and Durden decomposition and dominant scattering properties. San Francisco image taken by the airborne system AIRSAR (Lee and Pottier 2009).

The Cloude and Pottier decomposition results in three polarimetric parameters derived from the $[T_3]$ coherence matrix:

- The alpha angle (α) measures the dominant backscattering mechanism. A α value of 0°, 45° and 90° corresponds to a surface scattering, a volume scattering, and a double bounce, respectively.
- The entropy (H) is related to the randomness of the diffusion. If H = 0, there is a single scattering mechanism that dominates (case of water surfaces); If H = 1, several scattering mechanisms are present, thus, the signal is depolarized.
- The anisotropy (A) characterizes the importance of secondary scattering mechanisms compared to the primary scattering mechanism. This parameter is used in addition to the entropy parameter. It becomes interesting for high entropy values. If A = 0, the two secondary mechanisms are mixed in equal proportions. If A = 1, the secondary mechanism dominates.

Other polarimetric parameters can be used to characterize the targets from the $[C_3]$ covariance matrix. In this thesis, we use Shannon entropy (SE) because of its high potential to characterize the vegetation (Betbeder et al. 2014a, 2016b). The SE measures the randomness of the scattering of a pixel that may be due to the variation of power or backscatter polarization. For example, a complex structure induces an increase in SE. It is calculated from the following equation (Eq. 2.9):

$$SE = \log\left(\frac{(\pi^2 e^3(C_3)}{3}\right) \tag{2.9}$$

Where

$$SE_i = 3log\left(\frac{\pi e T_r(C_3)}{3}\right)$$

$$SE_p = log\left(27\frac{|C_3|}{T_r(C_3)^3}\right)$$

And $|.|$ is the determinat of the matrix and $T_r(.)$ is the trace of the matrix.

Polarimetric decompositions are suitable for processing quad-polarized SAR data. However, for dual-polarized data, one of the polarization channel is missing. The $[C_3]$ is therefore adapted in $[C_2]$. For example, the covariance matrix of S-1 is (Eq. 2.10):

$$C_2 = \begin{bmatrix} \langle S_{vv}S_{vv}^* \rangle & \langle S_{vv}S_{vh}^* \rangle \\ \langle S_{vh}S_{vv}^* \rangle & \langle S_{vh}S_{vh}^* \rangle \end{bmatrix} \tag{2.10}$$

2.3. Identification and characterization of the elements constituting ecological continuities using remote sensing data

The identification and characterization of the elements potentially constituting ecological continuities is one of the major challenges facing humanity in a context of rapid decline in biodiversity. Today, the notion of ecological continuity is a key concept in public policies dealing with environmental protection laws, protected areas, land use planning tools, etc from the international level to local level. The identification and characterization of ecological continuities are at the basis of biodiversity conservation strategies and represent a major scientific challenge due to the structural and functional complexity of ecological systems. In this context, remote sensing data are an important tool for the identification and characterization of the ecological elements constituting continuities. Optical remote sensing data have been more widely used than SAR for this purpose, in part due to their older operational history. Indeed, the first optical satellite, Landsat-1, was launched in 1972, while SAR satellite systems are available since the 1990s, first with JERS-1 and ERS-1. Optical data are sensitive to physiology of vegetation (chlorophyll content, pigments) while SAR data are sensitive to canopy structure and soil surface characteristics (roughness, moisture). Optical remote sensing data have already shown a high potential to identify and characterize ecological characteristics of landscape elements. However, they have some limitations such as their sensitivity to cloud cover and atmospheric effects. More specifically concerning vegetation, the optical waves do not penetrate the canopy and the signal saturates at high biomass levels. SAR sensors overcome these limitations since microwaves are insensitive to clouds and able to penetrate vegetation. SAR images also have limitations such as the presence of speckle noise and geometric distortions; in addition, the sensitivity of the signal to soil moisture is problematic in rainy conditions. This section provides an overview of research using optical and SAR remote sensing data for the identification and characterization of ecological characteristics from wooded to crop-dominated landscapes. While this thesis evaluates the Sentinel-1 and 2 data, special attention is given to them.

2.3.1. Identification and characterization of land cover types using remote sensing data

Satellite images are an ideal tool for mapping land cover types patterns since they cover large areas with a high frequency revisit time. Since several decades, MODIS, AVHRR and Landsat optical time series have been used extensively for global land cover classification due to their high temporal resolution and large spatial coverage (Congalton et al. 2014; Gómez et al. 2016). The S-2 sensor launched in 2014 improved the characteristics of available images to map land cover with a higher resolution (10m, 20m and 60m), a 5-day revisit time and 13 spectral bands. The associated SAR S-1 data offer a good complement to optical data, especially for cloudy areas. In addition, Sentinel data are freely available unlike most SAR data (e.g., TerraSAR-X, ALOS2, RADARSAT-2, COSMO-Sky Med) and high resolution optical data (e.g., SPOT, Quickbird, WorldView, Geo-Eye, Ikonos). Recent studies have demonstrated the potential of S-2 data for mapping land cover types from a single-date image (Immitzer et al. 2016; Clark 2017; Colkesen and Kavzoglu 2017; Haas and Ban 2018; Mongus and Žalik 2018) and time series (Inglada et al. 2017; Phiri et al. 2020). Some studies have demonstrated the potential of the S-1 signal intensity to map 5 global land cover types (Abdikan et al. 2016) and some CORINE land cover classes such as broadleaf and coniferous

forests, inland waters and non-irrigated arable land (Balzter et al. 2015). Use of S-1 data combined with S-2 or Landsat data increases the classification accuracy (Kussul et al. 2017; Zhou et al. 2017; Laurin et al. 2018; Reiche et al. 2018). Liu et al. (2019) demonstrated that the efficiency of optical and SAR data fusion is modulated by the algorithmic method selected. Although convolutional neural network approach remains ultimately more efficient, fusion has brought more to classical methods (random forest (RF), support vector machine (SVM)).

2.3.2. Identification and characterization of ecological entities in wooded landscapes using remote sensing data

As described in Chapter 1, deforestation and forest degradation are key points for studying ecological characteristics of wooded landscapes. Very high spatial resolution data are required to detect forest degradation (Zhu 2017; Bourgoin 2019). Spectral unmixing analysis has proven to be a relevant method to distinguish degraded vegetation, non-degraded vegetation and bare soil using remote sensing optical images (Tritsch et al. 2016). Time series are required to analyze the dynamics of degradation and the resilience of disturbed environments (Mitchell et al. 2017). While Landsat data are widely used for the detection of deforestation and forest degradation (Bourgoin 2019), more recently, high performance was found using S-2 optical data (Nuthammachot et al. 2018; Sedano et al. 2020). Although LiDAR data are particularly relevant for estimating aboveground biomass (Asner et al. 2012; Meyer et al. 2013), these data are unsuitable for monitoring large areas with a high revisit time. In tropical zones, high cloud cover is a major constraint to detect forest degradation using optical data. In this context, SAR data offer very interesting possibilities. They can be an alternative to LiDAR data since they are also sensitive to the geometrical structure of vegetation. Bourgoin et al. (2018) have demonstrated the performance of S-1 and ALOS-1 PALSAR data to estimate above ground biomass in a degraded Amazonian forest. Finally, the combined use of optical and SAR data allows to obtain denser data series essential for monitoring degradation dynamics. S-2 data are also promising to classify forest types and tree species (Immitzer et al. 2016; Persson et al. 2018; Hościło and Lewandowska 2019). The red-edge and SWIR bands are important for differentiating spectral signatures of species and the multitemporal nature of the data is a key point for capturing the different phenology of species at key periods.

2.3.3. Indentification and characterization of ecological entities in crop-dominated landscapes using remote sensing data

2.3.3.1. Semi-natural elements

Wooded elements and grasslands, which are commonly considered « semi-natural elements » by the scientific community, are essential for biodiversity in crop-dominated landscapes (Burel et al. 2013). Many remote sensing studies have addressed the identification of hedgerows (Betbeder 2015). The definition of hedgerows varies according to studies and this confusion is a problem for the extraction of hedgerows from satellite images because the maps obtained are not based on the same characteristics, making them incomparable (Baudry and Jouin 2003). Baudry and Jouin (2003) defined a hedgerow as "a linear element of the landscape composed of trees or shrubs and managed by man". Manual discrimination from aerial photographs was first used to identify hedgerows network. However, maps represented hedgerows as lines and manual discrimination was time consuming and

difficult to transfer on large areas. Automatic methods were therefore developed using optical satellite images such as QuickBird, SPOT-5 and WorldView-2 images (Thornton et al. 2006; Vannier and Hubert-Moy 2008; Aksoy et al. 2009; Fauvel et al. 2012). Spatial resolution is a key point for hedgerow mapping because fine hedges can only be detected with very high spatial resolutions (Vannier and Hubert-Moy 2014). LiDAR data and its derived raster products are particularly efficient for this purpose (Vannier and Hubert-Moy 2014; Lucas et al. 2019) and are increasingly used due to their growing availability (Lucas et al. 2019). Very few studies use SAR sensors to identify and characterize hedgerows despite some promising results (Bargiel 2013; Betbeder et al. 2014a). The hedgerows characterization remains little studied, either with optical or SAR satellite data. For example, Wiseman et al. (2009) developed a method to discriminate tree species in shelterbelts based on the spectral characteristics of SPOT 5 images. Czerepowicz et al. (2012) explained 70% of the variance in shelterbelt biomass using spatial and spectral characteristics of QuickBird images. Finally, only one study demonstrated the potential of SAR data to characterize hedgerows by estimating the canopy aperture using SE derived from TerraSAR-X images (Betbeder et al. 2014a).

Concerning grasslands, optical satellite data such as MODIS or AVHRR with coarse spatial resolution (>205m) and wide coverage are sufficient for global scale applications. On the other hand, sensors such as SPOT, S-2, GeoEye, RapidEye and Quickbird with higher spatial resolution (>10m) are required to retrieve grassland characteristics such as biophysical parameters, quality, growth, degradation and grazing capacity (Ali et al. 2016). Spectral resolution is a key factor to discriminate species, while temporal resolution is beneficial to estimate yields or monitor phenological stages and grassland management. SAR data have been less used than optical data but they remain promising (Ali et al. 2016). Wang et al. (Wang et al. 2019) found that the combination of S-1, S-2 and Landsat-8 data improved estimates of LAI and above ground biomass of grasslands compared to S-1 alone with low vegetation cover and compared to S-2 with high vegetation cover. Fauvel et al. (2020) predicted grasslands plant diversity by combining Sentinel-1 and 2 data. They showed thatS-1 did not improve results obtained using only S-2 data but only the signal intensity was used. Dusseux et al. (2014) found that the discrimination between grasslands and crops is more accurate using a full polarimetric RADARSAT-2 time series than an optical time series (SPOT and Landsat). Polarimetry also showed a high potential for monitoring grassland cutting practices (Voormansik et al. 2016). El Hajj et al. (2019) demonstrated that L-band was more relevant to characterize grasslands than C-band because of its higher penetration capacity.

2.3.3.2. Crops

Until the late 1990s, the optical Landsat and SPOT images were the most relevant to discriminate crop types with a spatial resolution of 30m and 20m, respectively (Bauer et al. 1979; Büttner and Csillag 1989). In 1990s, the launch of very high spatial resolution optical satellites such as Quickbird and IKONOS offered new opportunities to accurately identify crop types (Yang et al. 2007; Turker and Ozdarici 2011). The misclassifications of crop types are mainly due to spectral similarities between crops and spatial and spectral variability within fields. A high spectral resolution of optical sensors is essential to discriminate crops, especially spectrally similar crops. A high temporal resolution is also highly useful to

discriminate crops by enabling to monitor crop rotation and phenological cycles. The S-2 sensors, launched in 2015 and 2017, are a very good tool for crop identification and characterization since they combine high spatial, temporal and spectral resolutions (Immitzer et al. 2016; Inglada et al. 2016; Veloso et al. 2017; Belgiu and Csillik 2018; Vuolo et al. 2018; Ghosh et al. 2018). The use of SAR images alone have a good potential in identifying crop types, as shown with with TerraSAR-X (McNairn and Brisco 2004; Kenduiywo et al. 2016), RADARSAT-2 (Jiao et al. 2014) and S-1 (Denize et al. 2019b; Mandal et al. 2020) data. The temporal resolution of SAR data appears more important than the polarimetric information (McNairn and Brisco 2004; Kenduiywo et al. 2016, 2017; Denize et al. 2019b) and quad polarization outperforms dual polarization (McNairn and Brisco 2004; Denize et al. 2019b). Since 2014, the use of optical and SAR data fusion for crop type discrimination is increasing (Blaes et al. 2005; Inglada et al. 2016; Denize et al. 2019a; Orynbaikyzy et al. 2019). Landsat and RADARSAT sensors are the most widely used sensors while the fusion methods are mostly layer-stacking of optical and SAR bands. The optical and SAR data fusion improves the accuracy of classifications (Orynbaikyzy et al. 2019). Orynbaikyzy et al. (2019) noted that studies using optical and SAR data fusion used small study areas and the reproducibility of the methods is lacking.

Optical data (AVHRR, SPOT, Landsat, MODIS, IRS, IKONOS, QuickBird, Formosat-2, S-2) have been widely used for crop characterization (Quarmby et al. 1993; Doraiswamy et al. 2004; Mulla 2013; Bontemps et al. 2015; Pan et al. 2015; Betbeder et al. 2016b; Bégué et al. 2018). The spectral bands, vegetation indices and biophysical variables derived from these data have a high potential for estimating crop parameters such as yield, biomass, LAI and phenological stages of various crops. More specifically, S-2 data perform well in estimating LAI (Delegido et al. 2011b; Frampton et al. 2013; Clevers et al. 2017; Pan et al. 2018; Wang et al. 2019), biomass (Veloso et al. 2017; Ghosh et al. 2018; Ganeva et al. 2019) and phenological stages (Veloso et al. 2017; Ghosh et al. 2018; Stendardi et al. 2019) of grasslands and crops. Red-edge and SWIR bands of S-2 are relevant for estimating LAI of various crop types (Pan et al. 2018). Many studies demonstrate the value of satellite (RADARSAT, TerraSAR-X, ALOS, S-1) and airborne SAR data for identifying crop parameters (Steele-Dunne et al. 2017). Polarimetric parameters derived from RADARSAT-2 or TerraSAR-X are relevant for estimating phenological stages, height and LAI of various crops (Jiao et al. 2009; Wiseman et al. 2014; Mascolo et al. 2015; Jin et al. 2015; Betbeder et al. 2016b; Pacheco et al. 2016; Canisius et al. 2018; McNairn et al. 2018; Homayouni et al. 2019). We do not know any study using polarimetric indicators derived from S-1 to characterize crops. More specifically about S-1, recent studies show the interest of backscatter coefficients and VH:VV ratio for crop classification (Bargiel 2017), changes detection in the structure of rapeseed, maize and winter cereals (Vreugdenhil et al. 2018), identification of wheat phenological stages (Song and Wang 2019) and estimation of biomass, moisture content and LAI of wheat (Kumar et al. 2018). Some studies have used both optical and SAR data for crop characterization (Betbeder et al. 2016a; Veloso et al. 2017; El Hajj et al. 2019). However, most of them use optical data as a reference for evaluating SAR data. Although the combination of optical and SAR data improves classification results, it remains little used to predict crop parameters (Jin et al. 2015; Stendardi et al. 2019).

2.4. Functional assessment of ecological continuities identified by remote sensing data

While remote sensing is commonly used to map the elements constitutive of ecological continuities, be they semi-natural features, permanent grasslands, or cultivated plots, it is also is commonly used in landscape ecology to study landscape structure, change and function (Crowley and Cardille 2020). Landscape function can be assessed by combining these indicators with information from landscape ecology models (e.g., spatial distribution of a species, meteorological measurements). Ecological continuities are identified using modeling of the interactions between map data and species observations. Indicators used for this purpose can be images with continuous values such as vegetation indices (Moreno et al. 2020) or polarimetric indicators (Betbeder et al. 2015) or discrete land cover and land use classes (De la Fuente et al. 2018).

At the national level, in Spain, Fuente et al. (2018) have produced a map of ecological corridors relevant for forest mammal movements. They used a least-cost path modeling, based on resistance surfaces to link Natura 2000 sites with corridors. In the case of woodland species, movement was restricted outside woodlands, i.e. in crops, urban areas or through transport infrastructures. Therefore, high movement resistance values were assigned to these land cover/land use classes. The resistance surface was derived from the forest map of Spain, and the Corine land cover and OpenStreetMap databases.

In France, the mapping of the green and blue network is carried out in most regions in three stages. First, sub-networks such as wooded areas, hedgerows, wet grasslands or coastlines are identified. Aerial photographs and field inventories are the main sources of information. Second, biodiversity reservoirs are identified from existing protected areas (e.g. Natura 2000 and Natural Areas of Ecological, Faunistic and Floristic Interest), scientific databases (tree species, habitat), and modeling of species movement capacity according to the environment encountered. Third, corridors are identified using photo-interpretation of land cover/use. Two methods are used: 1) the identification of corridors using the least-cost method 2) the use of methods based on permeability of environments generally integrated into GIS (Betbeder 2015).

At the regional level, Hubert-Moy et al. (2012) mapped corridors in Brittany, France. They used high and medium spatial resolution optical data to identify agro-natural elements (woodlands, heathlands, thickets and permanent grasslands). Then, an aggregation index was applied to the different elements identified in order to detect structural continuities in this agricultural landscape.

Croley and Cardille (Crowley and Cardille 2020) identified future contributions of remote sensing to landscape ecology by examining studies of the last five years, including intra-annual monitoring for landscape analysis, comparison between different landscapes and the use of continuous rather than discrete classes of data. They outlined that ecological continuities maps do not consider the crop mosaic despite beneficial effects of heterogeneous landscape including semi-natural elements on biodiversity. They also highlighted that the temporal dynamics of ecological continuities such as hedgerow trimming or crop rotation

are never integrated despite their effects on landscape functions. These issues could be taken into consideration using remote sensing time series data, given their high potential to identify and characterize crop-dominated landscapes.

CHAPTER 3

Study areas and data

Contents

3.1. Introduction

The identification and characterization of ecological continuities were conducted over eight study areas in four countries: one in Brazil, one in Spain, three in France and three in Belgium. Firstly, this chapter presents the study areas: (i) the forest agriculture mosaics (Cantabrian range and Paragominas) used to map land cover types and (ii) the crop-dominated landscapes (Brittany, Picardy, Wallonia) used for crop characterization and ecological assessment of agricultural networks. Secondly, the data used are described, i.e. remote sensing data, field measurements and species data.

3.2. Study areas

3.2.1. Forest-agriculture mosaics

3.2.1.1. Cantabrian range (Spain)

The study area named "Cantabrian range" is a forest-agriculture mosaic that covers 35 700 km² and four regions of Spain, i.e. Lugo in the East, Cantabria in the West, Principality of Asturias in the North and Castilla y Leon in the South (Figure 3-). The region includes the entire Cantabrian Range with an elevation of 0-2468m (mean = 800m). The climate is Atlantic with mild temperatures and short cool summers (Mateo-Sánchez et al. 2016; García-León et al. 2019). The landscape is dominated by forested areas, shrublands and croplands dominated by vines, wheat, barley, rye, sunflower and oat (Mateo-Sánchez et al. 2016). The crops are located in the south of the study area (Castilla y Leon), most of them being irrigated.

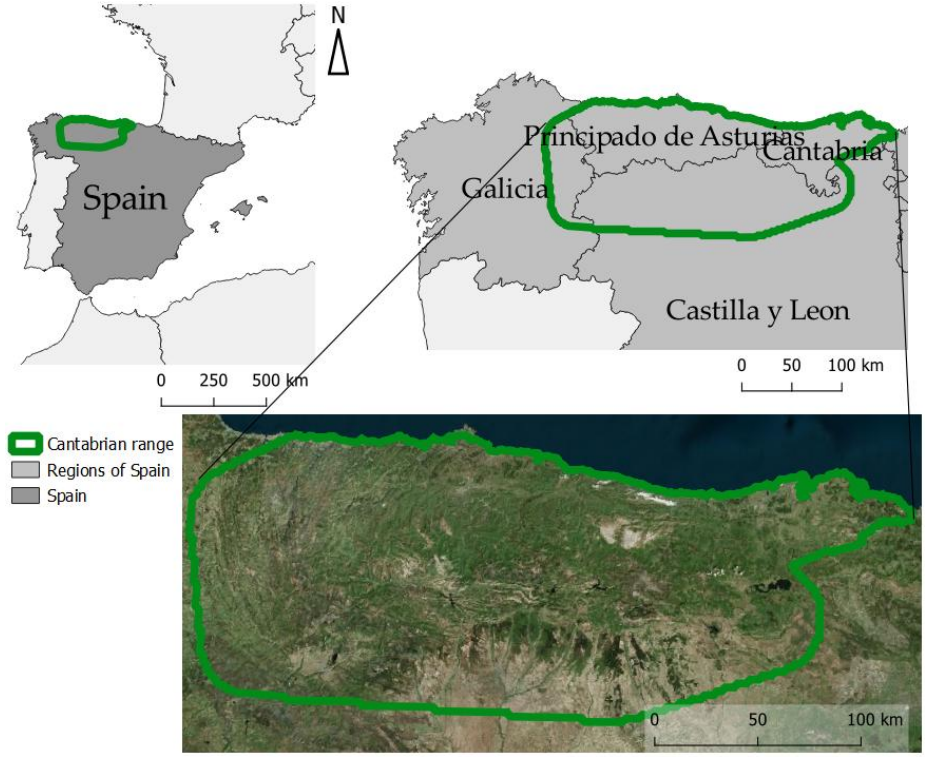

Figure 3-1. Location of the Cantabrian range study area. Satellite imagery accessed through Bing Aerial (Microsoft® Bing™ Maps).

Three thousand years ago, large patches of natural forests were converted to pasturelands (traditional cattle ranging and selective logging), leading to major decrease in forest area. Thus, the current landscape contains remnant forest fragments that are distinct from a non-forest matrix composed mainly of pastures, heathlands in abandoned meadows (García et al. 2005). Some parts of the region include small scattered villages while others are composed of extensive urban and agricultural lands connected by roads, highways, and railways (Sánchez et al. 2014). More recent forest decrease is due to anthropogenic pressures such as surface mining, road construction, creation of forest plantations and anthropogenic fires. Mature beech forests of Cantabrian range provide habitat for threatened species (capercaillie and brown bear). In the past 40 years, regional and national reserves were established to preserve forested habitats. Legal restrictions on new land uses are imposed in reserves such as road construction, mining and timber deforestation (García et al. 2005).

3.2.1.2. Paragominas (Brazil)

Paragominas is a municipality located in the eastern Brazilian Amazonia, in Pará State, 217 km south of Belem. The municipality covers 19342 km² with an elevation of 0-190 m (Figure 3-2). The climate is tropical with a wet season from December to May and a dry season from June to November, an average annual temperature of 26.3°C and an annual rainfall of 1693m (Andrade 2011).

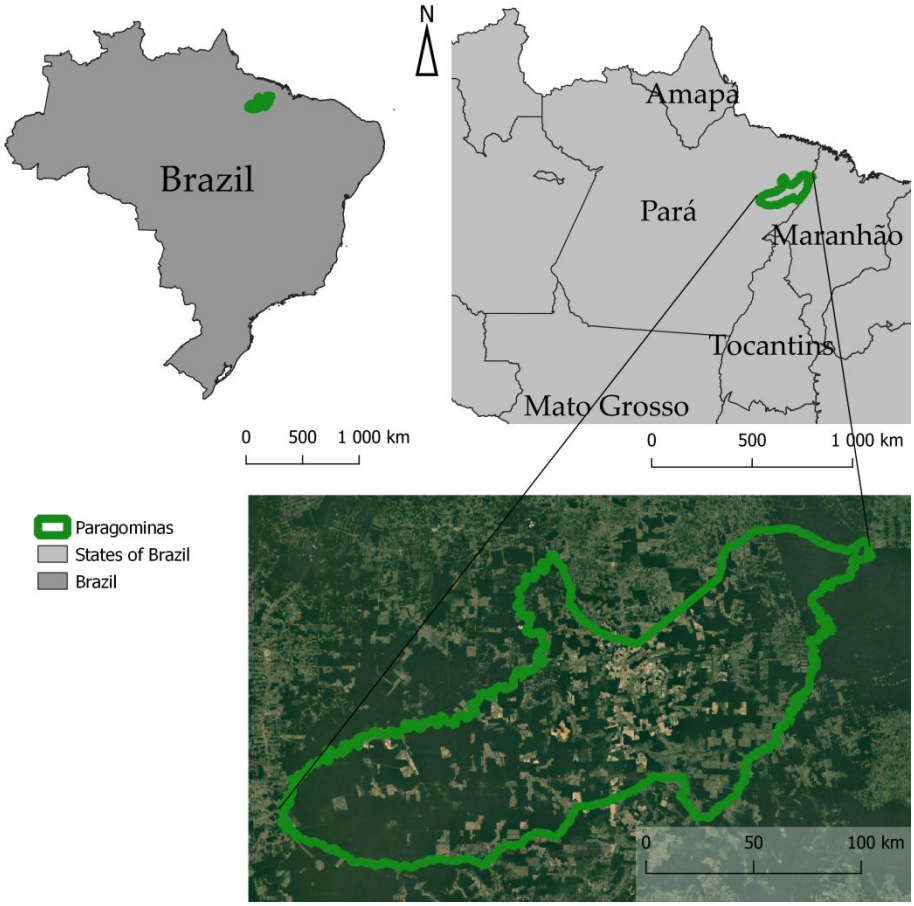

Figure 3-2. Location of Paragominas. Image Landsat Copernicus (© 2020 Google).

From the 1960s to 2010, there has been a period of deforestation mainly caused by soybean and maize cultivation, creation of forest plantations and cattle ranching. The remnant forest areas were degraded due to overlogging and fires (Tritsch et al. 2016). In

1990, Paragominas was the main producer of wood in Brazil. Landscape and forest disturbances in the municipality have caused biodiversity loss, with significant negative effects on species of high conservation and functional value (Barlow et al. 2016). In 2005, in the context of the new federal policy to fight deforestation, a new model of local governance, called "Municipio Verde", was adopted by the municipality (Viana et al. 2012). Its aims were to combat deforestation and strengthen the capacity of local institutions to develop specific environmental policies based on the Brazilian forestry code. Since then, Paragominas represents a spectacular case of deforestation that became a national reference for municipal-level anti-deforestation policies with annual deforestation rates decreasing by up to 80%.

3.2.2. Crop-dominated landscapes

3.2.2.1. Picardy (France)

The two study areas of Picardy are 5 km squares located in northern France (Figure 3-3). The climate is oceanic with an average annual temperature of 10°C and mean average precipitation of 702 mm (Météo France).

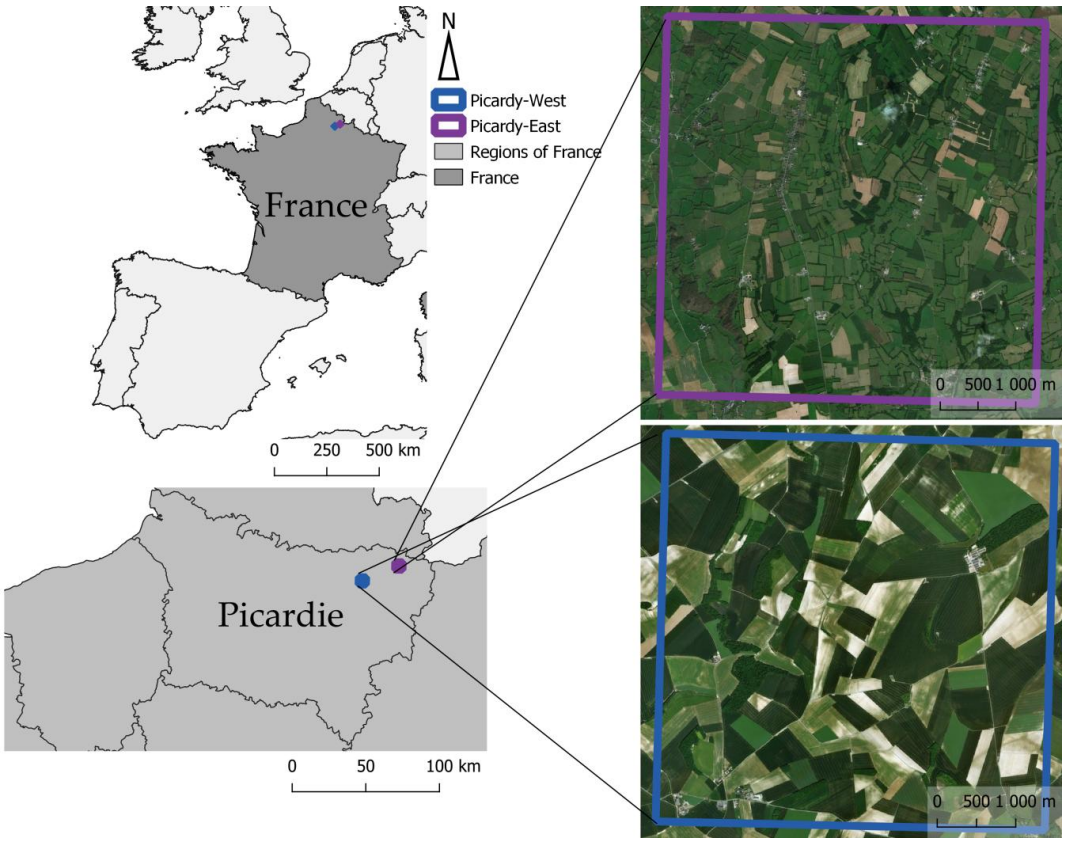

Figure 3-3. Location of the study areas of Picardy. Aerial photographs accessed through Bing Aerial (Microsoft® Bing™ Maps).

The site named “Picardy-West” is an open field landscape with intensive cultivation of cereals and sugar beet. The site named “Picardy-East” is a “bocage” landscape dominated by grasslands and less intensive farming activities (mainly dairy cattle), the fields being smaller and tending to be surrounded by hedgerows. In both landscapes, managed forest fragments are used for hunting and production of wood (Jamoneau 2010). These study areas are quite

flat with an elevation of 125-224 m (mean = 180 m) and 72-158 m (mean = 114 m), for the "bocage" and open field landscapes, respectively.

3.2.2.2. Brittany (France)

The study area of Brittany named "Zone Atelier Armorique" (ZAA) is located in the southern part of the Bay of Mont-Saint-Michel, France and covers 130km² (Figure 3-4). It is a Long-Term Ecological Research (LTER) accredited by the National Center for Scientific Research (CNRS) which is part of European LTER and International LTER networks (https://osur.univ-rennes1.fr/za-armorique). The ZAA was created in 1993 to perform long-term research around three main themes: planning, public policy and landscape dynamics; the relationship between spatio-temporal landscape dynamics and biodiversity; and influence of spatial-temporal landscape dynamics on ecosystem processes. The climate is temperate with an average annual temperature of 12 °C and an average annual precipitation of 650 mm. Cropland includes mainly maize, wheat, grassland and barley. Grasslands which represent 30% of the utile agricultural area are located in the northwestern and southern part of the study area. The crops are more or less surrounded by hedges, the density of the hedge network increasing from north to south.

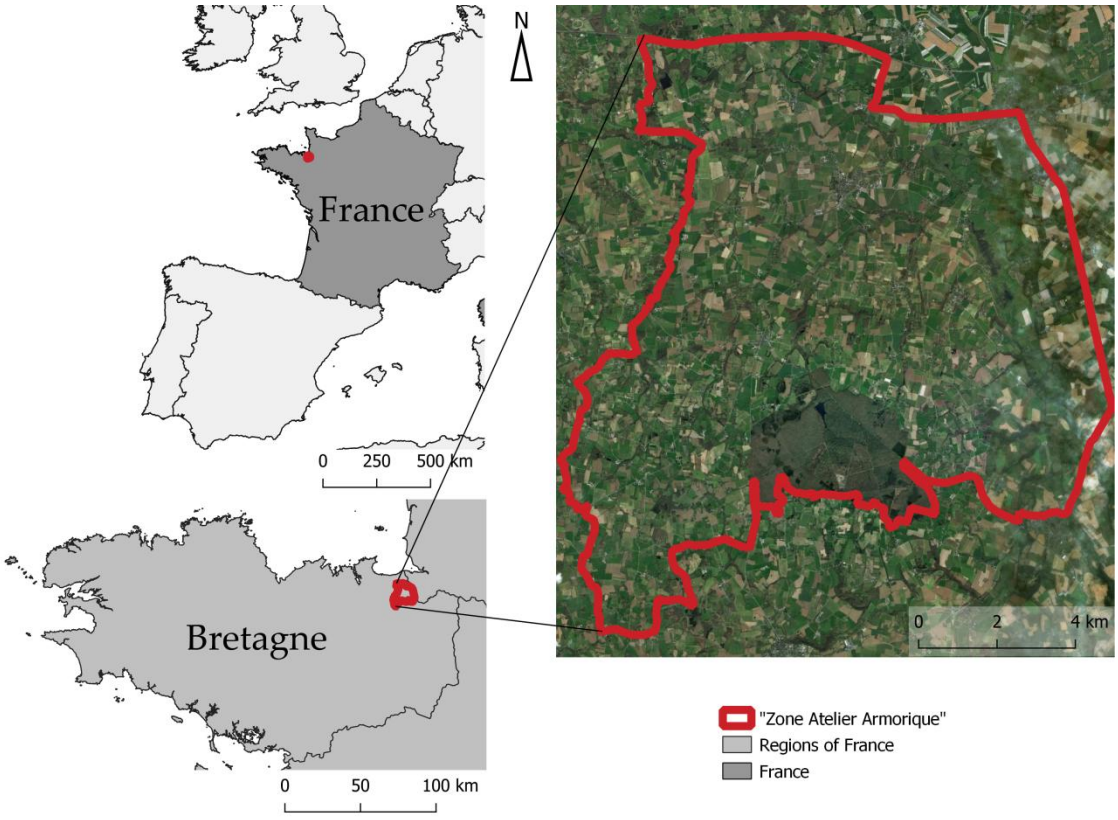

Figure 3-4. Location of the study area of Britanny. Satellite images accessed through Bing Aerial (Microsoft® Bing™ Maps).

3.2.2.3. Wallonia (Belgium)

The three Belgian study areas are located in Wallonia (Figure 3-5). The climate is temperate with annual mean temperature of 9.4-10.5°C and average annual precipitation of 822-912 mm (en.climate-data.org). The site named "Wallonia-Northeast" is an openfield landscape dominated by intensive cultivation of wheat and beet, and high proportions of potato and maize. The site named "Wallonia-Northwest" has an intermediate landscape grain with mainly grasslands and to a lesser extent wheat, maize, potato, barley and beet. The site named "Wallonia-South" ranges from an intermediate to coarse landscape grain with wheat, beet, barley, grassland and in smaller proportions potato and rapeseed depending on the year.

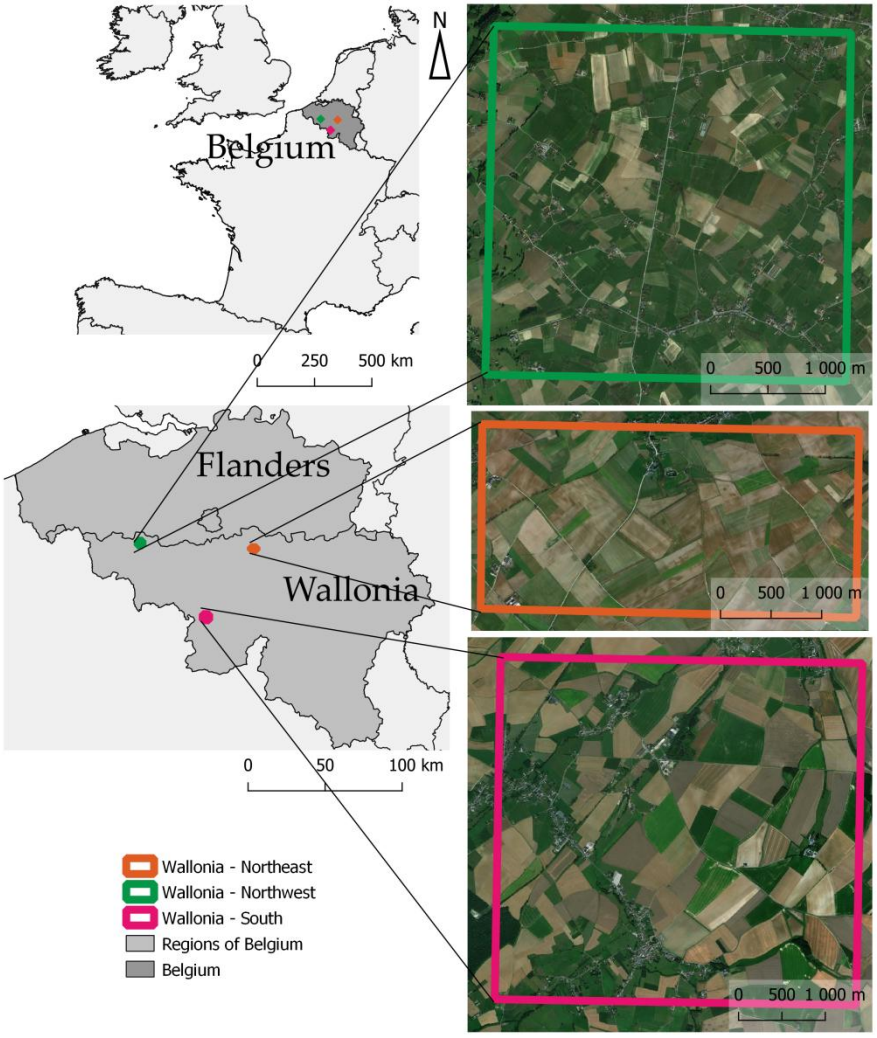

Figure 3-5. Location of the study areas of Wallonia. Aerial photographs accessed through Bing Aerial (Microsoft® Bing™ Maps).

3.3. Remote sensing data

The remote sensing data used in this thesis were exclusively SAR S-1 and optical S-2 images. In this section, the characteristics of optical and SAR images are first described, then the image pre-processing is presented.

3.3.1. Optical Sentinel-2 images

S-2 MSI products are organized in 110 X 110 km tiles with a 10 km overlap and 13 spectral bands in UTM/WGS84 projection. A total of 96 S-2 tiles were downloaded from the Copernicus Open Access Hub (https://scihub.copernicus.eu/). The images were acquired with spatial resolutions of 10 and 20 m (i.e. 10 spectral bands) were downloaded (Table 3-3).

Table 3-1. Main characteristics of S-2 MSI L1C / L2A images used.

Spatial and spectral resolutions	*10 × 10 m* B2 (490 nm), B3 (560 nm), B4 (665 nm) and B8 (842 nm) *20 × 20 m* B5 (705 nm), B6 (740 nm), B7 (783 nm), B8a (865 nm), B11 (1610 nm), B12 (2190nm)
Temporal resolution	5 days
Swath	290km

3.3.1.1. Forest-agriculture mosaics

The number of tiles required to cover the Spanish and Brazilian study areas were 8 and 9, respectively. For the Cantabrian range, six mosaics were acquired from December to August 2017 (The tiles were downloaded in level 2A for Cantabrian range and level 1C for Paragominas (level 2A was not yet available during processing). Level-1C and 2A products are orthorectified and provide top-of-atmosphere and top-of-canopy reflectances, respectively.

Table 3-2). Tiles were acquired on July 20 and 27, 2017 on Paragominas due to the frequent heavy cloud cover. The tiles were downloaded in level 2A for Cantabrian range and level 1C for Paragominas (level 2A was not yet available during processing). Level-1C and 2A products are orthorectified and provide top-of-atmosphere and top-of-canopy reflectances, respectively.

Table 3-2. Details of Sentinel-2 dates downloaded on the Spanish study area.

Mosaic / Tiles	Dec./Jan.	Feb./March	April/May	June	July	August
T29TPJ	2017-01-25	2017-03-16	2017-04-05	2017-06-14	2017-07-04	2017-08-13
T29TQJ	2017-01-25	2017-03-16	2017-05-25	2017-05-25	2017-07-04	2017-08-13
T29TPH	2017-01-25	2017-03-16	2017-04-05	2017-06-14	2017-07-04	2017-08-13
T29TQH	2017-01-25	2017-03-16	2017-04-05	2017-06-14	2017-07-04	2017-08-13
T30TUP	2016-12-13	2017-02-21	2017-04-22	2017-06-21	2017-07-11	2017-08-20
T30TVP	2016-12-13	2017-03-23	2017-04-22	2017-06-21	2017-07-11	2017-08-20
T30TUN	2016-12-13	2017-02-21	2017-04-22	2017-06-21	2017-07-11	2017-08-20
T30TVN	2016-12-13	2017-02-21	2017-04-22	2017-06-21	2017-07-11	2017-08-20

3.3.1.2. Crop-dominated landscapes

S-2 images were downloaded from January to July 2017 for Brittany and Picardy study areas, corresponding to the entire wheat and rapeseed crop cycles (

Table 3-3). In all crop-dominated landscapes, S-2 images were acquired from April to July 2017 and 2018 for the ecological assessment of the agricultural networks (
Table 3-3). These images were cloud-free and in level 2A providing top-of-canopy reflectance.

Table 3-3. S-2 dates downloaded on Brittany, Picardy and Wallonia study areas.

Brittany	Picardy	Wallonia-South	Wallonia-Northwest	Wallonia-Northeast
2017-01-19	2017-01-26	2017-05-06	2017-05-06	2017-05-06
2017-04-09	2017-02-15	2017-05-26	2017-05-26	2017-05-26
2017-05-09	2017-03-27	2017-07-05	2017-07-05	2017-07-05
2017-06-21	2017-05-26	2018-04-21	2018-04-21	2018-04-21
2018-04-22	2017-07-05	2018-05-18	2018-05-26	2018-05-26
2018-05-17	2018-04-21	2018-06-27	2018-06-30	2018-06-27
2018-06-26	2018-05-06			
	2018-06-30			

3.3.2. SAR Sentinel-1 images

3.3.2.1. Forest-agriculture mosaics

For the forest-agriculture mosaics (Spain and Brazil), Sentinel-1A images were downloaded in dual-polarization (VV and VH), Interferometric Wide (IW) swath mode and in Ground Range Detected (GRD) level-1 (Table 3-4). The IW swath mode acquires data with a 250km swath using Terrain Observation with Progressive Scans SAR (TOPSAR). Level-1 GRD products consist of focused SAR data that have been detected, multi-looked and projected to ground range using an Earth ellipsoid model (sentinel.esa.int). Phase information is lost, which enables to extract only the backscattering coefficients. The resulting product has approximately square spatial resolution and square pixel spacing with reduced speckle due to the multi-look processing. The range and azimuth spatial resolutions were 20 and 22 m, respectively, and the pixel spacing was 10 x 10 m (Table 3-4).

Table 3-4. Main characteristics of S-1 L1C images

Band	C (center frequency of 5 405 GHz)
Mode	Interferometric Wide Swath
Product type	Ground Range Detected
Pixel resolution	20 × 22 m (range × azimuth)
Pixel spacing	10 × 10 m (range × azimuth)
Temporal resolution	6 days (Spain) and 12 days (Brazil)
Orbit	Ascending
Polarization	VV & VH
Swath	250 km
Incidence angle (°)	29.1-46.0

For Cantabrian range, 22 mosaics of 3 images (66 images in total) were produced from December 2016 to September 2017. For Paragominas, 14 mosaics of 3 images (42 images in total) were produced from November 2016 to December 2017.

3.3.2.2. Crop-dominated landscapes

For crop-dominated landscapes, S-1 images were used in Brittany and Picardy to characterize crop parameters from January to July 2017 (**Erreur ! Source du renvoi**

ntrouvable.). S-1 images were acquired in dual polarization (VV and VH), Interferometric Wide (IW) swath mode and in Single Look Complex (SLC) format (**Erreur ! Source du renvoi ntrouvable.**). SLC products contain both amplitude and phase information, which enables to derive polarimetric indicators. The incidence angle of images ranged from 30.6-51.3° and the spatial resolution was 2.3 × 13.9 m.

Table 3-5. Main characteristics of S-1 SLC images.

Band	C (center frequency of 5 405 GHz)	
Mode	Interferometric Wide Swath	
Product type	Single Look Complex	
Ground Resolution	2.3 m	
Azimuth resolution	13.9 m	
Temporal resolution	6 days	
Orbit	Ascending	
Polarization	Dual (VV & VH)	
Swath	250 km	
Incidence angle	29.1-46.0°	
	Brittany	**Picardy**
Dates(Y-M-D)	2017-01-28	2017-01-21
	2017-03-17	2017-02-14
	2017-04-22	2017-03-10
	2017-05-16	2017-04-08
	2017-06-21	2017-05-02
		2017-06-02
		2017-06-14
		2017-07-01

3.3.3. Time-series pre-processing

3.3.3.1. Pre-processing of optical Sentinel-2 time series

S-2 images were downloaded from the Copernicus Open Access Hub providing level-1C and level-2A products. ESA used the Sen2Cor processor algorithm to perform atmospheric corrections on Level-2A products, thus we transformed Level-1C products to level-2A using the Sen2Cor application (Sen2Cor, ESA, http://step.esa.int/main/third-party-plugins-2/sen2cor/). The Sen2Cor processor algorithm performs atmospheric corrections adapted to S-2 data (Main-Knorn et al. 2017). It uses a scene classification algorithm (Louis et al. 2010) resulting in three different classes for clouds, and six classes for shadows, cloud shadows, vegetation, not vegetated, water and snow. The algorithm is based on a series of threshold tests that are derived from band ratios and indices (.e.g. NDVI). Cloud screening allows retrieving accurate atmospheric and surface parameters. The aerosol type and optical thickness of the atmosphere are calculated using the DDV (Dense Dark Vegetation) algorithm (Kaufman and Sendra 1988). These parameters are preferably determined from dense dark vegetation and water bodies whose reflectance behavior is well known. The Atmospheric Pre-Corrected Differential Absorption (APDA) algorithm uses the bands 8a and 9 (NIR-narrow and Cirrus) to perform water vapour retrieval over land (Schläpfer et al. 1998). Finally, the atmospheric correction is performed using a set of look-up tables generated via libRadtran (Emde et al. 2016)

The images were projected onto the appropriate coordinate system for each study area : ETRS89-TM3/ETRS0 system (EPSG 3042) for Cantabrian range, WGS84/UTM 22S system (EPSG 32722) for Paragominas, RGF93/Lambert-93 system (EPSG 2154) for Brittany and Picardy, and ETRS89/Belgian Lambert 2008 (EPGS 3812) for Wallonia.

In total, fourteen vegetation indices were calculated (Table 3-6): the NDVI, the Green Normalized Difference Vegetation Index (GNDVI), the NDWI, the EVI, the Red-Edge Inflation Point (REIP) index, the Inverted Red-Edge Chlorophyll Index (IRECI), the S2REP index, the Modified Chlorophyll Absorption in Reflectance Index (MCARI), the MERIS Terrestrial Chlorophyll Index (MTCI), the SAVI, the MSAVI, the WDVI, the Pigment Specific Simple Ratio (PSSRa) and the Normalized Difference Index (NDI).

LAI was also derived from S-2 images in Picardy using the PROSAIL radiative transfer model implemented in SNAP (Sentinel Application Platform) v6.0 software. This biophysical variable describes the state of vegetation cover and provides information on the density of green vegetation (Bréda 2003).

Table 3-6. Vegetation indices calculated from S-2 images. G = Green, R = Red, RE = Red-Edge.

Index	Equation	Sentinel-2 bands used	Original author
EVI	2.5×(NIR-R)/(NIR+6×R-7.5×B)+1)	2.5×(B8-B4)/(B8+6×R-7.5×B2)+1)	(Huete et al. 2002)
GNDVI	(RE3 - G) / (RE3 + G)	(B7 - B3) / (B7 + B3)	(Gitelson et al. 1996)
IRECI	(RE3 - R) / (RE1 / RE2)	(B7 - B4) / (B5 / B6)	(Guyot and Baret 1988)
MCARI	[(RE1 - R) 0.2(RE1 - G)] * (RE1 - R)	[(B5 - B4) - 0.2(B5 - B3)] * (B5 - B4)	(Daughtry et al. 2000)
MSAVI	(1 + L) * (NIR- R) / (NIR + R + 0.5) L = 1 – 2 * 0.5 * (RE3 – R) / (RE3 + R) * (NIR – 0.5 * R)	(1 + L) * (B8- B4) / (B8 + B4 + 0.5) L = 1 – 2 * 0.5 * (B7 – B4) / (B7+B4) * (B8 – 0.5 * B4)	(Qi et al. 1994)
MTCI	(RE2 - RE1)/(RE1 - R)	(B6 - B5)/(B5 - B4)	(Dash and Curran 2004)
NDI	(RE1 - R) / (RE1 + R)	(B5 - B4) / (B5 + B4)	(Delegido et al. 2011a)
NDVI	(RE3-R)/(RE3+R)	(B7-B4)/(B7+B4)	(Rouse et al. 1973)
NDWI	(NIR-G)/(NIR+G)	(B8-B3)/(B8+B3)	(Gao 1996)
PSSRa	RE3/R	B7/B4	(Blackburn 1998)
REIP	700 + 40 * ((R + RE3)/2 - RE1) / (RE2 - RE1)	700 + 40 * ((B4 + B7)/2 - B5) / (B6 - B5)	(Guyot and Baret 1988)
S2REP	705 + 35 * ((((RE3 + R)/2) - RE1)/(RE2 - RE1))	705 + 35 * ((((B7 + B4)/2) B5)/(B6 - B5))	(Guyot and Baret 1988)
SAVI	(1 + 0.5) * (NIR- R) / (NIR + R + 0.5)	(1 + 0.5) * (B8- B4) / (B8 + B4 + 0.5)	(Huete 1988)
WDVI	(NIR – 1.5 * R)	(B8 – 1.5 * B4)	(Clevers 1988)

3.3.3.2. Pre-processing of SAR Sentinel-1 images

3.3.3.2.1. Backscattering coefficients

The backscattering coefficient extraction process was performed using the S-1 Toolbox (ESA, http://step.esa.int/main/toolboxes/sentinel-1-toolbox/).

First, the images were radiometrically calibrated to transform the digital number of each pixel into a basckscattering coefficient ($\sigma\circ$VV, $\sigma\circ$VH) on a linear scale using the following equation (Miranda and Meadows 2015):

$$value(i) = \frac{|DN_i|}{A_i^2} \qquad (1)$$

where DN is the digital number of each pixel (i) (amplitude of the backscattering signal) and A is the information necessary to convert SAR reflectivity into physical units and provided in the Calibration Annotation Data Set in the image metadata.

Second, a Lee refined 7 x 7 filter was applied to reduce speckle noise (Lee et al. 1994).

Third, the images were geo-coded using Shuttle RaDAR Topography Mission (SRTM) data (Farr et al. 2007) to correct topographic deformations and were projected onto the appropriate coordinate system for each study area : ETRS89-TM3/ETRS0 system (EPSG 3042) for Cantabrian range, WGS84/UTM 22S system (EPSG 32722) for Paragominas, RGF93/Lambert-93 system (EPSG 2154) for Brittany and Picardy, and ETRS89/Belgian Lambert 2008 (EPGS 3812) for Wallonia.

Fourth, the $\sigma\circ$VH:$\sigma\circ$VV ratio was calculated from the backscattering coefficients.

Finally, the backscattering coefficients and the ratio were converted from linear to decibel (dB) scale using the following equation:

$$\sigma^0(db) = 10 \times log_{10}(\sigma^0) \qquad (2)$$

3.3.3.2.2. Polarimetric indicators

The polarimetric indicators extraction process was performed using PolSARpro version 5.1.3 software (Pottier and Ferro-Famil 2012).

First, a 2 × 2 covariance matrix (C_2) was extracted from the scattering matrix S of each S-1 SLC image.

Second, a Lee refined 7 x 7 filter was applied to reduce speckle noise (Lee et al. 1994).

Third, four polarimetric indicators were extracted: the span, the SE, the intensity (SE_i) and the degree of polarization (SE_p). The SE was calculated from the covariance matrix (C_2) using the following equation:

$$SE = \log(\pi^2 e^2 |C_2|) = SE_i + SE_p \qquad (3)$$

where SE_i is related to the intensity and SE_p to the degree of polarization.

Finally, SE, SE_i and SE_p were normalized as $SE\ norm$, $SE_i\ norm$ and $SE_p\ norm$.

3.4. Field surveys

3.4.1. Land cover surveys in forest-agriculture-mosaics

In order to identify and characterize the land cover types in forest-agriculture mosaics (Cantabrian range and Paragominas) using Sentinel-1 and 2 time series, samples were produced with a field campaign and aerial photographs in Paragominas and Forest Map of Spain and aerial photographs in Cantabrian range.

For Paragominas, a set of 328 GPS points were collected in September 2017 during a 3-week field mission. Then, polygons were manually discriminated around the GPS points using aerial photographs. The 7 land cover classes discriminated were bare soils, artificial surfaces, water bodies, forested areas, croplands, pastures, and "young secondary forests" (fallow land with dense but low vegetation representing early regeneration stages of forests after abandonment of agriculture or pasture).

For Cantabrian range, a set of 828 polygons was manually discriminated using the Forest Map of Spain (MAPAMA-Ministerio de Agricultura y Pesca, Alimentación y Medio Ambiente 1997) and aerial photographs. The Forest Map of Spain is the official national forest inventory consisting of polygons associated to land cover and land use attributes. The version used was developed from 1997–2006 and based on interpretation of aerial photographs and field inventory data. The 8 land cover classes discriminated were permanent bare soils, artificial surfaces, water bodies, forested areas, shrublands, permanent herbaceous vegetation (herbaceous vegetation containing chlorophyll throughout the year), summer herbaceous vegetation, and winter herbaceous vegetation.

3.4.2. Crop parameters measurements in crop-dominated landscapes of France

The following data were published as a data paper by Mercier et al (2021).

Phenological stages were identified in Picardy and Brittany to classify them using Sentinel-1 and 2 time series. In Picardy, field surveys were conducted on 36 wheat fields and 19 rapeseed fields (Figure 3-6) on 8 dates from January to July 2017 (Table 3-7). The wheat and rapeseed fields ranged from 0.77-35.09 ha (mean=7.31 ha), median=4.63) and 1.35-23.91 ha (mean=4.82 ha, median=2.84 ha) in size, respectively.

In Brittany, field surveys were conducted on 3 wheat fields and 3 rapeseed fields (Figure 3-7) on 5 dates from January to July 2017 (Table 3-7). Wheat field sizes were 4.26, 10.33 and 12.81 ha, and rapeseed field sizes were 6.02, 10.11 and 11.35 ha.

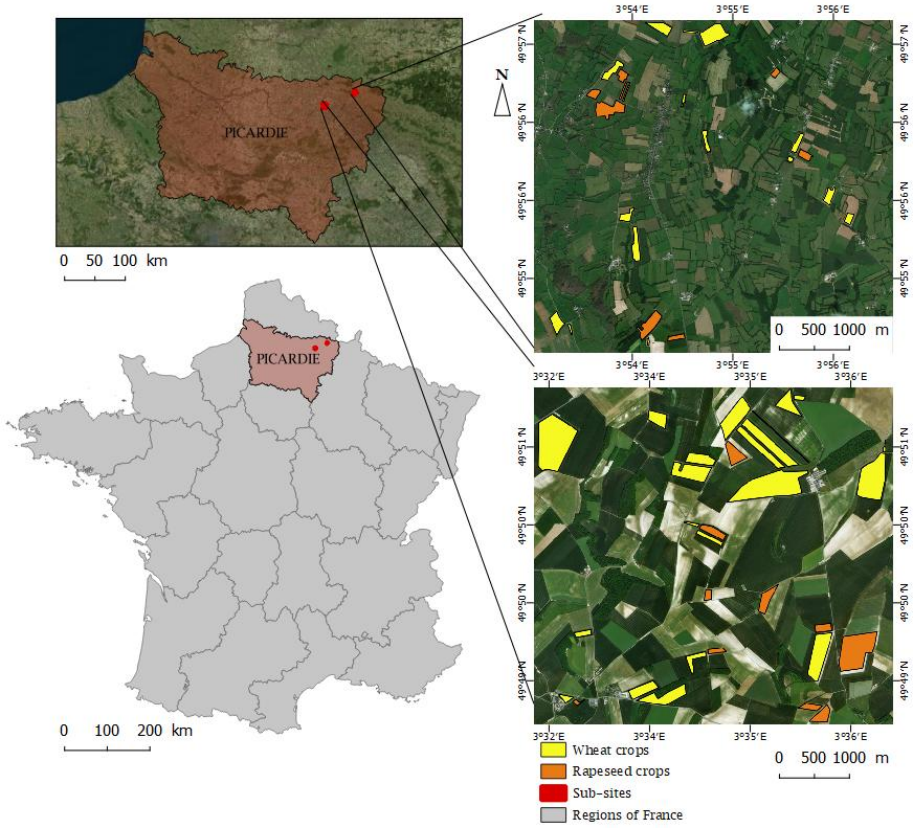

Figure 3-6. Location of crop parameters field surveys in Picardy. Satellite images and aerial photographs accessed through Bing Aerial (Microsoft® Bing™ Maps).

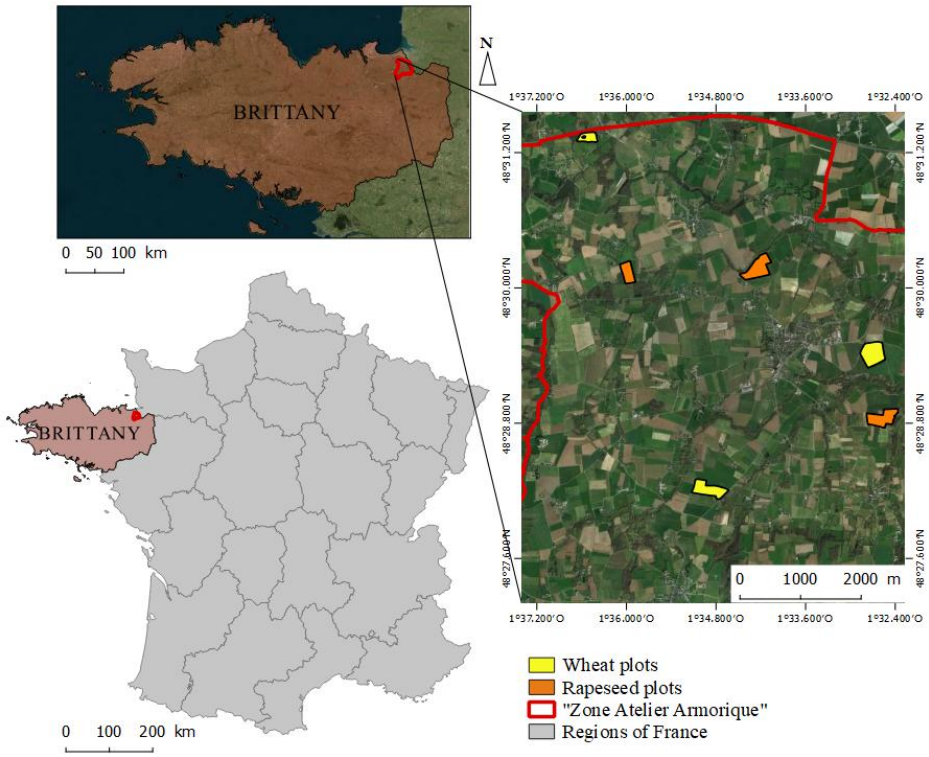

Figure 3-7. Location of crop parameters field surveys in Brittany. Satellite images and aerial photographs accessed through Bing Aerial (Microsoft® Bing™ Maps).

Table 3-7. Dates of crop parameters field surveys s in Brittany and Picardy.

Brittany		Picardy
Wheat	Rapeseed	Wheat and rapeseed
2017-03-16	2017-01-25	2017-01-18
2017-04-25	2017-03-16	2017-02-14
2017-05-17	2017-0425	2017-03-13
2017-07-05	2017-05-17	2017-04-10
	2017-07-05	2017-05-04
		2017-06-01
		2017-06-12
		2017-07-04

3.4.2.1. Phenological stages in Picardy and Brittany

The Biologische Bundesanstalt, Bundessortenamt and CHemical industry (BBCH) scale (Bleiholder, et al. 2001) was used to identify phenological stages.

In Picardy, for both crops, 5 principal phenological stages were identified. More specifically, 29 and 15 secondary phenological stages were observed for wheat and rapeseed, respectively. The samples of secondary phenological stages available for wheat and rapeseed were grouped into sub-classes to obtain a sufficient number of samples per class to train and validate the classifications.

In Brittany, four and five principal phenological stages were observed for wheat and rapeseed, respectively.

3.4.2.2. Leaf area index in Brittany

Approximately 10 hemispherical photographs were taken on the sampled plots for each field survey date. The digital hemispherical photographs were then processed using CAN-EYE software to estimate LAI (https://www6.paca.inra.fr/can-eye). Finally, LAI values were averaged per date and field sample.

3.4.2.3. Biomass and water content in Brittany

Biomass measurements were performed in homogeneous areas of 20 × 20 m (Betbeder et al. 2016b). For wheat and rapeseed, five samples of 50 cm on the ground and five plants were collected per field sample, respectively. The WB of each sample was directly weighed in situ, and the DB was measured after drying the crop (oven, 65°C, 48 h). WC in the plant equals WB minus DB.

3.4.2.4. Meteorological data

Meteorological data was used to ensure that SAR signal was not affected by rainfall or freezing on acquisition dates. Temperatures and rainfall were recorded at the Meteo-France weather stations in Saint Quentin (49°49′06″N, 3°12′22″E, located 24 km from the open field site and 52 km from the "bocage" site) for Picardy and in Vieux-Viel (48°30′47″ N, 1°33′31″W located in the middle of the ZAA) for Brittany.

3.5. Species data

3.5.1. Carabid beetles sampling in crop-dominated landscapes

We used carabid beetle samples to study the influence of wheat phenology derived from S-2 images on biodiversity. Carabid beetles were collected in 40 and 39 wheat fields from April to July in 2017 and 2018, respectively (Table 3-8). Pitfall traps filled with 200 mL of water saturated with salt and a few drops of soap were used to catch adult carabid beetles. There were two sampling station per wheat field, one located 40m from the hedgerow edge and the other 40 m from the grassed strip edge. One sampling station consisted of two pitfall traps set 1m apart. Traps were left open for two weeks prior to field collection. Finally, carabid beetles were identified to the species level (Jeannel 1941, 1942; Roger et al. 2013). In this thesis, we analyzed the two most abundant agricultural carabid beetles species named *Pterostichus Melanarius* and *Poecilus Cupreus*, to assess the ecological function of the agricultural network.

Table 3-8. Dates of carabid beetles sampling in crop-dominated landscapes.

Brittany	Picardy	Wallonia-South	Wallonia-Northwest	Wallonia-Northeast
2017-04-18/21	2017-05-02	2017-05-11	2017-05-10	2017-05-12
2017-05-23	2017-05-30	2017-06-01	2017-05-31	2017-06-02
2017-06-20	2017-06-27	2017-07-12	2017-07-11	2017-07-14
2018-04-24	2018-04-23	2018-04-23	2018-04-25	2018-04-27
2018-05-29	2018-05-29	2018-05-28	2018-05-30	2018-05-31
2018-06-26	2018-06-26	2018-07-02	2018-07-04	2018-07-06

II

IDENTIFICATION AND DESCRIPTION OF LAND COVER TYPES IN FOREST–AGRICULTURE MOSAICS USING SENTINEL-1 AND -2 TIME SERIES

Contents

Introduction

The second part of this manuscript consists of a comparative evaluation of the potential of variables derived from S-1 and S-2 data to identify and characterize the elements constituting ecological continuities in wooded landscapes. Land cover was identified and characterized in wooded landscapes in Brazil and Spain to answer the following research question: What are the most efficient Sentinel sensor and variables to identify the potential constitutive elements of ecological continuities in wooded landscapes?

In chapter 4, we evaluate the potential of S-1 data alone, S-2 data alone and the combined S-1 and S-2 data to identify and characterize land cover in forest-agricultural mosaic landscapes. The study focuses on two wooded landscapes with contrasting vegetation gradients: a temperate mountainous landscape in the Cantabrian Range (Spain) and a tropical humid forest landscape in Paragominas (Brazil). The satellite images were classified using an incremental procedure based on the ranks of importance of the input variables derived from S-1 and S-2 time series. The developed algorithm automatically selects the relevant variables and time periods to be used to best classify land cover and land use in each landscape.

CHAPTER 4

Evaluation of Sentinel-1 and 2 time Series for land cover classification of forest–agriculture mosaics in temperate and tropical landscapes

Contents

Reproduced from the article:

Mercier A, Betbeder J, Rumiano F, et al. (2019) Evaluation of Sentinel-1 and 2 Time Series for Land Cover Classification of Forest–Agriculture Mosaics in Temperate and Tropical Landscapes. Remote Sensing 11:979. https://doi.org/10.3390/rs11080979

4.1. Introduction

Mapping forest-agriculture mosaics is essential for understanding effects of land cover changes on economic (e.g. agricultural and silvicultural production, timber extraction, ecotourism) and non-market ecosystem services (e.g. carbon sequestration, water quality, stream flow, species conservation) (Gardner et al. 2013). Cropland and pastures are the largest use of Earth's ice-free land (Foley et al. 2011) and have particularly high biodiversity potential (Altieri 1999). However, this capacity refers to landscapes with heterogeneous semi-intensive agricultural systems and semi-natural elements (hedgerows, wetlands, forests) (Krebs et al. 1999; Billeter et al. 2008; Fahrig et al. 2011). In many parts of the world, land cover changes affect landscapes, causing habitat loss and fragmentation (Fahrig 2003). Habitat fragmentation decreases the size of habitats and populations and increases distances between patches of habitat, which may result in species loss (Hanski 2011).

Each species uses different kinds of habitats and requires different amounts of them (Fahrig 2003). Many species perceive landscapes in ways more complex than as a "habitat-matrix" dichotomy (i.e. dividing the landscape into "habitat", which contains all necessary resources, and "matrix", which is hostile) and use resources from different cover types (Fahrig et al. 2011). Thus, landscape management can be considered a complex process that requires characterizing the landscape composition and structure suitable for the target species. Habitat selection and resistance models are widely used as a decision support tool, since they can apply to multiple groups of species (e.g. insects, birds, herpetofauna, mammals, plants). Landscape maps are essential for developing these models, and most environmental features used in the models are derived from remote sensing imagery (Zeller et al. 2012).

Remotely sensed imagery is a common tool for straightforward land cover classification. The main difficulty is that the land cover classes in forest-agriculture mosaics are distributed along a landscape gradient, which results in misclassification. Images with high and very high spatial resolutions provide greater spatial detail and precise information (Aplin 2004; Wulder et al. 2004; Chen et al. 2017; Estes et al. 2018). However, the low temporal resolution of such data does not enable monitoring vegetation dynamics to better discriminate land cover classes that are spectrally similar. In contrast, satellite time series provide great opportunities for this purpose.

MODIS and Landsat optical time series have been used extensively for land cover classification since the 1970s. Despite a 1-2 days revisit time, however, land cover derived from MODIS has low local accuracy due to the maximum spatial resolution of 250m. The Landsat constellation has an 8-day revisit time but has a higher spatial resolution (30m) than MODIS. The S-2 satellite has even higher capacities, with a 5-day revisit time and a 10m spatial resolution (Gómez et al. 2016). Despite these high capacities, optical images sometimes cannot be used (e.g. lack of cloud-free periods) or are at the limit of their utility (e.g. optical reflectance provides information only about the top layer of vegetation). In this context, SAR images provide a reliable alternative to optical images because they are not greatly influenced by atmospheric conditions and can be acquired during the day or night. Several scattering mechanisms, including single bounce, double bounce, and volume

scattering can contribute to SAR backscatter over distributed targets such as agricultural fields (Lee and Pottier 2009), depending on crop properties (e.g. biomass, architecture, height) (Baghdadi et al. 2009; Fieuzal et al. 2013; Wiseman et al. 2014) and soil conditions (e.g. roughness, moisture) (McNairn and Brisco 2004; Baup et al. 2007; Álvarez-Mozos et al. 2009). Unlike optical data, however, SAR data are rarely used to map land cover. Some studies have focused on the complementarity of SAR and optical data, concluding that using them together provided better results than using them separately (Joshi et al. 2016). The SAR signal is sensitive to the geometry (e.g. roughness, texture, internal structure) and wetness of the observed targets, while optical reflectance is influenced by their physiology. Thus, these two spectral domains provide complementary information.

The recent SAR S-1 and optical S-2 time series provide a great opportunity to monitor forest-agriculture mosaics due to their high spatial and temporal resolutions, with a 5-day revisit time and decametric resolution. They are freely available under an open license, unlike most SAR data (e.g. TerraSAR-X, ALOS2, RADARSAT-2, COSMO-Sky Med) and optical data (e.g. SPOT, Quickbird, WorldView, Geo-Eye, Ikonos). Recent studies have demonstrated the potential of S-2 data for mapping 6-12 land cover classes from a single-date image (Immitzer et al. 2016; Clark 2017; Colkesen and Kavzoglu 2017; Haas and Ban 2018; Mongus and Žalik 2018). Studies that use S-2 time series focus on one or a few specific land cover classes, usually on homogeneous agricultural or forested landscapes located in the same climatic region . Use of S-1 data has been limited to combining them with S-2 or Landsat data, which increases classification accuracy (Inglada et al. 2016; Kussul et al. 2017; Zhou et al. 2017; Laurin et al. 2018; Reiche et al. 2018). Hence, the use of S-1 time series alone for mapping land cover classes has not yet been evaluated.

The objective of this study was to assess the potential of S-1 data alone, S-2 data alone, and combined S-1 & 2 data for mapping land cover in forest-agriculture mosaics. We focused on two landscapes with contrasting vegetation gradients: a temperate mountainous landscape in the Cantabrian Range (Spain) and a humid tropical forested landscape in Paragominas (Brazil). Although these forest-agriculture mosaics differ greatly, they perform similar ecological functions, such as conserving high levels of biodiversity and storing carbon.

Satellite images were classified using an incremental procedure based on the rank of importance of input features derived from S-1 and S-2 time series. The method automatically selects the relevant features (spectral bands and/or vegetation indices) and time periods to use to best classify land cover types in the forest-agriculture mosaics.

4.2. Study Area and Data

4.2.1. Study area

The Spanish study area is located in northwestern Spain, extending from eastern Lugo to western Cantabria. Covering the entire Cantabrian Range, it has an area of 35 700 km² (Figure 4-a). The region has an elevation of 0-2 468 m, an Atlantic climate, and remnant forest fragments that are distinct from a non-forest matrix composed mainly of pastures and heathlands in abandoned meadows (García et al. 2005; Gastón et al. 2017). Croplands constitute 22% of the study area and are composed of vines and cereals crops including wheat, barley, rye, sunflower and oats (Mateo-Sánchez et al. 2016). These crops are located in the south of the study area(Castile-Leon), most of them are irrigated (fao.org). In northern slopes of the Cantabrian range, oaks (*Quercus robur* and *Q. petraea*), beeches (*Fagus sylvatica*) and chestnuts (*Castanea sativa*) are the main species found in forested areas, while southern slopes are dominated by semi-deciduous oaks (*Q. pyrenaica* and *Q. faginea*) and evergreen oaks (*Q. ilex*), *Pinus sp*. and *Eucalyptus globulus* being relatively abundant . The major decrease in the forest area dates back to 3 000 years BP, with the transformation of large patches of natural forests into pasturelands (traditional cattle grazing and selective timber extraction). More recently, additional forests were lost due to road construction, surface mining, increased frequency of anthropogenic fires, and creation of forest plantations. In the past 20 years, reserves were established that impose legal restrictions on new land uses (García et al. 2005). Many studies focused on habitat quality for brown bear and wood grouse, two native species of the Cantabrian Range, indicating that the forest cover is essential to their presence (Quevedo et al. 2006; Gastón et al. 2017). Brown bear home ranges include forests, shrublands, rocky areas, and grasslands (Gastón et al. 2017).

The second study area is the municipality of Paragominas, Pará State, in the eastern Brazilian Amazonia, 217 km south of Belem (Figure 4-b). The municipality extends for 19 342 km², has an elevation up to 190 m, and has a tropical climate. It experienced a continuous period of deforestation from the 1960s to 2010, due mainly to cattle ranching, soybean and corn cultivation, and creation of forest plantations. Overlogging and fires degraded the remaining forests greatly (Tritsch et al. 2016; Bourgoin et al. 2018). The municipality was the main timber-producing region in Brazil in 1990. A biodiversity survey performed in the municipality showed that both landscape and within-forest disturbances contributed to biodiversity loss, with the greatest negative effects on species of high conservation and functional value (Barlow et al. 2016). In 2005, in the context of the new federal policy to fight deforestation, Paragominas was asked to establish measures against deforestation. The municipality established a new local governance model, called “Municipio Verde” (Viana et al. 2012), which aimed to fight deforestation and strengthen the ability of local institutions to develop specific environmental policies based on the Brazilian forest code. Since then, annual deforestation rates have decreased by up to 80%. Paragominas represents a case of remarkable deforestation that became a national reference for municipal-level anti-deforestation policies.

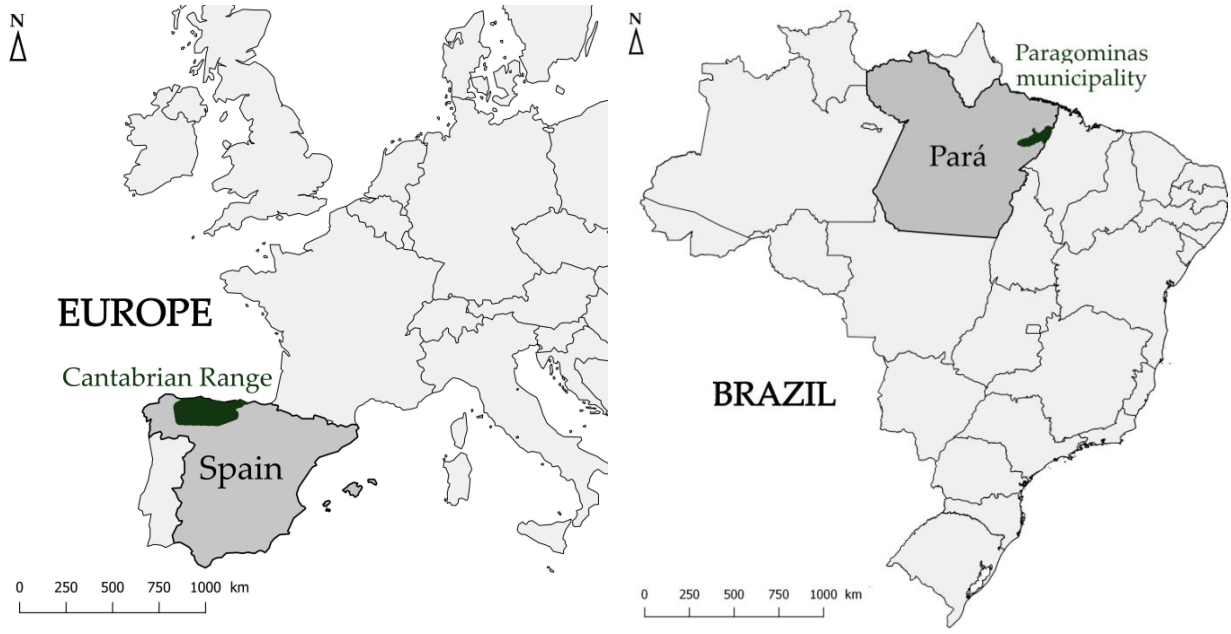

Figure 4-1.Location of (a) the Spanish study area (© EuroGeographics for the country boundaries) and (b) the Brazilian study area (© 2018 GADM for the state boundaries).

4.2.2. Data

4.2.2.1. Reference data

A set of 828 polygons was manually discriminated on the Spanish study area using aerial photographs and the Forest Map of Spain (mapama.go.es), which was developed from 1997-2006 and is the official forest inventory of the country. Its minimum mapping unit is 2.25 ha. The map is composed of polygons containing land cover and land use attributes derived from interpretation of aerial photographs and field inventory data. The 8 land cover classes discriminated in the sample data were permanent bare soils, artificial surfaces, water bodies, forested areas, shrublands, permanent herbaceous vegetation (herbaceous vegetation containing chlorophyll throughout the year), summer herbaceous vegetation, and winter herbaceous vegetation. The total area of samples per class ranged from 260-290 ha.

A set of 328 GPS points was recorded during a 3-week field mission in Paragominas in September 2017. The samples were produced by calculating polygons around the GPS points and using aerial photographs for photo-interpretation. The 7 land cover classes discriminated were bare soils, artificial surfaces, water bodies, forested areas, croplands, pastures, and "young secondary forests" (fallow land with dense but low vegetation representing early regeneration stages of forests after abandonment of agriculture or pasture). The total area of samples per class ranged from 14 ha (bare soil) to 530 ha (forested area).

4.2.2.2. Sentinel-1 time series

S-1 GRD products were acquired in Interferometric Wide Swath mode and delivered with VV and VH polarizations and an incidence angle ranging from 30.6-46.0° (Table 4-). GRD products provide multilook intensity (5 and 1 looks according to slant range and

azimuthal direction, respectively) and are projected to a ground range based on an Earth ellipsoid model (https://sentinel.esa.int/web/sentinel/user-guides/sentinel-1-sar). The range and azimuth spatial resolutions were 20 and 22 m, respectively, and the pixel spacing was 10 x 10m (Table 4-).

Table 4-1. Main characteristics of S-1A L1C images (https://sentinel.esa.int/web/sentinel/user-guides/sentinel-1-sar).

Band	C (center frequency of 5.405 GHz)
Mode	Interferometric Wide Swath
Product type	Ground Range Detected
Pixel resolution	20 × 22 m (range × azimuth)
Pixel spacing	10 × 10 m (range × azimuth)
Temporal resolution	5 days (Spain) and 12 days (Brazil)
Orbit	Ascending
Polarization	VV & VH
Swath	250 × 350 km
Incidence angle (°)	30.6-46.0

Sets of 66 and 42 S-1A images were downloaded for the Spanish and Brazilian study areas, respectively. S-1A images were acquired on two orbits (5-day and 12-day revisit time for Spain and Brazil, respectively), and 3 images were required to cover each study area. In total, 22 mosaics were produced from December 2016 to September 2017 for the Spanish study area, while 14 mosaics were produced from November 2016 to December 2017 for the Brazilian study area.

4.2.2.3. Sentinel-2 time series

The S-2 sensor acquired optical images during the same periods, with spatial resolutions of 10 and 20 m, and a spectral resolution of 10 bands (Table 4-12). For the Spanish study area, a series of 6 S-2 mosaics was acquired from December 2016 to August 2017. The tiles were downloaded in level 2A, which provides Top Of Canopy (TOC) reflectances and a cloud and shadow mask (sentinel.esa.int/web/sentinel/user-guides/sentinel-2-msi). Eight S-2 tiles were necessary to cover the entire study area (7-43 days between 2 tiles). Tiles with minimum cloud cover were selected. The mosaics were projected onto the ETRS89/ETRS-TM30 system (EPSG 3042).

For the Brazilian study area, only one mosaic was produced due to the frequent heavy cloud cover (July 2017). The tiles were downloaded in level 1C, which provides Top Of Atmosphere reflectances and orthorectified images mask (sentinel.esa.int/web/sentinel/user-guides/sentinel-2-msi). Nine S-2 tiles were necessary to cover the entire study area (no more than 12 days between 2 tiles). The mosaic was projected onto the WGS84/UTM 22S system.

Table 4-2. Main characteristics of S-2 L1C/ L2A images (sentinel.esa.int/web/sentinel/user-guides/sentinel-2-msi).

Spatial and spectral resolutions	*10 × 10 m* B2 (490 nm), B3 (560 nm), B4 (665 nm) and B8 (842 nm) *20 × 20 m* B5 (705 nm), B6 (740 nm), B7 (783 nm), B8a (865 nm), B11 (1610 nm), B12 (2190nm)
Temporal resolution	5 days
Swath	290km
Tile size	100 x 100 km

4.3. Methodology

The method was developed to assess the potential of S-1 data alone, S-2 data alone, and combined S-1 & 2 data for mapping land cover of forest-agriculture mosaics (Figure 4-2).We focused on automatically selecting the relevant features (spectral bands and/or vegetation indices) and time periods to classify land cover types. The method used to select and classify features into land cover types was based on the incremental classification developed by Inglada et al. (Inglada et al. 2016).

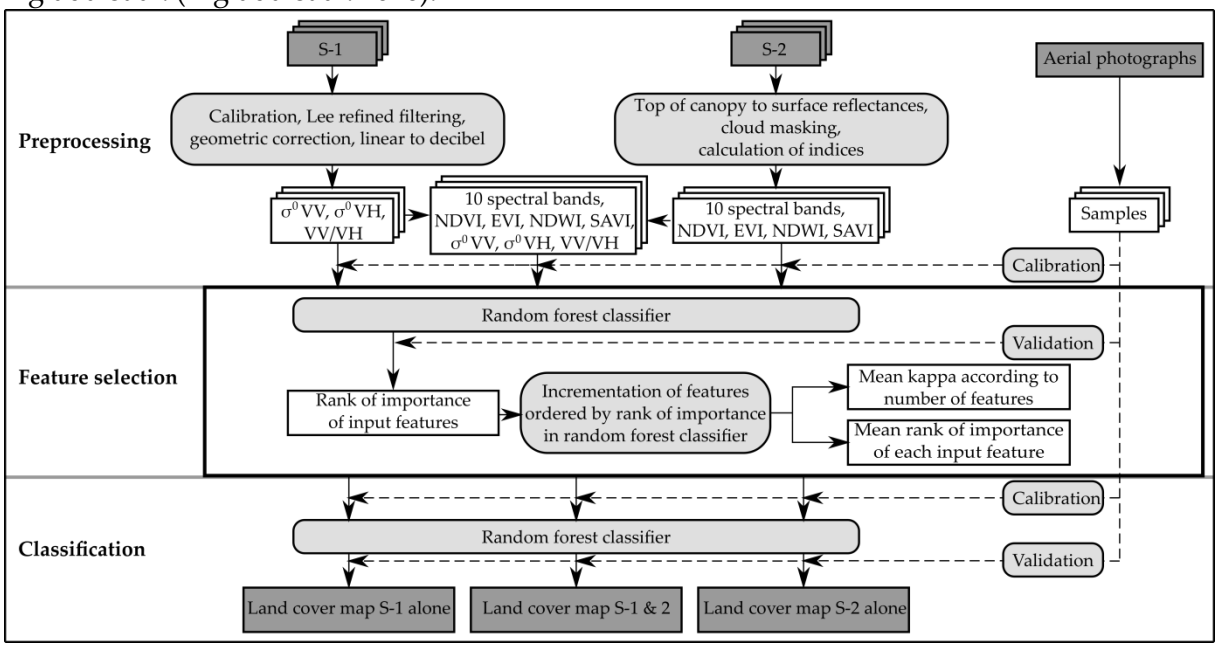

Figure 4-2. Flowchart of the image processing procedure.

4.3.1. Samples selection

A set of 30 pairs of training and validation polygons were randomly selected from the reference polygons with a 50/50 ratio. The 30 random pairs were performed in order to perform 30 trainings and 30 corresponding validations, allowing to compute average performances with confidence intervals (Inglada et al. 2016). The 50/50 ratio allows a more reliable comparison between training and validation samples than a ratio with a lower proportion of validation samples.} For each set of selected training polygons, 300 and 1000 pixels per class were randomly selected for the Brazilian and Spanish study areas, respectively. The same random selection of pixels was applied to each set of associated validation polygons. This selection was performed to avoid over-representing large polygons

at the expense of small polygons in the training and validation samples and to have the same number of samples for each class.

4.3.2. Preprocessing

The S-1 images were preprocessed using the ESA Toolbox, (http://step.esa.int/main/toolboxes/sentinel-1-toolbox/). The images were first radiometrically calibrated to extract the backscattering coefficients (σ^0VV, σ^0VH) (Figure 4-2).

A speckle filter was then applied (Lee refined, with a 7 x 7 window, (Lee et al. 1994). The images were geo-coded using SRTM data to correct topographic deformations (geometric correction accuracy < 1 pixel) and were projected onto the ETRS89-TM3/ETRS0 system (EPSG 3042) and the WGS84/UTM 22S system (EPSG 32722) for the Spanish and the Brazilian study areas, respectively. A ratio channel was produced (VV/VH) from the backscattering coefficient images. All images were then converted from linear to decibel (dB).

Spectral bands and indices were derived from S-2 images. For the Brazilian study area, the Sen2Cor application (Sen2Cor, ESA, http://step.esa.int/main/third-party-plugins-2/sen2cor/) was used to transform L1C tiles to level L2A (TOC). Four vegetation indices commonly used in remote sensing were calculated for each S-2 mosaic for both study areas: EVI, NDVI, NDWI, and SAVI (Table 4-3). Each mosaic was composed of 10 spectral bands and 4 vegetation indices.

Table 4-3. Vegetation indices calculated from S-2 images for the Spanish study area. B= Blue band, G = Green band, R = Red band.

Vegetation index	Formula	S-2 band used	Original author
NDVI	(NIR-R)/(NIR+R)	(B8-B4)/(B8+B4)	(Rouse et al. 1973)
NDWI	(NIR-G)/(NIR+G)	(B8-B3)/(B8+B3)	(Gao 1996)
EVI	2.5×(NIR-R)/(NIR+6×R-7.5×B)+1)	2.5×(B8-B4)/(B8+6×R-7.5×B2)+1)	(Huete et al. 2002)
SAVI	(NIR-R)×1.5/(NIR+R+0.5)	(B8-B4) ×1.5/(B8+B4+0.5)	(Huete 1988)

4.3.3. Feature selection and classification

Incremental classification was performed using a RF classifier. Two output analyses – mean rank of importance of each input feature and mean kappa index as a function of the number of features – were used to select the relevant features to use in the final classification. Incremental classification analyzes mapping quality as the type and number of features used are added, thus determining at what combination and number of features the classification reaches an acceptable quality (Inglada et al. 2016). For each training and validation set (30 pairs), a RF algorithm was first applied to all of the features (dates and bands) to rank them in order of importance based on the mean decrease in the Gini index. Calle and Urea (2011) demonstrated more robust results for exploring ranking stability using the mean decrease in the Gini index instead of the mean decrease in accuracy. The mean rank of importance of each feature was derived from the 30 ranks obtained from the 30 pairs of training and validation samples. We then ran as many RF algorithms as number of features, starting with the two most important features and then adding the less important features until all of the features were processed. The kappa index was calculated for each classification to estimate the accuracy of the land cover classifications (Cohen 1960). Rosenfield and Fitzpatrick-Lins (1986) advised using the kappa index to measure classification accuracy.

We chose the RF algorithm (Breiman 2001) due to its advantages of having low sensitivity to feature selection, simple parameterization, and short calculation time (Belgiu and Drăguţ 2016; Pelletier et al. 2017). We used it to select and classify features. In both cases, the number of trees was set to 100 to reduce calculation time since Pelletier et al. (2016) demonstrated that it can be set to 100 without a major loss in accuracy. The experiments were performed using the randomForest package of R software (randomForest package version 4.6-14, Andy Liaw, https://cran.r-project.org). We used the OrfeoToolbox to calculate the final RF prediction (OrfeoToolbox version 6.6.1., CNES, https://www.orfeo-toolbox.org}).

4.3.4. Percentage of pixels confused

For both study areas, the features selected from analyses of S-1 data alone and S-2 data alone were used to calculate 30 RF classifiers. For each pair of classes, we calculated the percentage of confused pixels in relation to the total number of misclassified pixels. The following equation (Eq. 4.1):

$$P_{conf\ Pixel\ pairs\ (i,j)} = \frac{NbPixels[i,j]\ +\ NbPixels[j,i]}{TotalPixels\ -\ (\Sigma(PixelDiagonal))} \quad (4.1)$$

where i and j are the classes in the pair, was applied to the 30 confusion matrices derived from the 30 RF classifications using the 30 pairs of training and validation samples. The mean of the percentages was calculated for each pair of classes. We then calculated the mean percentage of confused pixels per pair of classes in relation to the total number of misclassified pixels using the most important S-1 features and most important S-2 features.

4.3.5. Comparison of classifications

We used McNemar's X^2 test to analyze the significance of the difference or resemblance between the classifications derived from S-1 data alone vs. S-2 data alone, S-1 data alone vs. the combined S-1 & 2 data, and S-2 data alone vs. the combined S-1 & 2 data. This test, based on a binary 2 x 2 contingency matrix, shows the proportion of pixels correctly and incorrectly classified in two classification runs and allows the use of non-independent samples. A X^2 value lower than 3.14 means that the two classifications compared are non significantly different (Foody 2004).

4.4. Results

4.4.1. Contribution of Sentinel 1 & 2 time series to map land cover

To estimate the contribution of the optical and SAR Sentinel time series, we analyzed the mean kappa index as a function of the number of input features. The combined use of S-1 & 2 data provided the best results for both study areas (Figure 4-3). However, for the standard deviation of the kappa index, results of the combined use of S-1 & 2 data were similar to those of S-2 data alone. The improvement in classification due to combining S-1 & 2 data rather than using S-2 data alone was perceptible up to 30 input features for the Spanish study area. For the Spanish study area, using the top 10 S-2 features out of the 84 total S-2 features increased the mean kappa index by ca. 0.25 (i.e. from 0.58 to 0.83); the mean kappa index continued to increase slightly up to 40 input features and then stabilized. For the Brazilian study area, using the top 7 S-2 features out of the 14 total S-2 features increased the mean

kappa index by ca. 0.15 (i.e. from 0.70 to 0.85); the mean kappa index continued to increase slightly up to 9 input features and then stabilized.

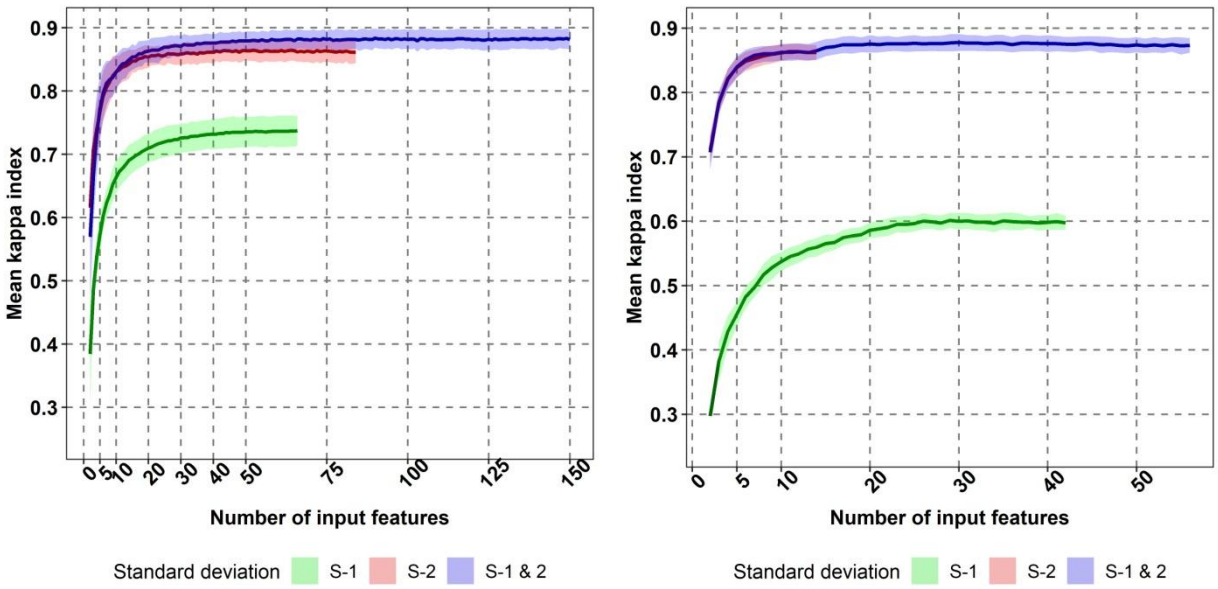

Figure 4-3. Mean kappa index of the incremental classifications for S-1 data alone (green), S-2 data alone (red), and combined Sentinel-1 & 2 data (blue) as a function of the number of input features for (a) the Spanish study area and (b) the Brazilian study area.

Using S-1 data alone yielded the lowest accuracy for both study areas. The mean kappa index was higher for the Spanish area than for the Brazilian area, as was the maximum kappa index (ca. 0.73 and 0.60, respectively). Compared to the mean kappa indices of S-2 data alone, those of S-1 data alone were lower by 0.08-0.20 for the Spanish study area and by 0.28-0.40 for the Brazilian study area.

4.4.2. Importance of input features

When using S-2 data alone, bands 11 and 12 (the SWIR domain) were the most important features for both study areas (mean rank of importance of 1.77 (B11) and 4.07 (B12), and of 1.43 (B12) and 1.63 (B11) for the Spanish and Brazilian study areas respectively) (Figure 4-4). For the Spanish area, the vegetation indices were relevant, with 11 of them among the top 20: 4 SAVI and 4 NDVI (1 each in January, March, June, and July), 2 NDWI (in January and March) and, although less relevant for classifying forest-agriculture mosaics, EVI. For the Brazilian study area, NDWI was the most relevant index (ranked 3rd,), while other spectral bands were more relevant than EVI, NDVI, or SAVI.

When assessing the relevance of time periods using S-2 data alone (Figure 4-4a), January was the most important month for discriminating the 8 land cover classes, since it was the month of the top 6 features (mean rank of importance=1.77-11). In addition, March and July appeared among the top 10 features. The least important months were August and April.

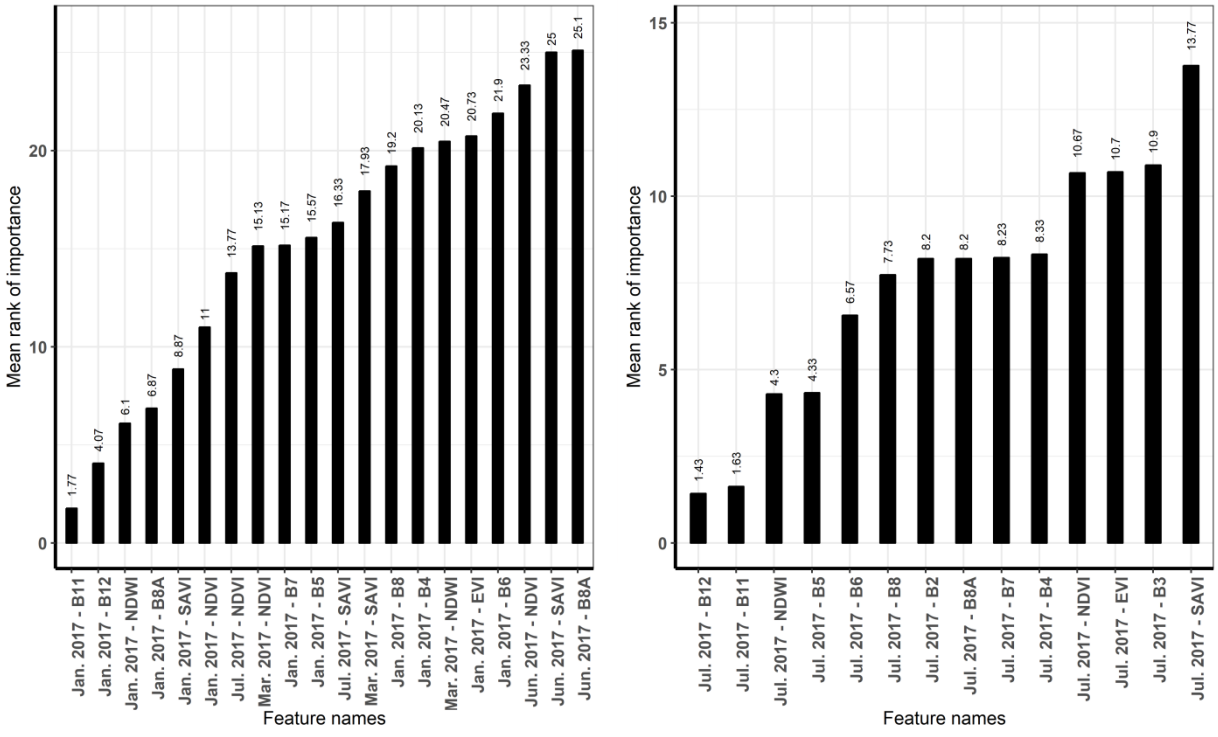

(a) (b)

Figure 4-4. Mean rank of importance of the most important features for S-2 data alone for (a) the Spanish study area and (b) the Brazilian study area.

When using S-1 data alone, the VV/VH ratio was not useful for mapping land cover in these two forest-agriculture mosaics. For both study areas, VV polarization was the most important feature. For the Spanish and Brazilian study areas, the VV mean ranks of importance were of 2.03 and 2.13, respectively (Figure 4-5). The top 20 features, however, had a nearly equal number of VV and VH features (10 VV and 9 VH polarization dates for the Spanish study area, 11 VV and 9 VH polarization dates for the Brazilian study area). When assessing the relevance of time periods using S-1 data alone, the months from December to May were relevant for the Spanish study area. In contrast, months from both dry and wet seasons were among the top 10 features (January, March, April, July, September, November, December) for the Brazilian study area.

When combining S-1 & 2 data, the top 20 important features were all S-2 features for the Spanish study area and mostly S-2 features (the top 14) for the Brazilian study area (Figure 4-6).

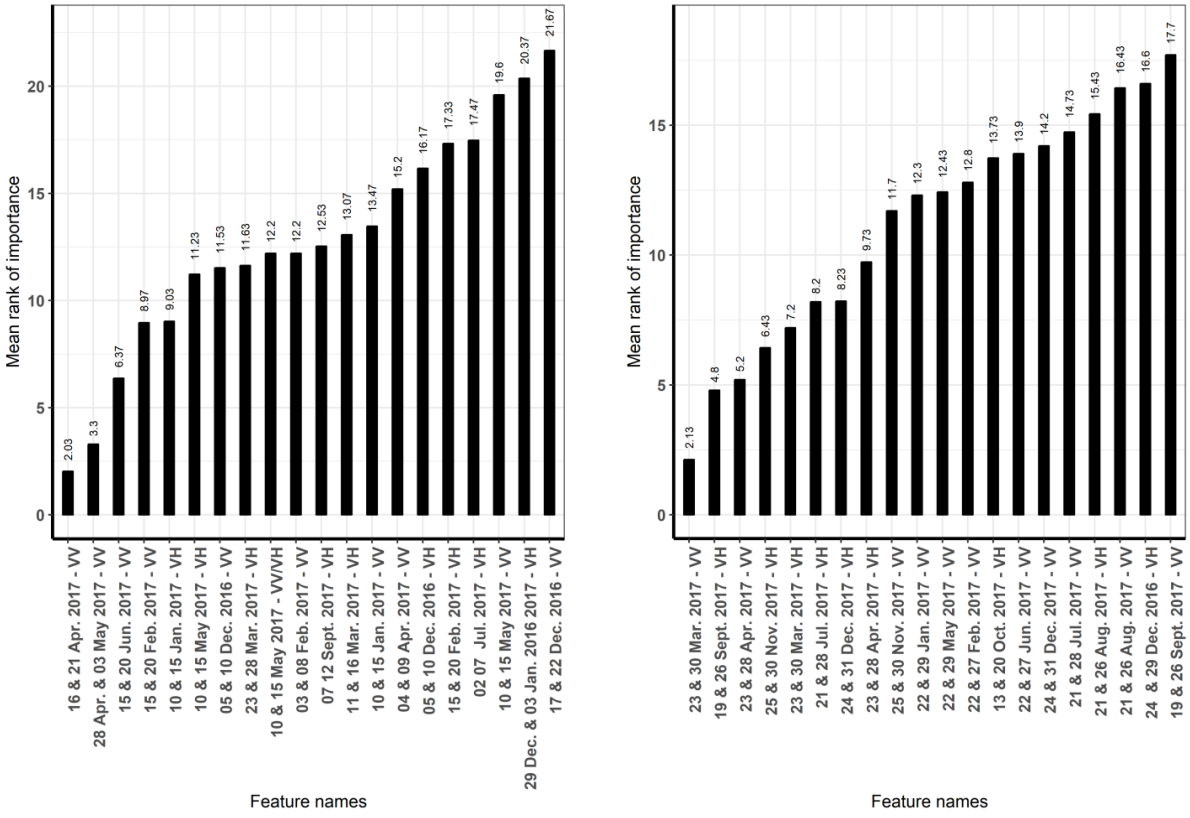

(a) (b)

Figure 4-5. Mean rank of importance of the most important features for S-1 data alone for (a) the Spanish study area and (b) the Brazilian study area.

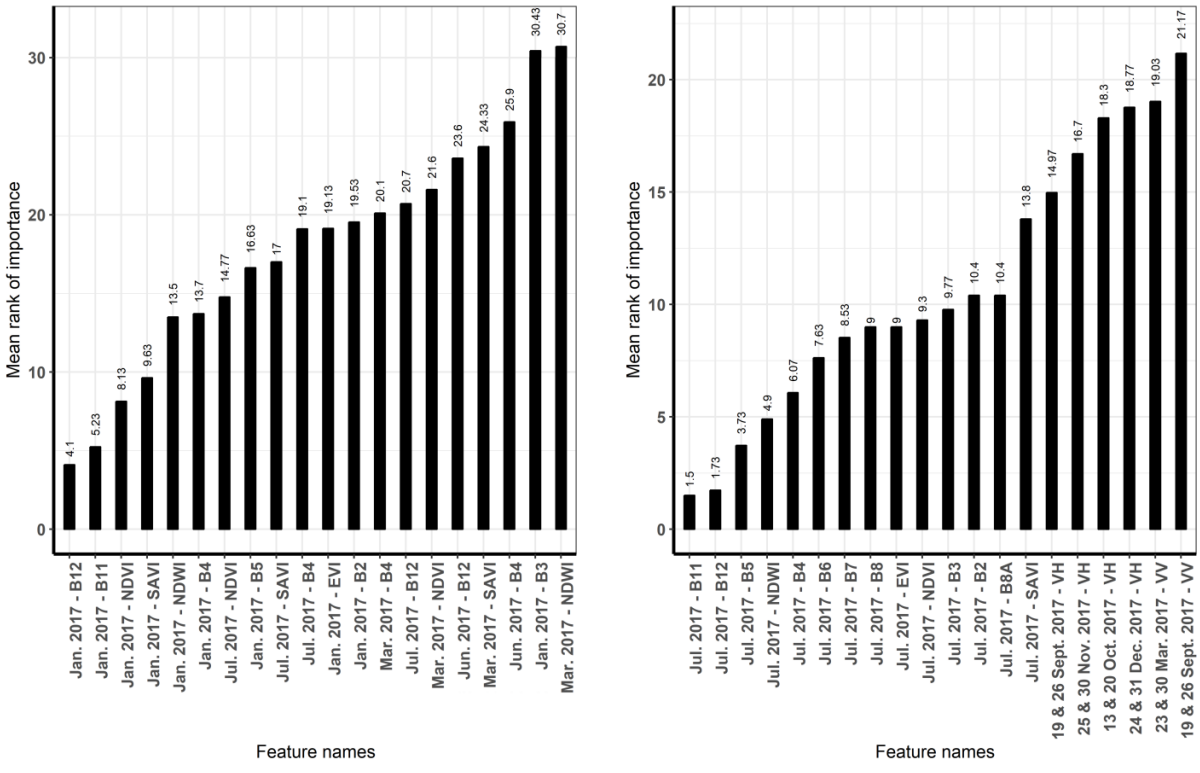

(a) (b)

Figure 4-6. Mean rank of importance of the most important features for the combined use of Sentinel-1 & 2 data for (a) the Spanish study area and (b) the Brazilian study area.

As a trade-off between accuracy and processing time, we decided to maintain a minimum but sufficient number of features for classification (Table 4-4). In the following experiments, we choose to keep the 20 most important S-1 features and 10 S-2 features, and the 10 most important S-1 features and 7 S-2 features on the Spanish and Brazilian study areas, respectively (Table 4-4). Due to the large majority of S-2 features in the top 20 important features of combined S-1 & 2 data (Figure 4-7), we decided to combine the previously selected features of S-1 data alone and S-2 data alone to predict the land cover classes combining S-1 & 2 data (Table 4-4).

Table 4-4. Number of top important features selected for predictions for the Spanish and Brazilian case studies.

Type of Data	Spain	Brazil
S-1 alone	20	10
S-2 alone	10	7

4.4.3. Confusion between classes

Using the S-1 features for the Spanish study area, forested areas vs. shrublands, shrublands vs. permanent herbaceous vegetation, and bare soils vs. winter vegetation were the pairs of classes most often confused (Figure Figure 4-7a). Using the S-2 features, bare soils vs. artificial surfaces, bare soils vs. winter vegetation, and forested areas vs. shrublands were the most confused pairs of classes (Figure 4-7b). Forested areas and shrublands were not well discriminated using S-1 or S2 features. Shrublands vs. permanent vegetation were better discriminated using S-2 data than S-1 data.

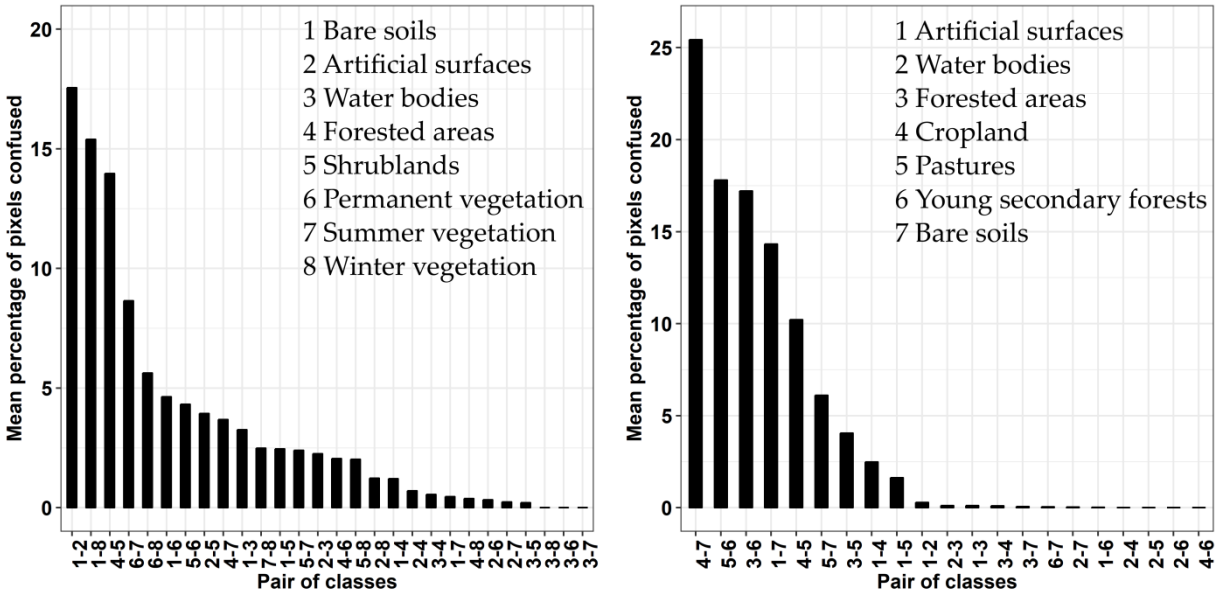

(a) (b)

Figure 4-7. Mean percentage of pixels confused per pair of classes in relation to the total number of misclassified pixels using (a) the top 20 S-1 features and (b) the top 10 S-2 features of the Spanish study.

Using the S-1 features for the Brazilian study area, most forested areas and young secondary forests pair of classes was confused, unlike the other pairs of classes, including forested areas vs. pastures (Figure 4-8a). Using the S-2 features, cropland vs. bare soils, pastures vs. young secondary forests, and forested areas vs. young secondary forests were

the most confused pairs of classes (Figure 4-8b). Forested areas vs. young secondary forests were better discriminated by S-2 than S-1 features. However, pastures and young secondary forests were better discriminated by S-1 than S-2 features. On both study areas, bare soils vs. artificial surfaces were discriminated better by S-1 data than S-2 data features.

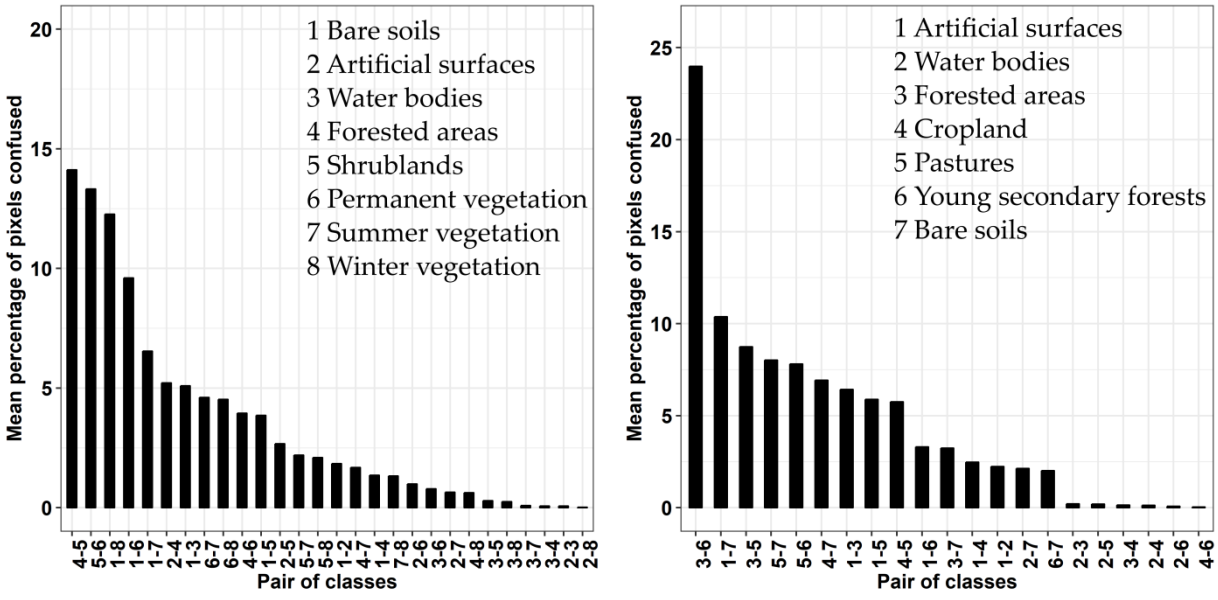

(a) (b)

Figure 4-8. Mean percentage of pixels confused per pair of classes in relation to the total number of misclassified pixels using (a) the top 10 S-1 features area and (b) the top 7 S-2 features of the Brazilian study area.

4.4.4. Prediction of selected features

Misclassification errors in the land cover map of forest-agriculture mosaics of the Spanish study area – due to cloud confusions using S-2 data alone and slopes using S-1 data alone – were partly corrected using combined S-1 (Figure 4-9).

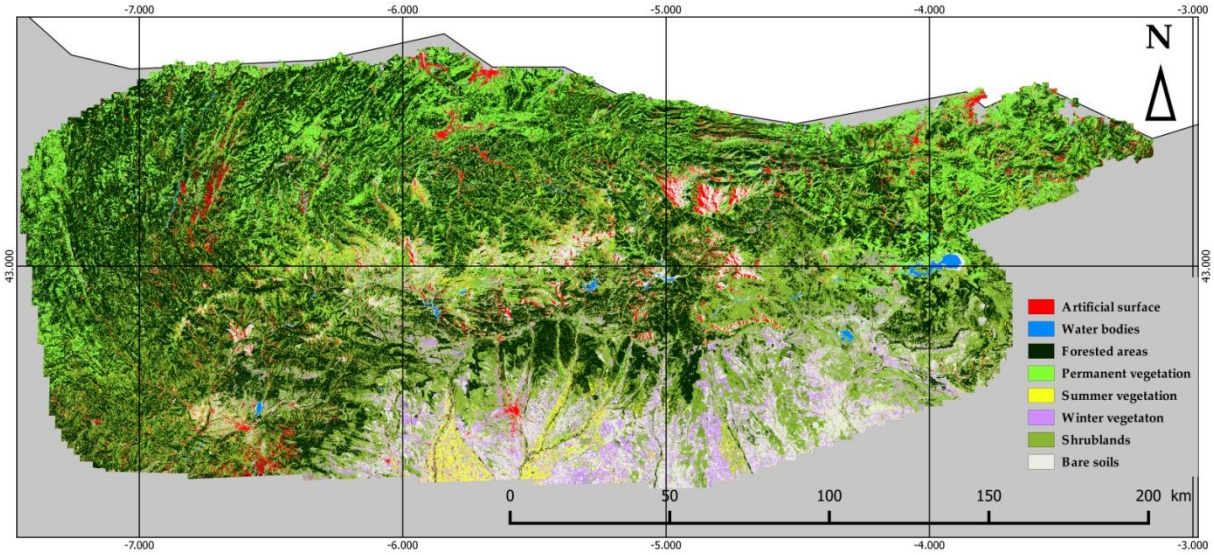

Figure 4-9.Classification of the Spanish study area using combined Sentinel-1 & 2 data.

The combined S-1 & 2 classification of the Brazilian study area (Figure 4-10) was more accurate than classification by S-2 data alone. Misclassification of cropland, which was confused with artificial surfaces using S-2 data alone, was partly corrected with combined S-1 & 2 data.

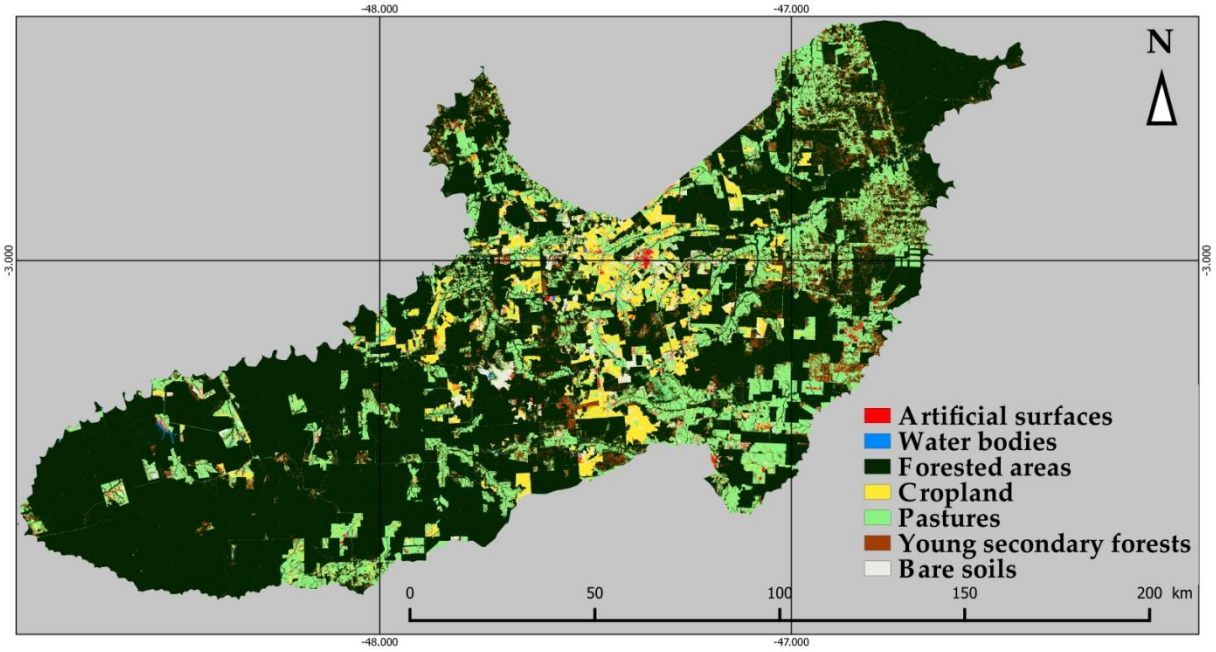

Figure 4-10. Classification of the Brazilian study area using combined Sentinel-1 & 2 data.

4.4.5. McNemar X^2 test results.

According to McNemar's X^2 test, all land cover class predictions differed significantly ($X^2 > 3.14$), and S-2 data alone vs. combined S-1 & 2 data for the Brazilian study area is not significant (p-value=NS) (Table 4-5). Thus, we concluded that all classifications differed.

Table 4-5. McNemar's X^2 test results for the Spanish and Brazilian case studies. The X^2 value less than 3.14 indicates that the two classifications were not significantly different.

	Spain		Brazil	
Classifications compared	X^2	p-value	X^2	p-value
S-1 data alone vs. S-2 data	113.23	<0.0001	368.47	<0.0001
S-1 data alone vs. S-1 & 2	379.82	<0.0001	439.00	<0.0001
S-2 data alone vs. S-1 & 2	105.39	<0.0001		NS

4.5. Discussion

4.5.1. Relative contributions of S-1 and S-2 data to map land cover of forest-agriculture mosaics

The land cover classes that comprise forest-agriculture mosaics are distributed along a landscape gradient, with transition classes such as shrublands to forest or pasture to young secondary forests, which result in misclassifications. S-1 data alone were least accurate for mapping land cover of forest-agriculture mosaics, with a best mean kappa index of 0.73, vs. 0.87 and 0.89 for S-2 data alone and combined S-1 & 2 data, respectively (Figure 4-3). For example, S-2 data discriminated forested areas from young secondary forests better than S-1 data for the Brazilian study area (Figure 4-8). This may be because SAR sensors are sensitive

to vegetation structure, while optical sensors are sensitive to chlorophyll content. Thus, when observed at a 10m resolution, broad vegetation classes were discriminated more easily by their physiology than their physical structure. Also, VV and VH polarizations were the most important S-1 features for discriminating land cover classes, while the VV/VH ratio was not useful (Figure 4-5). While it is known that VH polarization is more sensitive to vegetation than VV polarization (Patel et al. 2006), results show that both polarizations had an equivalent low contribution to classify forest-agriculture mosaics, as well as the ratio VV/VH. We can conclude that in this case the C-band of S-1 was not relevant to classify vegetation classes. In general, the C-band SAR is less suitable than L-Band for forest change monitoring due to a lower penetration depth and a rapid saturation of the signal (Woodhouse 2017). For example, Patel et al. (2006) demonstrated that L-band is more sensitive to plant density than C-band, and that C-band interacts mostly with the primary branches of the canopy while L-band within the vegetation canopy. We used S-1 GRD products that record backscattering coefficients (VV and VH) because they require less processing time than SLC products, which preserve the phase information. However, using texture, coherence, and polarimetric indices derived from full-polar RaDAR data, such as RADARSAT-2 data, could improve classification based on S-1 data alone (Ranson et al. 2001; Sonobe et al. 2015; Du et al. 2018; Roychowdhury). Thus, although Bagdhadi et al. (2016) concluded that using polarimetric indices (SE and span) derived from polSAR RADARSAT-2 images did not improve estimates of soil moisture and vegetation parameters, Betbeder et al. (2014) demonstrated the greater utility of the SE index than backscattering coefficients for mapping wetland vegetation using dual-pol TerraSAR-X time series. The best mean kappa index achieved with S-1 data was higher for the Spanish study area than for the Brazilian study area (0.73 vs 0.60, respectively) (Figure 4-3). This could be due to differences in the classification methods (different numbers of classes and land cover types) and to the number of S-1 images used to classify land cover types (22 dates for the Spanish study area vs. 14 dates for the Brazilian study area). %More misclassification errors were observed in high-relief areas, which is consistent with the literature (Lee and Pottier 2009).

For the Spanish study area, the classification results achieved using S-1 data alone show that misclassification errors are most often located on mountain slopes. These errors are due to the acquisition of SAR images in slant range geometry that causes layover and foreshortening effects (Lee and Pottier 2009). Moreover, it is known that soil moisture and roughness influence the RaDAR backscatter depending on frequency, polarization and the incidence angle of the incoming microwave. Holah et al. (2005) found that the sensitivity to surface roughness is more important using HH and HV polarizations than VV polarization. However, Baghdadi et al. (2008) demonstrated that the soil moisture was not very dependent on polarization. The effects of soil moisture on forest-agriculture classification are rather limited using C-band due to a low penetration depth of the microwaves compared to L-band (Ulaby et al. 1996), however C-band is more sensitive to roughness (Mattia et al. 1997). Lastly, the higher the incidence angle, the more important the sensitivity of the SAR to surface roughness(Fung and Chen 1992).

However, S-1 data sometimes discriminated better than S-2 data – for bare soils and artificial surfaces – (Figure 4-7Figure 4-8) because the SAR signal reacts differently to these two land cover classes, with double-bounce on buildings and single-bounce on flat bare soils (Lee and Pottier 2009), while their spectral signatures in the optical domain are similar (high

reflectance values in green, blue and red bands). When using S-2 data alone, SWIR bands were the most important features for discriminating land cover classes (Figure 4-2Figure 4-4). The importance of S-2 SWIR bands has been demonstrated for mapping vegetation and forest (Immitzer et al. 2016; Chrysafis et al. 2017). Vegetation indices derived from S-2 data (e.g. SAVI, NDVI, NDWI) discriminated better than spectral bands for the Spanish study area, while NDWI was the most important vegetation index for the Brazilian study area. The sensitivity of the blue band to water contained in vegetation could explain why NDWI is well suited to tropical vegetation, while NDVI saturates at high biomass values (Huete et al. 2002; Jackson et al. 2004). The EVI, which was developed for MODIS, was a less important feature than other vegetation indices for both study areas. It could be interesting to calculate other vegetation indices that are used for crop discrimination such as S2REP, IRECI, MTCI or SRI (Simple Ratio Index) (Jordan 1969; Frampton et al. 2013).

The best mean kappa index using combined S-1 & 2 data (0.88) did not differ greatly from that using S-2 data alone (0.86) (Figure 4-3). Thus, the use of S-2 data alone was sufficient to discriminate the land cover classes with high accuracy. However, the backscattering intensity from S-1 data alone provided additional relevant information, since predictions of land cover classes using S-1 data alone, S-2 data alone, and combined S-1 & 2 data differed according to McNemar's X^2 test (Table 4-5). For example, the misclassification between cropland and artificial surfaces for the Brazilian study area when using S-2 data alone was partly corrected using combined S-1 & 2 data (Figure 4-10).

4.5.2. Using S-1 and S-2 data to identify the key time periods for classifying land cover

Based on the classification results using S-1 data alone, S-2 data alone, and combined S-1 & 2 data, classification accuracy was strongly related to the number of dates. Classification accuracy increased when dates were added to the RF classifier (Figures Figure 4-3Figure 4-4aFigure 4-5Figure 4-6). The relevance of high temporal resolution underlines the importance of describing and taking into account the phenology of vegetation to map forest-agriculture mosaics. For the Spanish study area, January, March, June, and July features are among the top 20 important S-2 features (Figure 4-4a). This may have been because the S-2 sensor is sensitive to chlorophyll content in vegetation, and these months are key periods of chlorophyll activity. The features of the months from December to May were among the top 20 S-1 features for this study area, while the summer period was not relevant (Figure 4-5a). This is probably because SAR sensors, which are sensitive to the internal structure of elements, penetrate vegetation better during the leaf-off period. Only one S-2 date was used for the Brazilian study area, which precluded studying the importance of time period. In addition, no clear time periods emerged from the importance ranks of the S-1 time series (Figure 4-5b). Thus, no intra-annual time period seems more important than others for S-1 time series for discriminating land cover types in Paragominas. Unlike the Cantabrian Range, where the seasons differ, temperatures and precipitation are relatively constant in Pará, with a drier season from July to October (https://www. worldweatheronline.com/para-weather/para/br.aspx). In addition, the dynamics of human practices in pastures, forested areas, and plantations are inter-annual rather than intra-annual (Piketty et al. 2015).

4.5.3. The robustness of the method for different landscapes

The results show that the method can be applied to forest-agriculture mosaics in two landscapes with contrasting climates (i.e. tropical, temperate) and vegetation types (e.g. tropical forests, shrublands, coniferous and deciduous forests). S-1 and S-2 features were selected according to their respective importance in each study area, which highlighted relevant features and time periods for the two areas. Land cover maps of the two study areas were produced with a high degree of accuracy and a short processing time. Time series are used to map the land cover of forest-agriculture mosaics, but processing them requires high computational capacity. The method enabled focusing on specific time periods and features to reduce the time required for image processing.

4.6. Conclusion

An incremental procedure based on ranking the importance of the input features derived from S-1 and S-2 time series was used to discriminate land cover classes in forest-agriculture mosaics. The method automatically selected relevant features (spectral bands and/or vegetation indices) and time periods to classify land cover types in such landscapes. S-2 data alone were more relevant than S-1 data alone for mapping the land cover of forest-agriculture mosaics, and combining S-1 & 2 data slightly improved results compared to those of S-2 data alone. Using polarimetric indices, such as the SE index, which has already shown potential for characterizing vegetation, can improve predictions of S-1 data alone. Indeed, SAR data are useful in cloudy regions; the high cloud cover in the S-2 time series was the main source of misclassification errors.

III CHARACTERIZATION OF CROPS USING SENTINEL-1 AND 2 TIME SERIES

Contents

Introduction

This part of the manuscript aims at answering the following question: What are the most efficient Sentinel sensor and variables to identify and characterize the potential constitutive elements of ecological continuities in crop-dominated landscapes? Our assumption is that crop phenonologies play a major role in the structure of these continuities. For that purpose, we comparatively evaluated the potential of variables derived from S-1 and S-2 data to estimate phenological stages and biophysical variables in wheat and rapeseed crops.

In chapter 5, we evaluate the potential of S-1 data alone, S-2 data alone and the combined of S-1 and S-2 data to identify the principal and secondary phenological stages of wheat and rapeseed in Picardy (France). More specifically, the aim of this study was to evaluate the interest of polarimetric indicators derived from S-1 data and to determine the number and type of S-1 and S-2 variables necessary to discriminate the phenological stages of wheat and rapeseed. We estimated the performance of spectral bands and vegetation indices derived from S-2 and backscatter coefficients and polarimetric indicators derived from S-1. Satellite images were classified using the incremental method developed in the previous study (Mercier et al. 2019b).

In chapter 6, we continue our research on crop characterization by evaluating the potential of S-1 and S-2 data to estimate the LAI, WB, DB and WC of wheat and rapeseed in Brittany (France). We compared the predictive power of spectral bands and vegetation indices derived from S-2 and backscatter coefficients and polarimetric indicators derived from S-1 using GPR.

CHAPTER 5

Evaluation of Sentinel-1 and 2 time series for predicting wheat and rapeseed phenological stages

Contents

Reproduced from the article:

Mercier A, Betbeder J, Baudry J, et al. (2020a) Evaluation of Sentinel-1 & 2 time series for predicting wheat and rapeseed phenological stages. ISPRS Journal of Photogrammetry and Remote Sensing 163:231–256. https://doi.org/10.1016/j.isprsjprs.2020.03.009

5.1. Introduction

Monitoring crops is important for many agricultural and ecological applications, such as estimating crop yields (Maas 1988; Jin et al. 2018), preventing disease and insect infestation (Hatfield and Pinter 1993), applying fertilizer (Diacono et al. 2013; Bouchet et al. 2016) and managing water resources (Duchemin et al. 2015). Identifying and predicting phenological stages provide essential information for precision agriculture. Considering specific phenological stages can optimize irrigation and fertilizer application schedules (Sakamoto et al. 2005; Bouchet et al. 2016). Some phenological stages are more sensitive to pests and diseases, thus identifying and predicting these stages can prevent pest outbreaks and diseases and reduce the use of pesticides (Vreugdenhil et al. 2018). Finally, phenological stages can be used as indicators of global warming on terrestrial ecosystems (Menzel et al. 2006). One of the main current challenges is to identify principal and secondary phenological stages of wheat and rapeseed that are two of the most important crops in the world in terms of harvested area (Food and Agriculture Organization of the United Nations 2017). Principal phenological stages are defined as long-duration developmental phases of plants, while secondary stages are short developmental steps within them (Bleiholder, et al. 2001).

The recent SAR S-1 and optical S-2 sensors, which acquire image time-series at a high temporal frequency (every 5-12 days, depending on the acquisition mode and location in the world) and high spatial resolution (2.3 m and 13.9 m in range and azimuth directions, respectively, for S-1 bands; 10, 20 and 60 m spatial resolutions for S-2 bands), provide a unique opportunity to monitor crops regularly at fine grain scale. Moreover, S-1 & 2 data are freely available under an open license.

Several features (i.e. spectral bands, vegetation indices and biophysical variables) derived from optical remotely sensed data have demonstrated their great potential to predict crop parameters such as yield, biomass and phenological stages (Quarmby et al. 1993; Doraiswamy et al. 2004; Mulla 2013; Bontemps et al. 2015; Pan et al. 2015; Betbeder et al. 2016b). For S-2 time series, significant relationships have been found between S-2 and vegetation indices: LAI, leaf chlorophyll concentration and canopy chlorophyll content for potato crops in the Netherlands (Clevers et al. 2017) and for maize, garlic, oat, onion, potato, sunflower, alfalfa and grape crops in Spain and Italy (Frampton et al. 2013). The potential of S-2 red-edge bands for estimating LAI was demonstrated for maize, wheat, rapeseed, barley, sugar beet, sunflower, onion and other vegetable crops in Spain and Germany and for winter wheat in northern China (Pan et al. 2018). Veloso et al. (2017) found that S-2 NDVI was highly sensitive to the phenological stages of winter and summer crops in southern France. Despite these abilities, a continuous time-series of optical images is difficult – if not impossible – to acquire due to the cloud-free dependence of optical acquisitions and the signal provides information only about the top layer of vegetation. In this context, Synthetic-Aperture RaDAR (SAR) images are a reliable alternative to the limitations of optical images since microwaves are not sensitive to atmospheric or light conditions. Unlike optical reflectance, backscattering coefficients depend on soil conditions (roughness and moisture) during early plant phenological stages (McNairn and Brisco 2004; Baup et al. 2007; Álvarez-Mozos et al. 2009) and later on crop properties (biomass, architecture, height) (Baghdadi et al. 2009; Fieuzal et al. 2013; Wiseman et al. 2014).

Many studies have demonstrated the relevance of airborne and spatial SAR data for identifying phenological stages (Steele-Dunne et al. 2017). In recent years, several studies have shown the value of S-1 data for monitoring crop phenology. Bargiel (2017) improved crop classification in northern Germany using phenological stages based on S-1 time series. Vreugdenhil et al. (2018) demonstrated the high sensitivity of S-1 backscattering coefficients and the ratio of VH:VV polarizations in detecting changes in vegetation structure for rapeseed, maize and winter cereals. S-1 VV and VH polarizations have shown great potential for identifying phenological stages of wheat (Song and Wang 2019) and rice (Mandal et al. 2018b) based on analyzing temporal behavior of backscattering coefficients, but phenological stages were not classified in these studies. Studies using polarimetric features derived from RADARSAT-2 or TerraSAR-X satellite images to identify crop parameters showed that polarimetric indicators were highly sensitive to phenological stages (Pacheco et al. 2016; McNairn et al. 2018), crop height (Jin et al. 2015; Betbeder et al. 2016b; Canisius et al. 2018), crop biomass (Wiseman et al. 2014; Betbeder et al. 2016b; Homayouni et al. 2019; Jin et al. 2015) and LAI (Jiao et al. 2009; Betbeder et al. 2016b; Canisius et al. 2018). To our knowledge, polarimetric indicators derived from S-1 data have not been used to study crop parameters.

A few studies used both optical and RaDAR data to monitor crop phenology. Most used optical data as a reference and predicted biophysical parameters from SAR data. Betbeder et al. (2016) revealed the high potential of RADARSAT-2 polarimetry using NDVI derived from Formosat-2, SPOT-4 and SPOT-5 as references. El Hajj et al. (2019) described the ability of the S-1 C-band to penetrate crops when biomass is high (NDVI > 0.7) for maize, and the lack of this ability for wheat and grassland. Veloso et al. (2017) showed the value of S-1 data for monitoring crop growth through analysis of temporal profiles of VV and VH polarizations and the VH:VV ratio for winter and summer crops in southern France. Although these studies highlighted the value of SAR data, they did not evaluate the potential of combining SAR and optical data to predict crop parameters. Stendardi et al. (2019) concluded that combining SAR S-1 and optical S-2 data shows promise for detecting the phenology of mountain meadows in northern Italy. Jin et al. (2015) studied the potential of vegetation indices derived from the Huanjing-1A/B optical satellite and polarimetric indicators derived from RADARSAT-2 to estimate the LAI and biomass of winter wheat. They found the highest correlations when optical and RaDAR data were combined. While these studies evaluated SAR and optical time-series and their combined use to estimate LAI and biomass, to our knowledge, no study has explored the value of SAR S-1 and optical S-2 data for predicting phenological stages.

The objective of this study was to assess the potential of S-1 data alone, S-2 data alone, and their combined use to identify principal and secondary phenological stages of wheat and rapeseed. More specifically, this study aimed to evaluate the value of polarimetric indicators to discriminate wheat and rapeseed phenological stages and determine the number of relevant S-1 & 2 features that are needed to discriminate principal and secondary phenological stages of these crops. We evaluated the performance of spectral bands and vegetation indices derived from S-2 time-series and backscattering coefficients and polarimetric indicators derived from S-1 time-series. We first analyzed temporal profiles of features derived from S-1 and S-2 time-series for wheat and rapeseed crops. Satellite images were then classified using an incremental procedure based on the importance rank of these input features (Mercier et al. 2019b). This method automatically selects important features to classify the phenological stages of wheat and rapeseed.

The novelties of this work are threefold: (i) The use of S-1 polarimetric indicators to identify principal and secondary phenological stages of wheat and rapeseed; (ii) The statistical analysis of optical data, SAR data and their combined use to discriminate phenological stages of wheat and rapeseed; (iii) Mapping of wheat and rapeseed secondary phenological stages using remotely sensed data.

5.2. Materials

5.2.1. Study area

The study area consisted of two 5 × 5 km sub-sites in northern France (Figure 5-1). Their climate is oceanic with a mean annual temperature of 10°C and mean annual precipitation of 702 mm (Météo France). The western site is located in an open field landscape with intensive cultivation of cereals and sugar beet. The eastern site is located in a "bocage" landscape dominated by grasslands and is characterized by less intensive farming activities (mainly dairy cattle) and smaller fields that tend to be enclosed by hedgerows. Both landscapes contain managed forest fragments that are used mainly for hunting and production of wood (Jamoneau 2010)). The topography of the study area is quite flat, elevation of the "bocage" and open field landscapes ranging from 125 to 224 m (mean = 180 m) and 72 to 158 m (mean = 114 m), respectively. The geological substrate is composed of chalk in the open field landscape and silt in the "bocage" landscape (Jamoneau 2010).

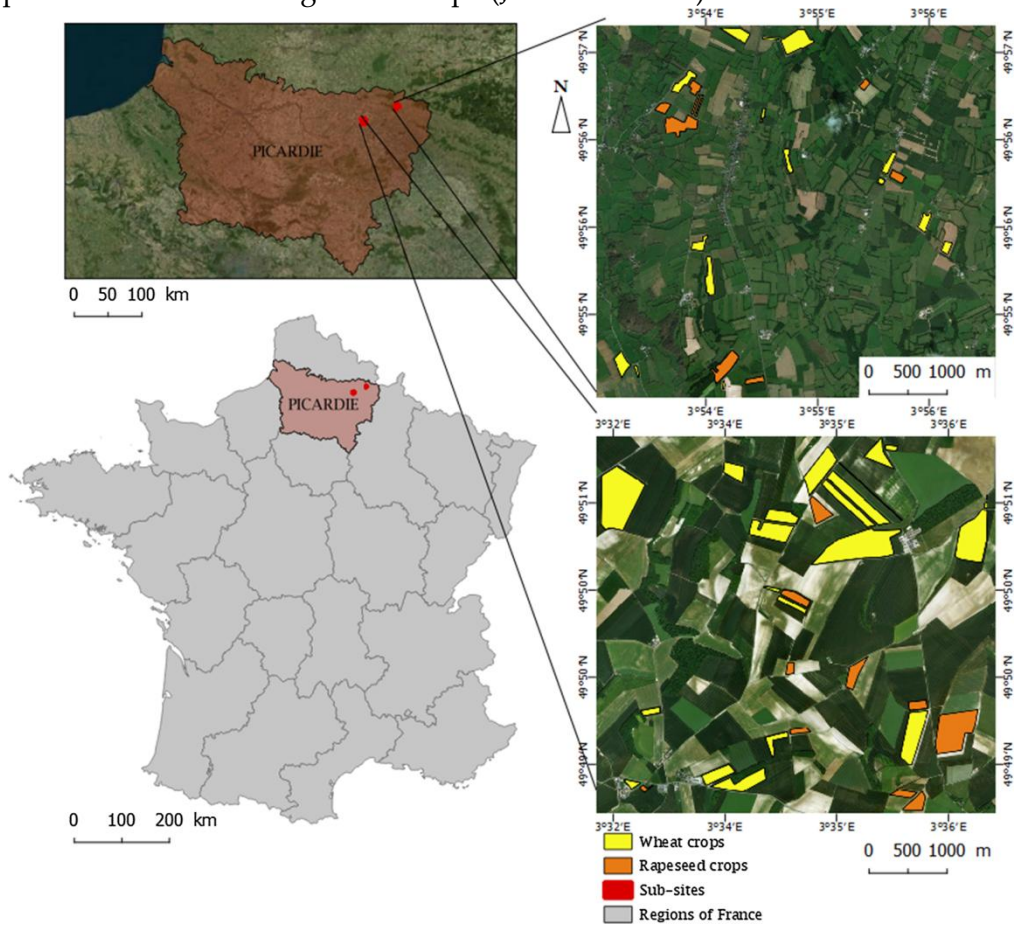

Figure 5-1. Location of the two sub-sites of the study area (bocage at the top, open field at the bottom) and the sampled fields. Satellite imagery and aerial photographs accessed through Bing Aerial using OpenLayers QGIS plugin 1.4.8 (Microsoft®Bing™Maps).

5.2.2. Satellite imagery

A series of five optical S-2 and eight SAR S-1 images were downloaded from January to July 2017 to cover crop cycles of wheat and rapeseed (Figure 5-2). The S-1 images were acquired in Interferometric Wide (IW) swath mode and delivered with VV and VH polarizations. We used the SLC product, which consists of focused SAR data that use the full C-signal bandwidth and preserve the phase information, to derive polarimetric indicators. The incidence angle of images ranged from 30.6-46.0° (Table 1). The ground spatial resolution was 2.5 m and the azimuth spatial resolution was 13.9 m (Table 5-1).

According to data recorded at the Météo-France weather station in Saint Quentin (49°49'06"N, 3°12'22"E, located 24 km from the open field site and 52 km from the "bocage" site), two S-1 images (DOY 69 and 182) were acquired after a rainfall event. The weather station recorded a rainfall of 2.6 mm and 10.1 mm on days 68 and 182, respectively. However, the RaDAR signal was not affected by rainfall or freezing on acquisition dates, no peak being observed in the temporal profiles of VH and VV polarizations (Figure 5-2).

Table 5-1. Main characteristics of S-1 SLC images.

Band	C (center frequency of 5 405 GHz)
Mode	Interferometric Wide Swath
Product type	Single Look Complex
Ground Resolution	2.3 m
Azimuth resolution	13.9 m
Temporal resolution	6 days
Orbit	Ascending
Polarization	Dual (VV & VH)
Swath	250 km
Incidence angle	30.6-46.0°

The S-2 images were acquired with spatial resolutions of 10 and 20 m, and a spectral resolution of 10 bands (Table 5-2). The tiles were downloaded in level 2A, which provides Top of Canopy reflectance and a cloud and shadow mask (ESA, 2019b). Only two S-2 images were acquired between DOY 72 and 163 due to heavy cloud cover during the spring.

Table 5-2. Main characteristics of S-2 MSI L2A images.

Spatial and spectral resolutions	*10 × 10 m* B2 (490 nm), B3 (560 nm), B4 (665 nm) and B8 (842 nm) *20 × 20 m* B5 (705 nm), B6 (740 nm), B7 (783 nm), B8a (865 nm), B11 (1610 nm), B12 (2190
Temporal resolution	5 days
Swath	290 km

5.2.3. Field data collection

Field surveys were conducted on 36 and 19 fields of wheat (*Triticum aestivum L.*) and rapeseed (*Brassica napus L.*), respectively (Figure 5-1). Sizes of wheat and rapeseed fields ranged from 0.77-35.09 ha (mean=7.31 ha), median=4.63) and 1.35-23.91 ha (mean=4.82 ha, median=2.84 ha), respectively. Phenological stages were identified on 8 dates from January to July 2017 (Figure 5-2) based on the Biologische Bundesanstalt, Bundessortenamt and CHemical industry (BBCH) scale (Bleiholder, et al. 2001). Five principal phenological stages

were observed for both crops, and 29 and 15 secondary phenological stages were identified for wheat (Table 5-3) and rapeseed (Table 5-4), respectively. The samples of secondary phenological stages available for wheat and rapeseed were grouped into sub-classes to obtain a sufficient number of samples per class to train and validate the classifications.

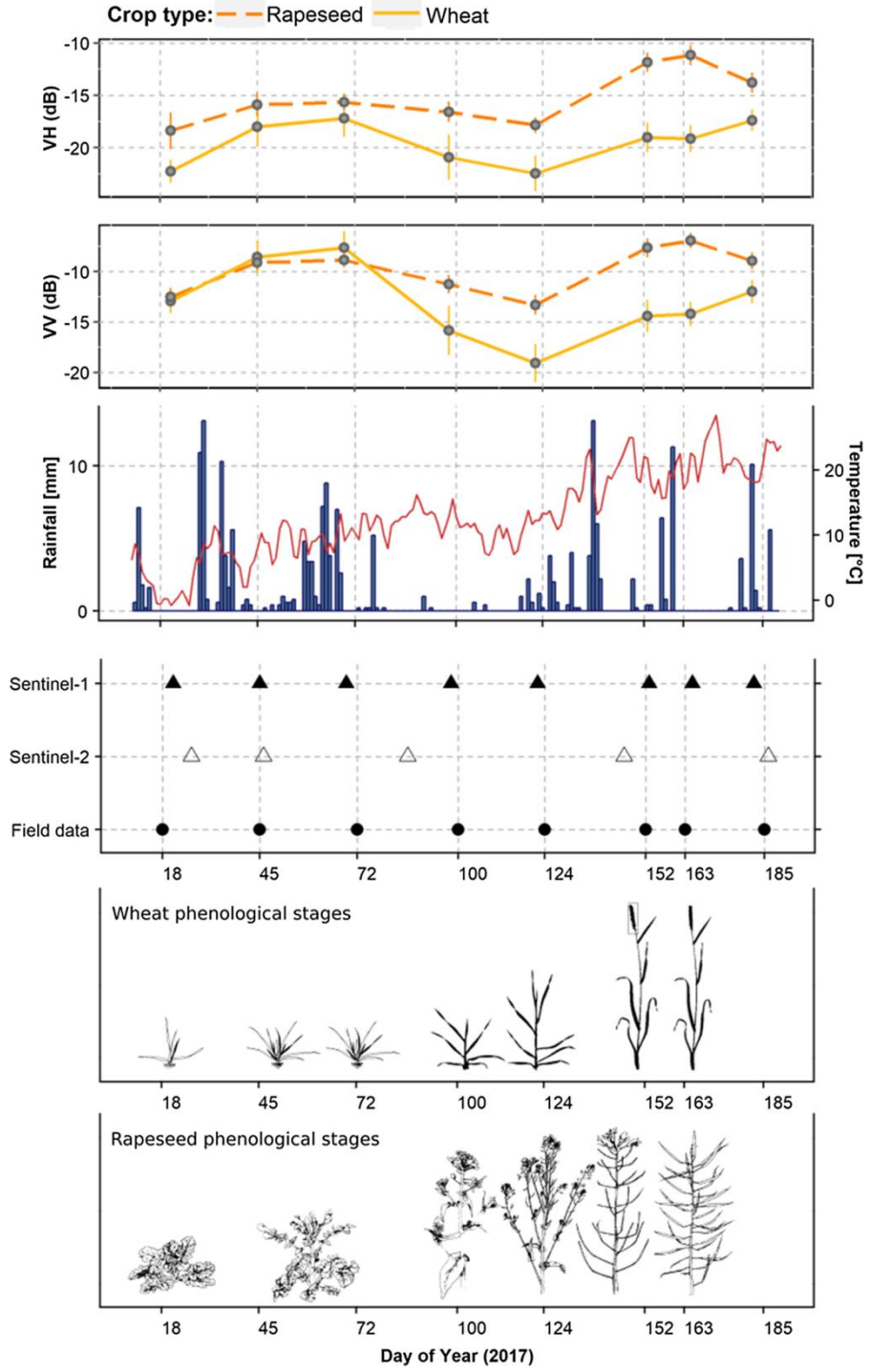

Figure 5-2. Days of year of satellite images (triangular shape), field surveys (circular shape) and main crop phenological stages for wheat and rapeseed (drawings) (Bleiholder, et al. 2001). The ombrothermal diagram (Météo France) shows climatic conditions on the image acquisition dates and temporal profiles show the mean and standard deviation of the S-1 backscattering coefficients for wheat and rapeseed. The RaDAR signal was not affected by rainfall (blue columns) or freezing (red lines) on acquisition dates.

Table 5-3. Phenological stages of wheat considered in this study and number of field observations for each secondary stage

Principal stage	Sub-class	2° stage	Description	Number of observations
Tillering	1	20	No tillers	1
		21	Beginning of tillering: first tiller detectable	14
		22	2 tillers detectable	16
		23	3 tillers detectable	18
	2	24	4 tillers detectable	22
		25	5 tillers detectable	6
		26	6 tillers detectable	8
		29	9 tillers detectable	20
Stem elongation	3	30	Beginning of stem elongation	4
		31	First node at least 1 cm above tillering node	25
		32	Node 2 at least 2 cm above node 1	6
		33	Node 3 at least 2 cm above node 2	24
		34	Node 4 at least 2 cm above node 3	9
		35	Node 5 at least 2 cm above node 4	3
Flowering, anthesis	4	65	Full flowering: 50% of anthers mature	3
		66	Full flowering: 60% of anthers mature	2
		67	Full flowering: 70% of anthers mature	3
		68	Full flowering: 80% of anthers mature	4
		69	End of flowering	9
Development of fruit	5	71	Watery ripe: first grains have reached half their final size	14
		72	Watery ripe / Early milk	2
		73	Early milk (the content of the kernel is milky)	13
		75	Medium milk: grain content milky, grains reached final size, still green	19
		77	Late milk	4
Ripening	6	83	Early dough (the content of the kernel is doughy)	10
		84	Early dough/ Soft dough ((the content of the kernel is doughy)	5
		85	Soft dough: grain content soft but dry. Fingernail impression not held	3
	7	87	Hard dough: grain content solid. Fingernail impression held	9
		89	Fully ripe: grain hard, difficult to divide with thumbnail	8

Table 5-4. Phenological stages of rapeseed considered in this study and number of field observations for each secondary stage

Principal stage	Sub-class	2° stage	Description	Number of observations
Leaf development	1	17	7 leaves unfolded	4
		18	Beginning of tillering: first tiller detectable	7
		19	2 tillers detectable	7
Inflorescence emergence	2	50	Flower buds present, still enclosed by leaves	10
		51	Flower buds visible from above (“green bud”)	26
Flowering	3	60	First flowers open	1
		62	20% of flowers on main raceme open	1
		63	30% of flowers on main raceme open	5
		64	40% of flowers on main raceme open	5
	4	65	Full flowering	7
		67	Flowering declining: majority of petals fallen	7
		69	End of flowering	12
Development of fruit	5	77	70% of pods have reached their final size	1
		79	Nearly all pods have reached final size	12
Ripening	6	80	Beginning of ripening	25
	7	89	Fully ripe	19

5.3. Methods

We developed a method to analyze temporal behaviors of S-1 and S-2 features and predict phenological stages of wheat and rapeseed (Figure 5-3). First, the SAR S-1 and optical S-2 signals were preprocessed and the median was computed at the field scale with a negative buffer of 15m. Second, temporal profiles were plotted based on the mean and standard deviation derived from the median for all sampled wheat and rapeseed fields. Field surveys were used to analyze the temporal profiles of the spectral bands and vegetation indices derived from S-2 and RaDAR backscattering coefficients and polarimetric indicators derived from S-1. Finally, we assessed the potential of S-1 data alone, S-2 data alone, and combined S-1 & 2 data to predict principal and secondary phenological stages of wheat and rapeseed using an incremental method developed by Mercier et al. (2019b)and field data were used as reference data to train the classifier.

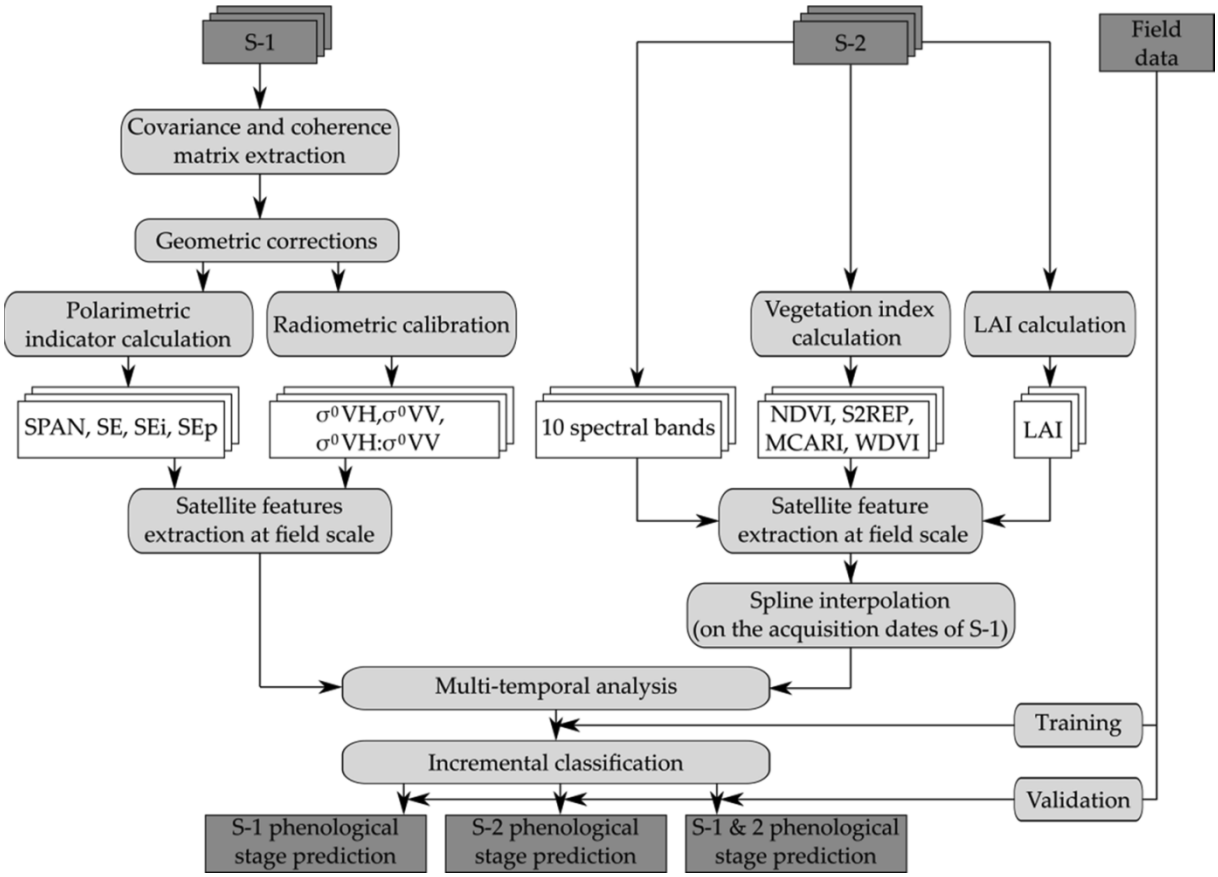

Figure 5-3. Flowchart of the image processing procedure applied to S-1 and S-2 time series to identify wheat and rapeseed secondary phenological stages.

5.3.1. SAR Sentinel-1 image preprocessing

5.3.1.1. Backscattering coefficients

Backscattering coefficients from S-1 images were extracted using the Sentinel-1 Toolbox (ESA, http://step.esa.int/main/toolboxes/sentinel-1-toolbox/). The images were first radiometrically calibrated to transform the digital number (DN, amplitude of the backscattering signal) of each pixel into backscattering coefficients ($\sigma\circ$VV, $\sigma\circ$VH) on a linear scale using the following equation (Eq. 5.1) (Miranda and Meadows 2015):

$$\text{value(i)} = \frac{|\text{DN}_\text{i}|}{\text{A}_\text{i}{}^2} \quad (5.1)$$

where A is the information necessary to convert SAR reflectivity into physical units provided in the Calibration Annotation Data Set in the image metadata.

A refined Lee filter was then applied in a window of 7 × 7 pixels to reduce speckle noise (Lee et al. 1994). The images were geocoded using SRTM data to correct topographic deformations (geometric correction accuracy < 1 pixel). A backscattering ratio was calculated by dividing $\sigma\circ$VH by $\sigma\circ$VV. All images were then converted from linear to decibel (dB) scale using the following equation (Eq. 5.2):

$$\sigma^0(db) = 10 \times log_{10}(\sigma^0) \quad (5.2)$$

5.3.1.2. Polarimetric indicators

A 2 × 2 covariance matrix (C_2) was first extracted from the scattering matrix S of each SLR image using PolSARpro version 5.1.3 software (Pottier and Ferro-Famil 2012). A refined Lee filter was then applied in a window of 7 × 7 pixels to reduce speckle noise (Lee et al. 1994). Then, we calculated the total scattered power called span in the case of a polarimetric RaDAR system (Ferro-Famil and Pottier 2014). SE, which measures the randomness of scattering of a pixel (e.g. due to variation in backscattering power or polarization), was calculated from the covariance matrix (C_2) using the following equation (Eq. 5.3):

$$SE = \log(\pi^2 e^2 |C_2|) = SE_i + SE_p \quad (5.3)$$

where SE_i is related to the intensity and SE_p to the degree of polarization.

Finally SE, SE_i and SE_p were normalized as $SE\ norm$, $SE_i\ norm$ and $SE_p\ norm$ using PolSARpro version 5.1.3 software.

5.3.2. Optical Sentinel-2 image preprocessing

Twelve vegetation indices were calculated since their potential to monitor crop parameters (LAI, chlorophyll content and phenological stages) using S-2 data has been demonstrated (Daughtry et al. 2000; Frampton et al. 2013; Herrmann et al. 2011; Clevers and Gitelson 2013; Clevers et al. 2017). We calculated NDVI, the GNDVI, the REIP index, the

IRECI, the S2REP index, the MCARI, the MTCI, the SAVI, the MSAVI, the WDVI, the PSSRa and the NDI. Based on analysis of their temporal profiles and on correlation matrices (Appendix B), we ultimately selected four of these indices: NDVI, S2REP, MCARI and WDVI (Table 5-5). First, we selected NDVI because it is a very commonly used vegetation index sensitive to chlorophyll content, calculated from bands 4 and 7 of S-2 (Hermann et al., 2011; Frampton et al., 2013). Second, we chose the S2REP because this index is a version of the REP estimate for S-2 derived from a linear interpolation that incorporates bands 5 and 6 positioned on the red-edge slope (Guyot and Baret 1988; Clevers et al. 2002). MCARI and WDVI were also selected, because they had the lowest correlations with the other features derived from S-2 for both crop types. The MCARI, which was developed to study variations in chlorophyll and minimize effects of non-photosynthetic materials, was derived from bands 3, 4 and 5 of S-2 (Daughtry et al. 2000). The WDVI, which is related to the chlorophyll content of the canopy was used to estimate LAI to avoid destructive measurements. It is a two-dimensional greenness index derived from bands 4 and 8 of S-2 (Bouman et al. 1992).

Table 5-5. Vegetation indices calculated from S-2 images. G = Green, R = Red, RE = Red-Edge.

Index	Equation	S-2 bands used	Original author
NDVI	(NIR-R)/(NIR+R)	(B7-B4)/(B7+B4)	(Rouse et al. 1973)
S2REP	705 + 35 - ((((NIR + R)/2) - RE1)/(RE2 -RE1))	705 + 35 * ((((B7 + B4)/2) B5)/(B6 B5))	(Guyot and Baret 1988)
MCARI	[(RE - R) 0.2(RE - G)] * (RE - R)	[(B5 - B4) - 0.2(B5 - B3)] * (B5 - B4)	(Daughtry et al. 2000)
WDVI	(NIR – 0,5 * R)	(B8 – 0,5 * B4)	(Clevers 1988)

LAI, a biophysical variable that describes the state of vegetation cover and provides information on the density of green vegetation, was also derived from S-2 images using the PROSAIL radiative transfer model implemented in SNAP v6.0 software. The spectral bands, vegetation indices and LAI were interpolated daily using a spline method to match the dates of SAR S-1 acquisition using the stats package of R software. All S-1 and S-2 images were projected onto the RGF93/Lambert-93 system (EPSG 2154) and resampled to the resolution of 10 m. In total, we preprocessed 120 S-2 features (10 spectral bands, 4 vegetation indices and 1 biophysical variable × 8 dates) and 56 S-1 features (2 backscattering coefficients, 1 backscatter ratio and 4 polarimetric indicators × 8 dates). Due to strong correlations between the S-2 spectral bands, we subsequently selected a sub-set of bands for the incremental classification based on their temporal behaviors.

5.3.3. Incremental classification

From an operational point of view, it is necessary to minimize the time between data acquisition and delivery of results to decision-makers (Hatfield et al. 2019). The time-consuming processing of multi-temporal remote sensing data is a limitation for this purpose. Therefore, we used an incremental procedure based on the importance rank of the input features to find a trade-off between accuracy and processing time (Mercier et al. 2019b). This method automatically selects important features to maintain a minimum but sufficient number of features to classify the phenological stages of wheat and rapeseed. This method was applied to predict the principal and sub-classes of secondary phenological stages of wheat (Table 5-3) and rapeseed (Table 5-4) (Figure 5-4).

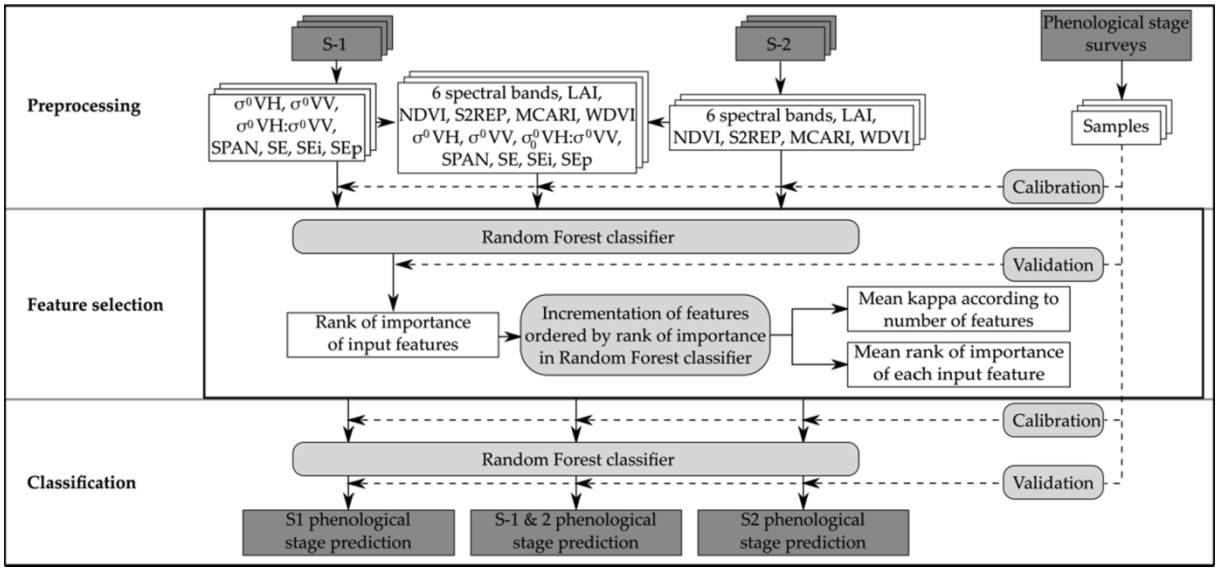

Figure 5-4. Detailed flowchart of the incremental classification procedure applied to S-1 data alone, S-2 data alone and combined S-1 & 2 data.

Incremental classification was performed using a Random Forest (RF) classifier applied to S-1 data alone, S-2 data alone, and combined S-1 & 2 data. A total set of 50 pairs of training and validation fields in a 70:30 ratio were randomly selected to classify all wheat and rapeseed phenological stages. For each of the pairs, the selected fields were the same for S-1 data alone, S-2 data alone, and combined S-1 & 2 data. A maximum number of randomly selected samples per class was set to rebalance the classes, since the RF classifier underperforms with unbalanced classes (Khoshgoftaar et al. 2007). The number of samples per pair ranged from 21 (5 principal phenological stages) or 18 (7 sub-classes of secondary phenological stages) to 52 for wheat, and from 13 to 35 for rapeseed (both types of phenological stages) (Table 5-6).

Table 5-6. Number of samples per pair (training + validation samples) used to classify phenological stages of wheat and rapeseed. OS = observed samples in the field, SS = selected samples for classification

Class code	Wheat fields				Rapeseed fields			
	Principal stages		Sub-classes		Principal stages		Sub-classes	
	OS	SS	OS	SS	OS	SS	OS	SS
1	105	52	49	49	18	18	18	18
2	72	52	56	52	36	35	36	35
3	21	21	72	52	38	35	12	12
4	52	52	21	21	13	13	26	26
5	35	35	52	52	44	35	13	13
6			18	18			25	25
7			17	17			19	19

Two output analysis – mean rank of importance of each input feature and mean kappa index (Cohen 1960; Rosenfield and Fitzpatrick-Lins 1986) as a function of the number of features - were used to select the most important features to include in the final classification. Incremental classification is used to assess mapping quality as the types and numbers of features increase. Thus, it determines the combination and number of features in the classification necessary to obtain acceptable quality (Inglada et al. 2016). For each training and validation set (50 pairs), an RF algorithm was first applied to all of the features to rank them in order of importance based on the mean decrease in the Gini index which assessed the reliably of the incremental classification (Calle and Urrea 2011). The mean rank of importance of each feature was derived from the 50 ranks obtained from the 50 pairs of training and validation samples. We then ran as many RF algorithms as the number of features, starting with the two most important features and then adding the less important features until all features were processed. The number of features selected for the final predictions was determined automatically: when kappa increased by less than 0.02 for three consecutive feature additions, the first of the three features marked the end of the selection for prediction. To visualize differences in performance between classes, we calculated user's accuracy (UA) and producer's accuracy (PA) (Congalton 1991) as a function of the number of features. We used the RF algorithm to select and classify features and to calculate the final prediction. In both cases, the number of trees was set to 100 (Pelletier et al. 2016). The analyses were performed using the randomForest package of R software.

5.4. Results

5.4.1. Analysis of time-series of Sentinel-2 features

For wheat and rapeseed, the highest signal variations in temporal profiles for S-2 reflectance were observed for bands 6 and 7 (red-edge) and bands 8 and 8A (NIR) (Figure 5-5).

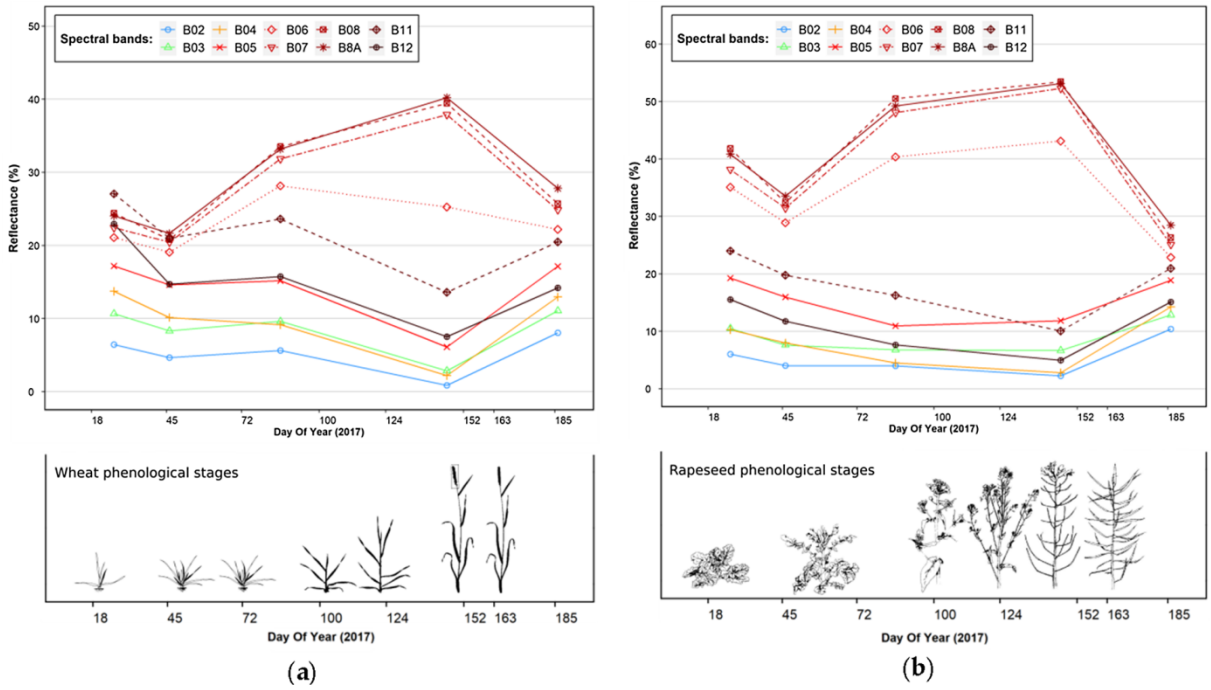

Figure 5-5. Mean temporal profiles of S-2 reflectance and main phenological stages for (a) wheat and (b) rapeseed (Bleiholder, et al. 2001) (B02 = blue, B03 = green, B04 = red, B05 = Red-edge 1, B06 = Red-edge 2, B07 = Red-edge 3, B08 = NIR wide, B8A = NIR narrow, B11= SWIR1, B12= SWIR2).

For wheat, all S-2 bands saturated before and during the maximum peak corresponding to stem elongation (DoY 100-124), inflorescence and flowering (DoY 152) (Figure 5-5a). For rapeseed, all S-2 bands saturated during flowering and development of fruit (DoY 100, BBCH stages ~ 60-65, DoY 124, BBCH stages ~67-69, and DoY 152 and 163, BBCH stage ~80) (Figure 5-5b). Based on these observations, we selected S-2 bands 3, 5, 6, 7, 8 and 8A as input for the incremental classification.

In the temporal profiles of S-2-based vegetation indices and LAI for wheat and rapeseed, the standard deviation peaked on DoY 146, which corresponded to the end of inflorescence for wheat (DoY 124, BBCH stage ~55) and the end of development of fruit for rapeseed (DoY 124, BBCH stages ~67-69) (Figure 5-6).

For wheat, LAI, NDVI and MCARI began to increase at the beginning of tillering, and S2REP and WDVI at the end of tillering. They all decreased during ripening.

For rapeseed, decreases are observed during ripening. NDVI increased until the development of fruit. However, it is not possible to observe its saturation due to the poor number of S-2 dates. LAI and WDVI were similar: they began to increase at the beginning of inflorescence (DoY 46) until the beginning of flowering (DoY 86). WDVI was the only vegetation index sensitive to leaf development (DoY 18-45).

For both crop types, MCARI had a high standard deviation. Thus, MCARI can produce inaccurate predictions of phenological stages.

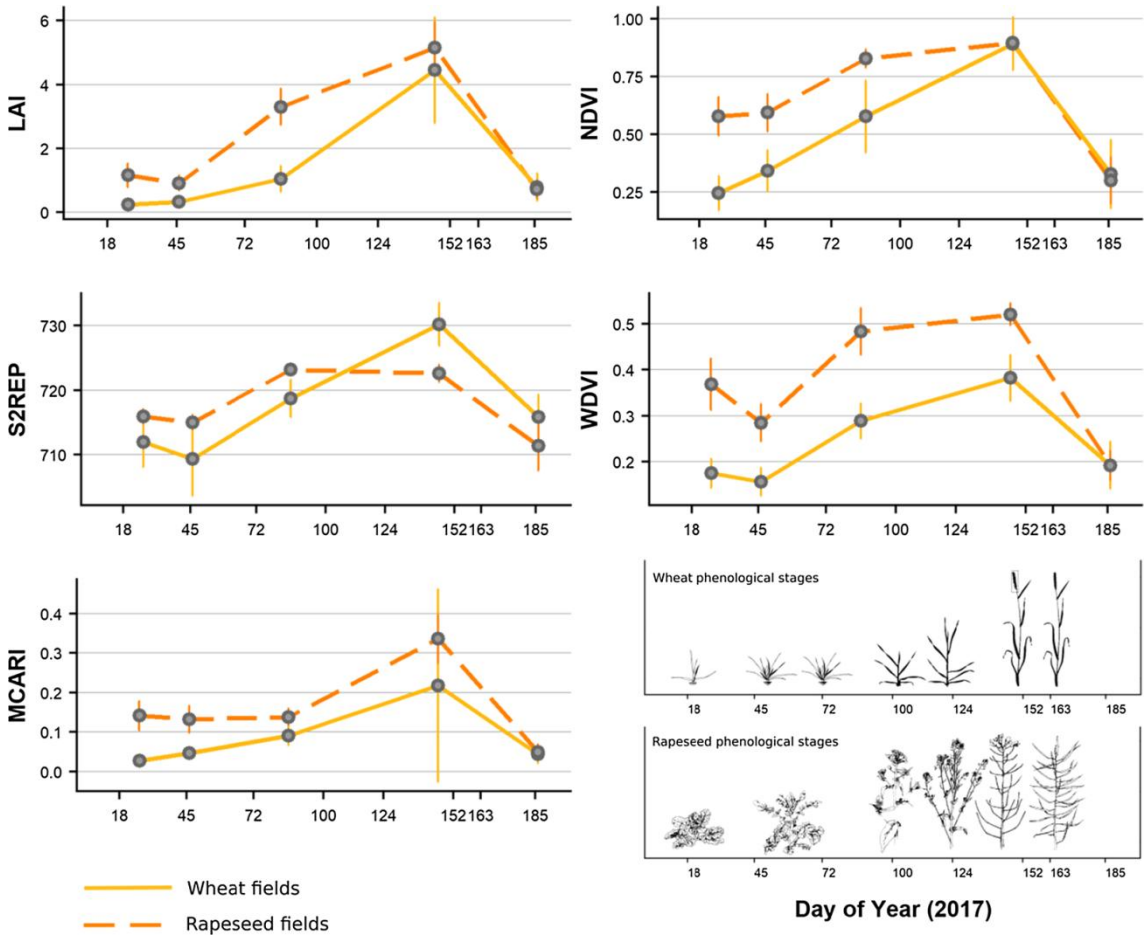

Figure 5-6. Mean temporal profiles of S-2 vegetation indices and LAI and main crop phenological stages for wheat and rapeseed (Bleiholder, et al. 2001). Error bars indicate 1 standard deviation.

5.4.2. Analysis of time series of Sentinel-1 features

For wheat, while trends in the temporal profiles for σ^0VH and σ^0VV were similar, σ^0VV was influenced more by wheat growth than σ^0VH (Figure 5-7). Both polarizations increased during tillering (DoY 18-72). Both σ^0VH and σ^0VV decreased throughout stem elongation (DoY 72-124) but increased from inflorescence to ripening. The $\sigma^0VH{:}\sigma^0VV$ ratio has varied little during tillering stages. The ratio increased strongly during stem elongation and slightly from the beginning of inflorescence to ripening. The polarimetric indices were also sensitive to wheat phenological stages, according to their temporal behaviors (Figure 5-7). The temporal behaviors of $SPAN$, σ^0VH and σ^0VV were similar. The normalized SE index and its intensity ($SE_i\ norm$) were similar. The influence of polarization ($SE_p norm$) on SE was weak, with values ranging from -0.9 to 0.8 dB, while $SE_i\ norm$ ranged from -5 to -1 dB. $SE\ norm$ and $SE_i\ norm$ initially increased at tillering but then decreased during stem elongation and inflorescence. $SE_p\ norm$ initially varied little but then significantly increased during stem elongation. $SE_p\ norm$ decreased linearly from the end of flowering to ripening.

For rapeseed, the trends for σ^0VH and σ^0VV were similar, showing that they were sensitive to phenological stages, while the $\sigma^0VH{:}\sigma^0VV$ ratio was affected only slightly (Figure 5-7). VH and VV polarizations increased slightly during leaf development, varied little during inflorescence and decreased during flowering. Both polarizations increased

from development of fruit to the beginning of ripening. They decreased until the end of ripening. Like for wheat, the temporal profiles of span, σ^0VH and σ^0VV for rapeseed were similar. $SE_p\ norm$ varied little throughout the rapeseed cycle. Temporal changes in $SE\ norm$ and $SE_i\ norm$ were similar to those of wheat, $SE_i\ norm$ increased during flowering and decreased during ripening.

SAR S-1 features were more sensitive to the development of fruit stage for rapeseed (Figure 5-7) than optical S-2 features, which saturated from development of fruit (DoY 86) to beginning of ripening (DoY 163) (Figure 5-5 and 6).

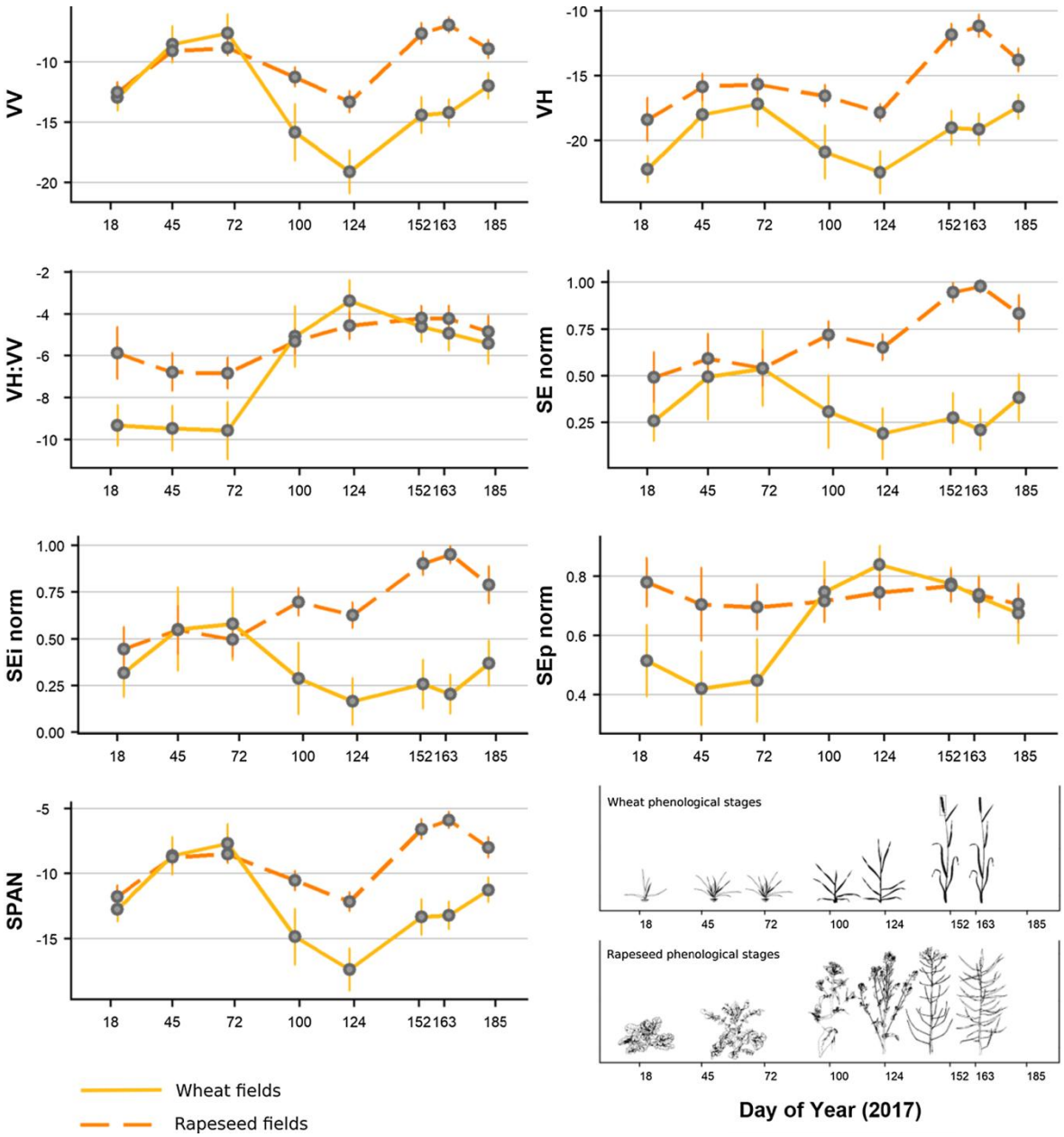

Figure 5-7. Mean and standard deviation of the S-1 backscattering coefficients and polarimetric indicators and main crop phenological stages for wheat and rapeseed (Bleiholder, et al. 2001) (VH = σ^0VH, VV = σ^0VV, VH:VV = σ^0VH: σ^0VV, $SPAN$ = total scattered power, $SE\ norm$ = normalized SE, $SE_i\ norm$ = normalized SE Intensity, $SE_p\ norm$ = normalized SE Polarization). Error bars indicate 1 standard deviation.

5.4.3. Contribution of Sentinel 1 & 2 time series to monitoring wheat and rapeseed phenology

5.4.3.1. Contribution of Sentinel 1 & 2 time series to identifying principal phenological stages of wheat and rapeseed

The combined use of S-1 & 2 data outperformed use of S-1 or S-2 data alone in detecting the principal crop stages of wheat and rapeseed (maximum mean kappa index of 0.82 and 0.91, respectively) (Figure 5-8). However, considering the standard deviation of the mean kappa index, results of the combined use of S-1 & 2 data were similar to those of S-2 data alone. The number of features automatically selected to predict the principal phenological stages were 4, 6 and 6 for wheat and 4, 5 and 5 for rapeseed for S-1 data alone, S-2 data alone and their combined use, respectively. For wheat, the mean kappa indices of S-1 and S-2 data alone were equal up to 3 input features, after which the S-1 mean kappa index changed little (0.60 ± 0.07), while that for S-2 continued to increase up to 5 input features (0.74 ± 0.07) (Figure 5-8a). Using the top 6 S-1 & 2 features out of all 18 features increased the mean kappa index by ca. 0.24 (i.e. from 0.53 ± 0.11 for 2 features to 0.77 ± 0.07 for 6 features). For rapeseed, S-1 data alone underperformed S-2 data alone based on the standard deviation of the mean kappa index (Figure 5-8b). Using the top 5 S-1 & 2 features out of all 18 features increased the mean kappa index by ca. 0.16 (i.e. from 0.74 ± 0.12 for 2 features to 0.90 ± 0.07).

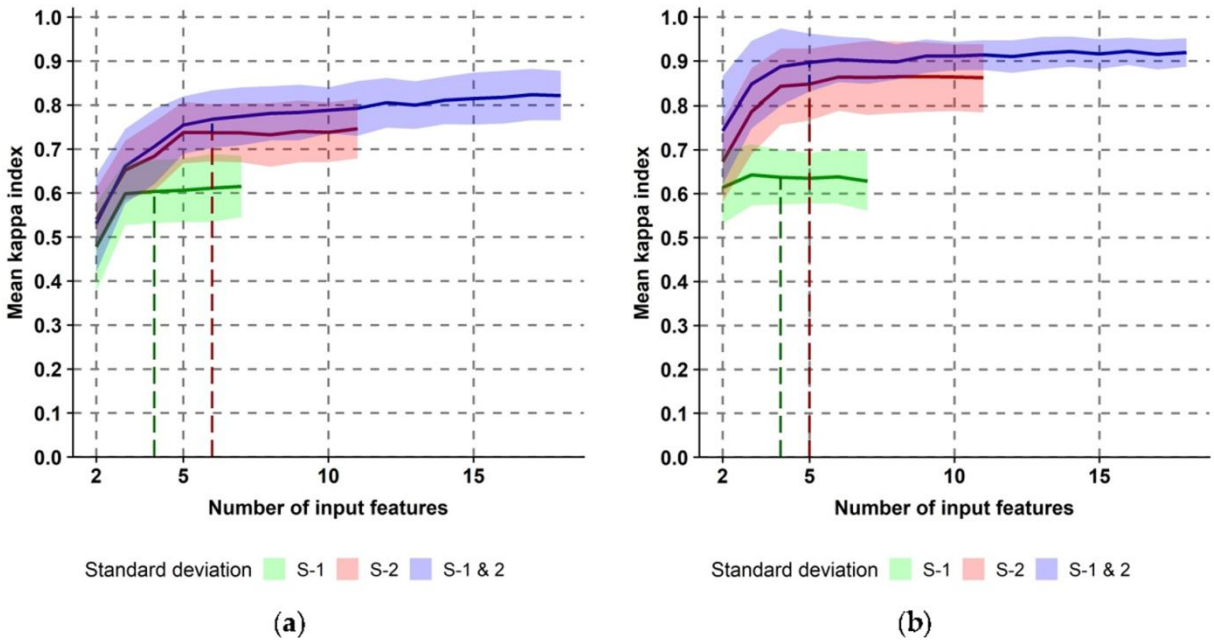

Figure 5-8. Mean kappa index of incremental classifications of principal phenological stages for S-1 data alone, S-2 data alone, and combined Sentinel-1 & 2 data as a function of the number of input features for **(a)** wheat and **(b)** rapeseed. The dashed lines indicate the number of features automatically selected for the predictions. The combined use of S-1 & 2 data outperformed use of S-1 or S-2 data alone in detecting the principal crop stages of wheat and rapeseed.

When using S-2 data alone for wheat (Figure 5-9b), LAI was the most important feature, followed by S2REP, red-edge2 (B06) and WDVI, NDVI and red edge1 (B05). For rapeseed (Figure 5-9e), the top 3 features were NDVI, S2REP and band 3 (green) (mean ranks of 1.4, 2.1

and 4 respectively). They were followed by LAI and WDVI (mean ranks of 4.3 and 5.3 respectively).

When using S-1 data alone, the $\sigma^0VH{:}\,\sigma^0VV$ ratio ranked first for both crops, while σ^0VV ranked third for wheat (Figures 5-9a and 9d). Polarimetric indicators were important for wheat and rapeseed: several of them were among the 4 input features selected for predictions for both crops. For wheat, the polarization of the SE ($SE_p norm$) ranked second (Figures 5-9a), for rapeseed, the intensity of the SE ($SE_i\, norm$) ranked fourth (Figure 5-9d).

When using combined S-1 & S2 data, an S-1 feature was the most important for both crops: $\sigma^0VH{:}\,\sigma^0VV$ for wheat (Figure 5-9c) and σ^0VH for rapeseed (Figure 5-9f). Among the top 10 important features, 6 were S-1 features for both crop types. For S-2 features, LAI was the most important for wheat and the NDVI and S2REP for rapeseed, since they were the only features out of the 6 and 5 features selected for prediction using the combined use of S-1 & 2 data. MCARI was the least important S-2 index for both crops.

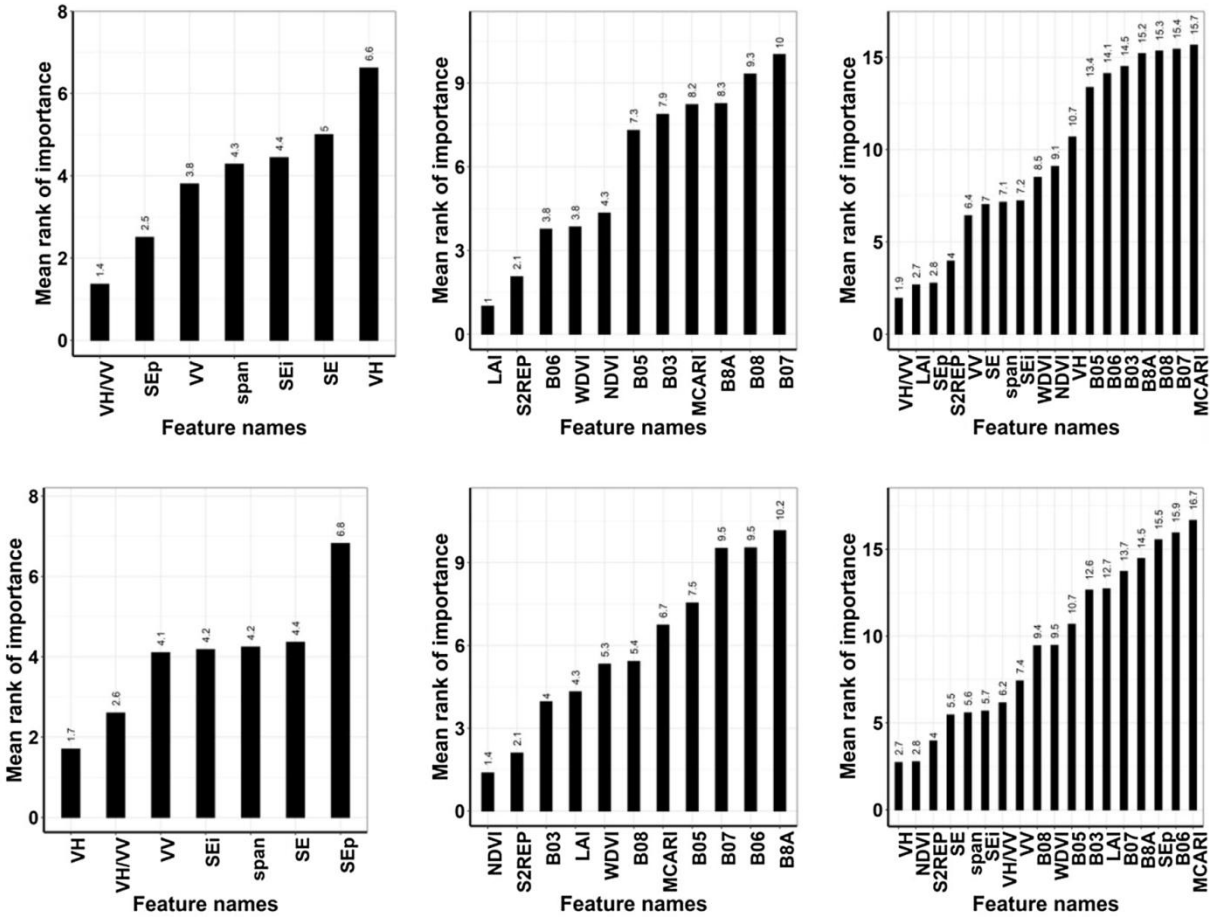

Figure 5-9. Mean rank of importance of the most important features to identify the 5 principal phenological stages of **(a, b, c)** wheat and **(d, e, f)** rapeseed for **(a, d)** S-1 data alone, **(b, e)** S-2 data alone and **(c, f)** combined Sentinel-1 & 2 data. The $\sigma^0VH{:}\,\sigma^0VV$ ratio was a relevant feature using S-1 data alone for both crops, while LAI and NDVI were the most important features using S-2 data alone for wheat and rapeseed, respectively.

Concerning classification results for wheat, tillering was the phenological stage most accurately classified using S-1 data alone, S-2 data alone and their combined use (Figures 5-

10a-c and 11a-c). Based on the UA and PA results, similar results were obtained using S-1 or S-2 data alone for the stem elongation stage. The tillering stage was identified better using S-1 than S-2 data, while the flowering, development of fruit and ripening stages were identified better using S-2 than S-1 (Figures 5-10a and 10b). Combined use of S-1 & 2 data improved the UA of tillering, stem elongation and ripening; only the PA of the stem elongation and flowering stages underperformed that of S-2.

For rapeseed, development of fruit was the most difficult phenological stage to identify using S-1 data alone and the combined use of S-1 & 2 data, due to confusion with ripening (Appendix C, Table C-4 and C-6 and Figures 5-10d and 10f, 11d and 11f). S-2 data alone provided better results than S-1 data alone for all classes (Figures 5-10d-e, 11d-e), while their combined use improved the PA of the leaf development stage from 0.8 (S-2) to 1 (S-1 & 2) (Figures 5-10e-f, 11e-f).

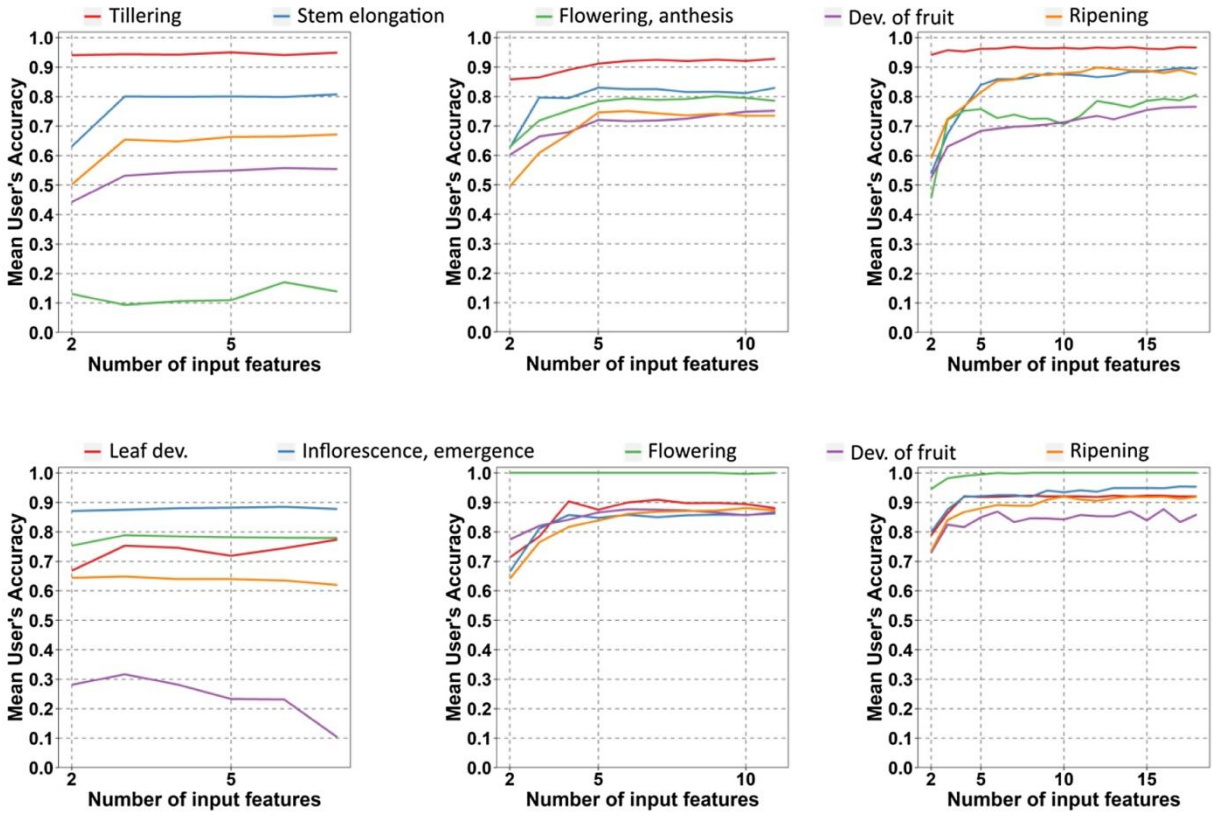

Figure 5-10. Mean UA of incremental classifications as a function of the number of input features to identify the 5 principal phenological stages of wheat and rapeseed. The colored lines refer to the crop phenological stages.

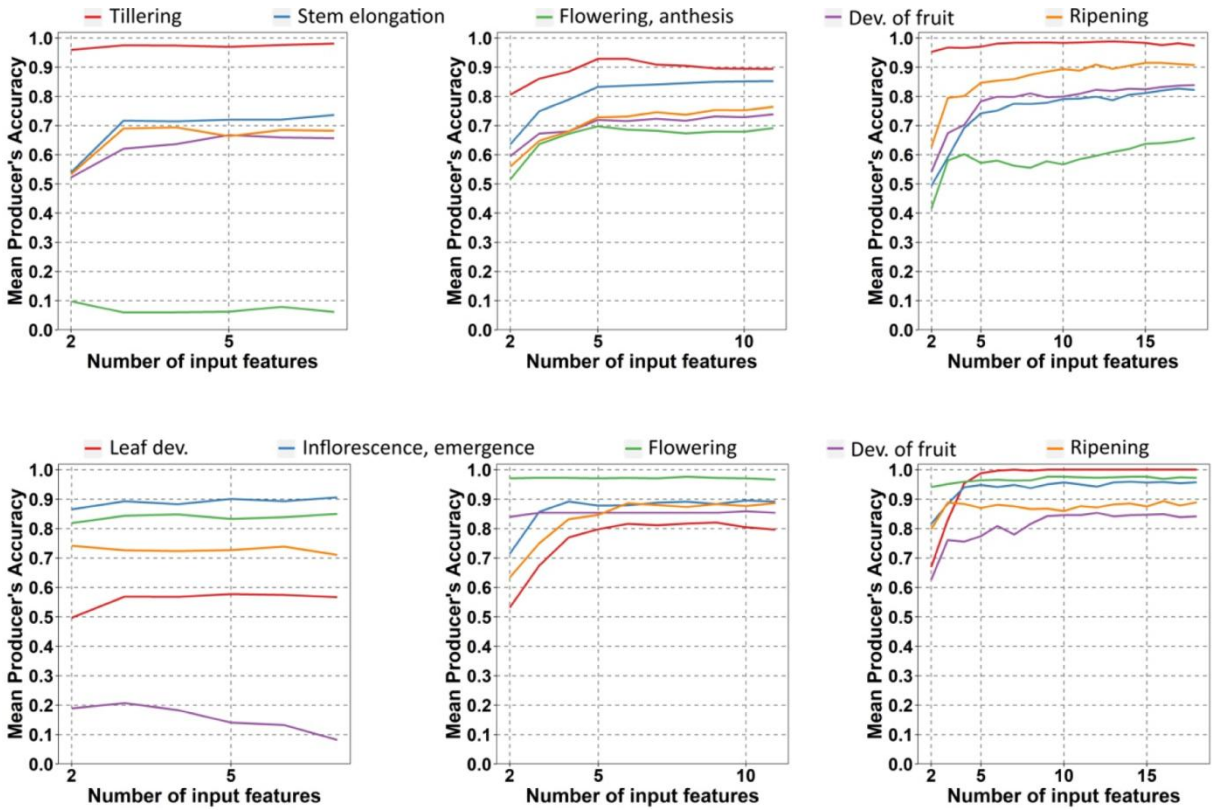

Figure 5-11. PA of incremental classifications as a function of the number of input features to identify the 5 principal phenological stages of wheat and rapeseed. The colored lines refer to the crop phenological stages.

5.4.3.2. *Contribution of Sentinel 1 & 2 time series to identifying secondary phenological stages of wheat and rapeseed*

The number of features automatically selected to predict secondary phenological stages were 4, 4 and 7 for wheat (Figure 12a) and 4, 4 and 5 for rapeseed (Figure 5-12b) for S-1 data alone, S-2 data alone and their combined use, respectively. For S-2 data alone, the mean kappa indices of wheat were similar to those for the principal phenological stages using the number of features automatically selected (0.72 ± 0.05 and 0.74 ± 0.06), whereas the secondary phenological stages of rapeseed were identified weaker than principal phenological stages (0.77 ± 0.07 and 0.86 ± 0.07, respectively). S-1 data alone did not discriminate secondary phenological stages well, since their mean kappa indices were significantly lower than those for the principal phenological stages (0.53 ± 0.06 and 0.60 ± 0.07, respectively, for wheat and 0.55 ± 0.07 and 0.63 ± 0.06, respectively, for rapeseed). For combined S-1 & 2 data, mean kappa indices for secondary phenological stages were also lower than those of principal phenological stages (0.72 ± 0.07 and 0.77 ± 0.06, respectively, for wheat and 0.79 ± 0.06 and 0.9 ± 0.07, respectively, for rapeseed). The use of S-1 & 2 data combined was similar to those of S-2 data alone for both crops (Figures 5-12a and 12b). Several S-1 features were present in the top ranks of importance for the combined S-1 & 2 data (Figures 5-13c and 13f). Considering standard deviation of the mean kappa index, the classification accuracy using S-2 data alone or combined S-1 & 2 was not significantly different. For rapeseed, the mean kappa index was very similar regardless of the number of input features. For wheat, S-2 data alone results were superior to combined S-1 & 2 results until 5 inputs features.

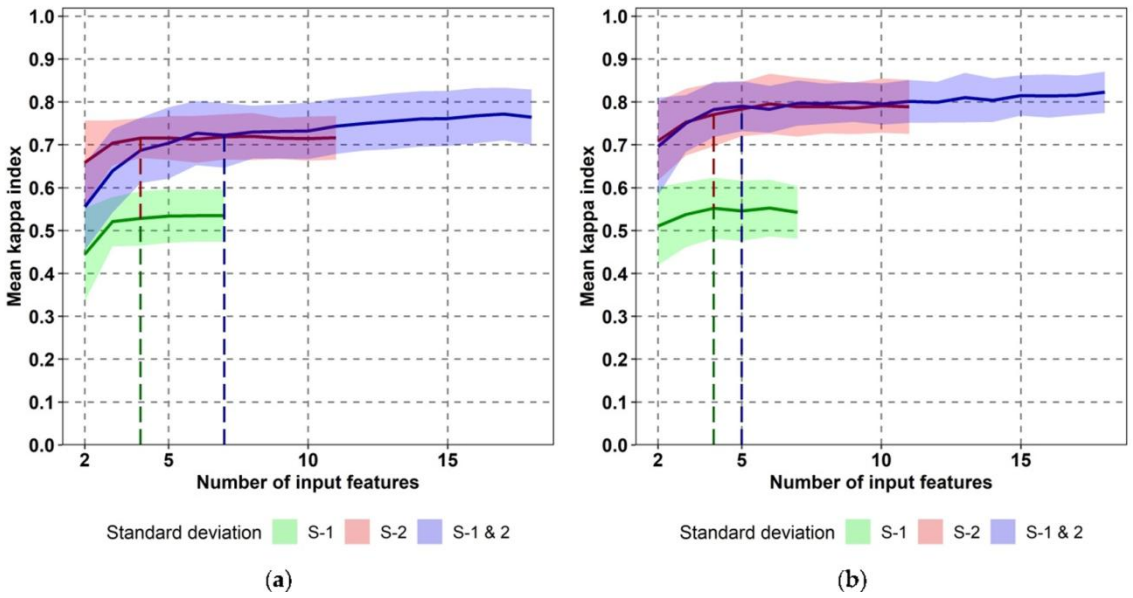

Figure 5-12. Mean kappa index of incremental classifications of secondary phenological stages for S-1 data alone (green), S-2 data alone (red), and combined Sentinel-1 & 2 data (blue) as a function of the number of input features for (a) wheat and (b) rapeseed. The classification accuracy using S-2 data alone or combined S-1 & 2 was not significantly different.

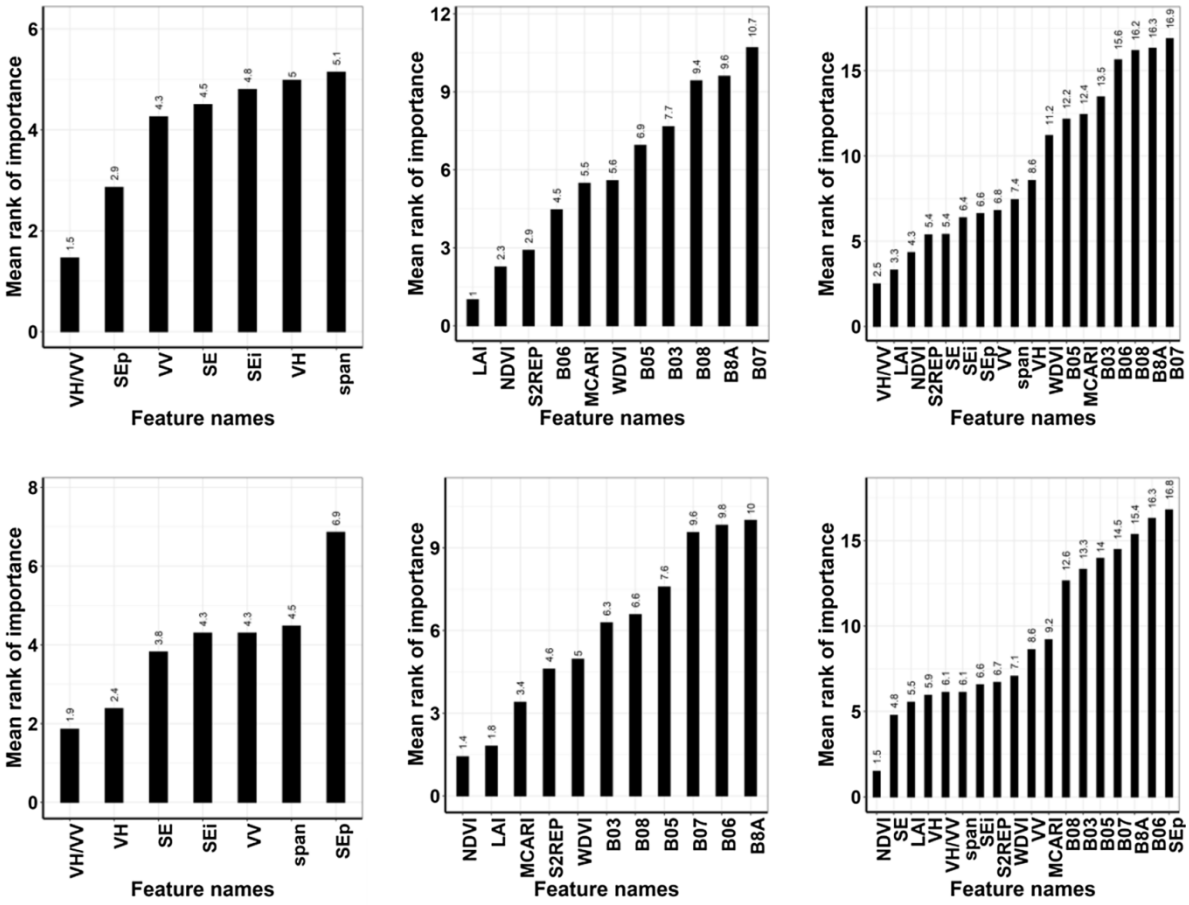

Figure 5-13. Mean rank of importance of the most important features to identify the 7 secondary phenological stages of wheat and rapeseed. The $\sigma^0VH:\sigma^0VV$ ratio was the most important feature using S-1 data alone for both crops, while LAI, NDVI and S2REP were the most important features using S-2 data alone.

When using S-2 features alone, LAI, NDVI and S2REP for both crop types remained, like those for the principal phenological stages, the most important features (Figures 5-11e and 13e). For rapeseed, band 3 (green), which had been ranked third for identifying the principal phenological stages (Figure 5-10e) decreased to the sixth rank for identifying the secondary phenological stages (Figure 5-13e).

The $\sigma^0VH{:}\sigma^0VV$ ratio was the most important feature using S-1 data alone for both crops (Figures 5-13a and 13d), and the first and seventh feature using S-1 & 2 data combined (Figures 5-13c and 13f) for wheat and rapeseed, respectively.

When using S-1 features alone, σ^0VV and $SE_p\,norm$ for wheat (Figure 5-13a) and σ^0VV and $SE\,norm$ for rapeseed (Figure 5-13d) were also highly important for identifying secondary phenological stages. $SE\,norm$ appeared more important for discriminating secondary phenological stages than principal phenological stages, increasing by 3 ranks for both crops, while the rank of span decreased from third and first for wheat and rapeseed, respectively.

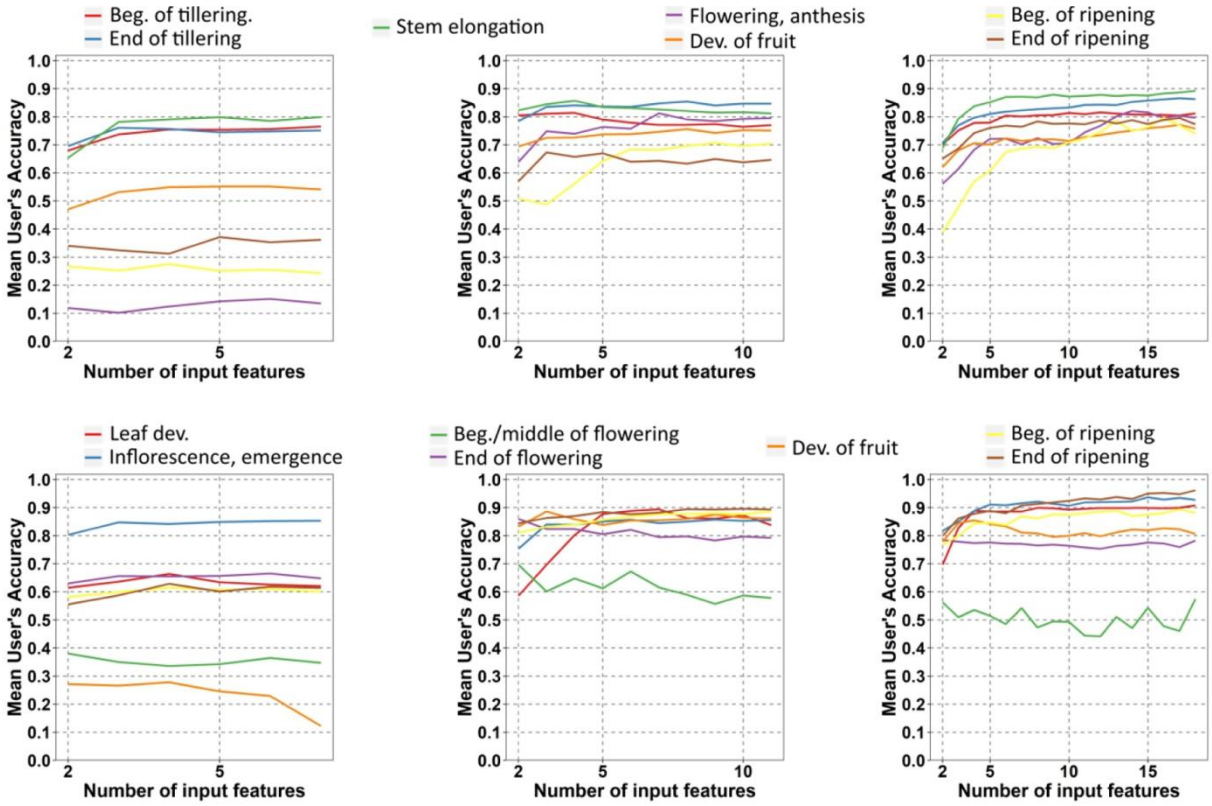

Figure 5-14. Mean UA of incremental classifications as a function of the number of input features to identify the 7 secondary phenological stages of wheat and rapeseed. The colored lines refer to thesecondary phenological stages.

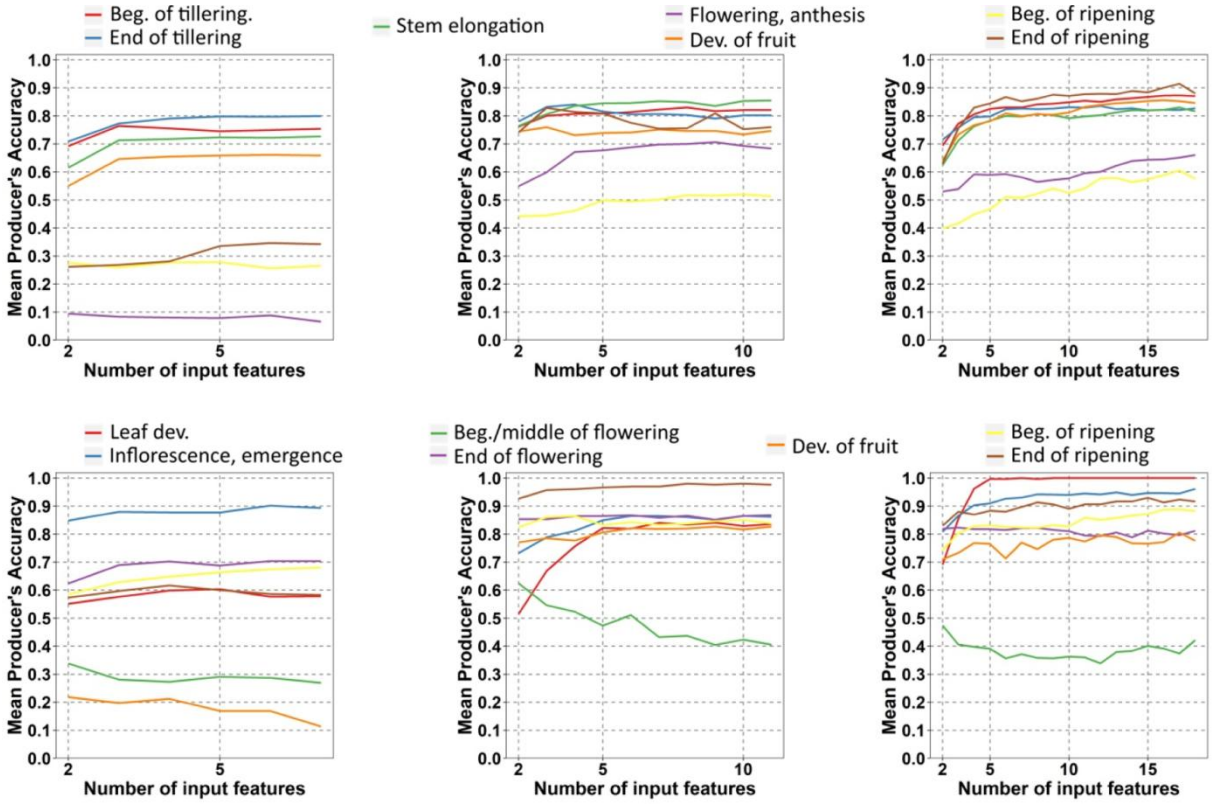

Figure 5-15. Mean PA of incremental classifications as a function of the number of input features to identify the 7 secondary phenological stages of wheat and rapeseed. The colored line refer to the secondary phenological stages.

For classification results for wheat, S-1 data alone (Figures 5-14a and 15a) underperformed S-2 data alone (Figures 5-14b and 15b) and combined S-1 & 2 data (Figures 5-14c and 15c) in classifying flowering, development of fruit and the beginning and end of ripening. However, by combining S-1 & 2 features (Figures 5-14c and 15c), the accuracy of the secondary phenological stages was either similar to those of S-2 data alone (Figures 5-14b and 15b) or higher, except for the flowering and the end of ripening stages based on the PA.

For classification results for rapeseed, the leaf development, the beginning/middle of flowering and the end of development of fruit were the stages least well predicted using S-1 data alone (Figures 5-14d and 15d) or S-2 data alone (Figures 5-14e and 15e). Combined use of S-1 & 2 data increased the accuracy of identifying the leaf development stage (Figures 5-14f and 15f).

5.5. Discussion

5.5.1. The relationship between Sentinel-2 features and phenological stages of wheat and rapeseed

For both crop types, the temporal profiles of S-2 bands were consistent with those observed by Ashourloo et al. (2019). Saturation was observed from stem elongation to flowering for wheat and from flowering to development of fruit for rapeseed (Figure 5). However, it should be noted that the analysis of the temporal profiles was done from only 5 dates due to the heavy cloud cover over the study area between DOY 72 and 152, i.e. during

the stem elongation, booting and early flowering stages for wheat and the flowering and development of fruit stages for rapeseed. Wilson et al. (2014) mentioned signal saturation for wheat and rapeseed when using hyperspectral data within a 400-900 nm range and identified optimal bands for identifying crops in green, red-edge and NIR wavelengths. Based on this study and our observations, we selected S-2 bands 3, 5, 6, 7, 8 and 8A as input for the incremental classification

In the temporal profiles of S-2-based vegetation indices and LAI, the standard deviation peaked at the end of inflorescence for wheat and the end of development of fruit for rapeseed (Figures 5-6). Thus, the heterogeneity in crop phenology among fields during the field surveys peaked earlier during the middle of stem elongation for wheat and the beginning of development of fruit for rapeseed. All vegetation indices saturated when the LAI was high (1-2 for wheat and 3-4 for rapeseed, depending on the vegetation index), which confirms observations of Haboudane et al. (2004) for wheat.

For wheat, the vegetation indices and LAI began to increase when the chlorophyll content increased at the tillering stage. They all decreased during ripening, as plants dried.

For rapeseed, decreases are observed during ripening due to the decrease in chlorophyll content as plants dried. LAI and WDVI began to increase at the beginning of inflorescence until the beginning of flowering as plant area expanded. WDVI decreased during the leaf development as leaves unfolded.

5.5.2. The relationship between Sentinel-1 backscatter coefficients and phenological stages of wheat and rapeseed

For wheat, while trends in the temporal profiles for σ^0VH and σ^0VV were similar, σ^0VV was higher than σ^0VH especially during the first phenological stages (i.e. tillering and stem elongation), since σ^0VV is influenced more by wheat growth than σ^0VH (Figures 5-7). This is consistent with observations of Cookmartin et al. (2000) who showed that σ^0VV is particularly sensitive to vegetation wetness and of Fieuzal et al. (2013) who observed maximum WC at the stem elongation stage. Both polarizations increased during tillering (DoY 18-72). The increase in the number of stems per plant and the length of stems results in an increase in VH polarization, which is dominated by double-bounce and volume-scattering mechanisms (Lopez-Sanchez et al. 2013; Wiseman et al. 2014; Veloso et al. 2017) and a strong increase in VV polarization, which is dominated by the influence of soil and canopy. Both σ^0VH and σ^0VV decreased throughout stem elongation but increased from inflorescence to ripening, as observed by Fieuzal et al. (2013), due to an increase in crop absorption when vegetation was wet, and decreased as vegetation dried. VV polarization is attenuated by vertical transformation of the structure of wheat during stem elongation (Brown et al. 2003). The $\sigma^0VH{:}\sigma^0VV$ ratio has varied little during tillering stages, which does not help identify secondary phenological stages. This ratio correlates more to fresh biomass than to photosynthetic activity (Veloso et al. 2017). For rapeseed, VH and VV polarizations increased slightly during leaf development as biomass increased. They varied little during inflorescence and decreased during flowering. Indeed, rapeseed's vertical transformation from a thick rosette of leaves to a flowering stalk attenuated VV polarization, while its low density attenuated VH polarization. Both polarizations increased from development of fruit to the beginning of ripening, which was also observed in other studies (Fieuzal et al., 2013; Lopez-Sanchez et al., 2013; Wiseman et al., 2014; Veloso et al., 2017). The progressive

development of structure without preferred orientations results in a more complex geometry, inducing a strong increase in the volume-scattering mechanism (Betbeder et al. 2016b). VH and VV polarizations decreased until the end of ripening due to the decrease in WC in the top layer of rapeseed. VV polarization is particularly sensitive to the WC of vegetation (Cookmartin et al. 2000), and VH is attenuated by the increase in wave penetration into the soil.

5.5.3. The relationship between Sentinel-1 polarimetric indicators and phenological stages of wheat and rapeseed

For both crop types, the temporal behaviors of $SPAN$, $\sigma^0 VH$ and $\sigma^0 VV$ were similar since span is the total scattered power. For wheat, $SE\ norm$ and $SE_i\ norm$ initially increased at tillering but then decreased during stem elongation and inflorescence. The increase in $SE_i\ norm$ was related to stem development during tillering. This complexity of plant structure increased the disorder encountered in the RaDAR signal. The opposite was observed during stem elongation, due to the less complex structure of wheat, which resulted in a decrease in backscatter power. Betbeder et al. (2016) demonstrated a strong positive correlation (r^2=0.7) between topsoil moisture and SE_i during leaf development and tillering due to a low wave penetration into the soil. $SE_p\ norm$ initially varied little but then significantly increased during stem elongation, indicating that polarization varied greatly due to heterogeneity in plant structures in wheat fields. $SE_p\ norm$ decreased linearly from the end of flowering to ripening, as wheat was becoming homogeneous at the field scale. $SE\ norm$ and $SE_i\ norm$ could identify the development of fruit stage, unlike the other S-1 features, since they decreased slightly during this stage. For rapeseed, the temporal changes in $SE\ norm$ and $SE_i\ norm$ were similar to those of wheat. As mentioned by Betbeder et al. (2016), the intensity of SE was sensitive to different phenological stages. The slight increase in $SE_p\ norm$ during flowering was associated with changes in rapeseed structure from a thick rosette of leaves to a flowering stalk, resulting in a strong variation in backscattering polarization (Betbeder et al. 2016b). $SE_i\ norm$ increased as rapeseed biomass increase; thus, it increased during flowering and decreased during ripening (Betbeder et al. 2016b).

5.5.4. Relative contributions of S-1 and S-2 data to mapping of wheat and rapeseed phenological stages

Concerning the prediction of principal phenological stages of wheat using S-2 data alone (Figures 5-9b), LAI was the most important feature, followed by S2REP, red-edge2 (B06) WDVI, NDVI and red edge1 (B05). For rapeseed (Figures 5-9e), the most important 5 features were NDVI, S2REP, band 3 (green), LAI and WDVI. Principal and secondary phenological stages of wheat and rapeseed were well identified by LAI derived from S-2 data, since this index is related to the density of green vegetation. The incremental classification results demonstrated the relevance of the S2REP index for both crop types, which is consistent with results of Frampton et al. (2013). S2REP, which is highly sensitive to chlorophyll content, is calculated from red-edge bands of S-2 that respond to high large changes in leaf reflectance (Hatfield et al. 2008). The importance of the S-2 red-edge bands has been demonstrated for predicting green LAI in crop fields, including wheat in Spain and Germany (Delegido et al. 2011b). We noted the potential of WDVI for predicting rapeseed phenology based on our analysis of temporal profiles; it was the only index sensitive to the leaf development stage.

Wilson et al. (2014) explained that rapeseed had higher reflectance in the green and red portions of the spectrum than other crops because of its yellow flowers.

Concerning principal and secondary phenological stages classification of wheat using S-1 data alone, the $\sigma^0VH{:}\sigma^0VV$ ratio ranked first for both crops, while σ^0VV ranked third (Figures 5-9a and 9d). Previous studies demonstrated the suitability of backscattering coefficients (σ^0VH, σ^0VV) and the polarization ratio ($\sigma^0VH{:}\sigma^0VV$) for estimating biomass and LAI of wheat (Dente et al. 2008; Betbeder et al. 2016b) and maize (Gao et al. 2013). Veloso et al. (2017) concluded that the influence of the ground was similarly reduced for wheat using $\sigma^0VH{:}\sigma^0VV$ compared to σ^0VH and σ^0VV, and was generally more consistent for wheat and rapeseed. For rapeseed, the $\sigma^0VH{:}\sigma^0VV$ ratio was the most important feature using S-1 data alone for classify principal and secondary phenological stages. The $\sigma^0VH{:}\sigma^0VV$ ratio had shown high performance in identifying principal phenological stages of both crops, confirming its high reliability for identifying principal and secondary phenological stages.

Consistent with results of Betbeder et al. (2016), polarimetric indicators were important for wheat and rapeseed: several of them were among the 4 input features selected based on the threshold automatically defined for predictions of principal and secondary phenological stages for both crops. SEp and span were selected to predict principal phenological stages of wheat and SEi was selected for rapeseed, while for secondary phenological stages, the selection included SEp and SE for wheat and SEi and SE for rapeseed.

This study aimed to evaluate the potential of S-1 data alone, S-2 data alone, and their combined use to predict wheat and rapeseed phenological stages. For wheat, the combined use of S-1 & 2 data outperformed use of S-1 or S-2 data alone in detecting the principal phenological stages of wheat and rapeseed. The secondary phenological stages of wheat were identified better using S-2 than S-1 data. Based on the standard deviation of the mean kappa index, similar results were obtained using S-2 data alone or combined S-1 & 2 data for the secondary phenological stages of wheat. The tillering was the principal and secondary phenological stage most accurately classified using S-1 data alone, S-2 data alone and their combined use (Figures 5-10a-c and 11a-c). From DOY 18 to 72, wheat was at tillering stage and a specific temporal behavior of S-1 and S-2 features was observed in comparison to all other phenological stages. However, the tillering stage was identified better using S-1 than S-2 data, while the flowering, development of fruit and ripening stages were identified better using S-2 than S-1 (Figures 10a and 10b). The SAR signal is sensitive to the geometry (e.g. roughness, texture, internal structure) and wetness of the observed targets, while optical reflectance is influenced by their physiology. Thus, we can conclude that the tillering stage of wheat was better discriminated by the structure of the wheat field rather than its physiology. From the stem elongation stage, the geometry of the wheat became vertical and varied little until ripening, while chlorophyll content increased and then decreased. Thus, S-2 features were more efficient than S-1 features to discriminate these phenological stages of wheat. For principal phenological stages of wheat, combined use of S-1 & 2 data improved the UA of tillering, stem elongation and ripening; only the PA of the stem elongation and flowering stages underperformed that of S-2. This is consistent with previous studies that have shown

saturation of the C-band (El Hajj et al. 2019) and optical bands (Haboudane et al. 2004) at high levels of wheat biomass.

For rapeseed principal phenological stages, the mean kappa index using combined S-1 & 2 data was higher and strongly higher than those obtained with S-2 data alone and S-1 data alone respectively. For secondary phenological stages, results of the combined use of S-1 & 2 data were similar to those obtained with S-2 data alone. However, combined use of S-1 & 2 data increased the accuracy of identifying the leaf development stage of rapeseed thanks to the capture of additional information about physiology from S-2 and geometry from S-1. Development of fruit was the most difficult principal phenological stage to identify using S-1 data alone and the combined use of S-1 & 2 data, due to confusion with ripening (Appendix C and E, Table C-4, C-6, E-1 and E-2 and Figures 5-10d and 10f, 11d and 11f). The most important features using S-1 data alone were σ^0VH, $\sigma^0VH{:}\sigma^0VV$ and σ^0VV. The temporal profiles showed that the $\sigma^0VH{:}\sigma^0VV$ ratio was stable between development of fruit and ripening, while σ^0VH and σ^0VV slightly increased. The structure of rapeseed stages is very similar during development of fruit and ripening, with randomly oriented canopy components. This high similarity can be explained by the fact that field observations were conducted during successive phenological stages (i.e. the end of development of fruit (BBCH = 77 and 79) and the beginning and end of ripening (BBCH = 80 and 89)). However, while, the development of fruit was considerably better classified using combined S-1 & 2 data (UA max = 0.87, PA max = 0.75) than using S-1 data alone (UA max = 0.32, PA max = 0.21), this phenological stage was the least well predicted. The most important features using combined S-1 & 2 data were σ^0VH derived from S-1 followed by NDVI and S2REP derived from S-2 and then $SE\ norm$, span, $SE_i\ norm$, $\sigma^0VH{:}\sigma^0VV$ and σ^0VV derived from S-1. Thus, SAR S-1 features increased confusion between development of fruit and ripening stages. The development of fruit was the most difficult secondary phenological stage to identify using S-1 data alone while the beginning and middle of flowering was the least well predited using S-2 data alone and combined S-1 & 2 data (Figures 5-14e and 14f, 15e and 15f). Prediction errors occurred between the two secondary phenological stages of flowering (Appendix D and E, Tables D-5, D-6, E-7 and E-8), the first corresponding to first flowers open until 40% of flowers on main raceme open and the second to the the full flowering until the end of flowering while the petals are fallen. It should be noted that this period coincided to the lack of S-2 data due to cloud cover, while S-1 temporal profiles showed little variation.

Classification results for combined use of S-1 & 2 data pointed out the large contribution of S-1 features for rapeseed. Combined used of S-1 & 2 data identified better principal phenological stages of rapeseed than S-2 data alone; moreover, the identification of the leaf development stage was improved adding S-1 features (Figures 5-11c, 11f). Results were more balanced for secondary phenological stages of wheat since S-2 data alone results were similar to those of combined S-1 & 2 data, except for the tillering stage.

5.6. Conclusion

This study evaluated the potential of SAR S-1, optical S-2 time-series and the combined use of S-1 & 2 data to identify principal and secondary phenological stages of wheat and rapeseed. More specifically, we have shown that:

- Combined use of S-1 & 2 data (mean kappa = 0.53-0.82 and 0.74-0.92 for wheat and rapeseed, respectively) was more accurate than using S-1 data alone (mean kappa = 0.48-0.61 and 0.61-0.64 for wheat and rapeseed, respectively) or S-2 data alone (mean kappa = 0.54-0.75 and 0.67-0.86 for wheat and rapeseed, respectively), in identifying principal and secondary phenological stages for both crops.
- S-2 data alone provided better results than S-1 data alone for both crop types.
- Concerning S-1 features, the $\sigma^0VH{:}\sigma^0VV$ ratio and polarimetric indicators were important for obtaining accurate classifications of phenological stages for both crops. These features were the most important for discriminating both crop types using S-1 data alone and combined S-1 & 2 data.
- Concerning S-2 features, LAI, NDVI and S2REP were the most important features for both crop types while the MCARI was less important.
- The number of Sentinel features automatically selected to predict phenological stages of wheat and rapeseed ranged from 4 to 7.

Overall, this study highlighted the value of using polarimetric indicators (SE and span) and combining Sentinel-1 and 2 data to monitor wheat and rapeseed phenology.

To confirm these results, this method should be based on a larger sample size, especially for identifying secondary phenological stages. Also, to test the robustness of combining S-1 & 2 data to predict principal and secondary phenological stages, the final predictive models should be applied to other study areas.

CHAPTER 6

Evaluation of Sentinel-1 and 2 time series for estimating LAI and biomass of wheat and rapeseed crop types

Contents

Reproduced from the article:

Mercier A, Betbeder J, Rapinel S, et al. (2020b) Evaluation of Sentinel-1 and -2 time series for estimating LAI and biomass of wheat and rapeseed crop types. JARS 14:024512. https://doi.org/10.1117/1.JRS.14.024512

6.2. Introduction

Crop monitoring is essential for managing agricultural resources to decrease environmental impacts. Indeed, natural resources (soil, forest, water) gradually decrease in the context of agricultural intensification, while food insecurity increases (Pinstrup-Andersen and Pandya-Lorch 1998). The challenge is to develop practices that are both economically and environmentally sustainable (Pinstrup-Andersen and Pandya-Lorch 1998) to meet the needs for food and feed, ecosystem services and human health. Land managers need timely and accurate information to help them manage agricultural resources efficiently.

Crop biophysical parameters, which are key variables that address this challenge, are required for several reasons: to estimate crop yield as model inputs (Maas 1988; Jin et al. 2018); to prevent disease and pest outbreaks (Hatfield and Pinter 1993; Vreugdenhil et al. 2018) since the plants are more sensitive during specific phenological stages; to optimize water resource management by accurately calculating crop needs and synchronizing irrigation schedules with vegetation stages during which water needs are minimal (Duchemin et al. 2015) and to decrease fertilizer application (Diacono et al. 2013; Bouchet et al. 2016). Crop biophysical parameters can also be used as indicators to study impacts of global warming (Menzel et al. 2006).

Most crop biophysical parameters commonly used for these purposes (e.g. LAI, DB, WB, WC) are obtained using time-consuming ground surveys and thus cannot be collected at the landscape scale. Remote sensing data can provide a solution to this issue because they can be used to map large areas at a fine scale. The free availability of SAR S-1 and optical S-2 time series offers a unique opportunity to monitor crops at a high temporal frequency (5-days) and high spatial resolution (10 m).

Many studies have focused on the use of satellite optical data (AVHRR, SPOT, Landsat, MODIS, IRS, IKONOS, QuickBird, Formosat-2, S-2 images) to estimate crop biophysical parameters, demonstrating the high performance of some spectral bands, vegetation indices, and biophysical variables (Quarmby et al. 1993; Doraiswamy et al. 2004; Mulla 2013; Bontemps et al. 2015; Betbeder et al. 2016b). More specifically, S-2 time series showed great potential for estimating grassland and crop LAI (Delegido et al. 2011b; Frampton et al. 2013; Clevers et al. 2017; Pan et al. 2018; Wang et al. 2019), biomass (Veloso et al. 2017; Ghosh et al. 2018; Ganeva et al. 2019) and phenological stages (Veloso et al. 2017; Ghosh et al. 2018; Stendardi et al. 2019). The importance of the S-2 red-edge bands has been demonstrated for predicting green LAI in crop fields, including wheat in Spain and Germany (Delegido et al. 2011b); however, Gosh et al. (2018) concluded that S-2 red-edge bands did not improve estimation of potato LAI compared to NIR bands. Ganeva et al. (2019) highlighted the importance of SWIR bands for estimating vegetation height and the vegetation fraction of rapeseed and wheat. The vegetation indices that emerged from the S-2 studies conducted in Europe were NDVI, IRECI, MCARI and NDI for several crops (wheat, rapeseed, barley, oat, onion, potato, sunflower, alfalfa, and grapevine). GNDVI and WDVI also performed well when estimating the parameters for potato. However, optical data have limitations because they are sensitive to weather conditions, capture only top-of-canopy information, and saturate at high levels of biomass and LAI. For example, for wheat, Wang et al. (2016a) estimated the saturation of visible and red-edge bands from 2.5 $m^2.m^{-2}$ for LAI and 1 $kg.m^{-2}$ for aboveground biomass. In contrast, although soil conditions (roughness and moisture) affect the SAR signal (McNairn

and Brisco 2004; Chaube et al. 2019), SAR data can be collected regardless of weather or light conditions, and microwaves are sensitive to the internal structure of vegetation (Fieuzal et al. 2013; Wiseman et al. 2014).

Several studies have evaluated the potential of satellite SAR data (RADARSAT, TerraSAR-X, ALOS, S-1) for estimating crop biophysical parameters (Steele-Dunne et al. 2017), and S-1 time series have demonstrated their high value for this purpose (Mandal et al. 2018b, a; Vreugdenhil et al. 2018; Kumar et al. 2018; Song and Wang 2019; Nasrallah et al. 2019). The high potential of backscattering coefficients and the VH:VV polarization ratio was observed when detecting changes in vegetation structure for rapeseed, maize and winter cereals (Vreugdenhil et al. 2018). Mandal et al. (2018a) found good correlations between S-1 polarization combination (VH+VV) and WB and plant area index (half the surfaces of all green organs) of rapeseed. The S-1 VV polarization has shown high correlations with the WC, WB, DB and LAI of wheat (Kumar et al. 2018), while the VH and VV polarizations were important for identifying the phenological stages of wheat (Song and Wang 2019; Nasrallah et al. 2019) and rice (Mandal et al. 2018b).

In addition, polarimetric indicators derived from RADARSAT-2 and TerraSAR-X have shown high sensitivity to crop biomass (Betbeder et al. 2016b; Wiseman et al. 2014; Homayouni et al. 2019; Yang et al. 2019), LAI (Betbeder et al. 2016b; Jin et al. 2015; Jiao et al. 2009; Canisius et al. 2018) and phenological stages (Mascolo et al. 2015; McNairn et al. 2018; Pacheco et al. 2016). Betbeder et al. (2016b) showed that the VV polarization was more effective than the NDVI at estimating wheat parameters from RADARSAT-2 images, and that while polarimetric indicators did not outperform VV, they were effective at estimating rapeseed crop height and DB. Wiseman et al. (2014) demonstrated that entropy had the highest accuracy among 21 SAR parameters derived from RADARSAT-2 images (linear and circular backscatter coefficients, linear copolarization and cross-polarization ratios, and polarimetric indicators) when estimating the DB of rapeseed. Entropy also emerged as important for estimating phenological stages of onion (Mascolo et al. 2015) using RADARSAT-2 and of rapeseed using RADARSAT-2 or TerraSAR-X (Pacheco et al. 2016). Despite these encouraging results, to our knowledge, polarimetric indicators derived from S-1 data have not been used to study crop biophysical parameters.

Yang et al. (2019) demonstrated a higher saturation point and better accuracy when estimating rapeseed biomass using quad-polarization SAR data derived from RADARSAT-2 rather than dual polarimetric data. However, even though quad-polarization data express several backscattering mechanisms better than dual-polarization data, quad-polarization mode always yields a smaller swath width and lower spatial resolution than dual-polarization mode, which is not yet suitable for application over large areas. In addition, no quad-polarization data are freely available, unlike dual-polarization data (S-1).

Several modeling approaches were investigated for estimating crop biophysical parameters using optical and SAR satellite images. It is well known that many remote sensing-based indicators show a non-linear relationship with crop biophysical parameters, which can be explained by the Beer-Lambert extinction law for radiation penetration in plant canopies (Tan et al. 2020). Several studies have shown the value of non-linear machine learning methods to estimate the crop biomass (Wang et al. 2016b; Ahmadian et al. 2019), as well as LAI, WC WB, DB and plant height (Kumar et al. 2018). Among machine learning methods, Gaussian processes regression (GPR), which is a non-parametric kernel-based model (Williams and Barber 1998), is one of the most robust regression algorithm for

monitoring crop biophysical parameters (Ganeva et al. 2019; Verrelst et al. 2012; Upreti et al. 2019; Pipia et al. 2019). For example, Upreti et al. (2019) demonstrated the superiority of GPR over eight machine-learning methods including RFs, neural networks and regression trees for estimating wheat biophysical parameters using S-2 images.

The objective of this study was to evaluate the potential of S-1 and S-2 images to estimate LAI, WB, DB and WC. We focused on wheat and rapeseed, which are two of the most important crops in the world in terms of harvested area (FAO, 2017). We evaluated the predictive power of 22 optical S-2 features (10 spectral bands and 12 vegetation indices) and 7 SAR S1-features (2 backscattering coefficients, 1 ratio and 4 polarimetric indicators). We estimated crop biophysical parameters of wheat (from tillering to ripening stages) and rapeseed (from leaf development to ripening stages) using a GPR approach.

6.3. Materials and Methods

6.3.1. Study area

The study area is a LTER site named ZAA located in the southern part of the Bay of Mont-Saint-Michel, France (Figure 6-1).

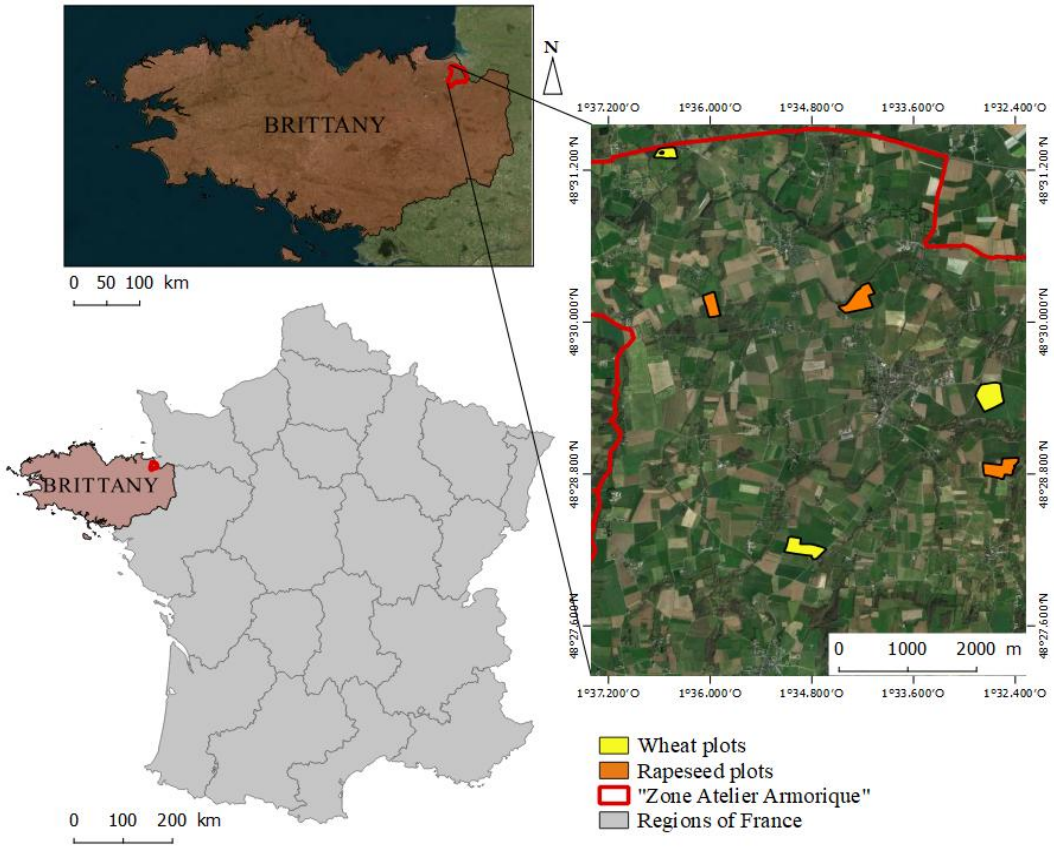

Figure 6-1. Location of the study area. Satellite imagery and aerial photographs accessed through Bing Aerial using OpenLayers QGIS plugin 1.4.8 (Microsoft®Bing™Maps).

It is part of European LTER and international ILTER networks (https://osur.univ-rennes1.fr/za-armorique). The ZAA was created in 1993 to perform long-term research around three main themes: planning, public policy and landscape dynamics; the relationship between spatio-temporal landscape dynamics and biodiversity; and influence of spatial-

temporal landscape dynamics on ecosystem processes. This 130 km² area has a temperate climate with an annual mean temperature of 12 °C and annual mean precipitation of 650 mm. Maize, wheat, rapeseed and barley are the main crops grown in this agricultural area. The crops are surrounded by hedges to differing degrees, with density of the hedge network increasing from north to south.

6.3.2. Satellite imagery

Four optical S-2 and five SAR S-1 images were collected from January to July 2017 throughout the entire crop cycles of wheat and rapeseed (Figure 6-2).

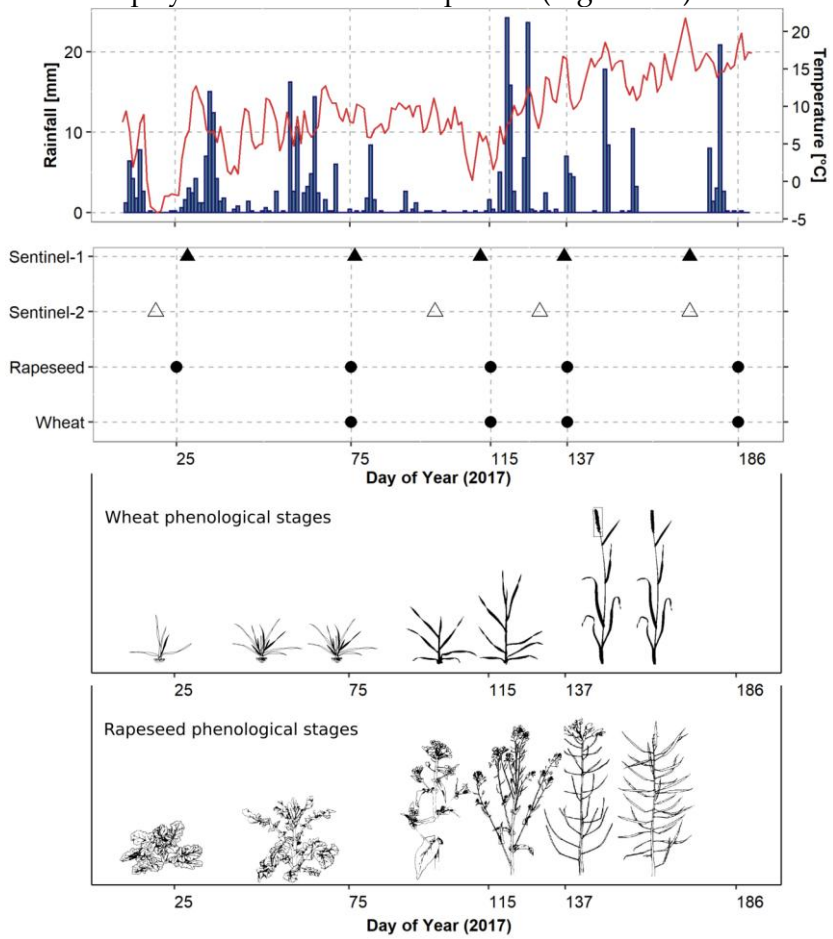

Figure 6-2. Days of year of satellite images, field surveys and main crop phenological stages for wheat and rapeseed (Bleiholder, et al. 2001). The ombrothermal diagram (Météo France) shows the climate conditions during image acquisition.

The S-1 images were acquired in Interferometric Wide (IW) swath mode and delivered with VV and VH polarizations. We used the SLC product, which consists of focused SAR data that use the full C-signal bandwidth and preserve the phase information, to derive polarimetric indicators. The incidence angle of images ranged from 36.9-51.3° (Table 6-1). The spatial resolution was 2.3 × 13.9 m (Figure 6-2 and Table 6-1).

Table 6-1. Main characteristics of S-1 SLC images used in this study.

Frequency	C-band (center frequency of 5 405 GHz)
Mode	Interferometric Wide Swath
Product type	Single Look Complex
Ground resolution	2.3 m
Azimuth resolution	13.9 m
Temporal resolution	6 days
Orbit	Descending
Polarization	Dual (VV & VH)
Swath	250 km
Incidence angle	36.9-51.3°

For the S-2 images, 10 bands with spatial resolutions of 10 and 20 m were selected (Table 6-2). The tiles were downloaded from the Europe Copernicus web site in level 2A, which provides top-of-canopy reflectance.

Table 6-2. Main characteristics of S-2 MSI L2A images used in this study.

Spatial and spectral resolutions	*10 × 10 m* B2 (490 nm), B3 (560 nm), B4 (665 nm) and B8 (842 nm) *20 × 20 m* B5 (705 nm), B6 (740 nm), B7 (783 nm), B8a (865 nm), B11 (1610 nm), B12 (2190 nm)
Temporal	5 days
Swath	290 km

6.3.3. Field data collection

Ground surveys were conducted on 3 wheat fields and 3 rapeseed fields (Figure 6-3). The wheat fields were 4.26, 10.33 and 12.81 ha in size, while the rapeseed fields were 6.02, 10.11 and 11.35 ha. Phenological stages were identified from January to July 2017 (Figure 6-2) based on the Biologische Bundesanstalt, Bundessortenamt and CHemical industry (BBCH) scale (Bleiholder, et al. 2001). Four and five principal phenological stages were observed in Brittany for wheat and rapeseed, respectively (Tables 3 and 4). Approximately 10 hemispherical photos were taken of each sampled plot on each date. LAI was estimated from digital hemispherical photographs using CAN-EYE software (https://www6.paca.inra.fr/can-eye) and averaged per date and field sample. At the same time, biomass measurements were performed (Betbeder et al. 2016b). In homogeneous areas (20 × 20 m), 5 samples of wheat 50 cm on the ground and 5 rapeseed plants were collected. The WB of each sample was directly weighed in situ, and the DB was measured after drying the crop (oven, 65°C, 48 h). WC in the plant equals WB minus DB. Figure 3 shows the temporal profiles of the wheat and rapeseed parameters and Table 6-5 summarizes the crop biophysical parameters for all wheat and rapeseed fields sampled.

Table 6-3. Phenological stages of wheat considered in the study area.

Principal stage	BBCH	Description
Tillering	23	3 tillers detectable
Stem elongation	31	First node at least 1 cm above tillering node
Inflorescence	55	Middle of heading: half of inflorescences emerged
Ripening	89	Fully ripe: grain hard, difficult to divide with thumbnail

Table 6-4. Phenological stages of rapeseed considered in the study area.

Principal stage	BBCH	Description
Leaf development	18	Beginning of tillering: first tiller detectable
Inflorescence emergence	53	Flower buds raised above the youngest leaves
Flowering	67	Flowering declining: most petals fallen
Development of fruit	71	10% of pods have reached their final size
Ripening	89	Fully ripe

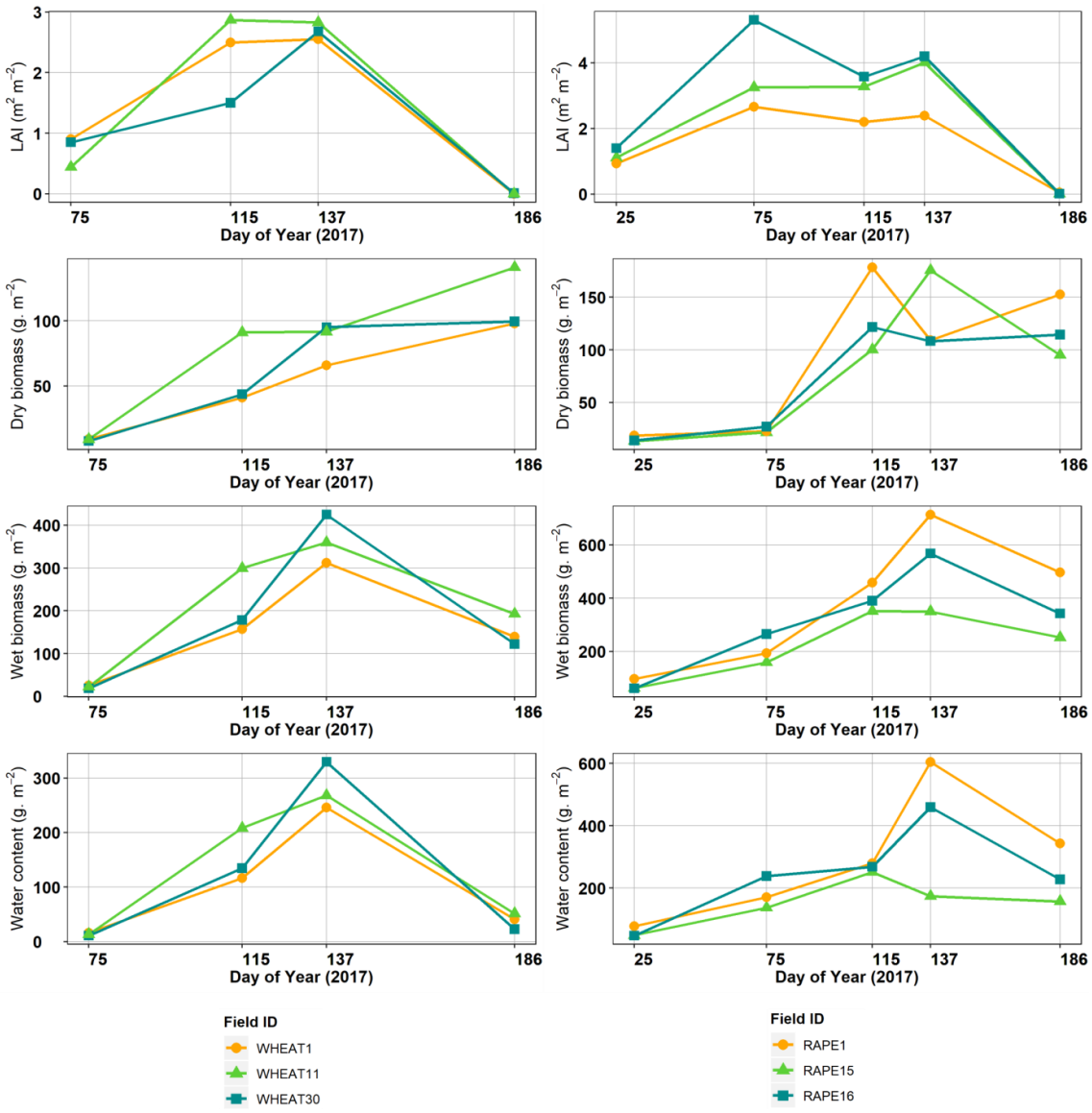

Figure 6-3. Temporal profiles of crop biophysical parameters for the wheat and rapeseed fields sampled.

Table 6-5. Crop biophysical parameters for wheat and rapeseed fields.

	Wheat				Rapeseed			
Parameter	**LAI**	**WB**	**DB**	**WC**	**LAI**	**WB**	**DB**	**WC**
Minimum	0.00	18.70	7.78	10.92	0.01	61.30	13.38	47.48
Maximum	2.87	424.74	141.20	329.56	5.31	713.80	178.42	604.80
Mean	1.43	187.71	66.15	121.56	2.29	317.40	84.82	232.93
Standard deviation	1.19	136.02	43.62	114.44	1.67	190.26	60.40	151.22

6.3.4. Data processing

First, we preprocessed the SAR S-1 and optical S-2 signals. Second, we used GPR to estimate LAI, WB, DB, WC of the wheat and rapeseed crops using the field samples and the S-1 and S-2 features, before quantifying the predictive power of the best models using cross-validation and the "k-folds " method.

6.3.4.1. SAR Sentinel-1 image preprocessing

We used the S-1 Toolbox (ESA, SNAP) to extract backscattering coefficients from the S-1 images.

Calibration was performed to convert digital pixel values into radiometrically calibrated backscatter (σ^0VV, σ^0VH) using the following equation (Eq. 6.1) (Miranda and Meadows 2015):

$$\text{value(i)} = \frac{|\text{DN}_\text{i}|}{{\text{A}_\text{i}}^2} \tag{6.1}$$

where DN is the digital number and A is the information necessary to convert SAR reflectivity into physical units provided in the Calibration Annotation Data Set in the image metadata.

The presence of speckle in SAR images was reduced using a refined Lee filter in a 7 × 7 pixel sliding window (Lee et al. 1994). The Range Doppler orthorectification method was applied to correct topographical distortions; the operator used orbit state vector information, RaDAR timing annotations, slant-to-ground-range conversion parameters and a reference DEM (SRTM). We calculated a ratio by dividing σ^0VH by σ^0VV. Then, the resulting images were transformed from a linear into a decibel (dB) scale using the following equation (Eq. 6.2):

$$\sigma^0(db) = 10 \times log_{10}(\sigma^0) \tag{6.2}$$

We used PolSARpro version 5.1.3 software to derive polarimetric indicators from the S-1 images (Pottier and Ferro-Famil 2012).

First, we extracted the 2 × 2 covariance matrix (C_2) from the scattering matrix S. Second, the presence of speckle in SAR images was reduced using a refined Lee filter in a 7 × 7 pixel sliding window (Lee et al. 1994). Third, we calculated the scattered power called span in the case of a polarimetric RaDAR system (Ferro-Famil and Pottier 2014), and the SE (randomness of scattering of a pixel) was calculated using the following equation (Eq. 6.3):

$$\text{SE} = \log(\pi^2 \text{e}^2 |\text{C}_2|) = \text{SE}_\text{i} + \text{SE}_\text{p} \tag{6.3}$$

where SE_i is the intensity and SE_p is the degree of polarization.

Finally, SE, SE_i and SE_p were normalized into SE norm, SE_i norm and SE_p norm.

6.3.4.2. Optical Sentinel-2 image preprocessing

We calculated 12 vegetation indices (Table 6-6) that are frequently used to monitor crop biophysical parameters (LAI, biomass, chlorophyll content and phenological stages) in studies using S-2 data (Frampton et al. 2013; Clevers et al. 2017; Daughtry et al. 2000; Herrmann et al. 2011; Clevers and Gitelson 2013). The indices included the GNDVI, IRECI, MCARI, MSAVI, MTCI, NDI, NDVI, PSSRa, REIP index, S2REP index, SAVI and WDVI.

Finally, we applied a spline method to interpolate daily the 10 spectral bands, and 12 vegetation indices derived from the S-2 images to match the dates of SAR S-1 acquisition using the "stats" package of R software (TEAM, R. Core et al. 2018). Then, S-1 and S-2 features were projected onto the RGF93/Lambert-93 system (EPSG 2154).

In total, we preprocessed 110 S-2 features (10 spectral bands and 12 vegetation indices × 5 dates) and 35 S-1 features (2 backscattering coefficients, 1 backscatter ratio and 4 polarimetric indicators × 5 dates).

Table 6-6. Vegetation indices calculated from S-2 images. G = Green, R = Red, RE = Red-Edge.

Index	Equation	S-2 bands used	Original author
GNDVI	(RE3 - G) / (RE3 + G)	(B7 - B3) / (B7 + B3)	(Gitelson et al. 1996)
IRECI	(RE3 - R) / (RE1 / RE2)	(B7 - B4) / (B5 / B6)	(Guyot and Baret 1988)
MCARI	[(RE1 - R) 0.2(RE1 - G)] * (RE1 - R)	[(B5 - B4) - 0.2(B5 - B3)] * (B5 - B4)	(Daughtry et al. 2000)
MSAVI	(1 + L) * (NIR- R) / (NIR + R + 0.5) L = 1 – 2 * 0.5 * (RE3 – R) / (RE3 + R) * (NIR – 0.5 * R)	(1 + L) * (B8- B4) / (B8 + B4 + 0.5) L = 1 – 2 * 0.5 * (B7 – B4) / (B7+B4) * (B8 – 0.5 * B4)	(Qi et al. 1994)
MTCI	(RE2 - RE1)/(RE1 - R)	(B6 - B5)/(B5 - B4)	(Dash and Curran 2004)
NDI	(RE1 - R) / (RE1 + R)	(B5 - B4) / (B5 + B4)	(Delegido et al. 2011a)
NDVI	(RE3-R)/(RE3+R)	(B7-B4)/(B7+B4)	(Rouse et al. 1973)
PSSRa	RE3/R	B7/B4	(Blackburn 1998)
REIP	700 + 40 * ((R + RE3)/2 - RE1) / (RE2 - RE1)	700 + 40 * ((B4 + B7)/2 - B5) / (B6 - B5)	(Guyot and Baret 1988)
S2REP	705 + 35 * ((((RE3 + R)/2) - RE1)/(RE2 - RE1))	705 + 35 * ((((B7 + B4)/2) B5)/(B6 - B5))	(Guyot and Baret 1988)
SAVI	(1 + 0.5) * (NIR- R) / (NIR + R + 0.5)	(1 + 0.5) * (B8- B4) / (B8 + B4 + 0.5)	(Huete 1988)
WDVI	(NIR – 1.5 * R)	(B8 – 1.5 * B4)	

6.3.4.3. Estimating crop biophysical parameters

GPRs were performed using crop biophysical parameters of the wheat and rapeseed fields sampled and S-1 & S-2 features. GPR is a probabilistic non-parametric approach to regression (Williams and Barber 1998). A Gaussian process is a stochastic process which can be specified by its mean function $\mu(x)$ and its covariance function $C(x, x')$; any finite set of points will have a joint multivariate Gaussian distribution. Gaussian process model assumes that the noise model is gaussian with zero-mean and variance $\sigma^2 I$, then the predicted mean (Eq. 6.4) and variance (Eq. 6.5) at x_* are given by:

$$\hat{y}(x_*) = k^T(x_*)(K + \sigma^2 I)^{-1} t \quad (6.4)$$

$$\sigma^2_{\hat{y}}(x_*) = C(x_*, x_*) - k^T(x_*)(K + \sigma^2 I)^{-1} k(x_*) \quad (6.5)$$

where $[K]_{ij} = C(x_i, x_j)$ and $k(x_*) = (C(x_*, x_1), \ldots, C(x_*, x_n))^T$.

A radial basis function kernel (Eq. 6.6) was used, defined as:

$$K(x, x') = \exp(-\sigma \| x - x' \|^2) \quad (6.6)$$

where σ is a parameter that sets the « spread » of the kernel.

GPR models were calibrated and validated using 10 repeated 3-fold cross-validation. More folds were not possible due to the sparse calibration dataset (n = 12 for wheat and n = 15 for rapeseed). The σ parameter of the radial basis function kernel was optimized with a tuning parameter grid value ranging from 0 to 4 (with a 0.05 step) to limit overfitting. For each relation, we calculated the adjusted R^2, related to the proportion of variance explained by the model, and the relative root mean square error (rRMSE), calculated by dividing the RMSE by the mean of observed data. We also calculated the means and standard deviations of adjusted R^2 and rRMSE among the 10 repeats.

GPR was performed with software "R" version 3.6.3 (R. Core Team, 2020) using packages "caret" version 6.0 (Kuhn et al. 2020).

6.4. Results and discussion

To estimate the crop biophysical parameters of the wheat and rapeseed, we compared the respective value of S-1 and S-2 features to model crop LAI, WB, DB and WC using GPR.

6.4.1. Estimating crop biophysical parameters using S-2 images

Concerning estimation of wheat crop biophysical parameters using S-2 features, correlations were high using green and NIR bands and all indices except MCARI and NDI45 to estimate LAI and WC (adj. $R^2 > 0.85$ and 0.70 respectively) (Figure 6-4). More specifically, figure 5 shows the best relationships obtained between wheat crop biophysical parameters and S-2 features. There was a linear and positive relation between LAI and NIR-band 8, the NIR reflectance increasing with the chlorophyll content. The lowest LAI values were observed during the ripening (BBCH = 89) and the highest ones during the stem elongation (BBCH = 33) and inflorescence (BBCH = 51). The WC decreased with the green band reflectances from inflorescence (BBCH = 55) to tillering (BBCH = 23). These results are consistent with previous studies that have shown greater sensitivity of green or NIR spectral domains (Fu et al. 2014; Wilson et al. 2014) and of some indices such as MSAVI (Haboudane et al. 2004), IRECI and NDVI (Frampton et al. 2013) to wheat biomass. Clevers et al. (2017) also demonstrated good performance of WDVI to estimate LAI of potato ($R^2 = 0.809$).

In contrast, the predictive power of models for DB (adj. R^2 max = 0.72) and WB (adj. R^2 max = 0.71) was low (Figure 4). More specifically, DB and WB values were high at ripening (BBCH = 89) when wheat is fully ripe, while MTCI and WDVI values were low when wheat is brown in color (Figure 6-5). Then, MTCI and WDVI values increased from tillering (BBCH = 23) to inflorescence (BBCH =55).

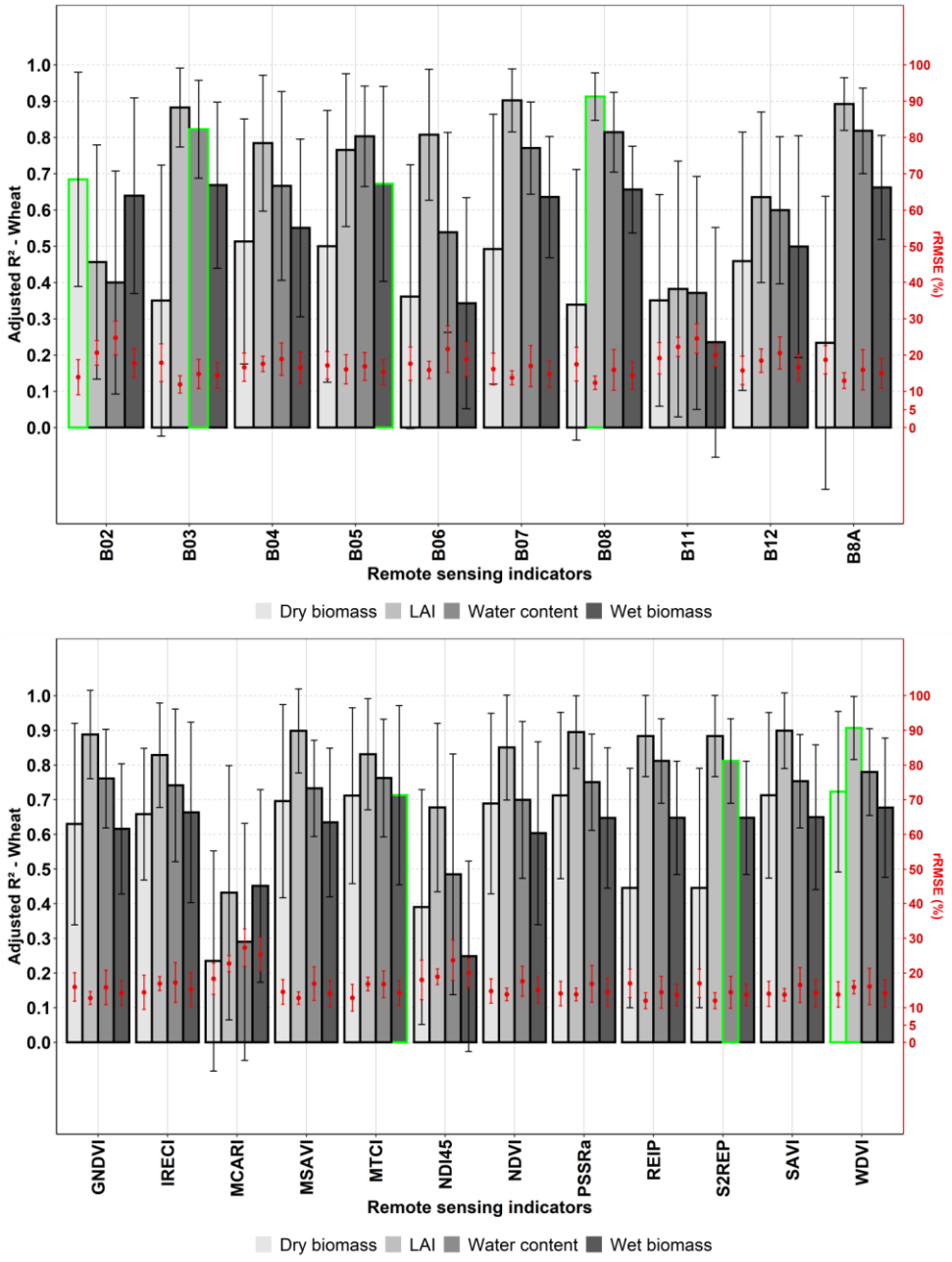

Figure 6-4. Adjusted R^2 and rRMSE (red dots) of empirical relationships between S-2 features and crop biophysical parameters (LAI, DB, WB and WC) of wheat fields. The highest adjusted R^2 values are highlighted in green.

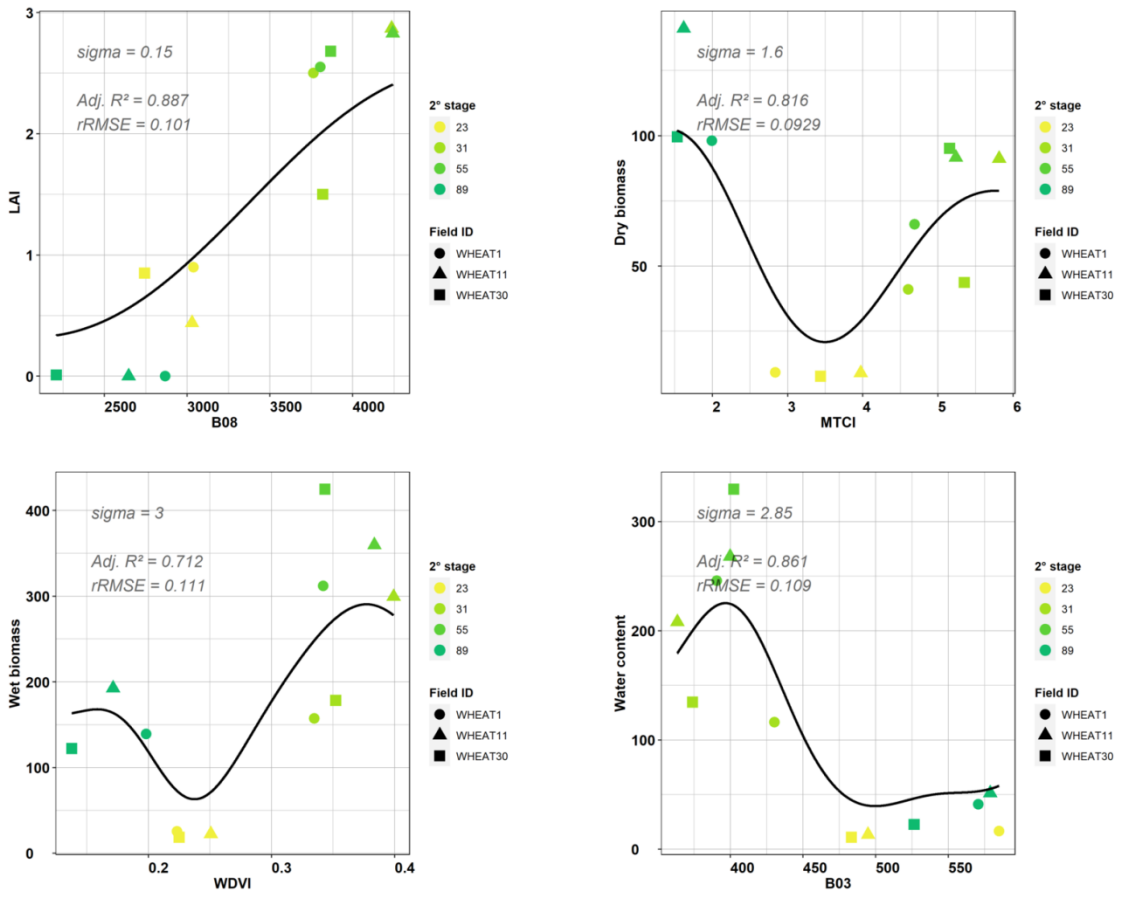

Figure 6-5. Best relationships obtained between wheat LAI, DB, WB and WC and S-2 features.

For rapeseed, the best results for DB and WB were obtained from bands 11 and 12, which correspond to the SWIR domain (adj. R^2 max = 0.85 and 0.77 respectively), while vegetation indices were not useful (adj. R^2 max < 0.55) (Figure 6-6). In contrast, the predictive power of models for WC and LAI (adj. R^2 max = 0.60 and 0.64 respectively) was low. More specifically, figure 7 shows the best relationships obtained between rapeseed LAI, DB, WB and WC and S-2 features. The more WB, DB and WC increased, the more the SWIR reflectance decreased. The results of estimating WC were poor, no relation being found between WC and SWIR-band 11 from 200 to 300 $g.m^{-2}$. When LAI was high (2.5-3), MTCI saturated at the inflorescence (BBCH = 53), flowering (BBCH = 67) and development of fruit (BBCH =71) stages.

These results are consistent with other studies that have demonstrated the high performance of the SWIR bands for mapping vegetation (Schultz et al. 2015; Immitzer et al. 2016) and estimating the nitrogen concentration in biomass, height and vegetation fraction of wheat and rapeseed (Ganeva et al. 2019). Wang et al. (2008) also demonstrated that WC increases with the decreasing of SWIR reflectances, with a saturation from LAI of 3. Besides, we showed that MTCI saturated when the LAI was high, which confirms observations of Mercier et al. (2020) over rapeseed fields in northern France.

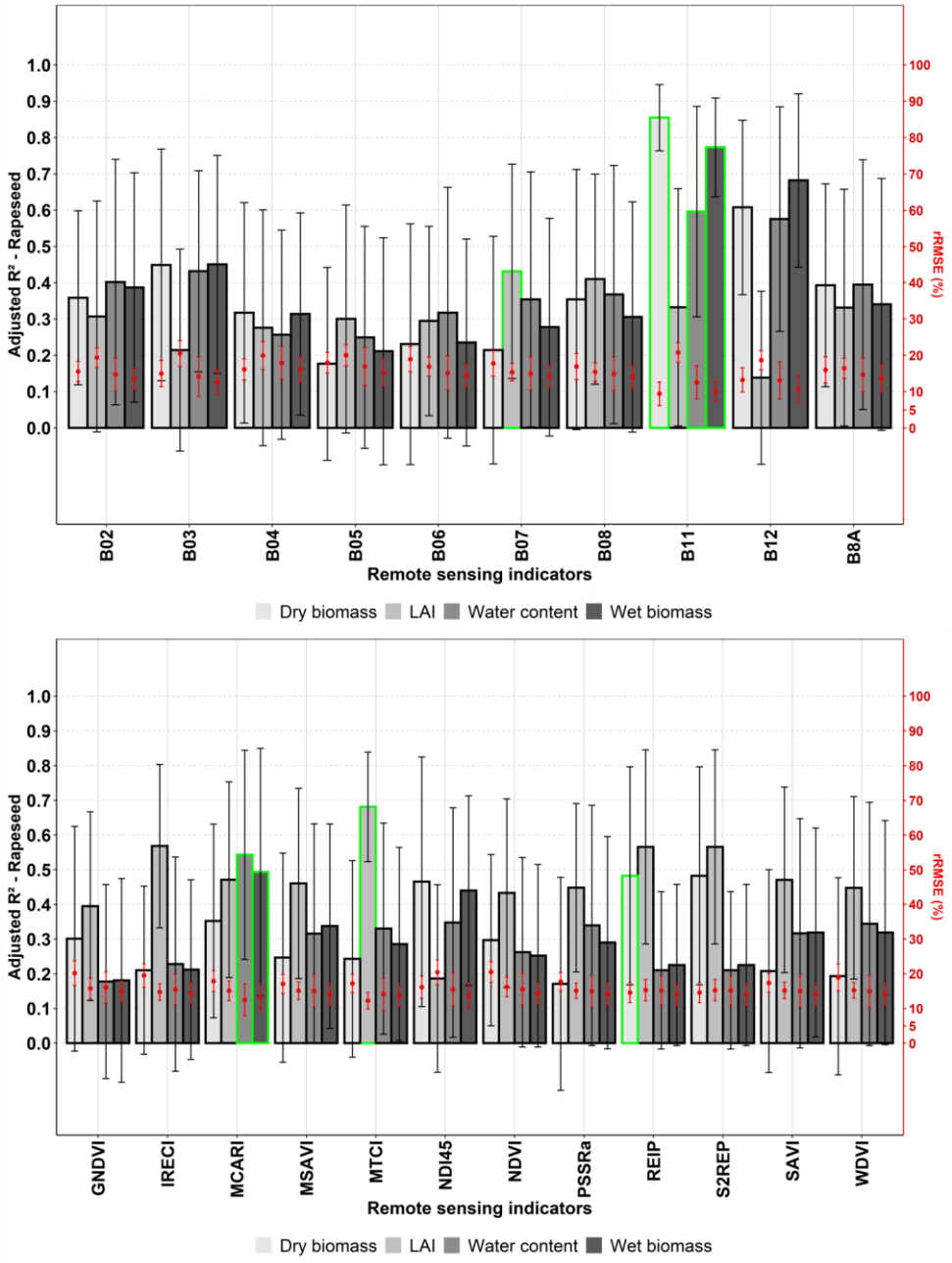

Figure 6-6. Adjusted R^2 and rRMSE (red dots) of empirical relationships between S-2 features and crop biophysical parameters (LAI, DB, WB and WC) of rapeseed fields. The highest adjusted R^2 values are highlighted in green.

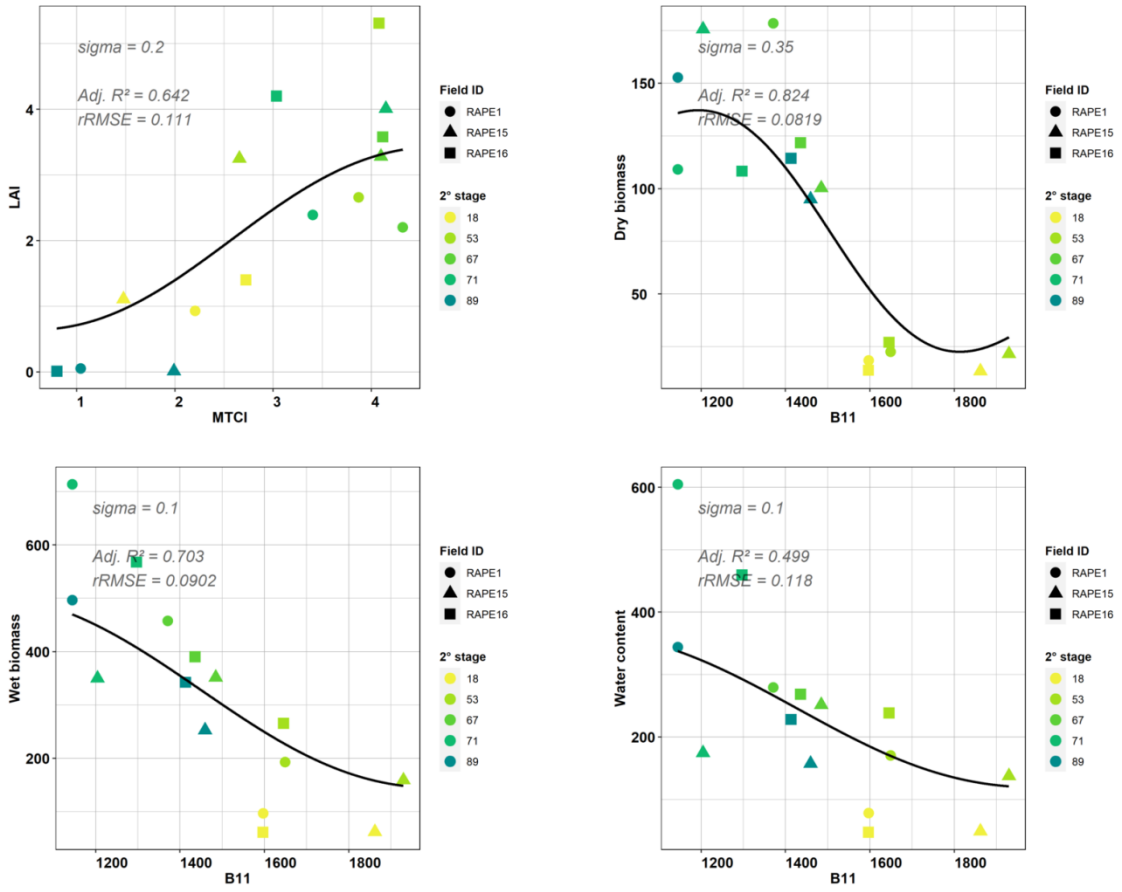

Figure 6-7 .Best relationships obtained between rapeseed LAI, DB, WB and WC and S-2 features.

6.4.2. Estimating crop biophysical parameters using S-1 images

Concerning estimation of wheat crop biophysical parameters using S-1 features, the σ^0VH: σ^0VV ratio was the most strongly correlated feature with LAI (adj. R^2 max = 0.91) (Figure 6-8). More specifically, figure 9 shows the best relationships obtained between wheat crop biophysical parameters and S-1 features. The LAI increased with the σ^0VH: σ^0VV ratio and saturated when LAI was high (2.5-3). Previous studies demonstrated the suitability of polarization ratios for estimating LAI of wheat (Dente et al. 2008; Jin et al. 2015). Veloso et al. (2017) concluded that the influence of the ground was similarly reduced for wheat using σ^0VH: σ^0VV compared to σ^0VH and σ^0VV.

SE_i norm performed best for estimating WB (adj. R^2 = 0.66) (Figure 6-8). More specifically, there was a linear and negative relation between WB and SE_i norm (Figure 6-9). The tillering (BBCH = 18) and ripening (BBCH = 89) stages had low WB values, while the stem elongation (BBCH = 31) and inflorescence (BBCH = 55) stages had higher WB values, Because tillering and ripening stages have a more fragmented and less vertical structure than the other two stages; they cause more disorder in the signal. The SE is influenced more by complex geometry during growth stages (Betbeder et al. 2016a).

SE_p norm performed best for estimating WC (adj. R^2 max = 0.78) (Figure 6-8). There was a sigmoidal and positive relation between WC and SE_p norm, (Figure 6-9), because the increase of the WC of the wheat crop induced lower wave penetration into the soil (Betbeder et al. 2016b). This is consistent with observations of Betbeder et al. (2016b) who showed a

decrease of SE_p norm during the first phenological stages of wheat, an increase from the beginning of the leaf development stage and a saturation at the end of this stage.

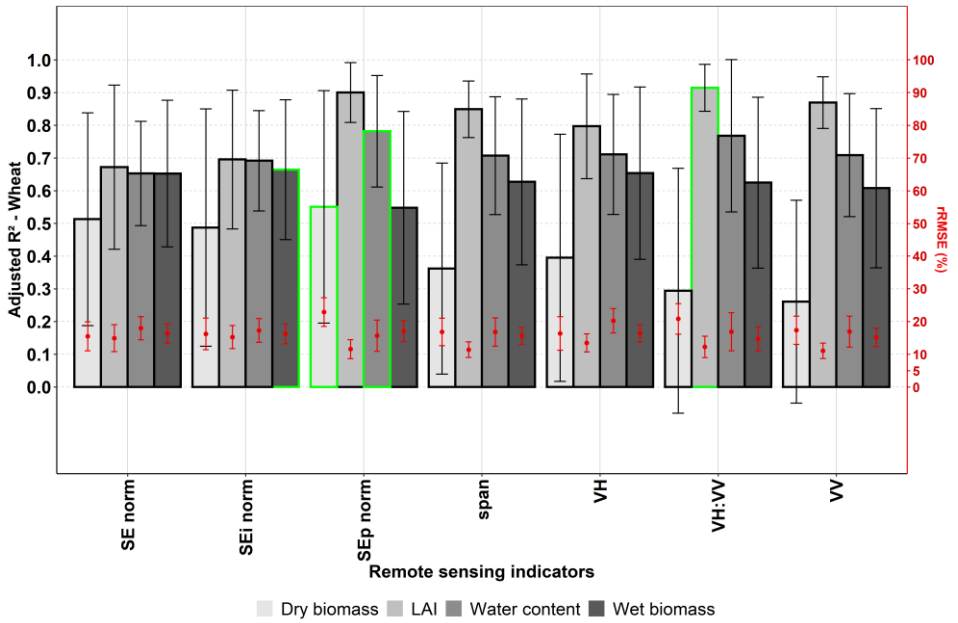

Figure 6-8. Adjusted R^2 and rRMSE (red dots) of empirical relationships between S-1 features and crop biophysical parameters (LAI, DB, WB and WC) of wheat fields. The highest adjusted R^2 values are highlighted in green.

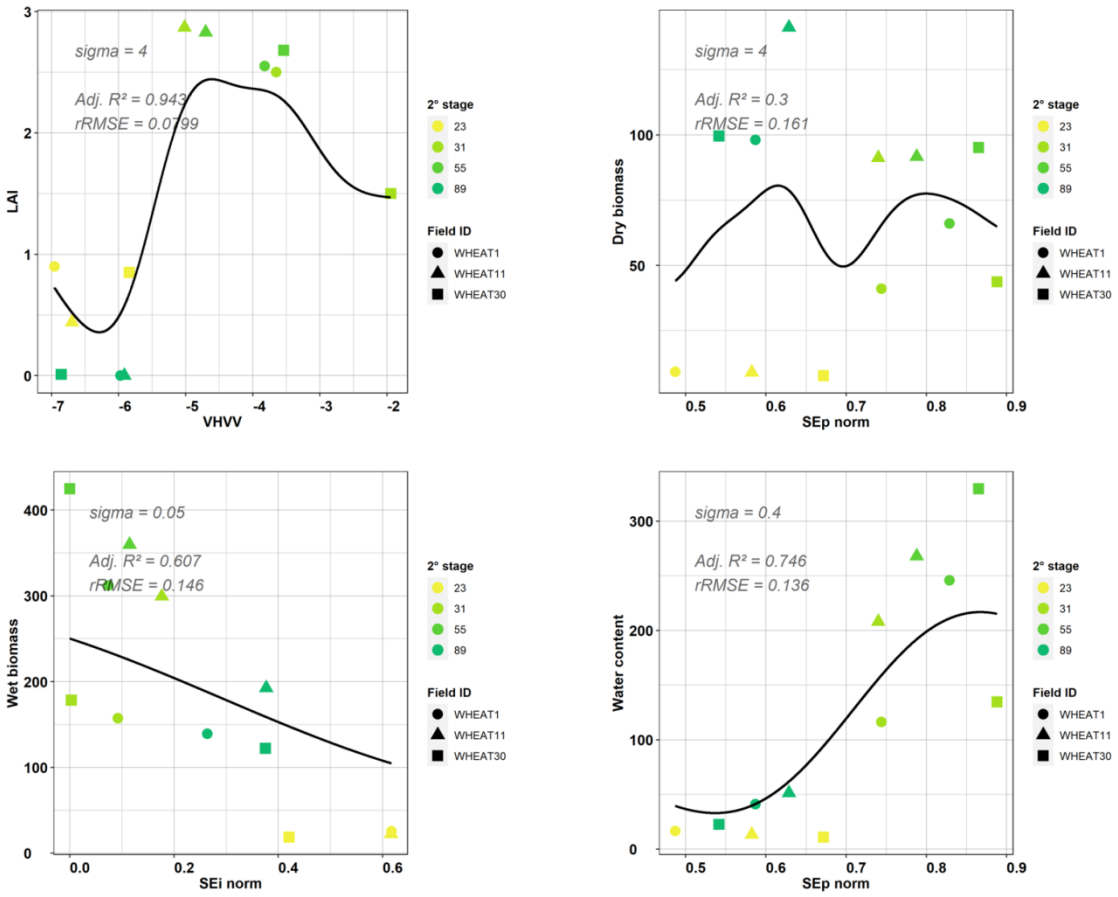

Figure 6-9. Best relationships obtained between wheat LAI, DB, WB and WC and S-1 features.

Correlations between DB and S-1 features did not exceed an adj. R^2 of 0.55 (Figure 6-8). However, Kumar et al. (2018) found an R^2 of 0.68 between S-1 VV-polarization and the DB of wheat in northern India based on 112 samples; thus, either our results underestimated the performance of S-1 data, or the weak relationship was due to external conditions related to the study area, such as the moisture content in the top few cm of the soil, the roughness of the soil surface, or the absorption and scattering characteristics of the vegetation canopy.

For rapeseed, the $\sigma^0VH:\sigma^0VV$ ratio and SE_p norm performed best for estimating DB and WB (Figure 6-10) and increased as the rapeseed crop biophysical parameters increased (Figure 6-11). Rapeseed has a complex structure, with stems that develop without a preferred orientation, which results in an increase in the volume-scattering mechanism (VH) (Betbeder et al. 2016a), while the VV polarization is particularly sensitive to the WC of vegetation (Cookmartin et al. 2000). However, Veloso et al. (2017) concluded that $\sigma^0VH:\sigma^0VV$ compared to σ^0VH and σ^0VV was generally more consistent for rapeseed. Betbeder et al. (2016b) found that the volume scattering (= σ^0VH) decreased due to a strong decline of the WC of the top vegetation layer inducing higher wave penetration into the soil and thus a decrease of the volume scattering. The adj. R^2 of the VV and VH polarization was higher for wheat than for rapeseed biomass (Figures 6-8 and 10), as Ahmadian et al. (2019) found with TerraSAR-X and Betbeder et al. (2016b) with RADARSAT-2.

The results of estimating LAI and WC of rapeseed were poor with a maximum adj. R^2 of 0.60 and 0.35, respectively (Figure 6-10). More specifically, no relation was found between LAI and σ^0VV at leaf development (BBCH = 18), inflorescence (BBCH = 53) and development of fruit (BBCH = 71) stages (Figure 6-11). The WC values in the "RAPE15" field were similar for all field samples (Figure 6-11) reducing the variance of the dataset. Thus, the model showed a low predictive power.

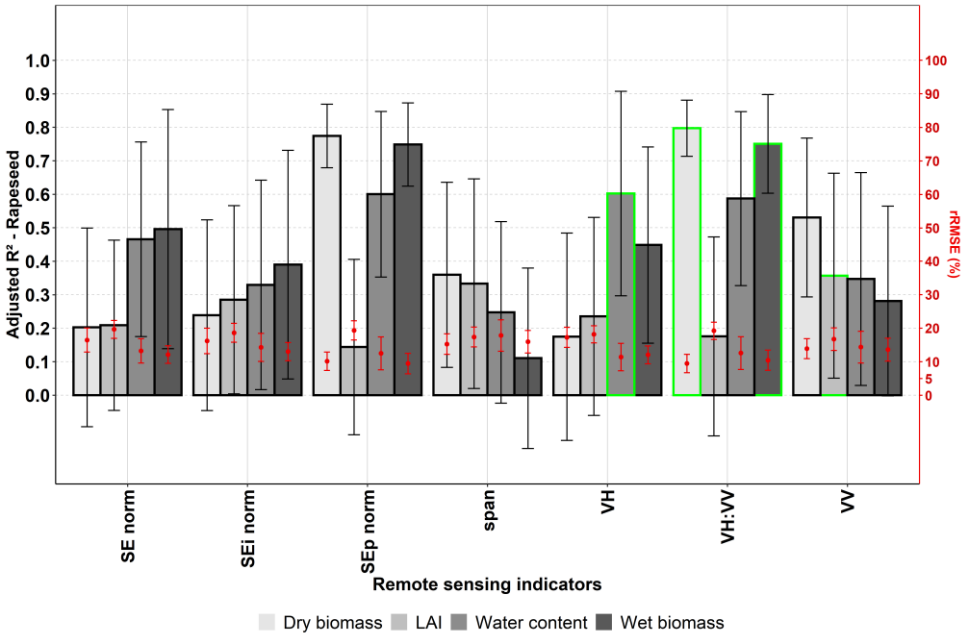

Figure 6-10. Adjusted R^2 and rRMSE (red dots) of empirical relationships between S-1 features and crop biophysical parameters (LAI, DB, WB and WC) of rapeseed fields. The highest adjusted R^2 values are highlighted in green.

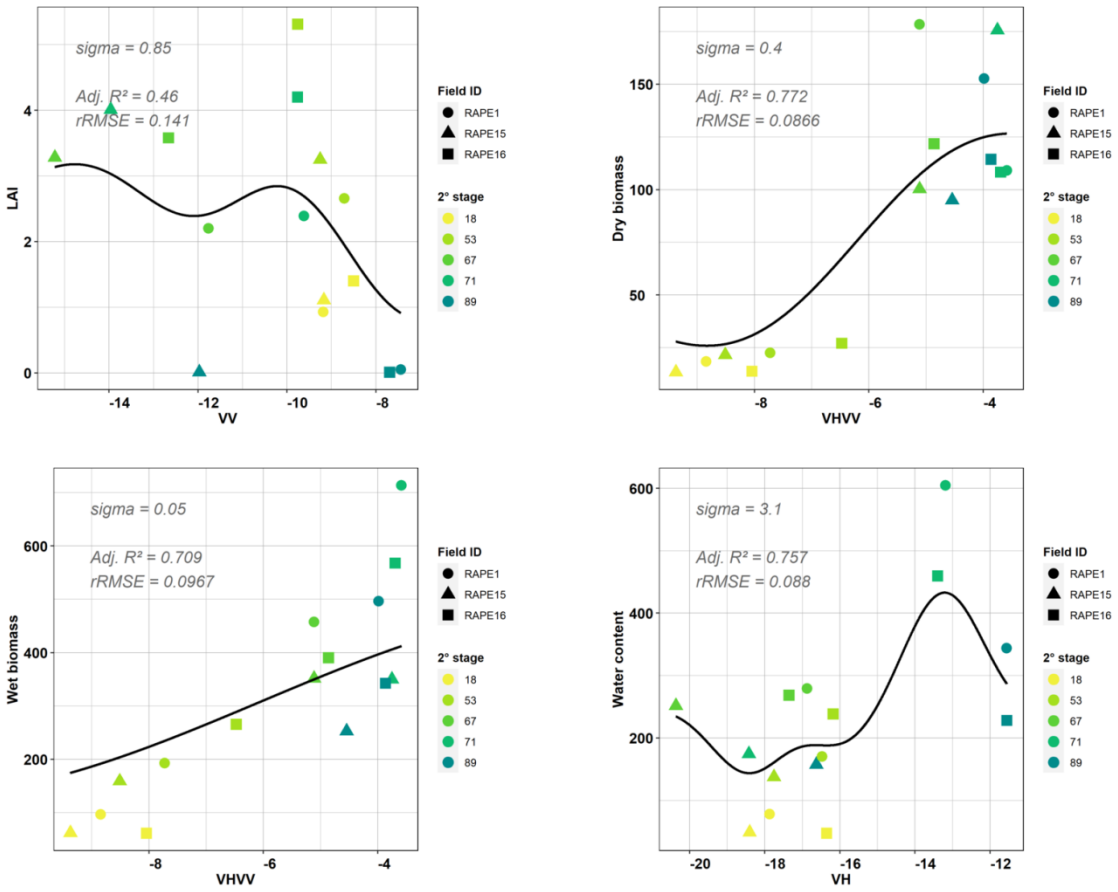

Figure 6-11. Best relationships obtained between rapeseed LAI, DB, WB and WC and S-1 features.

6.4.3. Relative contributions of S-1 and S-2 images for estimating crop biophysical parameters

The GPR results obtained with S-2 features were similar or better to those obtained with S-1 features to estimate crop biophysical parameters of wheat and rapeseed crops (Table 6-7). For example, the goodness of fit using S-1 features was similar to the one obtained using S-2 for wheat LAI (adj. R^2 = 0.91) and rapeseed WC (adj. R^2 = 0.60). We can note that the results for estimating rapeseed DB and WB using S-1 features were good, with a maximum adj. R^2 of 0.80 and 0.75, respectively. While C-band polarizations have shown good results for estimating crop biophysical parameters (Betbeder et al. 2016b; Mandal et al. 2018b; Vreugdenhil et al. 2018; Kumar et al. 2018; Song and Wang 2019; Nasrallah et al. 2019), this study highlighted the importance of the VH:VV ratio and the polarization of SE for estimating wheat LAI and WC (adj. R^2 > 0.75) and rapeseed WB and WC (Figure 6-8 and 10 and Table 6-7). These results are very promising since a continuous time-series of optical images is difficult – if not impossible – to acquire due to the cloud-free dependence of optical acquisitions.

Table 6-7. Adjusted coefficient of determination (Adj. R2) and rRMSE of the best relationships between the crop biophysical parameters of wheat and rapeseed and S-1 and S-2 features. CP, crop parameters. The bold characters highlight the best results obtained for the crop biophysical parameters.

		S-2			S-1	
CP	**Feature**	**Mean Adj. R^2**	**Mean rRMSE**	**Feature**	**Mean Adj. R^2**	**Mean rRMSE**
Wheat						
LAI	Band 8	0.91	0.124	VH:VV	0.91	0.122
DB	WDVI	0.72	0.138	SE_p norm	0.55	0.229
WB	MTCI	0.71	0.142	SE_i norm	0.66	0.163
WC	Band 3	0.82	0.148	SE_p norm	0.78	0.157
Rape						
LAI	MTCI	0.68	0.122	VV	0.36	0.167
DB	Band 11	0.85	0.094	VH:VV	0.80	0.095
WB	Band 11	0.77	0.100	VH:VV	0.75	0.105
WC	Band 11	0.60	0.126	VH	0.60	0.114

The small number of field surveys was a limiting factor when testing statistical models, most of studies using at least thirty field samples to perform GPR for monitoring crop biophysical parameters (Verrelst et al. 2012; Upreti et al. 2019; Ganeva et al. 2019; Pipia et al. 2019). The lower the sample size, the lower the power of the statistical test, that is the probability of rejecting the null hypothesis when it is false (the absence of statistical relationship in this study). Small sample size can lead to over-fitting, although cross-validation can address this issue. In this study, we used a cross-validation procedure to avoid over-fitting and reduce the bias in the classification performance estimate. We applied a repeated cross-validation since Chen et al. (2012). and Rodriguez et al. (2010). have shown that this method stabilizes the prediction error estimation, and thus reduces the variance of the K-fold cross-validation estimator, especially for small samples. Some resampling methods such as leave-one-out or bootstrap are also well suited to small sample sizes. However, the leave-one-out method is an unbiased estimator but suffers from a high variance (Devroye et al. 2013), while the bootstrap method has a smaller variance and a shorter confidence interval but suffers from a bias problem (Jain et al. 1987). Other methods could be tested with a larger set of samples (e.g. random forest algorithm), given the good performance they demonstrated for estimating wheat and rapeseed crop biophysical parameters using optical and SAR data. Wang et al. (2016b) estimated the DB of wheat using vegetation indices derived from HJ-CCD and had better results using RF compared to support vector regression and an artificial neural network. Kumar et al. (2018) also demonstrated that RF provided better results than support vector regression, linear regression, and artificial neural network regression for estimating the crop parameters of wheat (LAI, WC WB, DB and plant height) using S-1 VV polarization. Ahmadian et al. (2019) estimated the DB and WB of wheat, barley and rapeseed using a combination of polarizations derived from TerraSAR-X. They concluded that the RF approach provided better results than a stepwise regression approach and the approach they used (i.e. the "Water Cloud Model").

Future studies could focus on comparing the use of C- and L-bands for wheat and rapeseed, since the L-band signal has a longer wavelength and thus penetrates vegetation more deeply than the C-band (Woodhouse 2017). Inoue et al. (2002) showed that the C-band

was more effective for estimating the LAI of rice, while the L-band was better for estimating fresh biomass. Hosseini and McNairn (2017) demonstrated that the C-band outperformed the L-band in estimating biomass and soil moisture of wheat. However, they indicated that it was difficult to compare the two frequencies directly due to variance in the temporal sequence of data collection and the acquisition of the C-band by satellite and of the L-band by airborne remote sensing.

6.5. Conclusion

This study demonstrated the potential of SAR S-1 and optical S-2 time series to estimate crop biophysical parameters (LAI, WB, DB and WC) of wheat and rapeseed. The results show that best S-2 based models were achieved using the green band, NIR bands and vegetation indices for the wheat WC, LAI and biomass respectively, and the SWIR bands for rapeseed biomass. Concerning S-1 based models, the σ^0VH: σ^0VV ratio was the most relevant feature for wheat LAI and rapeseed biomass, and the SE polarization contribution best performed for wheat WC. Results obtained using S-2 features were similar or higher to those obtained using of S-1 features for estimating crop biophysical parameters of wheat and rapeseed crops. For wheat, the highest correlations using S-1 features were the σ^0VH: σ^0VV polarization ratio with LAI (adj. R^2 = 0.91) and the SE polarization contribution with WC (adj. R^2 = 0.78), while best S-2 based models were achieved using the green band for WC (adj. R^2 = 0.82), NIR-band 8 for LAI (adj. R^2 = 0.91), WDVI for DB (adj. R^2 = 0.72) and MTCI for WB (adj. R^2 = 0.71). For rapeseed, the highest correlations were the σ^0VH: σ^0VV ratio and the SE polarization contribution with WB and DB (adj. R^2 > 0.75), while the SWIR bands of S-2 appeared promising for estimating DB (adj. R^2 = 0.85) and WB (adj. R^2 = 0.77). The results also highlighted, for the first time, the importance of polarimetric indicators (SE and span) derived from S-1 time series for estimating biophysical crop biophysical parameters of wheat and rapeseed.

IV FUNCTIONAL ASSESSMENT OF THE ECOLOGICAL CONTINUITIES IDENTIFIED AND CHARACTERIZED BY SENTINEL-1 AND 2

Contents

Introduction

The last and fourth part of this manuscript is devoted to the analysis of the relationships between maps of landscape metrics derived from Sentinel images and species surveys. We propose to use the WDVI derived from S-2 images to evaluate landscape biophysical heterogeneity, i.e. the spatial diversity of the phenological stages in the crop mosaic in Brittany, Picardy and Wallonia study areas.

In chapter 7, we analyze the influence of biophysical heterogeneity on wheat phenology and associated biodiversity First; we analyzed the relationships between crop mosaic, landscape grain and biophysical heterogeneity. Then, we studied the effect of biophysical heterogeneity on wheat phenology. Finally, the distribution of two carabid beetle species was estimated using the biophysical heterogeneity metric.

CHAPTER 7

Sentinel-2 images bring out functional biophysical heterogeneities in crop mosaics

Contents

Reproduced from the article:

Mercier A, Hubert-Moy L, Baudry J (2021b) Sentinel-2 images reveal functional biophysical heterogeneities in crop mosaics. Landscape Ecol. https://doi.org/10.1007/s10980-021-01331-6

7.1. Introduction

In crop-dominated landscapes, spatial and temporal heterogeneities are key elements for biodiversity (Baudry et al. 2003). The more diverse the land use types and the more complex their configuration, the higher the spatial heterogeneity is (Fahrig et al. 2011). Furthermore, temporal heterogeneities result from the crop rotation, crop phenology and farming practices (Vasseur et al. 2013). These heterogeneities influence the movement and distribution of species across the landscape (Baudry et al. 2003; Fahrig et al. 2011; Vasseur et al. 2013). Many studies describe the influence of the landscape on protecting crops against pests (With et al. 2002; Gagic et al. 2011; Gurr et al. 2018; Chaplin-Kramer et al. 2019). They show the importance of wooded elements (woods, hedgerows) as refuge for predators. Before these studies in landscape ecology, the role of wooded elements as windbreaks to protect crops had been demonstrated in many regions (Kawatani and Meroney 1970; Kort 1988). Their effects have been studied mainly at the field scale (Cleugh 2002; Kanzler et al. 2019; Kučera et al. 2020). Results of these studies indicate that microclimatic heterogeneity is a major factor that influences crop development (Cleugh 2002; Kanzler et al. 2019; Kučera et al. 2020). The diverse plant cover (crops and non-crops) produces heterogeneity in surface temperatures that causes energy fluxes (Ryszkowski and Kędziora 1987). Heterogeneity in crop phenology results in differences in albedo and evapotranspiration between crops, which generates lateral fluxes. For example, when a tractor lifts dust, some of the dust floats away, but some of it returns to fields surrounded by hedgerows, which may be warmer (Figure 7-1). Few scientific literature focuses on this type of heterogeneity caused by energy fluxes (Ryszkowski and Kędziora 1987). The direct relationship between the landscape mosaic and crop phenology at the field scale has not been investigated. This hinders understanding of crop dynamics and associated biodiversity. The heterogeneity of phenological stages of crop/vegetation cover induces differences in solar energy capture and evaporation at the field scale (Ryszkowski and Kędziora 1987). Since thermodynamics states that this kind of heterogeneity generates heat fluxes, we hypothesized that the overall landscape mosaic has an effect on the dynamics of crop phenology and associated biodiversity. Veste et al. (2020) quantified effects of a tree hedgerow planted in a vineyard on wind speed and evapotranspiration, which decreased by up to 20% to about five times the hedgerow height. These effects can improve growing conditions of crops in the local climate and increase the soil water content. Crop phenology also influences energy fluxes. Wind speed is related in part to the surface roughness of the field (Kawatani and Meroney 1970), which differs between maturity and senescence. As the wheat grows, its canopy attenuates the net radiation, which influences the soil heat flux (Choudhury et al. 1987) or albedo (Clothier et al. 1986). Evaporative processes dominate in vegetative-stage vegetation, while radiative processes dominate in senescent vegetation (Jacob et al. 2002).

Remote sensing images are commonly used in landscape ecology (Crowley and Cardille 2020). Optical and radar images from unmanned aerial vehicles (UAVs) and airborne and spaceborne systems have been used to study the structure, change and function of the landscape (Crowley and Cardille 2020). Satellite images and field samples are used to classify land-cover types (e.g. forest, hedgerow, grassland, wetland) to analyze landscape structure. Remote sensing images collected on different dates are used to detect changes in landscape structure over space and time. Landscape function can be assessed by combining

information from remote sensing data (e.g. topography derived from radar data, vegetation indices derived from optical data) and from landscape ecology datasets (e.g. spatial distribution of species, meteorological measurements). Energy flux models commonly incorporate remote sensing data (Schmugge et al. 1998; Olioso et al. 1999; Bindlish et al. 2001; Bastiaanssen et al. 2005). Soil-vegetation-atmosphere transfer models (SVAT) simulate energy and mass transfers between soil, vegetation and the atmosphere based on radiative, turbulent, heat and water transfers. Remote sensing data provide input data to SVAT models such as canopy structure, surface temperature and surface soil moisture (Olioso et al. 1999). For example, thermal images provide a picture of surface temperature heterogeneity (Zellweger et al, 2019). Bastiaanssen et al. (2005) developed the surface energy balance algorithm for land (SEBAL), which estimates wind speed and air temperature based on the spatial variability in convective fluxes. They demonstrated that remote sensing is a direct method to estimate evapotranspiration without prior knowledge about soil, crop and management conditions. Schmugge et al. (1998) predicted surface heat fluxes in an arid watershed in Arizona, USA, using surface temperatures derived from an airborne thermal infrared sensor and land cover from a Landsat Thematic Mapper image. Bindlish et al. (2001) used soil moisture derived from a passive microwave sensor (ASTER) to estimate heat fluxes. These measures are complex and time consuming. In the present study, we used a landscape heterogeneity metric as a proxy of energy fluxes and its relationships with crop phenology and biodiversity.

Satellite images can be used to identify landscape heterogeneities. Mercier et al. (2020b, a) showed that features of radar Sentinel-1 and optical Sentinel-2 satellite images can accurately predict phenological stages and crop biophysical parameters of wheat. For example, the most accurate Sentinel-2 based models used the green band, near-infrared (NIR) bands and vegetation indices to determine wheat's water content, leaf area index and biomass, respectively (Mercier et al. 2020b). In the present study, we explored the potential of remote sensing to derive spatio-temporal ecological metrics that may be related to energy flows. We used the weighted difference vegetation index (WDVI) derived from Sentinel-2 satellite images as an index of wheat plant growth due to its demonstrated ability to monitor phenological stages and crop biophysical parameters of wheat (Mercier et al. 2020b, a).

We analyzed the ecological function of biophysical heterogeneity using carabid beetle samples. Ground beetles (Coleoptera, Carabidae) are relevant indicators of environmental quality or change (Pearson and Hawksworth 1994). The objectives of this article are to (i) evaluate optical remote sensing data to measure the biophysical heterogeneity generated by landscape mosaic heterogeneity at the field scale, and (ii) assess the influence of the biophysical heterogeneity on the distribution of carabid beetles at the landscape scale.

Figure 7-1. Evidence of dust fluxes moving in different directions in an agricultural landscape (Source: Air Papillon)

7.2. Study area

We analyzed three study sites in France (Brittany and Picardy) and three in Belgium (Wallonia) (Figure 7-2). These six landscapes are distributed along gradients of landscape grain and spatial heterogeneity (Appendix F, G and C and https://woodnetweb.wordpress.com). The landscape grain is related to the spatial organization of hedgerows and woods (Le Féon et al. 2013). Landscape grain chaHacterizes structures from fine to coarse grain. This metric, which incorporates hedgerow density and mesh shape (elongated meshes interact more with surrounding hedgerows than compact, square, ones) is useful to measure the effect of the hedgerow network on the surrounding landscape. In this study, landscape grain varies from fine grain, (*i.e.* closed landscapes), to coarse, (*i.e.* open landscape with few hedgerows and little interface with fields). The value of landscape grain ranges from 0 (fine grain) to 1 (coarse grain) (see section 3.1.3).

The study site in Brittany, located to the south of the Bay of Mont Saint Michel, France, covers 130 km² (Figure 7-2). It is a Long-Term Ecological Research (LTER) site called "Zone Atelier Armorique" that is part of the European LTER and international ILTER networks (https://osur.univ-rennes1.fr/za-armorique/). Its climate is temperate, with a mean annual temperature of 12°C and mean annual precipitation of 650 mm (Source: Meteo France weather station of Trans-la-Forêt). The study site is dominated by maize, wheat, grassland and barley. Its landscape grain is the finest of the six study landscapes (Appendix F), and the density of its hedgerow network increases from north to south (Appendix G).

The two study sites in Picardy (West and East) are two 5 km × 5 km areas (Figure 7-2). Their climate is oceanic, with a mean annual temperature of 10°C and mean annual precipitation of 702 mm (Source: Meteo France weather station of Saint Quentin). The West site is the most open of the six study landscapes, with intensively cultivated wheat and sugar beet. The East site is located in a "bocage" landscape (fields enclosed by a network of hedgerows) (Forman and Baudry 1984). dominated mainly by grassland, with some maize and wheat fields. Both landscapes contain fragments of managed forests used mainly for hunting and timber production (Jamoneau 2010).

The three study sites in Belgium (Northeast, Northwest and South) are located in western Wallonia (Figure 7-2). Their climate is temperate, with a mean annual temperature of 9.4-10.5°C and mean annual precipitation of 822-912 mm (http://en.climate-data.org). The Northeast site is an open (i.e. coarse-grain) landscape dominated mainly by wheat, but also has a high proportion of beet, potato and maize. Grassland is the main land cover of the Northwest site, followed by wheat, maize, potato, barley and beet. This landscape has an intermediate grain (landscape grain metric = 0.3 - 0.6). The South site is dominated by wheat, beet, barley, grassland and, to a lesser extent, potato and rapeseed, depending on the year. These crops vary in their distance to hedgerows depending on the coarseness of the landscape grain.

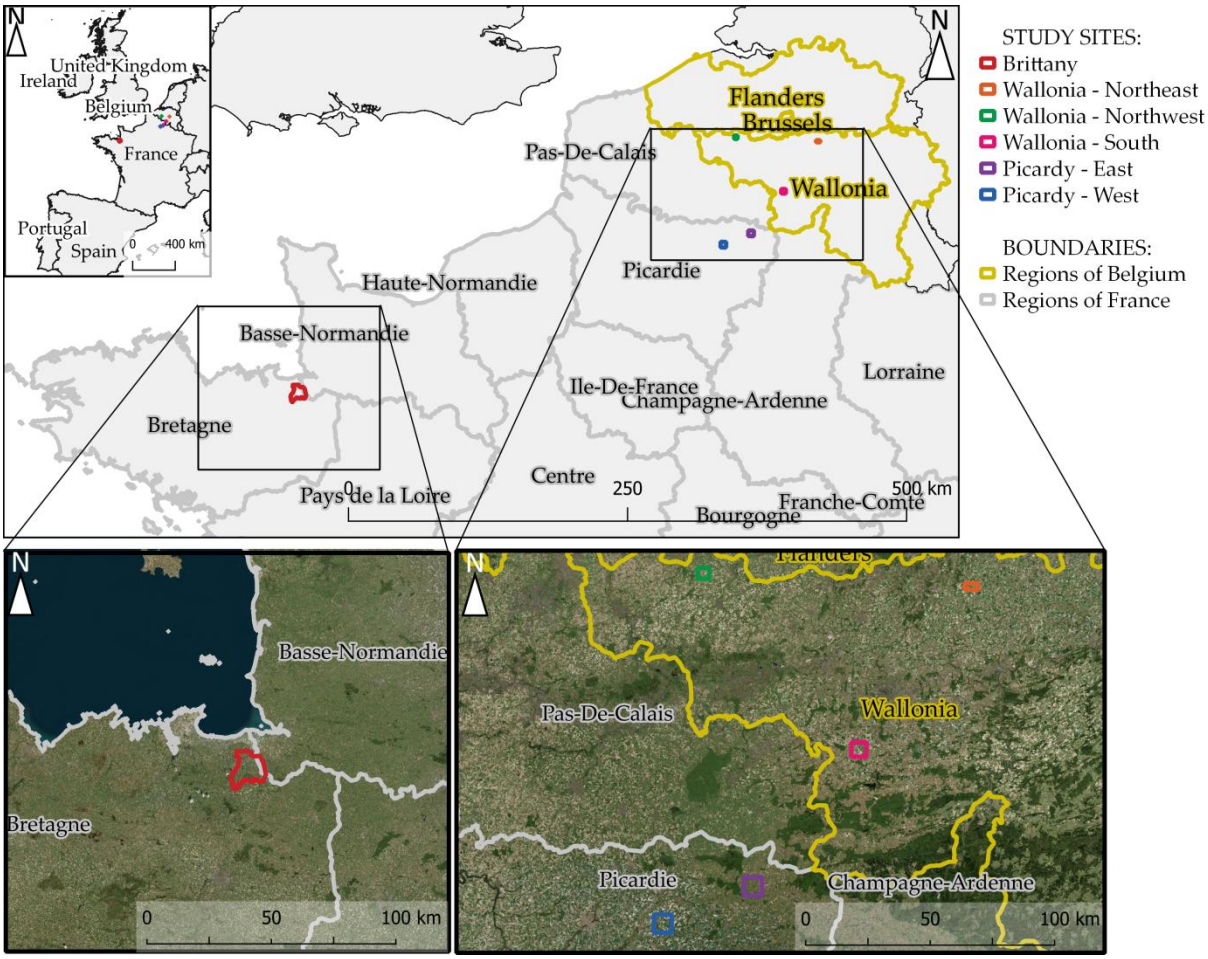

Figure 7-2. Location of study sites in France and Belgium © EuroGeographics for the administrative boundaries

7.3. Materials and methods

The WDVI (Clevers, 1988) derived from Sentinel-2 images was used as an indicator of wheat phenology named Diff WDVI and metric of biophysical heterogeneity (WDVI SD) (detailed in section 3.1.2, Figure 7-3). First, we computed the crop mosaic heterogeneity reflecting the diversity of crops and their spatial distribution (detailed in section 3.1.1) and landscape grain (detailed in section 3.1.3, Figure 7-3). Then, we analyzed the relationships between landscape grain, crop mosaic heterogeneity and biophysical heterogeneity (WDVI SD) (detailed in section 3.3.1, Figure 7-3). Second, we studied the effects of biophysical heterogeneity (WDVI SD) on wheat phenology (detailed in section 3.3.2, Figure 7-3). Last, we used WDVI SD to estimate the distribution of carabid beetles (detailed in section 3.3.3, Figure 7-3).

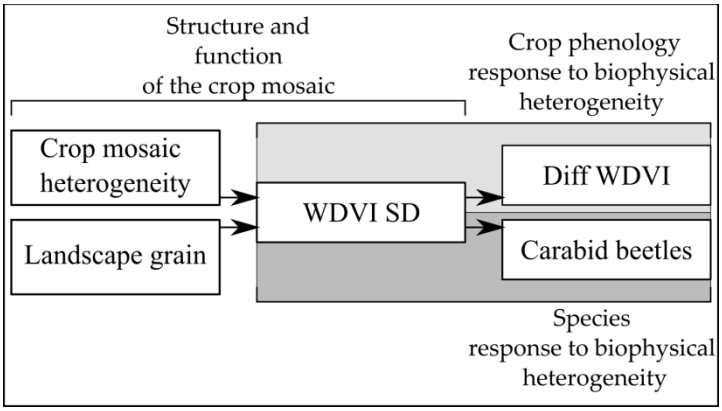

Figure 7-3. Flowchart describing the relationships hypothesized among carabid beetles, crop phenology and the crop mosaic.

7.3.1. Maps and landscape heterogeneities

We analyzed heterogeneity in 1) the crop mosaic, 2) its phenological stages and 3) the associated hedgerow network. This required three types of maps, which had a 2 km buffer around each study site to avoid edge effects when calculating the metrics. The metrics (crop mosaic heterogeneity, landscape grain and biophysical heterogeneity) were calculated using the "Chloé - métriques paysagères" software, developed by INRAE (Boussard and Baudry 2017), which is a mapping analysis tool based on landscape ecology concepts. For all of the analyses, we calculated all metrics in circular windows of five different radii (255, 505, 1005, 1505 and 2005 m). Circular windows used for computing the metrics were defined along a gradient of spatial scales from field scale (255m radius) to landscape scale (2005m radius).

7.3.1.1. Land-cover/ maps

The crop mosaic was the first type of heterogeneity. We used the agricultural Land Parcel Information System (LPIS), a European Union (EU) system to monitor agriculture (Inan et al. 2010), to determine the land cover of the study sites in 2017 and 2018 . In it, polygons that correspond to fields are mapped at 1:15 000 scale, and farmers declare the main land cover types per polygon each year. The French LPIS, called the "Registre Parcellaire Graphique", is produced annually by the National Institute of Geographic and Forestry Information (https://www.data.gouv.fr/fr/datasets/registre-parcellaire-graphique-

rpg-contours-des-parcelles-et-ilots-culturaux-et-leur-groupe-de-cultures-majoritaire/). The Walloon LPIS, called the "Parcelle agricole anonyme", is produced by the Public Service of Wallonia (http://geoportail.wallonie.be/catalogue/44b10a46-4025-4020-a943-e8ffd5ccbd21.html).

We used two national land-cover maps to supplement the non-agricultural areas of these maps. For France, we used the OSO Land Cover product developed by the Land Cover Scientific Expertise Centre of the French Theia Land Data and Services Centre (http://osr-cesbio.ups-tlse.fr/~oso/). The land-cover maps were produced using a fully automated method for processing Sentinel-2 and Landsat-8 time series and contained 17 classes at 20 m spatial resolution and 23 classes at 10 m for 2017 and 2018, respectively (Inglada et al. 2017). For Wallonia, we used a 2 m land-cover map with 10 land cover classes (Radoux et al. 2019) .

For hedgerow networks at the French study sites, maps of woods and hedgerows were produced by the French company KERMAP (https://kermap.com/). Hedgerows were extracted automatically with a 0.20 m spatial resolution from aerial photographs from 2013 in Picardy and 2015 in Brittany and were corrected manually. For Wallonia, we extracted woods and hedgerows from a 2 m land-cover map developed in the Lifewatch-WB project, funded by the Fédération Wallonie-Bruxelles (Radoux et al. 2019). This map is composed of ecotopes, *i.e.* small ecologically homogeneous landscape units, which resulted in 10 land cover classes. This map is based on a majority classification system computed from analysis of aerial, LiDAR and Sentinel-2 images. To optimize the calculation time, we scaled the hedgerow maps to 10 m spatial resolution. We grouped land-use classes to compare Belgium and France and merged maps of hedgerows, crop types and land cover at 10 m spatial resolution. The final land-use maps had 30 land-use classes for France and 45 for Wallonia (Appendix H). There are differences in the number of classes in the final output maps because the crop type classes in Wallonia were more detailed than those in France. The classes of Wallonia with a high level of detail (i.e. cereals, cereals and vegetables and greenhouse vegetables) occupy little area and do not influence the crop mosaic heterogeneity since this metric is derived from the main crop types in terms of area.

To measure the crop mosaic heterogeneity, we used the number of pairs of adjacent pixels of land-use classes of the main crop types: wheat, grassland, maize, rapeseed, beet, barley and potato. We performed correspondence factor analysis (CFA) of the interface metrics (number of pairs (i, j), with i and j as the land-use classes) using the "FactoMineR" v. 2.3 package (Lê et al. 2008) of R software v. 3.6.3 (TEAM, R. Core et al. 2018). CFA is a multivariate technique that detects associations and oppositions among data and measures their contribution to the total inertia for each factor (Teil 1975). We used factor 1 of the CFA as a measure of crop mosaic heterogeneity.

7.3.1.2. Heterogeneity in phenological stages in the crop mosaic

We downloaded Sentinel-2 images from the EU's Copernicus website (https://scihub.copernicus.eu) in level 2A, which provides top-of-canopy reflectance, for dates as close as possible to the sampling dates of the carabid beetles (Table 7-1). The WDVI, which is related to the chlorophyll content of the canopy, is a two-dimensional greenness index derived from bands 4 (red) and 8 (NIR) of Sentinel-2 images (Bouman et al. 1992).

Mercier et al. (2020b) found a positive correlation between WDVI and leaf area index or water content of wheat (Appendix I). They also observed that biomass is high at ripening, while WDVI is low when wheat turns brown. Consequently, WDVI increases from tillering to flowering (Appendix I). Wheat, the target crop, was present in each landscape. The other crops were diverse: maize, beets, grassland and rapeseed. They have different phenologies, cover the soil differently and mature at different dates. Therefore, their chlorophyll activity generates the heterogeneity in WDVI across the landscapes. We used the standard deviation (SD) of the WDVI as a proxy of the heterogeneity in crop development. We developed this method following articles showing the potential of WDVI for wheat monitoring (Mercier et al 2020a, b). The two landscape metrics were the 1) hedgerow network grain and 2) SD of the WDVI in the given buffer. The objective was to detect effects of both metrics. WDVI indices were calculated using the Sentinel-2 NIR and red bands at 10 m spatial resolution as follows (Clevers 1988):

$$WDVI = NIR - 1.5 \times RED \quad (1)$$

We calculated the SD from all pixels with vegetated landscape elements except for hedgerows and woods. WDVI SDs were calculated around the carabid beetle sampling points in circular windows of five different radii (255, 505, 1005, 1505 and 2005 m) (Figure 7-4). Changes in the WDVI (Diff WDVI) of wheat fields were calculated around the carabid beetle sampling points using a buffer of 15 m radius. We measured the median WDVI from Sentinel-2 images at 3 dates delimiting two periods: (1) wheat's stem-extension period, from date 1 to 2 and (2) ripening period, from dates 2 to 3. The phenological stages of wheat were based on the field surveys of the Brittany and Picardy study sites used by Mercier et al. (2020b, a). Diff WDVI was calculated as follows:

$$DiffWDVI_{(t+1)-t} = WDVI_{(t+1)} - WDVI_t \quad (2)$$

where t corresponds to an acquisition date of Sentinel-2 images.

The WDVI SD in windows around the carabid beetle sampling point was calculated at each scale as follows:

$$WDVISD_{(t+1)-t} = \sqrt{\frac{1}{n}\sum\left|DiffWDVI - \overline{DiffWDVI}\right|^2} \quad (3)$$

where n is the number of pixels in the circular window around the carabid beetle sampling point.

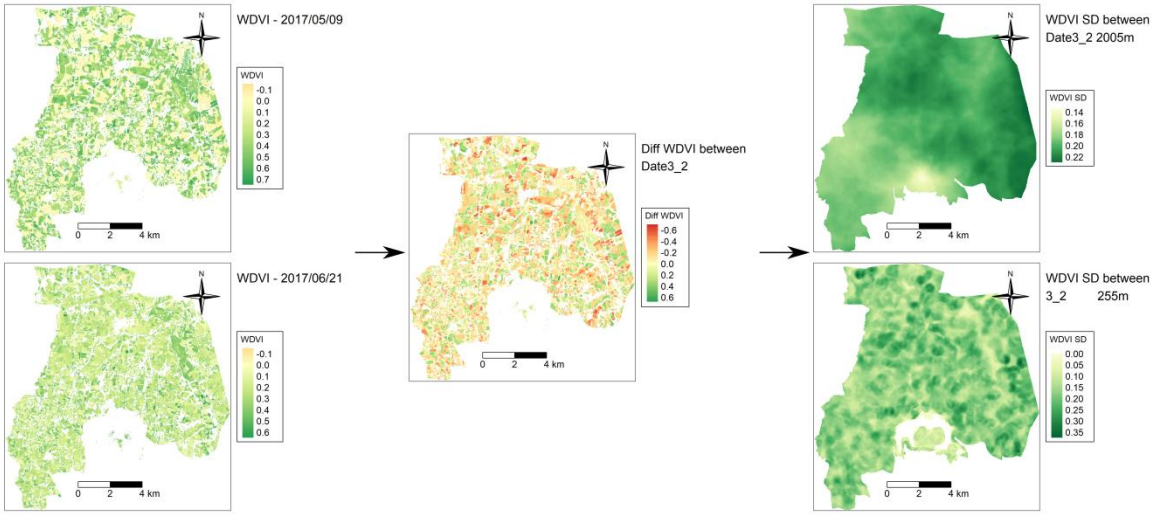

Figure 7-4. Flowchart describing the derivation of Diff WDVI and then WDVI SD from Sentinel-2 images during the ripening period of wheat in Brittany.

7.3.1.3. Landscape grain

Hedgerow density does not assess the influence of hedgerow networks on landscapes well since it has no spatial dimension. We previously showed that landscape grain, which has a spatial dimension, performs better (Le Féon et al. 2013). The landscape grain metric incorporates both hedgerow density and mesh shape (elongated meshes interact more with surrounding hedgerows than compact, square ones). We used the metric "MD", which corresponds to a distance weighted by the landscape-grain distance. It equals the mean distance to a hedgerow, with distances truncated at 100 m because hedgerows have no windbreak effect beyond this distance. MD was calculated in sliding windows using the following equation:

$$d_{WE>100m} = 100m \quad (4)$$

$$MD = \frac{mean(d_{WE})}{100} \quad (5)$$

where d is the distances to the wooded elements.

7.3.2. Carabid beetle data

Carabid beetles were sampled at the six sites from April-July in 2017 and 2018 in 40 and 39 wheat fields, respectively, which yielded 157 sampling points (Table 7-1, Appendix G and H). Adult beetles were caught in pitfall traps filled with 200 ml of water saturated with salt and a few drops of soap. Two sampling stations were located in each wheat field (except in one field in Picardy-East in 2018): one 40 m from a hedgerow edge and one 40 m from a grassed strip edge. Each sampling station consisted of two pitfall traps set 1 m apart. Traps were left open for two weeks before they were collected from the field. The number of carabid beetles trapped is their activity-density, a combination of the overall density and their movement causing their trapping. In this study, we analyzed only two carabid beetle species for the sake of clarity. Since it focuses on the phenology of wheat fields, we selected the two most abundant species in agricultural areas: *Poecilus cupreus* and *Pterostichus melanarius*. Both species are common in fields, move more by walking than by flying, are

predators and contribute to biological control (Holland et al. 2005). *P. cupreus* and *P. melanarius* reproduce in spring-summer and autumn, respectively.

Table 7-1. Dates of field sampling of carabid beetles and corresponding Sentinel-2 images

Study site	Field sampling	Sentinel-2 images
Brittany	2017-04-21	2017-04-09
	2017-05-23	2017-05-09
	2017-06-20	2017-06-21
	2018-04-24	2018-04-22
	2018-05-29	2018-05-17
	2018-06-26	2018-06-26
Picardy	2017-05-02	2017-03-27
	2017-05-30	2017-05-26
	2017-06-27	2017-07-05
	2018-04-23	2018-04-21
	2018-05-29	2018-05-06
	2018-06-26	2018-06-30
Wallonia-South	2017-05-11	2017-05-06
	2017-06-01	2017-05-26
	2017-07-12	2017-07-05
	2018-04-23	2018-04-21
	2018-05-28	2018-05-18
	2018-07-02	2018-06-27
Wallonia-Northwest	2017-05-10	2017-05-06
	2017-05-31	2017-05-26
	2017-07-11	2017-07-05
	2018-04-25	2018-04-21
	2018-05-30	2018-05-26
	2018-07-04	2018-06-30
Wallonia-Northeast	2017-05-12	2017-05-06
	2017-06-02	2017-05-26
	2017-07-14	2017-07-05
	2018-04-27	2018-04-21
	2018-05-31	2018-05-26
	2018-07-06	2018-06-27

7.3.3. Data analysis

7.3.3.1. Relationship between crop mosaic heterogeneity and biophysical heterogeneity

We performed linear regressions between WDVI SD and CFA factor 1 to understand the influence of crop mosaic heterogeneity (CFA factor 1) on biophysical heterogeneity (WDVI SD). The relationships were calculated during the stem-extension and ripening periods of wheat, with 2017 and 2018 data pooled, using the "stats" v. 3.6.3 package of R. For each relationship, we calculated the adjusted R^2 (i.e. a modified version of R-squared useful for comparing models as it is adjusted for the number of predictors in the model) and the relative root mean square error (rRMSE) (i.e. RMSE divided by the mean of the observed data).

7.3.3.2. *Relationship between biophysical heterogeneity and wheat phenology at field scale*

We used generalized additive models (GAMs), a modeling technique commonly used by ecologists, to understand effects of biophysical heterogeneity (WDVI SD) on wheat phenology (Diff WDVI) during the stem-extension and ripening periods of wheat. GAMs with regression splines were created using the "caret" v. 6.0 package of R (Kuhn et al. 2020). A GAM is a non-parametric model that is an extended version of a generalized linear model (Hastie and Tibshirani 1990). The smoothing operator, here a regression spline, was used to estimate the unknown function that described the relationship between the dependent and independent variables. The degree of freedom, which indicates the degree of smoothing, was optimized with a tuning parameter that ranged from 1-4 (with a step of 0.5) to avoid overfitting. The relationships between WDVI SD and Diff WDVI was investigated at the carabid beetle sampling points and for each landscape scale (5 in total). The Diff WDVI value correspond to the median value in the analysis window (landscape scale) around the carabid beetle sampling point. In total, we created 20 GAMs (2 periods × 2 years × 5 landscape scales). For each relationship, we calculated adj. R^2 and RMSE.

7.3.3.3. *Species response to biophysical heterogeneity*

To describe dynamics of the activity-density of *P. cupreus* and *P. melanarius*, we computed a CFA per year (Figure 7-5). CFAs were computed using a matrix of *P. cupreus* and *P. melanarius* activity-density from all samples at the end of the stem-extension (date 2) and ripening (date 3) periods. Then, we created GAMs between WDVI SD and CFA factor 1 (Figure 7-5) to understand effects of biophysical heterogeneity during the stem-extension and ripening periods of wheat on the activity-density of carabid beetles at the end of these periods.

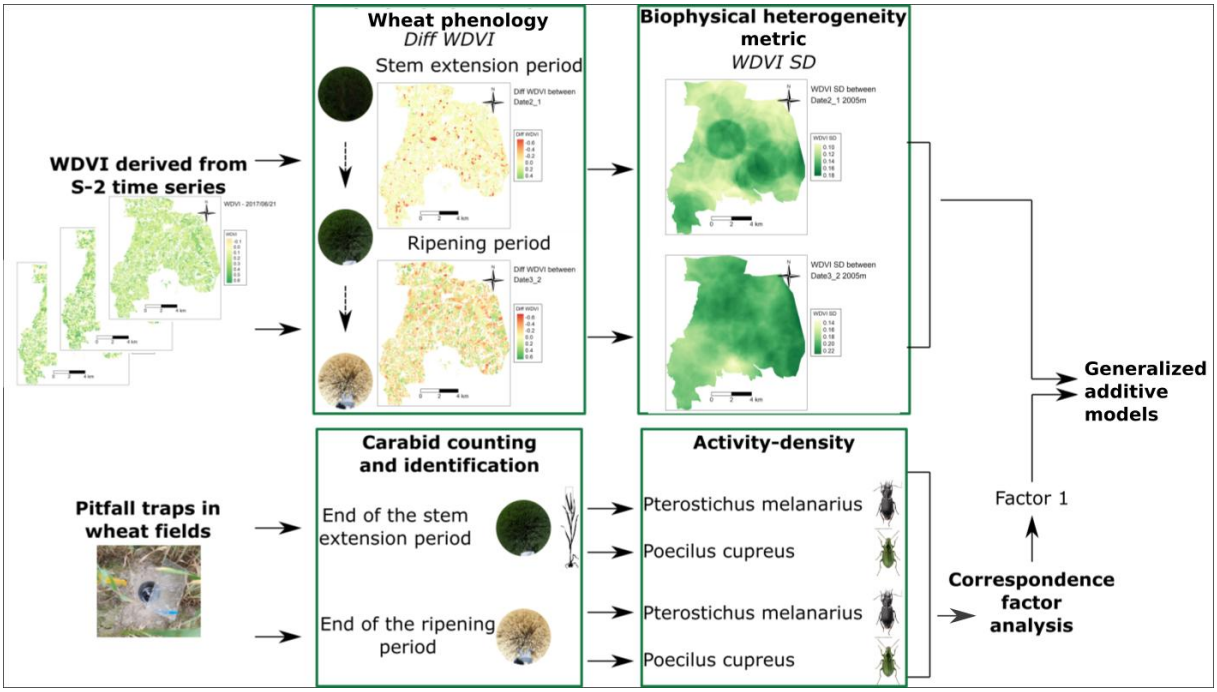

Figure 7-5. Flowchart describing the carabid beetle species response to biophysical heterogeneity in Brittany.

7.4. Results

7.4.1. Structural and functional evaluation of the crop mosaic

In the biplot resulting from CFA of 2005 m circular windows, factor 1 explained 58.8% of the variance, while factor 2 explained 20.7% (Figure 7-6). Interfaces with maize were most common in the Brittany landscape, while interfaces with grassland were most common in Picardy-East. In Picardy-West, interfaces with beet and wheat dominated. The landscapes in Wallonia varied more, with interfaces mainly between potato, wheat, beet and barley in Wallonia-South; barley, wheat and beet in Wallonia-Northeast; and grassland, potato and rapeseed in Wallonia-Northwest. A gradient was observed for factor 1 from Picardy-East to Picardy-West that described extensive (dominated by permanent and multi-annual grassland) to intensive (dominated by annual crops) landscapes (Appendix E). Relationships between WDVI SD and factor 1 varied (the 2005 m scale in Figure 7-7; see Appendix G for the other scales). During the stem-extension period (Dates 2-1), WDVI SD decreased as the landscape intensified, while the opposite was observed during the ripening period (Dates 3-2). The crop mosaic gradient expressed by factor 1 explained 37% of the variance of WDVI SD during stem extension (adj. R^2=0.37) and 53% during ripening (adj. R^2=0.53). Linear regressions showed strong positive relationships between landscape grain and factor 1 that increased as the scale increased (Appendix F); the strongest relationship (adj. R^2 = 0.81) was at the 2005 m scale (Figure 7-7).

WDVI SD changed completely from the stem-extension period to the ripening period along the same crop mosaic gradient (Figure 7-7). During the former, landscapes dominated by grassland or maize were highly heterogeneous, while those dominated by wheat and other annual crops were homogeneous. The crop types that increase WDVI SD were maize and grassland (Figure 7-8). In spring, maize fields were first bare, and then maize developed a little until June, which explains the high WDVI SD. Grassland may have been heterogeneous as well (in term of biomass and photosynthesis activity). Some of it was grazed (low biomass), some mown for silage (yellowish), and some used to make hay (green and high biomass). At the other end of the crop mosaic gradient, wheat dominated. During the ripening period, the WDVI SD of wheat and beet, and to a lesser extent, rapeseed, barley and potato, increased. Thus, WDVI SD inverted between the stem-extension and ripening periods: it increased and then decreased in landscapes with maize and grassland, while it decreased and then increased in landscapes with wheat, beet, barley, potato and rapeseed.

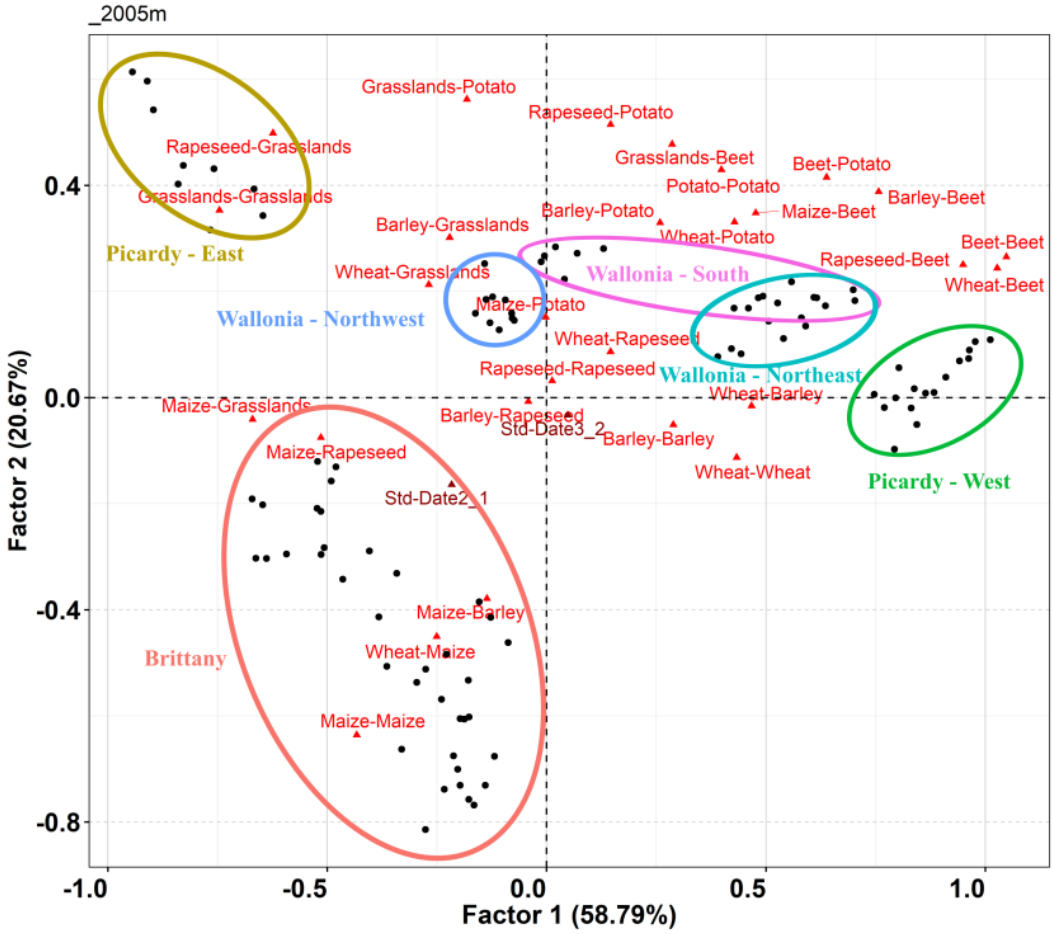

Figure 7-6. Correspondence factor analysis biplot of the number of interfaces (triangles) in the six landscapes. Circles represent carabid beetle sampling points. The closer the symbols (of each type), the more similar are their profiles. The colored ellipsoids correspond to the 6 study sites.

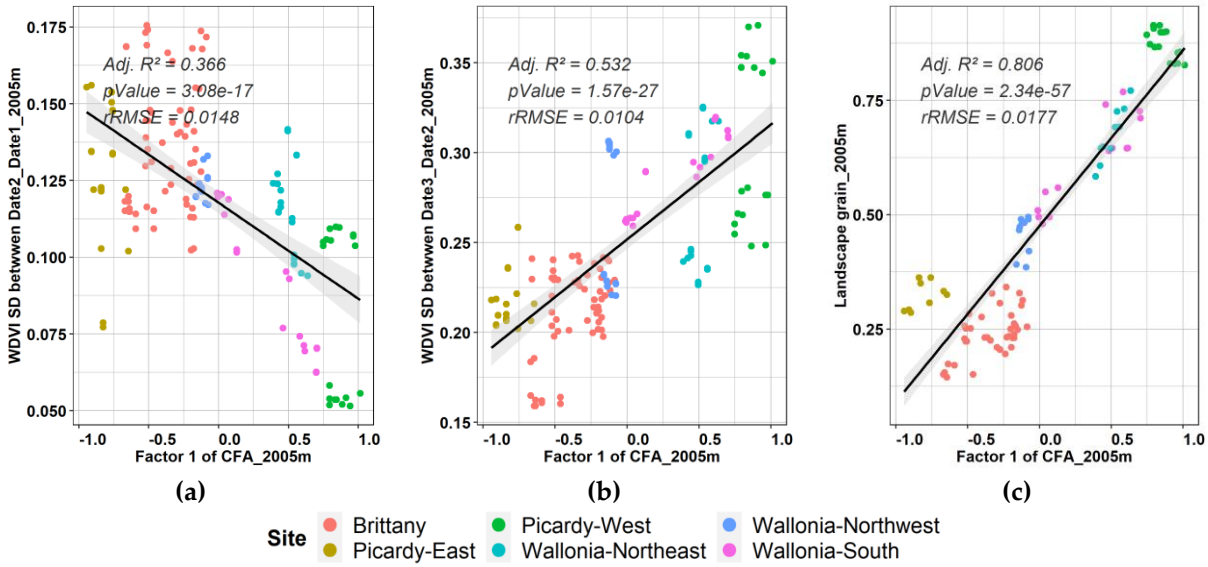

Figure 7-7. Best linear regressions between WDVI SD and factor 1 of the correspondence factor analysis (CFA) at the 2005 m scale for the six study landscapes during (a) stem extension (Date2_Date1) and (b) ripening (Date3_Date2) of wheat, and (c) between landscape grain and factor 1. Grey zone = the 95% confidence interval.

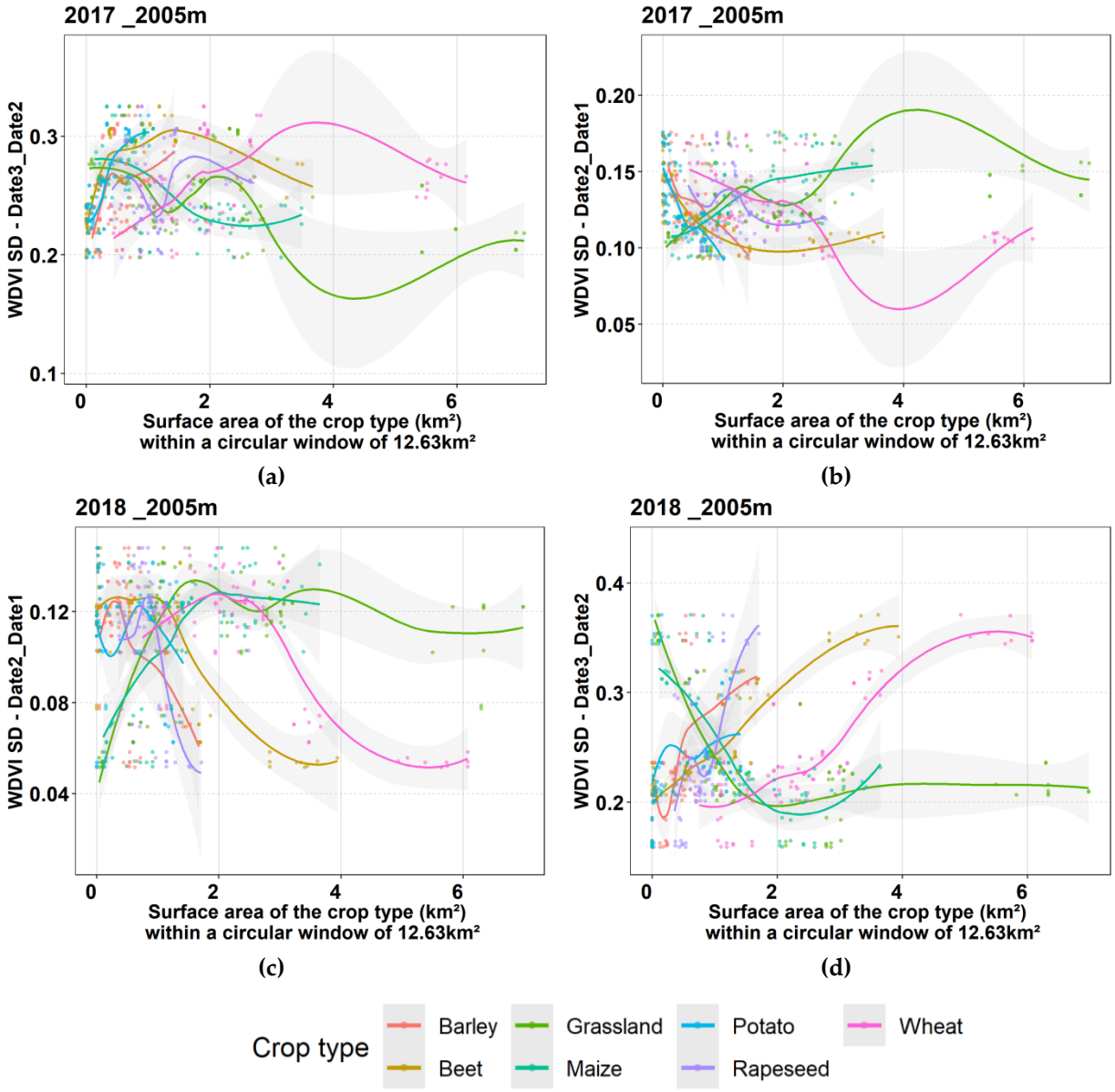

Figure 7-8. Relationships between WDVI SD and surface area of crop types at the 2005 m scale during the (a, c) stem-extension (Dates 2-1) and (b, d) ripening (Dates 3-2) periods of wheat in (a, b) 2017 and (c, d) 2018. Grey zone = the 95% confidence interval.

7.4.2. Effects of biophysical heterogeneity on wheat phenology

During the stem-extension period, the increase in WDVI is explained by the higher chlorophyll content of wheat (Mercier et al. 2020a) and biophysical parameters increase (e.g. biomass, leaf area index, water content) as WDVI increases (Mercier et al. 2020b) (Appendix I). Thus, the higher the WDVI, the greater is the wheat growth. Conversely, during the ripening period, WDVI decreases as the chlorophyll content decreases, as the wheat dries (Mercier et al. 2020a), while the water content and leaf area index decrease as the biomass continues to increase (Mercier et al. 2020b) (Appendix I).

Based on the best results (highest adj. R^2) of the GAMs between Diff WDVI and WDVI SD, for the stem-extension period in 2017, Diff WDVI increased as WDVI SD increased, while in 2018, the relationship was negative and then positive (Figure 7-9). In 2017, only the 255 m

scale was significant, with an adj. R^2 of 0.11. In 2018, all scales were significant, and the adj. R^2 ranged from 0.19 (505 m) to 0.32 (1505 m) (Table 7-2). During the ripening period, the relationship was negative and slightly positive in 2017 but negative in 2018 (Figure 7-9). The scales of analysis were significant from 1005 m upwards, and the larger the scale, the stronger was the correlation (Table 7-2).

The landscapes exhibited different patterns, some of them significant (Figure 7-10, Table 7-3). The landscapes with the finest grain, Brittany and Picardy-East, had positive relationships between Diff WDVI and WDVI SD during the stem-extension period in both years but negative relationships during the ripening period in 2017. Picardy-East, Wallonia-South and Picardy-West, which have the most intensive and open landscapes, had negative relationships during the stem-extension period in 2018, while Picardy-West and Wallonia-Northwest had a positive relationship during the ripening period in 2017. Conversely, in the open field landscape of Wallonia-Northeast, the relationship was positive during the stem-extension period of 2017 but negative during the ripening period of 2018.

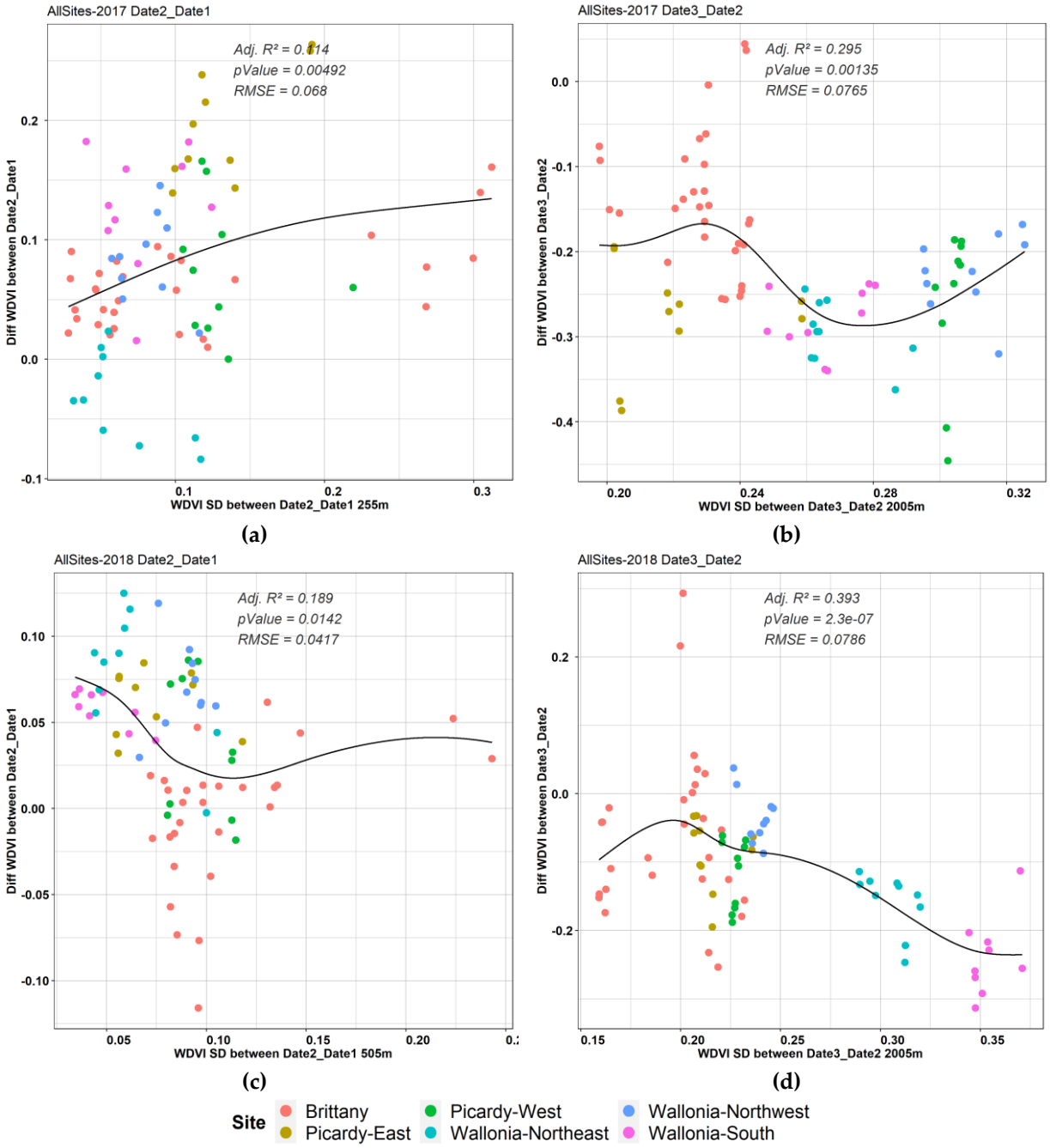

Figure 7-9. The best relationships (i.e. highest adj. R^2) between Diff WDVI and WDVI SD for the six study landscapes during the (a, c) stem-extension (Date2_Date1) and (b, d) ripening (Date3_Date2) periods of wheat in (a, b) 2017 and (c, d) 2018.

Table 7-2. Adjusted R^2 and root mean square error (RMSE) associated with significant relationships between Diff WDVI and WDVI SD. Scale refers to the length of radii of circular windows.

Year	2017	2017		2018					2018		
Period	Dates2-1	Dates3-2		Dates2-1					Dates3-2		
Scale (m)	255	1505	2005	255	505	1005	1505	2005	1005	1505	2005
Adj. R^2	0.11	0.25	0.29	0.23	0.19	0.31	0.32	0.26	0.23	0.36	0.39
RMSE	0.07	0.08	0.08	0.04	0.04	0.04	0.04	0.04	0.09	0.08	0.08

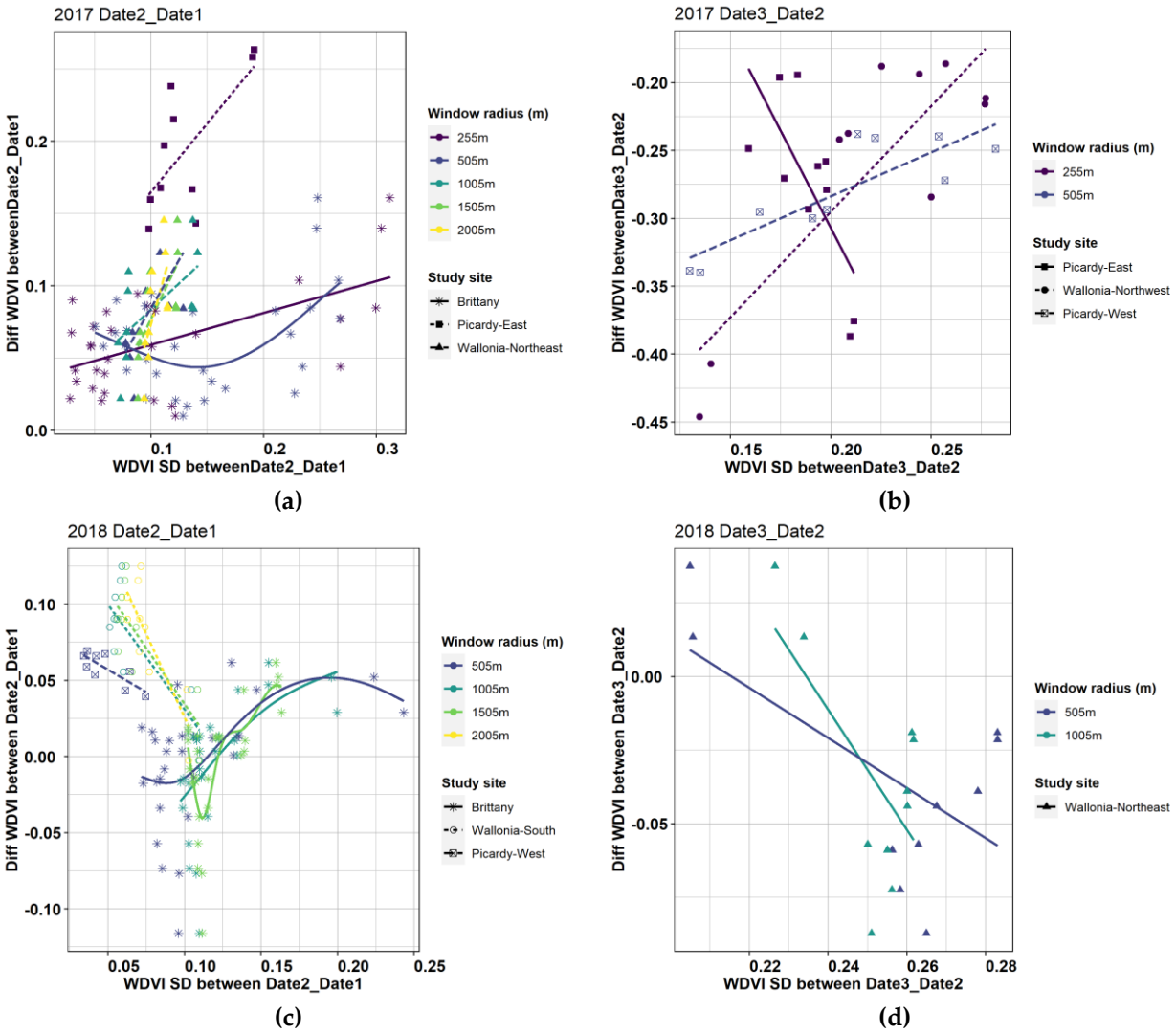

Figure 7-10. Significant relationships between Diff WDVI and WDVI SD per study site during the (a, c) stem-extension (Date2_Date1) and (b, d) ripening (Date3_2) periods in (a, b) 2017 and (c, d) 2018.

Table 7-3. Adjusted R^2 and root mean square error (RMSE) associated with significant relationships between Diff WDVI and WDVI SD during stem-extension and ripening periods per study site. "+" = Positive trend, "-" = Negative trend. Scale refers to the length of radii of circular windows.

Year	Period	Study site	Scale	Trend	Adj. R^2	RMSE
2017	Stem extension	Brittany	255 m	+	0.30	0.03
			505 m	+	0.36	0.03
		Picardy-East	255 m	+	0.42	0.03
		Wallonia-Northeast	505 m	+	0.39	0.02
			1005 m	+	0.33	0.03
			1505 m	+	0.46	0.02
			2005 m	+	0.36	0.03
2017	Ripening	Picardy-East	255 m	-	0.47	0.04
		Wallonia-Northwest	255 m	+	0.70	0.04
		Picardy-West	505 m	+	0.69	0.02
2018	Stem extension	Brittany	505 m	+	0.26	0.03
			1005 m	+	0.35	0.03
			1505 m	+	0.63	0.02
		Wallonia-South	1005 m	-	0.58	0.02
			1505 m	-	0.59	0.02
			2005 m	-	0.65	0.02
		Picardy-West	505 m	-	0.58	0.01
2018	Ripening	Wallonia-Northeast	505 m	-	0.32	0.03
			1005 m	-	0.34	0.03

7.4.3. Species response to biophysical heterogeneity at the landscape scale

The dynamics of the number of the two species captured varied among the landscapes in 2017 and 2018 (Figure 7-11). The CFA results (Figure 7-12) highlight the characteristics of study sites regarding activity-density of carabid beetles per year. We analyzed the effect of WDVI SD during the stem-extension and ripening periods of wheat on the activity-density of carabid beetles at the end of these periods. Brittany and Picardy-East, the landscapes with the finest grain, had the most *P. cupreus* and fewest *P. melanarius*, while the opposite was observed in Wallonia-South, Picardy-West and Wallonia-Northeast, the most open landscapes. Wallonia-Northwest was intermediate, with few carabid beetles in both years, without either species dominating. CFA factor 1 explained 61.0% and 60.2% of the variance in activity-density in 2017 and 2018, respectively (Figure 7-12). It described a gradient from *P. cupreus* to *P. melanarius* and also from fine (Brittany) to coarse grain (Wallonia-South).

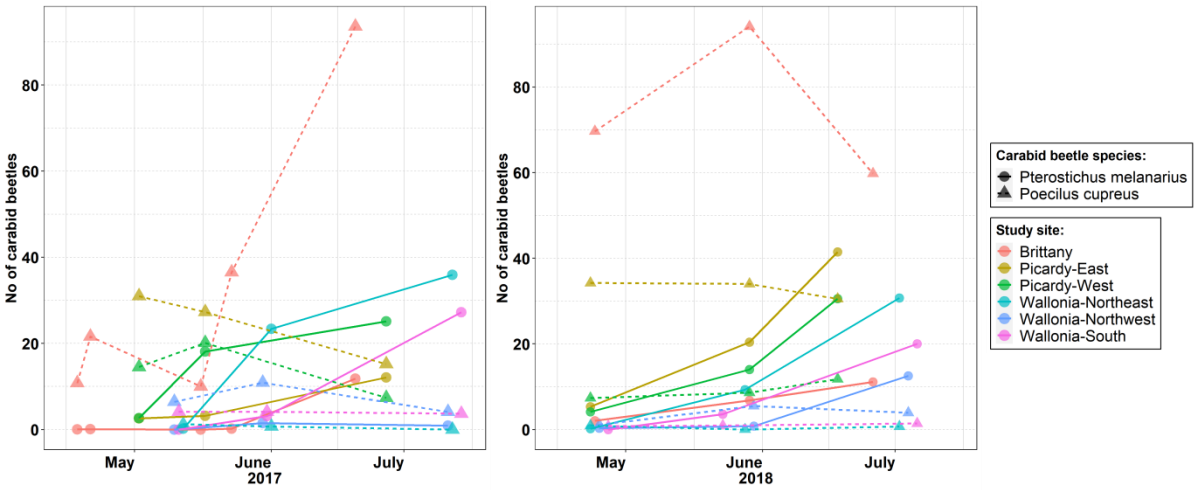

Figure 7-11. Dynamics of the number of carabid beetles *Poecilus cupreus* and *Pterostichus melanarius* captured in 2017 and 2018.

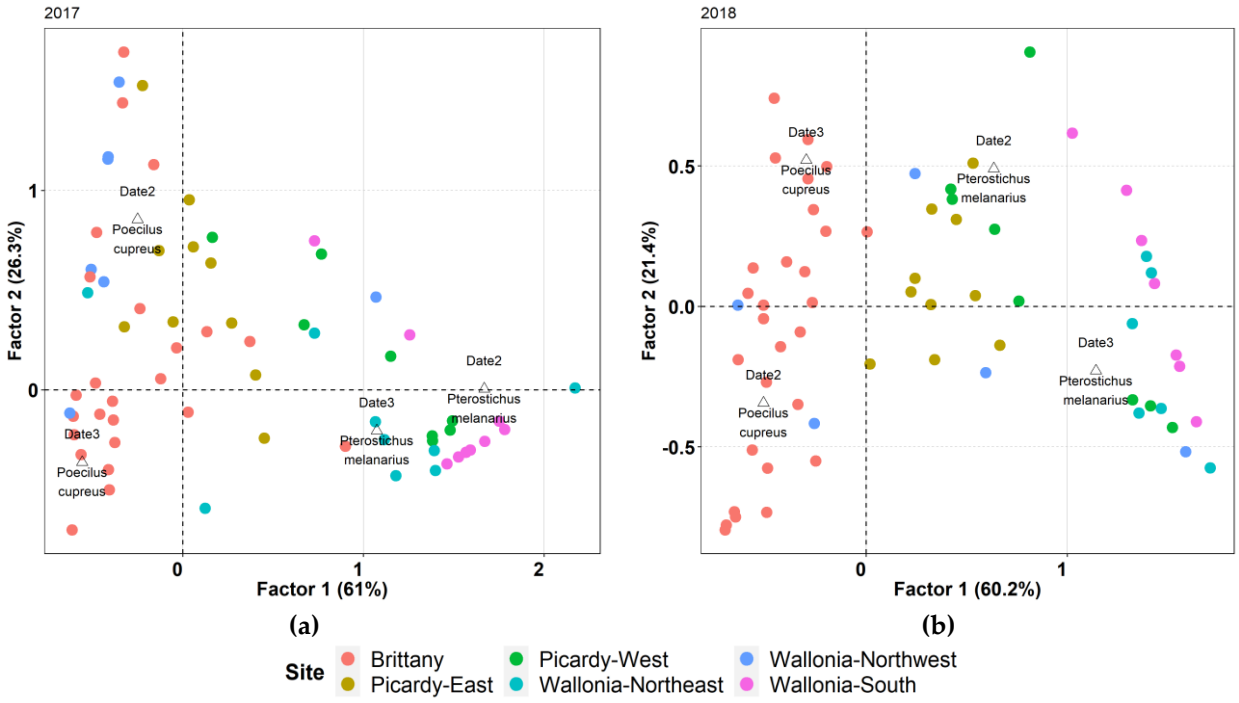

Figure 7-12. Correspondence analysis biplot of the activity-density of *Poecilus cupreus* and *Pterostichus melanarius* in the six study landscapes at the end of the stem-extension (Date 2) and ripening (Date 3) period in (a) 2017 and (b) 2018.

Highly significant correlations were found between factor 1 and WDVI SD at the 2005 m scale (Figure 7-13). The relationships were negative during the stem-extension period, with an adj. R^2 of 0.62 in 2017 and 0.24 in 2018. During the ripening period, the relationship was positive in 2017, with an adj. R^2 of 0.47, but in 2018, factor 1 increased with WDVI SD and then decreased (adj. R^2 = 0.62). A high activity-density of *P. cupreus* corresponded to negative values of factor 1, while a high activity-density of *P. melanarius* corresponded to positive values from 1-2. As mentioned, in fine-grain landscapes, the biophysical heterogeneity (WDVI SD) increased during the stem-extension period and decreased during the ripening

period, while the opposite was observed for coarse-grain landscapes. Thus, during the stem-extension period, biophysical heterogeneity, fine landscape grain and/or extensive crop mosaics were favorable to *P. cupreus* but unfavorable to *P. melanarius*. During the ripening period, biophysical heterogeneity, coarse landscape grain and/or intensive crop mosaics were favorable to *P. melanarius* but unfavorable to *P. cupreus*.

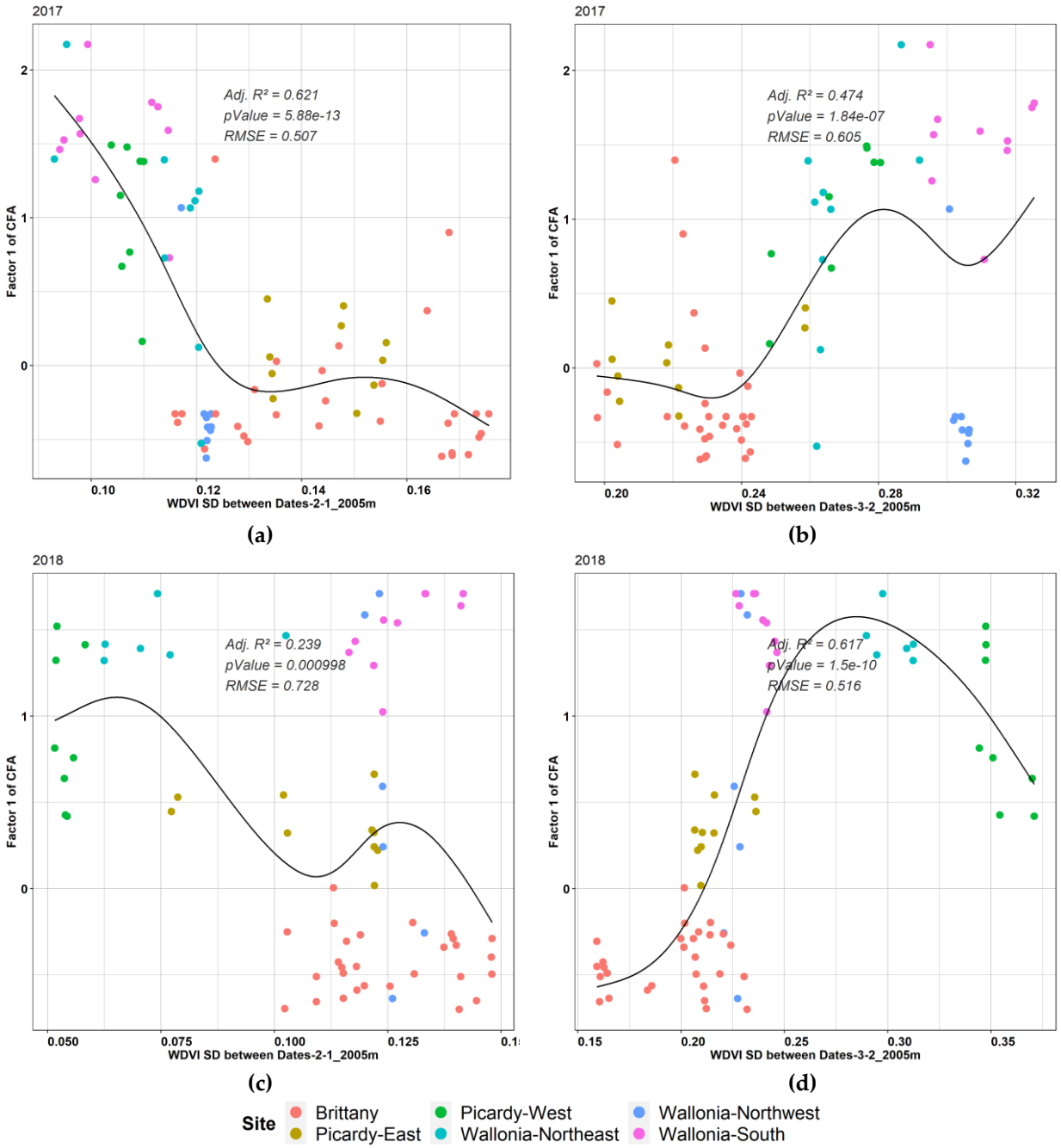

Figure 7-13. Relationships between factor 1 of the correspondence factor analysis and WDVI SD at the 2005 m scale for the six study landscapes during the (a, c) stem-extension (Dates 2-1) and (b, d) ripening (Dates 3-2) periods of wheat in (a, b) 2017 and (c, d) 2018.

7.5. Discussion

7.5.1. Effects of landscape structure on biophysical heterogeneity

The landscape grain correlated strongly with the crop mosaic gradient; indeed, land-use organization depends on the hedgerow density (Thenail 2002). From 1940-1990 in France, much of the hedgerow network was removed due to land consolidation programs to support agricultural intensification (Baudry and Burel 1984). Fine-grain landscapes are related mostly to extensive livestock and grassland systems (fodder, cattle), while coarse-grain landscapes are dominated more by crop rotations. For example, at the Brittany study site, the proportion of maize increases and grassland decreases from fine- to coarse-grain landscapes (Thenail and Baudry 2004). This explains why this study site often extended over larger sections of gradients in this study. The sampling points in Brittany extend more widely on the x-axis or y-axis of the established relationships compared to the other sites (Figures 7-7 and 9). The fragmentation of farming territories in fine-grain landscapes has simplified crop successions and circulating cattle lots. Conversely, large fields in coarse-grain landscapes are likely to have similar physical conditions; therefore, many land islets formed into a single field are used for cash crops. The finest-grain landscapes were found in Brittany, Picardy-West and Wallonia-Northwest, which contained mainly grassland and variable proportions of wheat and maize. The coarsest-grain landscapes were found in Wallonia-South, Wallonia-Northeast and Picardy-West, which contained mainly beet and wheat. The landscape grain of the six study sites appears along the crop mosaic gradient since it represents a gradient from grassland and maize to wheat and beet (Figure 7-6). The two factors, landscape grain and crop mosaic, are confounded, however, so their effects on wheat phenology may be either confounded or complementary. Either the effect of landscape grain has an effect on crop mosaic (or inversely), thus one of them influences wheat phenology, or their effects are merged (by addition for example) and affect wheat phenology together.

7.5.2. Effects of biophysical heterogeneity on wheat phenology

Based on the combined analysis of all sites, biophysical heterogeneity (WDVI SD) had a positive effect on wheat growth (Diff WDVI) during the ripening period, since Diff WDVI decreased as WDVI SD increased. Biophysical heterogeneity causes lateral energy flows that benefit wheat growth. However, analysis of individual sites showed that biophysical heterogeneity (WDVI SD) appears to benefit wheat growth in fine-grain landscapes but is a disadvantage in coarse-grain landscapes. Thus, fluxes are beneficial exchanges in fine-grain landscapes but are disturbances in coarse-grain landscapes. This phenomenon is likely explained by the nature of fluxes in each landscape. Alford et al. (2018) found that open landscapes are warmer than complex landscapes, which have more extreme and variable temperatures. Local temperatures increase because the coarse-grain landscape is exposed to more shortwave radiation during the daytime (Chen et al. 1999). In fine-grain landscapes, hedgerows function as windbreaks that reduce local wind speed and increase the relative humidity by condensing fresh dense air (Kort 1988). Alford et al. (2018) observed that the passage from winter to spring increased vegetation growth and buffered temperatures. Differences between landscapes decrease, but fine-grain landscapes remain colder than coarse-grain landscapes. Temperature differences between day and night are largest on sunny days, and woods intercept solar radiation, which reduces the amplitude of the daytime temperature (Zellweger et al. 2019). Thus, biophysical heterogeneity in coarse-grain

landscapes would cause temperature fluxes and extreme temperatures that reduce wheat growth.

7.5.3. Importance of the landscape scale

Relationships between the crop mosaic gradient and biophysical heterogeneity (WDVI SD) had higher adj. R^2 at larger scales. As the scale of analysis increased, the variability within each study site decreased, but the variability among study sites increased. Thus, if a relationship exists between two metrics analyzed in windows, it will be stronger at larger scales.

Landscape structure influenced changes in wheat within the field. For all sites analysis, the scales that explained the most variance between biophysical heterogeneity (WDVI SD) and wheat phenology (Diff WDVI) had a radius larger than 1505 m, except for the stem-extension period in 2017 (Table 7-2).

For some sites, the 255 and 505 m scales showed significant relationships between biophysical heterogeneity (WDVI SD) and wheat phenology (Diff WDVI) during wheat ripening in 2017 and 2018 (Table 7-3, Figure 7-14). However, these scales were no longer present when all sampling points from the six study sites were considered (Table 7-2, Figure 7-14). As the extent of the WDVI SD maps increased, WDVI SDs became more homogeneous. At the European scale, the diversity of local practices contributes increasingly less to the explanation of differences among sites as the scale increases. However, the 255 m scale was significant during the stem-extension period in both years, which indicates that local practices influence wheat growth more during this period.

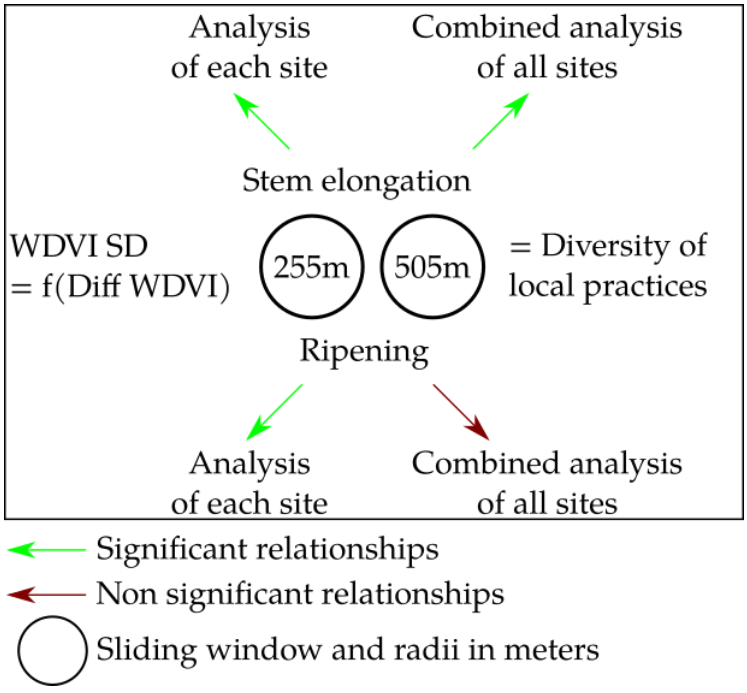

Figure 7-14. Scematic explanation of relationships between WDVI SD and Diff WDVI with 255 and 505m radii sliding windows.

7.5.4. Distribution of *P. melanarius* and *P. cupreus* at the landscape scale

P. melanarius and *P. cupreus* were found in different landscapes and locations. Thomas et al. (2001) observed spatial separation between these species in different fields. These two carabid beetle species have different ecological requirements. *P. cupreus* was more abundant in the fine-grain landscapes of Brittany and Picardy-East, while *P. melanarius* was more abundant in the coarse-grain landscapes of Picardy-West and Wallonia-South. *P. cupreus* remains near hedgerows, while *P. melanarius* remains further from them (Winder et al. 2001; Rouabah et al. 2015), although neither species crosses hedgerows (Holland et al. 2004). *P. melanarius* is adapted to temperature variations (Holland et al. 2005), and open landscapes have more extreme and variable temperatures than complex landscapes (Alford et al. 2018). Thus, this biological feature of *P. melanarius* makes it suitable for coarse-grain landscapes.

Some habitat preferences of *P. melanarius* and *P. cupreus* remain unclear due to opposite results. For example, Thomas et al. (2001) found *P. cupreus* in fields, while Rouabah et al. (2015) found them near hedgerows. Hassan et al. (2013) found lower abundance of *P. cupreus* in fine-grain landscapes, which is opposite to our results. These contrasting results may be due to other factors that influence carabid beetle distribution, such as crop types, hedgerow age, soil moisture, prey density, competitive exclusion, mutual predation and the management system (Winder et al. 2001; Holland et al. 2004; Rouabah et al. 2015).

7.5.5. Using remote sensing to characterize landscapes

Free remote sensing images, such as Sentinel data, can address data collection limitations and the financial cost of images. Crowley and Cardille (2020) reviewed landscape ecology research from the past five years and identified future contributions of remote sensing to landscape ecology. Based on this review, innovations in our study are the use of intra-annual monitoring to analyze landscapes, comparison of different landscapes and use of continuous values (WDVI) rather than discrete classes. Sentinel-2 time series provide the opportunity to monitor landscape dynamics regularly at the field scale. Using a variety of study sites generated a continuous landscape gradient, which allowed us to identify patterns that developed along gradients, while each landscape maintained its own identity. This is in contrast with many studies pooling data from different landscapes without making them distinct in the analysis (e.g. Alignier et al. 2020). In our study, patterns emerged due to the diversity of landscapes. It is difficult to map the crop mosaic accurately and consistently using satellite images of different study areas or over a large scale. The accuracy of a map can be measured using quality estimators (e.g. kappa statistic, overall accuracy, F-score). Nevertheless, assessing accuracy depends greatly on the validation data, and uncertainty is unavoidable due to classification errors that occur at different stages of map production (Friedl et al. 2001; Congalton et al. 2014). Continuous values such as WDVI overcome this problem because WDVI uses two variables (red and NIR bands) that were measured consistently in all images. Crowley and Cardille (2020) recommended shifting from categorical indices to continuous values for habitat assessments to better evaluate impacts of landscape change on biodiversity and quantify error in landscape ecology models. Several authors (e.g. McGarigal et al. 2009; Lausch et al. 2015) recommend shifting the representation of landscapes from a mosaic to a gradient. Moreover, continuous values are the most suitable for capturing gradients in a landscape. Optical remote sensing reflects the phenological

dynamics of crops (Diff WDVI) independent of neighboring crops. Mercier et al. (2020b) found that variables (backscattering coefficients and polarimetric indicators) derived from the radar sensor Sentinel-1 were suitable for monitoring phenological stages and crop biophysical parameters of wheat. The microwave domain (radar) captures the geometry of wheat, while the optical domain is sensitive to the chlorophyll content. Moreover, the roughness of wheat, related to its geometry, influences wind speed directly (Kawatani and Meroney 1970). Therefore, it would be interesting to compare the results of Sentinel-1 and Sentinel-2 to study biophysical heterogeneity. No fluxes were measured or modeled in this study, so further research is needed to confirm the ability of WDVI SD to represent the physical energy of landscapes. However, this study provides a framework for sampling fluxes in landscapes. WDVI SD could be used at relevant scales as an indicator for targeted areas. Previous studies developed methods to produce microclimate maps that incorporate remote sensing data, such as those from LiDAR, (George et al. 2015), unmanned aerial vehicles (Maes et al. 2017) and the MODIS satellite (Metz et al. 2014; Fick and Hijmans 2017). Future studies could analyze correlations between WDVI SD and microclimate maps or field sampling.

7.5.6. Using remote sensing to understand biodiversity

We showed that the distributions of *P. melanarius* and *P. cupreus* were related to biophysical heterogeneity (WDVI SD). However, biophysical heterogeneity (WDVI SD) correlated strongly with the crop mosaic gradient and landscape grain. Therefore, we could not quantify the effect of each variable on *P. melanarius* and *P. cupreus*; however, the landscape effect (landscape grain and crop mosaic gradient) can be assessed using WDVI SD. Remote sensing enables carabid beetle distribution to be studied without the need for a land-use or hedgerow map. In this study, we use continuous values independent of *any classification system*. In addition, it is consistent across crop types and locations, which makes it possible to address ecological issues using free images that are available for any area on Earth (Sentinel data available at https://scihub.copernicus.eu). Conversely, for fixed variables such as crop mosaics, WDVI SD varies over time. The relationship between WDVI SD and CFA factor 1 explains a state (i.e. the distribution of two carabid beetle species) but not its dynamics. Since WDVI SD is a spatio-temporal index, future studies could use it to focus on the dynamics of species.

7.5.7. Synthesis of the discussion

The strong correlation between landscape grain and crop mosaic gradient is explained by the dependence of land-use organization to hedgerow density. As a result, the effects of landscape grain and crop mosaic on wheat phenology may be either confounded or complementary.

The analysis per site showed that biophysical heterogeneity (WDVI SD) appears to benefit wheat growth (Diff WDVI) in fine-grain landscapes but is a disadvantage in coarse-grain landscapes. Thus, while fluxes are beneficial exchanges in fine-grain landscapes (higher relative humidity, lower amplitude of the daytime temperature), they are disturbances in coarse-grain landscapes (more extreme and variable temperature).

The combined analysis of all sites shows that the relationships between biophysical heterogeneity (WDVI SD) and wheat phenology (Diff WDVI) were significant at local scale

(255m and 505m) during the stem extension period but not during the ripening period. Thus, local agricultural practices influence wheat growth more during the stem-extension period.

We showed that the distributions of *P. melanarius* and *P. cupreus* were related to biophysical heterogeneity (WDVI SD). Remote sensing images enable carabid beetle distribution to be studied without the need for a land--cover or hedgerow map. Only optical bands are required to compute WDVI SD. They are continuous values independent of any classification system, they vary over time and overcome the problem of map accuracy assessment.

No fluxes were measured or modeled in this study, so further research is needed to confirm the ability of WDVI SD to represent landscape energy . Future studies could analyze correlations between WDVI SD and microclimate maps or field sampling.

P. cupreus and *P. melanarius* species have different ecological requirements. Our results showed that *P. cupreus* was more abundant in fine-grain landscapes while *P. melanarius* was more abundant in coarse-grain landscapes. This is consistent with other studies founding that *P. cupreus* is present near hedgerows, while *P. melanarius* moves further from them (Winder et al. 2001; Rouabah et al. 2015). *P. melanarius* is adapted to temperature variations (Holland et al. 2005) higher in open landscapes than in complex landscapes (Alford et al. 2018).

7.6. Conclusion

This study aimed to understand the influence of biophysical heterogeneity on wheat phenology and biodiversity using optical satellite images. More specifically, we showed that:

- In all cases, the larger the scale, the stronger was the correlation.
- Landscape grain and the crop mosaic gradient were strongly correlated (maximum adj. R^2=0.81 at the 2005 m scale).
- WDVI SD inverted between the stem-extension and ripening periods: it increased and then decreased in landscapes with maize and grassland, while it decreased and then increased in landscapes with wheat, beet, barley, potato and rapeseed.
- For the combined analysis of all sites, biophysical heterogeneity (WDVI SD) appeared beneficial for wheat phenology (Diff WDVI) during the ripening period, since Diff WDVI decreased as WDVI SD increased.
- Analysis of each site showed that biophysical heterogeneity (WDVI SD) appeared to benefit wheat growth in fine-grain landscapes but disadvantage it in coarse-grain landscapes during the stem-extension and ripening periods.
- Biophysical heterogeneity (WDVI SD) estimated the distribution of carabid beetle species accurately (max adj. R^2 = 0.62) at the 2005 m scale. During the stem-extension period, biophysical heterogeneity, fine landscape grain and/or extensive crop mosaics were beneficial to *P. cupreus* but unfavorable to *P. melanarius*, while the opposite was observed during the ripening period.
- We can consider the crop mosaic as a green infrastructure to manage landscape scale biodiversity. Local farming organization could design these infrastructures as they do to combat erosion (Joannon et al. 2004).

Overall, the study highlighted the benefit of using optical remote sensing data to understand wheat dynamics and their associated biodiversity. To understand the ecological function of biophysical heterogeneity further, the WDVI SD developed should be compared

to energy flux measurements. It also would be interesting to evaluate the contribution of radar images, since the microwave domain is sensitive to plant structure.

GENERAL CONCLUSION AND PERSPECTIVES

The objective of the thesis was twofold : 1) comparatively evaluate the S-2 optical and S-1 SAR time series to identify and characterize the constituent elements of ecological continuities using land cover and land use classifications and crop characterization in wooded and crop-dominated landscapes, 2) assess the influence of the spatio-temporal structuring these landscape mosaics on biodiversity using metrics derived from S-1 and S-2 time series.

We exposed in the first part of the thesis the challenges posed by landscape ecology and remote sensing applied to ecological continuities.

The second part consisted of a comparative evaluation of the potential of variables derived from S-1 and S-2 data to identify and characterize the elements constituting ecological continuities in wooded landscapes. Land cover was identified and characterized in forest-agriculture mosaics in Brazil and Spain.

In a third part, we comparatively evaluated the potential of variables derived from S-1 and S-2 data to identify and characterize the elements constituting ecological continuities in crop-dominated landscapes. S-1 and S-2 sensors were also evaluated to estimate phenological stages and biophysical variables in wheat and rapeseed crops.

A fourth section was dedicated to the analysis of the relationships between maps of landscape metrics derived from Sentinel images and species surveys. We analyzed the influence of biophysical heterogeneity derived from S-2 on wheat phenology and the distribution of two agricultural carabid beetle species in six crop-dominated landscapes.

More specifically, the second part of the thesis aimed at answering the question: What are the most efficient Sentinel sensor and variables to identify the potential constitutive elements of ecological continuities in wooded landscapes?

To answer this question, we evaluated the potential of S-1 data alone, S-2 data alone and combined S-1 and S-2 data to identify and characterize land cover types in forest-agricultural mosaic landscapes. The study focused on two wooded landscapes with contrasting vegetation gradients: a temperate mountainous landscape in the Cantabrian Range (Spain) and a tropical humid forest landscape in Paragominas (Brazil). Although these landscape mosaics differ greatly, they have similar ecological functions (biodiversity conservation and carbon storage). The satellite images were classified using an incremental procedure based on the ranks of importance of the input variables derived from S-1 and S-2 time series. The S-2 data alone produced better results (mean kappa index=0.59-0.83) than the S-1 data alone (mean kappa index=0.28-0.72), while the combination of the two types of data slightly improved the results (mean kappa index=0.55-0.85). The method used allows defining the number and type of variables that optimally discriminate the land use classes according to the type of landscape considered. The best configuration for the Spanish and Brazilian study areas includes respectively 5 and 10 variables for the S-2 data and 10 and 20 variables for the S-1 data. The NIR and the VV and VH polarizations are the most discriminating variables for the S-2 and S-1 data, respectively. In addition, the method allowed the definition of key periods for the discrimination of land cover and land use classes according to the type of images used. For example, in the Cantabrian Mountains, winter and summer are key periods for the S-2 time series, while spring and winter are key periods for the S-1 time series.

The third part of the thesis aimed at answering the question: What are the most efficient Sentinel sensor and variables to identify and characterize the potential constitutive elements of ecological continuities in crop-dominated landscapes? This part focuses on crop characterization with the study of wheat and rapeseed, which are two of the most important crops in the world in terms of harvested area.

We evaluated the potential of S-1 data alone, S-2 data alone and of combined S-1 and S-2 data to identify the main and secondary phenological stages of wheat and rapeseed in Picardy (France). More specifically, the aim of this study was to evaluate the interest of polarimetric indicators derived from S-1 data and to determine the number and type of S-1 and S-2 variables necessary to discriminate the phenological stages of wheat and rapeseed. We estimated the performance of spectral bands and vegetation indices derived from S-2 and backscatter coefficients and polarimetric indicators derived from S-1. Satellite images were classified using the incremental method developed in the previous study (Mercier et al. 2019b). Results showed that the combined use of S-1 and S-2 data (mean kappa = 0.53-0.82 and 0.74-0.92 for wheat and rapeseed, respectively) provided higher accuracy than the use of S-1 data alone (mean kappa = 0. 48-0.61 and 0.61-0.64 for wheat and rapeseed, respectively) or S-2 alone (mean kappa = 0.54-0.75 and 0.67-0.86 for wheat and rapeseed, respectively) for the identification of principal and secondary phenological stages. The most important variables were the VH:VV ratio and polarimetric indicators for S-1 and NDVI and S2REP indices and the biophysical variable, LAI, for S-2. Overall, this study highlighted the interest of polarimetric indicators and the combined use of S-1 and S-2 data to monitor the phenology of wheat and rapeseed.

We continued our research on crop characterization by evaluating the potential of S-1 and S-2 images to estimate the LAI, WB, DB and moisture content of wheat and rapeseed. We compared the predictive power of 22 S-2 optical variables (10 spectral bands and 12 vegetation indices) and 7 S-1 SAR variables (2 backscatter coefficients, 1 ratio and 4 polarimetric indicators) using GPR. This study, applied to the study area of Brittany, showed the potential of S-1 and S-2 data to estimate these 4 crop parameters for wheat and rapeseed. The performance of the S-2 variables is equivalent or superior to that of S-1 variables. The best models obtained with S-1 use the green, NIR bands and vegetation indices respectively for LAI (adjusted R^2 = 0.91), biomass (adjusted R^2 > 0.70) and WC (adjusted R^2 = 0.82) of wheat, and SWIR bands for DB (adjusted R^2 = 0.85) and WB (adjusted R^2 = 0.77) of rapeseed. For the S-1 variables, the VH:VV ratio was most relevant for wheat LAI (adjusted R^2 = 0.91) and rapeseed biomass (adjusted R^2 >0.75), versus SE for wheat WC (adjusted R^2 = 0.78). While confirming the interest of S-2 data, the results highlighted, in an unprecedented way, the importance of polarimetric indicators derived from S-1 for the estimation of biophysical parameters of wheat and rapeseed.

Finally, the fourth and last part of the thesis aimed at answering the question: What is the impact of landscape structure on crop phenology and biodiversity in crop-dominated landscapes?

Based on the results obtained in the previous part, we assessed the impact of the spatio-temporal structuring of the crop mosaic on biodiversity. For that purpose, we analyzed the influence of biophysical heterogeneity on wheat phenology and associated biodiversity in

Brittany, Picardy and Wallonia study areas. The vegetation index named WDVI calculated from S-2 data was used as a metric of biophysical heterogeneity and as an indicator of wheat phenology. First, we analyzed the relationships between crop mosaic, landscape grain and biophysical heterogeneity. Then, we studied the effect of biophysical heterogeneity on wheat phenology. Finally, the distribution of two carabid beetle species was estimated using the biophysical heterogeneity metric. The results showed that landscape grain and crop mosaic gradient were highly correlated (maximum adjusted $R^2 = 0.81$). For the joint analysis of all sites, biophysical heterogeneity was beneficial for wheat phenology during the ripening period. The analysis by site showed that biophysical heterogeneity was beneficial for wheat growth in the fine grain but disadvantaged it in the open field landscapes both during stem extension and ripening periods. The biophysical heterogeneity metric was used to accurately estimate the distribution of two carabid beetle species (maximum adjusted $R^2 = 0.62$). This study highlighted the value of using S-2 data to understand wheat dynamics and associated biodiversity.

In general, this thesis assessed the potential of S-2 optical and S-1 SAR time series to identify and characterize ecological continuities in wooded and crop-dominated landscapes. More specifically, we showed that although S-2 data are more suitable than S-1 data for discriminating land cover/land use types as well as phenological stages and biophysical variables of wheat and rapeseed, the combined use of S-2 and S-1 data improves the accuracy of the classifications, with S-1 data also showing high interest in cloudy areas. Our research also showed the interest of polarimetric indicators derived from S-1 data to characterize wheat and rapeseed crops inserted in crop-dominated landscapes. Finally, this thesis highlighted the interest of the biophysical heterogeneity metric derived from S-2 data that allowed estimating precisely the distribution of two carabid beetle species. The crop mosaic can be considered as a green infrastructure to manage biodiversity at the landscape scale. The biophysical heterogeneity metric derived from S-2 images is continuous, consistent across locations and crop types and able to address ecological issues using free satellite images available for any area on Earth.

Based on these findings, we also highlight several issues that need to be addressed in ongoing and future work.

Concerning the combination of S-1 and S-2 data to identify constituent elements of ecological continuities, the fusion methods used in this thesis are called low-level or pre-classification fusions because they consist in combining optical and SAR « raw » variables. High-level fusions (or post-classification fusions) consist in combining information extracted from independent data sets. For example, in the case of land cover maps, the classes best identified by the S-2 data alone and S-1 data alone could be combined to form a final map. However, this method requires an initial analysis of the classifications derived from each independent data set and decision making appropriate to the study objective to obtain a relevant final map. Therefore, it would be interesting to comparatively evaluate fusion methods with different semantic levels in order to optimize the fusion of SAR and optical data to identify and characterize the potential elements constituting ecological continuities.

Regarding the phenological stage prediction model that we developed in the second part of this thesis on the study area located in Picardy, we evaluated the robustness of the model

by applying it on the study area of Brittany. The results show that principal phenological stages of rapeseed have been very well predicted (kappa = 0.75, OA = 80%) while numerous misclassifications have been observed for secondary phenological stages. For wheat, the interpretation of results was more difficult due to different typologies between the training (Picardy) and validation samples (Brittany). However, results showed a correct prediction of the stem elongation stage and a coherent succession of principal and secondary phenological stages. These results confirmed that the method used was robust in predicting the principal phenological stages of rapeseed and promising for the principal and secondary phenological stages of wheat. These results have been valued in the SPIE Remote Sensing International Symposium (Mercier et al. 2019a). Besides, the use of samples collected in several study areas could also contribute to test the robustness of the model applied to the estimate crop biophysical variables (Part 2), especially since the sampling used was small. Small number of crops surveys for the estimation of crop biophysical variables derived from S-1 and S-2 data was a limiting factor when testing statistical models. Indeed, the lower the sample size, the lower the predictive power of the statistical test. A larger sample size would allow testing more powerful modeling methods such as RF or SVM.

The biophysical heterogeneity (WDVI SD) measured from S-2 data is a continuous metric that reflects a biophysical state rather than discretized classes of crops. This continuous value is relevant for generalist species. Indeed, these species are not specialized in one type of land cover/land use or plant species, since they use several types of land cover/land use during their life cycle. Moreover, in crop-dominated landscapes, the landscape heterogeneity is generally beneficial for generalist species. Habitat suitability maps could be derived from the WDVI SD to highlight the connectivity or fragmentation of potential habitats. Finally, WDVI variations around an element beneficial for a specialist species could be studied to better understand the resistance of landscape elements to the movement of this species. Finally, the influence of hedgerow network on biophysical heterogeneity could be studied with the use of a very high spatial resolution satellite data such as SPOT-6 images.

During this thesis, a study has started in close collaboration with the Spanish team of the WOODNET project. We used a brown bear habitat suitability model developed by the Spanish team and detailed in an article published by Gastón et al. (2017). Landscape metrics that we calculated from land cover maps derived from the combined use of S-1 and S-2 data were incorporated into the brown bear habitat suitability model. This study aimed to evaluate the value of the Spanish land cover maps produced in Mercier et al. (2019b) for the identification and characterization of ecological continuities for brown bears. Landscape metrics were derived from the most accurate land cover map, i.e., the map derived from the combined use of Sentinel-1 and 2 data. These landscape metrics correspond to landscape heterogeneity (Appendix M, Figure M-1), landscape grain (Appendix M, Figure M-2) and interfaces between land cover types (Appendices M, Figures M-3 and M-4). First results showed that the proportion of brown bear increases with fine grain and decreases with landscape heterogeneity. Overall, interfaces containing "bare soil" class have a negative effect on the proportion brown bears while interfaces including forested surfaces have a positive effect. Perspectives emerged from these first results and further work will be done in close collaboration with the Spanish team of the WOODNET project. We plan to further analyze the choice of input parameters of the model by removing the interface metrics including

misclassified land cover types (water and artificial surfaces) and create new landscape parameters by combining other land cover types (scrubland/bare soil) at different spatial scales.

Finally, the database we developed in the second part of this thesis to characterize wheat and rapeseed will soon be available in a data paper to share the data further with the scientific community.

REFERENCES

Abdikan S, Sanli FB, Ustuner M, Calò F (2016) Land cover mapping using sentinel-1 SAR data. The International Archives of Photogrammetry, Remote Sensing and Spatial Information Sciences 41:757

Ahmadian N, Ullmann T, Verrelst J, et al (2019) Biomass Assessment of Agricultural Crops Using Multi-temporal Dual-Polarimetric TerraSAR-X Data. PFG. https://doi.org/10.1007/s41064-019-00076-x

Aksoy S, Akçay HG, Wassenaar T (2009) Automatic mapping of linear woody vegetation features in agricultural landscapes using very high resolution imagery. IEEE Transactions on Geoscience and Remote Sensing 48:511–522

Alford L, Tougeron K, Pierre J-S, et al (2018) The effect of landscape complexity and microclimate on the thermal tolerance of a pest insect. Insect Science 25:905–915. https://doi.org/10.1111/1744-7917.12460

Ali I, Cawkwell F, Dwyer E, et al (2016) Satellite remote sensing of grasslands: from observation to management. J Plant Ecol 9:649–671. https://doi.org/10.1093/jpe/rtw005

Alignier A, Solé-Senan XO, Robleño I, et al (2020) Configurational crop heterogeneity increases within-field plant diversity. Journal of Applied Ecology 57:654–663. https://doi.org/10.1111/1365-2664.13585

Altieri MA (1999) The ecological role of biodiversity in agroecosystems. Agric Ecosyst Environ 74:19–31. https://doi.org/10.1016/B978-0-444-50019-9.50005-4

Álvarez-Mozos J, Verhoest NEC, Larrañaga A, et al (2009) Influence of Surface Roughness Spatial Variability and Temporal Dynamics on the Retrieval of Soil Moisture from SAR Observations. Sensors 9:463–489. https://doi.org/10.3390/s90100463

Andrade FS (2011) Variabilidade da precipitação pluviometrica de um município do estado do Pará. ngenharia Ambiental - Espírito Santo do Pinhal 8:138–145

Angelsen A, Kaimowitz D (1999) Rethinking the Causes of Deforestation: Lessons from Economic Models. World Bank Res Obs 14:73–98. https://doi.org/10.1093/wbro/14.1.73

Aplin P (2004) Remote sensing: land cover. Progress in Physical Geography: Earth and Environment 28:283–293. https://doi.org/10.1191/0309133304pp413pr

Ashourloo D, Shahrabi HS, Azadbakht M, et al (2019) Automatic canola mapping using time series of sentinel 2 images. ISPRS Journal of Photogrammetry and Remote Sensing 156:63–76. https://doi.org/10.1016/j.isprsjprs.2019.08.007

Asner GP, Mascaro J, Muller-Landau HC, et al (2012) A universal airborne LiDAR approach for tropical forest carbon mapping. Oecologia 168:1147–1160

Aviron S, Kindlmann P, Burel F (2007) Conservation of butterfly populations in dynamic landscapes: The role of farming practices and landscape mosaic. Ecological Modelling 205:135–145. https://doi.org/10.1016/j.ecolmodel.2007.02.012

Baghdadi N, Boyer N, Todoroff P, et al (2009) Potential of SAR sensors TerraSAR-X, ASAR/ENVISAT and PALSAR/ALOS for monitoring sugarcane crops on Reunion Island. Remote Sensing of Environment 113:1724–1738. https://doi.org/10.1016/j.rse.2009.04.005

Baghdadi N, Cerdan O, Zribi M, et al (2008) Operational performance of current synthetic aperture radar sensors in mapping soil surface characteristics in agricultural environments: application to hydrological and erosion modelling. Hydrological Processes: An International Journal 22:9–20

Baghdadi N, El Hajj M, Zribi M, Fayad I (2016) Coupling SAR C-band and optical data for soil moisture and leaf area index retrieval over irrigated grasslands. IEEE J Sel Top Appl Earth Obs Remote Sens 9:1129–1244. https://doi.org/10.1109/IGARSS.2016.7729919

Bailey D, Schmidt-Entling MH, Eberhart P, et al (2010) Effects of habitat amount and isolation on biodiversity in fragmented traditional orchards. Journal of Applied Ecology 47:1003–1013. https://doi.org/10.1111/j.1365-2664.2010.01858.x

Balzter H, Cole B, Thiel C, Schmullius C (2015) Mapping CORINE land cover from Sentinel-1A SAR and SRTM digital elevation model data using random forests. Remote Sensing 7:14876–14898

Bargiel D (2013) Capabilities of high resolution satellite radar for the detection of semi-natural habitat structures and grasslands in agricultural landscapes. Ecological informatics 13:9–16

Bargiel D (2017) A new method for crop classification combining time series of radar images and crop phenology information. Remote Sens Environ 198:369–383. https://doi.org/10.1016/j.rse.2017.06.022

Barlow J, Gardner TA, Araujo IS, et al (2007) Quantifying the biodiversity value of tropical primary, secondary, and plantation forests. PNAS 104:18555–18560. https://doi.org/10.1073/pnas.0703333104

Barlow J, Lennox GD, Ferreira J, et al (2016) Anthropogenic disturbance in tropical forests can double biodiversity loss from deforestation. Nature 535:144–147. https://doi.org/10.1038/nature18326

Bastiaanssen WGM, Noordman EJM, Pelgrum H, et al (2005) SEBAL Model with Remotely Sensed Data to Improve Water-Resources Management under Actual Field Conditions. Journal of Irrigation and Drainage Engineering 131:85–93. https://doi.org/10.1061/(ASCE)0733-9437(2005)131:1(85)

Baudry J, Bunce RGH, Burel F (2000) Hedgerows: An international perspective on their origin, function and management. Journal of Environmental Management 60:7–22. https://doi.org/10.1006/jema.2000.0358

Baudry J, Burel F (1984) "Remembrement": Landscape consolidation in France. Landscape Planning 11:235–241. https://doi.org/10.1016/0304-3924(84)90047-9

Baudry J, Burel F, Aviron S, et al (2003) Temporal variability of connectivity in agricultural landscapes: do farming activities help? Landscape Ecol 18:303–314. https://doi.org/10.1023/A:1024465200284

Baudry J, Jouin A (2003) De la haie aux bocages. Organisation, dynamique et gestion. Editions Quae

Bauer ME, Cipra JE, Anuta PE, Etheridge JB (1979) Identification and area estimation of agricultural crops by computer classification of Landsat MSS data. Remote Sensing of Environment 8:77–92

Baup F, Mougin E, de Rosnay P, et al (2007) Surface soil moisture estimation over the AMMA Sahelian site in Mali using ENVISAT/ASAR data. Remote Sensing of Environment 109:473–481. https://doi.org/10.1016/j.rse.2007.01.015

Bégué A, Arvor D, Bellon B, et al (2018) Remote Sensing and Cropping Practices: A Review. Remote Sensing 10:99. https://doi.org/10.3390/rs10010099

Beier P, Noss RF (1998) Do Habitat Corridors Provide Connectivity? Conservation Biology 12:1241–1252. https://doi.org/10.1111/j.1523-1739.1998.98036.x

Belgiu M, Csillik O (2018) Sentinel-2 cropland mapping using pixel-based and object-based time-weighted dynamic time warping analysis. Remote Sensing of Environment 204:509–523. https://doi.org/10.1016/j.rse.2017.10.005

Belgiu M, Drăguţ L (2016) Random forest in remote sensing: A review of applications and future directions. ISPRS Journal of Photogrammetry and Remote Sensing 114:24–31. https://doi.org/10.1016/j.isprsjprs.2016.01.011

Bennett G (2004) Integrating Biodiversity Conservation and Sustainable Use: Lessons Learned from Ecological Networks. IUCN

Bertrand F, Fournier M (2009) Les politiques européennes d'environnement et l'aménagement des territoires. Armand Colin

Betbeder J (2015) Evaluation des données de télédétection pour l'identification et la caractérisation des continuités écologiques

Betbeder J, Fieuzal R, Baup F (2016a) Assimilation of LAI and Dry Biomass Data From Optical and SAR Images Into an Agro-Meteorological Model to Estimate Soybean Yield. IEEE J Sel Top Appl Earth Obs Remote Sens 9:2540–2553. https://doi.org/10.1109/JSTARS.2016.2541169

Betbeder J, Fieuzal R, Philippets Y, et al (2016b) Contribution of multitemporal polarimetric synthetic aperture radar data for monitoring winter wheat and rapeseed crops. Journal of Applied Remote Sensing 10:026020. https://doi.org/10.1117/1.JRS.10.026020

Betbeder J, Hubert-Moy L, Burel F, et al (2015) Assessing ecological habitat structure from local to landscape scales using synthetic aperture radar. Ecological Indicators 52:545–557. https://doi.org/10.1016/j.ecolind.2014.11.009

Betbeder J, Nabucet J, Pottier E, et al (2014a) Detection and Characterization of Hedgerows Using TerraSAR-X Imagery. Remote Sens 6:3752–3769. https://doi.org/10.3390/rs6053752

Betbeder J, Rapinel S, Corpetti T, et al (2014b) Multitemporal classification of TerraSAR-X data for wetland vegetation mapping. JARS, JARSC4 8:083648. https://doi.org/10.1117/1.JRS.8.083648

Billeter R, Liira J, Bailey D, et al (2008) Indicators for biodiversity in agricultural landscapes: a pan-European study. J Appl Ecol 45:141–150. https://doi.org/10.1111/j.1365-2664.2007.01393.x

Bindlish R, Kustas WP, French AN, et al (2001) Influence of near-surface soil moisture on regional scale heat fluxes: model results using microwave remote sensing data from SGP97. IEEE Transactions on Geoscience and Remote Sensing 39:1719–1728. https://doi.org/10.1109/36.942550

Blackburn GA (1998) Spectral indices for estimating photosynthetic pigment concentrations: A test using senescent tree leaves. International Journal of Remote Sensing 19:657–675. https://doi.org/10.1080/014311698215919

Blaes X, Vanhalle L, Defourny P (2005) Efficiency of crop identification based on optical and SAR image time series. Remote Sensing of Environment 96:352–365. https://doi.org/10.1016/j.rse.2005.03.010

Bleiholder, H, Weber E, Hess M, et al (2001) Growth Stages of Mono- and Dicotyledonous Plants, BBCH Monograph, Federal Biological Research Centre for Agriculture and Forestry: Berlin/Braunschweig, Germany

Bolund P, Hunhammar S (1999) Ecosystem services in urban areas. Ecological Economics 29:293–301. https://doi.org/10.1016/S0921-8009(99)00013-0

Bontemps S, Arias M, Cara C, et al (2015) Building a Data Set over 12 Globally Distributed Sites to Support the Development of Agriculture Monitoring Applications with Sentinel-2. Remote Sensing 7:16062–16090. https://doi.org/10.3390/rs71215815

Born C-H, Dufrêne M, Peeters A (2014) La biodiversité en Wallonie, 40 ans après l'adoption de la loi sur la conservation de la nature. Aménagement-environnement: urbanisme et droit foncier 2014:

Bouchet A-S, Laperche A, Bissuel-Belaygue C, et al (2016) Nitrogen use efficiency in rapeseed. A review. Agron Sustain Dev 36:38. https://doi.org/10.1007/s13593-016-0371-0

Bouman BAM, van Kasteren HWJ, Uenk D (1992) Standard relations to estimate ground cover and LAI of agricultural crops from reflectance measurements. European Journal of Agronomy 1:249–262. https://doi.org/10.1016/S1161-0301(14)80077-4

Bourgoin C (2019) A framework for evaluating forest ecological vulnerability in tropical deforestation fronts from the assessment of forest degradation in a landscape approach : Case studies from Brazil and Vietnam. Phdthesis, Institut agronomique, vétérinaire et forestier de France

Bourgoin C, Blanc L, Bailly J-S, et al (2018) The Potential of Multisource Remote Sensing for Mapping the Biomass of a Degraded Amazonian Forest. Forests 9:303. https://doi.org/10.3390/f9060303

Boussard H, Baudry J (2017) Chloe2012: a software for landscape pattern analysis

Bréda NJJ (2003) Ground-based measurements of leaf area index: a review of methods, instruments and current controversies. J Exp Bot 54:2403–2417. https://doi.org/10.1093/jxb/erg263

Breiman L (2001) Random Forests. Machine Learning 45:5–32. https://doi.org/10.1023/A:1010933404324

Brown SCM, Quegan S, Morrison K, et al (2003) High-resolution measurements of scattering in wheat canopies-implications for crop parameter retrieval. IEEE Transactions on Geoscience and Remote Sensing 41:1602–1610. https://doi.org/10.1109/TGRS.2003.814132

Burel F, Aviron S, Baudry J, et al (2013) The Structure and Dynamics of Agricultural Landscapes as Drivers of Biodiversity. In: Fu B, Jones KB (eds) Landscape Ecology for Sustainable Environment and Culture. Springer Netherlands, Dordrecht, pp 285–308

Burel F, Baudry J (2003) Landscape Ecology: Concepts, Methods, and Applications. Science Publishers

Burel F, Baudry J, Butet A, et al (1998) Comparative biodiversity along a gradient of agricultural landscapes. Acta Oecologica 19:47–60. https://doi.org/10.1016/S1146-609X(98)80007-6

Büttner G, Csillag F (1989) Comparative study of crop and soil mapping using multitemporal and multispectral SPOT and landsat thematic mapper data. Remote Sensing of Environment 29:241–249. https://doi.org/10.1016/0034-4257(89)90003-5

Calle ML, Urrea V (2011) Letter to the Editor: Stability of Random Forest importance measures. Brief Bioinform 12:86–89. https://doi.org/10.1093/bib/bbq011

Canisius F, Shang J, Liu J, et al (2018) Tracking crop phenological development using multi-temporal polarimetric Radarsat-2 data. Remote Sensing of Environment 210:508–518. https://doi.org/10.1016/j.rse.2017.07.031

Chaplin-Kramer R, O'Rourke M, Schellhorn N, et al (2019) Measuring What Matters: Actionable Information for Conservation Biocontrol in Multifunctional Landscapes. Front Sustain Food Syst 3:. https://doi.org/10.3389/fsufs.2019.00060

Chaube NR, Chaurasia S, Tripathy R, et al (2019) Crop phenology and soil moisture applications of SCATSAT-. CURRENT SCIENCE 117:10

Chen B, Huang B, Xu B (2017) Multi-source remotely sensed data fusion for improving land cover classification. ISPRS Journal of Photogrammetry and Remote Sensing 124:27–39. https://doi.org/10.1016/j.isprsjprs.2016.12.008

Chen C, Wang Y, Chang Y, Ricanek K (2012) Sensitivity Analysis with Cross-Validation for Feature Selection and Manifold Learning. In: Wang J, Yen GG, Polycarpou MM (eds) Advances in Neural Networks – ISNN 2012. Springer, Berlin, Heidelberg, pp 458–467

Chen J, Saunders SC, Crow TR, et al (1999) Microclimate in Forest Ecosystem and Landscape EcologyVariations in local climate can be used to monitor and compare the effects of different management regimes. BioScience 49:288–297. https://doi.org/10.2307/1313612

Choudhury BJ, Idso SB, Reginato RJ (1987) Analysis of an empirical model for soil heat flux under a growing wheat crop for estimating evaporation by an infrared-temperature based energy balance equation. Agricultural and Forest Meteorology 39:283–297. https://doi.org/10.1016/0168-1923(87)90021-9

Chrysafis I, Mallinis G, Siachalou S, Patias P (2017) Assessing the relationships between growing stock volume and Sentinel-2 imagery in a Mediterranean forest ecosystem. Remote Sens Letters 8:508–517. https://doi.org/10.1080/2150704X.2017.1295479

Clark ML (2017) Comparison of simulated hyperspectral HyspIRI and multispectral Landsat 8 and Sentinel-2 imagery for multi-seasonal, regional land-cover mapping. Remote Sensing of Environment 200:311–325. https://doi.org/10.1016/j.rse.2017.08.028

Clark RN (1999) Spectroscopy of rocks and minerals, and principles of spectroscopy. Manual of remote sensing 3:2–2

Claverie M (2012) Estimation spatialisée de la biomasse et des besoins en eau des cultures à l'aide de données satellitales à hautes résolutions spatiale et temporelle : application aux agrosystèmes du sud-ouest de la France. Phd, Université de Toulouse, Université Toulouse III - Paul Sabatier

Cleugh H (2002) Field measurements of windbreak effects on Airflow, turbulent exchanges and microclimates

Clevers JGPW (1988) The derivation of a simplified reflectance model for the estimation of leaf area index. Remote Sensing of Environment 25:53–69. https://doi.org/10.1016/0034-4257(88)90041-7

Clevers JGPW, Gitelson AA (2013) Remote estimation of crop and grass chlorophyll and nitrogen content using red-edge bands on Sentinel-2 and -3. International Journal of Applied Earth Observation and Geoinformation 23:344–351. https://doi.org/10.1016/j.jag.2012.10.008

Clevers JGPW, Jong SMD, Epema GF, et al (2002) Derivation of the red edge index using the MERIS standard band setting. International Journal of Remote Sensing 23:3169–3184. https://doi.org/10.1080/01431160110104647

Clevers JGPW, Kooistra L, Van den Brande MMM (2017) Using Sentinel-2 Data for Retrieving LAI and Leaf and Canopy Chlorophyll Content of a Potato Crop. Remote Sensing 9:405. https://doi.org/10.3390/rs9050405

Clobert J, Baguette M, Benton TG, Bullock JM (2012) Dispersal ecology and evolution. Oxford University Press

Clothier BE, Clawson KL, Pinter PJ, et al (1986) Estimation of soil heat flux from net radiation during the growth of alfalfa. Agricultural and Forest Meteorology 37:319–329. https://doi.org/10.1016/0168-1923(86)90069-9

Cloude SR, Pottier E (1996) A review of target decomposition theorems in radar polarimetry. IEEE Transactions on Geoscience and Remote Sensing 34:498–518. https://doi.org/10.1109/36.485127

Cohen J (1960) A Coefficient of Agreement for Nominal Scales. Educational and Psychological Measurement 20:37–46. https://doi.org/10.1177/001316446002000104

Colkesen I, Kavzoglu T (2017) Ensemble-based canonical correlation forest (CCF) for land use and land cover classification using sentinel-2 and Landsat OLI imagery. Remote Sens Letters 8:1082–1091. https://doi.org/10.1080/2150704X.2017.1354262

Congalton R, Gu J, Yadav K, et al (2014) Global Land Cover Mapping: A Review and Uncertainty Analysis. Remote Sens 6:12070–12093. https://doi.org/10.3390/rs61212070

Congalton RG (1991) A review of assessing the accuracy of classifications of remotely sensed data. Remote Sensing of Environment 37:35–46. https://doi.org/10.1016/0034-4257(91)90048-B

Cookmartin G, Saich P, Quegan S, et al (2000) Modeling microwave interactions with crops and comparison with ERS-2 SAR observations. IEEE Transactions on Geoscience and Remote Sensing 38:658–670. https://doi.org/10.1109/36.841996

Crowley MA, Cardille JA (2020) Remote Sensing's Recent and Future Contributions to Landscape Ecology. Curr Landscape Ecol Rep 5:45–57. https://doi.org/10.1007/s40823-020-00054-9

Csillik O, Belgiu M (2017a) Cropland mapping from Sentinel-2 time series data using object-based image analysis. Wageningen, The Netherlands

Csillik O, Belgiu M (2017b) Cropland mapping from Sentinel-2 time series data using object-based image analysis. 5

Czerepowicz L, Case BS, Doscher C (2012) Using satellite image data to estimate aboveground shelterbelt carbon stocks across an agricultural landscape. Agriculture, ecosystems & environment 156:142–150

Dash J, Curran PJ (2004) The MERIS terrestrial chlorophyll index. International Journal of Remote Sensing 25:5403–5413. https://doi.org/10.1080/0143116042000274015

Daughtry CST, Walthall CL, Kim MS, et al (2000) Estimating Corn Leaf Chlorophyll Concentration from Leaf and Canopy Reflectance. Remote Sensing of Environment 74:229–239. https://doi.org/10.1016/S0034-4257(00)00113-9

De la Fuente B, Mateo-Sánchez MC, Rodríguez G, et al (2018) Natura 2000 sites, public forests and riparian corridors: The connectivity backbone of forest green infrastructure. Land Use Policy 75:429–441. https://doi.org/10.1016/j.landusepol.2018.04.002

de Snoo GR, van der Poll RJ (1999) Effect of herbicide drift on adjacent boundary vegetation. Agriculture, Ecosystems & Environment 73:1–6. https://doi.org/10.1016/S0167-8809(99)00008-0

Defourny P, Bontemps S, Bellemans N, et al (2019) Near real-time agriculture monitoring at national scale at parcel resolution: Performance assessment of the Sen2-Agri automated system in various cropping systems around the world. Remote Sensing of Environment 221:551–568. https://doi.org/10.1016/j.rse.2018.11.007

Delattre P, De Sousa B, Fichet-Calvet E, et al (1999) Vole outbreaks in a landscape context: evidence from a six year study of Microtus arvalis. Landscape Ecology 14:401–412. https://doi.org/10.1023/A:1008022727025

Delattre T, Pichancourt J-B, Burel F, Kindlmann P (2010) Grassy field margins as potential corridors for butterflies in agricultural landscapes: A simulation study. Ecological Modelling 221:370–377. https://doi.org/10.1016/j.ecolmodel.2009.10.010

Delegido J, Vergara C, Verrelst J, et al (2011a) Remote Estimation of Crop Chlorophyll Content by Means of High-Spectral-Resolution Reflectance Techniques. Agronomy Journal 103:1834–1842. https://doi.org/10.2134/agronj2011.0101

Delegido J, Verrelst J, Alonso L, Moreno J (2011b) Evaluation of Sentinel-2 Red-Edge Bands for Empirical Estimation of Green LAI and Chlorophyll Content. Sensors 11:7063–7081. https://doi.org/10.3390/s110707063

Denize J, Hubert-Moy L, Betbeder J, et al (2019a) Evaluation of Using Sentinel-1 and -2 Time-Series to Identify Winter Land Use in Agricultural Landscapes. Remote Sens 11:37. https://doi.org/10.3390/rs11010037

Denize J, Hubert-Moy L, Pottier E (2019b) Polarimetric SAR Time-Series for Identification of Winter Land Use. Sensors 19:5574. https://doi.org/10.3390/s19245574

Dennis RLH, Dapporto L, Dover JW, Shreeve TG (2013) Corridors and barriers in biodiversity conservation: a novel resource-based habitat perspective for butterflies. Biodivers Conserv 22:2709–2734. https://doi.org/10.1007/s10531-013-0540-2

Dente L, Satalino G, Mattia F, Rinaldi M (2008) Assimilation of leaf area index derived from ASAR and MERIS data into CERES-Wheat model to map wheat yield. Remote Sensing of Environment 112:1395–1407. https://doi.org/10.1016/j.rse.2007.05.023

Desneux N, Decourtye A, Delpuech J-M (2007) The Sublethal Effects of Pesticides on Beneficial Arthropods. Annual Review of Entomology 52:81–106. https://doi.org/10.1146/annurev.ento.52.110405.091440

Devroye L, Györfi L, Lugosi G (2013) A Probabilistic Theory of Pattern Recognition. Springer Science & Business Media

Diacono M, Rubino P, Montemurro F (2013) Precision nitrogen management of wheat. A review. Agronomy for Sustainable Development 33:219–241. https://doi.org/10.1007/s13593-012-0111-z

Dirzo R, Raven PH (2003) Global State of Biodiversity and Loss. Annual Review of Environment and Resources 28:137–167. https://doi.org/10.1146/annurev.energy.28.050302.105532

Dondina O, Kataoka L, Orioli V, Bani L (2016) How to manage hedgerows as effective ecological corridors for mammals: A two-species approach. Agriculture, Ecosystems & Environment 231:283–290. https://doi.org/10.1016/j.agee.2016.07.005

Doraiswamy PC, Hatfield JL, Jackson TJ, et al (2004) Crop condition and yield simulations using Landsat and MODIS. Remote Sensing of Environment 92:548–559. https://doi.org/10.1016/j.rse.2004.05.017

Du Z, Ge L, Ng AH-M, et al (2018) Correlating the subsidence pattern and land use in Bandung, Indonesia with both Sentinel-1/2 and ALOS-2 satellite images. International Journal of Applied Earth Observation and Geoinformation 67:54–68. https://doi.org/10.1016/j.jag.2018.01.001

Duchemin B, Fieuzal R, Rivera MA, et al (2015) Impact of Sowing Date on Yield and Water Use Efficiency of Wheat Analyzed through Spatial Modeling and FORMOSAT-2 Images. Remote Sensing 7:5951–5979. https://doi.org/10.3390/rs70505951

Duru M, Therond O, Martin G, et al (2015) How to implement biodiversity-based agriculture to enhance ecosystem services: a review. Agron Sustain Dev 35:1259–1281. https://doi.org/10.1007/s13593-015-0306-1

Dusseux P, Corpetti T, Hubert-Moy L, Corgne S (2014) Combined Use of Multi-Temporal Optical and Radar Satellite Images for Grassland Monitoring. Remote Sensing 6:6163–6182. https://doi.org/10.3390/rs6076163

El Hajj M, Baghdadi N, Bazzi H, Zribi M (2019) Penetration Analysis of SAR Signals in the C and L Bands for Wheat, Maize, and Grasslands. Remote Sensing 11:31. https://doi.org/10.3390/rs11010031

Emde C, Buras-Schnell R, Kylling A, et al (2016) The libRadtran software package for radiative transfer calculations (version 2.0.1). Geoscientific Model Development 9:1647–1672. https://doi.org/10.5194/gmd-9-1647-2016

Ernoult A, Tremauville Y, Cellier D, et al (2006) Potential landscape drivers of biodiversity components in a flood plain: Past or present patterns? Biological Conservation 127:1–17. https://doi.org/10.1016/j.biocon.2005.07.008

Estes L, Chen P, Debats S, et al (2018) A large-area, spatially continuous assessment of land cover map error and its impact on downstream analyses. Glob Chang Biol 24:322–337. https://doi.org/10.1111/gcb.13904

Fahrig L (2017) Ecological Responses to Habitat Fragmentation Per Se. Annu Rev Ecol Evol Syst 48:1–23. https://doi.org/10.1146/annurev-ecolsys-110316-022612

Fahrig L (1992) Relative importance of spatial and temporal scales in a patchy environment. Theoretical Population Biology 41:300–314. https://doi.org/10.1016/0040-5809(92)90031-N

Fahrig L (2003) Effects of Habitat Fragmentation on Biodiversity. Annu Rev Ecol Evol Syst 34:487–515. https://doi.org/10.1146/annurev.ecolsys.34.011802.132419

Fahrig L, Arroyo-Rodríguez V, Bennett JR, et al (2019) Is habitat fragmentation bad for biodiversity? Biological Conservation 230:179–186. https://doi.org/10.1016/j.biocon.2018.12.026

Fahrig L, Baudry J, Brotons L, et al (2011) Functional landscape heterogeneity and animal biodiversity in agricultural landscapes. Ecol Lett 14:101–112. https://doi.org/10.1111/j.1461-0248.2010.01559.x

Farr TG, Rosen PA, Caro E, et al (2007) The Shuttle Radar Topography Mission. Reviews of Geophysics 45:. https://doi.org/10.1029/2005RG000183

Fauvel M, Arbelot B, Benediktsson JA, et al (2012) Detection of hedges in a rural landscape using a local orientation feature: from linear opening to path opening. IEEE Journal of Selected Topics in Applied Earth Observations and Remote Sensing 6:15–26

Fauvel M, Lopes M, Dubo T, et al (2020) Prediction of plant diversity in grasslands using Sentinel-1 and -2 satellite image time series. Remote Sensing of Environment 237:111536. https://doi.org/10.1016/j.rse.2019.111536

Feber RE, Smith H (1995) Butterfly conservation on arable farmland. In: Pullin AS (ed) Ecology and Conservation of Butterflies. Springer Netherlands, Dordrecht, pp 84–97

Ferro-Famil L, Pottier E (2014) Chapter 21 - Radar Polarimetry Basics and Selected Earth Remote Sensing Applications. In: Sidiropoulos ND, Gini F, Chellappa R, Theodoridis S (eds) Academic Press Library in Signal Processing. Elsevier, pp 1119–1244

Fick SE, Hijmans RJ (2017) WorldClim 2: new 1-km spatial resolution climate surfaces for global land areas. International Journal of Climatology 37:4302–4315. https://doi.org/10.1002/joc.5086

Fieuzal R, Baup F, Marais-Sicre C (2013) Monitoring Wheat and Rapeseed by Using Synchronous Optical and Radar Satellite Data—From Temporal Signatures to Crop Parameters Estimation. Advances in Remote Sensing 02:162–180. https://doi.org/10.4236/ars.2013.22020

Fitzgibbon CD (1997) Small Mammals in Farm Woodlands: The Effects of Habitat, Isolation and Surrounding Land-Use Patterns. Journal of Applied Ecology 34:530–539. https://doi.org/10.2307/2404895

Fletcher RJ, Didham RK, Banks-Leite C, et al (2018) Is habitat fragmentation good for biodiversity? Biological Conservation 226:9–15. https://doi.org/10.1016/j.biocon.2018.07.022

Foley JA, Ramankutty N, Brauman KA, et al (2011) Solutions for a cultivated planet. Nature 478:337–342. https://doi.org/10.1038/nature10452

Food and Agriculture Organization of the United Nations (2017) FAOSTAT. In: F. Statistical databases. http://www.fao.org/faostat/en/#data/QC. Accessed 17 May 2019

Foody GM (2004) Thematic map comparison: Evaluating the statistical significance of differences in classification accuracy. Photogramm Eng Remote Sens 70:. https://doi.org/627–633

Forman RTT, Baudry J (1984) Hedgerows and hedgerow networks in landscape ecology. Environmental Management 8:495–510. https://doi.org/10.1007/BF01871575

Frampton WJ, Dash J, Watmough G, Milton EJ (2013) Evaluating the capabilities of Sentinel-2 for quantitative estimation of biophysical variables in vegetation. ISPRS Journal of Photogrammetry and Remote Sensing 82:83–92. https://doi.org/10.1016/j.isprsjprs.2013.04.007

Freeman A, Durden SL (1998) A three-component scattering model for polarimetric SAR data. IEEE Transactions on Geoscience and Remote Sensing 36:963–973. https://doi.org/10.1109/36.673687

Freemark KE, Kirk DA (2001) Birds on organic and conventional farms in Ontario: partitioning effects of habitat and practices on species composition and abundance. Biological Conservation 101:337–350. https://doi.org/10.1016/S0006-3207(01)00079-9

Friedl MA, McGwire KC, McIver DK (2001) An Overview of Uncertainty in Optical Remotely Sensed Data for Ecological Applications. In: Hunsaker CT, Goodchild MF, Friedl MA, Case TJ (eds) Spatial Uncertainty in Ecology: Implications for Remote Sensing and GIS Applications. Springer, New York, NY, pp 258–283

Fu Y, Yang G, Wang J, et al (2014) Winter wheat biomass estimation based on spectral indices, band depth analysis and partial least squares regression using hyperspectral measurements. Computers and Electronics in Agriculture 100:51–59. https://doi.org/10.1016/j.compag.2013.10.010

Fung AK, Chen KS (1992) Dependence of the surface backscattering coefficients on roughness, frequency and polarization states. International journal of remote sensing 13:1663–1680

Gagic V, Tscharntke T, Dormann CF, et al (2011) Food web structure and biocontrol in a four-trophic level system across a landscape complexity gradient. Proceedings of the Royal Society B: Biological Sciences 278:2946–2953. https://doi.org/10.1098/rspb.2010.2645

Ganeva D, Roumenina E, Jelev G, et al (2019) Applicability of parametric and nonparametric regression models for retrieval of crop canopy parameters for winter rapeseed and wheat crops using Sentinel-2 multispectral data. In: Seventh International Conference on Remote Sensing and Geoinformation of the Environment (RSCy2019). International Society for Optics and Photonics, p 111740J

Gao B (1996) NDWI—A normalized difference water index for remote sensing of vegetation liquid water from space. Remote Sensing of Environment 58:257–266. https://doi.org/10.1016/S0034-4257(96)00067-3

Gao S, Niu Z, Huang N, Hou X (2013) Estimating the Leaf Area Index, height and biomass of maize using HJ-1 and RADARSAT-2. International Journal of Applied Earth Observation and Geoinformation 24:1–8. https://doi.org/10.1016/j.jag.2013.02.002

García D, Quevedo M, Obeso JR, Abajo A (2005) Fragmentation patterns and protection of montane forest in the Cantabrian range (NW Spain). Forest Ecology and Management 208:29–43. https://doi.org/10.1016/j.foreco.2004.10.071

García-León D, Contreras S, Hunink J (2019) Comparison of meteorological and satellite-based drought indices as yield predictors of Spanish cereals. Agricultural Water Management 213:388–396. https://doi.org/10.1016/j.agwat.2018.10.030

Gardner TA, Ferreira J, Barlow J, et al (2013) A social and ecological assessment of tropical land uses at multiple scales: the Sustainable Amazon Network. Phil Trans R Soc B 368:20130307. https://doi.org/10.1098/rstb.2013.0307

Gastón A, Ciudad C, Mateo-Sánchez MC, et al (2017) Species' habitat use inferred from environmental variables at multiple scales: How much we gain from high-resolution vegetation data? International Journal of Applied Earth Observation and Geoinformation 55:1–8. https://doi.org/10.1016/j.jag.2016.10.007

Gaublomme E, Hendrickx F, Dhuyvetter H, Desender K (2008) The effects of forest patch size and matrix type on changes in carabid beetle assemblages in an urbanized landscape. Biological Conservation 141:2585–2596. https://doi.org/10.1016/j.biocon.2008.07.022

George AD, III FRT, Faaborg J (2015) Using LiDAR and remote microclimate loggers to downscale near-surface air temperatures for site-level studies. Remote Sensing Letters 6:924–932. https://doi.org/10.1080/2150704X.2015.1088671

Ghazoul J, Burivalova Z, Garcia-Ulloa J, King LA (2015) Conceptualizing Forest Degradation. Trends in Ecology & Evolution 30:622–632. https://doi.org/10.1016/j.tree.2015.08.001

Ghosh P, Mandal D, Bhattacharya A, et al (2018) Assessing Crop Monitoring Potential of SENTINEL-2 in a Spatio-Temporal Scale. ISPRS - International Archives of the Photogrammetry, Remote Sensing and Spatial Information Sciences 425:227–231. https://doi.org/10.5194/isprs-archives-XLII-5-227-2018

Gitelson AA, Kaufman YJ, Merzlyak MN (1996) Use of a green channel in remote sensing of global vegetation from EOS-MODIS. Remote Sensing of Environment 58:289–298. https://doi.org/10.1016/S0034-4257(96)00072-7

Gómez C, White JC, Wulder MA (2016) Optical remotely sensed time series data for land cover classification: A review. ISPRS Journal of Photogrammetry and Remote Sensing 116:55–72. https://doi.org/10.1016/j.isprsjprs.2016.03.008

Gurr GM, Reynolds OL, Johnson AC, et al (2018) Landscape ecology and expanding range of biocontrol agent taxa enhance prospects for diamondback moth management. A review. Agron Sustain Dev 38:23. https://doi.org/10.1007/s13593-018-0500-z

Guyot G, Baret F (1988) Utilisation de la haute resolution spectrale pour suivre l'etat des couverts vegetaux. Spectral Signatures of Objects in Remote Sensing 287:279

Haas J, Ban Y (2018) Urban Land Cover and Ecosystem Service Changes based on Sentinel-2A MSI and Landsat TM Data. IEEE J Sel Top Appl Earth Obs Remote Sens 11:485–497. https://doi.org/10.1109/JSTARS.2017.2786468

Haboudane D, Miller JR, Pattey E, et al (2004) Hyperspectral vegetation indices and novel algorithms for predicting green LAI of crop canopies: Modeling and validation in the context of precision agriculture. Remote Sensing of Environment 90:337–352. https://doi.org/10.1016/j.rse.2003.12.013

Haddad NM, Brudvig LA, Damschen EI, et al (2014) Potential Negative Ecological Effects of Corridors. Conservation Biology 28:1178–1187. https://doi.org/10.1111/cobi.12323

Hall LS, Krausman PR, Morrison ML (1997) The Habitat Concept and a Plea for Standard Terminology. Wildlife Society Bulletin (1973-2006) 25:173–182

Hanski I (1999) Habitat Connectivity, Habitat Continuity, and Metapopulations in Dynamic Landscapes. Oikos 87:209–219. https://doi.org/10.2307/3546736

Hanski I (2011) Habitat Loss, the Dynamics of Biodiversity, and a Perspective on Conservation. AMBIO 40:248–255. https://doi.org/10.1007/s13280-011-0147-3

Hassan DA, Georgelin E, Delattre T, et al (2013) Does the presence of grassy strips and landscape grain affect the spatial distribution of aphids and their carabid predators? Agricultural and Forest Entomology 15:24–33. https://doi.org/10.1111/j.1461-9563.2012.00587.x

Hastie TJ, Tibshirani RJ (1990) Generalized Additive Models. CRC Press

Hatfield JL, Gitelson AA, Schepers JS, Walthall CL (2008) Application of Spectral Remote Sensing for Agronomic Decisions. Agronomy Journal 100:S-117. https://doi.org/10.2134/agronj2006.0370c

Hatfield JL, Prueger JH, Sauer TJ, et al (2019) Applications of Vegetative Indices from Remote Sensing to Agriculture: Past and Future. Inventions 4:71. https://doi.org/10.3390/inventions4040071

Hatfield PL, Pinter PJ (1993) Remote sensing for crop protection. Crop Protection 12:403–413. https://doi.org/10.1016/0261-2194(93)90001-Y

Heller NE, Zavaleta ES (2009) Biodiversity management in the face of climate change: A review of 22 years of recommendations. Biological Conservation 142:14–32. https://doi.org/10.1016/j.biocon.2008.10.006

Herrmann I, Pimstein A, Karnieli A, et al (2011) LAI assessment of wheat and potato crops by VENμS and Sentinel-2 bands. Remote Sensing of Environment 115:2141–2151. https://doi.org/10.1016/j.rse.2011.04.018

Holah N, Baghdadi N, Zribi M, et al (2005) Potential of ASAR/ENVISAT for the characterization of soil surface parameters over bare agricultural fields. Remote sensing of environment 96:78–86

Holland JM, Begbie M, Birkett T, et al (2004) The spatial dynamics and movement of Pterostichus melanarius and P. madidus (Carabidae) between and within arable fields in the UK. International Journal of Ecology and Environmental Sciences 30:35–53

Holland JM, Thomas CFG, Birkett T, et al (2005) Farm-scale spatiotemporal dynamics of predatory beetles in arable crops. Journal of Applied Ecology 42:1140–1152. https://doi.org/10.1111/j.1365-2664.2005.01083.x

Homayouni S, McNairn H, Hosseini M, et al (2019) Quad and compact multitemporal C-band PolSAR observations for crop characterization and monitoring. International Journal of Applied Earth Observation and Geoinformation 74:78–87. https://doi.org/10.1016/j.jag.2018.09.009

Hoover JP, Brittingham MC, Goodrich LJ (1995) Effects of Forest Patch Size on Nesting Success of Wood Thrushes. Auk 112:146–155. https://doi.org/10.2307/4088774

Hościło A, Lewandowska A (2019) Mapping Forest Type and Tree Species on a Regional Scale Using Multi-Temporal Sentinel-2 Data. Remote Sensing 11:929. https://doi.org/10.3390/rs11080929

Hosseini M, McNairn H (2017) Using multi-polarization C- and L-band synthetic aperture radar to estimate biomass and soil moisture of wheat fields. International Journal of Applied Earth Observation and Geoinformation 58:50–64. https://doi.org/10.1016/j.jag.2017.01.006

Huete A, Didan K, Miura T, et al (2002) Overview of the radiometric and biophysical performance of the MODIS vegetation indices. Remote Sensing of Environment 83:195–213. https://doi.org/10.1016/S0034-4257(02)00096-2

Huete AR (1988) A soil-adjusted vegetation index (SAVI). Remote Sensing of Environment 25:295–309. https://doi.org/10.1016/0034-4257(88)90106-X

Huete AR, Justice CO, Van Leeuwen WJD (1999) MODIS vegetation index (MOD 13). Version 3. Algorithm theoretical basis document. Greenbelt MD NASA Goddard Space Flight Cent, Greenbelt, MD, USA 7:

Immitzer M, Vuolo F, Atzberger C (2016) First Experience with Sentinel-2 Data for Crop and Tree Species Classifications in Central Europe. Remote Sens 8:166. https://doi.org/10.3390/rs8030166

Inan HI, Sagris V, Devos W, et al (2010) Data model for the collaboration between land administration systems and agricultural land parcel identification systems. Journal of Environmental Management 91:2440–2454. https://doi.org/10.1016/j.jenvman.2010.06.030

Inglada J, Vincent A, Arias M, et al (2017) Operational High Resolution Land Cover Map Production at the Country Scale Using Satellite Image Time Series. Remote Sens 9:95. https://doi.org/10.3390/rs9010095

Inglada J, Vincent A, Arias M, Marais-Sicre C (2016) Improved Early Crop Type Identification By Joint Use of High Temporal Resolution SAR And Optical Image Time Series. Remote Sens 8:362. https://doi.org/10.3390/rs8050362

Inoue Y, Kurosu T, Maeno H, et al (2002) Season-long daily measurements of multifrequency (Ka, Ku, X, C, and L) and full-polarization backscatter signatures over paddy rice field and their relationship with biological variables. Remote Sensing of Environment 81:194–204. https://doi.org/10.1016/S0034-4257(01)00343-1

Jackson TJ, Chen D, Cosh M, et al (2004) Vegetation water content mapping using Landsat data derived normalized difference water index for corn and soybeans. Remote Sensing of Environment 92:475–482. https://doi.org/10.1016/j.rse.2003.10.021

Jacob F, Olioso A, Gu XF, et al (2002) Mapping surface fluxes using airborne visible, near infrared, thermal infrared remote sensing data and a spatialized surface energy balance model. Agronomie 22:669–680. https://doi.org/10.1051/agro:2002053

Jacquemoud S, Verhoef W, Baret F, et al (2009) PROSPECT+SAIL models: A review of use for vegetation characterization. Remote Sensing of Environment 113:S56–S66. https://doi.org/10.1016/j.rse.2008.01.026

Jain AK, Dubes RC, Chen C-C (1987) Bootstrap Techniques for Error Estimation. IEEE Transactions on Pattern Analysis and Machine Intelligence PAMI-9:628–633. https://doi.org/10.1109/TPAMI.1987.4767957

Jamoneau A (2010) Relations entre les diversités alpha, béta et gamma de la flore vasculaire de fragments forestiers inclus dans des paysages agricoles contrastés. Doctoral dissertation, Université de Picardie Jules Verne

Jeannel R (1941) Coléoptères Carabiques, Faune de France. Lechevalier, Paris, France

Jeannel R (1942) Coléoptères Carabiques II, Faune de France. Lechevalier, Paris, France

Jiao X, Kovacs JM, Shang J, et al (2014) Object-oriented crop mapping and monitoring using multi-temporal polarimetric RADARSAT-2 data. ISPRS Journal of Photogrammetry and Remote Sensing 96:38–46. https://doi.org/10.1016/j.isprsjprs.2014.06.014

Jiao X, McNairn H, Shang J, et al (2009) The sensitivity of RADARSAT-2 quad-polarization SAR data to crop LAI. In: Remote Sensing and Modeling of Ecosystems for Sustainability VI. International Society for Optics and Photonics, p 74540O

Jin X, Kumar L, Li Z, et al (2018) A review of data assimilation of remote sensing and crop models. European Journal of Agronomy 92:141–152. https://doi.org/10.1016/j.eja.2017.11.002

Jin X, Yang G, Xu X, et al (2015) Combined Multi-Temporal Optical and Radar Parameters for Estimating LAI and Biomass in Winter Wheat Using HJ and RADARSAR-2 Data. Remote Sensing 7:13251–13272. https://doi.org/10.3390/rs71013251

Joannon A, Torre A, Souchere V, Martin P (2004) The determinants of local collective action on erosive runoff. An analysis of farmers' geographical proximities in Upper Normandy, France. International Journal of Sustainable Development 7:302–320. https://doi.org/10.1504/IJSD.2004.005959

Jokimäki J, Huhta E, Itämies J, Rahko P (1998) Distribution of arthropods in relation to forest patch size, edge, and stand characteristics. 28:5

Jönsson P, Cai Z, Melaas E, et al (2018) A Method for Robust Estimation of Vegetation Seasonality from Landsat and Sentinel-2 Time Series Data. Remote Sens 10:635. https://doi.org/10.3390/rs10040635

Jordan CF (1969) Derivation of leaf-area index from quality of light on the forest floor. Ecology 50:663–666

Joshi N, Baumann M, Ehammer A, et al (2016) A Review of the Application of Optical and Radar Remote Sensing Data Fusion to Land Use Mapping and Monitoring. Remote Sens 8:70. https://doi.org/10.3390/rs8010070

Kanzler M, Böhm C, Mirck J, et al (2019) Microclimate effects on evaporation and winter wheat (Triticum aestivum L.) yield within a temperate agroforestry system. Agroforest Syst 93:1821–1841. https://doi.org/10.1007/s10457-018-0289-4

Kaplan JO, Krumhardt KM, Zimmermann N (2009) The prehistoric and preindustrial deforestation of Europe. Quaternary Science Reviews 28:3016–3034. https://doi.org/10.1016/j.quascirev.2009.09.028

Kaufman YJ, Sendra C (1988) Algorithm for automatic atmospheric corrections to visible and near-IR satellite imagery. International Journal of Remote Sensing 9:1357–1381. https://doi.org/10.1080/01431168808954942

Kautz R, Kawula R, Hoctor T, et al (2006) How much is enough? Landscape-scale conservation for the Florida panther. Biological Conservation 130:118–133. https://doi.org/10.1016/j.biocon.2005.12.007

Kawatani T, Meroney RN (1970) Turbulence and wind speed characteristics within a model canopy flow field. Agricultural Meteorology 7:143–158. https://doi.org/10.1016/0002-1571(70)90011-7

Kenduiywo BK, Bargiel D, Soergel U (2016) CROP TYPE MAPPING FROM A SEQUENCE OF TERRASAR-X IMAGES WITH DYNAMIC CONDITIONAL RANDOM FIELDS. 9

Kenduiywo BK, Bargiel D, Soergel U (2017) Higher Order Dynamic Conditional Random Fields Ensemble for Crop Type Classification in Radar Images. IEEE Transactions on Geoscience and Remote Sensing 55:4638–4654. https://doi.org/10.1109/TGRS.2017.2695326

Khoshgoftaar TM, Golawala M, Hulse JV (2007) An Empirical Study of Learning from Imbalanced Data Using Random Forest. In: 19th IEEE International Conference on Tools with Artificial Intelligence(ICTAI 2007). pp 310–317

Kort J (1988) 9. Benefits of windbreaks to field and forage crops. Agriculture, Ecosystems & Environment 22–23:165–190. https://doi.org/10.1016/0167-8809(88)90017-5

Krauss J, Bommarco R, Guardiola M, et al (2010) Habitat fragmentation causes immediate and time-delayed biodiversity loss at different trophic levels. Ecology Letters 13:597–605. https://doi.org/10.1111/j.1461-0248.2010.01457.x

Krebs JR, Wilson JD, Bradbury RB, Siriwardena GM (1999) The second Silent Spring? Nature 400:611–612. https://doi.org/10.1038/23127

Krieger DJ (2001) Economic value of forest ecosystem services: a review

Kučera J, Podhrázská J, Karásek P, Papaj V (2020) The Effect of Windbreak Parameters on the Wind Erosion Risk Assessment in Agricultural Landscape. J Ecol Eng 21:150–156. https://doi.org/10.12911/22998993/116323

Kuhn M, Wing J, Weston S, et al (2020) caret: Classification and Regression Training. Version 6.0-86URL https://CRAN.R-project.org/package=caret

Kumar P, Prasad R, Gupta DK, et al (2018) Estimation of winter wheat crop growth parameters using time series Sentinel-1A SAR data. Geocarto International 33:942–956. https://doi.org/10.1080/10106049.2017.1316781

Kussul N, Lavreniuk M, Skakun S, Shelestov A (2017) Deep Learning Classification of Land Cover and Crop Types Using Remote Sensing Data. IEEE Trans Geosci Remote Sens Lett 14:778–782. https://doi.org/10.1109/LGRS.2017.2681128

Lambert M-J, Traoré PCS, Blaes X, et al (2018) Estimating smallholder crops production at village level from Sentinel-2 time series in Mali's cotton belt. Remote Sensing of Environment 216:647–657. https://doi.org/10.1016/j.rse.2018.06.036

Laurent F, Arvor D, Daugeard M, et al (2017) Le tournant environnemental en Amazonie : ampleur et limites du découplage entre production et déforestation. EchoGéo. https://doi.org/10.4000/echogeo.15035

Laurin GV, Balling J, Corona P, et al (2018) Above-ground biomass prediction by Sentinel-1 multitemporal data in central Italy with integration of ALOS2 and Sentinel-2 data. Journal of Applied Remote Sensing 12:016008

Lausch A, Blaschke T, Haase D, et al (2015) Understanding and quantifying landscape structure – A review on relevant process characteristics, data models and landscape metrics. Ecological Modelling 295:31–41. https://doi.org/10.1016/j.ecolmodel.2014.08.018

Le Féon V, Burel F, Chifflet R, et al (2013) Solitary bee abundance and species richness in dynamic agricultural landscapes. Agriculture, Ecosystems & Environment 166:94–101. https://doi.org/10.1016/j.agee.2011.06.020

Lê S, Josse J, Husson F (2008) **FactoMineR** : An *R* Package for Multivariate Analysis. J Stat Soft 25:. https://doi.org/10.18637/jss.v025.i01

Le Toan T (2007) SAR data for forestry and agriculture. 63

Lee JS, Jurkevich L, Dewaele P, et al (1994) Speckle filtering of synthetic aperture radar images: A review. Remote Sensing Reviews 8:255-267. https://doi.org/10.1080/02757259409532206

Lee J-S, Pottier E (2009) Polarimetric Radar Imaging: From Basics to Applications, 1sted edn. CRC Press, Taylor & Francis Group, Boca Raton, FL, USA

Lewis T (1969) The Distribution of Flying Insects Near a Low Hedgerow. Journal of Applied Ecology 6:443–452. https://doi.org/10.2307/2401510

Lillesand T, Kiefer RW, Chipman J (2015) Remote Sensing and Image Interpretation. John Wiley & Sons

Lindenmayer DB, Franklin JF, Fischer J (2006) General management principles and a checklist of strategies to guide forest biodiversity conservation. Biological Conservation 131:433–445. https://doi.org/10.1016/j.biocon.2006.02.019

Liu S, Qi Z, Li X, Yeh AG-O (2019) Integration of convolutional neural networks and object-based post-classification refinement for land use and land cover mapping with optical and sar data. Remote Sensing 11:690

Lopez-Sanchez JM, Vicente-Guijalba F, Ballester-Berman JD, Cloude SR (2013) Estimating Phenology Of Agricultural Crops From Space. p 115

Louis J, Charantonis A, Berthelot B (2010) Coud Detection for Sentinel-2. ESASP 686:510

Lucas C, Bouten W, Koma Z, et al (2019) Identification of Linear Vegetation Elements in a Rural Landscape Using LiDAR Point Clouds. Remote Sensing 11:292. https://doi.org/10.3390/rs11030292

Maas SJ (1988) Use of remotely-sensed information in agricultural crop growth models. Ecological Modelling 41:247–268. https://doi.org/10.1016/0304-3800(88)90031-2

Maes WH, Huete AR, Steppe K (2017) Optimizing the Processing of UAV-Based Thermal Imagery. Remote Sensing 9:476. https://doi.org/10.3390/rs9050476

Main-Knorn M, Pflug B, Louis J, et al (2017) Sen2Cor for Sentinel-2. In: Image and Signal Processing for Remote Sensing XXIII. International Society for Optics and Photonics, p 1042704

Mandal D, Kumar V, Bhattacharya A, et al (2018a) Crop Biophysical Parameters Estimation with a Multi-Target Inversion Scheme using the Sentinel-1 SAR Data. In: IGARSS 2018 - 2018 IEEE International Geoscience and Remote Sensing Symposium. pp 6611–6614

Mandal D, Kumar V, Bhattacharya A, et al (2018b) Sen4Rice: A Processing Chain for Differentiating Early and Late Transplanted Rice Using Time-Series Sentinel-1 SAR Data With Google Earth Engine. IEEE Trans Geosci Remote Sens Lett 1–5. https://doi.org/10.1109/LGRS.2018.2865816

Mandal D, Kumar V, Ratha D, et al (2020) Dual polarimetric radar vegetation index for crop growth monitoring using sentinel-1 SAR data. Remote Sensing of Environment 247:111954. https://doi.org/10.1016/j.rse.2020.111954

MAPAMA-Ministerio de Agricultura y Pesca, Alimentación y Medio Ambiente (1997) Mapa Forestal de España a Escala 1:50,000. In: http://www.mapama.gob.es/es/biodiversidad/servicios/bancodatos- naturaleza/informacion-disponible/mfe50.aspx. http://www.mapama.gob.es/es/biodiversidad/servicios/bancodatos-naturaleza/informacion-disponible/mfe50.aspx. Accessed 3 Aug 2018

Margono BA, Potapov PV, Turubanova S, et al (2014) Primary forest cover loss in Indonesia over 2000–2012. Nature Climate Change 4:730–735. https://doi.org/10.1038/nclimate2277

Mascolo L, Lopez-Sanchez JM, Vicente-Guijalba F, et al (2015) Retrieval of phenological stages of onion fields during the first year of growth by means of C-band polarimetric SAR measurements. International Journal of Remote Sensing 36:3077–3096. https://doi.org/10.1080/01431161.2015.1055608

Mateo-Sánchez MC, Gastón A, Ciudad C, et al (2016) Seasonal and temporal changes in species use of the landscape: how do they impact the inferences from multi-scale habitat modeling? Landscape Ecol 31:1261–1276. https://doi.org/10.1007/s10980-015-0324-z

Mattia F, Le Toan T, Souyris J-C, et al (1997) The effect of surface roughness on multifrequency polarimetric SAR data. IEEE Transactions on Geoscience and Remote Sensing 35:954–966

McFeeters SK (1996) The use of the Normalized Difference Water Index (NDWI) in the delineation of open water features. International Journal of Remote Sensing 17:1425–1432. https://doi.org/10.1080/01431169608948714

McGarigal K, Tagil S, Cushman SA (2009) Surface metrics: an alternative to patch metrics for the quantification of landscape structure. Landscape Ecol 24:433–450. https://doi.org/10.1007/s10980-009-9327-y

McNairn H, Brisco B (2004) The application of C-band polarimetric SAR for agriculture: a review. Can J Remote Sensing 30:525–542. https://doi.org/10.5589/m03-069

McNairn H, Jiao X, Pacheco A, et al (2018) Estimating canola phenology using synthetic aperture radar. Remote Sensing of Environment 219:196–205. https://doi.org/10.1016/j.rse.2018.10.012

Menzel A, Sparks TH, Estrella N, et al (2006) European phenological response to climate change matches the warming pattern. Global Change Biology 12:1969–1976. https://doi.org/10.1111/j.1365-2486.2006.01193.x

Mercier A, Betbeder J, Baudry J, et al (2020a) Evaluation of Sentinel-1 & 2 time series for predicting wheat and rapeseed phenological stages. ISPRS Journal of Photogrammetry and Remote Sensing 163:231–256. https://doi.org/10.1016/j.isprsjprs.2020.03.009

Mercier A, Betbeder J, Baudry J, et al (2019a) Evaluation of Sentinel-1 and -2 time series to derive crop phenology and biomass of wheat and rapeseed: northern France and Brittany case studies. In: Remote Sensing for Agriculture, Ecosystems, and Hydrology XXI. International Society for Optics and Photonics, p 1114903

Mercier A, Betbeder J, Denize J, et al (2021) Estimating crop parameters using Sentinel-1 and 2 datasets and geospatial field data. Data in Brief 38:107408. https://doi.org/10.1016/j.dib.2021.107408

Mercier A, Betbeder J, Rapinel S, et al (2020b) Evaluation of Sentinel-1 and -2 time series for estimating LAI and biomass of wheat and rapeseed crop types. JARS 14:024512. https://doi.org/10.1117/1.JRS.14.024512

Mercier A, Betbeder J, Rumiano F, et al (2019b) Evaluation of Sentinel-1 and 2 Time Series for Land Cover Classification of Forest–Agriculture Mosaics in Temperate and Tropical Landscapes. Remote Sensing 11:979. https://doi.org/10.3390/rs11080979

Metz M, Rocchini D, Neteler M (2014) Surface Temperatures at the Continental Scale: Tracking Changes with Remote Sensing at Unprecedented Detail. Remote Sensing 6:3822–3840. https://doi.org/10.3390/rs6053822

Meyer V, Saatchi SS, Chave J, et al (2013) Detecting tropical forest biomass dynamics from repeated airborne lidar measurements. Biogeosciences 10:5421

Miranda N, Meadows PJ (2015) Radiometric Calibration of S-1 Level-1 Products Generated by the S-1 ipf. Viewed at https://sentinel.esa.int/documents/247904/685163/S1-Radiometric-Calibration-V1.0.pdf

Mitchell AL, Rosenqvist A, Mora B (2017) Current remote sensing approaches to monitoring forest degradation in support of countries measurement, reporting and verification (MRV) systems for REDD+. Carbon Balance and Management 12:9

Mitchell MS, Hebblewhite M, Boitani L, Powell RA (2012) Carnivore habitat ecology: integrating theory and application. Carnivore ecology and conservation: a handbook of techniques (L Boitani and RA Powell, eds) Oxford University Press, London, United Kingdom 218–255

Mongus D, Žalik B (2018) Segmentation schema for enhancing land cover identification: A case study using Sentinel 2 data. International Journal of Applied Earth Observation and Geoinformation 66:56–68. https://doi.org/10.1016/j.jag.2017.11.004

Moreno R, Ojeda N, Azócar J, et al (2020) Application of NDVI for identify potentiality of the urban forest for the design of a green corridors system in intermediary cities of Latin America: Case study, Temuco, Chile. Urban Forestry & Urban Greening 55:126821. https://doi.org/10.1016/j.ufug.2020.126821

Mulla DJ (2013) Twenty five years of remote sensing in precision agriculture: Key advances and remaining knowledge gaps. Biosystems Engineering 114:358–371. https://doi.org/10.1016/j.biosystemseng.2012.08.009

Nasrallah A, Baghdadi N, El Hajj M, et al (2019) Sentinel-1 Data for Winter Wheat Phenology Monitoring and Mapping. Remote Sensing 11:2228. https://doi.org/10.3390/rs11192228

Norris K, Asase A, Collen B, et al (2010) Biodiversity in a forest-agriculture mosaic – The changing face of West African rainforests. Biological Conservation 143:2341–2350. https://doi.org/10.1016/j.biocon.2009.12.032

Nuthammachot N, Phairuang W, Wicaksono P, Sayektiningsih T (2018) Estimating aboveground biomass on private forest using Sentinel-2 imagery. Journal of Sensors 2018:

Olioso A, Chauki H, Courault D, Wigneron J-P (1999) Estimation of Evapotranspiration and Photosynthesis by Assimilation of Remote Sensing Data into SVAT Models. Remote Sensing of Environment 68:341–356. https://doi.org/10.1016/S0034-4257(98)00121-7

Orynbaikyzy A, Gessner U, Conrad C (2019) Crop type classification using a combination of optical and radar remote sensing data: a review. International Journal of Remote Sensing 40:6553–6595. https://doi.org/10.1080/01431161.2019.1569791

Ouin A, Paillat G, Butet A, Burel F (2000) Spatial dynamics of wood mouse (Apodemus sylvaticus) in an agricultural landscape under intensive use in the Mont Saint Michel Bay (France). Agriculture, Ecosystems & Environment 78:159–165. https://doi.org/10.1016/S0167-8809(99)00119-X

Pacheco A, McNairn H, Li Y, et al (2016) Using RADARSAT-2 and TerraSAR-X satellite data for the identification of canola crop phenology. In: Remote Sensing for Agriculture, Ecosystems, and Hydrology XVIII. International Society for Optics and Photonics, p 999802

Pan H, Chen Z, Ren J, et al (2018) Modeling Winter Wheat Leaf Area Index and Canopy Water Content With Three Different Approaches Using Sentinel-2 Multispectral Instrument Data. IEEE Journal of Selected Topics in Applied Earth Observations and Remote Sensing 1–11. https://doi.org/10.1109/JSTARS.2018.2855564

Pan Z, Huang J, Zhou Q, et al (2015) Mapping crop phenology using NDVI time-series derived from HJ-1 A/B data. International Journal of Applied Earth Observation and Geoinformation 34:188–197. https://doi.org/10.1016/j.jag.2014.08.011

Pargal S, Fararoda R, Rajashekar G, et al (2017) Inverting Aboveground Biomass?Canopy Texture Relationships in a Landscape of Forest Mosaic in the Western Ghats of India Using Very High Resolution Cartosat Imagery. Remote Sensing 9:228. https://doi.org/10.3390/rs9030228

Patel P, Srivastava HS, Panigrahy S, Parihar JS (2006) Comparative evaluation of the sensitivity of multi-polarized multi-frequency SAR backscatter to plant density. International Journal of Remote Sensing 27:293–305. https://doi.org/10.1080/01431160500214050

Pearson DL, Hawksworth DL (1994) Selecting indicator taxa for the quantitative assessment of biodiversity. Philosophical Transactions of the Royal Society of London Series B: Biological Sciences 345:75–79. https://doi.org/10.1098/rstb.1994.0088

Pelletier C, Valero S, Inglada J, et al (2017) Effect of Training Class Label Noise on Classification Performances for Land Cover Mapping with Satellite Image Time Series. Remote Sens 9:173. https://doi.org/10.3390/rs9020173

Pelletier C, Valero S, Inglada J, et al (2016) Assessing the robustness of Random Forests to map land cover with high resolution satellite image time series over large areas. Remote Sensing of Environment 187:156–168. https://doi.org/10.1016/j.rse.2016.10.010

Persson M, Lindberg E, Reese H (2018) Tree Species Classification with Multi-Temporal Sentinel-2 Data. Remote Sens 10:1794. https://doi.org/10.3390/rs10111794

Petit S (1994) Diffusion of forest carabid beetles in hedgerow network landscapes. In: Desender K, Dufrêne M, Loreau M, et al. (eds) Carabid Beetles: Ecology and Evolution. Springer Netherlands, Dordrecht, pp 337–341

Petit S, Boursault A, Le Guilloux M, et al (2011) Weeds in agricultural landscapes. A review. Agronomy Sust Developm 31:309–317. https://doi.org/10.1051/agro/2010020

Phiri D, Simwanda M, Salekin S, et al (2020) Sentinel-2 Data for Land Cover/Use Mapping: A Review. Remote Sensing 12:2291. https://doi.org/10.3390/rs12142291

Piketty M-G, Piraux M, Laurent F, et al (2017) Chapitre 7 - « Municípios Verdes » : passer du zéro-déforestation à la gestion durable des ressources naturelles en Amazonie brésilienne. In: Des territoires vivants pour transformer le monde. Editions Quæ, pp 54–57

Piketty M-G, Poccard-Chapuis R, Drigo I, et al (2015) Multi-level Governance of Land Use Changes in the Brazilian Amazon: Lessons from Paragominas, State of Pará. Forests 6:1516–1536. https://doi.org/10.3390/f6051516

Pimm SL, Russell GJ, Gittleman JL, Brooks TM (1995) The Future of Biodiversity. Science 269:347–350. https://doi.org/10.1126/science.269.5222.347

Pinstrup-Andersen P, Pandya-Lorch R (1998) Food security and sustainable use of natural resources: a 2020 Vision. Ecological Economics 26:1–10. https://doi.org/10.1016/S0921-8009(97)00067-0

Pipia L, Muñoz-Marí J, Amin E, et al (2019) Fusing optical and SAR time series for LAI gap filling with multioutput Gaussian processes. Remote Sensing of Environment 235:111452. https://doi.org/10.1016/j.rse.2019.111452

Pottier E, Ferro-Famil L (2012) PolSARPro V5.0: An ESA educational toolbox used for self-education in the field of POLSAR and POL-INSAR data analysis. In: 2012 IEEE International Geoscience and Remote Sensing Symposium. pp 7377–7380

Puletti N, Chianucci F, Castaldi C (2017) Use of Sentinel-2 for forest classification in Mediterranean environments. Ann Silvic Res 42:

Putz FE, Redford KH (2010) The Importance of Defining 'Forest': Tropical Forest Degradation, Deforestation, Long-term Phase Shifts, and Further Transitions. Biotropica 42:10–20. https://doi.org/10.1111/j.1744-7429.2009.00567.x

Qi J, Chehbouni A, Huete AR, et al (1994) A modified soil adjusted vegetation index. Remote Sensing of Environment 48:119–126. https://doi.org/10.1016/0034-4257(94)90134-1

Quarmby NA, Milnes M, Hindle TL, Silleos N (1993) The use of multi-temporal NDVI measurements from AVHRR data for crop yield estimation and prediction. International Journal of Remote Sensing 14:199–210. https://doi.org/10.1080/01431169308904332

Quevedo M, Bañuelos MJ, Obeso JR (2006) The decline of Cantabrian capercaillie: How much does habitat configuration matter? Biological Conservation 127:190–200. https://doi.org/10.1016/j.biocon.2005.07.019

Radoux J, Bourdouxhe A, Coos W, et al (2019) Improving Ecotope Segmentation by Combining Topographic and Spectral Data. Remote Sensing 11:354. https://doi.org/10.3390/rs11030354

Ranson KJ, Sun G, Kharuk VI, Kovacs K (2001) Characterization of Forests in Western Sayani Mountains, Siberia from SIR-C SAR Data. Remote Sensing of Environment 75:188–200. https://doi.org/10.1016/S0034-4257(00)00166-8

Reiche J, Hamunyela E, Verbesselt J, et al (2018) Improving near-real time deforestation monitoring in tropical dry forests by combining dense Sentinel-1 time series with Landsat and ALOS-2 PALSAR-2. Remote Sensing of Environment 204:147–161. https://doi.org/10.1016/j.rse.2017.10.034

Resasco J (2019) Meta-analysis on a Decade of Testing Corridor Efficacy: What New Have we Learned? Curr Landscape Ecol Rep 4:61–69. https://doi.org/10.1007/s40823-019-00041-9

Ribeiro MC, Metzger JP, Martensen AC, et al (2009) The Brazilian Atlantic Forest: How much is left, and how is the remaining forest distributed? Implications for conservation. Biological conservation 142:1141–1153

Rodriguez JD, Perez A, Lozano JA (2010) Sensitivity Analysis of k-Fold Cross Validation in Prediction Error Estimation. IEEE Transactions on Pattern Analysis and Machine Intelligence 32:569–575. https://doi.org/10.1109/TPAMI.2009.187

Roger J-L, Jambon O, Bouger G (2013) Clé de détermination des Carabides-Paysages agricoles du nord ouest de la France

Rosenfield GH, Fitzpatrick-Lins K (1986) A coefficient of agreement as a measure of thematic classification accuracy. Photogrammetric Engineering and Remote Sensing 52:5

Rouabah A, Villerd J, Amiaud B, et al (2015) Response of carabid beetles diversity and size distribution to the vegetation structure within differently managed field margins. Agriculture, Ecosystems & Environment 200:21–32. https://doi.org/10.1016/j.agee.2014.10.011

Rouse JWJ, Haas RH, Schell JA, Deering DW (1973) Monitoring vegetation systems in the Great Plains with ERTS. NASA,Washington, DC, USA

Roy V, de Blois S (2008) Evaluating hedgerow corridors for the conservation of native forest herb diversity. Biological Conservation 141:298–307. https://doi.org/10.1016/j.biocon.2007.10.003

Roychowdhury K Comparison between Spectral, Spatial and Polarimetric Classification of Urban and Periurban Landcover Using Temporal Sentinel-1 Images. Prague, Czech Republic

Ryszkowski L, Kędziora A (1987) Impact of agricultural landscape structure on energy flow and water cycling. Landscape Ecol 1:85–94. https://doi.org/10.1007/BF00156230

Sakamoto T, Yokozawa M, Toritani H, et al (2005) A crop phenology detection method using time-series MODIS data. Remote Sensing of Environment 96:366–374. https://doi.org/10.1016/j.rse.2005.03.008

Sánchez MCM, Cushman SA, Saura S (2014) Scale dependence in habitat selection: the case of the endangered brown bear (Ursus arctos) in the Cantabrian Range (NW Spain). International Journal of Geographical Information Science 28:1531–1546. https://doi.org/10.1080/13658816.2013.776684

Schläpfer D, Borel CC, Keller J, Itten KI (1998) Atmospheric Precorrected Differential Absorption Technique to Retrieve Columnar Water Vapor. Remote Sensing of Environment 65:353–366. https://doi.org/10.1016/S0034-4257(98)00044-3

Schmugge TJ, Kustas WP, Humes KS (1998) Monitoring land surface fluxes using ASTER observations. IEEE Transactions on Geoscience and Remote Sensing 36:1421–1430. https://doi.org/10.1109/36.718846

Schooley RL, Branch LC (2011) Habitat quality of source patches and connectivity in fragmented landscapes. Biodivers Conserv 20:1611–1623. https://doi.org/10.1007/s10531-011-0049-5

Schultz B, Immitzer M, Formaggio AR, et al (2015) Self-Guided Segmentation and Classification of Multi-Temporal Landsat 8 Images for Crop Type Mapping in Southeastern Brazil. Remote Sensing 7:14482–14508. https://doi.org/10.3390/rs71114482

Sedano F, Lisboa S, Duncanson L, et al (2020) Monitoring intra and inter annual dynamics of forest degradation from charcoal production in Southern Africa with Sentinel – 2 imagery. International Journal of Applied Earth Observation and Geoinformation 92:102184. https://doi.org/10.1016/j.jag.2020.102184

Shimada M, Itoh T, Motooka T, et al (2014) New global forest/non-forest maps from ALOS PALSAR data (2007–2010). Remote Sensing of environment 155:13–31

Simberloff D, Cox J (1987) Consequences and Costs of Conservation Corridors. Conservation Biology 1:63–71. https://doi.org/10.1111/j.1523-1739.1987.tb00010.x

Simberloff D, Farr JA, Cox J, Mehlman DW (1992) Movement Corridors: Conservation Bargains or Poor Investments? Conservation Biology 6:493–504. https://doi.org/10.1046/j.1523-1739.1992.06040493.x

Singh M, Malhi Y, Bhagwat S (2014) Biomass estimation of mixed forest landscape using a Fourier transform texture-based approach on very-high-resolution optical satellite imagery. International Journal of Remote Sensing 35:3331–3349. https://doi.org/10.1080/01431161.2014.903441

Song Y, Wang J (2019) Mapping Winter Wheat Planting Area and Monitoring Its Phenology Using Sentinel-1 Backscatter Time Series. Remote Sensing 11:449. https://doi.org/10.3390/rs11040449

Sonobe R, Tani H, Wang X, et al (2015) Discrimination of crop types with TerraSAR-X-derived information. Physics and Chemistry of the Earth, Parts A/B/C 83–84:2–13. https://doi.org/10.1016/j.pce.2014.11.001

Spellerberg IF, Gaywood MJ (1993) Linear features: linear habitats & wildlife corridors. Center for Environmental Sciences

Steele-Dunne SC, McNairn H, Monsivais-Huertero A, et al (2017) Radar Remote Sensing of Agricultural Canopies: A Review. IEEE Journal of Selected Topics in Applied Earth Observations and Remote Sensing 10:2249–2273. https://doi.org/10.1109/JSTARS.2016.2639043

Stendardi L, Karlsen SR, Niedrist G, et al (2019) Exploiting Time Series of Sentinel-1 and Sentinel-2 Imagery to Detect Meadow Phenology in Mountain Regions. Remote Sensing 11:542. https://doi.org/10.3390/rs11050542

Suorsa P, Helle H, Koivunen V, et al (2004) Effects of forest patch size on physiological stress and immunocompetence in an area-sensitive passerine, the Eurasian treecreeper (Certhia familiaris): an experiment. Proceedings of the Royal Society of London Series B: Biological Sciences 271:435–440. https://doi.org/10.1098/rspb.2003.2620

Tan C-W, Zhang P-P, Zhou X-X, et al (2020) Quantitative monitoring of leaf area index in wheat of different plant types by integrating NDVI and Beer-Lambert law. Sci Rep 10:1–10. https://doi.org/10.1038/s41598-020-57750-z

Taylor PD, Fahrig L, Henein K, Merriam G (1993) Connectivity Is a Vital Element of Landscape Structure. Oikos 68:571–573. https://doi.org/10.2307/3544927

TEAM, R. Core, TEAM, Maintainer R. Core, SUGGESTS, M. A. S. S., Matrix, SuppDists (2018) Package stats. The R Stats Package. The R Stats Package

Teil H (1975) Correspondence factor analysis: An outline of its method. Mathematical Geology 7:3–12. https://doi.org/10.1007/BF02080630

Thenail C (2002) Relationships between farm characteristics and the variation of the density of hedgerows at the level of a micro-region of bocage landscape. Study case in Brittany, France. Agricultural Systems 71:207–230. https://doi.org/10.1016/S0308-521X(01)00048-8

Thenail C, Baudry J (2004) Variation of farm spatial land use pattern according to the structure of the hedgerow network (bocage) landscape: a case study in northeast Brittany. Agriculture, Ecosystems & Environment 101:53–72. https://doi.org/10.1016/S0167-8809(03)00199-3

Thomas C f. g, Parkinson L, Griffiths GJK, et al (2001) Aggregation and temporal stability of carabid beetle distributions in field and hedgerow habitats. Journal of Applied Ecology 38:100–116. https://doi.org/10.1046/j.1365-2664.2001.00574.x

Thomas JA (1983) The Ecology and Conservation of Lysandra bellargus (Lepidoptera: Lycaenidae) in Britain. Journal of Applied Ecology 20:59–83. https://doi.org/10.2307/2403376

Thornton MW, Atkinson PM, Holland DA (2006) Sub-pixel mapping of rural land cover objects from fine spatial resolution satellite sensor imagery using super-resolution pixel-swapping. International Journal of Remote Sensing 27:473–491

Toth C, Lenzano M, Pereira A, et al (2014) GEOACTA - Revista de la Asociación Argentina de Geofísicos y Geodestas - Special Issue "Geomatics in Earth Sciences", Guest Editors

Tritsch I, Sist P, Narvaes I da S, et al (2016) Multiple Patterns of Forest Disturbance and Logging Shape Forest Landscapes in Paragominas, Brazil. Forests 7:315. https://doi.org/10.3390/f7120315

Tscharntke T, Klein AM, Kruess A, et al (2005) Landscape perspectives on agricultural intensification and biodiversity – ecosystem service management. Ecology Letters 8:857–874. https://doi.org/10.1111/j.1461-0248.2005.00782.x

Turker M, Ozdarici A (2011) Field-based crop classification using SPOT4, SPOT5, IKONOS and QuickBird imagery for agricultural areas: a comparison study. International Journal of Remote Sensing 32:9735–9768. https://doi.org/10.1080/01431161.2011.576710

Ulaby FT, Dubois PC, Van Zyl J (1996) Radar mapping of surface soil moisture. Journal of hydrology 184:57–84

Upreti D, Huang W, Kong W, et al (2019) A Comparison of Hybrid Machine Learning Algorithms for the Retrieval of Wheat Biophysical Variables from Sentinel-2. Remote Sensing 11:481. https://doi.org/10.3390/rs11050481

Vandermeer JH (1972) Niche Theory. Annual Review of Ecology and Systematics 3:107–132

Vannier C, Hubert-Moy L (2008) Detection of Wooded Hedgerows in High Resolution Satellite Images using an Object-Oriented Method. In: IGARSS 2008 - 2008 IEEE International Geoscience and Remote Sensing Symposium. p IV-731-IV–734

Vannier C, Hubert-Moy L (2014) Multiscale comparison of remote-sensing data for linear woody vegetation mapping. International Journal of Remote Sensing 35:7376–7399. https://doi.org/10.1080/01431161.2014.968683

Vasseur C (2012) Contrôles exercés par les mosaïques de systèmes de culture sur les dynamiques du carabe Pterostichus melanarius Illiger (Coleoptera, Carabidae). Phdthesis, Université de Rennes 1

Vasseur C, Joannon A, Aviron S, et al (2013) The cropping systems mosaic: How does the hidden heterogeneity of agricultural landscapes drive arthropod populations? Agriculture, Ecosystems & Environment 166:3–14. https://doi.org/10.1016/j.agee.2012.08.013

Veloso A, Mermoz S, Bouvet A, et al (2017) Understanding the temporal behavior of crops using Sentinel-1 and Sentinel-2-like data for agricultural applications. Remote Sensing of Environment 199:415–426. https://doi.org/10.1016/j.rse.2017.07.015

Verrelst J, Muñoz J, Alonso L, et al (2012) Machine learning regression algorithms for biophysical parameter retrieval: Opportunities for Sentinel-2 and -3. Remote Sensing of Environment 118:127–139. https://doi.org/10.1016/j.rse.2011.11.002

Veste M, Littmann T, Kunneke A, et al (2020) Windbreaks as part of climate-smart landscapes reduce evapotranspiration in vineyards, Western Cape Province, South Africa. Plant, Soil and Environment 66 (2020):119–127. https://doi.org/10.17221/616/2019-PSE

Viana C, Coudel E, Barlow J, et al (2012) From red to green: achieving an environmental pact at the municipal level in paragominas (Pará, Brazilian Amazon). In: 12th Biennial Conference of the International Society for Ecological Economics (ISEE 2012 Conference) "Ecological Economics and Rio+20: Challenges and Contributions for a Green Economy", 16-19 June 2012, Rio de Janeiro, Brazil. http://www.isee2012.org/anais/pdf/66.pdf. Accessed 8 Oct 2018

Vidal CY, Mangueira JR, Farah FT, et al (2016) 8. Biodiversity Conservation of Forests and their Ecological Restoration in Highly-modified Landscapes. In: Biodiversity in agricultural landscapes of Southeastern Brazil. Sciendo Migration, pp 136–150

Villemey A, Jeusset A, Vargac M, et al (2018) Can linear transportation infrastructure verges constitute a habitat and/or a corridor for insects in temperate landscapes? A systematic review. Environ Evid 7:5. https://doi.org/10.1186/s13750-018-0117-3

Virgós E (2001) Role of isolation and habitat quality in shaping species abundance: a test with badgers (Meles meles L.) in a gradient of forest fragmentation. Journal of Biogeography 28:381–389. https://doi.org/10.1046/j.1365-2699.2001.00552.x

Voormansik K, Jagdhuber T, Zalite K, et al (2016) Observations of Cutting Practices in Agricultural Grasslands Using Polarimetric SAR. IEEE Journal of Selected Topics in Applied Earth Observations and Remote Sensing 9:1382–1396. https://doi.org/10.1109/JSTARS.2015.2503773

Vreugdenhil M, Wagner W, Bauer-Marschallinger B, et al (2018) Sensitivity of Sentinel-1 Backscatter to Vegetation Dynamics: An Austrian Case Study. Remote Sensing 10:1396. https://doi.org/10.3390/rs10091396

Vuolo F, Neuwirth M, Immitzer M, et al (2018) How much does multi-temporal Sentinel-2 data improve crop type classification? International Journal of Applied Earth Observation and Geoinformation 72:122–130. https://doi.org/10.1016/j.jag.2018.06.007

Wang C, Feng M-C, Yang W-D, et al (2016a) Impact of spectral saturation on leaf area index and aboveground biomass estimation of winter wheat. Spectroscopy Letters 49:241–248. https://doi.org/10.1080/00387010.2015.1133652

Wang J, Xiao X, Bajgain R, et al (2019) Estimating leaf area index and aboveground biomass of grazing pastures using Sentinel-1, Sentinel-2 and Landsat images. ISPRS Journal of Photogrammetry and Remote Sensing 154:189–201. https://doi.org/10.1016/j.isprsjprs.2019.06.007

Wang L, Qu JJ, Hao X, Zhu Q (2008) Sensitivity studies of the moisture effects on MODIS SWIR reflectance and vegetation water indices. International Journal of Remote Sensing 29:7065–7075. https://doi.org/10.1080/01431160802226034

Wang L, Zhou X, Zhu X, et al (2016b) Estimation of biomass in wheat using random forest regression algorithm and remote sensing data. The Crop Journal 4:212–219. https://doi.org/10.1016/j.cj.2016.01.008

Wegmann M, Leutner B, Dech S (2016) Remote Sensing and GIS for Ecologists: Using Open Source Software. Pelagic Publishing Ltd

Wiens JA, Stenseth NChr, Van Horne B, Ims RA (1993) Ecological Mechanisms and Landscape Ecology. Oikos 66:369–380. https://doi.org/10.2307/3544931

Wilcove DS, McLellan CH, Dobson AP (1986) Habitat fragmentation in the temperate zone. Conservation biology 6:237–256

Williams CKI, Barber D (1998) Bayesian classification with Gaussian processes. IEEE Transactions on Pattern Analysis and Machine Intelligence 20:1342–1351. https://doi.org/10.1109/34.735807

Wilson J, Zhang C, Kovacs J (2014) Separating Crop Species in Northeastern Ontario Using Hyperspectral Data. Remote Sensing 6:925–945. https://doi.org/10.3390/rs6020925

Winder L, Alexander CJ, Holland JM, et al (2001) Modelling the dynamic spatio-temporal response of predators to transient prey patches in the field. Ecology Letters 4:568–576. https://doi.org/10.1046/j.1461-0248.2001.00269.x

Wiseman G, Kort J, Walker D (2009) Quantification of shelterbelt characteristics using high-resolution imagery. Agriculture, ecosystems & environment 131:111–117

Wiseman G, McNairn H, Homayouni S, Shang J (2014) RADARSAT-2 Polarimetric SAR Response to Crop Biomass for Agricultural Production Monitoring. IEEE Journal of Selected Topics in Applied Earth Observations and Remote Sensing 7:4461–4471. https://doi.org/10.1109/JSTARS.2014.2322311

With KA, Pavuk DM, Worchuck JL, et al (2002) Threshold Effects of Landscape Structure on Biological Control in Agroecosystems. Ecological Applications 12:52–65. https://doi.org/10.1890/1051-0761(2002)012[0052:TEOLSO]2.0.CO;2

Wohlfart C, Winkler K, Wendleder A, Roth A (2018) TerraSAR-X and Wetlands: A Review. Remote Sensing 10:916. https://doi.org/10.3390/rs10060916

Woodhouse IH (2017) Introduction to Microwave Remote Sensing. CRC Press

Wu M, Yang C, Song X, et al (2018) Monitoring cotton root rot by synthetic Sentinel-2 NDVI time series using improved spatial and temporal data fusion. Scientific Reports 8:2016. https://doi.org/10.1038/s41598-018-20156-z

Wulder MA, Hall RJ, Coops NC, Franklin SE (2004) High Spatial Resolution Remotely Sensed Data for Ecosystem Characterization. BioScience 54:511–521. https://doi.org/10.1641/0006-3568(2004)054[0511:HSRRSD]2.0.CO;2

Yang C, Everitt JH, Fletcher RS, Murden D (2007) Using high resolution QuickBird imagery for crop identification and area estimation. Geocarto International 22:219–233. https://doi.org/10.1080/10106040701204412

Yang H, Yang G, Gaulton R, et al (2019) In-season biomass estimation of oilseed rape (Brassica napus L.) using fully polarimetric SAR imagery. Precision Agric 20:630–648. https://doi.org/10.1007/s11119-018-9587-0

Zeller KA, McGarigal K, Whiteley AR (2012) Estimating landscape resistance to movement: a review. Landscape Ecol 27:777–797. https://doi.org/10.1007/s10980-012-9737-0

Zellweger F, De Frenne P, Lenoir J, et al (2019) Advances in Microclimate Ecology Arising from Remote Sensing. Trends in Ecology & Evolution 34:327–341. https://doi.org/10.1016/j.tree.2018.12.012

Zhou T, Zhao M, Sun C, Pan J (2017) Exploring the Impact of Seasonality on Urban Land-Cover Mapping Using Multi-Season Sentinel-1A and GF-1 WFV Images in a Subtropical Monsoon-Climate Region. ISPRS J Photogramm Remote Sens 7:3. https://doi.org/10.3390/ijgi7010003

Zhou X, Gu L, Ren R, Fan X (2018) Research of forest type identification based on multi-dimensional POLSAR data in Northeast China. In: Remote Sensing and Modeling of Ecosystems for Sustainability XV. International Society for Optics and Photonics, p 107670K

Zhu Z (2017) Change detection using landsat time series: A review of frequencies, preprocessing, algorithms, and applications. ISPRS Journal of Photogrammetry and Remote Sensing 130:370–384

APPENDICES

Appendix A: Mercier A, Betbeder J, Denize J, et al (2021) Estimating crop parameters using Sentinel-1 and 2 datasets and geospatial field data. Data in Brief 38:107408. https://doi.org/10.1016/j.dib.2021.107408

Data in Brief 38 (2021) 107408

Contents lists available at ScienceDirect

Data in Brief

journal homepage: www.elsevier.com/locate/dib

Data Article

Estimating crop parameters using Sentinel-1 and 2 datasets and geospatial field data

Audrey Mercier[a,*], Julie Betbeder[b,c], Julien Denize[a,d], Jean-Luc Roger[e], Fabien Spicher[f], Jérôme Lacoux[f], David Roger[f], Jacques Baudry[e], Laurence Hubert-Moy[a]

[a] *LETG Rennes UMR 6554, Université Rennes 2, Place du recteur Henri Le Moal, Rennes Cedex 35043, France*
[b] *CIRAD, Forêts et Sociétés, Montpellier 34398, France*
[c] *Ecosystems Modelling Unity, Forests, Biodiversity and Climate Change Program, Tropical Agricultural Research and Higher Education Center (CATIE), Turrialba, Cartago, Costa Rica*
[d] *Institute of Electronics and Telecommunications of Rennes IETR, UMR CNRS 6164, University of Rennes, Rennes 35000, France*
[e] *Institut Agro, UMR 0980 BAGAP, ESA, Rennes 35042, France*
[f] *Unité Ecologie et Dynamiques des Systèmes Anthropisés, UMR 7058 CNRS, Université de Picardie Jules Verne, 33 rue St-Leu, Amiens 80039, France*

ARTICLE INFO

Article history:
Received 29 June 2021
Revised 16 September 2021
Accepted 20 September 2021
Available online 21 September 2021

Keywords:
LAI
Biomass
Phenological stages
Water content
Remote sensing
Optical and SAR satellite images
Wheat
Rapeseed

ABSTRACT

Crop monitoring is essential for ensuring food security in a global context of population growth and climate change. Satellite images are commonly used to estimate crop parameters over large areas, and the freely available Synthetic Aperture Radar (SAR) Sentinel-1 (S-1) and optical Sentinel-2 (S-2) images are relevant for that purpose combining high temporal resolution and high spatial resolution. For this data article, field surveys were conducted from January to July 2017 in France to sample wheat and rapeseed crop parameters during the entire crops cycle. Phenological stages were identified in 83 wheat fields and 32 rapeseed fields in Brittany and Picardy regions. Moreover, Leaf Area Index (LAI), wet biomass, dry biomass and water content were sampled in three wheat fields and three rapeseed fields in Brittany. We assigned to each field sample 10 spectral bands and 12 vegetation indices from S-2 images and two backscattering coefficients, one backscattering ratio and four

DOI of original article: 10.1016/j.isprsjprs.2020.03.009
* Corresponding author.
E-mail address: audrey.mercier@cirad.fr (A. Mercier).

https://doi.org/10.1016/j.dib.2021.107408

polarimetric indicators from S-1 images. This dataset can be used for crop monitoring in other regions, as well as for modelling development.

Specifications Table

Subject	Agronomy and Crop Science
Specific subject area	Applied remote sensing; crop biophysical parameters
Type of data	Table Spatial data
How data were acquired	Spectral values and vegetation indices derived from S-2 images; backscattering coefficients and polarimetric indicators derived from S-1 images; LAI derived from hemispherical photographs using CAN-EYE software [5]; wet biomass, dry biomass and water content collected on the field.
Data format	Raw Analyzed
Parameters for data collection	S-1 and S-2 pixels completely included within wheat and rapeseed fields and associated crop parameters collected during the field surveys (phenological stages, LAI, wet biomass, dry biomass and water content) from January to July 2017.
Description of data collection	Field surveys were conducted from January to July 2017 to collect wheat and rapeseed crop parameters in 115 fields. Phenological stages were identified in 83 wheat fields and 32 rapeseed fields in Brittany and Picardy regions (France). LAI, wet biomass, dry biomass and water content were sampled in three wheat fields and three rapeseed fields in Brittany. As close as possible to the dates of field surveys, spectral values and vegetation indices were derived from S-2 images and backscattering coefficients and polarimetric indicators from S-1 images.
Data source location	Region: Brittany and Picardy Country: France
Data accessibility	With the article
Related research article	A. Mercier, J. Betbeder, J. Baudry, V. Le Roux, F. Spicher, J. Lacoux, D. Roger, L. Hubert-Moy, Evaluation of Sentinel-1 & 2 time series for predicting wheat and rapeseed phenological stages. ISPRS Journal of Photogrammetry and Remote Sensing. 163 (2020) 231-256. https://doi.org/10.1016/j.isprsjprs.2020.03.009

Value of the Data

- The datasets provide crop biophysical parameters (LAI, biomass and phenological stages) during the crop cycles of wheat and rapeseed and associated S-1 and S-2 features for crop monitoring.
- The datasets can be used in many fields of research (Agronomy, Climatology, Ecology...) to analyze the relationships between crop growth and agricultural practices, climatic variables, landscape structure or species distribution.
- These datasets can be used for crop monitoring in other regions, as well as for modelling development.

1. Data Description

The datasets include a vector GIS shapefile (RGF93/Lambert-93 system, ESPG 2154) containing 55 polygons located in Picardy [2,3] and 60 in Brittany regions [3,4] (France). The 115 polygons correspond to 32 rapeseed fields and 83 wheat fields sampled in 2017 during one crop cycle. Five

Table 1
List of acronyms and abbreviations.

Acronyms and abbreviations	Description	Unit
ID	Field identifier	Dimensionless
DOY	Day of year 2017	Day number
LAI	Leaf Area Index	Dimensionless
entropy_shannon_norm	Normalized shannon entropy	Dimensionless
entropy_shannon_I_norm	Normalized intensity of shannon entropy	Dimensionless
entropy_shannon_P_norm	Normalized polarization of shannon entropy	Dimensionless
span	Total scattered power	Decibel (dB)
VV	Sigma VV	Decibel (dB)
VH	Sigma VH	Decibel (dB)
VHVV	Sigma VH:Sigma VV	Decibel (dB)
Band 2	Blue band	Per ten thousand
Band 3	Green band	Per ten thousand
Band 4	Red band	Per ten thousand
Band 5	Red-edge band	Per ten thousand
Band 6	Red-edge band	Per ten thousand
Band 7	Red-edge band	Per ten thousand
Band 8	Near-infrared band	Per ten thousand
Band 8A	Near-infrared band	Per ten thousand
Band 11	Shortwave-infrared band	Per ten thousand
Band 12	Shortwave-infrared band	Per ten thousand
GNDVI	Green Normalized Vegetation Index	Dimensionless
IRECI	Inverted Red-Edge Chlorophyll Index	Dimensionless
MCARI	Modified Chlorophyll Absorption in Reflectance Index	Dimensionless
MSAVI	Modified Soil-Adjusted Vegetation Index	Dimensionless
MTCI	MERIS Terrestrial Chlorophyll Index	Dimensionless
NDI	Normalized Difference Index	Dimensionless
NDVI	Normalized Difference Vegetation Index	Dimensionless
PSSRa	Pigment Specific Simple Ratio	Dimensionless
REIP	Red-Edge Inflection Point	Dimensionless
SAVI	Soil-Adjusted Vegetation Index	Dimensionless
S2REP	Sentinel-2 Red Edge Position	Dimensionless
WDVI	Weighted Difference Vegetation Index	Dimensionless

attribute tables were assigned to each sampled field, which are crop types (wheat/rapeseed), LAI and biomass (*i.e.*, LAI, wet biomass, dry biomass, water content), phenological stages, S-1 features (i.e., backscattering coefficients and polarimetric indicators) and S-2 features (*i.e.*, spectral values and vegetation indices). The three last table columns that are labeled “DOY”, “Region” and “ID” correspond to the acquisition dates of satellite images or crop parameters in Day Of Year (DOY) 2017, region of France (Brittany or Picardy) and field identifier, respectively. Table 1 provides a full description of the acronyms and abbreviations used in this article.

2. Experimental Design, Materials and Methods

Concerning crop parameters, phenological stages were identified over the 115 field samples based on the Biologische Bundesanstalt, Bundessortenamt and Chemical industry (BBCH) scale [5]. These data were used in Mercier et al [2,3]. LAI, wet biomass, dry biomass and water content surveys were conducted on three wheat fields and three rapeseed fields in Brittany region. For this purpose, 10 digital hemispherical photographs were taken at each sampled field on each date. These data were used in Mercier et al [4]. LAI was estimated from the hemispherical photographs using CAN-EYE software [1] and averaged per date and field sample. Biomass measurements were performed in homogeneous areas (20 $\times$ 20 m) where five samples of wheat 50 cm and five rapeseed plants were collected during the field surveys. The wet biomass was directly weighed *in situ*, and the dry biomass was measured after drying the crop (oven, 65 °C, 48 h). Water content in the plant equals wet biomass minus dry biomass.

Concerning remote sensing features, S-1 and S-2 images were downloaded from the Copernicus Open Access Hub (https://scihub.copernicus.eu/). Cloud-free S-2 images used correspond to Level-2A products providing top of canopy reflectances. Twelve vegetation indices were calculated from S-2 spectral bands (Table 1). S-1 images used were acquired in Interferometric Wide (IW) swath mode and correspond to Single Look Complex (SLC) products. The backscattering coefficients (sigma VH and sigma VV) extraction process was performed using the S-1 Toolbox (http://step.esa.int/main/toolboxes/sentinel-1-toolbox/). This process includes (1) radiometric calibration, (2) speckle filtering using a Lee Refined 7 $\times$ 7 filter [6], (3) geometric corrections using Shuttle Radar Topography Mission data [7], (4) calculation of the sigma VH: sigma VV ratio and (5) conversion from linear to decibel values. The polarimetric indicators extraction process was performed using PolSARpro version 5.1.3 software [8]. This process includes (1) the extraction of a 2 $\times$ 2 covariance matrix, (2) a speckle filtering using a Lee Refined 7 $\times$ 7 filter, (3) the extraction of four polarimetric indicators (the Shannon entropy, the intensity, the degree of polarization and the span), (4) the normalization of the Shannon entropy, the intensity and the degree of polarization. Finally, all S-1 and S-2 images were projected onto the RGF93/Lambert-93 system (EPSG 2154) and resampled with bilinear interpolation to the resolution of 10 m. The median value was computed at the field scale with a negative buffer of 15 m and 10 m in Picardy and Brittany, respectively, to select only pixels fully contained within each field.

Declaration of Competing Interest

The authors declare that they have no known competing financial interests or personal relationships which have, or could be perceived to have, influenced the work reported in this article.

CRediT Author Statement

Audrey Mercier: Conceptualization, Methodology, Software, Validation, Data curation, Writing – original draft, Visualization; **Julie Betbeder:** Conceptualization, Methodology, Software, Supervision; **Julien Denize:** Resources, Data curation; **Jean-Luc Roger:** Resources; **Fabien Spicher:** Resources, Data curation; **Jérôme Lacoux:** Resources; **David Roger:** Resources; **Jacques Baudry:** Conceptualization, Writing – review & editing, Project administration, Funding acquisition; **Laurence Hubert-Moy:** Conceptualization, Supervision, Writing – review & editing, Project administration, Funding acquisition.

Acknowledgments

We thank Sébastien Rapinel for his helpful comments on database contents. This research was funded through the 2015-2016 BiodivERsA COFUND call for research proposals, with the national funders ANR, MINECO, and BELSPO, and was supported by the Kalideos project funded by the CNES, the Zone Atelier Armorique project, and a Ph.D. grant to A. Mercier from the Ministry of Research.

Supplementary Materials

Supplementary material associated with this article can be found in the online version at doi:10.1016/j.dib.2021.107408.

References

[1] F. Baret, M. Weiss, Can-Eye: processing digital photographs for canopy structure characterization, CAN EYE tutorial document, Avignon, France, 2004.

[2] A. Mercier, J. Betbeder, J. Baudry, V. Le Roux, F. Spicher, J. Lacoux, D. Roger, L. Hubert-Moy, Evaluation of Sentinel-1 & 2 time series for predicting wheat and rapeseed phenological stages, ISPRS J. Photogramm. Remote Sens. 163 (2020) 231–256, doi:10.1016/j.isprsjprs.2020.03.009.
[3] A. Mercier, J. Betbeder, J. Baudry, J. Denize, V. Leroux, J.L. Roger, F. Spicher, L. Hubert-Moy, Evaluation of Sentinel-1 and -2 time series to derive crop phenology and biomass of wheat and rapeseed: northern France and Brittany case studies, Remote Sensing for Agriculture, Ecosystems, and Hydrology XXI, International Society for Optics and Photonics, 2019, doi:10.1117/12.2533132.
[4] A. Mercier, J. Betbeder, S. Rapinel, N. Jegou, J. Baudry, L. Hubert-Moy, Evaluation of Sentinel-1 and -2 time series for estimating LAI and biomass of wheat and rapeseed crop types, JARS 14 (2020) 024512, doi:10.1117/1.JRS.14.024512.
[5] H. Bleiholder, E. Weber, M. Hess, H. Wicke, T. van den Boom, P.D. Lancashire, L. Buhr, H. Hack, F.R. Klose, R. Strauss, Growth Stages of Mono- and Dicotyledonous Plants, BBCH Monograph, Federal Biological Research Centre for Agriculture and Forestry, Berlin/Braunschweig, Germany, 2001.
[6] J.S. Lee, L. Jurkevich, P. Dewaele, P. Wambacq, A. Oosterlinck, Speckle filtering of synthetic aperture radar images: a review, Remote Sens. Rev. 8 (1994) 255–267, doi:10.1080/02757259409532206.
[7] T.G. Farr, P.A. Rosen, E. Caro, R. Crippen, R. Duren, S. Hensley, M. Kobrick, M. Paller, E. Rodriguez, L. Roth, D. Seal, S. Shaffer, J. Shimada, J. Umland, M. Werner, M. Oskin, D. Burbank, D. Alsdorf, The shuttle radar topography mission, Rev. Geophys. 45 (2007), doi:10.1029/2005RG000183.
[8] E. Pottier, L. Ferro-Famil, PolSARPro V5.0: An ESA educational toolbox used for self-education in the field of POLSAR and POL-INSAR data analysis, in: Proceedings of the IEEE International Geoscience and Remote Sensing Symposium, 2012, pp. 7377–7380, doi:10.1109/IGARSS.2012.6351925.

Appendix B: Correlation matrices of features derived from S-2 images

Appendix B-1. Correlation matrix of features devived from S-2 images for wheat.

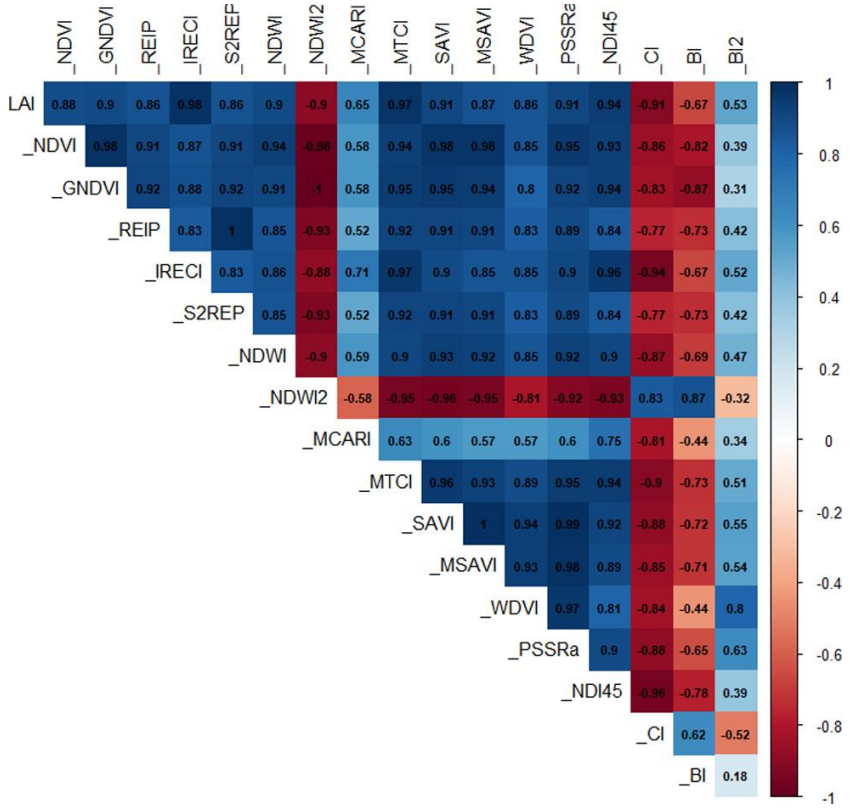

Appendix B-2. Correlation matrix of features devived from S-2 images for wheat

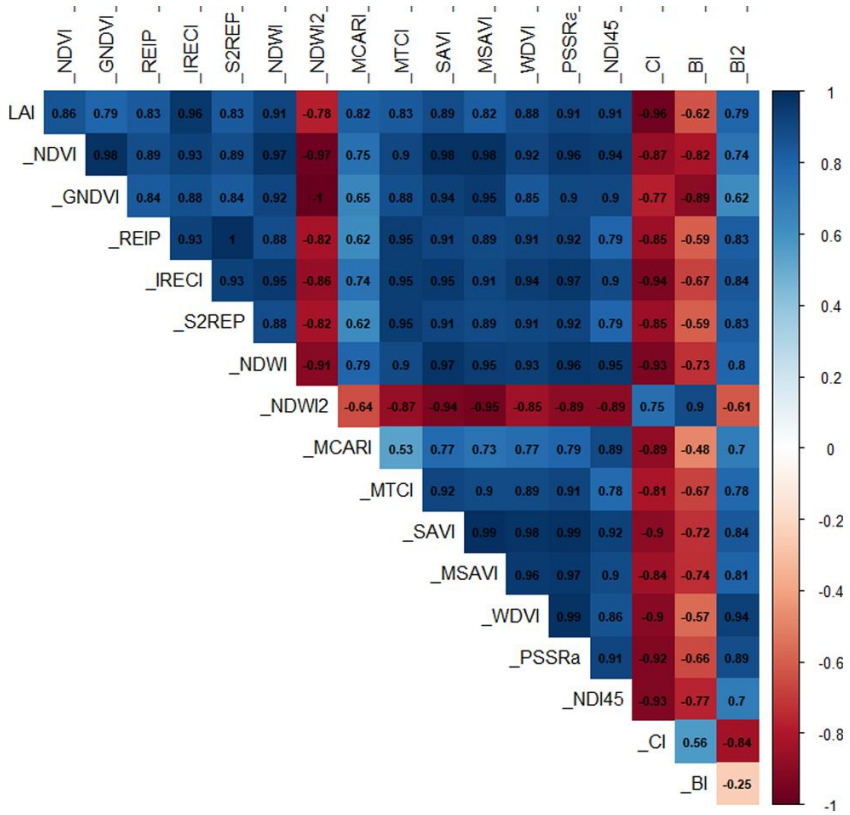

Appendix C: Confusion matrices of the classifications of wheat and rapeseed principal phenological stages.

Appendix C-1. Confusion matrix of the principal phenological stages of wheat classification derived from the 4 most important features of S-1 data alone (lines) and the validation (columns). The classification was performed using the first pair of randomly generated

Classification	Code	Validation					Total
		1	2	3	4	5	
Tillering	**1**	**13**				1	**14**
Stem elongation	**2**		**9**	1	2		**12**
Flowering	**3**		2	**1**	2	1	**6**
Development of fruit	**4**		1	5	**8**	2	**18**
Ripening	**5**					**7**	
Total		**14**	**13**	**8**	**14**	**11**	
Kappa index	**0.54**						
Overall Accuracy	**63%**						

Appendix C-2. Confusion matrix of the principal phenological stages of wheat classification derived from the 8 most important features of S-2 data alone (lines) and the validation (columns). The classification was performed using the first pair of randomly generated

Classification	Code	Validation					Total
		1	2	3	4	5	
Tillering	**1**	**13**					**13**
Stem elongation	**2**		**11**		1		**12**
Flowering	**3**			**6**	1		**7**
Development of fruit	**4**		2	2	**12**	4	**20**
Ripening	**5**	1				**7**	**8**
Total		**14**	**13**	**8**	**14**	**11**	
Kappa index	**0.77**						
Overall Accuracy	**82%**						

Appendix C-3. Confusion matrix of the principal phenological stages of wheat classification derived from the 9 most important features of combined S-1 & 2 data (lines) and the validation (columns). The classification was performed using the first pair of randomly generated training and validation samples.

Classification	Code	Validation					Total
		1	2	3	4	5	
Tillering	**1**	**13**				1	**14**
Stem elongation	**2**		**8**		2		**10**
Flowering	**3**			**6**			**6**
Development of fruit	**4**		4	2	**12**	1	**19**
Ripening	**5**	1	1			**9**	**11**
Total		**14**	**13**	**8**	**14**	**11**	
Kappa index	**0.75**						
Overall Accuracy	**80%**						

Appendix C-4. Confusion matrix of the principal phenological stages of rapeseed classification derived from the 4 most important features of S-1 data alone (lines) and the validation (columns). The classification was performed using the first pair of randomly generated training and validation samples.

Classification	Code	Validation					Total
		1	2	3	4	5	
Leaf development	**1**	**4**		**2**			**6**
Inflorescence emergence	**2**		**11**	**1**		**1**	**13**
Flowering	**3**	**2**		**9**			**11**
Development of fruit	**4**				**1**	**1**	**2**
Ripening	**5**		**1**		**4**	**8**	**12**
Total		**6**	**12**	**12**	**5**	**10**	
Kappa index	**0.65**						
Overall Accuracy	**73%**						

Appendix C-5. Confusion matrix of the principal phenological stages of rapeseed classification derived from the 6 most important features of S-2 data alone (lines) and the validation (columns). The classification was performed using the first pair of randomly generated training and validation samples.

Classification	Code	Validation					Total
		1	2	3	4	5	
Leaf development	**1**	**5**					**5**
Inflorescence emergence	**2**		**11**	**1**		**2**	**13**
Flowering	**3**			**11**			**11**
Development of fruit	**4**				**4**		**4**
Ripening	**5**	**1**	**1**		**1**	**8**	**11**
Total		**6**	**12**	**12**	**5**	**10**	
Kappa index	**0.83**						
Overall Accuracy	**87%**						

Appendix C-6. Confusion matrix of the principal phenological stages of rapeseed classification derived from the 10 most important features of combined S-1 & 2 data (lines) and the validation (columns). The classification was performed using the first pair of randomly generated training and validation samples.

Classification	Code	Validation					Total
		1	2	3	4	5	
Leaf development	**1**	**6**		1			**7**
Inflorescence emergence	**2**		**12**				**12**
Flowering	**3**			**11**			**11**
Development of fruit	**4**				**4**		**4**
Ripening	**5**				1	**10**	**11**
Total		**6**	**12**	**12**	**5**	**10**	
Kappa index	**96%**						
Overall Accuracy	**0.94**						

Appendix D: Confusion matrices of the classifications of wheat and rapeseed secondary phenological stages.

Appendix D-1. Confusion matrix of the secondary phenological stages of wheat classification derived from the 4 most important features of S-1 data alone (lines) and the validation (columns). The classification was performed using the first pair of randomly generated training and validation samples.

Classification	Code	Validation							Total
		1	2	3	4	5	6	7	
Beginning of tillering	**1**	**11**	2				1		**14**
Middle/end of tillering	**2**	2	**16**						**18**
Stem elongation	**3**			**9**		2			**11**
Flowering, anthesis	**4**			2	**1**	2	2		**7**
Development of fruit	**5**			2	6	**9**	2	1	**20**
Middle of ripening	**6**					1	**1**		**2**
End of ripening	**7**				1		3	**1**	**5**
Total		**13**	**18**	**13**	**8**	**14**	**9**	**2**	
Kappa index	**0.55**								
Overall Accuracy	**62%**								

Appendix D-2. Confusion matrix of the secondary phenological stages of wheat classification derived from the 5 most important features of S-2 data alone (lines) and the validation (columns). The classification was performed using the first pair of randomly generated training and validation samples.

Classification	Code	Validation							Total
		1	2	3	4	5	6	7	
Beginning of tillering	**1**	**11**	2						**13**
Middle/end of tillering	**2**	1	**16**				1		**17**
Stem elongation	**3**			**12**					**12**
Flowering, anthesis	**4**				**6**	1			**7**
Development of fruit	**5**			1	2	**12**	4		**19**
Middle of ripening	**6**					1	**2**		**3**
End of ripening	**7**	1					2	**2**	**5**
Total		**13**	**18**	**13**	**8**	**14**	**9**	**2**	
Kappa index	**0.75**								
Overall Accuracy	**79%**								

Appendix D-3. Confusion matrix of the secondary phenological stages of wheat classification derived from the 9 most important features of combined S-1 & 2 data (lines) and the validation (columns). The classification was performed using the first pair of randomly generated training and validation samples.

Classification	Code	Validation							Total
		1	2	3	4	5	6	7	
Beginning of tillering	**1**	**12**	1						**13**
Middle/end of tillering	**2**	1	**17**				1		**18**
Stem elongation	**3**			**9**	1	2			**12**
Flowering, anthesis	**4**				**5**				**5**
Development of fruit	**5**			3	2	**12**	1		**18**
Middle of ripening	**6**			1			**4**		**5**
End of ripening	**7**						3	**2**	**5**
Total		**13**	**18**	**13**	**8**	**14**	**9**	**2**	
Kappa index	**0.75**								
Overall Accuracy	**79%**								

Appendix D-4. Confusion matrix of the secondary phenological stages of rapeseed classification derived from the 4 most important features of S-1 data alone (lines) and the validation (columns). The classification was performed using the first pair of randomly generated training and validation samples.

Classification	Code	Validation							Total
		1	2	3	4	5	6	7	
Leaf development	**1**	**3**		2	1				**6**
Inflorescence emergence	**2**		**11**	1					**12**
Beginning/Middle of flowering	**3**	1			2				**3**
End of flowering	**4**	2			**6**				**8**
Development of fruit	**5**						1		**1**
Beginning of ripening	**6**					5	**6**	1	**12**
End of ripening	**7**							**5**	**5**
Total		**6**	**11**	**3**	**9**	**5**	**7**	**6**	
Kappa index	**0.59**								
Overall Accuracy	**66%**								

Appendix D-5. Confusion matrix of the secondary phenological stages of rapeseed classification derived from the 5 most important features of S-2 data alone (lines) and the validation (columns). The classification was performed using the first pair of randomly generated training and validation samples.

Classification	Code	Validation							Total
		1	2	3	4	5	6	7	
Leaf development	**1**	**2**					1		**7**
Inflorescence emergence	**2**	4	**10**						**11**
Beginning/Middle of flowering	**3**			**3**	2				
End of flowering	**4**		1		**7**				**8**
Development of fruit	**5**					**3**			**3**
Beginning of ripening	**6**		1			2	**6**		**9**
End of ripening	**7**							**6**	**6**
Total		**6**	**11**	**3**	**9**	**5**	**7**	**6**	
Kappa index	**0.74**								
Overall Accuracy	**79%**								

Appendix D-6. Confusion matrix of the secondary phenological stages of rapeseed classification derived from the 10 most important features of combined S-1 & 2 data (lines) and the validation (columns). The classification was performed using the first pair of randomly generated training and validation samples.

Classification	Code	Validation							Total
		1	2	3	4	5	6	7	
Leaf development	**1**	**6**							**6**
Inflorescence emergence	**2**		**11**						**11**
Beginning/Middle of flowering	**3**			**2**	1				**3**
End of flowering	**4**			1	**8**				**9**
Development of fruit	**5**					**3**			**3**
Beginning of ripening	**6**					2	**7**		**9**
End of ripening	**7**							6	**6**
Total		**6**	**11**	**3**	**9**	**5**	**7**	**6**	
Kappa index	**0.90**								
Overall Accuracy	**91%**								

Appendix E: Classifications of the principal and secondary phenological stages of wheat and rapeseed

Appendix E-1. Classification of the 5 principal phenological stages of wheat in the open field study site using combined Sentinel-1 & 2 data.

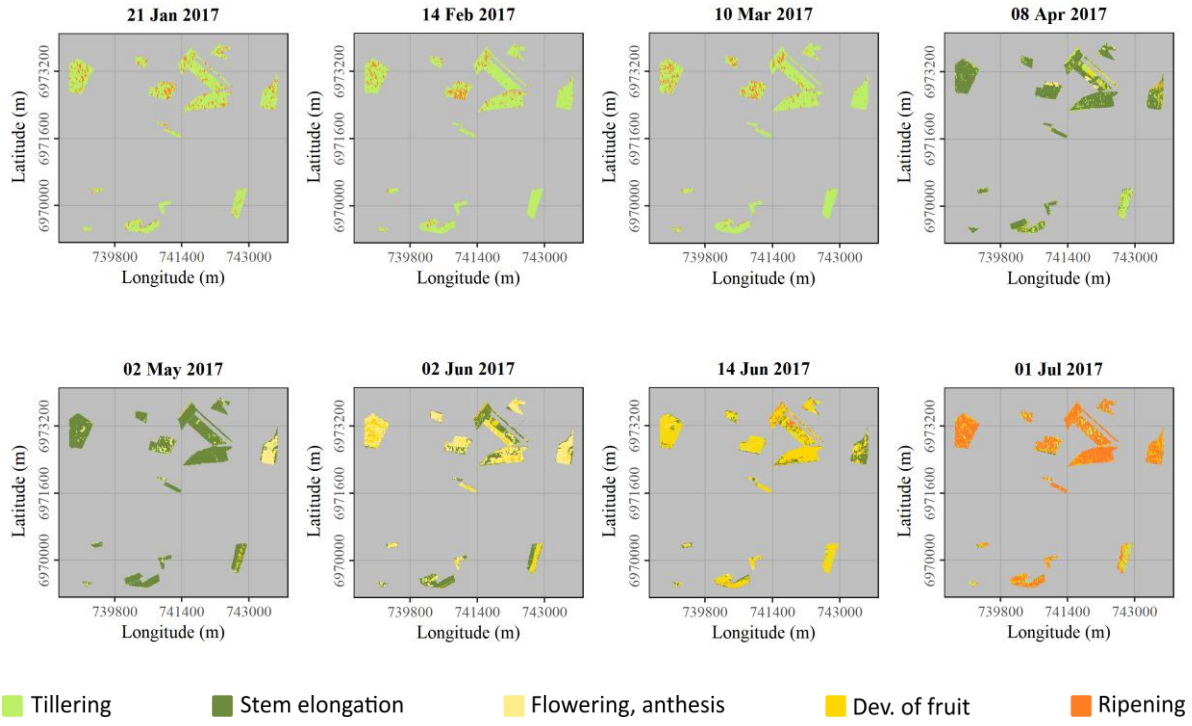

Appendix E-2. Classification of the 5 principal phenological stages of wheat in the bocage study site using combined Sentinel-1 & 2 data.

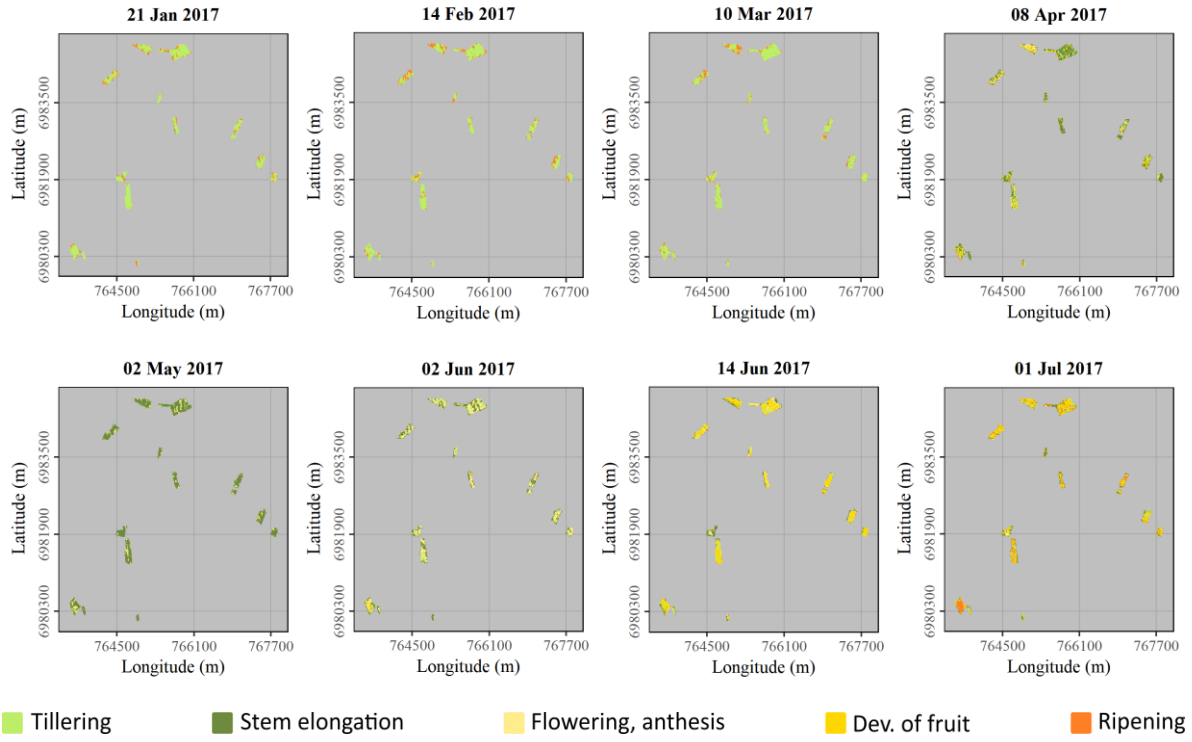

Appendix E-3. Classification of the 7 secondary phenological stages of wheat in the open field study site using combined Sentinel-1 & 2 data.

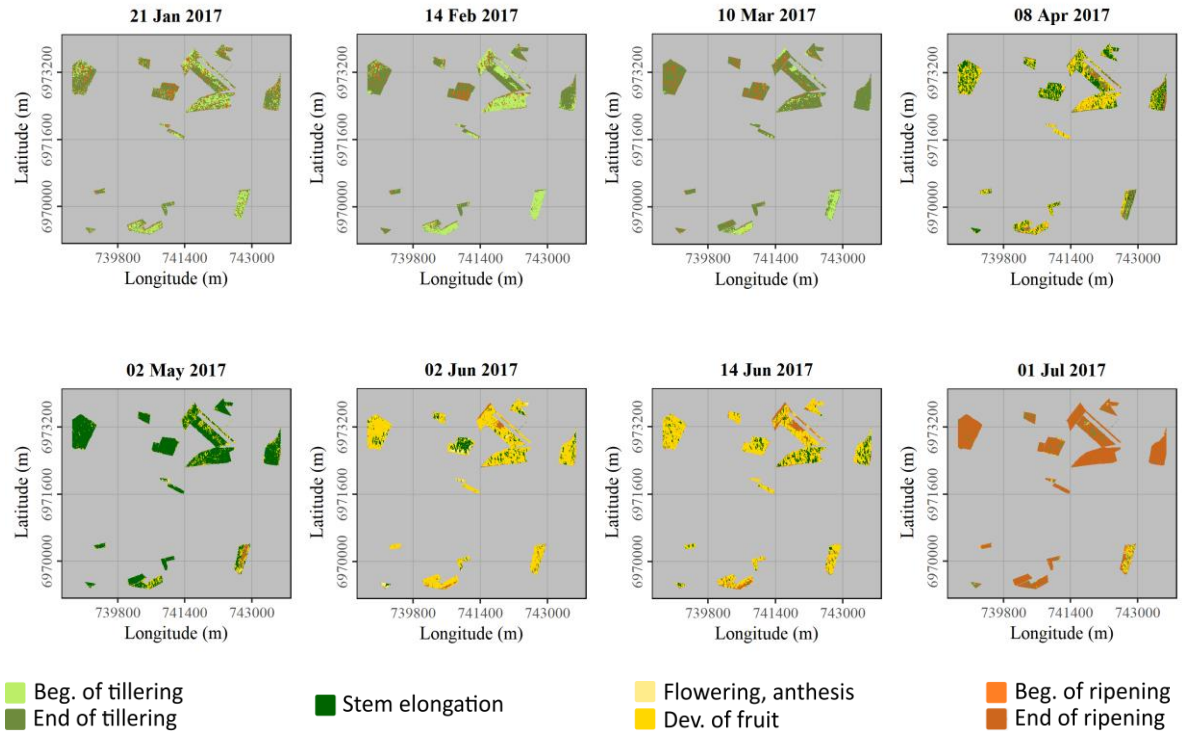

Appendix E-4. Classification of the 7 secondary phenological stages of wheat in the bocage study site using combined Sentinel-1 & 2 data.

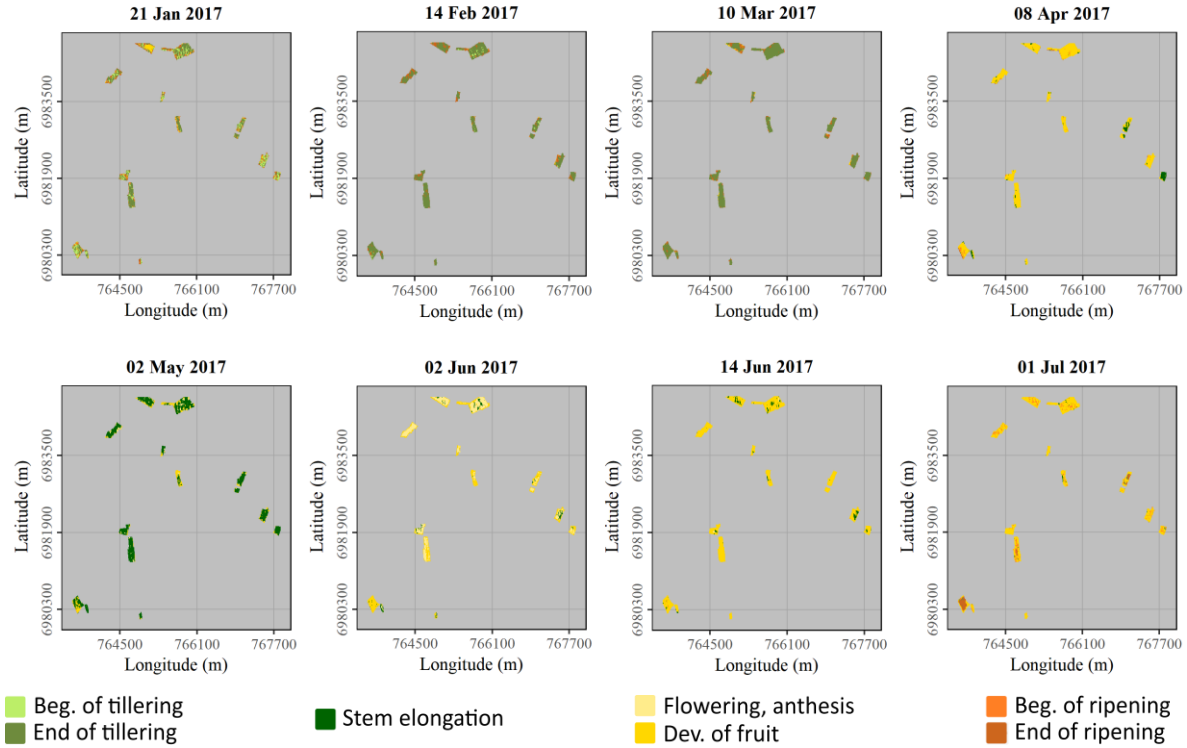

Appendix E-5. Classification of the 5 principal phenological stages of rapeseed in the open field study site using combined Sentinel-1 & 2 data.

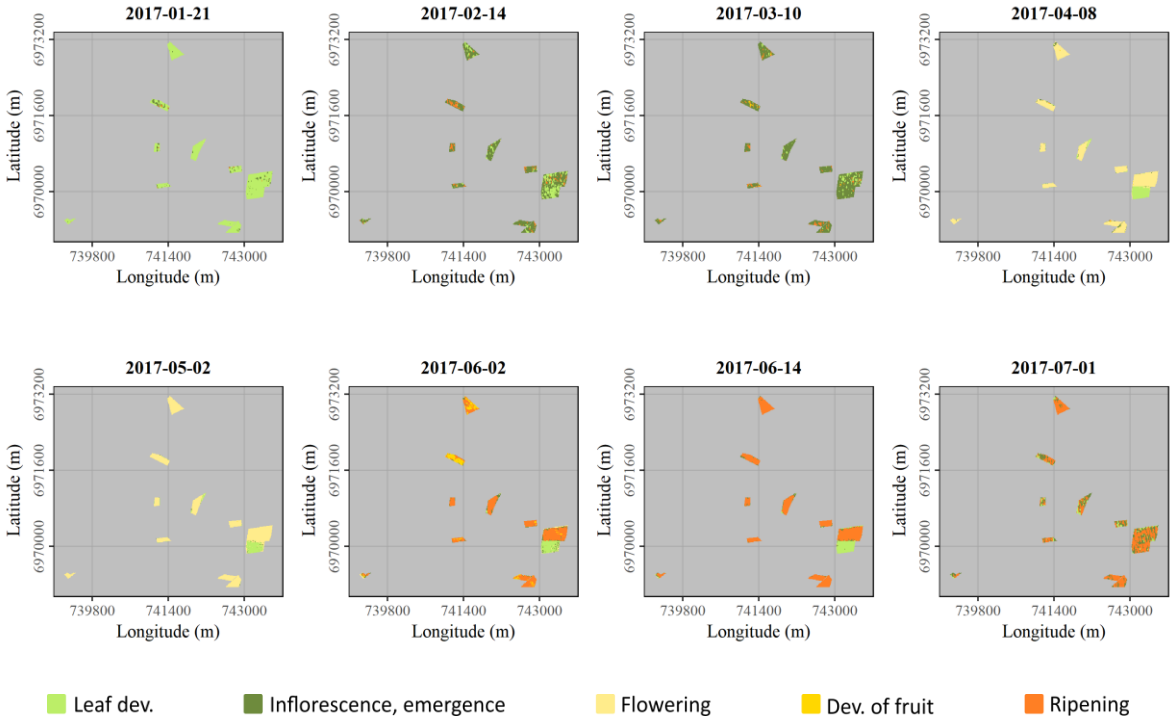

Appendix E-6. Classification of the 5 principal phenological stages of rapeseed in the bocage study site using combined Sentinel-1 & 2 data.

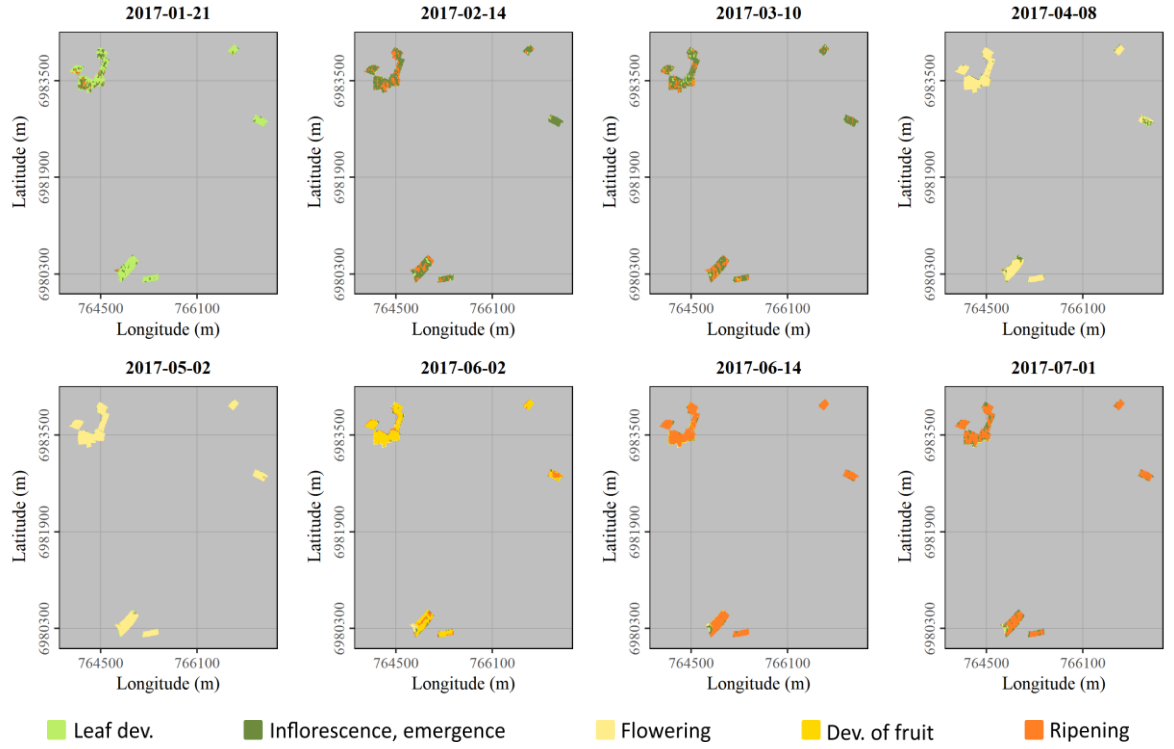

Appendix E-7. Classification of the 7 secondary phenological stages of rapeseed in the open field study site using combined Sentinel-1 & 2 data.

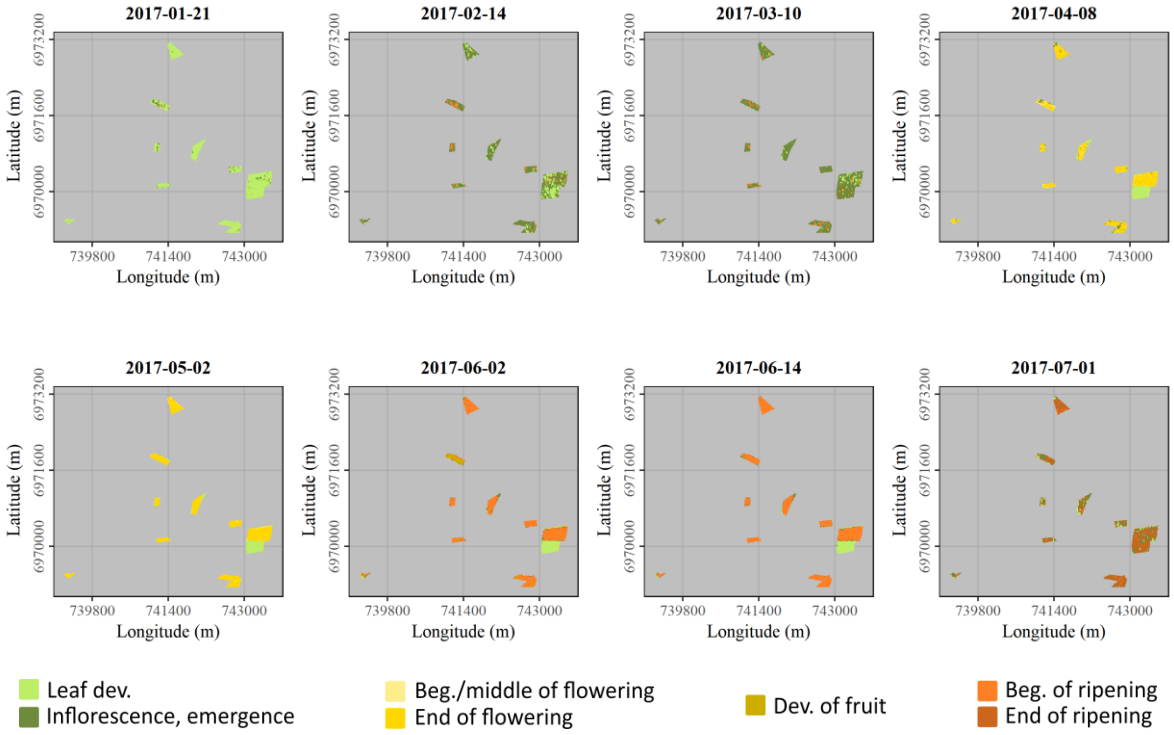

Appendix E-8. Classification of the 7 secondary phenological stages of rapeseed in the bocage study site using combined Sentinel-1 & 2 data.

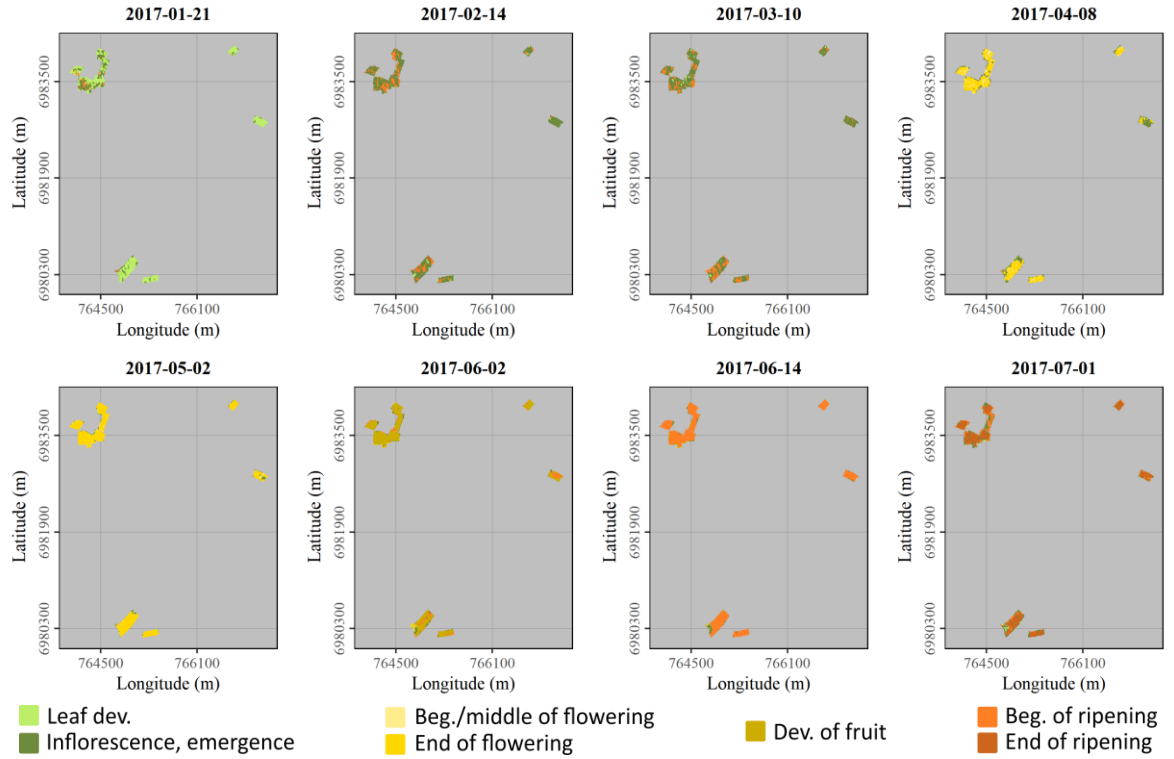

Appendix F: Landscape grain of crop-dominated landscapes 505 m circular window.

Appendix F-1. Landscape grain of study sites in 505 m circular window.

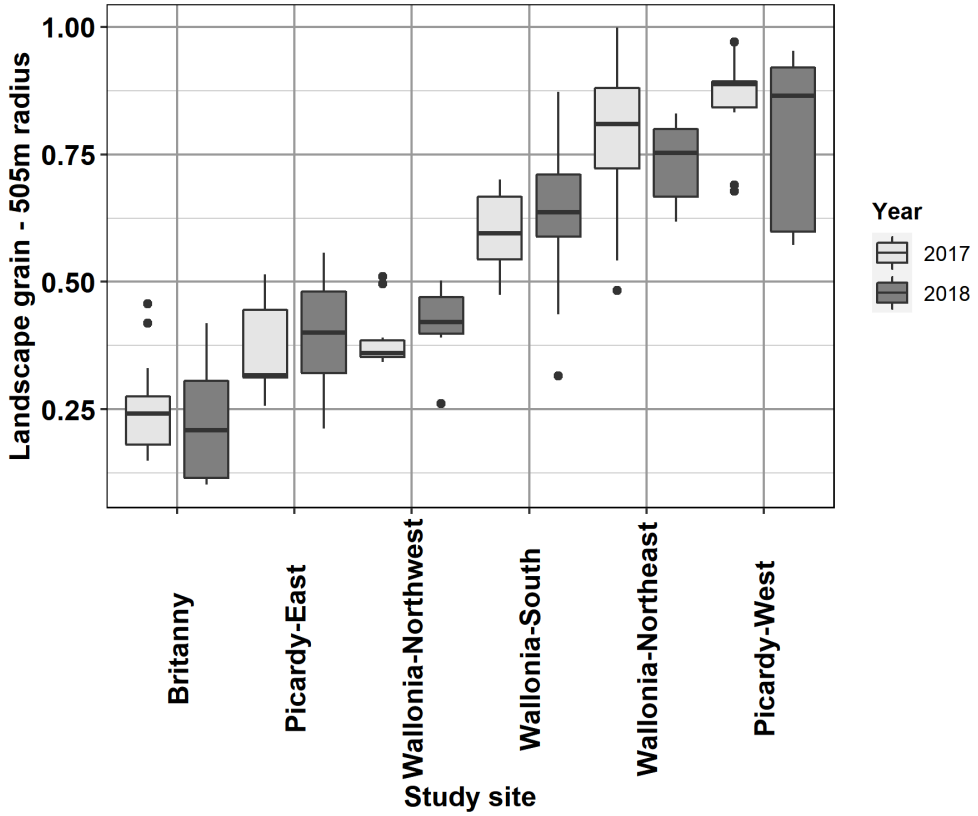

Appendix G: Landscape grain of crop-dominated landscapes and location of pitfall traps.

Appendix G-1. Landscape grain of Brittany and location of pitfall traps.

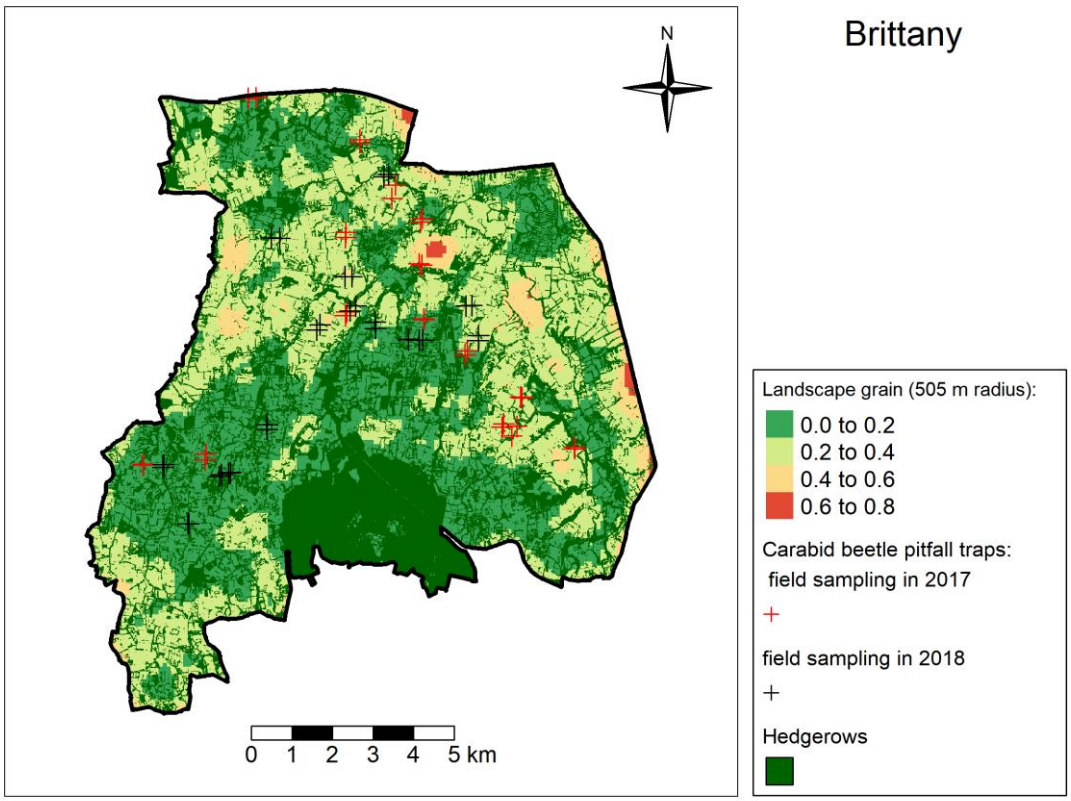

Appendix G-2. Landscape grain of Picardy-East and location of pitfall traps.

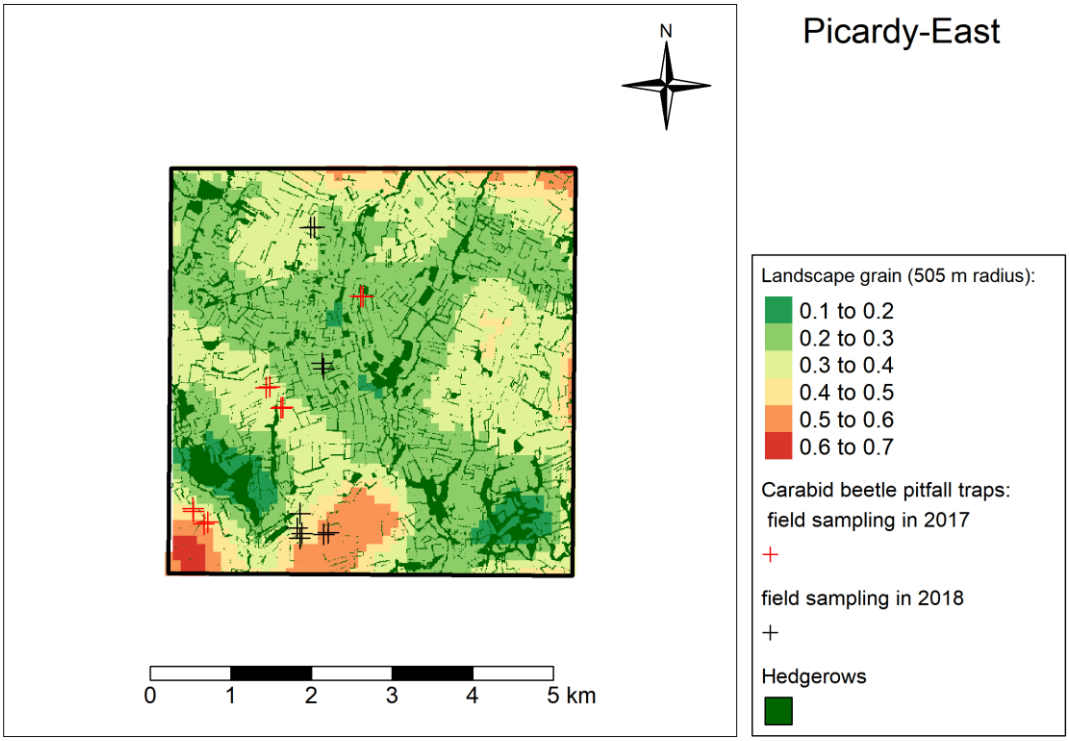

Appendix G-3. Landscape grain of Picardy-West and location of pitfall traps.

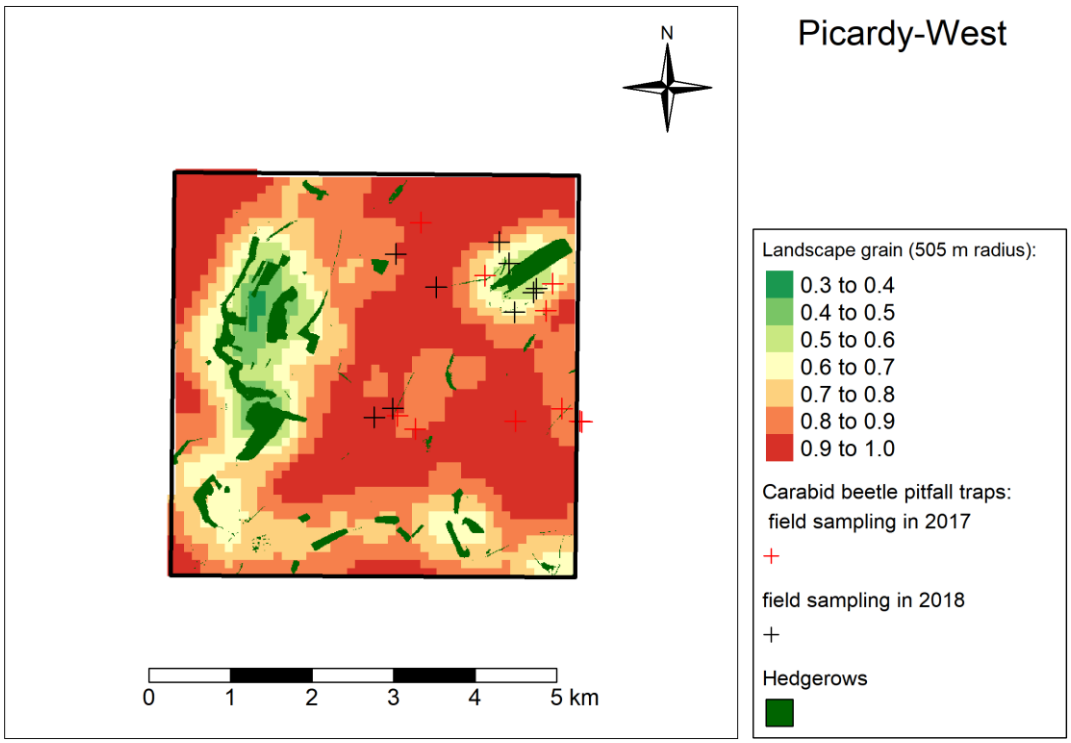

Appendix G-4. Landscape grain of Wallonia-South and location of pitfall traps.

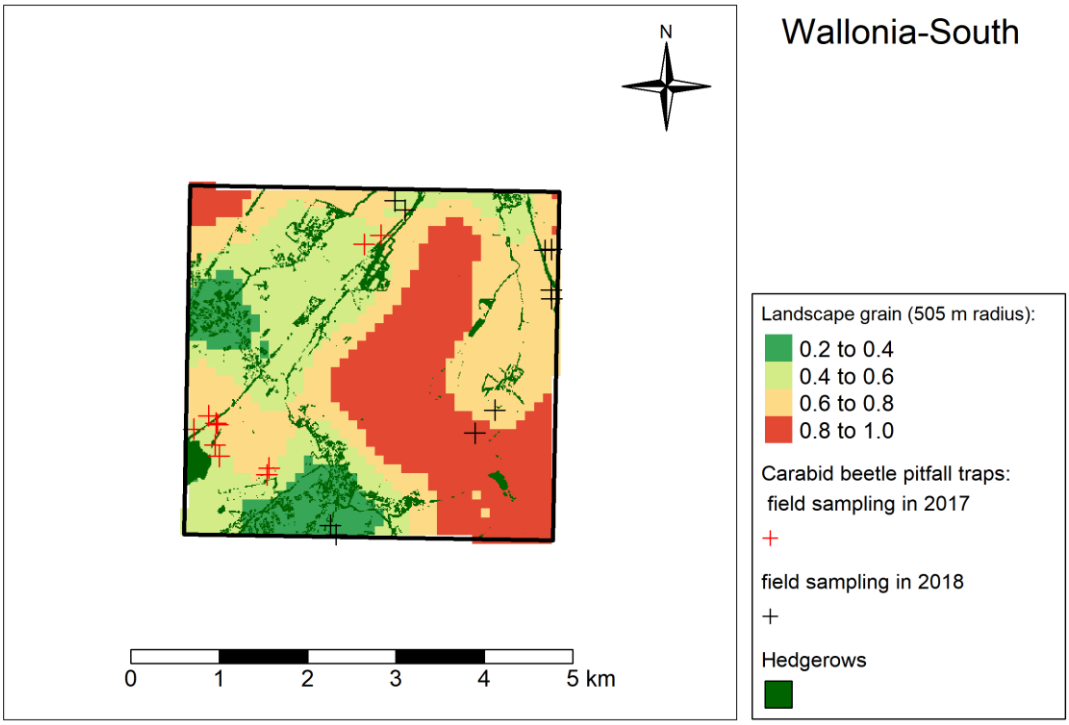

Appendix G-5. Landscape grain of Wallonia-Northwest and location of pitfall traps.

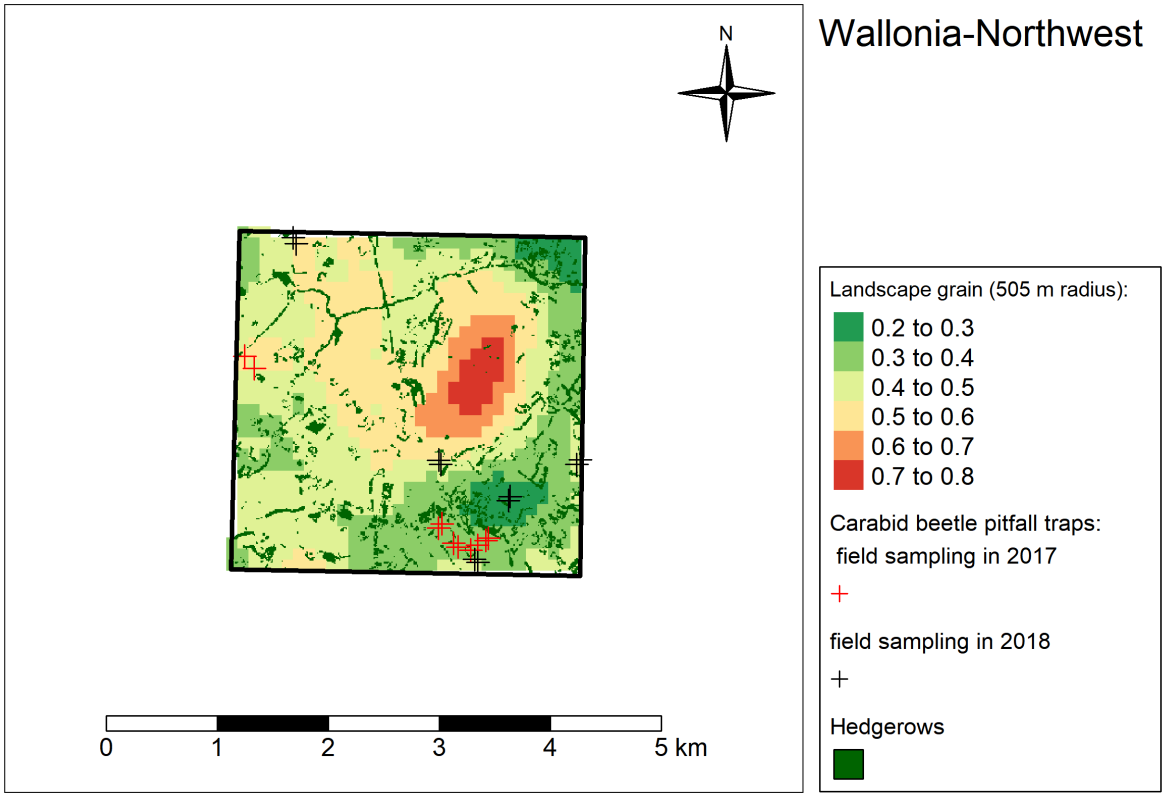

Appendix G-6. Landscape grain of Wallonia-Northeast and location of pitfall traps.

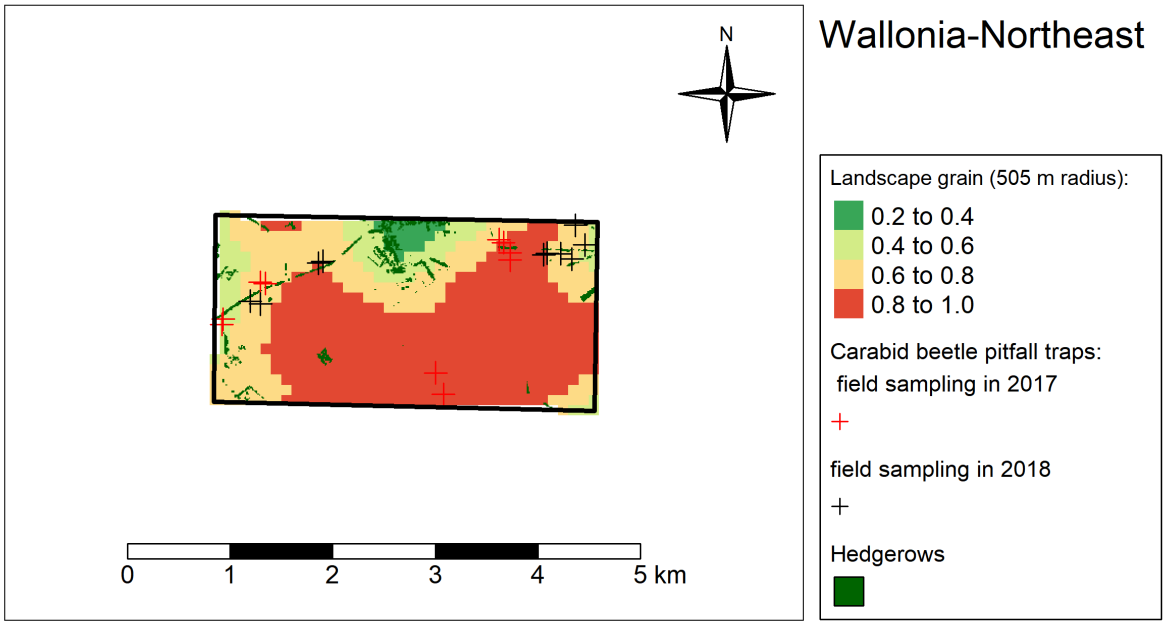

Appendix H: Final land use maps of the six crop-dominated landscapes and location of pitfall traps.

Appendix H-1. Final land use maps of the six landscapes and location of pitfall traps.

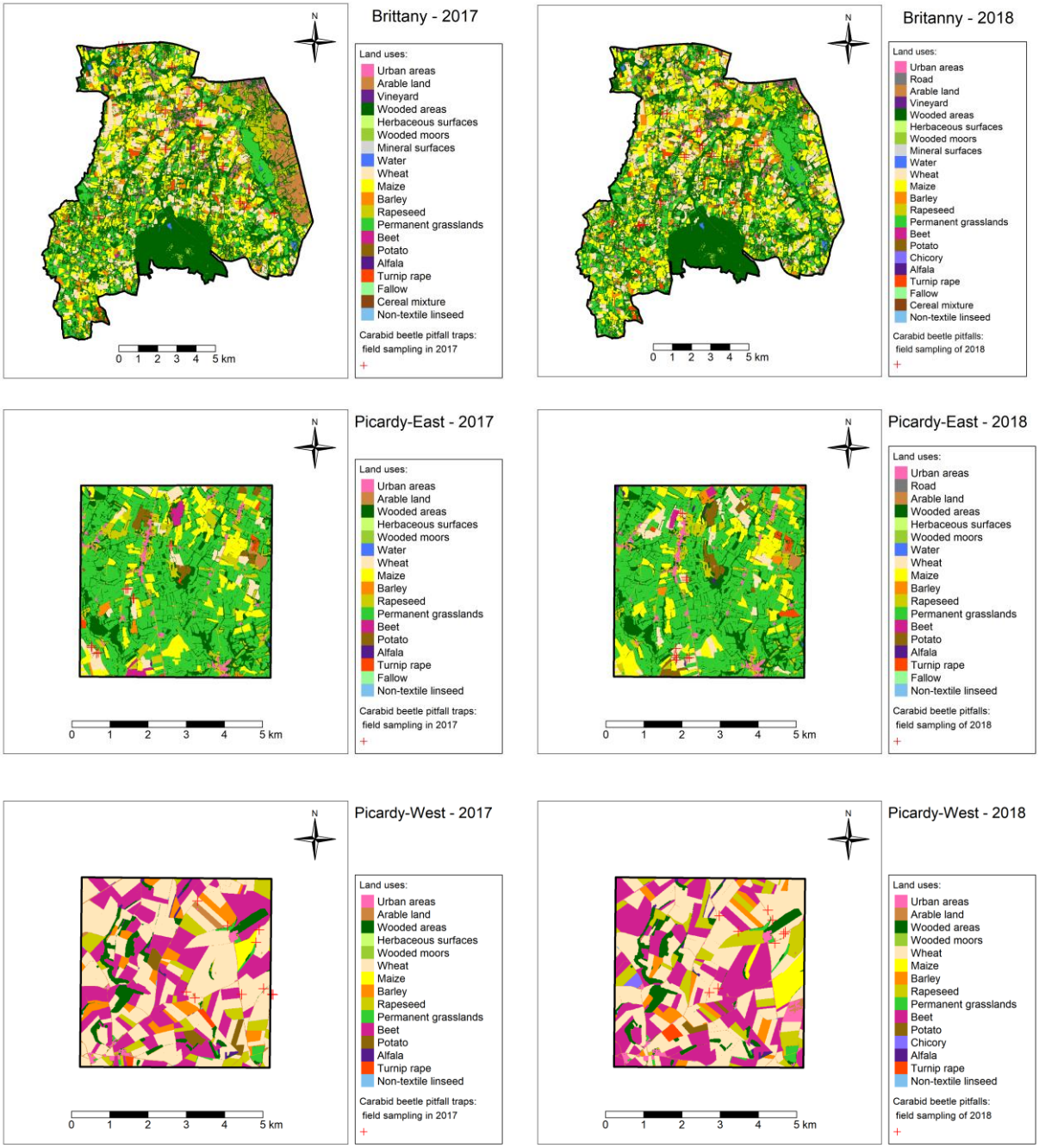

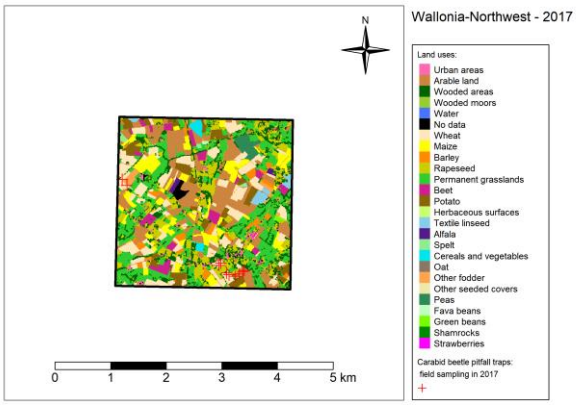
Wallonia-Northwest - 2017
N
0 1 2 3 4 5 km
Land uses:
Urban areas
Arable land
Wooded areas
Wooded moors
Water
No data
Wheat
Maize
Barley
Rapeseed
Permanent grasslands
Beet
Potato
Herbaceous surfaces
Textile linseed
Alfala
Spelt
Cereals and vegetables
Oat
Other fodder
Other seeded covers
Peas
Fava beans
Green beans
Shamrocks
Strawberries
Carabid beetle pitfall traps:
field sampling in 2017

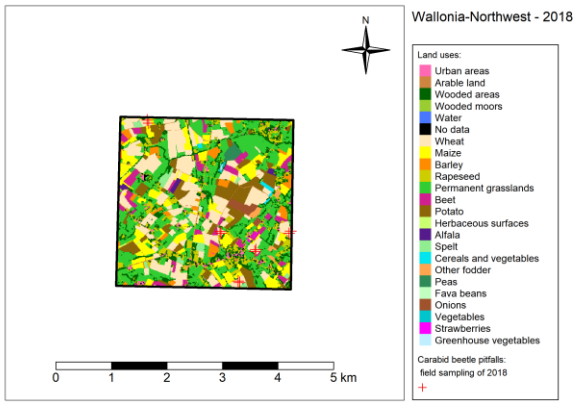
Wallonia-Northwest - 2018
N
0 1 2 3 4 5 km
Land uses:
Urban areas
Arable land
Wooded areas
Wooded moors
Water
No data
Wheat
Maize
Barley
Rapeseed
Permanent grasslands
Beet
Potato
Herbaceous surfaces
Alfala
Spelt
Cereals and vegetables
Other fodder
Peas
Fava beans
Onions
Vegetables
Strawberries
Greenhouse vegetables
Carabid beetle pitfalls:
field sampling of 2018

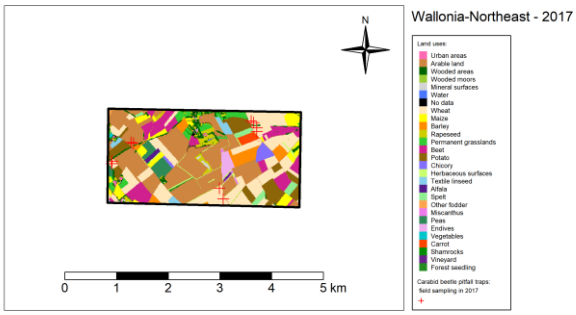
Wallonia-Northeast - 2017
N
0 1 2 3 4 5 km
Land uses:
Urban areas
Arable land
Wooded areas
Wooded moors
Mineral surfaces
Water
No data
Wheat
Maize
Barley
Rapeseed
Permanent grasslands
Beet
Potato
Chicory
Herbaceous surfaces
Textile linseed
Alfala
Spelt
Other fodder
Miscanthus
Peas
Endives
Vegetables
Carrot
Shamrocks
Vineyard
Forest seedling
Carabid beetle pitfall traps:
field sampling in 2017

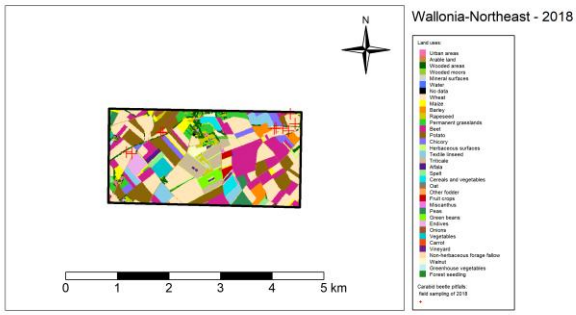
Wallonia-Northeast - 2018
N
0 1 2 3 4 5 km
Land uses:
Carabid beetle pitfalls:
field sampling of 2018

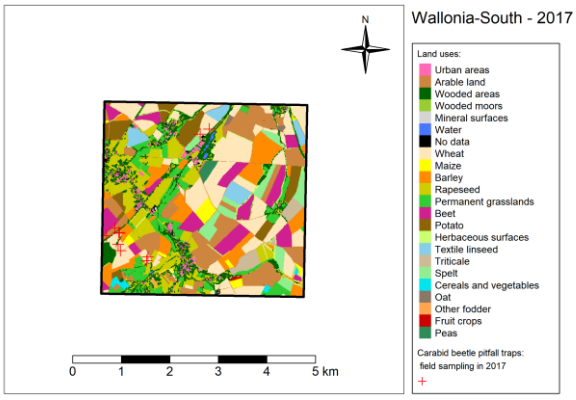
Wallonia-South - 2017
N
0 1 2 3 4 5 km
Land uses:
Urban areas
Arable land
Wooded areas
Wooded moors
Mineral surfaces
Water
No data
Wheat
Maize
Barley
Rapeseed
Permanent grasslands
Beet
Potato
Herbaceous surfaces
Textile linseed
Triticale
Spelt
Cereals and vegetables
Oat
Other fodder
Fruit crops
Peas
Carabid beetle pitfall traps:
field sampling in 2017

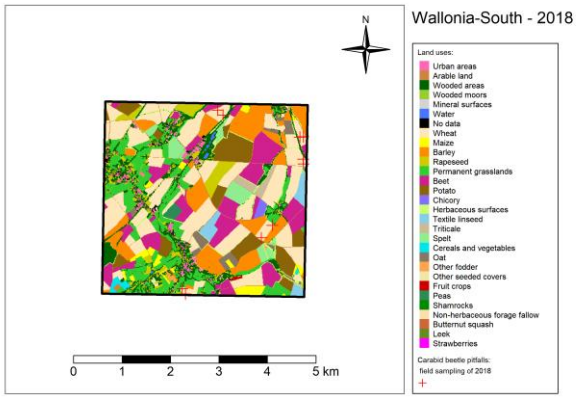
Wallonia-South - 2018
N
0 1 2 3 4 5 km
Land uses:
Urban areas
Arable land
Wooded areas
Wooded moors
Mineral surfaces
Water
No data
Wheat
Maize
Barley
Rapeseed
Permanent grasslands
Beet
Potato
Chicory
Herbaceous surfaces
Textile linseed
Triticale
Spelt
Cereals and vegetables
Oat
Other fodder
Other seeded covers
Fruit crops
Peas
Shamrocks
Non-herbaceous forage fallow
Butternut squash
Leek
Strawberries
Carabid beetle pitfalls:
field sampling of 2018

Appendix I: Relationships between wheat leaf area index, dry biomass, wet biomass, and water content and WDVI derived from S-2.

Appendix I-1. Relationships between wheat leaf area index, dry biomass, wet biomass, and water content and WDVI derived from S-2. .

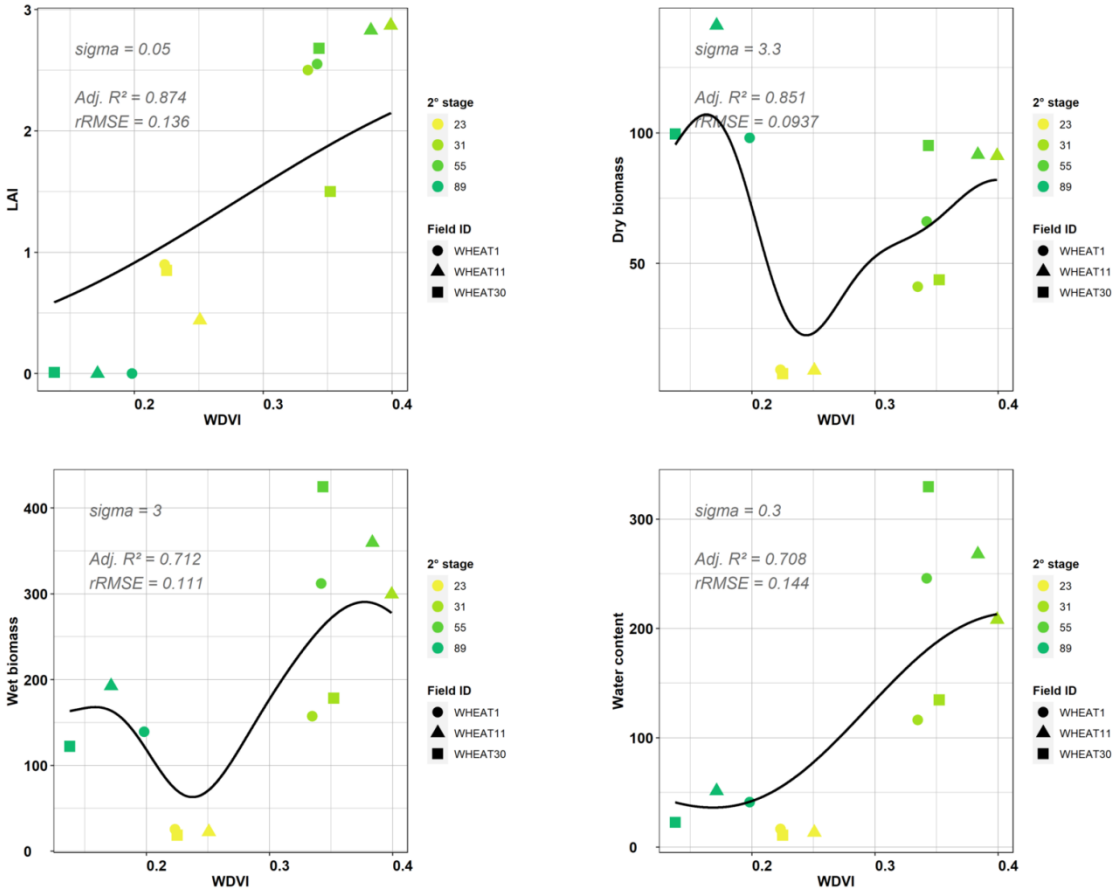

Appendix J: Correspondence factor analysis biplot of the number of interfaces in the crop-dominated landscapes.

Appendix J-1. Correspondence factor analysis biplot of the number of interfaces (triangles) at the 255 m (a), 505 m (b) 1005 m (c), 1505 m (d) and 2005 m (e) in the six landscapes. Circles represent carabid beetle sampling points.The closer the symbols (of each type), the more similar are their profiles.

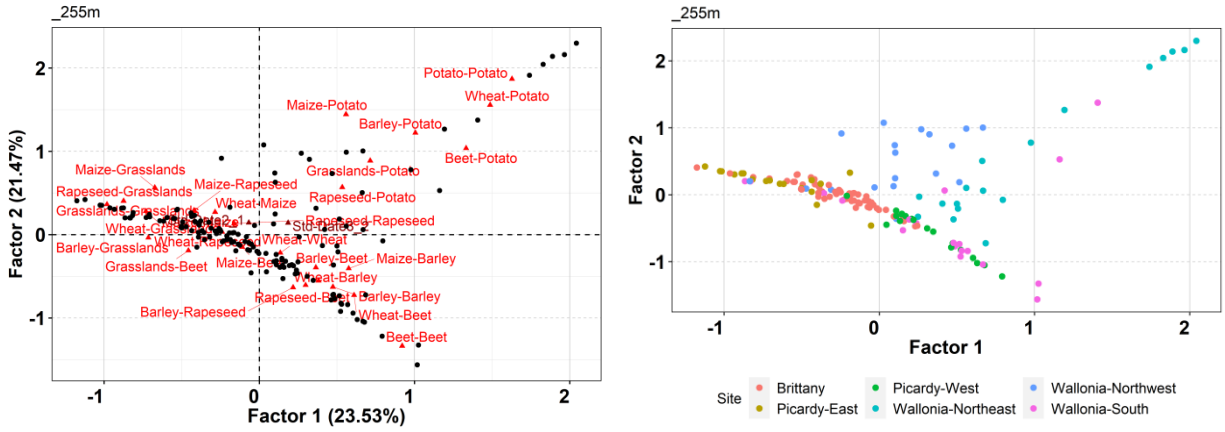

(a)

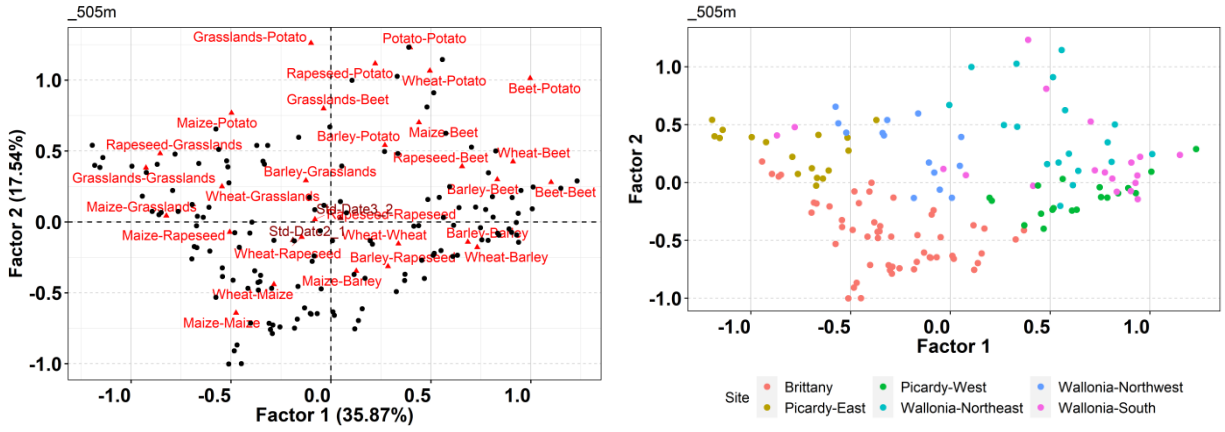

(b)

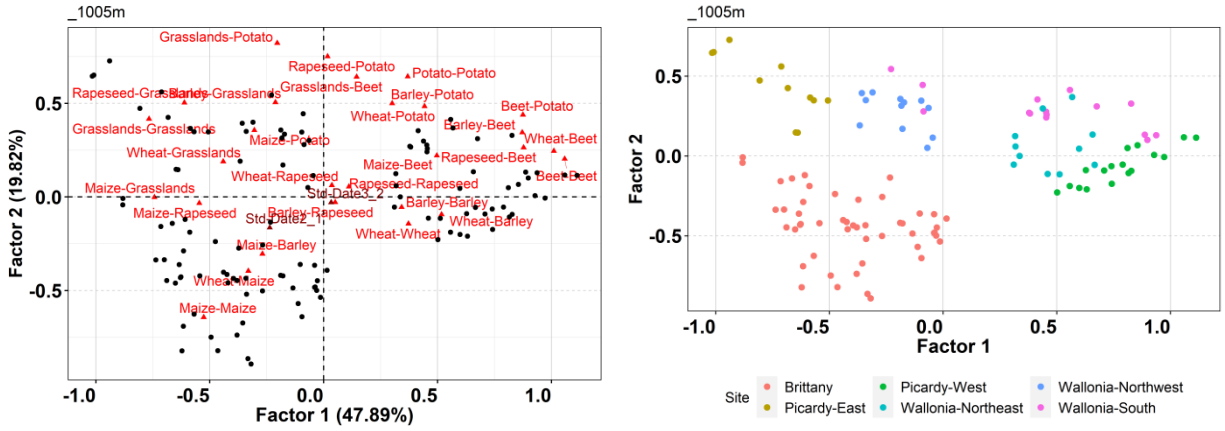

(c)

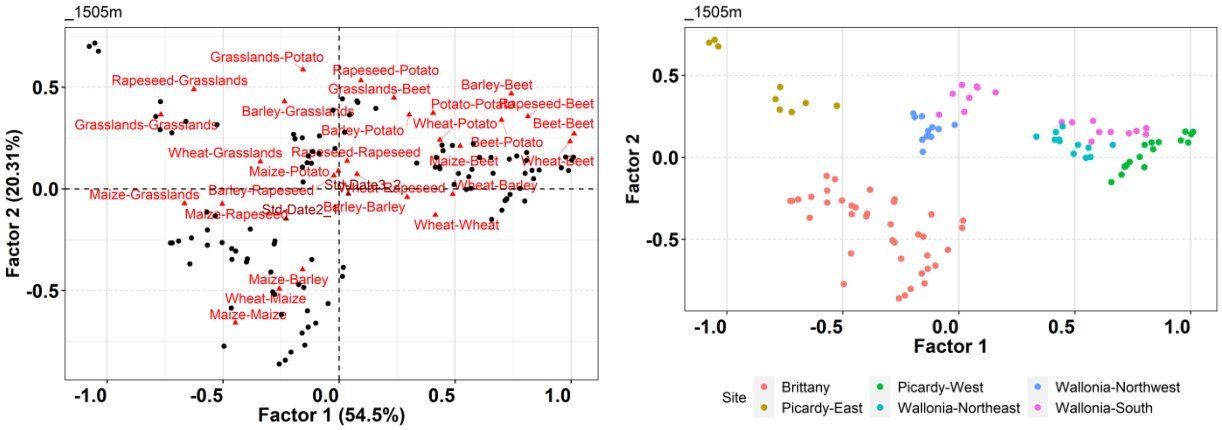
_1505m
Grasslands-Potato
Rapeseed-Potato
Rapeseed-Grasslands
Grasslands-Beet
Barley-Beet
Barley-Grasslands
Potato-Potato
Rapeseed-Beet
Grasslands-Grasslands
Barley-Potato
Wheat-Potato
Beet-Beet
Beet-Potato
Wheat-Grasslands
Rapeseed-Rapeseed
Maize-Beet
Wheat-Beet
Maize-Potato
Std-Date3_2
Maize-Grasslands
Barley-Rapeseed
Wheat-Rapeseed
Wheat-Barley
Std-Date2_1
Barley-Barley
Maize-Rapeseed
Wheat-Wheat
Maize-Barley
Wheat-Maize
Maize-Maize
Factor 2 (20.31%)
Factor 1 (54.5%)
0.5
0.0
-0.5
-1.0
1.0
_1505m
Factor 2
Factor 1
Site
Brittany
Picardy-West
Wallonia-Northwest
Picardy-East
Wallonia-Northeast
Wallonia-South

(d)

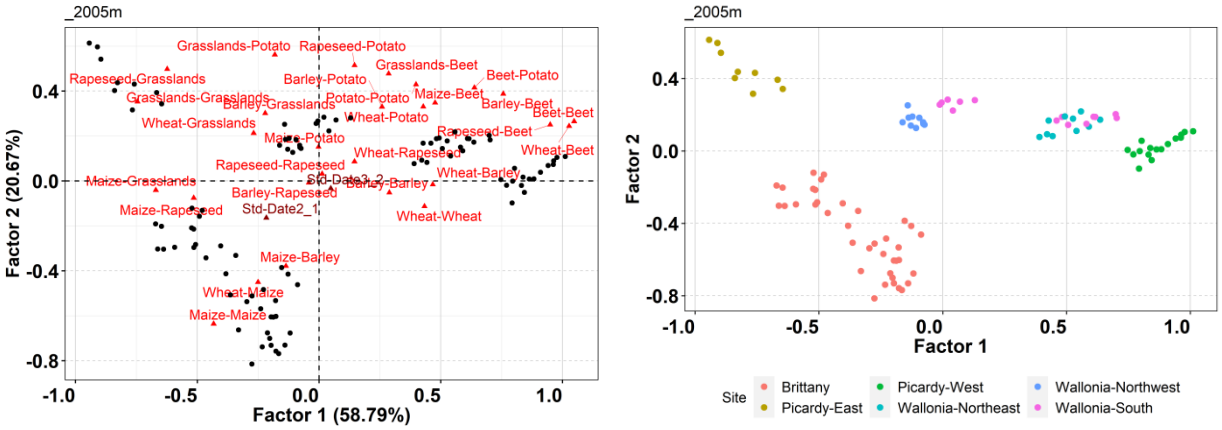
_2005m
Grasslands-Potato
Rapeseed-Potato
Grasslands-Beet
Rapeseed-Grasslands
Barley-Potato
Beet-Potato
Maize-Beet
Grasslands-Grasslands
Barley-Grasslands
Potato-Potato
Barley-Beet
Beet-Beet
Wheat-Grasslands
Wheat-Potato
Maize-Potato
Rapeseed-Beet
Wheat-Rapeseed
Wheat-Beet
Rapeseed-Rapeseed
Wheat-Barley
Maize-Grasslands
Std-Date3_2
Barley-Rapeseed
Barley-Barley
Maize-Rapeseed
Std-Date2_1
Wheat-Wheat
Maize-Barley
Wheat-Maize
Maize-Maize
Factor 2 (20.67%)
Factor 1 (58.79%)
0.4
0.0
-0.4
-0.8
-1.0
0.5
1.0
_2005m
Factor 2
Factor 1
Site
Brittany
Picardy-West
Wallonia-Northwest
Picardy-East
Wallonia-Northeast
Wallonia-South

(e)

Appendix K: Linear regressions between biophysical heterogeneity (WDVI SD) and factor 1 of the correspondence factor analysis (CFA).

Appendix K-1. Linear regressions between WDVI SD and factor 1 of the correspondence factor analysis (CFA) at the 255 m (a, b and c), 505 m (d, e and f), 1005 m (g, h and i), 1505 m (j, k and l) and 2005 m (m, n and o) scales for the six study landscapes during (a, d, g, j and m) stem extension (Date2_Date1) and (b, e, h, k and n) ripening (Date3_Date2) of wheat, and (c, f, i, l and o) between landscape grain and factor 1. Grey zone = the 95% confidence interval.

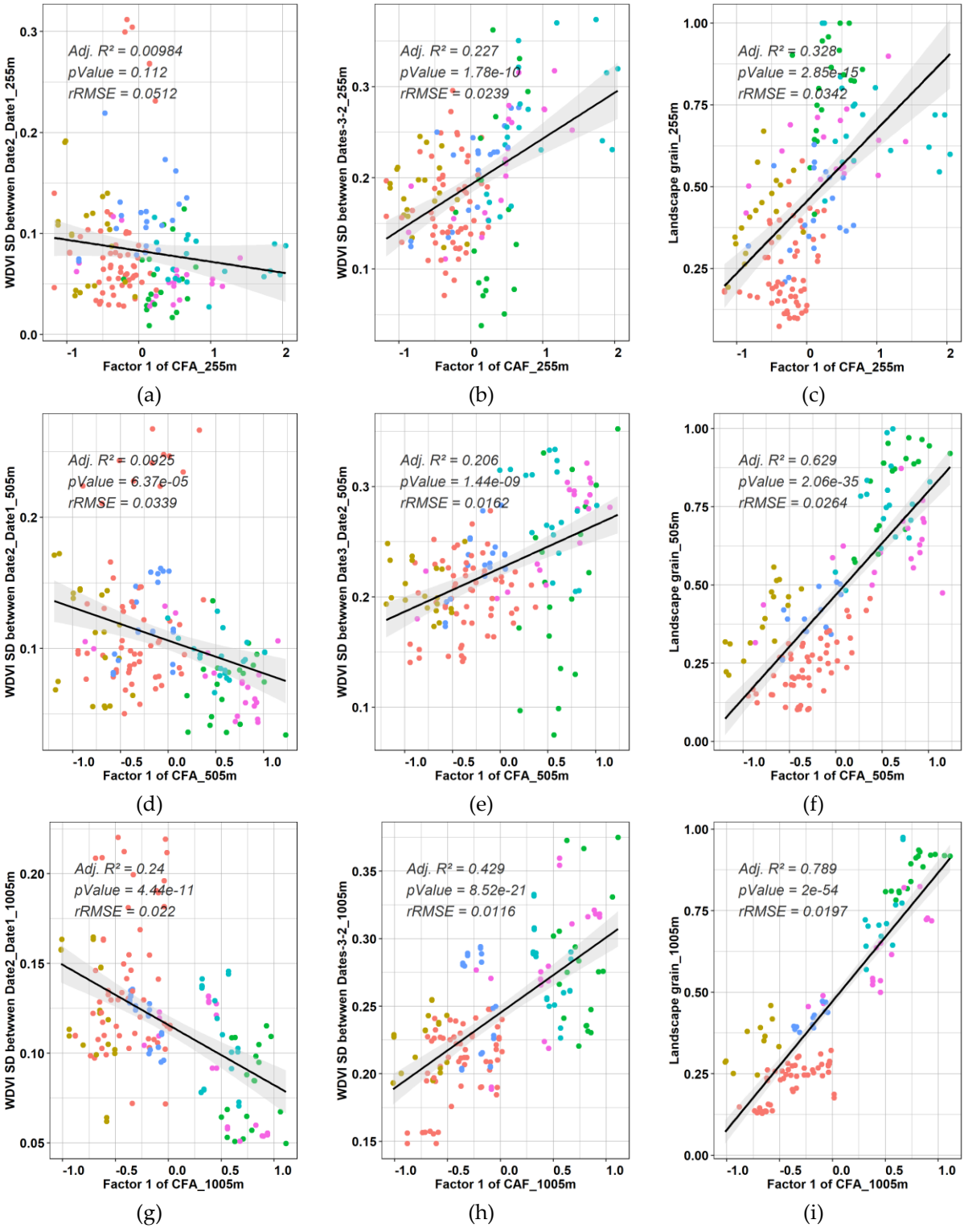

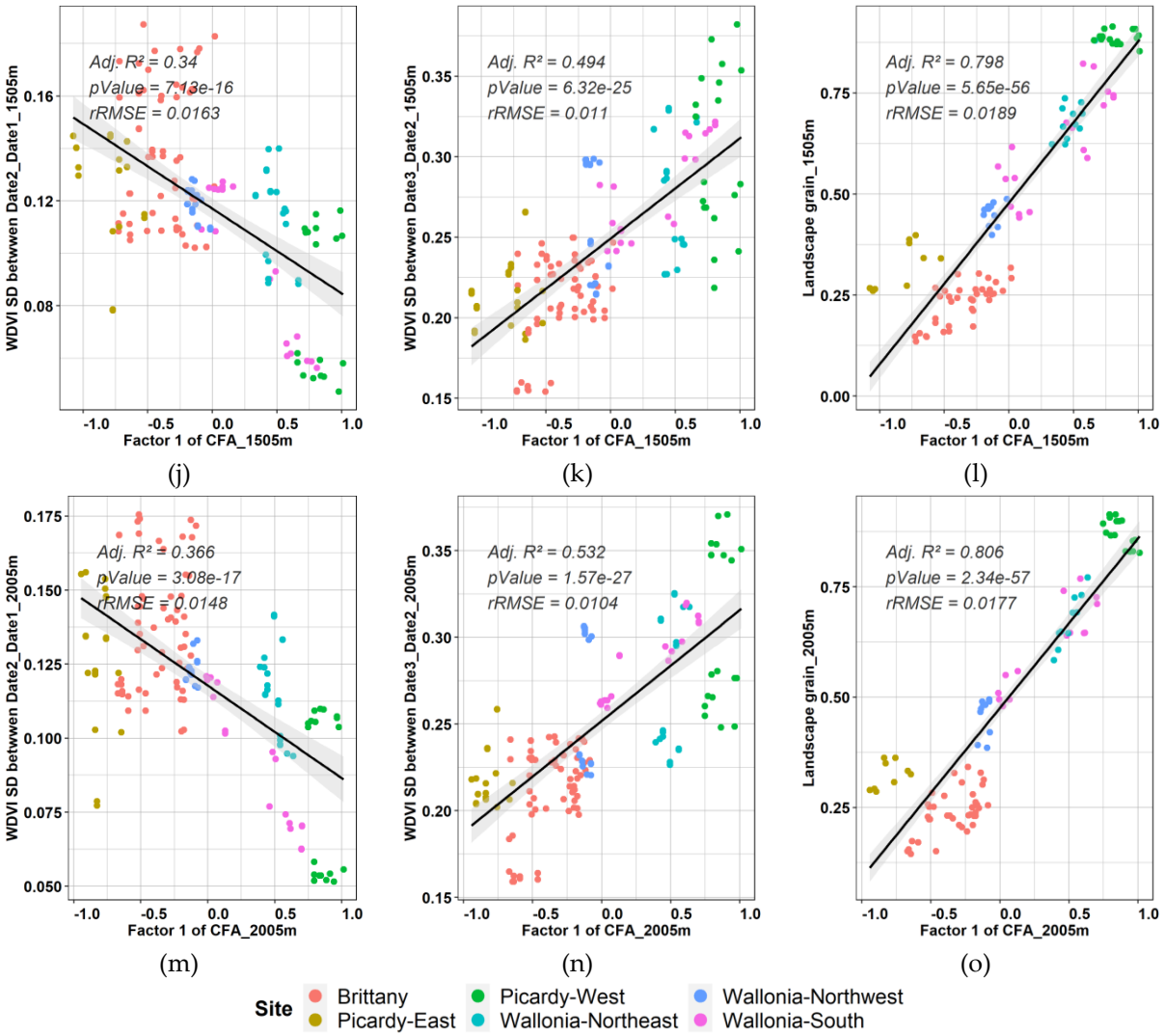
Adj. R² = 0.34
pValue = 7.13e-16
rRMSE = 0.0163
WDVI SD betwwen Date2_Date1_1505m
Factor 1 of CFA_1505m
(j)
Adj. R² = 0.494
pValue = 6.32e-25
rRMSE = 0.011
WDVI SD betwwen Date3_Date2_1505m
Factor 1 of CFA_1505m
(k)
Adj. R² = 0.798
pValue = 5.65e-56
rRMSE = 0.0189
Landscape grain_1505m
Factor 1 of CFA_1505m
(l)
Adj. R² = 0.366
pValue = 3.08e-17
rRMSE = 0.0148
WDVI SD betwwen Date2_Date1_2005m
Factor 1 of CFA_2005m
(m)
Adj. R² = 0.532
pValue = 1.57e-27
rRMSE = 0.0104
WDVI SD betwwen Date3_Date2_2005m
Factor 1 of CFA_2005m
(n)
Adj. R² = 0.806
pValue = 2.34e-57
rRMSE = 0.0177
Landscape grain_2005m
Factor 1 of CFA_2005m
(o)
Site
Brittany
Picardy-East
Picardy-West
Wallonia-Northeast
Wallonia-Northwest
Wallonia-South

Appendix L: Mercier A, Betbeder J, Baudry J, et al (2019a) Evaluation of Sentinel-1 and -2 time series to derive crop phenology and biomass of wheat and rapeseed: northern France and Brittany case studies. In: Remote Sensing for Agriculture, Ecosystems, and Hydrology XXI. International Society for Optics and Photonics, p 1114903

Evaluation of Sentinel-1 & 2 time series to derive crop phenology and biomass of wheat and rapeseed: northern France and Brittany case studies

Audrey Mercier*[a], Julie Betbeder[bc], Jacques Baudry[d], Julien Denize[ae], Vincent Leroux[f], Jean-Luc Roger[d], Fabien Spicher[f], Laurence Hubert-Moy[a]

[a]LETG Rennes, UMR 655, Université Rennes 2, Place du recteur Henri Le Moal, Rennes Cedex 35043, France; [b]CIRAD, Forêts et Sociétés, 34398 Montpellier, France; [c]Ecosystems Modelling Unity, Forests, Biodiversity and Climate Change Program, Tropical Agricultural Research and Higher Education Center (CATIE), Turrialba, Cartago, Costa Rica ; [d]INRA, UMR BAGAP, 65 rue de St-Brieuc CS 84215, Rennes Cedex 35042 ; [e]IETR, UMR CNRS 6164, University of Rennes, 35000 Rennes, France; [f]Unité Ecologie et Dynamiques des Systèmes Anthropisés, UMR 7058 CNRS Université de Picardie Jules Verne, 33 rue St-Leu, 80039 Amiens, France

ABSTRACT

Crop monitoring at a fine scale is critical from an environmental perspective since it provide crucial information to combine increased food production and sustainable management of agricultural landscapes. The recent Synthetic Aperture Radar (SAR) Sentinel-1 (S-1) and optical Sentinel-2 (S-2) time series offer a great opportunity to monitor cropland (structure, biomass and phenology) due to their high spatial and temporal resolutions. In this study, we assessed the potential of Sentinel data to derive Wet Biomass (WB), Dry biomass (DB), water content and crop Phenological Stages (PS). This study focuses on wheat and rapeseed, which represent two of the most important seasonal crops of the world in terms of occupied area. Satellites and ground data were collected over two French temperate agricultural landscapes, in northern France and Brittany. Spectral bands and vegetation indices were derived from the S-2 images and backscattering coefficients and polarimetric indicators from the S-1 images. We used linear models to estimate the Crop Parameters (CP) of wheat and rapeseed crops. Satellite images were then classified using a random forest incremental procedure based on the importance rank of the input features to discriminate PS. Results showed that S-1 features were more efficient than S-2 features to estimate CP of rapeseed while S-2 features were better for wheat. We demonstrated the high potential of S-1 & 2 to predict principal PS (kappa=0.75) while secondary PS were misclassified. For wheat, the succession of PS predicted was consistent, further research is required to confirm the potential of S-1 & 2.

Keywords: Remote sensing, agriculture, optical and SAR satellite images, linear regression, random forest

1. INTRODUCTION

Crop monitoring is crucial for many agricultural and ecological applications such as crop yield estimation [1,2], prevention of diseases and pest outbreaks [3,4], water resources management [5] and fertilizer application [6,7]. Leaf area index (LAI), DB, WB, water content and PS are commonly used for these purposes. Most of these data are acquired using time-consuming ground surveys and therefore cannot be collected at a landscape scale [8]. Remote sensing data can be used to map large spatial areas while maintaining a fine spatial resolution. The free availability of Synthetic Aperture Radar (SAR) Sentinel-1 (S-1) and optical Sentinel-2 (S-2) time series offers a unique opportunity to monitor crops at a high temporal frequency (5-days) and high spatial resolution (10m).

Many studies have focused on the use of optical data (AVHRR, SPOT, Landsat, MODIS, IRS, IKONOS, QuickBird, Formoat-2, Sentinel-2) to estimate crop parameters demonstrating the high performance of vegetation indices and biophysical variables [9–13]. More specifically about Sentinel-2 time series, they showed great potential on pasture and various crops in the estimation of LAI [14–18], biomass [19,20] and phenological stages [19,21]. However, optical data have limitations because they are sensitive to weather conditions and capture top of canopy information rather than vegetation structure. Radar data can be collected regardless of the weather or light conditions. Microwaves are sensitive to the internal structure of vegetation [22,23], but the signal is affected by soil conditions (roughness and moisture) [24]. Polarimetric indicators derived from RADARSAT-2 and TerraSAR-X have showed high sensitivity to biomass [23,25,13,26], LAI [27,25,13,28] and phenological stages [29,30] of various crops. Several studies have highlighted the potential of S-1 time series to estimate crop parameters. A high potential of backscattering coefficients and the ratio of VH:VV polarizations was found in detecting changes in vegetation

structure for rapeseed, maize and winter cereals [31]. The S-1 VV polarization have showed high correlations with water content, wet biomass, dry biomass and LAI of wheat [32], while the VH and VV polarizations were relevant for identifying phenological stages of wheat and rice [33,34]. Despite these encouraging results, to our knowledge, polarimetric indicators derived from S-1 data have not been used to study crop parameters.

The objective of this study was to assess the potential of S-1 data alone, S-2 data alone and their joint use to derive WB, DB, water content and crop PS. We evaluated the performance of spectral bands and vegetation indices derived from S-2 time-series and backscattering coefficients and polarimetric indicators derived from S-1 time-series. We focused on two of the most important crops in the world in terms of harvested area: wheat and rapeseed (Food and Agriculture Organization of the United Nations, 2017). We first assessed the potential of Sentinel data to estimate CP of wheat and rapeseed computing linear regressions between CP including WB, DB and water content and S-1 and S-2 features. Then, we classified principal and secondary PS of wheat and rapeseed. Principal PS are defined as long-duration developmental phases of plants, while secondary PS are short developmental steps within them [35]. In a precedent study [36], we demonstrated the high capacity of S-2 data alone and the combined S-1 & 2 data to predict principal and secondary PS of wheat and rapeseed over northern France. Combined use of S-1 & 2 data and S-2 data alone was significantly more accurate than using S-1 data alone with similar performances in identifying principal and secondary PS for both crops. The $\sigma^0VH{:}\sigma^0VV$ ratio and polarimetric indicators were important for obtaining accurate classifications for both crops. LAI, NDVI and S2REP were the most important features for both crop types while the MCARI was not important. In order to validate these results, we applied the best models developed on the northern France to the study area of Brittany.

2. MATERIALS

2.1 Study areas

Satellites and ground data were collected over two French temperate agricultural landscapes, in northern France and Brittany.

The study area of northern France consisted of two 5 × 5 km sub-sites (Fig. 1). The climate is oceanic with a mean annual temperature of 10°C and mean annual precipitation of 700 mm (Météo France). The western site is located in an open field landscape with intensive cultivation of cereals and sugar beet. The eastern site is located in a "bocage" landscape dominated by grasslands and is characterized by less intensive farming activities (mainly dairy cattle) and smaller fields that tend to be enclosed by hedgerows. Both landscapes contain managed forest fragments that are used mainly for hunting and production of wood [37].

The study area of Brittany is a Long Term Ecological Research site named 'Zone Atelier Armorique (130km²), located in the southern part of the Bay of the Mont-Saint-Michel, France (Fig. 2). The area has a temperate climate with an annual mean temperature of 12 °C and mean annual precipitation of 650 mm. The site contains ca. 7000 agricultural fields surrounded by a hedgerow network. The main annual crops are maize, wheat, rapeseed and barley.

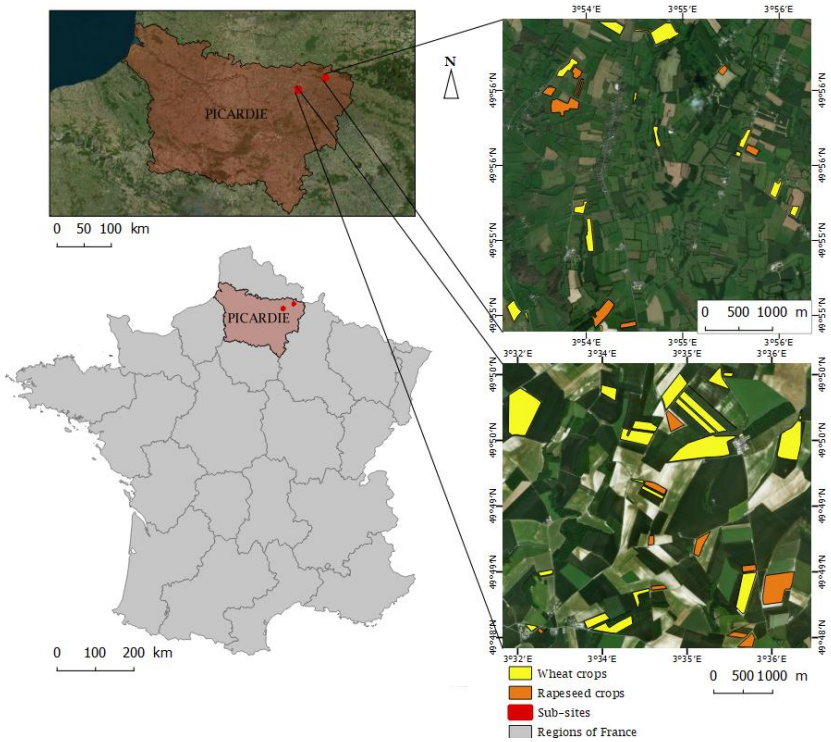

Figure 1. Location of the two sub-sites of the study area of northern France (Sources: © EuroGeographics for the administrative boundaries; Bing © 2019, Microsoft Corporation © 2019, and DigitalGlobe © CNES 2019 Distribution Airbus DS for aerial photographs).

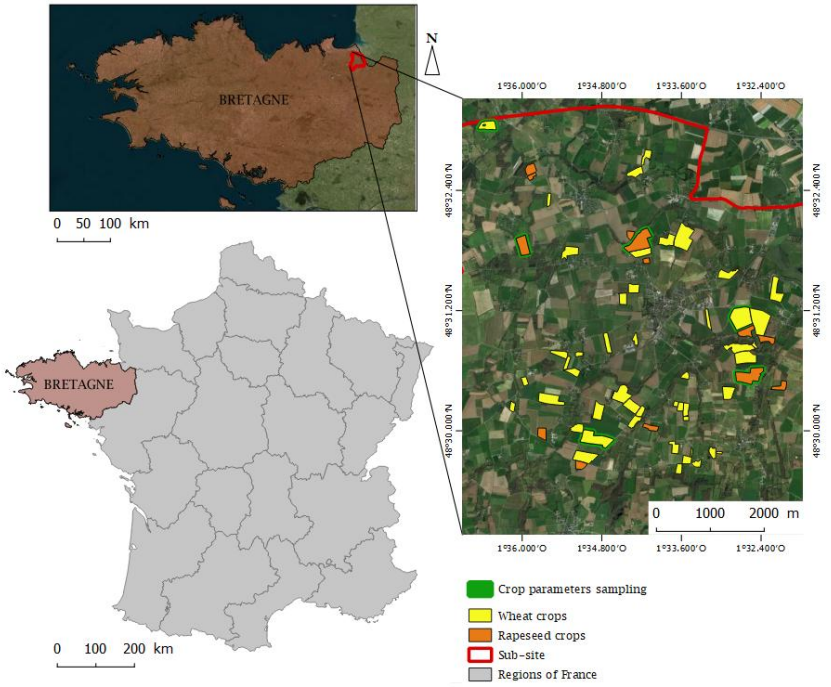

Figure 2. Location of the sub-site of the study area of Brittany (Sources: © EuroGeographics for the administrative boundaries; Bing © 2019, Microsoft Corporation © 2019, and DigitalGlobe © CNES 2019 Distribution Airbus DS for aerial photographs).

2.2 Satellite imagery

A series of five and four optical S-2 and eight and five SAR S-1 images were downloaded over the northern France and Brittany respectively. The entire crop cycles of wheat and rapeseed were recorded downloading images from January to July 2017 (Fig. 3). The S-1 images were acquired in Interferometric Wide (IW) swath mode and delivered with VV and VH polarizations). We used the Single Look Complex (SLC) product, which consists of focused SAR data that use the full C-signal bandwidth and preserve the phase information, to derive polarimetric indicators. The incidence angle of images ranged from 30.6-46.0° (Table 1). The spatial resolution ranged from 2.7-3.5 m, the azimuth spatial resolution was 22 m, and the pixel spacing was 2.3 × 14.1 m (Table 1). According to data recorded at the Météo-France weather station in Saint Quentin (49°49′N, 3°12′E) for northern France and Vieux-Viel for Brittany (48°51′N, 1°55′W), the radar signal was not affected by rainfall or freezing on acquisition dates (Fig. 3).

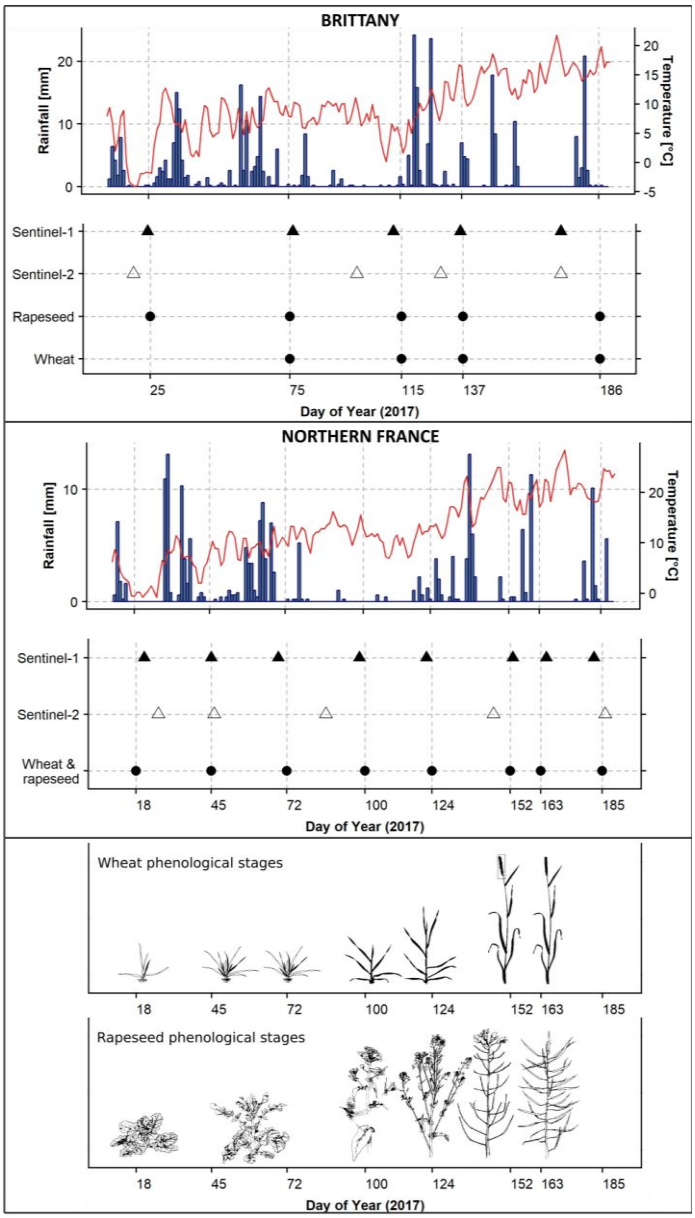

Figure 3. Days of year of satellite images, field surveys and main crop phenological stages over the study area of northern France for wheat and rapeseed [35]. The ombrothermal diagram (Météo France) shows climatic conditions on the image acquisition dates.

Table 1. Main characteristics of Sentinel-1 SLC images.

Band	C (center frequency of 5 405 GHz)
Mode	Interferometric Wide Swath
Product type	Single Look Complex
Ground Resolution	2.3 m
Azimuth resolution	13.9 m
Temporal resolution	6 days
Orbit	Ascending
Polarization	Dual (VV & VH)
Swath	250 km
Incidence angle	30.6-46.0°

The S-2 images were acquired with spatial resolutions of 10 and 20 m, and a spectral resolution of 10 bands (Table 2). The tiles were downloaded in level 2A, which provides Top of Canopy reflectance and a cloud and shadow mask (ESA, 2019b).

Table 2. Main characteristics of Sentinel-2 MSI L2A images.

Spatial and spectral resolutions	*10 × 10 m*
	B2 (490 nm), B3 (560 nm), B4 (665 nm) and B8 (842 nm)
	20 × 20 m
	B5 (705 nm), B6 (740 nm), B7 (783 nm), B8a (865 nm), B11 (1610 nm), B12 (2190 nm)
Temporal resolution	5 days
Swath	290 km

2.3 Field data collection

Ground surveys were conducted on 36 and 19 fields of wheat and rapeseed, respectively over the northern France study areas (Fig. 1) while 47 and 12 fields were sampled over the study area of Brittany (Fig.3). Sizes of wheat and rapeseed fields ranged from 0.27-31.65 ha (mean=5.69 ha) and 0.45-20.92 ha (mean=3.50 ha, median=1.83 ha), respectively. PS were identified on 8 and 5 dates from January to July 2017 over northern of France and Brittany respectively (Fig. 3) based on the Biologische Bundesanstalt, Bundessortenamt and CHemical industry (BBCH) scale [35]. Five principal PS were observed for both crops in the northern of France (Table 3 and 4) and 4 and 5 principal PS were observed in Brittany for wheat and rapeseed, respectively (Table 5 and 6). In addition, for the northern of France study areas, 29 and 15 secondary PS were identified for wheat (Table 3) and rapeseed (Table 4), respectively. The samples of secondary PS available for wheat and rapeseed were grouped into sub-classes to obtain a sufficient number of samples per class to train and validate the classifications.

Biomass measurements were performed in 3 fields of wheat and rapeseed (Fig. 3). In homogeneous areas (20 x 20m), 5 samples with a length of 50 cm were collected for wheat and 5 feet for rapeseed. The WB of each sample was directly weighed in situ, and the DB was measured after crop drying (oven, 65◦C, 48 h). The difference between total biomass and DB correspond to the water content in the plant.

Table 3. Phenological stages of wheat considered in the study area of northern France.

Principal stage	Sub-class	2° stage	Description	Number of observations
Tillering	1	20	No tillers	1
		21	Beginning of tillering: first tiller detectable	14
		22	2 tillers detectable	16
		23	3 tillers detectable	18
	2	24	4 tillers detectable	22
		25	5 tillers detectable	6
		26	6 tillers detectable	8
		29	9 tillers detectable	20
Stem elongation	3	30	Beginning of stem elongation	4
		31	First node at least 1 cm above tillering node	25
		32	Node 2 at least 2 cm above node 1	6
		33	Node 3 at least 2 cm above node	24
		34	Node 4 at least 2 cm above node 3	9
		35	Node 5 at least 2 cm above node 4	3
Flowering, anthesis	4	65	Full flowering: 50% of anthers mature	3
		66	Full flowering: 60% of anthers mature	2
		67	Full flowering: 70% of anthers mature	3
		68	Full flowering: 80% of anthers mature	4
		69	End of flowering	9
Development of fruit	5	71	Watery ripe: first grains have reached half their final size	14
		72	Early milk	2
		73	Early milk	13
		75	Medium milk: grain content milky, grains reached final size, still green	19
		77	Late milk	4
Ripening	6	83	Early dough	10
		84	Early dough	5
		85	Soft dough: grain content soft but dry. Fingernail impression not held	3
	7	87	Hard dough: grain content solid. Fingernail impression held	9
		89	Fully ripe: grain hard, difficult to divide with thumbnail	8

Table 4. Phenological stages of rapeseed considered in the study area of northern France.

Principal stage	Sub-class	2° stage	Description	Number of observations
Leaf development	1	17	7 leaves unfolded	4
		18	Beginning of tillering: first tiller detectable	7
		19	2 tillers detectable	7
Inflorescence emergence	2	50	Flower buds present, still enclosed by leaves	10
		51	Flower buds visible from above (“green bud”)	26
Flowering	3	60	First flowers open	1
		62	20% of flowers on main raceme open	1
		63	30% of flowers on main raceme open	5
		64	40% of flowers on main raceme open	5
	4	65	Full flowering	7
		67	Flowering declining: majority of petals fallen	7
		69	End of flowering	12
Development of fruit	5	77	70% of pods have reached their final size	1
		79	Nearly all pods have reached final size	12
Ripening	6	80	Beginning of ripening	25
	7	89	Fully ripe	19

Table 5. Phenological stages of wheat considered in the study area of Brittany.

Principal stage	2° stage	Description	Number of observations
Tillering	23	3 tillers detectable	47
Stem elongation	31	First node at least 1 cm above tillering node	47
Inflorescence	55	Middle of heading: half of inflorescence emerged	47
Ripening	89	Fully ripe: grain hard, difficult to divide with thumbnail	47

Table 6. Phenological stages of rapeseed considered in the study area of Brittany.

Principal stage	2° stage	Description	Number of observations
Leaf development	18	Beginning of tillering: first tiller detectable	12
Inflorescence emergence	53	Flower buds raised above the youngest leaves	12
Flowering	67	Flowering declining: majority of petals fallen	12
Development of fruit	71	10% of pods have reached their final size	12
Ripening	89	Fully ripe	12

3. METHODS

First, the SAR S-1 and optical S-2 signals were preprocessed and the median was computed at the field scale. Second, we used linear models to estimate the crop parameters (WB, DB, water content) of wheat and rapeseed crops. Finally, we classify principal and secondary PS of wheat and rapeseed using the model developed by [39], we applied the model trained with the northern of France data to the Brittany study area.

3.1 SAR Sentinel-1 image preprocessing

Backscattering coefficients from S-1 images were extracted using the Sentinel-1 Toolbox (ESA, http://step.esa.int/main/toolboxes/sentinel-1-toolbox/). The images were first radiometrically calibrated to transform the digital number (DN, amplitude of the backscattering signal) of each pixel into backscattering coefficients ($\sigma\circ$VV, $\sigma\circ$VH) on a linear scale using the following equation [40]:

$$value(i) = \frac{|DN_i|}{A_i{}^2} \ (1)$$

where A is the information necessary to convert SAR reflectivity into physical units provided in the Calibration Annotation Data Set in the image metadata.

A refined Lee filter was then applied in a window of 7 × 7 pixels to reduce speckle noise [41]. The images were geocoded using Shuttle Radar Topography Mission data to correct topographic deformations (geometric correction accuracy < 1 pixel). A backscattering ratio was calculated by dividing $\sigma\circ$VH by $\sigma\circ$VV. All images were then converted from linear to decibel (dB) scale using the following equation:

$$\sigma^0(db) = 10 \times log_{10}(\sigma^0) \ (2)$$

A 2 × 2 covariance matrix (C_2) was first extracted from the scattering matrix S of each SLR image using PolSARpro version 5.1.3 software [42]. A refined Lee filter was then applied in a window of 7 × 7 pixels to reduce speckle noise [41]. Then, we calculated the SPAN, which corresponds to the total scattered power (sum of volume-scattering, double-bounce scattering, and surface or single-bounce scattering mechanisms). Shannon Entropy (SE), which measures the randomness of scattering of a pixel (e.g. due to variation in backscattering power or polarization), was calculated from the covariance matrix (C_2) using the following equation:

$$SE = \log(\pi^2 e^2 |C_2|) = SE_i + SE_p \ (3)$$

where SE_i is related to the intensity and SE_p to the degree of polarization.

Finally, SE, SE_i and SE_p were normalized as $SE\ norm$, $SE_i\ norm$ and $SE_p\ norm$ using PolSARpro version 5.1.3 software.

3.2 Optical Sentinel-2 image preprocessing

Twelve vegetation indices were calculated since their potential to monitor crop parameters (LAI, chlorophyll content and PS) using S-2 data has been demonstrated [43,15,44,45,16]. We calculated NDVI, the Green Normalized Vegetation Index (GNDVI), the Red-Edge Inflation Point (REIP) index, the Inverted Red-Edge Chlorophyll Index (IRECI), the Sentinel-2 Red-Edge Position (S2REP) index, the Modified Chlorophyll Absorption in Reflectance Index (MCARI), the MERIS Terrestrial Chlorophyll Index (MTCI), the Soil-Adjusted Vegetation Index (SAVI), the Modified Soil-Adjusted Vegetation Index (MSAVI), the Weighted Difference Vegetation Index (WDVI), the Pigment Specific Simple Ratio (PSSRa) and the Normalized Difference Index (NDI).

Table 7. Vegetation indices calculated from Sentinel-2 images. G = Green, R = Red, RE = Red-Edge, NIR = Near-infrared.

Index	Equation	S-2 bands used	Original author
GNDVI	(RE3 - G) / (RE3 + G)	(B7 - B3) / (B7 + B3)	[46]
IRECI	(RE3 - R) / (RE1 / RE2)	(B7 - B4) / (B5 / B6)	[47]
MCARI	[(RE1 - R) 0.2(RE1 - G)] * (RE1 - R)	[(B5 - B4) - 0.2(B5 - B3)] * (B5 - B4)	[43]
MSAVI	(1 + L) * (NIR- R) / (NIR + R + 0,5)	(1 + L) * (B8- B4) / (B8 + B4 + 0,5)	[48]
	L = 1 – 2 * 0,5 * (RE3 – R) / (RE3 + R)	L = 1 – 2 * 0,5 * (B7 – B4) / (B7+B4)	
	* (NIR – 0,5 * R)	* (B8 – 0,5 * B4)	
MTCI	(RE2 - RE1)/(RE1 - R)	(B6 - B5)/(B5 - B4)	[49]
NDI	(RE1 - R) / (RE1 + R)	(B5 - B4) / (B5 + B4)	[50]
NDVI	(RE3-R)/(RE3+R)	(B7-B4)/(B7+B4)	[51]
PSSRa	RE3/R	B7/B4	[52]
REIP	700 + 40 * ((R + RE3)/2 - RE1) / (RE2 - RE1)	700 + 40 * ((B4 + B7)/2 - B5) / (B6 - B5)	[47]
S2REP	705 + 35 - ((((RE3 + R)/2) - RE1)/(RE2 -RE1))	705 + 35 * ((((B7 + B4)/2) B5)/(B6 - B5))	[47]
SAVI	(1 + 0,5) * (NIR- R) / (NIR + R + 0,5)	(1 + 0,5) * (B8- B4) / (B8 + B4 + 0,5)	[53]
WDVI	(NIR – 0,5 * R)	(B8 – 0,5 * B4)	[54]

LAI, fapar and fcover, three biophysical variables that describe the state of vegetation cover and provide information on the density of green vegetation, were also derived from S-2 images using the PROSAIL radiative transfer model implemented in SNAP v6.0 software. The spectral bands, vegetation indices and the biophysical variables were interpolated daily using a spline method to match the dates of SAR S-1 acquisition using the stats package of R software. All S-1 and S-2 images were projected onto the RGF93/Lambert-93 system (EPSG 2154).

In total, we preprocessed 325 S-2 features (10 spectral bands, 12 vegetation indices and 3 biophysical variable × 8 dates for northern France and 5 for Brittany) and 91 S-1 features (2 backscattering coefficients, 1 backscatter ratio and 4 polarimetric indicators × 8 dates for northern France and 5 for Brittany).

3.3 Crop parameters estimation

WB, DB, water content were transformed computing the binary logarithm (log2) to assess normal distribution. Then, linear regressions were established between S-1 & 2 features and the crop parameters using the following equation:

$$CP = a \times RSI + b \quad (4)$$

where CP is related to the crop parameter (WB, DB, water content) and RSI to the remote sensing indicator (S-1 or S-2 features). For each relation, we computed the adjusted R^2 related to the fraction of variance explained by the model and the relative root mean square error (rRMSE) calculated by dividing the RMSE by the mean observed data.

3.4 Phenological stages predictions

In order to validate the results obtained on the northern France in a precedent study [36], we applied the best model developed to the study area of Brittany using a random forest classifier. Based on the results of Mercier et al [36], for the prediction of the principal and secondary PS of wheat, the number of input S-1 & 2 features were 6 (VH:VV, LAI, SEp norm, S2REP, VV, and SE norm) and 7 (VH:VV, LAI, NDVI, S2REP, SE norm, SEi norm, SEp norm), respectively. For rapeseed, we selected VH, NDVI, S2REP, SE norm and span for the principal PS prediction and NDVI, SE norm, LAI, VH and VH:VV for the secondary PS. The kappa index and the overall accuracy were calculated to estimate the accuracy of the classifications of rapeseed principal PS [55], while visual analysis was conducted for principal PS classification of wheat due to different PS available between the northern France and Brittany study areas.

4. RESULTS AND DISCUSSION

4.1 Crop parameters estimation

Concerning the estimation of wheat CP using S-2 features, the correlations were highest with fcover, LAI, REIP and S2REP to estimate the water content (Fig. 4). The band 2 (blue) demonstrated the best performance for estimating DB and WB while other S-2 features demonstrated poor capacity (Fig. 4). The results of the blue band are to be confirmed because previous studies have showed better sensitivities of wheat biomass in the green or NIR spectral domains [56,57]. The relationships between wheat CP and the blue band (Fig. 6a) was very influenced by 3 points with a low biomass, the distribution of points along the regression line was not homogeneous, thus a larger sample size would confirm the performance of the blue band. For rapeseed, the best results for all CP were from the bands 11 and 12 corresponding to the SWIR domain, while vegetation indices appeared not useful (Fig. 5). Some studies have already demonstrated the high performance of the SWIR bands for vegetation mapping [58,59] but to our knowledge, none of them have studied its interest in rapeseed mapping, thus further research is warranted.

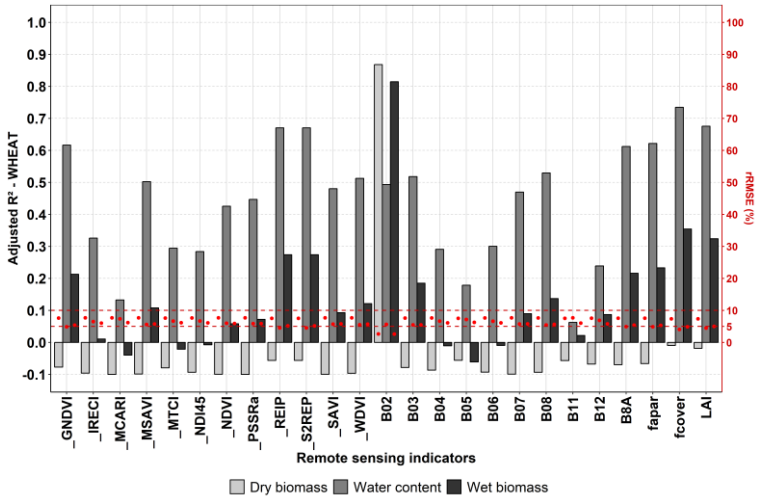

Figure 4. Adjusted R^2 and rRMSE of empirical relationships established between the S-2 features and the crop parameters on wheat fields.

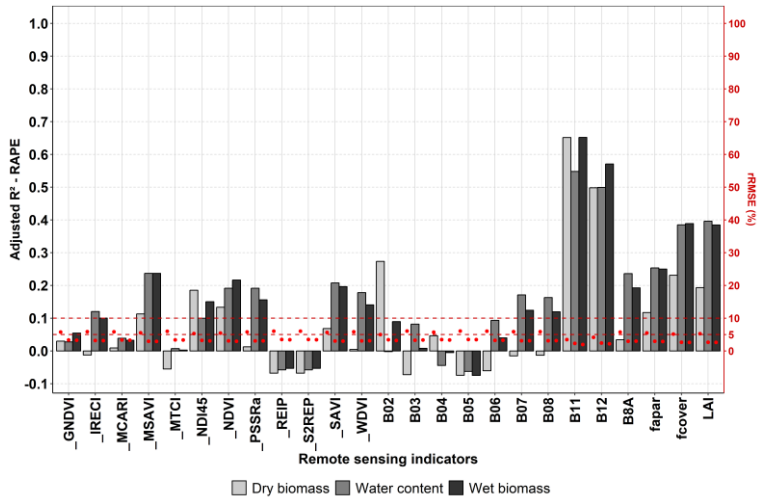

Figure 5. Adjusted R² and rRMSE of empirical relationships established between the S-2 features and the crop parameters on rapeseed fields.

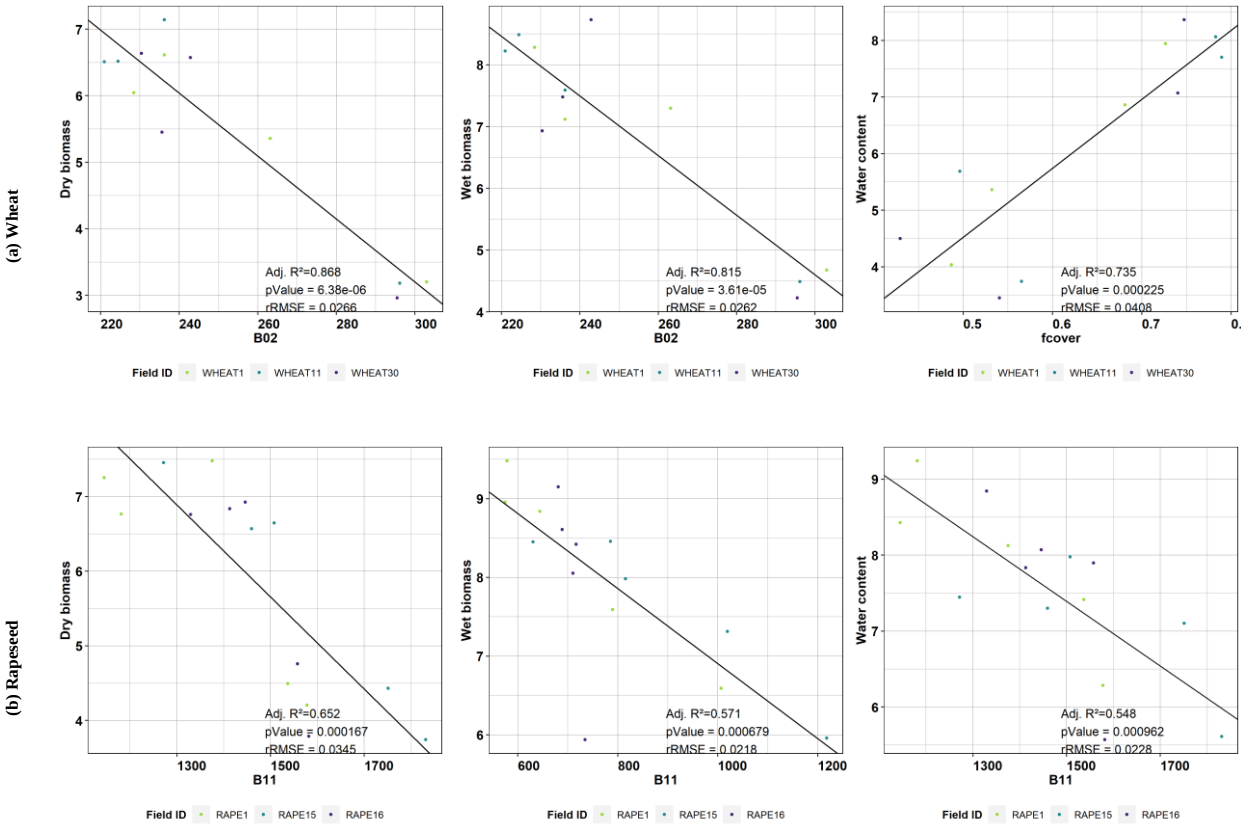

Figure 6. Best relationships obtained between wheat **(a)** and rapeseed **(b)** DB, WB and water content and S-2 features.

Table 8. Parameter values (a and b) of the best linear relationships established between the crop parameters of wheat and rapeseed and S-2 features. Their corresponding statistics for determination coefficient and relative root mean square error are also given.

Crop parameter	RSI	a	b	Adj. R²	rRMSE

Wheat					
DB	band 2	-0.047	17.399	0.87	0.03
WB	band 2	-0.048	19.068	0.81	0.03
Water content	fcover	12.188	-1.571	0.73	0.04
Rapeseed					
DB	band 11	-0.006	14.911	0.65	0.03
WB	Band 11	-0.005	14.980	0.57	0.02
Water content	band 11	-0.004	13.776	0.55	0.02

For both crop types, water content was better estimated using S-1 features than S-2 features (Fig. 7 and 8). For wheat, correlations between DB and S-1 features did not exceed 0.4 of adj. R^2 (Fig.7). This may be explained by the sensitivity of SAR signal to the wetness of the vegetation [22,60]. The ratio VH:VV polarizations and the polarization of the Shannon entropy showed the best performances for rapeseed (Fig.8) and the lowest for wheat (Fig.7). The Shannon entropy decreased with wheat biomass (Fig. 9a and table 9) and the ratio VH:VV increased with rapeseed biomass (Fig. 9b and table 9). Compared to wheat, rapeseed have a more complex structure with a development of the stems without preferred orientations, this induces an increase of the disorder encountered in the radar signal (Shannon entropy) and the volume-scattering mechanism (VH) [61].

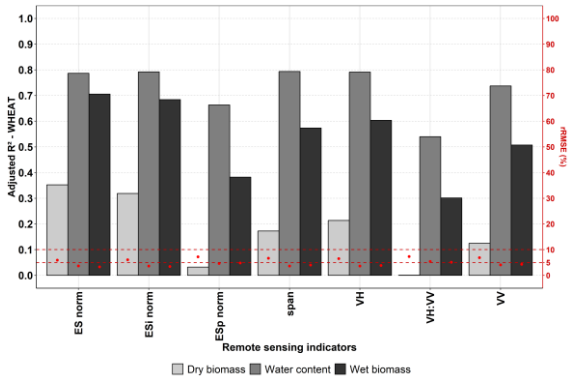

Figure 7. Adjusted R^2 and rRMSE of empirical relationships established between the S-1 features and the crop parameters on wheat fields.

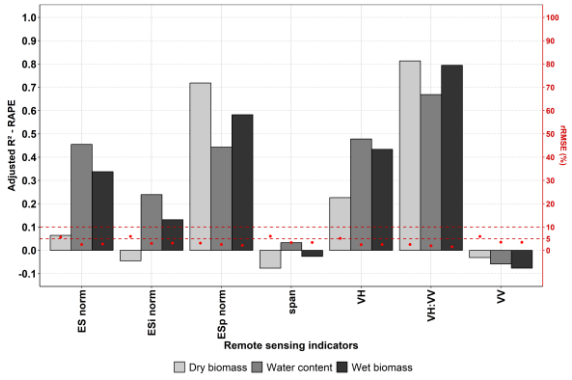

Figure 8. Adjusted R^2 and rRMSE of empirical relationships established between the S-1 features and the crop parameters on rapeseed fields.

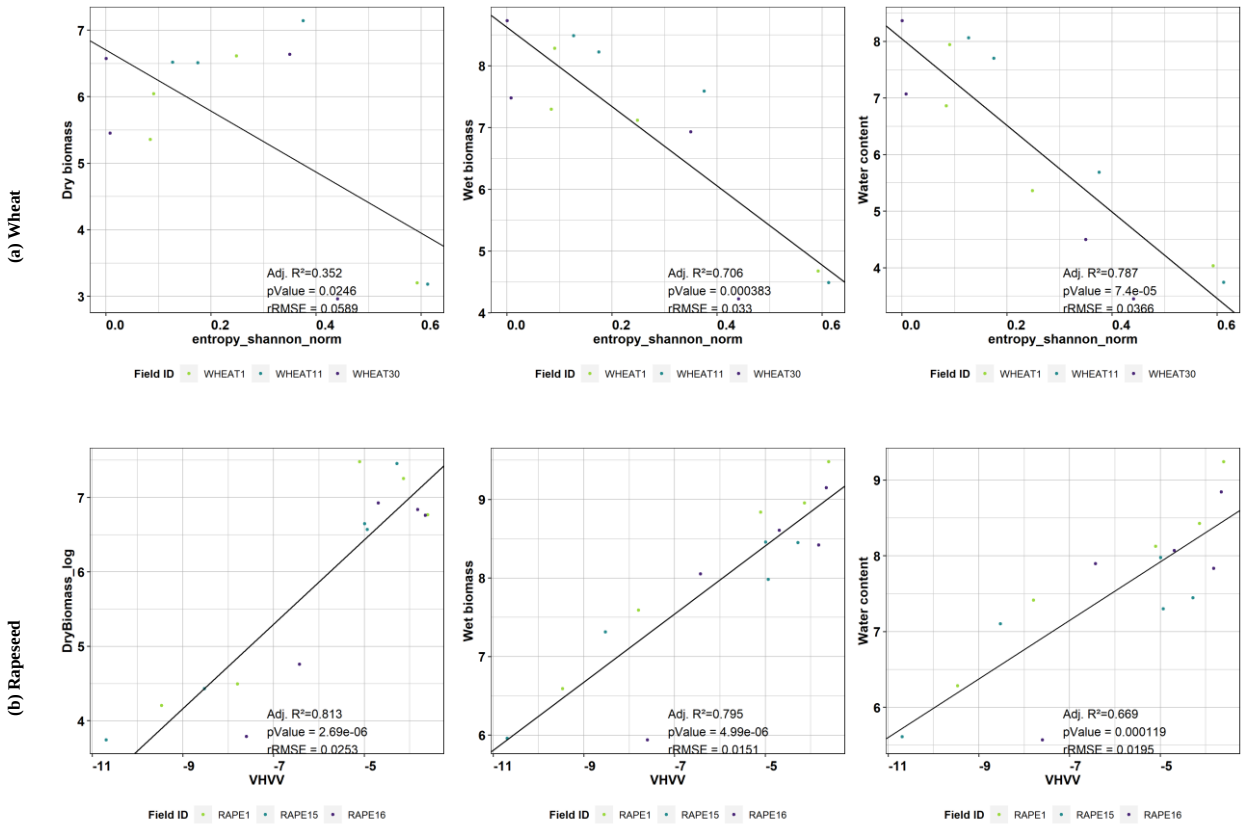

Figure 9. Best relationships obtained between wheat **(a)** and rapeseed **(b)** DB, WB and water content and S-1 features.

Table 9. Parameter values (a and b) of the best linear relationships established between the crop parameters of wheat and rapeseed and S-1 features. Their corresponding statistics for determination coefficient and relative root mean square error are also given.

Crop parameter	RSI	a	b	Adj. R^2	rRMSE
Wheat					
DB	ES norm	-4.59	5.70	0.35	0.06
WB	ES norm	-6.42	8.62	0.71	0.03
Water content	ES norm	-7.64	8.04	0.79	0.04
Rapeseed					
DB	VH:VV	0.56	9.27	0.81	0.02
WB	VH:VV	0.43	10.58	0.79	0.01
Water content	VH:VV	0.39	9.85	0.67	0.02

4.2 Phenological stages predictions

The figures 10 and 11 present the predictions of principal and secondary PS of wheat respectively, on the Brittany study area. Based on the ground surveys (Table 10), on January 24, 2017, the wheat was at the leaf development stage, this stage was not observed on the training data, in the northern France, thus the predictions of the first class “tillering” as the principal PS (Fig. 10) and “beginning of tillering” as the secondary PS (Fig. 11) were coherent. On March 3, 2017, there was much confusion between the observed stage “stem elongation” and the tillering and flowering stages for both PS typologies. On April 22, 2017, the map was correct by predicting the stem elongation stage. The inflorescence stage was observed on May 16, 2017, however, this stage was not present in the training data, the prediction of principal PS result was a prediction of stem elongation and flowering which is consistent since these are the two adjacent stages of the observed stage. Finally, on June 21, 2017, the classifier predicted development of fruit for principal and secondary PS while we supposed the wheat was at the beginning of ripening since we observed the end of ripening on July, 5 2017.

Table 10. Ground surveys dates for wheat

Principal stage	2° stage	Date of sample
Tillering	23	17 march 2017
Stem elongation	31	22 april 2017
Inflorescence	55	16 may 2017
Ripening	89	5 july 2017

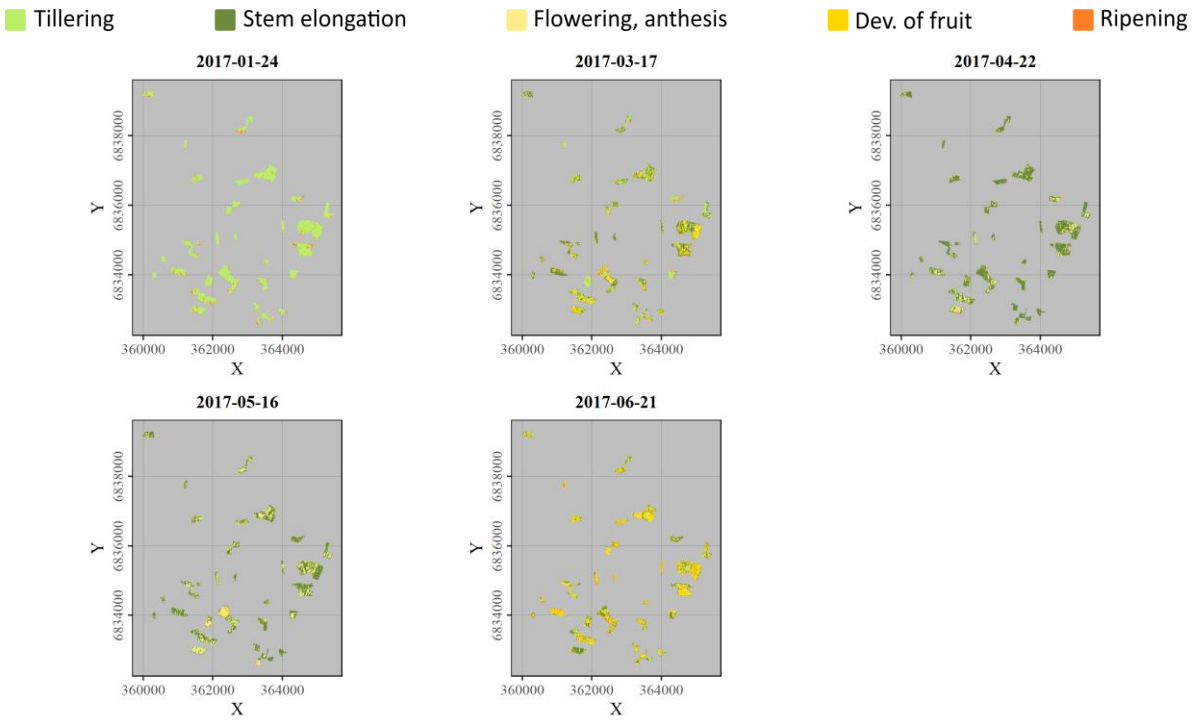

Figure 10. Classification of the principal phenological stages of wheat in the Brittany study area.

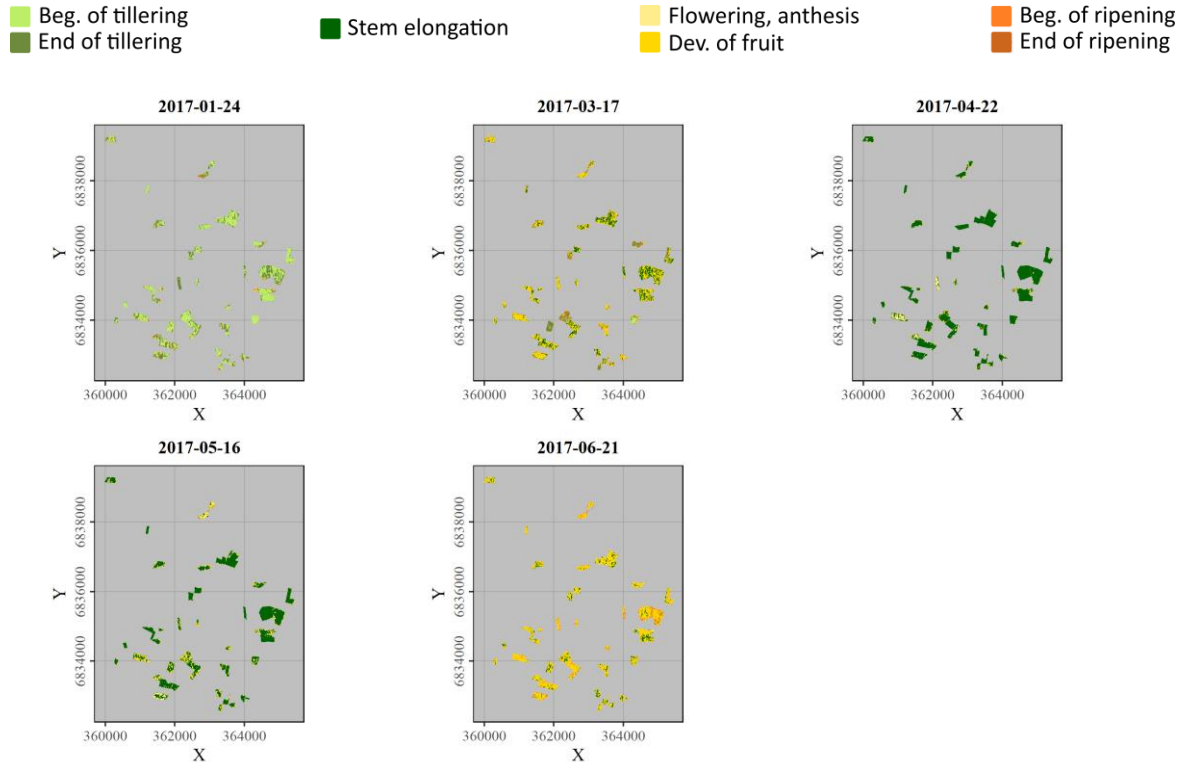

Figure 11. Classification of the secondary phenological stages of wheat in the Brittany study area.

The figures 12 and13 present the predictions of principal and secondary PS of rapeseed respectively, on the Brittany study area. The principal PS were very well predicted with a kappa of 0.75 and an overall accuracy of 80% (Table 12), only one confusion between fruit development and ripening occurred on May 16, 2017 (Table 11 and 12, Fig. 12). The secondary PS were misclassified except for the ripening on June 21, 2017 (Table 11, Fig. 13).

Table 11. Ground surveys dates for rapeseed

Principal stage	2° stage	Date of sample
Leaf development	18	24 january 2017
Inflorescence emergence	53	17 march 2017
Flowering	67	22 april 2017
Development of fruit	71	16 may 2017
Ripening	89	5 july 2017

Table 12. Confusion matrix of the principal phenological stages of rapeseed classification.

Classification	Code	Validation					Total
		1	2	3	4	5	
Leaf development	**1**	**13**	**1**				**14**
Inflorescence emergence	**2**		**12**				**12**
Flowering	**3**			**13**	1		**14**
Development of fruit	**4**				**2**		**2**
Ripening	**5**				10	**12**	**22**
Total		**13**	**13**	**13**	**13**	**12**	
Kappa index	**0.75**						
Overall Accuracy	**80%**						

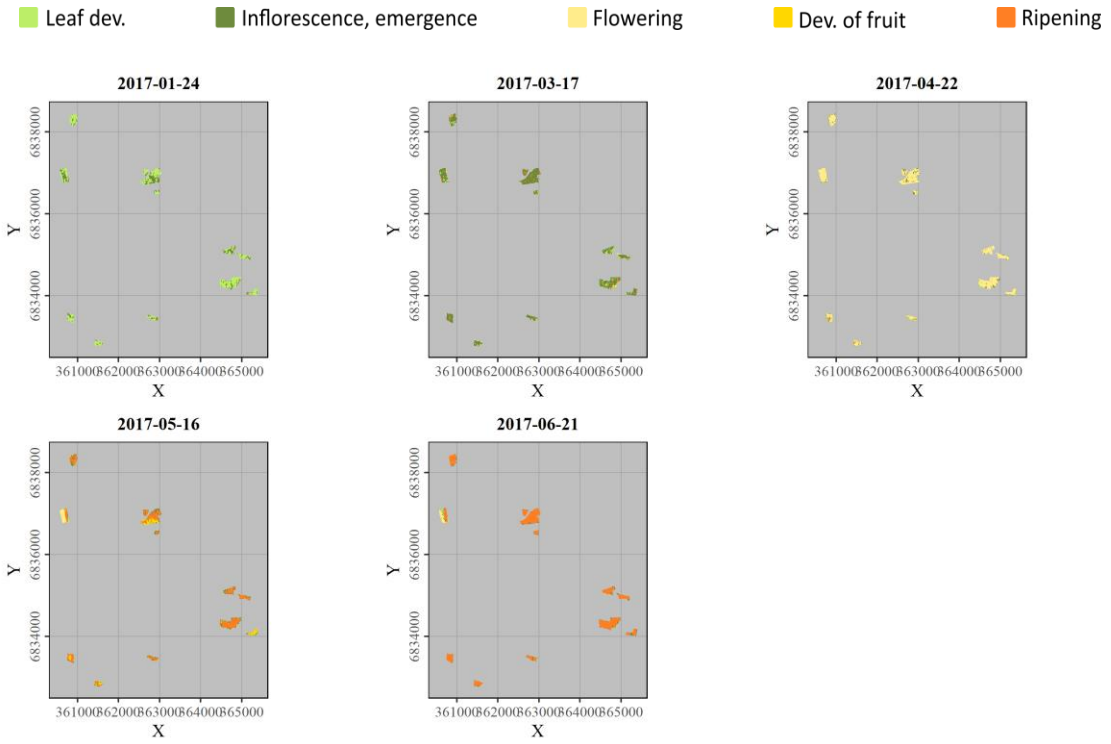

Figure 12. Classification of the principal phenological stages of rapeseed in the Brittany study area.

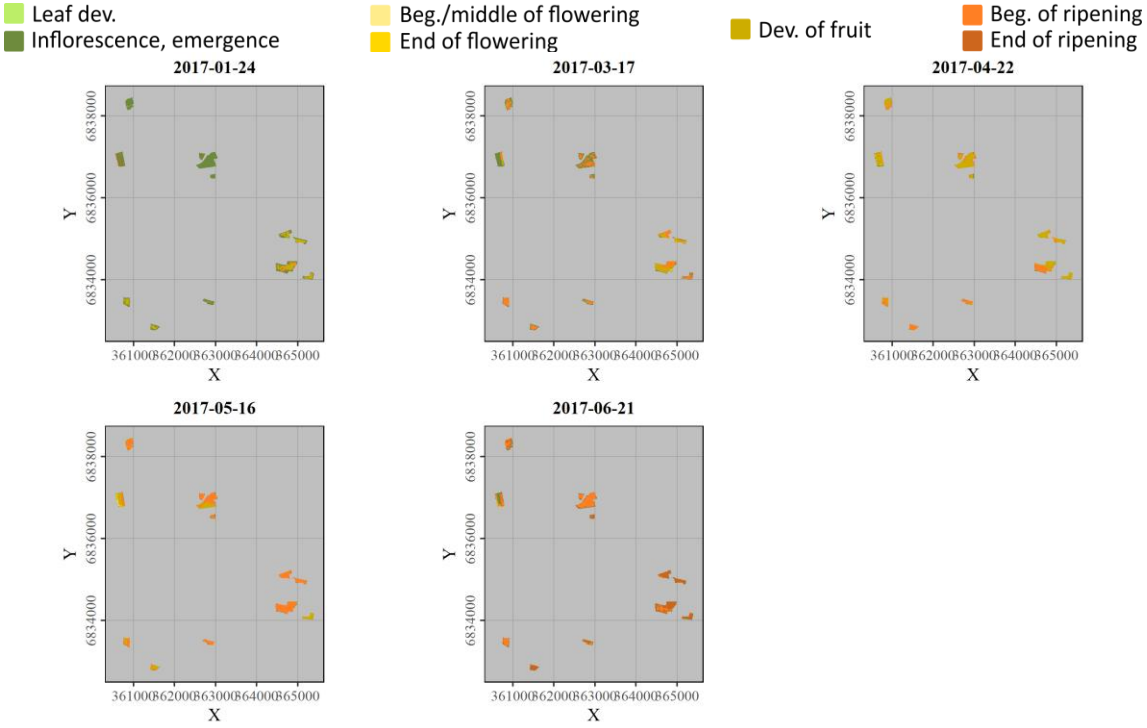

Figure 13. Classification of the secondary phenological stages of rapeseed in the Brittany study area.

The principal PS of rapeseed have been very well predicted with training using data from the northern France and validation from Brittany. However, numerous misclassifications have been observed to predict the secondary PS because they are more sensitive to phenomena occurring at landscape and local scales. For wheat, results of principal and secondary PS were moderate. Due to the typology of the validation samples, it was difficult to confirm each predicted class but we can note a correct prediction of the stem elongation stage and a consistent

succession of PS. These results confirmed that the method used was robust in predicting the principal PS of rapeseed and promising for the principal and secondary PS of wheat.

5. CONCLUSION

This study evaluated the potential of SAR S-1 and optical S-2 time series to estimate CP (WB, DB and water content), principal and secondary PS of wheat and rapeseed. For wheat CP estimation results, highest correlations were found using the blue band of S-2 and the Shannon entropy of S-1. Based on the distribution of points along the regression lines, the results obtained with S-1 features are more reliable than those obtained with S-2 features. For rapeseed, S-1 features showed better performance than S-2 features to estimate CP, the best performances were obtained using he ratio VH:VV polarizations (adj. $R^2 > 0.79$ for DB and WB). For PS predictions, the results confirmed that the incremental method used was robust by training the model on one site and validating on another. Combined used of S-1 & 2 was accurate to identify the principal PS of rapeseed while the results of wheat PS are promising.

Funding: This research was funded through the 2015-2016 BiodivERsA COFUND call for research proposals, with the national funders ANR, MINECO, and BELSPO and was supported by the Kalideos project, funded by the CNES and the Zone Atelier Armorique project and a Ph.D. grant from the Ministry of Research for A. Mercier.

Acknowledgments: We would like to thank Napo N'Bohn, Julien Racoux and David Roger for their help in collecting field data.

6. REFERENCES

[1] Maas, S. J., "Use of remotely-sensed information in agricultural crop growth models," Ecol. Model. **41**(3), 247–268 (1988).

[2] Jin, X., Kumar, L., Li, Z., Feng, H., Xu, X., Yang, G. and Wang, J., "A review of data assimilation of remote sensing and crop models," Eur. J. Agron. **92**, 141–152 (2018).

[3] Hatfield, P. L. and Pinter, P. J., "Remote sensing for crop protection," Crop Prot. **12**(6), 403–413 (1993).

[4] Vreugdenhil, M., Pfeil, I., Riffler, M., Kolitzus, D., Dorninger, P. and Wagner, W., "Monitoring vegetation dynamics using Sentinel-1 and Sentinel-2," presented at EGU General Assembly Conference Abstracts, 1 April 2018, 12559.

[5] Duchemin, B., Fieuzal, R., Rivera, M. A., Ezzahar, J., Jarlan, L., Rodriguez, J. C., Hagolle, O. and Watts, C., "Impact of Sowing Date on Yield and Water Use Efficiency of Wheat Analyzed through Spatial Modeling and FORMOSAT-2 Images," Remote Sens. **7**(5), 5951–5979 (2015).

[6] Diacono, M., Rubino, P. and Montemurro, F., "Precision nitrogen management of wheat. A review," Agron. Sustain. Dev. **33**(1), 219–241 (2013).

[7] Bouchet, A.-S., Laperche, A., Bissuel-Belaygue, C., Snowdon, R., Nesi, N. and Stahl, A., "Nitrogen use efficiency in rapeseed. A review," Agron. Sustain. Dev. **36**(2), 38 (2016).

[8] Duchemin, B., Maisongrande, P., Boulet, G. and Benhadj, I., "A simple algorithm for yield estimates: Evaluation for semi-arid irrigated winter wheat monitored with green leaf area index," Environ. Model. Softw. **23**(7), 876–892 (2008).

[9] Quarmby, N. A., Milnes, M., Hindle, T. L. and Silleos, N., "The use of multi-temporal NDVI measurements from AVHRR data for crop yield estimation and prediction," Int. J. Remote Sens. **14**(2), 199–210 (1993).

[10] Doraiswamy, P. C., Hatfield, J. L., Jackson, T. J., Akhmedov, B., Prueger, J. and Stern, A., "Crop condition and yield simulations using Landsat and MODIS," Remote Sens. Environ. **92**(4), 548–559 (2004).

[11] Mulla, D. J., "Twenty five years of remote sensing in precision agriculture: Key advances and remaining knowledge gaps," Biosyst. Eng. **114**(4), 358–371 (2013).

[12] Bontemps, S., Arias, M., Cara, C., Dedieu, G., Guzzonato, E., Hagolle, O., Inglada, J., Matton, N., Morin, D., Popescu, R., Rabaute, T., Savinaud, M., Sepulcre, G., Valero, S., Ahmad, I., Bégué, A., Wu, B., De Abelleyra, D., Diarra, A., et al., "Building a Data Set over 12 Globally Distributed Sites to Support the Development of Agriculture Monitoring Applications with Sentinel-2," Remote Sens. **7**(12), 16062–16090 (2015).

[13] Betbeder, J., Fieuzal, R., Philippets, Y., Ferro-Famil, L. and Baup, F., "Contribution of multitemporal polarimetric synthetic aperture radar data for monitoring winter wheat and rapeseed crops," J Appl Remote Sens **10**(2), 026020 (2016).

[14] Delegido, J., Verrelst, J., Alonso, L. and Moreno, J., "Evaluation of Sentinel-2 Red-Edge Bands for Empirical Estimation of Green LAI and Chlorophyll Content," Sensors **11**(7), 7063–7081 (2011).
[15] Frampton, W. J., Dash, J., Watmough, G. and Milton, E. J., "Evaluating the capabilities of Sentinel-2 for quantitative estimation of biophysical variables in vegetation," ISPRS J Photogramm Remote Sens **82**, 83–92 (2013).
[16] Clevers, J. G. P. W., Kooistra, L. and Van den Brande, M. M. M., "Using Sentinel-2 Data for Retrieving LAI and Leaf and Canopy Chlorophyll Content of a Potato Crop," Remote Sens. **9**(5), 405 (2017).
[17] Pan, H., Chen, Z., Ren, J., Li, H. and Wu, S., "Modeling Winter Wheat Leaf Area Index and Canopy Water Content With Three Different Approaches Using Sentinel-2 Multispectral Instrument Data," IEEE J Sel Top Appl Earth Obs Remote Sens, 1–11 (2018).
[18] Wang, J., Xiao, X., Bajgain, R., Starks, P., Steiner, J., Doughty, R. B. and Chang, Q., "Estimating leaf area index and aboveground biomass of grazing pastures using Sentinel-1, Sentinel-2 and Landsat images," ISPRS J. Photogramm. Remote Sens. **154**, 189–201 (2019).
[19] Veloso, A., Mermoz, S., Bouvet, A., Le Toan, T., Planells, M., Dejoux, J.-F. and Ceschia, E., "Understanding the temporal behavior of crops using Sentinel-1 and Sentinel-2-like data for agricultural applications," Remote Sens Env. **199**, 415–426 (2017).
[20] Ghosh, P., Mandal, D., Bhattacharya, A., Nanda, M. K. and Bera, S., "Assessing Crop Monitoring Potential of SENTINEL-2 in a Spatio-Temporal Scale," ISPRS - Int. Arch. Photogramm. Remote Sens. Spat. Inf. Sci. **425**, 227–231 (2018).
[21] Stendardi, L., Karlsen, S. R., Niedrist, G., Gerdol, R., Zebisch, M., Rossi, M. and Notarnicola, C., "Exploiting Time Series of Sentinel-1 and Sentinel-2 Imagery to Detect Meadow Phenology in Mountain Regions," Remote Sens. **11**(5), 542 (2019).
[22] Fieuzal, R., Baup, F. and Marais-Sicre, C., "Monitoring Wheat and Rapeseed by Using Synchronous Optical and Radar Satellite Data—From Temporal Signatures to Crop Parameters Estimation," Adv Remote Sens **02**(02), 162–180 (2013).
[23] Wiseman, G., McNairn, H., Homayouni, S. and Shang, J., "RADARSAT-2 Polarimetric SAR Response to Crop Biomass for Agricultural Production Monitoring," IEEE J Sel Top Appl Earth Obs Remote Sens **7**(11), 4461–4471 (2014).
[24] McNairn, H. and Brisco, B., "The application of C-band polarimetric SAR for agriculture: a review," Can J Remote Sens. **30**(3), 525–542 (2004).
[25] Jin, X., Yang, G., Xu, X., Yang, H., Feng, H., Li, Z., Shen, J., Lan, Y. and Zhao, C., "Combined Multi-Temporal Optical and Radar Parameters for Estimating LAI and Biomass in Winter Wheat Using HJ and RADARSAR-2 Data," Remote Sens. **7**(10), 13251–13272 (2015).
[26] Homayouni, S., McNairn, H., Hosseini, M., Jiao, X. and Powers, J., "Quad and compact multitemporal C-band PolSAR observations for crop characterization and monitoring," Int J Appl Earth Obs Géoinf **74**, 78–87 (2019).
[27] Jiao, X., McNairn, H., Shang, J., Pattey, E., Liu, J. and Champagne, C., "The sensitivity of RADARSAT-2 quad-polarization SAR data to crop LAI," Remote Sens. Model. Ecosyst. Sustain. VI **7454**, 74540O, International Society for Optics and Photonics (2009).
[28] Canisius, F., Shang, J., Liu, J., Huang, X., Ma, B., Jiao, X., Geng, X., Kovacs, J. M. and Walters, D., "Tracking crop phenological development using multi-temporal polarimetric Radarsat-2 data," Remote Sens. Environ. **210**, 508–518 (2018).
[29] McNairn, H., Jiao, X., Pacheco, A., Sinha, A., Tan, W. and Li, Y., "Estimating canola phenology using synthetic aperture radar," Remote Sens Env. **219**, 196–205 (2018).
[30] Pacheco, A., McNairn, H., Li, Y., Lampropoulos, G. and Powers, J., "Using RADARSAT-2 and TerraSAR-X satellite data for the identification of canola crop phenology," Remote Sens. Agric. Ecosyst. Hydrol. XVIII **9998**, 999802, International Society for Optics and Photonics (2016).
[31] Vreugdenhil, M., Wagner, W., Bauer-Marschallinger, B., Pfeil, I., Teubner, I., Rüdiger, C. and Strauss, P., "Sensitivity of Sentinel-1 Backscatter to Vegetation Dynamics: An Austrian Case Study," Remote Sens **10**(9), 1396 (2018).
[32] Kumar, P., Prasad, R., Gupta, D. K., Mishra, V. N., Vishwakarma, A. K., Yadav, V. P., Bala, R., Choudhary, A. and Avtar, R., "Estimation of winter wheat crop growth parameters using time series Sentinel-1A SAR data," Geocarto Int. **33**(9), 942–956 (2018).
[33] Mandal, D., Kumar, V., Bhattacharya, A., Rao, Y. S., Siqueira, P. and Bera, S., "Sen4Rice: A Processing Chain for Differentiating Early and Late Transplanted Rice Using Time-Series Sentinel-1 SAR Data With Google Earth Engine," IEEE Trans Geosci Remote Sens Lett, 1–5 (2018).
[34] Song, Y. and Wang, J., "Mapping Winter Wheat Planting Area and Monitoring Its Phenology Using Sentinel-1 Backscatter Time Series," Remote Sens. **11**(4), 449 (2019).
[35] Bleiholder, H., Weber, E., Hess, M., Wicke, H., van den Boom, T., Lancashire, P. D., Buhr, L., Hack, H., Klose, F. R. and Strauss, R., [Growth Stages of Mono- and Dicotyledonous Plants, BBCH Monograph,

Federal Biological Research Centre for Agriculture and Forestry:], Berlin/Braunschweig, Germany (2001).
[36] Mercier, A., Betbeder, J., Baudry, J., Leroux, V., Spicher, F. and Hubert-Moy, L., "Evaluation of Sentinel-1 & 2 time series for predicting wheat and rapeseed phenological stages," ISPRS J Photogramm Remote Sens (2019), submitted for publication.
[37] Jamoneau, A., "Relations entre les diversités alpha, béta et gamma de la flore vasculaire de fragments forestiers inclus dans des paysages agricoles contrastés" (2010).
[38] "User Guides—Sentinel-1 SAR—Level-1 Ground Range Detected—Sentinel Online.", <https://sentinel.esa.int/web/sentinel/user-guides/sentinel-1-sar> (7 March 2019).
[39] Mercier, A., Betbeder, J., Rumiano, F., Baudry, J., Gond, V., Blanc, L., Bourgoin, C., Cornu, G., Ciudad, C., Marchamalo, M., Poccard-Chapuis, R. and Hubert-Moy, L., "Evaluation of Sentinel-1 and 2 Time Series for Land Cover Classification of Forest–Agriculture Mosaics in Temperate and Tropical Landscapes," Remote Sens. **11**(8), 979 (2019).
[40] Miranda, N. and Meadows, P., "Radiometric Calibration of S-1 Level-1 Products Generated by the S-1 IPF, ESA-EOPG-CSCOP-TN-0002," European Space Agency (2015).
[41] Lee, J. S., Jurkevich, L., Dewaele, P., Wambacq, P. and Oosterlinck, A., "Speckle filtering of synthetic aperture radar images: A review," Remote Sens Rev **8**(4), 255–267. (1994).
[42] Pottier, E. and Ferro-Famil, L., "PolSARPro V5.0: An ESA educational toolbox used for self-education in the field of POLSAR and POL-INSAR data analysis," 2012 IEEE Int. Geosci. Remote Sens. Symp., 7377–7380 (2012).
[43] Daughtry, C. S. T., Walthall, C. L., Kim, M. S., de Colstoun, E. B. and McMurtrey, J. E., "Estimating Corn Leaf Chlorophyll Concentration from Leaf and Canopy Reflectance," Remote Sens. Environ. **74**(2), 229–239 (2000).
[44] Herrmann, I., Pimstein, A., Karnieli, A., Cohen, Y., Alchanatis, V. and Bonfil, D. J., "LAI assessment of wheat and potato crops by VENμS and Sentinel-2 bands," Remote Sens Env. **115**(8), 2141–2151 (2011).
[45] Clevers, J. G. P. W. and Gitelson, A. A., "Remote estimation of crop and grass chlorophyll and nitrogen content using red-edge bands on Sentinel-2 and -3," Int J Appl Earth Obs Géoinf **23**, 344–351 (2013).
[46] Gitelson, A. A., Kaufman, Y. J. and Merzlyak, M. N., "Use of a green channel in remote sensing of global vegetation from EOS-MODIS," Remote Sens. Environ. **58**(3), 289–298 (1996).
[47] Guyot, G. and Baret, F., "Utilisation de la haute resolution spectrale pour suivre l'etat des couverts vegetaux," Spectr. Signat. Objects Remote Sens. **287**, 279 (1988).
[48] Qi, J., Chehbouni, A., Huete, A. R., Kerr, Y. H. and Sorooshian, S., "A modified soil adjusted vegetation index," Remote Sens. Environ. **48**(2), 119–126 (1994).
[49] Dash, J. and Curran, P. J., "The MERIS terrestrial chlorophyll index," Int. J. Remote Sens. **25**(23), 5403–5413 (2004).
[50] Delegido, J., Vergara, C., Verrelst, J., Gandía, S. and Moreno, J., "Remote Estimation of Crop Chlorophyll Content by Means of High-Spectral-Resolution Reflectance Techniques," Agron. J. **103**(6), 1834–1842 (2011).
[51] Rouse, J. W. J., Haas, R. H., Schell, J. A. and Deering, D. W., "Monitoring vegetation systems in the Great Plains with ERTS," presented at Third ERTS-1 Symposium, 1973, NASA,Washington, DC, USA.
[52] Blackburn, G. A., "Spectral indices for estimating photosynthetic pigment concentrations: A test using senescent tree leaves," Int. J. Remote Sens. **19**(4), 657–675 (1998).
[53] Huete, A. R., "A soil-adjusted vegetation index (SAVI)," Remote Sens Env. **25**(3), 295–309 (1988).
[54] Clevers, J. G. P. W., "The derivation of a simplified reflectance model for the estimation of leaf area index," Remote Sens. Environ. **25**(1), 53–69 (1988).
[55] Cohen, J., "A Coefficient of Agreement for Nominal Scales," Educ Psychol Meas **20**(1), 37–46 (1960).
[56] Fu, Y., Yang, G., Wang, J., Song, X. and Feng, H., "Winter wheat biomass estimation based on spectral indices, band depth analysis and partial least squares regression using hyperspectral measurements," Comput. Electron. Agric. **100**, 51–59 (2014).
[57] Wilson, J., Zhang, C. and Kovacs, J., "Separating Crop Species in Northeastern Ontario Using Hyperspectral Data," Remote Sens. **6**(2), 925–945 (2014).
[58] Schultz, B., Immitzer, M., Formaggio, A. R., Sanches, I. D. A., Luiz, A. J. B. and Atzberger, C., "Self-Guided Segmentation and Classification of Multi-Temporal Landsat 8 Images for Crop Type Mapping in Southeastern Brazil," Remote Sens. **7**(11), 14482–14508 (2015).
[59] Immitzer, M., Vuolo, F. and Atzberger, C., "First Experience with Sentinel-2 Data for Crop and Tree Species Classifications in Central Europe," Remote Sens **8**(3), 166 (2016).
[60] Cookmartin, G., Saich, P., Quegan, S., Cordey, R., Burgess-Allen, P. and Sowter, A., "Modeling microwave interactions with crops and comparison with ERS-2 SAR observations," IEEE Trans. Geosci. Remote Sens. **38**(2), 658–670 (2000).

[61] Betbeder, J., Fieuzal, R. and Baup, F., “Assimilation of LAI and Dry Biomass Data From Optical and SAR Images Into an Agro-Meteorological Model to Estimate Soybean Yield,” IEEE J Sel Top Appl Earth Obs Remote Sens **9**(6), 2540–2553 (2016).

Appendix M: Landscape metrics derived in the Spanish study area from the land cover classification derived from S-1 & 2 (Mercier et al. 2019b)

Land cover classification derived from S-1 & 2 (Mercier et al. 2019b).

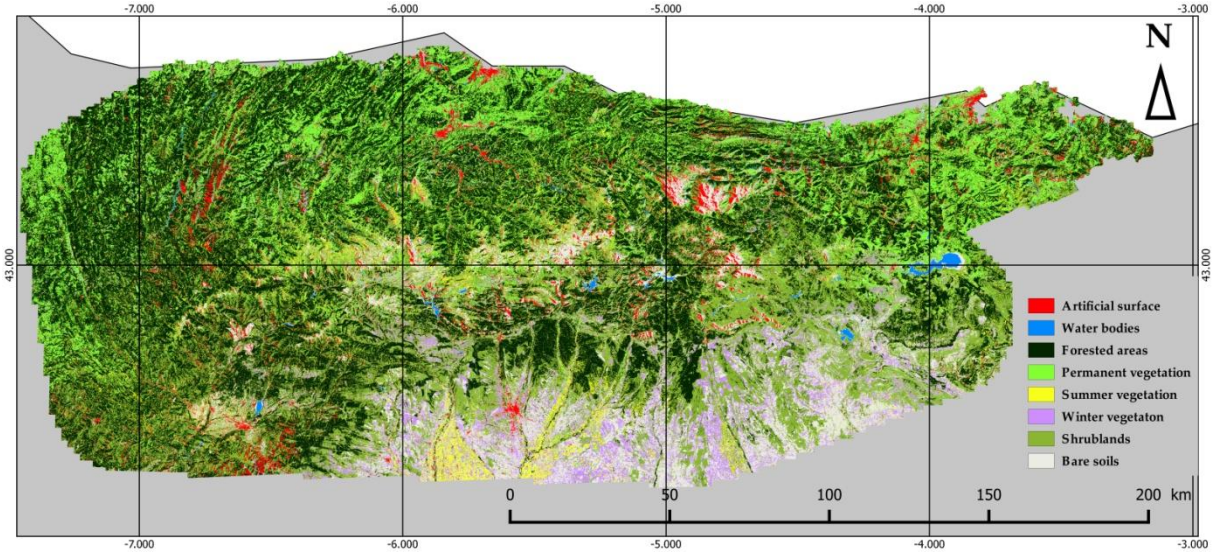

Appendix M-1. Landscape heterogeneity derived using a circular slidding window of 8km radii and derived from the land cover classification of Mercier et al (2019b). The higher theindex, the higher the heterogeneity.

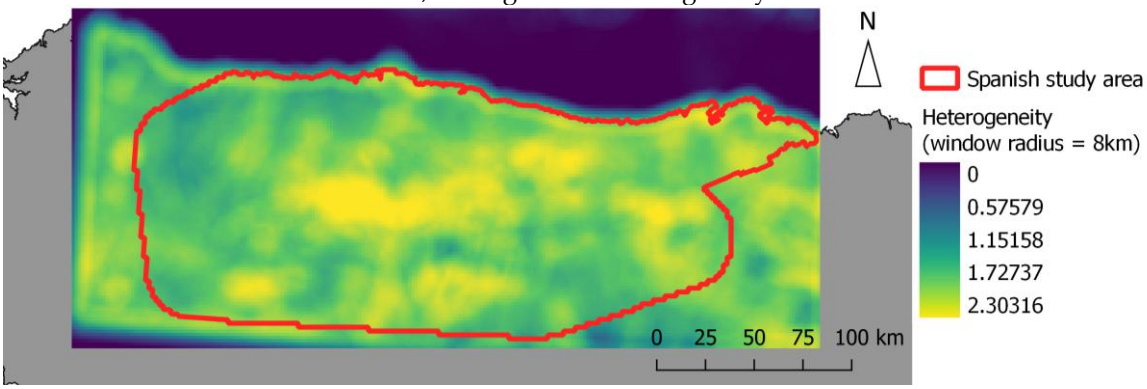

Appendix M-2. Landscape grain derived using a circular slidding window of 8km radii and derived from the land cover classification of Mercier et al (2019b). The finer the landscape grain, the higher the index.

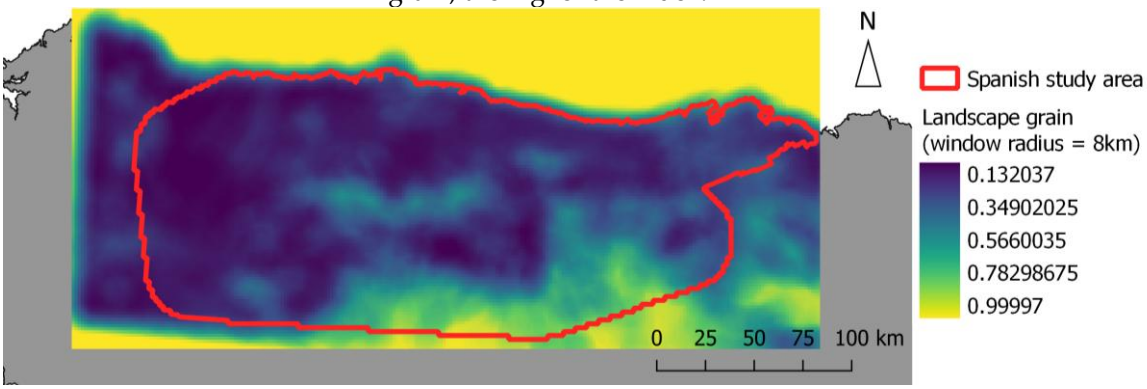

Appendix M-3.Number of interfaces between bare soil and permanent vegetation classes (in number of pixels) derived using a circular slidding window of 8km radii and derived from the land cover classification of Mercier et al (2019b). The more interfaces there are, the more the number of pixels increases.

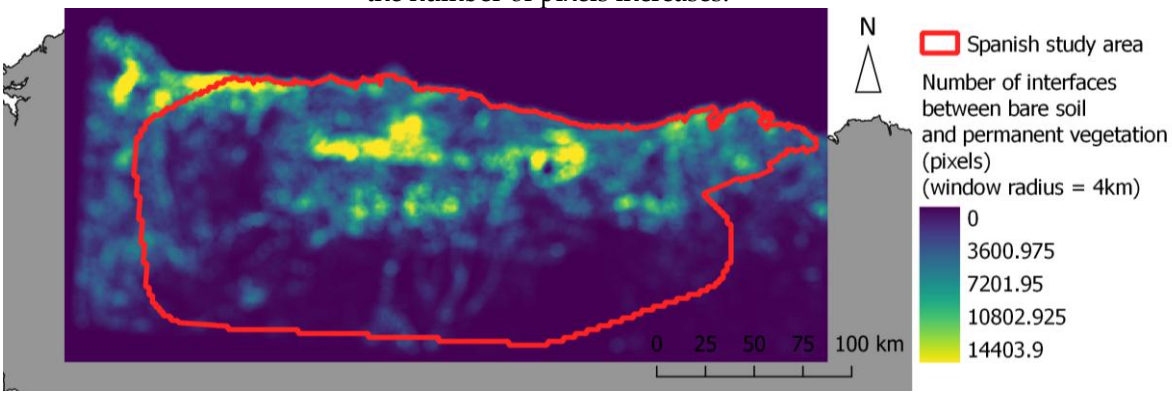

Appendix M-4. Number of interfaces between forested areas and shrublands classes (in number of pixels) derived using a circular slidding window of 8km radii and derived from the land cover classification of Mercier et al (2019b). The more interfaces there are, the more the number of pixels increases.

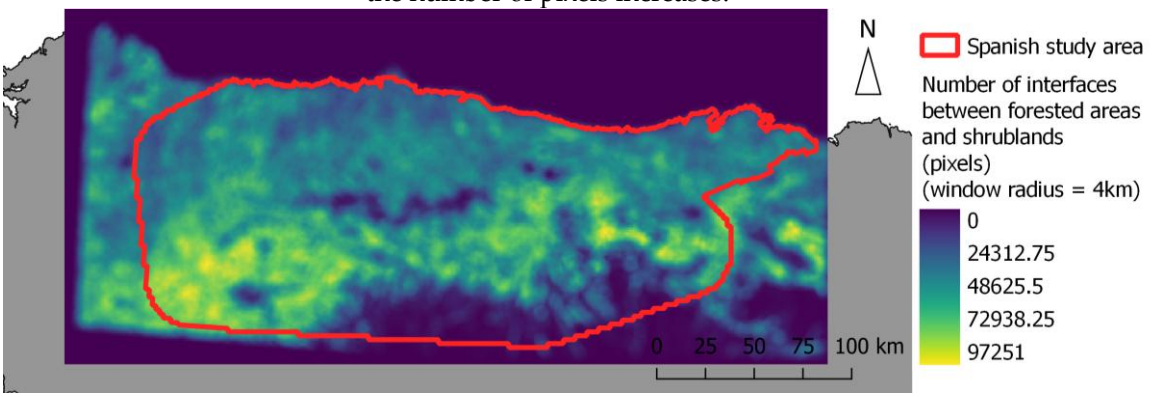

LIST OF ILLUSTRATIONS

LIST OF TABLES

LIST OF APPENDICES

RÉSUMÉ ÉTENDU

La Terre est menacée d'une crise d'extinction massive, avec un taux de disparition des espèces de 10 à 100 fois supérieur au taux naturel d'extinction (Pimm et al. 1995). Les pressions anthropiques telles que l'urbanisation et l'intensification agricole mènent à une dégradation et une perte des habitats, et la réduction de la taille des habitats et leur isolation conduisent à une perte de biodiversité (Hanski 2011). Or, le déplacement des espèces au cours de leur vie pour se nourrir, trouver refuge et se reproduire est indispensable à leur pérennité (Wiens et al. 1993). En outre, le brassage génétique améliore la résistance des individus aux maladies et diminue les risques de malformations (Clobert et al. 2012).

Les corridors écologiques permettent aux espèces de se déplacer entre les habitats, les habitats et les corridors formant les continuités écologiques (Bennett 2004). En plus de la conservation de la diversité biologique, les continuités écologiques assurent des services écosystémiques tels que la régulation du climat, le soutien à l'agriculture (fertilisation des sols, régulation des ravageurs), la production de ressources alimentaires et matérielles, ou la transformation des déchets et polluants (Bolund and Hunhammar 1999; Baudry et al. 2000; Krieger 2001) En milieu agricole, le réseau des continuités écologiques peut être constitué d'éléments semi-naturels et prairies permanentes, ou de parcelles cultivées entre des éléments semi-naturels, ou encore uniquement de parcelles cultivées (Burel et al. 2013).

L'inventaire et l'évaluation fonctionnelle des continuités écologiques, qui sont mis en œuvre dans le cadre de programmes d'aménagement du territoire tels que celui des trames vertes et bleues en France, s'appuient sur des cartes (http://www.trameverteetbleue.fr/). Dans les paysages boisés, la menace principale pour la biodiversité et la déforestation et la dégradation des forêts. Les forêts primaires et les grands patches d'habitats sont considérées comme les éléments paysagers les plus efficaces pour la conservation de la biodiversité dans les paysages boisés. Cependant, les forêts secondaires et les petits patches d'habitats jouent un rôle important pour la persistance des espèces en augmentant potentiellement la connectivité du paysage (Lindenmayer et al. 2006; Vidal et al. 2016). Dans les paysages agricoles, la cartographie des continuités écologiques s'effectue le plus souvent en prenant en compte exclusivement des éléments naturels ou semi-naturels et en excluant les cultures (Burel et al. 2013) alors qu'elles constituent le mode d'utilisation des terres le plus répandu sur notre planète (FAO, 2017), et qu'elles ont un fort potentiel de biodiversité dans des paysages hétérogènes caractéristiques des systèmes agricoles semi-intensifs, constitués d'éléments semi-naturels et de cultures (Billeter et al. 2008). En effet, si les cultures sont régulièrement inventoriées dans le cadre de programmes de suivi de politiques agricoles, elles ne sont pas intégrées aux cartographies officielles des continuités écologiques qui privilégient les boisements et les prairies permanentes. De plus, les cartes réalisées sur les continuités écologiques sont figées dans le temps alors que les éléments qui les constituent ont des dynamiques intra et inter-annuelles spécifiques. Ceci s'explique par le fait que le suivi des continuités écologiques sur le terrain et l'interprétation de photographies aériennes constitue un coût non négligeable en termes de temps et de main d'œuvre.

Dans ce contexte, les séries temporelles d'images satellite offrent une alternative pour cartographier et effectuer le suivi des éléments constituant les continuités écologiques dans les paysages agricoles et boisés sur de vastes étendues. Les images acquises par les satellites optiques ont déjà montré un fort potentiel pour identifier et caractériser les caractéristiques écologiques des éléments du paysage. Les capteurs optiques MODIS, AVHRR et Landsat ont

été largement utilisés pour cartographier l'occupation et l'usage des sols (Congalton et al. 2014; Gómez et al. 2016), la déforestation et la dégradation des forêts (Bourgoin 2019) à large échelle du fait de leur haute résolution temporelle et leur grande fauchée. Cependant la faible résolution spatiale des données acquises par ces capteurs (30m à 1,1km) ne permet pas d'identifier finement les éléments paysagers ou d'aller jusqu'à leur caractérisation. En revanche, les données à haute résolution spatiale comme les images SPOT et Formosat-2 (< 5m) et à très haute résolution spatiales telles que images Quickbird, WorldView et IKONOS (<1m) ont montré un bon potentiel pour identifier des haies fines (Vannier and Hubert-Moy 2014), estimer le rendement, l'indice de surface foliaire (ISF), la biomasse et le stade phénologique des cultures (Quarmby et al. 1993; Doraiswamy et al. 2004; Mulla 2013; Bontemps et al. 2015; Pan et al. 2015; Betbeder et al. 2016b) ou encore cartographier la biomasse de surface des forêts tropicales (Singh et al. 2014; Pargal et al. 2017). La résolution temporelle des capteurs est également un élément essentiel pour caractériser la dynamique temporelle des éléments paysagers. Par ailleurs, depuis les années 2000, des études ont montré l'intérêt des données satellitaires RSO à haute résolution spatiale pour cartographier les cultures et les caractériser (Steele-Dunne et al. 2017). Ainsi, les indicateurs polarimétriques dérivés de RADARSAT-2 ou TerraSAR-X se sont montré pertinents pour estimer les stades phénologiques, la hauteur et la biomasse de diverses cultures (Jiao et al. 2009; Wiseman et al. 2014; Mascolo et al. 2015; Jin et al. 2015; Betbeder et al. 2016b; Pacheco et al. 2016; Canisius et al. 2018; McNairn et al. 2018; Homayouni et al. 2019). Dans les paysages boisés, le capteur ALOS-SAR a permis de produire une carte globale forêt/non forêt (Shimada et al. 2014; Zhou et al. 2018). Toutefois, la faible répétitivité de ces capteurs, leur nécessaire programmation ainsi que le coût des images constituent des contraintes fortes pour le suivi des paysages agricoles et boisés.

Les données gratuites à hautes résolutions spatiale et temporelle acquises par les satellites RaDAR à Synthèse d'Ouverture (RSO) Sentinel-1 (S-1) depuis 2014 et optiques Sentinel-2 (S-2) depuis 2016 offrent de nouvelles possibilités pour la cartographie et le suivi des continuités écologiques. Des études récentes ont démontré le potentiel des séries temporelles S-2 pour cartographier l'occupation du sol dans des paysages boisés (Jönsson et al. 2018) et des paysages agricoles (Denize et al. 2019a). Concernant les cultures, les bandes spectrales, les indices de végétation et les variables biophysiques dérivés des données S-2 ont permis d'estimer avec une bonne précision l'ISF (Delegido et al. 2011b; Frampton et al. 2013; Clevers et al. 2017; Pan et al. 2018; Wang et al. 2019), la biomasse (Veloso et al. 2017; Ghosh et al. 2018; Ganeva et al. 2019) et les stades phénologiques (Veloso et al. 2017; Ghosh et al. 2018; Stendardi et al. 2019) des cultures**.** Cependant, l'exploitation de ces données optiques est limitée par la présence d'une couverture nuageuse. De plus, elles ne fournissent de l'information que sur la couche haute de la végétation et le signal sature avec un niveau élevé de biomasse et d'ISF (Wang et al. 2016a). En dépit du fait que les données S-1 sont sensibles aux conditions du sol (rugosité, humidité), elles constituent une alternative aux données S-2 car elles ne sont pas influencées par les conditions atmosphériques, et le signal RaDAR pénètre la canopée (Lee and Pottier 2009). Des études récentes ont montré l'intérêt des coefficients de rétrodiffusion et du ratio σ^0VH:σ^0VV dérivés des données S-1 pour la cartographie de cinq types d'occupation du sol globales (eau, forêt, urbain, sol nu et surface agricole) en Turquie (Abdikan et al. 2016) et la détection des forêts de conifères, des forêts de feuillus et des terres arables non irriguées en Allemagne (Balzter et al. 2015). Dans les paysages agricoles, le potentiel de ces mêmes variables S-1 a été démontré pour la détection

des changements dans la structure du colza, du maïs et des céréales d'hiver (Vreugdenhil et al. 2018), l'identification des stades phénologiques du blé (Song and Wang 2019) et l'estimation de la biomasse, la teneur en eau (WC) et l'ISF du blé (Kumar et al. 2018). Toutefois, à notre connaissance, aucune étude n'a été menée avec des indicateurs polarimétriques dérivés de S-1 pour caractériser les cultures.

En conséquence, l'utilisation combinée des capteurs optiques et RSO devrait permettre d'améliorer la cartographie des continuités écologiques. En effet, la fusion des données optiques et RSO améliore l'identification des occupations/usages des sols (Kussul et al. 2017; Zhou et al. 2017; Laurin et al. 2018; Reiche et al. 2018) et des types de cultures (Orynbaikyzy et al. 2019). Le domaine optique est sensible à la physiologie de la végétation, tandis que les micro-ondes sont influencées par la géométrie (rugosité, texture, structure interne) et l'humidité des surfaces. Cette complémentarité entre les domaines optique et RSO est peu exploitée pour caractériser les continuités écologiques. Quelques études ont utilisé à la fois les données optiques et RSO pour caractériser des cultures (Betbeder et al. 2016a; Veloso et al. 2017; El Hajj et al. 2019). Cependant, ces études utilisent l'indice de végétation, NDVI, dérivé des données optiques comme référence pour évaluer les données RSO. Bien que la réelle combinaison des données optiques et RSO améliore les résultats de classification de l'occupation du sol et des types de cultures, elle reste peu exploitée pour prédire les paramètres de cultures (Stendardi et al 2019, Jin et al 2015).

Si la télédétection est couramment utilisée pour cartographier les éléments constitutifs des continuités écologiques, qu'il s'agissent d'éléments semi-naturels, de prairies permanentes ou de parcelles cultivées, elle l'est aussi en écologie du paysage, notamment pour étudier la structure, le changement et la fonction du paysage (Crowley and Cardille 2020). La structure du paysage peut être analysée à partir d'indicateurs dérivés de données de télédétection (hétérogénéité du paysage, topographie,…). Les séries temporelles d'images satellite permettent d'identifier les changements intervenus dans le paysage à travers l'étude de l'évolution de ces indicateurs. La fonction du paysage peut être évaluée en combinant ces indicateurs et des informations issues de modèles d'écologie du paysage (distribution spatiale d'une espèce, mesures météorologiques,…).

C'est dans ce contexte que s'inscrivent ces travaux de thèse dont l'objectif est double : Evaluer comparativement les séries temporelles optiques S-2 et RSO S-1 pour identifier et caractériser les éléments constitutifs des continuités écologiques à travers des classifications de l'occupation et de l'utilisation des sols et la caractérisation de cultures dans les paysages de mosaïques boisées et agricoles ; Evaluer l'impact de la structuration spatio-temporelle de ces mosaïques paysagères sur la biodiversité en utilisant des métriques dérivées des séries temporelles Sentinel.

Plus précisément, les recherches ont été principalement concentrées sur quatre sites et deux espèces animales: les carabes en Bretagne, Picardie (France) et Wallonie (Belgique) et les ours bruns en Cantabrie (Espagne). D'une part, les travaux ont focalisé sur l'exploitation de séries temporelles S-1 et S-2 afin (1) d'effectuer un suivi intra-annuel de l'occupation et de l'utilisation des sols permettant d'identifier les éléments constitutifs des continuités écologiques et d'élaborer des métriques paysagères spatio-temporelles sur les sites d'étude et (2) de caractériser les cultures de blé et de colza qui sont des éléments clés de connectivité

dans les mosaïques agricoles étudiées. D'autre part, les travaux ont porté sur la mise en relation des cartes des métriques paysagères précédemment élaborées à partir des données Sentinel avec les relevés d'espèces afin d'évaluer l'impact de la structure des mosaïques paysagères sur la biodiversité.

Cette thèse contribue au projet WOODNET (Connectivity patterns and processes along a gradient of European landscapes with woody vegetation and spatial heterogeneity), qui fait partie du Programme européen BIODIVERSA. Il s'agit d'un projet interdisciplinaire qui combine l'écologie, la géographie, l'hydrologie, l'agronomie et le droit et implique des chercheurs de Belgique, de France et d'Espagne. Les recherches qui sont présentées dans cette thèse se concentrent sur l'une des principales activités du projet WOODNET, c'est-à-dire l'évaluation de nouvelles images satellites pour la cartographie des paysages (https://woodnetweb.wordpress.com/project/).

Nous avons tout d'abord évalué le potentiel des données S-1 seules, S-2 seules et des données S-1 et S-2 combinées pour identifier et caractériser l'occupation et l'utilisation du sol dans des paysages de mosaïques forêt-agriculture, le suivi de ces paysages étant crucial pour comprendre l'hétérogénéité des paysages et gérer la biodiversité. La cartographie de ces mosaïques à partir d'images de télédétection est un défi, car les gradients écologiques entre les zones forestières et agricoles rendent la caractérisation de la végétation plus difficile. L'étude a porté sur deux paysages aux gradients de végétation contrastés : un paysage montagneux tempéré dans les Monts Cantabriques (Espagne) et un paysage forestier tropical humide au Paragominas (Brésil). Bien que ces mosaïques paysagères diffèrent fortement, elles ont des fonctions écologiques similaires (conservation de la biodiversité et stockage du carbone).

Les images satellites ont été classées en utilisant une procédure incrémentale basée sur les rangs d'importance des variables d'entrée dérivées des séries temporelles S-1 et S-2. L'algorithme sélectionne automatiquement les variables et périodes de temps pertinentes à utiliser pour classifier au mieux l'occupation et l'utilisation du sol dans chaque paysage. Les données S-2 seules ont permis de produire de meilleurs résultats (indice de kappa moyen=0.59-0.83) que les données S-1 seules (indice de kappa moyen=0.28-0.72), la combinaison des deux types de données ayant légèrement amélioré les résultats (indice de kappa moyen=0.55-0.85). La méthode utilisée a permis de définir le nombre et le type de variables qui discriminent de manière optimale les classes d'occupation des sols en fonction du type de paysage considéré. La meilleure configuration pour les sites d'étude espagnol et brésilien comprend respectivement 5 et 10 variables pour les données S-2 et 10 et 20 variables pour les données S-1. Le proche infrarouge et les polarisations VV et VH sont les variables les plus discriminantes pour les données S-2 et S-1, respectivement. De plus, la méthode a permis de définir les périodes clés pour la discrimination des classes d'occupation et d'utilisation des sols en fonction du type d'images utilisées. Par exemple, dans les Monts Cantabriques, l'hiver et l'été sont des périodes clés pour les séries temporelles S-2, tandis que le printemps et l'hiver sont des périodes clés pour les séries temporelles S-1. L'identification des types d'occupation du sol dans ces deux paysages boisés est une première étape essentielle avant la cartographie des continuités écologiques. En effet, ces dernières peuvent être révélées par la mise en relation des cartes d'occupation du sol produites avec des données d'espèces. La caractérisation des éléments paysagers en termes de structure, composition, dynamiques spatio-temporelles permet une compréhension plus fine des diversités de fonctions écologiques existantes pour les espèces.

Plus précisément, ces recherches ont permis de mettre en exergue les trois points suivants :

1- Les contributions relatives des données S-1 et S-2 à la cartographie de l'occupation des sols des mosaïques forêt-agriculture :

Les classes d'occupation des sols qui composent les mosaïques forêt-agriculture sont réparties le long d'un gradient de paysage, avec des classes de transition telles que les arbustes vers la forêt ou les pâturages vers les jeunes forêts secondaires, ce qui entraîne des erreurs de classification. Les données S-1 seules sont les moins précises pour la cartographie de l'occupation des sols dans les mosaïques forêt-agriculture, avec un meilleur indice kappa

moyen de 0,73, contre 0,87 et 0,89 pour les données S-2 seules et les données S-1 et S-2 combinées, respectivement.

Par exemple, sur la zone d'étude brésilienne, les données S-2 ont permis de mieux distinguer les zones boisées des jeunes forêts secondaires que les données S-1. Cela peut s'expliquer par le fait que les capteurs RSO sont sensibles à la structure de la végétation, tandis que les capteurs optiques sont sensibles à la teneur en chlorophylle. Ainsi, lorsqu'elles ont été observées à une résolution de 10 m, les grandes classes de végétation ont été plus facilement discriminées par leur physiologie que par leur structure physique. De plus, les polarisations VV et VH sont les variables S-1 les plus importantes pour discriminer les classes d'occupation des sols, alors que le rapport σ^0VV:σ^0VH n'apparaît pas utile. Bien que l'on sache que la polarisation VH est plus sensible à la végétation que la polarisation VV (Patel et al. 2006), les résultats montrent que les deux polarisations contribuent peu à la classification des mosaïques forêt-agriculture, tout comme le ratio σ^0VV:σ^0VH. Nous pouvons conclure que dans ce cas, la bande C de S-1 n'est pas pertinente pour classer les classes de végétation. En général, le RSO en bande C est moins adapté que la bande L pour la surveillance des changements forestiers en raison d'une profondeur de pénétration plus faible et d'une saturation rapide du signal (Woodhouse 2017). Par exemple, Patel et al. (2006) ont démontré que la bande L est plus sensible à la densité de la végétation que la bande C, et que la bande C interagit principalement avec les premières branches de la canopée, tandis que la bande L pénètre l'intérieur de la canopée. Nous avons utilisé des produits GRD S-1 qui enregistrent les coefficients de rétrodiffusion (VV et VH) car ils nécessitent moins de temps de traitement que les produits SLC, qui préservent l'information de phase. Cependant, l'utilisation de la texture, de la cohérence et des indices polarimétriques dérivés des données RaDAR polarimétriques complètes, telles que les données RADARSAT-2, pourrait améliorer la classification basée ici sur les seules données S-1 (Roychowdhury ; Ranson et al. 2001 ; Sonobe et al. 2015 ; Du et al. 2018). Ainsi, bien que Bagdhadi et al. (2016) aient conclu que l'utilisation d'indices polarimétriques, tels que l'entropie de Shannon (SE) et le span, dérivés d'images polSAR RADARSAT-2 n'améliorait pas les estimations de l'humidité du sol et des paramètres de la végétation, Betbeder et al. (2014) ont démontré que SE était plus utile que les coefficients de rétrodiffusion pour cartographier la végétation des zones humides à l'aide de séries chronologiques TerraSAR-X à deux polarisations.

Le meilleur indice kappa moyen obtenu avec les données S-1 est plus élevé pour la zone d'étude espagnole que pour la zone d'étude brésilienne (0,73 contre 0,60, respectivement). Cela pourrait être dû à des différences dans les méthodes de classification (nombre différent de classes et de types d'occupation des sols) et au nombre d'images S-1 utilisées pour classifier les types d'occupation des sols (22 dates pour la zone d'étude espagnole contre 14 dates pour la zone d'étude brésilienne). Un nombre plus important d'erreurs de classification ont été observées dans les zones à fort relief, ce qui est conforme à la littérature (Lee et Pottier 2009). Pour la zone d'étude espagnole, les résultats de classification obtenus en utilisant uniquement les données S-1 montrent que les erreurs de classification sont le plus souvent localisées sur les pentes des montagnes. Ces erreurs sont dues à l'acquisition d'images RSO en géométrie oblique qui provoque des effets de repliement et de raccourcissement (Lee et Pottier 2009). De plus, on sait que l'humidité et la rugosité du sol influencent la rétrodiffusion RaDAR en fonction de la fréquence, de la polarisation et de l'angle d'incidence de la micro-onde. Holah et al. (2005) ont constaté que la sensibilité à la rugosité de surface est plus importante en utilisant les polarisations HH et HV que la polarisation VV. Cependant, Baghdadi et al. (2008) ont démontré que la sensibilité du capteur à l'humidité du sol

dépendait peu de la polarisation. Les effets de l'humidité du sol sur la classification forêt-agriculture sont plutôt limités en utilisant la bande C en raison d'une faible profondeur de pénétration des micro-ondes par rapport à la bande L (Ulaby et al. 1996), alors que la bande C est plus sensible à la rugosité (Mattia et al. 1997). Enfin, plus l'angle d'incidence est élevé, plus la sensibilité du RSO à la rugosité de surface est importante (Fung et Chen 1992).

Cependant, les données S-1 discriminent parfois mieux que les données S-2 les sols nus et les surfaces artificielles car le signal RSO réagit différemment à ces deux classes d'occupation des sols, avec un double rebond sur les bâtiments et un simple rebond sur les sols nus plats (Lee et Pottier 2009), alors que leurs signatures spectrales dans le domaine optique sont similaires (valeurs de réflectance élevées dans les bandes verte, bleue et rouge).

En utilisant uniquement les données S-2, les bandes SWIR sont les variables les plus importantes pour discriminer les classes d'occupation des sols. L'importance des bandes SWIR de S-2 a été démontrée pour la cartographie de la végétation et des forêts (Immitzer et al. 2016 ; Chrysafis et al. 2017). Les indices de végétation dérivés des données S-2 (par exemple SAVI, NDVI, NDWI) ont été plus pertinentes que les bandes spectrales pour la zone d'étude espagnole, tandis que le NDWI était l'indice de végétation le plus important pour la zone d'étude brésilienne. La sensibilité de la bande bleue à l'eau contenue dans la végétation pourrait expliquer pourquoi le NDWI est bien adapté à la végétation tropicale, alors que le NDVI sature à des valeurs de biomasse élevées (Huete et al. 2002 ; Jackson et al. 2004). L'indice EVI, qui a été développé pour MODIS, est une variable moins importante que les autres indices de végétation pour les deux zones d'étude. Il pourrait être intéressant de calculer d'autres indices de végétation qui sont utilisés pour la discrimination des cultures comme le S2REP, l'IRECI, le MTCI ou le SRI (Jordan 1969 ; Frampton et al. 2013).

L'indice de kappa moyen utilisant les données combinées S-1 et S-2 (0,88) diffère peu de celui qui utilise les données S-2 seules (0,86). Ainsi, l'utilisation des données S-2 seules est suffisante pour discriminer les classes d'occupation des sols avec une grande précision. Cependant, l'intensité de rétrodiffusion des données S-1 seules a fourni des informations supplémentaires pertinentes, puisque les prédictions des classes d'occupation des sols utilisant les données S-1 seules, les données S-2 seules et les données S-1 et S-2 combinées diffèrent selon le test X^2 de McNemar. Par exemple, l'erreur de classification entre les terres cultivées et les surfaces artificielles pour la zone d'étude brésilienne, lorsqu'on utilise les données S-2 seules, a été partiellement corrigée en utilisant les données S-1 et S-2 combinées.

2- L'utilisation des données S-1 et S-2 pour identifier les périodes clés pour la classification de l'occupation des sols :

Sur la base des résultats de la classification utilisant les données S-1 seules, les données S-2 seules et les données S-1 et S-2 combinées, la précision de la classification est fortement liée au nombre de dates. La précision de la classification augmente lorsque des dates sont ajoutées au classificateur random forest. La pertinence d'une haute résolution temporelle souligne l'importance de la description et de la prise en compte de la phénologie de la végétation pour cartographier les mosaïques forêt-agriculture.

Pour la zone d'étude espagnole, les variables de janvier, mars, juin et juillet figurent parmi les 20 variables S-2 les plus importantes. Cela peut s'expliquer par le fait que le capteur S-2 est sensible à la teneur en chlorophylle de la végétation, et que ces mois sont des périodes clés de l'activité chlorophyllienne. Les variables des mois de décembre à mai figurent parmi les 20 variables S-1 les plus importantes pour cette zone d'étude, alors que la période estivale n'est pas pertinente. Cela est probablement dû au fait que les capteurs RSO,

qui sont sensibles à la structure interne des éléments, pénètrent mieux dans la végétation pendant la période de feuillaison.

Une seule date S-2 a été utilisée pour la zone d'étude brésilienne, ce qui a empêché d'étudier l'importance de la période de temps. En outre, aucune période de temps précise n'est ressortie des rangs d'importance de la série temporelle S-1. Ainsi, aucune période intra-annuelle ne semble plus importante que les autres pour les séries temporelles S-1 pour discriminer les types d'occupation des sols à Paragominas. Contrairement à la chaîne cantabrique, où les saisons diffèrent, les températures et les précipitations sont relativement constantes au Pará, avec une saison plus sèche de juillet à octobre (https://www.worldweatheronline.com/para-weather/para/br.aspx). En outre, la dynamique des pratiques humaines dans les pâturages, les zones forestières et les plantations est interannuelle plutôt qu'intra-annuelle (Piketty et al. 2015).

3- La robustesse de la méthode pour différents paysages :

Les résultats montrent que la méthode peut être appliquée aux mosaïques forêt-agriculture dans des paysages au climat (tropical, tempéré) et au type de végétation contrastés (par exemple, forêts tropicales, arbustes, forêts de conifères et de feuillus). Les variables S-1 et S-2 ont été sélectionnées en fonction de leur importance respective dans chaque zone d'étude, ce qui a permis de mettre en évidence les variables et les périodes pertinentes pour les deux zones. Les cartes de l'occupation des sols des deux zones d'étude ont été produites avec un degré élevé de précision et un temps de traitement court. Les séries temporelles sont utilisées pour cartographier l'occupation des sols des mosaïques forêt-agriculture, mais leur traitement nécessite une grande capacité de calcul. La méthode a permis de se concentrer sur des périodes et des variables spécifiques afin de réduire le temps nécessaire au traitement des images.

En conclusion, une procédure incrémentale basée sur le classement de l'importance des variables d'entrée dérivées des séries temporelles S-1 et S-2 a été utilisée pour distinguer les classes d'occupation des sols dans les mosaïques forêt-agriculture. La méthode a automatiquement sélectionné les variables pertinentes (bandes spectrales et/ou indices de végétation) et les périodes de temps pour classer les types d'occupation des sols dans ces paysages. Les résultats montrent que les données S-2 seules sont plus pertinentes que les données S-1 seules pour cartographier l'occupation des sols des mosaïques forêt-agriculture, et que la combinaison des données S-1 et S-2 améliore légèrement les résultats par rapport à ceux des données S-2 seules. L'utilisation d'indices polarimétriques, tels que l'indice SE, qui a déjà montré son potentiel pour la caractérisation de la végétation, peut améliorer les prédictions des données S-1 seules. En effet, les données RSO sont utiles dans les régions nuageuses : la forte couverture nuageuse dans la série temporelle S-2 a été la principale source d'erreurs de classification.

Ensuite, nous nous sommes focalisés sur la caractérisation des cultures avec l'étude du blé et du colza, qui sont deux des cultures les plus importantes au monde en termes de surface récoltée (FAO, 2017). Nous avons évalué le potentiel des données S-1 seules, des données S-2 seules et de la combinaison des données S-1 et S-2 pour identifier les stades phénologiques principaux et secondaires du blé et du colza en Picardie (France).

Plus spécifiquement, cette étude avait pour but d'évaluer l'intérêt des indicateurs polarimétriques dérivés des données S-1 et de déterminer le nombre et le type de variables S-1 et S-2 nécessaires pour discriminer les stades phénologiques du blé et du colza.

Nous avons estimé la performance des bandes spectrales et des indices de végétations dérivés de S-2 et des coefficients de rétrodiffusion et indicateurs polarimétriques dérivés de S-1. Les images satellites ont été classées en utilisant la méthode incrémentale développée dans l'étude précédente (Mercier et al. 2019b). Globalement, les résultats ont montré que l'utilisation combinée des données S-1 et S-2 (kappa moyen = 0.53-0.82 et 0.74-0.92 pour le blé et le colza, respectivement) apporte une précision supérieure à l'utilisation des données S-1 seules (kappa moyen = 0.48-0.61 et 0.61-0.64 pour le blé et le colza, respectivement) ou S-2 seules (kappa moyen = 0.54-0.75 et 0.67-0.86 pour le blé et le colza, respectivement) pour l'identification des stades phénologiques principaux et secondaires. Les variables les plus importantes sont le ratio σ^0VH: σ^0VV et les indicateurs polarimétriques pour S-1 et les indices NDVI et S2REP et la variable biophysiques ISF pour S-2.

Plus précisément, ces recherches ont permis de mettre en exergue les quatre points suivants :

1- La relation entre les variables S-2 et les stades phénologiques du blé et du colza :

Pour les deux types de cultures, les profils temporels des bandes S-2 sont conformes à ceux observés par Ashourloo et al. (2019). Une saturation a été observée de l'allongement de la tige à la floraison pour le blé et de la floraison au développement des fruits pour le colza. Cependant, il convient de noter que l'analyse des profils temporels a été effectuée à partir de 5 dates seulement en raison de la forte couverture nuageuse sur la zone d'étude entre les jours de l'année (DoY) 72 et 152, c'est-à-dire pendant l'élongation de la tige, la montaison et les premiers stades de floraison pour le blé et la floraison et le développement du fruit pour le colza. Wilson et al. (2014) ont mentionné la saturation du signal pour le blé et le colza avec l'utilisation de données hyperspectrales dans une plage de 400-900 nm et ont identifié des bandes optimales pour l'identification des cultures dans les longueurs d'onde du vert, du bord rouge et du proche infrarouge. Sur la base de cette étude et de nos observations, nous avons sélectionné les bandes S-2 3, 5, 6, 7, 8 et 8A comme entrée pour la classification incrémentale. Sur les profils temporels des indices de végétation et de l'ISF dérivés de S-2, l'écart-type atteint son maximum à la fin de l'inflorescence pour le blé et à la fin du développement du fruit pour le colza. Ainsi, l'hétérogénéité de la phénologie des cultures entre les champs au cours des enquêtes sur le terrain atteint un pic lors de l'élongation de la tige pour le blé et au début du développement du fruit pour le colza. Tous les indices de végétation saturent lorsque l'ISF est élevé (1-2 pour le blé et 3-4 pour le colza, selon l'indice de végétation), ce qui confirme les observations de Haboudane et al. (2004) pour le blé.

Pour le blé, les indices de végétation et l'ISF commencent à augmenter lorsque la teneur en chlorophylle augmente au stade du tallage. Ils diminuent tous pendant la maturation, au fur et à mesure que les plantes sèchent.

Pour le colza, des diminutions sont observées pendant la maturation en raison de la diminution de la teneur en chlorophylle au fur et à mesure que les plantes sèchent. L'ISF et le « Weighted Difference Vegetation Index » (WDVI) commencent à augmenter au début de l'inflorescence jusqu'au début de la floraison, au fur et à mesure de l'expansion de la surface des plantes. Le WDVI diminue pendant le développement des feuilles au fur et à mesure que celles-ci se déploient.

2- La relation entre les coefficients de rétrodiffusion de S-1 et les stades phénologiques du blé et du colza :

Pour le blé, alors que les tendances des profils temporels de σ^0VH et σ^0VV sont similaires, σ^0VV est plus élevé que σ^0VH surtout pendant les premiers stades phénologiques (c'est-à-dire le tallage et l'élongation de la tige), puisque σ^0VV est plus influencé par la croissance du blé que σ^0VH. Cela correspond aux observations de Cookmartin et al. (2000) qui ont montré que σ^0VV est particulièrement sensible à l'humidité de la végétation et de Fieuzal et al. (2013) qui ont observé une WC maximum au stade de l'élongation de la tige. Les deux polarisations augmentent pendant le tallage (DoY 18-72). L'augmentation du nombre de tiges par plante et de la longueur des tiges entraîne une augmentation de la polarisation VH, qui est dominée par des mécanismes de double rebond et de diffusion volumique (Lopez-Sanchez et al. 2013 ; Wiseman et al. 2014 ; Veloso et al. 2017) et une forte augmentation de la polarisation VV, qui est dominée par l'influence du sol et du couvert végétal. Tant σ^0VH que σ^0VV diminuent tout au long de l'élongation de la tige mais augmentent de l'inflorescence à la maturation, comme l'ont observé Fieuzal et al. (2013), en raison d'une augmentation de l'absorption des cultures lorsque la végétation est humide, et diminue lorsque la végétation s'assèche. La polarisation VV est atténuée par la transformation verticale de la structure du blé pendant l'élongation de la tige (Brown et al. 2003). Le rapport σ^0VH:σ^0VV varie peu pendant les stades de tallage, ce qui ne permet pas d'identifier les stades phénologiques secondaires. Ce rapport est davantage corrélé à la biomasse fraîche qu'à l'activité photosynthétique (Veloso et al. 2017). Pour le colza, les polarisations VH et VV augmentent légèrement au cours du développement des feuilles à mesure que la biomasse augmente. Elles varient peu pendant l'inflorescence et diminuent pendant la floraison. En effet, la transformation verticale du colza atténue la polarisation VV, tandis que sa faible densité atténue la polarisation VH. Les deux polarisations augmentent du développement du fruit au début de la maturation, ce qui a également été observé dans d'autres études (Fieuzal et al., 2013 ; Lopez-Sanchez et al., 2013 ; Wiseman et al., 2014 ; Veloso et al., 2017). Le développement progressif de la structure sans orientations privilégiées entraîne une géométrie plus complexe, induisant une forte augmentation du mécanisme de diffusion volumique (Betbeder et al. 2016b). Les polarisations VH et VV diminuent jusqu'à la fin de la maturation en raison de la diminution de la WC dans la couche supérieure du colza. La polarisation VV est particulièrement sensible à la WC de la végétation (Cookmartin et al. 2000), et la polarisation VH est atténuée par l'augmentation de la pénétration des ondes dans le sol.

3- La relation entre les indicateurs polarimétriques S-1 et les stades phénologiques du blé et du colza :

Pour les deux types de cultures, les comportements temporels du span, de σ^0VH et de σ^0VV sont similaires puisque le span correspond à la puissance totale difusée.

Pour le blé, SE normalisée et l'intensité de l'entropie de Shannon (SE_i) normalisée augmentent d'abord lors du tallage mais diminuent ensuite pendant l'élongation de la tige et l'inflorescence. L'augmentation du SE_i normalisée est liée au développement de la tige pendant le tallage. Cette complexité de la structure de la plante augmente le désordre rencontré dans le signal RaDAR. Le contraire a été observé pendant l'élongation de la tige, en raison de la structure moins complexe du blé, ce qui entraîne une diminution de la puissance de rétrodiffusion. Betbeder et al. (2016) ont démontré une forte corrélation positive (r^2=0,7) entre l'humidité de la surface et SE_i pendant le développement des feuilles et le tallage en raison d'une faible pénétration des ondes dans le sol. La polarisation de l'entropie de Shannon (SE_p) normalisée varie peu dans un premier temps, mais augmente ensuite de manière significative pendant l'élongation de la tige, ce qui indique que la polarisation varie beaucoup en raison de l'hétérogénéité des structures végétales dans les champs de blé. SE_p normalisée diminue de façon linéaire de la fin de la floraison à la maturation, le blé devenant homogène à l'échelle du champ. SE normalisée et SE_i normalisée ont permis d'identifier le stade de développement des fruits, contrairement aux autres variables S-1, puisqu'elles diminuent légèrement au cours de ce stade.

Pour le colza, les changements temporels de SE normalisée et SE_i normalisée sont similaires à ceux observés sur le blé. Comme le mentionnent Betbeder et al. (2016), l'intensité de SE est sensible aux différents stades phénologiques. La légère augmentation de SE_p normalisée pendant la floraison est associée à des changements dans la structure du colza, ce qui entraîne une forte variation de la polarisation de rétrodiffusion (Betbeder et al. 2016b). L' SE_i normalisée augmente avec l'augmentation de la biomasse du colza ; ainsi, il augmente pendant la floraison et diminue pendant la maturation (Betbeder et al. 2016b).

4- Les contributions relatives des données S-1 et S-2 à la cartographie des stades phénologiques du blé et du colza :

En ce qui concerne la prédiction des principaux stades phénologiques du blé à l'aide des données S-2 seules, l'ISF est la variable la plus importante, suivie par le S2REP, le red-edge2 (B06), le WDVI, le NDVI et le red-edge1 (B05). Pour le colza, les variables les plus importantes sont le NDVI, le S2REP, la bande 3 (vert), l'ISF et le WDVI. Les stades phénologiques principaux et secondaires du blé et du colza ont été bien identifiés par l'indice ISF dérivé des données S-2, puisque cet indice est lié à la surface recouverte par la végétation verte. Les résultats de la classification incrémentale ont démontré la pertinence de l'indice S2REP pour les deux types de culture, ce qui est conforme aux résultats de Frampton et al. (2013). Le S2REP, qui est très sensible à la teneur en chlorophylle, est calculé à partir des bandes S-2 du red-edge qui réagissent à des changements importants de la réflectance des feuilles (Hatfield et al. 2008). L'importance des bandes rouges de S-2 a été démontrée pour l'estimation de l'IFS dans des parcelles cultivées, y compris le blé en Espagne et en Allemagne (Delegido et al. 2011b). Nous avions noté le potentiel du WDVI pour la prédiction des stades phénologiques du colza sur la base de notre analyse des profils temporels; il s'agit du seul indice sensible au stade de développement des feuilles. Wilson et al. (2014) ont

expliqué que le colza avait une réflectance plus élevée dans les parties verte et rouge du spectre que les autres cultures en raison de ses fleurs jaunes.

Concernant la classification des stades phénologiques principaux et secondaires du blé en utilisant uniquement les données S-1 seules, le rapport σ^0VH:σ^0VV s'est classé premier pour les deux cultures, tandis que σ^0VV s'est classé troisième. Des études antérieures ont démontré la pertinence des coefficients de rétrodiffusion (σ^0VH, σ^0VV) et du rapport de polarisation (σ^0VH:σ^0VV) pour l'estimation de la biomasse et de l'ISF du blé (Dente et al. 2008 ; Jin et al. 2015b ; Betbeder et al. 2016b) et du maïs (Gao et al. 2013). Veloso et al. (2017) ont conclu que l'influence du sol était réduite pour le blé en utilisant σ^0VH:σ^0VV par rapport à σ^0VH et σ^0VV.

Pour le colza, le rapport σ^0VH:σ^0VV est la variable la plus importante en utilisant uniquement les données S-1 pour classer les stades phénologiques principaux et secondaires.

Le rapport σ^0VH:σ^0VV s'est révélé très performant pour l'identification des principaux stades phénologiques des deux cultures, confirmant sa grande fiabilité pour l'identification des stades phénologiques principaux et secondaires.

Conformément aux résultats de Betbeder et al. (2016), les indicateurs polarimétriques sont importants pour le blé et le colza : plusieurs d'entre eux figurent parmi les 4 variables d'entrée sélectionnées sur la base du seuil défini automatiquement pour les prédictions des stades phénologiques principaux et secondaires des deux cultures. SE_p et le span ont été sélectionnés pour prédire les stades phénologiques principaux du blé et SE_i a été sélectionné pour le colza, tandis que pour les stades phénologiques secondaires, la sélection comprenait SE_p et SE pour le blé et SE_i et SE pour le colza.

De façon générale, cette étude visait à évaluer le potentiel des données S-1 seules, des données S-2 seules, et leur utilisation combinée pour prédire les stades phénologiques du blé et du colza. Pour le blé, l'utilisation combinée des données S-1 et S-2 a été plus performante que l'utilisation des données S-1 ou S-2 seules pour détecter les principaux stades phénologiques du blé et du colza.

Les stades phénologiques secondaires du blé ont été mieux identifiés en utilisant les données S-2 qu'en utilisant les données S-1. Sur la base de l'écart-type de l'indice kappa moyen, des résultats similaires ont été obtenus en utilisant les données S-2 seules ou les données S-1 et S-2 combinées pour les stades phénologiques secondaires du blé. Le tallage est le stade phénologique principal et secondaire le plus précisément classé en utilisant les données S-1 seules, les données S-2 seules et leur utilisation combinée. Du DoY 18 à 72, le blé est au stade du tallage et un comportement temporel spécifique des variables S-1 et S-2 a été observé par rapport à tous les autres stades phénologiques. Cependant, le stade de tallage a été mieux identifié en utilisant les données de S-1 que celles de S-2, tandis que les stades de floraison, de développement du fruit et de maturation ont été mieux identifiés en utilisant S-2 que S-1. Le signal RSO est sensible à la géométrie (par exemple la rugosité, la texture, la structure interne) et à l'humidité des cibles observées, tandis que la réflectance optique est influencée par leur physiologie. Ainsi, nous pouvons conclure que le stade de tallage du blé a été mieux discriminé par la structure du champ de blé plutôt que par sa physiologie. À partir du stade de l'élongation de la tige, la géométrie du blé est verticale et varie peu jusqu'à la maturation, tandis que la teneur en chlorophylle augmente puis diminue. Ainsi, les variables S-2 sont plus efficaces que les variables S-1 pour discriminer ces stades phénologiques du blé. Pour les principaux stades phénologiques du blé, l'utilisation combinée des données S-1 et S-2 a permis d'améliorer la précision utilisateur (UA) du tallage, de l'élongation de la tige

et de la maturation ; seule l'UA des stades d'élongation de la tige et de floraison a été inférieure à celle de S-2. Ceci est cohérent avec les études précédentes qui ont montré la saturation de la bande C (El Hajj et al. 2019) et des bandes optiques (Haboudane et al. 2004) à des niveaux élevés de biomasse de blé.

Pour les principaux stades phénologiques du colza, l'indice de kappa moyen en utilisant les données combinées S-1 et S-2 est plus élevé et fortement supérieur à ceux obtenus avec les données S-2 seules et les données S-1 seules respectivement. Pour les stades phénologiques secondaires, les résultats de l'utilisation combinée des données S-1 et S-2 sont similaires à ceux obtenus avec les données S-2 seules. Cependant, l'utilisation combinée des données S-1 et S-2 a permis d'augmenter la précision de l'identification du stade de développement des feuilles du colza grâce à des informations complémentaires sur la physiologie à partir de S-2 et la géométrie à partir de S-1. Le développement du fruit est le principal stade phénologique le plus difficile à identifier en utilisant les données S-1 seules et l'utilisation combinée des données S-1 et S-2, en raison de la confusion avec le stade de maturation. Les variables les plus importantes en utilisant les données S-1 seules sont σ^0VH, le σ^0VH:σ^0VV et σ^0VV. L'analyse des profils temporels a montré que le rapport σ^0VH:σ^0VV est stable entre le développement du fruit et la maturation, tandis que σ^0VH et σ^0VV augmentent légèrement. La structure des stades du colza est très similaire pendant le développement du fruit et la maturation, les éléments de la canopée étant orientées de manière aléatoire. Cette grande similitude peut s'expliquer par le fait que les observations sur le terrain ont été effectuées au cours de stades phénologiques successifs (c'est-à-dire la fin du développement du fruit (BBCH = 77 et 79) et le début et la fin de la maturation (BBCH = 80 et 89)). Cependant, bien que le développement du fruit ait été beaucoup mieux classé en utilisant les données S-1 et S-2 combinées (UA max = 0,87, précision producteur (PA) max = 0,75) qu'en utilisant les données S-1 seules (UA max = 0,32, PA max = 0,21), ce stade phénologique est le moins bien prédit. Les variables les plus importantes en utilisant des données combinées S-1 et S-2 sont σ^0VH dérivé de S-1 suivi du NDVI et du S2REP dérivés de S-2 et ensuite SE, le span, SE_i normalisée, et le σ^0VH:σ^0VV et le σ^0VV dérivés de S-1. Ainsi, l'utilisation des données RSO S-1 entraîne une confusion accrue entre le développement du fruit et les stades de maturation. Le développement du fruit est le stade phénologique secondaire le plus difficile à identifier en utilisant uniquement les données S-1, tandis que le début et le milieu de la floraison sont les moins bien prédits en utilisant uniquement les données S-2 et les données combinées S-1 et S-2. Des erreurs de prédiction se sont produites entre les deux stades phénologiques secondaires de la floraison, le premier correspondant aux premières fleurs ouvertes et le second à la pleine floraison jusqu'à la fin de la floraison. Il convient de noter que cette période coïncide avec l'absence de données S-2 en raison de la couverture nuageuse, tandis que les profils temporels S-1 montrent peu de variation.

Les résultats de la classification obtenue avec l'utilisation combinée des données S-1 et S-2 ont mis en évidence la grande contribution des variables S-1 pour le colza. L'utilisation combinée des données S-1 et S-2 a permis de mieux identifier les principaux stades phénologiques du colza que les données S-2 seules ; en outre, l'identification du stade de développement des feuilles a été améliorée par l'ajout des variables S-1. Les résultats sont plus équilibrés pour les stades phénologiques secondaires du blé, car les résultats des données S-2 seules sont similaires à ceux obtenus avec des données S-1 et S-2 combinées, sauf pour le stade de tallage.

Globalement, cette étude a permis de souligner l'intérêt des indicateurs polarimétriques et de la combinaison des données S-1 et S-2 pour suivre la phénologie du blé et du colza. Nous avons appliqué les modèles finaux développés en Picardie sur le site breton et avons obtenu des résultats similaires, ce qui confirme l'intérêt des données Sentinel et la robustesse de la méthode utilisée pour l'identification des stades phénologiques des cultures.

Nous avons ensuite poursuivi nos recherches sur la caractérisation des cultures en cherchant à évaluer le potentiel des images S-1 et S-2 pour estimer l'ISF, la biomasse humide (WB), la biomasse sèche (DB) et la WC du blé et du colza.

Nous avons comparé le pouvoir prédictif de 22 variables optiques S-2 (10 bandes spectrales et 12 indices de végétation) et 7 variables RSO S-1 (2 coefficients de rétrodiffusion, 1 ratio et 4 indicateurs polarimétriques) en utilisant des régressions par processus gaussien.

Cette étude, appliquée au site breton, a montré le potentiel des données S-1 et S-2 pour estimer ces 4 paramètres de cultures pour le blé et le colza.

Cette étude a démontré le potentiel des séries chronologiques RSO S-1 et optiques S-2 pour estimer les paramètres biophysiques des cultures (ISF, WB, DB et WC) du blé et du colza. Les résultats montrent que les performances des variables S-2 sont équivalentes ou supérieures à celles des variables S-1.

Les meilleurs modèles obtenus avec S-2 utilisent les bandes vertes, proche-infrarouge et les indices de végétation respectivement pour l'ISF (R^2 ajusté = 0.91), la biomasse (R^2 ajusté > 0.70) et la WC (R^2 ajusté = 0.82) du blé, et les bandes infrarouge-courtes pour la DB (R^2 ajusté = 0.85) et la biomasse humide (R^2 ajusté = 0.77) du colza.

En ce qui concerne les modèles basés sur S-1, le rapport σ^0VH:σ^0VV s'avère être la variable la plus pertinente pour l'ISF du blé et la biomasse du colza, et la contribution de la polarisation SE la plus performante pour la WC du blé. Les résultats obtenus en utilisant les variables S-2 étaient similaires ou supérieurs à ceux obtenus en utilisant les caractéristiques S-1 pour l'estimation des paramètres biophysiques des cultures de blé et de colza.

Pour le blé, les corrélations les plus élevées en utilisant les variables S-1 étaient le ratio σ^0VH:σ^0VV avec l'ISF (R^2 = 0,91) et la contribution de la polarisation de SE avec la WC (R^2 = 0,78), tandis que les meilleurs modèles basés sur S-2 ont été obtenus en utilisant la bande verte pour la WC (R^2 = 0,82), la bande proche infrarouge 8 pour l'ISF (R^2 = 0,91), l'indice WDVI pour la DB (R^2 = 0,72) et l'indice MTCI pour la WC (R^2 = 0,71). Pour le colza, les corrélations les plus élevées étaient le rapport σ^0VH:σ^0VV et la contribution de la polarisation de SE avec la WB et la DB (R^2 ajusté > 0,75), tandis que les bandes SWIR de S-2 semblaient prometteuses pour l'estimation de la DB (R^2 ajusté = 0,85) et de la WB (R^2 ajusté = 0,77). Les résultats ont également mis en évidence, pour la première fois, l'importance des indicateurs polarimétriques (SE et portée) dérivés des séries temporelles de S-1 pour l'estimation des paramètres biophysiques des cultures de blé et de colza.

Sur la base des résultats obtenus dans les deux études précédentes, nous avons cherché à évaluer l'impact de la structuration spatio-temporelle des mosaïques paysagères forêt-agriculture sur la biodiversité.

Pour cela, nous avons analysé l'influence de l'hétérogénéité biophysique sur la phénologie du blé et la biodiversité qui y est associée sur les sites en Bretagne, en Picardie et en Wallonie. L'indice de végétation WDVI a été utilisé comme métrique de l'hétérogénéité biophysique et indicateur de la phénologie du blé. D'abord, nous avons analysé les relations entre la mosaïque des cultures, le grain du paysage et l'hétérogénéité biophysique. Puis, nous avons étudié l'effet de l'hétérogénéité biophysique sur la phénologie du blé. Enfin, la distribution des espèces de carabes a été estimée en utilisant la métrique d'hétérogénéité biophysique.

Les résultats ont montré que le grain du paysage et le gradient de mosaïque des cultures était fortement corrélés (R^2 ajusté maximum = 0.81). En ce qui concerne l'analyse conjointe de tous les sites, l'hétérogénéité biophysique était bénéfique pour la phénologie du blé pendant la période de maturation. L'analyse par site a montré que l'hétérogénéité biophysique était bénéfique pour la croissance du blé dans le grain fin mais la désavantageait dans les paysages de plein champ tant pendant la période d'extension de la tige que la maturation. La métrique d'hétérogénéité biophysique a permis d'estimer avec précision la distribution des espèces de carabes (R^2 ajusté maximum = 0,62). Cette étude a souligné l'intérêt d'utiliser les données S-2 pour comprendre la dynamique du blé et la biodiversité qui lui est associée.

Plus précisément, ces recherches ont permis de mettre en exergue les six points suivants:

1- L'intérêt de l'utilisation de la télédétection pour caractériser les paysages :

Les images de télédétection gratuites, telles que les données Sentinel, permettent de remédier aux limites de la collecte de données et au coût financier des images. Crowley et Cardille (2020) ont passé en revue les recherches sur l'écologie du paysage des cinq dernières années et ont identifié les contributions futures de la télédétection à l'écologie du paysage. Sur la base de cette revue, les innovations de notre étude sont l'utilisation d'un suivi intra-annuel pour analyser les paysages, la comparaison de différents paysages et l'utilisation de valeurs continues (WDVI) plutôt que de classes discrètes.

Les séries temporelles S-2 permettent de suivre régulièrement la dynamique des paysages à une échelle fine. L'utilisation d'une variété de zones d'étude a généré un gradient continu du paysage, ce qui nous a permis d'identifier des modèles de paysage qui se développent le long des gradients, alors que chaque paysage conservait sa propre identité. Cela contraste avec de nombreuses études qui mettent en commun des données provenant de différents paysages sans les rendre distinctes dans l'analyse (par exemple, Alignier et al. 2020).

Dans notre étude, les modèles de paysage sont apparus en raison de la diversité des paysages. Il est difficile de cartographier la mosaïque des cultures de manière précise et cohérente en utilisant des images satellites de différentes zones d'étude ou à grande échelle. La précision d'une carte peut être mesurée en utilisant des estimateurs de qualité (par exemple, l'indice de kappa, la précision globale, le F-score). Néanmoins, l'évaluation de la précision dépend en grande partie des données de validation, et l'incertitude est inévitable en raison des erreurs de classification qui se produisent à différents stades de la production

de la carte (Friedl et al. 2001 ; Congalton et al. 2014). Les valeurs continues telles que le WDVI permettent de surmonter ce problème car le WDVI utilise deux variables (bandes rouge et proche-infrarouge) qui ont été mesurées de manière cohérente sur toutes les images. Crowley et Cardille (2020) ont recommandé de passer d'indices catégoriels à des valeurs continues pour les évaluations d'habitats afin de mieux évaluer les impacts des changements de paysages sur la biodiversité et de quantifier les erreurs dans les modèles d'écologie des paysages. Plusieurs auteurs (par exemple McGarigal et al. 2009 ; Lausch et al. 2015) recommandent de passer d'une représentation des paysages en mosaïque à une représentation en gradient. En outre, les valeurs continues sont les plus adaptées pour saisir les gradients d'un paysage.

La télédétection optique reflète la dynamique phénologique des cultures avec la différenced de WDVI (Diff WDVI) indépendamment des cultures voisines. Mercier et al. (2020b) ont constaté que les variables (coefficients de rétrodiffusion et indicateurs polarimétriques) dérivées du capteur RSO S-1 étaient adaptées à la surveillance des stades phénologiques et des paramètres biophysiques des cultures de blé. Le domaine des micro-ondes (RaDAR) capture la géométrie du blé, tandis que le domaine optique est sensible à la teneur en chlorophylle. De plus, la rugosité du blé, liée à sa géométrie, influence directement la vitesse du vent (Kawatani et Meroney 1970). Il serait donc intéressant de comparer les résultats de S-1 et S-2 pour étudier l'hétérogénéité biophysique.

Aucun flux n'a été mesuré ou modélisé dans cette étude, de sorte que des recherches supplémentaires sont nécessaires pour confirmer la capacité de la métrique d'hétérogénéité biophysique (WDVI SD) à représenter l'énergie physique des paysages. Cependant, cette étude fournit un cadre pour l'échantillonnage des flux dans les paysages. Le WDVI SD pourrait être utilisé à des échelles pertinentes comme indicateur pour les zones ciblées. Des études antérieures ont permis de développer des méthodes pour produire des cartes de microclimat qui intègrent des données de télédétection, comme celles du LiDAR, (George et al. 2015), des drônes (Maes et al. 2017) et des données satellite MODIS (Metz et al. 2014 ; Fick et Hijmans 2017). De futures études pourraient analyser les corrélations entre le WDVI SD et les cartes de microclimat ou l'échantillonnage sur le terrain.

2- Les effets de la structure du paysage sur l'hétérogénéité biophysique :

Le grain du paysage est fortement corrélé avec le gradient de la mosaïque des cultures ; en effet, l'organisation de l'utilisation des terres dépend de la densité des haies (Thenail 2002). De 1940 à 1990 en France, une grande partie du réseau de haies a été supprimée en raison des programmes de remembrement des terres visant à soutenir l'intensification agricole (Baudry et Burel 1984). Les paysages à grains fins sont principalement liés à des systèmes d'élevage extensif et de prairies (fourrage, bétail), tandis que les paysages à grains grossiers sont davantage dominés par la rotation des cultures. Par exemple, dans la zone d'étude bretonne, la proportion de maïs augmente et les prairies diminuent, passant de paysages à grains fins à des paysages à grains grossiers (Thenail et Baudry 2004). Cela explique pourquoi, dans cette étude, la zone d'étude s'étendait souvent sur de plus grandes sections de gradients. La fragmentation des territoires agricoles dans les paysages à grains fins a simplifié les successions de cultures et la diversité du bétail en circulation. À l'inverse, les grands champs dans les paysages à grains grossiers sont susceptibles d'avoir des conditions physiques similaires ; c'est pourquoi de nombreux îlots de terre formés en un seul champ sont utilisés pour des cultures de rente. Dans notre étude, les paysages à grains fins se trouvaient en Bretagne, en Picardie-Ouest et en Wallonie-Nord-Ouest, qui contenaient

principalement des prairies et des proportions variables de blé et de maïs. Les paysages à grains grossiers se trouvaient en Wallonie-Sud, en Wallonie-Nord-Est et en Picardie-Ouest, qui contenaient principalement de la betterave et du blé. Le grain des paysages des six zones d'étude apparaît le long du gradient de la mosaïque de cultures puisqu'il représente un gradient allant des prairies et du maïs, au blé et à la betterave (figure 7-5). Les deux facteurs, grain paysager et mosaïque de cultures, sont toutefois confondus, de sorte que leurs effets sur la phénologie du blé peuvent être soit confondus, soit complémentaires.

3- Les effets de l'hétérogénéité biophysique sur la phénologie du blé :

Sur la base de l'analyse combinée de tous les sites, l'hétérogénéité biophysique (WDVI SD) a eu un effet positif sur la croissance du blé (Diff WDVI) pendant la période de maturation, puisque la Diff WDVI a diminué alors que la WDVI SD a augmenté. L'hétérogénéité biophysique provoque des flux d'énergie latéraux qui favorisent la croissance du blé. Cependant, l'analyse des sites individuels a montré que l'hétérogénéité biophysique (WDVI SD) semble être bénéfique à la croissance du blé dans les paysages à grains fins, mais qu'elle est un inconvénient dans les paysages à grains grossiers. Ainsi, les flux sont des échanges bénéfiques dans les paysages à grains fins mais sont des perturbations dans les paysages à grains grossiers. Ce phénomène s'explique probablement par la nature des flux dans chaque paysage. Alford et al. (2018) ont constaté que les paysages ouverts sont plus chauds que les paysages complexes, qui ont des températures plus extrêmes et plus variables. Les températures locales augmentent parce que le paysage à grains grossiers est exposé à plus de rayonnement à ondes courtes pendant la journée (Chen et al. 1999). Dans les paysages à grains fins, les haies fonctionnent comme des brise-vent qui réduisent la vitesse du vent local et augmentent l'humidité relative en condensant l'air frais et dense (Kort 1988). Alford et al. (2018) ont observé que le passage de l'hiver au printemps augmentait la croissance de la végétation et amortissait les températures. Les différences entre les paysages diminuent, mais les paysages à grains fins restent plus froids que les paysages à grains grossiers. Les différences de température entre le jour et la nuit sont plus importantes les jours ensoleillés, et les bois interceptent le rayonnement solaire, ce qui réduit l'amplitude de la température diurne (Zellweger et al. 2019). Ainsi, l'hétérogénéité biophysique dans les paysages à grain grossier provoquerait des flux de température et des températures extrêmes qui réduisent la croissance du blé.

4- L'importance de l'échelle du paysage :

Les relations entre le gradient de la mosaïque des cultures et l'hétérogénéité biophysique (WDVI SD) avaient un R^2 ajusté plus élevé à des échelles plus grandes. À mesure que l'échelle d'analyse augmentait, la variabilité au sein de chaque zone d'étude diminuait, mais la variabilité entre les zones d'étude augmentait. Ainsi, si une relation existe entre deux mesures analysées dans des fenêtres, elle sera plus forte à des échelles plus grandes. La structure du paysage a influencé les changements dans le blé au sein du champ. Pour tous les sites, les échelles qui expliquaient le plus de variance avaient un rayon supérieur à 1505 m, sauf pour la période d'extension des tiges en 2017. Pour certains sites, les échelles de 255 et 505 m ont montré des relations significatives entre l'hétérogénéité biophysique (WDVI SD) et la phénologie du blé (Diff WDVI) pendant la maturation du blé en 2017 et 2018. Toutefois, ces échelles n'étaient plus présentes lorsque tous les points d'échantillonnage des six zones d'étude ont été pris en compte. À mesure que l'étendue des cartes WDVI SD augmentait, les valeurs de WDVI SD devenaient plus homogènes. À l'échelle européenne, la diversité des

pratiques locales contribue de moins en moins à l'explication des différences entre les sites à mesure que l'échelle augmente. Cependant, l'échelle de 255 m était significative pendant la période d'extension des tiges les deux années, ce qui indique que les pratiques locales influencent davantage la croissance du blé pendant cette période.

5- La répartition de *Pterostichus melanarius* (*P. melanarius)* et *Poecilus cupreus* (*P. cupreus*) à l'échelle du paysage :

P. melanarius et P. cupreus ont été trouvés dans des paysages et des lieux différents. Thomas et al. (2001) ont observé une séparation spatiale entre ces espèces dans différents domaines. Ces deux espèces de carabes ont des exigences écologiques différentes. *P. cupreus* était plus abondant dans les paysages à grains fins de Bretagne et de Picardie-Est, tandis que *P. melanarius* était plus abondant dans les paysages à grains grossiers de Picardie-Ouest et de Wallonie-Sud. *P. cupreus* reste près des haies, tandis que *P. melanarius* en est plus éloigné (Winder et al. 2001 ; Rouabah et al. 2015), bien qu'aucune des deux espèces ne traverse les haies (Holland et al. 2004). *P. melanarius* est adapté aux variations de température (Holland et al. 2005), et les paysages ouverts ont des températures plus extrêmes et variables que les paysages complexes (Alford et al. 2018). Ainsi, cette caractéristique biologique de *P. melanarius* le rend adapté aux paysages à grains grossiers. Certaines préférences d'habitat de *P. melanarius et P. cupreus* restent floues en raison de résultats opposés. Par exemple, Thomas et al. (2001) ont trouvé *P. cupreus* à l'intérieur des champs, tandis que Rouabah et al. (2015) les ont trouvés près de haies. Hassan et al. (2013) ont trouvé une abondance plus faible de *P. cupreus* dans des paysages à grains fins, ce qui est contraire à nos résultats. Ces résultats contrastés peuvent être dus à d'autres facteurs qui influencent la distribution des carabes, tels que les types de cultures, l'âge des haies, l'humidité du sol, la densité des proies, l'exclusion compétitive, la prédation mutuelle et le système de gestion (Winder et al. 2001; Holland et al. 2004; Rouabah et al. 2015).

6- L'utilisation de la télédétection pour comprendre la biodiversité :

Nous avons montré que les distributions de *P. melanirus* et *P. cupreus* étaient liées à l'hétérogénéité biophysique (WDVI SD). Cependant, l'hétérogénéité biophysique (WDVI SD) était fortement corrélée avec le gradient de la mosaïque des cultures et le grain du paysage. Par conséquent, nous n'avons pas pu quantifier l'effet de chaque variable sur *P. melanirus* et *P. cupreus* ; cependant, l'effet du paysage (grain du paysage et gradient de la mosaïque des cultures) peut être évalué à l'aide du WDVI SD. La télédétection permet d'étudier la distribution des carabes sans avoir besoin d'une carte de l'utilisation des terres ou des haies. En outre, elle est cohérente entre les types de cultures et les lieux, ce qui permet d'aborder les questions écologiques en utilisant des images gratuites qui sont disponibles pour n'importe quelle zone de la Terre (données Sentinel disponibles sur https://scihub.copernicus.eu). Inversement, pour des variables fixes telles que les mosaïques de cultures, le WDVI SD varie dans le temps. La relation entre le WDVI SD et le facteur 1 de l'analyse factorielle par correspondances explique un état (c'est-à-dire la répartition de deux espèces de carabes) mais pas sa dynamique. Comme le WDVI SD est un indice spatio-temporel, les futures études pourraient l'utiliser pour se concentrer sur la dynamique des carabes.

Dans l'ensemble, l'étude a mis en évidence l'intérêt d'utiliser les données de télédétection optique pour comprendre la dynamique du blé et la biodiversité qui lui est associée. Pour mieux comprendre la fonction écologique de l'hétérogénéité biophysique, il convient de

comparer le SD WDVI développé aux mesures de flux d'énergie. Il serait également intéressant d'évaluer la contribution des images RSO, car le domaine des micro-ondes est sensible à la structure des plantes.

L'objectif de la thèse était double : 1) évaluer comparativement les séries temporelles optiques S-2 et RSO S-1 pour identifier et caractériser les éléments constitutifs des continuités écologiques en utilisant les classifications d'occupation des sols et d'utilisation des sols et la caractérisation des cultures dans les paysages boisés et dominés par les cultures, 2) évaluer l'influence de la structuration spatio-temporelle de ces mosaïques de paysages sur la biodiversité en utilisant les mesures dérivées des séries temporelles S-2.

Nous avons exposé dans la première partie de la thèse les défis posés par l'écologie paysagère et la télédétection appliquées aux continuités écologiques.

La deuxième partie a consisté en une évaluation comparative du potentiel des variables dérivées des données S-1 et S-2 pour identifier et caractériser les éléments constituant les continuités écologiques dans les paysages boisés. L'occupation et l'utilisation des sols ont été identifiées et caractérisées dans des mosaïques forêt-agriculture au Brésil et en Espagne.

Dans une troisième partie, nous avons évalué de manière comparative le potentiel des variables dérivées des données S-1 et S-2 pour identifier et caractériser les éléments constituant les continuités écologiques dans des paysages dominés par les cultures. Les capteurs S-1 et S-2 ont également été évalués pour estimer les stades phénologiques et des variables biophysiques dans les cultures de blé et de colza.

Une quatrième partie a été consacrée à l'analyse des relations entre les cartes des mesures du paysage dérivées des images Sentinel et les données relevées sur les espèces. Nous avons analysé l'influence de l'hétérogénéité biophysique dérivée de S-2 sur la phénologie du blé et la distribution de deux espèces de carabes agricoles dans six paysages dominés par des cultures.

Plus précisément, la deuxième partie de la thèse visait à répondre à la question : Quels sont les capteurs et les variables Sentinel les plus efficaces pour identifier les éléments potentiellement constitutifs des continuités écologiques dans les paysages boisés ?

Pour répondre à cette question, nous avons évalué le potentiel des données S-1 seules, des données S-2 seules et des données S-1 et S-2 combinées pour identifier et caractériser les types d'occupation des sols dans des paysages de mosaïque forêt-agriculture. L'étude s'est concentrée sur deux paysages boisés présentant des gradients de végétation contrastés : un paysage montagneux tempéré dans la monts cantabriques (Espagne) et un paysage forestier tropical humide à Paragominas (Brésil). Bien que ces mosaïques de paysages soient très différentes, elles ont des fonctions écologiques similaires (conservation de la biodiversité et stockage du carbone). Les images satellites ont été classées selon une procédure incrémentielle basée sur le rang d'importance des variables d'entrée dérivées des séries temporelles S-1 et S-2. Les données S-2 seules ont donné de meilleurs résultats (indice kappa moyen = 0,59-0,83) que les données S-1 seules (indice kappa moyen = 0,28-0,72), tandis que la combinaison des deux types de données a légèrement amélioré les résultats (indice kappa moyen = 0,55-0,85). La méthode utilisée permet de définir le nombre et le type de variables qui discriminent de manière optimale les classes d'utilisation des terres en fonction du type de paysage considéré. La meilleure configuration pour les zones d'étude espagnole et brésilienne comprend respectivement 5 et 10 variables pour les données S-2 et 10 et 20 variables pour les données S-1. Le PIR et les polarisations VV et VH sont les variables les plus discriminantes pour les données S-2 et S-1, respectivement. En outre, la méthode a permis de définir des périodes clés pour la discrimination des classes d'occupation et d'utilisation des sols selon le type d'images utilisées. Par exemple, dans les montagnes cantabriques, l'hiver et l'été sont des périodes clés pour la série temporelle S-2, tandis que le printemps et l'hiver sont des périodes clés pour la série temporelle S-1.

La troisième partie de la thèse visait à répondre à la question : Quels sont le capteur et les variables Sentinel les plus efficaces pour identifier et caractériser les éléments constitutifs potentiels des continuités écologiques dans les paysages dominés par les cultures ? Cette partie se concentre sur la caractérisation des cultures avec l'étude du blé et du colza, qui sont deux des cultures les plus importantes au monde en termes de surface récoltée.

Nous avons évalué le potentiel des données S-1 seules, des données S-2 seules et des données S-1 et S-2 combinées pour identifier les stades phénologiques principaux et secondaires du blé et du colza en Picardie (France). Plus spécifiquement, le but de cette étude était d'évaluer l'intérêt des indicateurs polarimétriques dérivés des données S-1 et de déterminer le nombre et le type de variables S-1 et S-2 nécessaires pour discriminer les stades phénologiques du blé et du colza. Nous avons estimé la performance des bandes spectrales et des indices de végétation dérivés de S-2 et des coefficients de rétrodiffusion et des indicateurs polarimétriques dérivés de S-1. Les images satellites ont été classées en utilisant la méthode incrémentale développée dans l'étude précédente (Mercier et al. 2019b). Les résultats ont montré que l'utilisation combinée des données S-1 et S-2 (kappa moyen = 0,53-0,82 et 0,74-0,92 pour le blé et le colza, respectivement) offrait une plus grande précision que l'utilisation des données S-1 seules (kappa moyen = 0. 48-0,61 et 0,61-0,64 pour le blé et le colza, respectivement) ou S-2 seules (kappa moyen = 0,54-0,75 et 0,67-0,86 pour le blé et le colza, respectivement) pour l'identification des stades phénologiques principaux et secondaires. Les variables les plus importantes étaient le ratio σ^0VH:σ^0VV et les indicateurs polarimétriques pour S-1 et les indices NDVI et S2REP et la variable biophysique, ISF, pour S-2. Dans l'ensemble, cette étude a souligné l'intérêt des indicateurs polarimétriques et de l'utilisation combinée des données S-1 et S-2 pour suivre la phénologie du blé et du colza.

Nous avons ensuite poursuivi nos recherches sur la caractérisation des cultures en évaluant le potentiel des images S-1 et S-2 pour estimer l'ISF, la WB, la DB et la WC du blé et du colza. Nous avons comparé le pouvoir prédictif de 22 variables optiques S-2 (10 bandes spectrales et 12 indices de végétation) et de 7 variables RSO S-1 (2 coefficients de rétrodiffusion, 1 rapport et 4 indicateurs polarimétriques) en utilisant la régression par processus gaussien (GPR). Cette étude, appliquée à la zone d'étude de la Bretagne, a montré le potentiel des données S-1 et S-2 pour estimer ces 4 paramètres de culture pour le blé et le colza. La performance des variables S-2 est équivalente ou supérieure à celle des variables S-1. Les meilleurs modèles obtenus avec S-1 utilisent les bandes verte, PIR et les indices de végétation respectivement pour l'ISF (R^2 ajusté = 0,91), la biomasse (R^2 ajusté > 0,70) et la WC (R^2 ajusté = 0,82) du blé, et les bandes infraouge-courtes pour la DB (R^2 ajusté = 0,85) et la WB (R^2 ajusté = 0,77) du colza. Pour les variables S-1, le ratio σ^0VH:σ^0VV était le plus pertinent pour l'ISF du blé (R^2 ajusté = 0,91) et la biomasse du colza (R^2 ajusté > 0,75), par rapport à SE pour la WC du blé (R^2 ajusté = 0,78). Tout en confirmant l'intérêt des données S-2, les résultats ont mis en évidence, de manière inédite, l'importance des indicateurs polarimétriques dérivés de S-1 pour l'estimation des paramètres biophysiques du blé et du colza.

Enfin, la quatrième et dernière partie de la thèse visait à répondre à la question : Quel est l'impact de la structuration spatio-temporelle du paysage sur la phénologie des cultures et la biodiversité dans les paysages dominés par les cultures ?

Sur la base des résultats obtenus dans la partie précédente, nous avons évalué l'impact de la structuration spatio-temporelle de la mosaïque de cultures sur la biodiversité. Pour cela, nous avons analysé l'influence de l'hétérogénéité biophysique sur la phénologie du blé et la biodiversité associée dans les zones d'étude de Bretagne, de Picardie et de Wallonie.

L'indice de végétation nommé WDVI calculé à partir des données S-2 a été utilisé comme mesure de l'hétérogénéité biophysique et comme indicateur de la phénologie du blé. Nous avons d'abord analysé les relations entre la mosaïque des cultures, le grain du paysage et l'hétérogénéité biophysique. Ensuite, nous avons étudié l'effet de l'hétérogénéité biophysique sur la phénologie du blé. Enfin, la distribution de deux espèces de carabes a été estimée en utilisant la métrique de l'hétérogénéité biophysique. Les résultats ont montré que les gradients de la mosaïque des céréales et des cultures étaient fortement corrélés (R^2 maximum ajusté = 0,81). Pour l'analyse conjointe de tous les sites, l'hétérogénéité biophysique a été bénéfique pour la phénologie du blé pendant la période de maturation. L'analyse par site a montré que l'hétérogénéité biophysique était bénéfique pour la croissance du blé à grain fin mais la défavorisait dans les paysages de plein champ tant pendant la période d'extension des tiges que pendant la période de maturation. La mesure de l'hétérogénéité biophysique a été utilisée pour estimer avec précision la distribution de deux espèces de carabes (R^2 maximum ajusté = 0,62). Cette étude a souligné l'intérêt d'utiliser les données S-2 pour comprendre la dynamique du blé et la biodiversité associée.

D'une façon générale, cette thèse a permis d'évaluer le potentiel des séries temporelles optiques S-2 et RSO S-1 pour identifier et caractériser les continuités écologiques dans des paysages boisés et dominés par les cultures. Plus spécifiquement, nous avons montré que bien que les données S-2 soient plus appropriées que les données S-1 pour discriminer les types d'occupation et d'utilisation des terres ainsi que les stades phénologiques et les variables biophysiques du blé et du colza, l'utilisation combinée des données S-1 et S-2 améliore la précision des classifications, les données S-1 montrant également un grand intérêt pour les zones nuageuses. Nos recherches ont également montré l'intérêt des indicateurs polarimétriques dérivés des données S-1 pour caractériser les cultures de blé et de colza insérées dans des paysages dominés par les cultures. Enfin, cette thèse a mis en évidence l'intérêt de la métrique d'hétérogénéité biophysique dérivée des données S-2 qui a permis d'estimer précisément la distribution de deux espèces de carabes. La mosaïque de cultures peut être considérée comme une infrastructure verte pour gérer la biodiversité à l'échelle du paysage. La mesure de l'hétérogénéité biophysique dérivée des images S-2 est continue, cohérente entre les lieux et les types de cultures et capable de traiter des questions écologiques en utilisant des images satellites gratuites disponibles partout sur la Terre.

Sur la base de ces résultats, nous mettons également en évidence plusieurs questions qui doivent être abordées dans le cadre des travaux en cours et futurs.

Concernant la combinaison des données S-1 et S-2 pour identifier les éléments constitutifs des continuités écologiques, les méthodes de fusion utilisées dans cette thèse sont appelées fusion de bas niveau ou de pré-classification car elles consistent à combiner des variables "brutes" optiques et RSO. Les fusions de haut niveau (ou fusions de post-classification) consistent à combiner des informations extraites de jeux de données indépendants. Par exemple, dans le cas des cartes d'occupation des sols, les classes les mieux identifiées par les données S-2 seules et les données S-1 seules pourraient être combinées pour former une carte finale. Cependant, cette méthode nécessite une analyse initiale des classifications dérivées de chaque ensemble de données indépendant et une prise de décision adaptée à l'objectif de l'étude pour obtenir une carte finale pertinente. Par conséquent, il serait intéressant d'évaluer comparativement les méthodes de fusion avec différents niveaux sémantiques afin d'optimiser la fusion des données RSO et optiques pour identifier et caractériser les éléments constitutifs des continuités écologiques.

Concernant le modèle de prédiction des stades phénologiques que nous avons développé dans la deuxième partie de cette thèse sur la zone d'étude située en Picardie, nous avons évalué la robustesse du modèle en l'appliquant sur la zone d'étude de la Bretagne.

Les résultats montrent que les principaux stades phénologiques du colza ont été très bien prédits (kappa = 0,75, OA = 80%) alors que de nombreuses erreurs de classification ont été observées pour les stades phénologiques secondaires.

Pour le blé, l'interprétation des résultats a été plus difficile en raison des différentes typologies entre les échantillons de formation (Picardie) et de validation (Bretagne). Cependant, les résultats ont montré une prédiction correcte du stade d'élongation de la tige et une succession cohérente des stades phénologiques principaux et secondaires.

Ces résultats ont confirmé que la méthode utilisée était robuste pour la prédiction des principaux stades phénologiques du colza et prometteuse pour les stades phénologiques principaux et secondaires du blé. Ces résultats ont été valorisés lors du Symposium international de télédétection de SPIE (Mercier et al. 2019a).

Par ailleurs, l'utilisation d'échantillons collectés dans plusieurs zones d'étude pourrait également contribuer à tester la robustesse du modèle appliqué à l'estimation des variables biophysiques des cultures (partie 2), d'autant plus que l'échantillonnage utilisé était de petite taille. Le petit nombre d'enquêtes sur les cultures pour l'estimation des variables biophysiques des cultures dérivées des données S-1 et S-2 a constitué un facteur limitant lors de l'essai des modèles statistiques. En effet, plus la taille de l'échantillon est faible, plus le pouvoir prédictif du test statistique est faible. Une taille d'échantillon plus importante permettrait de tester des méthodes de modélisation plus puissantes telles que le random forest ou le support vector machine.

L'hétérogénéité biophysique (WDVI SD) mesurée à partir des données S-2 est une mesure continue qui reflète un état biophysique plutôt que des classes de cultures discrètes. Cette valeur continue est pertinente pour les espèces généralistes. En effet, ces espèces ne sont pas spécialisées dans un type d'occupation/utilisation des terres ou d'espèces végétales, car elles utilisent plusieurs types d'occupation/utilisation des terres au cours de leur cycle de vie. En outre, dans les paysages dominés par les cultures, l'hétérogénéité du paysage est généralement bénéfique pour les espèces généralistes. Des cartes d'adéquation des habitats pourraient être dérivées du WDVI SD pour mettre en évidence la connectivité ou la fragmentation des habitats potentiels. Enfin, les variations du WDVI autour d'un élément bénéfique pour une espèce spécialisée pourraient être étudiées pour mieux comprendre la résistance des éléments du paysage au déplacement de cette espèce. Enfin, l'influence du réseau de haies sur l'hétérogénéité biophysique pourrait être étudiée grâce à l'utilisation de données satellitaires à très haute résolution spatiale telles que les images SPOT-6.

Au cours de cette thèse, une étude a été lancée en étroite collaboration avec l'équipe espagnole du projet WOODNET. Nous avons utilisé un modèle de capacité d'habitat de l'ours brun développé par l'équipe espagnole et détaillé dans un article publié par Gastón et al. (2017). Les métriques paysagères que nous avons calculées à partir des cartes d'occupation des sols dérivées de l'utilisation combinée des données S-1 et S-2 ont été incorporées dans le modèle de capacité d'habitat de l'ours brun. Cette étude visait à évaluer la valeur des cartes espagnoles d'occupation des sols produites dans Mercier et al. (2019b) pour l'identification et la caractérisation des continuités écologiques pour les ours bruns. Les mesures du paysage ont été dérivées de la carte d'occupation des sols la plus précise, c'est-à-

dire la carte dérivée de l'utilisation combinée des données S-1 et S-2. Ces mesures du paysage correspondent à l'hétérogénéité du paysage, au grain du paysage et aux interfaces entre les types d'occupation des sols. Les premiers résultats ont montré que la proportion d'ours bruns augmente avec le grain fin et diminue avec l'hétérogénéité du paysage.

Dans l'ensemble, les interfaces contenant la classe "sol nu" ont un effet négatif sur la proportion d'ours bruns, tandis que les interfaces comprenant des surfaces boisées ont un effet positif.

Des perspectives se sont dégagées de ces premiers résultats et des travaux complémentaires seront effectués en étroite collaboration avec l'équipe espagnole du projet WOODNET. Nous prévoyons d'analyser plus profondémment le choix des paramètres d'entrée du modèle en supprimant les métriques d'interface incluant des types d'occupation des sols mal classés (eau et surfaces artificielles), et de créer de nouvelles métriques paysagères en combinant d'autres d'occupation des sols (formations arbustives/sol nu) à différentes échelles spatiales.

Enfin, la base de données que nous avons développée dans la deuxième partie de cette thèse pour caractériser le blé et le colza sera bientôt disponible dans un document de données afin de partager plus largement les données avec la communauté scientifique

DOCTORAT SOCIETES BRETAGNE TEMPS LOIRE TERRITOIRES

UNIVERSITÉ RENNES 2

Titre : Evaluation des séries temporelles Sentinel-1 & 2 pour l'identification et la caractérisation des continuités écologiques, des paysages boisés aux paysages agricoles.

Mots clés : Télédétection, Agriculture, images satellite optiques et RSO, écologie du paysage

Résumé : La perte des habitats est aujourd'hui considérée comme l'une des plus sérieuses menaces sur la biodiversité. Si de nombreuses études se sont concentrées sur le rôle de « conduit » des éléments boisés, très peu d'entre elles se sont focalisées sur le rôle des continuités écologiques au sein des mosaïques agricoles. Les objectifs de cette thèse étaient (1) d'évaluer la synergie des séries temporelles Sentinel 1 et 2 pour identifier et caractériser les éléments constitutifs des continuités écologiques à travers des classifications de l'occupation et de l'utilisation des sols et la caractérisation de cultures dans les paysages boisés et agricoles et (2) d'estimer l'impact de la structuration spatio-temporelle de ces paysages sur la biodiversité en utilisant des métriques dérivées des séries temporelles Sentinel. Les résultats ont mis en évidence que bien que les données S-2 soient plus adaptées que les données S-1 pour la discrimination des types d'occupation du sol dans les paysages boisés et des stades phénologiques du blé et du colza dans les paysages agricoles, l'usage combiné des données S-2 et S-1 améliore la précision des classifications les données S-1 présentant de surcroît un fort intérêt dans les zones nuageuses. Ils ont aussi montré l'intérêt des indicateurs polarimétriques dérivés des données S-1 pour caractériser les cultures du blé et de colza. Enfin, ils ont permis de souligner l'intérêt de la métrique d'hétérogénéité biophysique dérivée des données S-2 pour estimer précisément la distribution des espèces de carabes. L'usage de cette métrique, calculée avec des images gratuites et disponibles partout sur la Terre, continue et cohérente d'un site à l'autre et d'un type de culture à l'autre, devrait contribuer à l'étude de l'impact des continuités écologiques sur la biodiversité.

Title : Evaluation of Sentinel-1 & 2 time series for the identification and characterization of ecological continuities, form wooded to crop domined landscapes.

Keywords : Remote sensing, Agriculture, Optical and SAR satellite images, landscape ecology

Abstract : Habitat loss is now considered one of the most serious threats to biodiversity. While many studies have focused on the circulation role of woodland features, very few have focused on the role of ecological continuities within agricultural mosaics. The objectives of this thesis were (1) to assess the combined use of Sentinel 1 and 2 time series to identify and characterize the elements of ecological continuities through land cover classifications and crop characterization in wooded and crop-dominated landscapes and (2) to estimate the impact of the spatio-temporal structuring of these landscape on biodiversity using metrics derived from Sentinel time series. The results showed that although S-2 data are more adapted than S-1 data to discriminate between land cover/land use types in wooded landscapes and phenological stages of wheat and rapeseed in crop-dominated landscapes, the combined use of S-2 and S-1 data improves their accuracy of the classifications, with S-1 data also showing a strong interest in cloudy areas. They also showed the interest of polarimetric indicators derived from S-1 data to characterize wheat and rapeseed crops. Finally, they highlighted the interest of the biophysical heterogeneity metrics derived from S-2 data to accurately estimate the distribution of carabid beetle species. The use of this metric, calculated with free images available everywhere on Earth, continuous and consistent from one site to another and from one type of crop to another, should contribute to the study of the impact of ecological continuities on biodiversity.